



**UNIVERSIDAD
DE GRANADA**

Tesis doctoral

PROGRAMA DE DOCTORADO EN BIOMEDICINA

**Generation of chondroinductive scaffolds
with improved biomechanical properties and
development of a bioreactor for cartilage
tissue engineering**

DANIEL MARTÍNEZ MORENO

Directores: JUAN ANTONIO MARCHAL CORRALES, GUILLERMO RUS
CARLBORG y PATRICIA GÁLVEZ MARTÍN

Editor: Universidad de Granada. Tesis Doctorales
Autor: Daniel Martínez Moreno
ISBN: 978-84-1195-462-4
URI: <https://hdl.handle.net/10481/95838>

El doctorando **Daniel Martínez Moreno** y los directores de la tesis **Juan Antonio Marchal Corrales**, CATEDRÁTICO DEL DEPARTAMENTO DE ANATOMÍA Y EMBRIOLOGÍA HUMANA; **Guillermo Rus Carlborg**, CATEDRÁTICO DEL DEPARTAMENTO DE MECÁNICA DE ESTRUCTURAS; y **Patricia Gálvez Martín**, RESPONSABLE DE PROYECTOS DE I+D+I EN SALUD HUMANA Y ANIMAL DE BIOIBÉRICA S.A.U.;

GARANTIZAMOS, al firmar esta tesis doctoral, que el trabajo ha sido realizado durante los años 2017-2022 por el doctorando bajo la dirección de los directores de la tesis. Y, hasta donde nuestro conocimiento alcanza en la realización del trabajo, se han respetado los derechos de otros autores a ser citados, cuando se han utilizado sus resultados o publicaciones.

Granada, a 23 de febrero de 2023.

Directores de la tesis:

JUAN ANTONIO MARCHAL CORRALES

GUILLERMO RUS CARLBORG

PATRICIA GÁLVEZ MARTÍN

Doctorando:

DANIEL MARTÍNEZ MORENO

Para optar a la mención de “Doctor Internacional”, el doctorando realizó, durante el período de formación, una estancia de tres meses (Septiembre de 2022 – Diciembre 2022) en el laboratorio del Professor Daniel Kelly en Trinity Centre for Bioengineering (TCBE) situado en el Trinity College of Dublin.

Parte de los resultados de esta tesis doctoral han sido aceptados en las siguientes publicaciones que cumplen con los criterios de calidad exigidos:

Martínez-Moreno, D.; Jiménez, G.; Gálvez-Martín, P.; Rus, G.; Marchal, J.A. Cartilage biomechanics: a key factor for osteoarthritis regenerative medicine. *Biochimica et Biophysica Acta - Molecular Basis of Disease*. 2019 Jun 1;1865(6):1067-1075. JIF (JCR): 4.352. Q1.

Martínez-Moreno D, Jiménez G, Chocarro-Wrona C, Carrillo E, Montañez E, Galocha-León C, Clares-Naveros B, Gálvez-Martín P, Rus G, de Vicente J, Marchal JA. Pore geometry influences growth and cell adhesion of infrapatellar mesenchymal stem cells in biofabricated 3D thermoplastic scaffolds useful for cartilage tissue engineering. *Mater Sci Eng C Mater Biol Appl*. 2021 Mar;122:111933. doi: 10.1016/j.msec.2021.111933. Epub 2021 Feb 3. PMID: 33641924. JIF (JCR): 8.457. Q1

Martínez-Moreno D, Venegas-Bustos D, Rus G, Gálvez-Martín P, Jiménez G, Marchal JA. Chondro-Inductive b-TPUe-Based Functionalized Scaffolds for Application in Cartilage Tissue Engineering. *Adv Healthc Mater*. 2022 Oct;11(19):e2200251. doi: 10.1002/adhm.202200251. Epub 2022 Jul 29. PMID: 35857383. JIF (JCR): 11.092. Q1

“Life on earth is more like a verb. It repairs, maintains, re-creates, and outdoes itself.”

“La vida en la tierra es más bien un verbo. Se repara, se mantiene, se recrea y se supera a sí misma.”

Lynn Margulis

Index

1. Abstract	3
2. Resumen	6

Introduction

3. Regenerative medicine	13
3.1. Background	13
3.2. Definition.....	16
3.3. Stem cell treatment.....	17
3.3.1. Pluripotency	18
3.3.2. Multipotency	19
3.3.3. Unipotency (or Singlepotency)	21
3.4. Gene Therapy	22
4. Tissue Engineering	25
4.1. Background	25
4.2. Definition.....	27
4.3. Challenges and advances in TE.....	28
5. Biomaterials	31
5.1. Background	31
5.2. Definition.....	31
5.3. Relevant terms related to biomaterials.....	33
5.4. Evolution of biomaterials.....	34
5.5. The importance of the ECM.....	37
5.5.1. Collagens.....	38
5.5.2. Elastic fibers	38

5.5.3.	Proteoglycans (PGs).....	40
5.5.4.	Glycoproteins.....	41
6.	Biomechanics.....	43
6.1.	Background.....	43
6.2.	Basic solid mechanical concepts.....	43
6.2.1.	Stress in solid mechanics.....	45
6.2.2.	Strain in solid mechanics.....	46
6.2.3.	Hooke's law.....	47
6.3.	Pressure waves.....	48
6.3.1.	Linear wave propagation equation.....	48
6.4.	Basic Fluid mechanics concepts.....	50
6.5.	Perfusion flow.....	53
6.5.1.	Laminar flow through a cylindrical pipe	56
6.6.	Mechanotransduction.....	60
6.6.1.	Mechanoreceptors.....	60
6.6.2.	Tensegrity.....	62
6.7.	Finite Element Analysis.....	64
6.7.1.	Finite element models in biomechanics	65
7.	Biofabrication.....	69
7.1.	Background.....	69
7.2.	Definition.....	70
7.3.	Biofabrication technologies.....	71
7.3.1.	Light-based technologies.....	71
7.3.2.	Wet-spun (aka wet-spinning).....	74
7.3.3.	Electrowiring.....	75
7.3.4.	Fused Deposition Modeling - 3D printing.	76

8.	Bioprinting.....	79
8.1.	Background.....	79
8.2.	Definition.....	82
8.3.	Bioinks.....	83
8.3.1.	Hydrogels.....	85
8.3.2.	Decellularized Extracellular Matrix.....	86
8.3.3.	Microcarriers based bioinks	87
8.3.4.	Tissue spheroids-based bioinks	88
8.4.	3D bioprinting techniques.....	88
8.4.1.	Droplet-based bioprinting (DBB):.....	88
8.4.2.	Extrusion-based bioprinting (EBB):.....	89
8.4.3.	Laser-assisted bioprinting (LAB):	89
8.4.4.	Laser-based bioprinting (LBB):.....	90
8.5.	Steps of the 3D bioprinting process	93
8.5.1.	Pre-bioprinting	94
8.5.2.	Bioprinting.....	94
8.5.3.	Post-bioprinting	94
9.	Bioreactors	96
9.1.	Background.....	96
9.2.	Definition.....	97
9.3.	Relevant design aspects.....	98
9.3.1.	Scaffold seeding.....	99
9.3.2.	Nutrient transport.....	100
9.3.3.	Biomechanical stimuli.....	101
9.4.	Sensors.....	102
9.4.1.	Gas phase monitoring	103

9.4.2.	Liquid phase monitoring	103
9.4.3.	Solid phase monitoring	104
9.4.4.	Soft sensors.....	105
9.5.	Types of bioreactors.....	106
9.5.1.	Bioreactors for mimicking pathological conditions and drug screening.....	107
9.5.2.	Single-use bioreactors	108
10.	Cartilage.....	112
10.1.	Main aspects	112
10.2.	Anatomy.....	112
10.2.1.	Histology and surface characterization	114
10.3.	Cartilage functions	115
10.4.	Pathophysiology.....	116
10.5.	Chondrogenesis.....	118
10.5.1.	Biochemistry of chondrogenesis.....	121
10.6.	Articular cartilage.....	123
10.6.1.	Cartilage collagens.....	124
10.6.2.	Proteoglycans	124
10.6.3.	Glycosaminoglycans.....	125
10.6.4.	ECM organization of AC.....	126
10.6.5.	Mechanical aspects of AC.....	127
11.	Osteoarthritis	129
11.1.	Background	129
11.2.	Definition.....	130
11.3.	Development of OA.....	131
11.3.1.	Biochemical and biomechanical pathways	132

12.	Cartilage Tissue Engineering.....	137
12.1.	Background.....	137
12.2.	Cell source: mature chondrocytes or MSCs?	139
12.3.	Biomaterials for cartilage tissue engineering.....	140
12.3.1.	Scaffold architecture.....	141
12.4.	Biomechanics for <i>in vitro</i> cartilage development.....	143
12.4.1.	Hydrostatic Pressure.....	144
12.4.2.	Mechanical loads	146
12.4.3.	Ultrasound	148
12.5.	Future Perspectives of CTE.....	150
13.	Motivation.....	152
13.1.	Clinical development process	152
13.2.	No time for old drugs.....	153
13.3.	A paradigm shift.....	154
13.4.	Multidisciplinary: the role of bioengineering	155
13.5.	A bioreactor for cartilage.....	159

Hypothesis and objectives

14.	Hypothesis.....	163
15.	Objectives.....	167
15.1.	Specific Objectives of Chapter I.....	167
15.2.	Specific Objectives of Chapter II	167
15.3.	Specific Objectives of Chapter III.....	168

Chapter I: Pore geometry influences growth and cell adhesion of infrapatellar mesenchymal stem cells in biofabricated 3D thermoplastic scaffolds useful for cartilage tissue engineering

16.	Abstract of Chapter I	171
17.	Background for Chapter I.....	173
18.	Materials and methods for Chapter I	176
18.1.	Bioprinter setup	176
18.2.	Isolation and culture of IPFP-MSCs	176
18.3.	Cell adhesion and proliferation assays in 3D scaffolds.....	177
18.4.	Porosity estimation and surface/volume ratio	178
18.5.	Wettability	178
18.6.	Angle Frequency	178
18.7.	Mechanical testing of the scaffolds	179
18.8.	Characterization of the microstructure throughout μ CT technology	180
18.9.	DNA quantification.....	180
18.10.	Environmental scanning electron microscope (ESEM).....	180
18.11.	Statistical Analysis	181
19.	Results and discussions from Chapter I	182
19.1.	Fabrication approach.....	182
19.2.	Cell Adhesion/Proliferation assay	184
19.3.	Correlation of proliferation with experimental porosity and S/V ratio	188
19.4.	Mechanical testing	191
19.5.	Characterization of the microstructure	194
19.6.	DNA Quantification.....	195

19.7.	Study of interactions between cells and biomaterials by ESEM	198
19.8.	Conclusions	198

Chapter II: Chondro-inductive b-TPUe-based functionalized scaffolds for application in cartilage tissue engineering

20.	Abstract of Chapter II	203
21.	Background for Chapter II.....	205
22.	Materials & methods for Chapter II	208
22.1.	Sample processing	208
22.2.	Printing of 3D scaffolds.....	208
22.3.	Functionalization with PBA	209
22.4.	Functionalization with type I collagen.....	209
22.5.	Magnifying glass and AFM.....	209
22.6.	Immunofluorescence of type I collagen and PBA after the functionalization process.....	210
22.7.	Seeding of the scaffolds with cells.....	210
22.8.	Metabolic activity	210
22.9.	Cell Viability	211
22.10.	DNA and GAG quantification	211
22.11.	Cartilage gene expression.....	211
22.12.	Scanning electron microscopy.....	212
22.13.	Statistical analysis	212
23.	Results from Chapter II.....	214
23.1.	Characterization and verification of functionalization protocols on b-TPUe	214

23.2.	Evaluation of cell metabolic activity and cell viability in PBA and type I collagen functionalized-scaffolds	219
23.3.	Evaluation of the chondrogenic potential of functionalized scaffolds	223
23.4.	Analysis of cell morphology and ECM appearance by scanning electron microscopy	226
24.	Discussions from Chapter II	229
24.1.	Conclusions	233
 Chapter III: Induction and real time ultrasonic monitoring of 3D cartilage-like tissue by a low shear stresses-based bioreactor		
25.	Abstract of Chapter III	237
26.	Background for Chapter III	239
27.	Materials and methods for Chapter III	242
27.1.	Bioreactor design and construction	242
27.2.	Cells isolation and culture	243
27.3.	Printing 3D scaffolds	243
27.4.	Scaffolds functionalization	244
27.5.	Seeding cells in scaffolds	244
27.6.	Metabolic activity	244
27.7.	DNA and collagen quantification	244
27.8.	Immunofluorescence	245
27.9.	Scanning electron microscopy (SEM)	246
27.10.	Statistical Analysis	246
27.11.	In silico model	246
28.	Results from Chapter III	249
28.1.	Perfusion bioreactor with pulsed ultrasound characterization	249

28.2.	Acoustic Pressure Wave Propagation Model	254
28.3.	Viability and chondrogenic characterization	258
28.4.	Biomechanical correlation analysis	263
29.	Discussions from Chapter III	268
29.1.	Conclusions	274

Final discussion

30.	Final discussion.....	277
30.1.	Overarching concerns.....	277
30.2.	The role of microstructure	278
30.3.	Tissues as dynamic systems	281
30.4.	Future perspectives.....	283
30.4.1.	Technical implications.....	283
30.4.2.	Biological implications	285
30.4.3.	Ethical implications.....	286
30.4.4.	Clinical application.....	286
30.5.	Closing argument.....	287

Conclusions

31.	Conclusions.....	291
32.	Conclusiones.....	293

Annexes

33.	Printing settings.....	297
33.1.	The slicing step	297
33.2.	Parameters affecting the printing process	299
33.2.1.	Layer height.....	299
33.2.2.	Nozzle speed	300

33.2.3.	Extrusion rate	301
33.2.4.	Infill	301
33.3.	Future outlook	303
34.	Piezoelectric effect.....	304
34.1.	Piezoelectric effect.....	304
34.1.1.	Electric Displacement	306
34.2.	Ultrasonic transducers.....	306
35.	Supplementary Material C1.....	309
35.1.	Workflow of Chapter I.....	309
35.2.	Volume ratio and surface/volume	310
35.3.	IPFP-MSCs characterization	312
35.3.1.	Flow cytometry analysis	312
35.3.2.	Differentiation assays	314
35.4.	Mechanical analysis.....	314
35.5.	ESEM	317
35.6.	Supplementary Tables.....	318
36.	Supplementary Material C2.....	321
36.1.	Characterization and verification of functionalization protocols on b-TPUe	321
36.2.	MSCs characterization.....	322
36.3.	Preparation of the ninhydrin standard curve. Aminolysis and ninhydrin treatment.	324
36.4.	Metabolic activity & Viability of Collagen with and without Glutaraldehyde	325
37.	Supplementary Material C3.....	327
37.1.	Design concepts.....	327

37.2.	Model validation	328
37.3.	MSCs characterization.....	331
37.4.	Quantification Standard Curves.....	332
38.	Literature	XLVI
39.	Curriculum Vitae.....	CXXII
39.1.	Educational background	CXXII
39.1.1.	Courses	CXXII
39.2.	Contracts	CXXII
39.3.	Publications.....	CXXIII
39.4.	Contributions to congress	CXXIV
39.5.	Fellowships and Grants	CXXV
39.6.	Patents.....	CXXV

Figure Index

Figure 1. Timeline of organ transplantation. The history of these procedures is divided by three remarkable landmarks: the first successful organ transplantation at 1944, the invention of immunosuppressors as cyclosporine at late 1970s, and, the start of implementation of vascular grafts thanks to new advanced immunosuppressors. (Figure adapted from Salvatori et al. 2015 with permission).	14
Figure 2. Representation of the three technical approaches for Regenerative Medicine. ..	17
Figure 3. Cell potent lineage.	18
Figure 4 MSCs differentiation potential.	21
Figure 5. Gene therapy pathway.	22
Figure 6. Scheme of the three main pillars of TE. They must be seen as a fully integrated structure with various distinct action channels connecting them.	25
Figure 7. Time-line of more relevant TE history events. The black line represents the most accepted beginning of current TE. Red circle envelops the first iteration of a commercial cartilage TE product, a significant historical landmark for this work.	26
Figure 8. Pathway of TE as an applied therapy.	28
Figure 9. Scheme of new advances acquired in TE during last decade.	29
Figure 10. Representation of the Foreign-Body Response steps. At the early stages, the nude scaffold is covered by a layer of coating proteins to attract the macrophages. The phagocytosis is frustrated due to biomaterial size, and, finally the biomaterials is encapsulated by a fibrous layer mostly made by collagen.	32
Figure 11. Classificatory scheme of biomaterials depending on their chemical composition.	35

Figure 12. A fragment of a collagen molecule that demonstrates how the alpha chains are wrapped into a triple helix. The amino acids are similarly organized in a helix within each chain, with glycine facing the triple helix's core. The dots stand in for the other amino acids. 38

Figure 13. A representation of elastic fibers with a microfibril-containing elastin core is shown. 39

Figure 14. Representation of a conventional PGs with an amplification of their monomers. In the dotted line square there is the Hyaluronic acid obtained by the mixture of the hyaluronan (core molecule) with other PGs..... 40

Figure 15. Representation of the most relevant glycoproteins. Osteopontin and link protein are not included due to small size..... 42

Figure 16. Elastic behaviour from the interatomic forces...... 44

Figure 17. Cartesian representation of tridimensional stresses and the plane stress. 45

Figure 18. Planar representation of normal and shear strains in Cartesian coordinates.... 47

Figure 19. Representation of a linear planar mechanical wave propagation front. 49

Figure 20. Scheme of different pore shapes. Porous materials present different kind of behaviour for fluid mechanics depending if they are: closed, dead-ended or opened at both sides. This effect cannot be measured by porosity ratio. 55

Figure 21. Representation of an ideal Hagen-Poiseuille flow through a capillary. 59

Figure 22. The most common mechanoreceptors and their relationship to gene expression via various signalling pathways are depicted schematically. As previously stated, the cytoskeleton plays a critical role in the mechanotransduction process. 62

Figure 23. Tensegrity implies a level of prestressing of a whole fiber network connected from the ECM to the cell nucleus. Thanks to this phenomenon, all cells in the same ECM niche are connected and intercommunicated for external stimuli. 63

Figure 24. Flow diagram of the developing steps for a FEM.	66
Figure 25. Scheme explaining how the different scientific technologies interact between them.	71
Figure 26. Scheme for SLS fabrication technique.	72
Figure 27. Scheme for SLA fabrication technique.	73
Figure 28. Scheme of WS synthesis process.	74
Figure 29. Scheme of electrowiring process.	76
Figure 30. Scheme of 3D printing techniques applied in biofabrication. A) Corresponds to FDM method and B) to 3DF.	77
Figure 31. Timeline of 3D bioprinting.	80
Figure 32. Representation of bioink and biomaterial ink compositions. In biomaterial inks, the cells are added in parallel or after bioprinting step.	84
Figure 33. Representation of an arbitrary hydrogel bioink and their three different crosslinking methods applied in bioprinting.	85
Figure 34. Pathway for dECM bioink synthesis.	87
Figure 35. Representation of a microcarrier bioink. Adhesion cells are attached to these microcarriers allowing high expansion of them.	87
Figure 36. The pathway developed by Mironov to develop tubular structures (e.g., capillaries).	88
Figure 37. Representation of the most common bioprinting methods.	90
Figure 38. Outline of the development process of a 3D bioprinting TE graft.	93
Figure 39. Timeline representing the most relevant advances in BR history.	96

Figure 40. A schematic representation of the main aspects that a BR destined for TE must have.	98
Figure 41. A spider diagram of the diverse bioprocess variables and their most common applied sensors.	102
Figure 42. Classification of biosensors depending on their interaction with the BR.	103
Figure 43. Basic types of BRs are classified depending on the kind of mechanical stimuli that they exert.	106
Figure 44. Bio-MEMs are chip kind BRs that can simulate tissues or organs. SUBs are very relevant BRs to produce TE products under sterile conditions.	107
Figure 45. Image of human cartilage tissue. Graphical representations expose and example of hyaline cartilage in the knee joint. Chondroblasts are embedded in the perichondrium.	113
Figure 46. Most relevant pathologies present in cartilage tissues.	118
Figure 47. Graphical representation of the chondrogenic process and the endochondral ossification process.	120
Figure 48. AC zones and their different cell distribution and ECM organization.	126
Figure 49. Radiography of a healthy knee joint VS. an OA knee joint. Image obtained by perimissions of Shivanand et al. ⁷⁶⁸.	131
Figure 50. Osteoarthritis mechanical feedback cycle.	132
Figure 51. Schematic representation of the diverse biochemical and biomechanical pathways affecting OA joints.	134
Figure 52. Time-line of CTE.	138
Figure 53. For CTE, it is very important to adequate the architecture of the final graft because it will affect cell metabolism.	142

Figure 54. Schematic representation of the biomechanical pathways involved in cartilage synthesis. Hydrostatic Pressure (HP) enhances Ca²⁺ and Na⁺ channels and the Na⁺/K⁺ pump which interacts with PKA that regulates chondrogenesis (Sox9/CREB). Shear stress induced by flow stimulate the primary cilium of chondrocytes that also plays a key role in the Sox9/CREB cycle. Finally, US stimulation activates the TRPV4 channels and actin polymerization that induces chondrogenesis as well.....149

Figure 55. Basis of Biomedical Engineering of the future of cartilage tissue engineering.151

Figure 56. The current drug development process has an acute bottleneck that is still unsolved.152

Figure 57. Evolution pipeline of ATMPs divided in different techniques. Figure exposed with permission of the European Federation of Pharmaceutical Industries and Associations (EFPIA)⁹⁸⁶.154

Figure 58. Precision medicine involves one hypothetical scenario where every person will receive a personalized and specific treatment.156

Figure 59. A system envelops a complex connection web: green arrows represent, multidisciplinary connections, black arrows the interdisciplinary ones, and the blue circle is the transdisciplinary field of biomedicine.....158

Figure 60. Graphical abstract of Chapter I. Porosity is an important feature in biomechanics and cell-biomaterial interaction.172

Figure 61. A-C) STL models of the scaffolds of each layer-down topography (PS 1.5 mm). In A) layers 1,2,3,4 are inserted periodically one on top of the next one. B) The hexagonal pattern only has one layer which is repeated along Z axis. C) In the Square pattern there are two different layers intercalated repeatedly. D-E) Cross-sectional images of the fabricated scaffolds. Scale bars correspond to 2 mm in all cases.184

Figure 62. A & D) Normalized Proliferation assays for b-TPUe and PCL materials, respectively. B) Absorbance of fluorescence emitted at 590 nm for b-TPUe at day 1. C) Same as B at day 21.

E) Absorbance of fluorescence emitted at 590 nm for PCL at day 1. F) Same as E at day 21. P-Value less than 0.05 was represented *; P-Value < 0.01 with ** and P-Value < 0.001 ***. Brackets means significance different with the rest of PS inside the same geometry. 185

Figure 63. A) Fluorescence units (590 nm) from AlamarBlue® assay for b-TPUe and PCL scaffolds against their experimental porosity at days 1, 7, 14 and 21 (n=3). B) Fluorescence units (590 nm) from AlamarBlue® assay for b-TPUe and PCL scaffolds against their S/V ratio at days 1, 7, 14 and 21 (n=3). C) Angle frequency (AF) for each geometry as obtained from the frequency resulted by dividing the number of angles for each geometry by the total number of angles for all geometries. D) Infographic scheme of how stresses was applied on the scaffolds together with the representation of PS and the different printed angles which affects in cell adhesion..... 190

Figure 64. A-H) Stress-strain curves for the optimal architectures in comparison with the average curve from Cartilage samples. A-D) Samples with perimeters. E-H) Samples without perimeters. Each curve corresponds to the average curve applying linear interpolation (n=3). 193

Figure 65. -D) μ CT cross-sectional images (coronal and sagittal middle planes) of T1.5 and T2 geometries. Inside orange circles are presented the ‘pilars’ formed because of filament superposition among layers. Color bars represents the real distance among those ‘pilars’ (which should be PS), in the legend they are aligned for comparing sizes between samples. Orange bar corresponds to T1.5 b-TPUe, red bar T1.5 PCL, green bar T2 b-TPUe and blue bar T2 PCL. E) Porosity ratio obtained from segmentation image analysis from μ CT technique for b-TPUe and PCL, geometries: T1.5 and T2. P-Value less than 0.001 was represented with *** for b-TPUe and with ### for PCL. (n=3) F) DNA content for PCL and b-TPUe in T1.5 and T2 geometries. P-Value less than 0.05 was represented *; P-Value < 0.01 with ** and P-Value < 0.001 *** among equal material. P-Value < 0.001 ### with respect the rest of cases. G) ESEM images of b-TPUe T1. In the amplified picture, it is localized what seems ECM from ifpMSCs. b-TPUe seems to present some rugosity at microstructure, and, consequently there are found more cells attached..... 196

Figure 66. Graphical abstract of Chapter II. Scheme of the whole procedure followed in Part II.....204

Figure 67. AFM topography analyses. (A-F) Height images captured from AFM for, (A) Mili Q water as control, (B) ethanol 70% (mixed with Mili Q water), used to sterilized scaffolds, (C) 2-propanol 100% buffer, used to diluted hexamethylenediamine (necessary to PBA functionalization) and (D) KH₂PO₄ 0.16 % Glutaraldehyde buffer used to crosslinked collagen fibers in the collagen type I functionalization. (E) Height images for collagen functionalized scaffolds, whereas (F) exposes a PBA functionalized fiber. In all cases, the ROI was 5x5 μm . (G) PSD curves from AFM buffer analyses compared with control. (H) PSD of functionalized scaffolds versus control.216

Figure 68. Macroscopic and microscopic characterization. (A) Images captured by magnifying glass under transmitted light from different buffers. Control was Mili Q water, 70% ethanol mixed with Mili Q water, pure isopropanol, and KH₂PO₄ 0.16 % Glutaraldehyde buffer. (B) Ninhydrin standard absorbance curve is done by a spectrophotometer. (C) Ninhydrin assay for aminated scaffolds (scaffolds embedded inside hexamethylenediamine 2-prop buffer) and control (naïve scaffolds). (D) Confocal images from autofluorescence of bTPUe scaffolds functionalized with PBA, and control (non-functionalized). (E) Confocal images from immunohistochemistry scaffolds, Immunolabeling as type I collagen functionalization, and control as naïve scaffolds. Magnifying was 10X.....219

Figure 69. Metabolic and cell proliferation of bTPUe functionalized scaffold loaded with IPFP-MSCs. (A) Alamar Blue reduction fluorescence response ($\lambda = 570 \text{ nm}$) for bTPUe scaffolds without treatment (control), PBA functionalized scaffolds, and type I collagen functionalized scaffolds at days 1, 3, 7, 14, and, 21. (B) Alamar Blue reduction/DNA fold increase (obtained by dividing Supplementary Figure S4A BY S4B) curves for PBA functionalized scaffolds and type I collagen functionalized scaffolds along 21 days. (n=3) (***, $p < 0.001$; *, $p < 0.05$; N.S., not significance), (C-K) Confocal images from Live/Dead assay (Thermo Fisher Scientific) of naïve bTPUe scaffolds as control and both functionalization protocols. Magnifying was 10X.....222

Figure 70. Chondro-inductive properties of bTPUe functionalized scaffold loaded with IPFP-MSCs. (A) GAG concentrations obtain through papain assay for naïve bTPUe scaffold and both

functionalization protocols on day 1 and day 21. (B) DNA concentrations were obtained through papain assay for naïve bTPUe scaffolds and both functionalization protocols on day 1 and day 21. (C) GAG/DNA ratios for naïve bTPUe scaffolds and both functionalization protocols at day 1 and day 21 (n=3). (***, $p < 0.001$; *, $p < 0.05$; ###, $p < 0.001$; ^^, $p < 0.001$). (D) Gene expression fold increase obtained through qPCR. Control used were IPFP-MSCs cultured at day 0. PBA was scaffolds functionalized with PBA under normal cell medium, PBA Dif was the same scaffolds under chondrogenic medium, both at day 21. Collagen scaffolds were collagen type I functionalized scaffolds under normal medium, Collagen Dif was same scaffolds under chondrogenic medium, both at day 21. Col2 was COL2A1. Sox9 was the Transcription factor SOX-9. Acan was Aggrecan. Col1 was COL1A1. (n=3) (***, $p < 0.001$; *, $p < 0.05$; ###, $p < 0.001$; ^^, $p < 0.001$; N.S., Not Significance). Black bars correlated chondrogenic markers of functionalized scaffolds versus control. N.S: implies exception in previous correlation. Blue # correlates control concerning others. Grey bars correlate PBA with PBA Dif. Green bars correlate Collagen with Collagen Dif. 226

Figure 71. SEM images from control, PBA functionalized and type I collagen functionalized scaffolds at day 21. (A-E) Control images, where (B) shows a magnification of a viable cell. (E) shows poor cell-biomaterial interaction. (F-J) PBA images, (F) clearly show the presence of ECM over scaffold fibers, (G) represents cell-cell interactions. (J) Shows cell-ECM interactions. Collagen images, where (I) shows the presence of ECM over scaffold surface, (K) shows cell-biomaterial interaction and ECM preserved morphology and, (L) shows a chondrocyte-like cell..... 228

Figure 72. Diagram of the work framework from Chapter III..... 238

Figure 73. Bioreactor (BR) design. (A) Final design (cell chamber and transducers coupled) renderization. (B) Render image of cell chamber BR and input and output (IO) cylinders. (C) IO channels render images. (D) The visual concept of the transducer with the coupling system. (E) (a) represents the Olympus preamplifier that was connected after the recording oscilloscope (b) and the receiver transducer (c); (d) the cell chamber and BR heart; e) transmitter transducer, which was directly connected to the wave generator (f); (g) Raspberry PI that is uncharged of received the signals from the Oscilloscope and to control the Arduino board; (h) Arduino Uno that regulates pump rotation speed and flow rate; (i) peristaltic pump

that exerts the laminar fluid flow through the bioreactor; (j) the medium reservoir with a 0.22 μm filter for O_2 and CO_2 exchange.....250

Figure 74. BR final arrangement and global parameters. (A) Photography of the final assembly of the BR inside a laminar hood. (B) Photography of the Arduino circuit that controls the peristaltic pump. (C) Output signals recorder by Raspberry PI. Red represents the functionalized scaffold with seeded cells, and in black, the same scaffold without cells. (D) Pressure amplitude of P-Wave vs. Voltage amplitude exciting transducer. (E) Results from flow rate calibration, Flow rate vs. Voltage amplitude of peristaltic pump. (F) A 2D fluid dynamic model in FEM to evaluate the incidence flow speed (a and c) over scaffold fibers and their corresponding shear stresses (b and d) depending on the flow rate. Two flow rates are represented $0.5 \text{ mL}\cdot\text{min}^{-1}$ and $0.8 \text{ mL}\cdot\text{min}^{-1}$254

Figure 75. FEM model of P-wave propagation phenomena. (A) 2D representation of the different domains of the FEM model. (B) Thermal image of the “u” component of the displacement of the transmitter ultrasound transducer (i.e., X component) at $t = 0.5 \mu\text{s}$ (a) and $t = 1 \mu\text{s}$ (b). (C) P-wave propagation at different times: (a) $t = 0.5 \mu\text{s}$, (b) $t = 1 \mu\text{s}$, (c) $t = 15 \mu\text{s}$, (d) $t = 18 \mu\text{s}$, (e) $t = 34 \mu\text{s}$, and (f) $t = 50 \mu\text{s}$. (D) Thermal image of the “u” component (i.e., X component) of the displacement of the receiver ultrasound transducer at $t = 35 \mu\text{s}$ (a) and $t = 40 \mu\text{s}$. (b). (E) The final electrical modeled signal was obtained from the FEM model.....256

Figure 76. (A) Alamar Blue assay with different flow rates and control. Values were normalized for day 1. (B) DNA quantification at day 7 of experimentation of control and BR $0.8 \text{ mL}\cdot\text{min}^{-1}$. (C) General collagen quantification with Sirius Red assay of the control and BR samples ($0.8 \text{ mL}\cdot\text{min}^{-1}$). (D) Collagen type II quantification using Elisa kit for both control and BR ($0.8 \text{ mL}\cdot\text{min}^{-1}$) samples. (E) SEM images at day 7 of both scaffolds and scale bars are expressed in microns. (* means $p\text{-value} < 0.001$; cont. = continuous perfusion flow, disct. = discrete perfusion flow).....259

Figure 77. Immunofluorescence merges images without primary antibody (i.e., negative) of the control sample (A) and BR sample (B). (C) Control and BR samples with primary type II collagen antibody + 2^{nd} Ab and primary aggrecan antibody + 2^{nd} Ab. Cell Tracker™ green is

represented in green. Secondary Ab (Alexa 647 nm) is shown in red. In blue, the DAPI marker is represented. 261

Figure 78. (A) P-wave arbitrary signals obtained from the cell content scaffolds during BR experimentation. (B) P-wave arbitrary signals obtained from the blank scaffolds (no cells) during BR experimentation. (C) Amplitude evolution curve of average amplitude signals. (D) Time of flight (ToF) curves. (E) Thermal 2D images of fluid shear stress (CFD) model using different scaffold fiber diameters. (F) Output Flow speed from the BR vs. the scaffold fiber diameter (FD) in black; and the instant velocity of the middle point ($X = 0, Y = 0$) inside the scaffold domain. (G) Density evolution along time of BR cell content in scaffold samples and blank scaffolds obtained by cross-correlation empirical signals with synthetical ones. (H) Speed of sound of scaffold domain (c_{SD}) (scaffold + water) obtained by cross-correlation. (*: P -value < 0.001). 265

Figure 79. Word cloud of the role of microstructure. 279

Figure 80. Word cloud of tissues as dynamic systems. 281

Figure 81. The slicing step is divided in two main steps: i) the STL-file formation and ii) the GCODE formation. 297

Figure 82. Diagram of layer height and its relation with the critical layer height. 299

Figure 83. Scheme of different infill arrangements. Image adapted from that one published by Domingo et al. ¹⁰⁴⁴ 302

Figure 84. Scheme of piezoelectric effect. 304

Figure 85. Cross section of an ultrasound transducer and its components. Image courtesy of Dr Rachael Nightingale, Radiopaedia.org, rID: 54040 307

Figure 86. Nine different geometries were proposed for the proliferation assay, each one was carefully studied. After, some of those geometries were discarded to simplify deeper analyses, reducing sample number. Finally, selected geometries were exposed to mechanical assays, microarchitecture analyses, viability tests and cell-material interactions inquiries. 309

Figure 87. A) Scheme of fiber distribution and dependency of fiber length as a function of scaffold radius (R_s). B) In the hexagonal geometry, the real length of the filaments was slightly larger than square and triangular conformations. It was extracted calculating the number of hexagons approximating a straight filament divided by the apothem (a_{hex}). l_f : length of the filament. D_s : scaffold diameter.311

Figure 88. A) FACS markers for stemness. B) Differentiation capacity. Controls were IPFP-MSCs with DMEM, 10%FBS and 1%P/S. Differentiated mediums were: Osteogenic medium applied was StemMACS OsteoDiff 130-091-678, Miltenyi. Adipogenic medium applied was StemMACS adipoDiff 130-091-677, Miltenyi. Chondrogenic medium applied was DMEM supplemented with 10 ng/ml TGF- β 1, 0.1 μ M dexamethasone, 40 μ g/ml L-proline, 50 μ g/ml L-Ascorbate-2-Phosphate, and 50 mg/ml ITS. (Scale bar = 110 μ m).313

Figure 89. A-B) Stress vs. Strain curve of cube b-TPUe scaffold under compression pattern in the rheometer and UTM for Triangular geometry and PS 1.5 mm, A) 'in plane', and B) 'out of plane'. C-D) Stress vs. Strain curve of cube b-TPUe scaffold under compression pattern in the rheometer and UTM for Triangular geometry and PS 2 mm, C) 'in plane', and D) 'out of plane'. E-F) Stress vs. Strain curve of cube PCL scaffold under compression pattern in the rheometer and UTM for Triangular geometry and PS 1.5 mm, E) 'in plane', and F) 'out of plane'. G-H) Stress vs. Strain curve of cube PCL scaffold under compression pattern in the rheometer and UTM for Triangular geometry and PS 1.5 mm, G) 'in plane', and H) 'out of plane'. ($n=3$) ..314

Figure 90. Same as previous figure without perimeters ($n=3$).317

Figure 91. ESEM images of PCL, although there are cells attached to the fibers, it seems to be a coating layer above the scaffold. Possibly due to material degradation because of the assay.317

Figure 92. AFM topography analyses. (A-B) Height images captured from AFM for, A) ethanol 70% (mixed with Mili Q water), used to sterilized scaffolds, B) ethanol 70% (mixed with Mili Q water), used to sterilized scaffolds C) PSD curves from AFM ethanol buffers analyses.321

Figure 93. A) FACS markers for stemness. B) Differentiation capacity. Controls were IPFP-MSCs with DMEM, 10%FBS and 1%P/S. Differentiated mediums were: Osteogenic medium applied

was StemMACS OsteoDiff 130-091-678, Miltenyi. Adipogenic medium applied was StemMACS adipoDiff 130-091-677, Miltenyi. Chondrogenic medium applied was DMEM supplemented with 10 ng/ml TGF- β 1, 0.1 μ M dexamethasone, 40 μ g/ml L-proline, 50 μ g/ml L-Ascorbate-2-Phosphate, and 50 mg/ml ITS. (Scale bar = 110 μ m). 322

Figure 94. A), B) Metabolic activity study carried out on days 0 and 3 using the Alamar Blue reagent. FF scaffolds have been functionalized with collagen using different concentrations of glutaraldehyde (0%; 0.16% and 0.625%) and glycine (0M, 0.5M, 0.2M, respectively). The positive control has only been seeded without previous functionalization. (***) $p < 0.001$. Images obtained with the confocal microscope Nikon Eclipse Ti after the treatment of FF scaffolds with the LIVE/DEAD[®] cytotoxicity/viability kit. C) Positive control. D) 0% glutaraldehyde and 0M glycine E) 0.16% glutaraldehyde and 0.5M glycine. F) 0.625% glutaraldehyde and 0.2M glycine. 324

Figure 95. A) Alamar Blue fold increase obtained normalizing Alamar Blue reduction assay fluorescence raw results by day 1. B) DNA fold increase obtained by normalizing fluorescence raw results by day 1. (n=3) (***) $p < 0.001$; *, $p < 0.05$; N.S., not significance)..... 326

Figure 96. (A) Front view of Input/Output (IO) channels, (B) Profile view of IO channels. (C) Profile view of Scaffold chamber and IO channels. Ultrasound (US) field is represented in orange whereas the perfusion flow are represented in blue. 327

Figure 97. (A) Pearson coefficients obtained from Pearson correlation between water experimental signal and FEM (Finite Element Model) synthetical signals. (B) Pearson coefficients obtained from Pearson correlation between PLA (polylactic acid) experimental signal and FEM (Finite Element Model) synthetical signals. (C) Comparison of experimental water signal with the modeled one. (D) Comparison of experimental PLA signal with the modeled one. (ρ = Pearson coefficient)..... 328

Figure 98. Modeled signals of our pressure wave sweeping mesh size (Δx), each step was 100 μ m; thus, the parametric sweep varied from 1 mm to final 100 μ m. (Δx =distance of mesh size, is equal in both directions X and Y 330

Figure 99. (A) FACS markers for stemness. (B) Differentiation capacity. Controls were IPFP-*MSCs* with DMEM, 10%FBS and 1%P/S. Differentiated mediums were: Osteogenic medium applied was StemMACS OsteoDiff 130-091-678, Miltenyi. Adipogenic medium applied was StemMACS adipoDiff 130-091-677, Miltenyi. Chondrogenic medium applied was DMEM supplemented with 10 ng/ml TGF- β 1, 0.1 μ M dexamethasone, 40 μ g/ml L-proline, 50 μ g/ml L-Ascorbate-2-Phosphate, and 50 mg/ml ITS. (Scale bar = 200 μ m).330

Figure 100. (A) Standard curve of DNA quantification. DNA content was estimated using a fluorometric marker (DAPI staining) and DNA standard curve was done using DNA from Calf Thymus (Sigma-Aldrich). (B) Standard curve of general collagen quantification. Collagen content was measured via Sirius Red assay, absorbance supernatant was measured in a microplate reader at 540 nm (Synergy HT, BIO-TEK), for standard collagen from calf skin was used (Sigma). (C) Standard curve of type II collagen quantification following manufacturer's protocols by Chondrex. (R^2 is the coefficient of determination for linearity, 1 means completely linearity, 0 means no linearity).332

Abbreviation index

#

2PP *Two Photon Polymerization*

A

AAV *Associated Viral Vectors*

AC *Articular Cartilage*

ACAN *Aggrecan gen*

ACI *Autologous Chondrocyte
Implantation*

ACL *Anterior Cruciate Ligament*

ADA-encoding RV *Adenosine
Deaminase Retroviral Vector*

ADAMTS *A Desintegrin and
Metalloproteinases with
Thrombospondin Motifs*

AF *Angle Frequency*

AFM *Atomic Force Microscopy*

ALK *Alkaline Phosphatase*

ARGET *Activators Regenerated by
Electron Transfer*

ASC *Adult Stem Cells*

ATMPs *Advanced Therapeutical
Medical Products*

ATRP *Chain-Transfer Polymerization*

B

bFGF *essential Fibroblast Growth
Factor*

Bio-MEMs *Biomimetic Microsystems*

BMLs *Bone Marrow Lesions*

BMP-2 *Bone Morphogenetic Protein 2*

BMPs *Bone Morphogenetic Proteins*

BR *Bioreactor*

b-TPUe *1,4-butanediol Thermoplastic
Polyurethane*

C

CA *Contact Angle*

CAD *Computer-Aided Design*

CARM1 *Coactivator-Associated
Arginine Methyltransferase 1*

CCN2 *Connective TFG*

CNC *Computer Numerical Control*

COL2A1 *type II collagen gen*

CT *Computed Tomography*

COX *Cyclooxygenases*

CPCs *Chondrogenitor Cells*

CREB *Camp Response Element-Binding*

CS A *Chondroitin Sulfate 4*

CS C *Chondroitin Sulfate 6*

CTE *Cartilage Tissue Engineering*

CWP *Cartilage Wear Particles*

D

DALY *Disability-Adjusted Life Years*

DBB *Droplet Based Bioprinting*

DDR2 *Discoidin Domain Receptor 2*

dECM *decellularized Extracellular Matrix*

DL *Deep Learning*

DLPTM *Digital Light Processing*

DMEM *Dulbecco's Modified Eagle Medium*

DS (also CS B) *Dermatan Sulfate*

E

E *Young's Modulus*

EBB *Extrusion Based Bioprinting*

ECM *Extracellular Matrix*

EGFR *Epidermal Growth Factor Receptor*

EPO *European Patent Office*

ERK *Extracellular Regulated Kinase*

ESC *Embryonic Stem Cells*

EUSTM *European Society of Translational Medicine*

F

FBR *Foreign Body Reaction*

FCD *Fixed Charge Density*

FD *Fiber Diameter*

FDM *Fused Deposition Modeling*

FEA *Finite Element Analysis*

FEM *Finite Element Models*

FGF *Fibroblast Growth Factor*

FIA *Flow Injection Analysis*

G

GAG *Glycosaminoglycan*

GBD *Global Burden of Disease*

GDF5 *Growth Differentiation Factor 5*

GFRs *Growth Factor Receptors*

GH *Growth Hormone*

GMP *Good Manufacturing Practice*

GPCRs *G Protein Coupled Receptors*

GSED *Gaseous SE Detector*

GUI *Graphical User Interface*

H

H *Hexagonal*

HA *Hyaluronic Acid*

HCS *Human Chondrosarcoma-Derived Chondrocytic Cell Line*

HMG *High Mobility Group*

HP *Hydrostatic Pressure*

HS *Heparan Sulfate*

HSC *Hematopoietic Stem Cells*

I

IFT *Intra-Flagellar Transport*

Ihh *Indian hedgehog*

IKK *Inhibitor of Kinases*

IL-1 β *Interleukin Beta*

IL-2 *Interleukin-2*

IMPACT *Instant MSC Product
Accompanying Autologous Chondron
Transplantation*

IPFP-MSCs *Infrapatellar Fat Pad-
Derived Mesenchymal Stem Cells*

iPSCs *Induced Pluripotent Stem Cells*

ISCT *International Society for Cellular
Therapy*

ISM *in situ Microscopy*

IUPAC *International Union of Pure and
Applied Chemistry*

K

KS *Keratan Sulfate*

L

LAB *Laser-Assisted Bioprinting*

LH *Layer Height*

LIPUS *Low Intensity Pulsed Ultrasound*

LV *Lentiviral Vector*

M

MACI *Second-Generation ACI (aka.
Matrix associated ACI)*

MRI *Magnetic Resonance Imaging*

MAPK *Mitogen-Activated Protein
Kinase*

MCP-1 *Monocyte Chemotactic Protein
1*

ME *Medical Electric*

MEK *Mitogen-Activated Signal
Regulated Kinase*

MIP-1 β *Macrophage Inflammatory
Protein 1*

MIR *Mid-Infrared*

MMPs *Metalloproteinases*

mRNAs *messenger Ribonucleic Acids*

MSC *Mesenchymal Stem Cells*

μ *Poisson's ratio*

O

OA *Osteoarthritis*

OD *Optical Density*

P

P *Porosity*

P/S *Penicillin/Streptomycin*

PBA 1 *Pyrene Butyric Acid*

XXX

PBS *Phosphate-Buffered Saline*
PCAST *President's Council of Advisors
on Science and Technology*
PCB *Printed Circuit Board*
PCL *Polycaprolactone*
PCM *Pericellular Matrix*
PDMS *Poly-Dimethyl Siloxane*
PE *Protective Earth*
PEG *Polyethylene Glycol*
PG *Proteoglycan*
PGA *Poly-Glycolic Acid*
PHB *Poly-3-Hydroxybutyrate*
PHEMA *Poly-Hydroxyethyl Ethyl
Methacrylate*
PKA *Protein Kinase A*
PLA *Poly-Lactic Acid*
PLGA *Poly-Lactic-Co/Glycolic Acid*
PMMA *Poly-Methyl Methacrylate*
PNIPAM *Poly-N-Isopropyl Acrylamide*
PS *Pore Size*
PTHrP/Ihh *Parathyroid Hormone-
Related Protein*

R

RA *Rheumatoid Arthritis*
RAGE *Receptor for Advanced Glycation
End Products*
Re *Reynolds number*

RGD *Arg-Gly-Asp*
Rho/ROCK *Rho-Associated Protein
Kinase*
RM *Regenerative Medicine*
ROS *Reactive Oxygen Species*

S

S *Square*
S/N *Signal to Noise Ratio*
S/V *Surface Volume Ratio*
SAM *Significance Analysis of
Microarrays*
SCID *Severe Combined Immune
Deficiency*
SCTMP *Somatic Cell Therapy
Medicinal Products*
SDF-1 *Secrete Derived Factor 1*
sFRP3 *Secreted Frizzled-Related
Protein 3*
SLA *Stereolithography*
SLS *Selective Laser Sintering*
Smad3 *Mothers Against
Decapentaplegic Homolog 3*
SME *Shape-Morphing Effect*
SSLS *Surface Selective Laser Sintering*
STL *STereoLithography file*
SUB *Single Use Bioreactor*
SZP *Superficial Zone Protein*

T

T *Triangular*

TE *Tissue Engineering*

TEP *Tissue Engineering Products*

TERM *Tissue Engineering and
Regenerative Medicine*

TGF- β *Transforming Growth Factor
Beta*

TLRs *Toll-Like Receptors*

TM *Translational Medicine*

TNF- α *Tumor Necrosis Factor Alfa*

TRPV4 *Transient Receptor Potential
Vanilloid 4*

TSSC *Tissue Specific Stem Cells*

U

UV *Ultraviolet*

US *Ultrasound*

V

VEGF *Vascular Endothelial Growth
Factor*

W

WS *Wet Spun*

Agradecimientos

Tenemos presente en el acervo colectivo la idea, influenciada en parte por la ficción, de que la ciencia la desarrollan científicos. Y claro, cabe preguntarnos, ¿qué es un científico? La respuesta fácil caería en definir como tal a aquél que trabaja en base o para la ciencia. Si bien, el saber popular tiene por cierta la imagen de una persona introvertida, encerrada en sus pensamientos y trabajando sobremanera encerrada entre cuatro paredes llenas de “trastos” a las que gustamos llamar laboratorios. Me temo que la realidad difiere bastante.

Porque, ante todo, los científicos son personas. Y, pese a la mitología popular, personas más comunes de lo que pueda parecer. Es esta alienación con la realidad la que, en mi humilde opinión, aleja a la ciencia cotidiana —aquella que se explica a lo largo de este trabajo— de la proyección mental que la mayoría de la población tiene de la misma.

La realidad es que la gran mayoría, sino todos, de los grandes avances científicos de nuestra sociedad siempre son avances colectivos. La ciencia, no es un resultado individual, y tampoco es inmediato. Los grandes descubrimientos, al fin de cuentas, lo son porque la gente los aclama como tal. A sí, permitirme que describa la ciencia como una herramienta hecha por personas para personas, una herramienta que nos permite crecer, comprender y entender. Y, a medida que se avanza en este camino sobre el aumento de consciencia general, uno se da cuenta de dos cosas: primero, lo que uno sabe es más bien poco; y segundo, lo que uno hace tampoco es que sea mucho.

¡Pero qué dice este “loco”! ¿Y la cantidad de horas —años en mi caso— que lleva hacer algo “nuevo”? Sí, es cierto, la ciencia es difícil, entender cómo funcionan las cosas es complejo. La Naturaleza es infinitamente enrevesada y abismal, y a la misma vez simple. Puede que nunca la lleguemos a entender en su totalidad. Creo, si se me permite la interpretación, que el problema recae en la escala; y es que nuestra escala de percepción es humana, medimos el tiempo en relación a nosotros y eso nos hace delimitar la realidad. A quién se le ocurre mirar al abismo a los ojos y descubre la mota de polvo que somos, corre el riesgo

de perder la cordura si permanece mucho tiempo ahí sentado. Pero, si miras la realidad de refilón, con la mente abierta y sin miedo a equivocarte puedes llegar a ver la belleza de la vida. Entender, durante un breve instante, que el océano es un mar de gotas, tal y como dijeron los budistas. Y la Ciencia, como no puede ser de otra manera, es una suma de esfuerzo, voluntad, saber y autosuperación no de una sino de muchas personas que al final luchan también contra la ignorancia y el paso del tiempo.

Con esta imagen que he descrito en la imaginación del lector, me gustaría mostrar como el trabajo aquí realizado es, a fin de cuentas, una colaboración inmensa que engloba varios años y termina repercutiendo en mi persona.

En primer lugar, quiero agradecer la existencia de este trabajo a mi tutor (también primer director), Juan Antonio Marchal Corrales, catedrático del Departamento de Anatomía y Embriología humana por la universidad de Granada. Parece mentira que la relación que nos traemos entre manos vaya ya a ser una relación de más de siete años. Empezó siendo una relación extraña donde entré *in extremis* en el máster que a fecha de este escrito él dirige. Durante el desarrollo del proyecto de fin de máster, el profesor Marchal me dejó mucha libertad. Palabras suyas son: “Sé que dándote libertad harás cosas”. Así, gracias a su confianza, que sigue arrastrando todos estos años, este proyecto ha salido a la luz.

En segundo lugar, a Guillermo Rus Carlborg, catedrático del Departamento de Mecánica de Estructura de la universidad de Granada. La primera vez que fui a su laboratorio me sorprendió y asustó. No por el número total de cables— a día de hoy sigo sin saber exactamente cuántos hay, entre muchos y muchísimos— sino por el complejo mundo de los ultrasonidos que desarrolló dentro de la facultad. En parte fue un revolucionario, pues se opuso a la idea de que un ingeniero de caminos sólo hace carreteras, puentes y presas. Se atrevió a instaurar en su facultad la bioingeniería, y puede que por ello no le

asustó que un ingeniero biomédico — por entonces, éramos pocos en España— quisiera colaborar con su grupo.

En tercer lugar, a Patricia Gálvez Martín, responsable de proyectos de I+D de Bioibérica S.A.U. Nuestro primer encuentro fue complejo, y es que la doctora Patricia impone. Es una profesional fuerte, valiente, con las ideas claras que sabe dirigir y sabe mucho de I+D. Confrontar a alguien tan “potente” siendo un simple estudiante abrumba. Y, aún así, ella no te trata como un mero estudiante, a menos nunca me trató así. Su trato siempre ha sido profesional, educado y productivo. Tiene una gran ambición que se manifiesta en las ideas y aportes a los proyectos. Sin duda los resultados son mejores gracias a ella. También posee una gran paciencia, pues aguantarme no es fácil, y le agradezco sinceramente haberlo hecho todos estos años, así como haber depositado su confianza.

En cuarto lugar, agradezco a Gema Jiménez González, doctora de la Universidad de Granada, su apoyo en este trabajo. No solo desde el nivel profesional, donde me ha enseñado y ayudado a mejorar considerablemente. Sino también en momentos que, sin duda, espero que recuerde. El camino arduo en las estelas del doctorado ha sido menos árido gracias a ella. Es un ejemplo de perseverancia y fortaleza, de saber estar, de realismo y esfuerzo que sin duda me ha hecho mejor trabajador y mejor persona. Por ello, gracias Gema.

En quinto lugar, a Juan de Vicente Álvarez Manzaneda, catedrático del Departamento de Física Aplicada de la Universidad de Granada. Creo que sólo conozco una persona más educada que este hombre, mi abuelo que en paz descansa. Le agradezco sinceramente su apoyo a este mero ingeniero que no se puede comparar a los inmensos —a menos eso me parecieron— conocimientos que este hombre posee de los conceptos físicos. Una vez perdida la vergüenza por mi sincera ignorancia, me enseñó un mundo fascinante del que estudiar. Decir, que siempre me abrió su laboratorio, pese a no ser parte de él. Y su ayuda, enseñanza y amabilidad son algo que en este mundo se agradecen por su escasez.

En sexto lugar, a Antonio Callejas Zafra, doctor por la universidad de Granada. Por nuestras conversaciones a las diez de la noche, por vivir de la misma forma los avances como yo y por darle vueltas la cabeza tanto como yo. Mucho has dado, y este trabajo sin ti tampoco existiría.

En séptimo lugar, quiero agradecer a mis compañeros —porque los compañeros lo siguen siendo allá donde estén cada uno— Cristina Antich Acedo y Carlos Chocarro Wrona, ambos de mi quinta y doctores ya. Hemos pasado muchos momentos juntos en el edificio al que llaman CIBM. Tantos, que a día de hoy no puedo separar mi doctorado del aprendizaje que hemos realizado juntos. Puede que un ingeniero no sea un experto en caballitos de mar, pero no podrán negar que mis chistes son buenos — no me lo creo ni yo, lo sé.

En octavos lugares, porque aquí hay muchas. Quiero agradecer a todas mis compañeras del CIBM su compañerismo, su amabilidad, su ayuda, su escucha, su habla, sus dudas, sus alegrías, sus esfuerzos, también sus derrotas, su cercanía, sus risas, sus críticas, sus historias...

Entre ellas, gracias a Carmen Griñán Lisón porque sí, porque no hacen falta palabras para ella.

Gracias a Elena López Ruiz, por abrir camino, que no es tan fácil como se cree.

Gracias a Saúl Navarro Marchal, porque es majo, cercano y siempre me ha ayudado cuando se lo he pedido.

Gracias a Julia López de Andrés, porque seamos sinceros, sin sus apuntes de cultivos la vida sería peor. Es concienzuda como pocas y hacedme caso, muy perseverante. Estoy convencido de que algún día leeré noticias sobre ella.

Gracias Paula Pleguezuelos Beltrán y Eli Nygren Jiménez, que oye, se atrevieron a ir a Dublín, además de que son muy trabajadoras, buenas personas y simpáticas. Os pido perdón por la caña que os di, pero espero que os vaya bien — u os esté yendo bien si me leéis desde el futuro—.

A Ana Voltres Martínez, por las terceras, cuartas y quintas oportunidades. Por escuchar, por saber regañar cuando toca y también por no darte por vencida conmigo. Eres un tesoro, y estés donde estés, sé que te irá bien.

A Yaiza Jiménez Martínez, otro tesorito, ¿te puedo llamar hermana de tesis?

A Jesús Peña López y Pablo Graván Jiménez, compañeros de pedidos y de pádel. Hacéis bien, hacedme caso, el laboratorio es mucho más fácil gracias a vosotros.

A, Pablo Hernández Camarero, un héroe invisible, un referente, un sabio. A tus pies me pongo como investigador y como persona. Mucho tienes que enseñar, pena me da quien no lo vea.

A Jesús Ruíz Espígares, por ser tan original. Viniste con Desiré y aún me sigues enseñando cosas a día de hoy. Gracias.

A Aitor González Titos, por ser tú, porque haces más ameno todo. Las mañanas sin tu risa atronadora son menos mañanas. Ánimo, Aitor, eres fuerte. Yo confío en ti. También agradecer a Belén Toledo Cutillas, Belén García Ortega, Gloria Ruíz Alcalá, Manuel Picón Ruíz, MariPaz Zafra Martín, Alfonso Rubio Navarro y quién se me quede en el tintero por ser grandes compañeras/os y hacer del grupo un lugar más acogedor.

Y también agradezco a mis estudiantes, Desiré Venegas Bustos y Helena Contreras Vigo, porque las dos me habéis ayudado más de lo que os podáis imaginar.

Ahora con los novenos lugares, que tampoco son pocos. Quiero agradecer a todos mis compañeros de la ETS de la Universidad de Granada.

Empezando por Manuel Hurtado Estévez, diciendo que es una muy buena persona, un muy buen colega y una persona muy trabajadora. Sé que serás el siguiente.

A José Cortés Cortés, un gran compañero que me debe una vuelta en bicicleta — sin caernos, eso sí.

A Beatriz Blanco Besteiro, por no matarme por chistes de gallegos.

A Inás Faris Al Azzawi, nuestra madre dentro del grupo de ultrasonidos.

A Rafa Marqués Gómez por ser tan entusiasta del diseño, de las IAs, de todo. Porque aprendes mucho con él y encima te diviertes.

A Jorge Torres Pérez, gracias señor, un honor trabajar con usted. Bromas aparte, es un muy buen ingeniero, muy buen investigador y muy buen compañero.

A Antonio Gómez Fernández, por su buen hacer. A Juanma por haberme ayudado y escuchado tanto, siento ser tan pesado, pero es que los matemáticos abundáis muy poco.

A Hiras Shamimi Noori, por cambiar las minas por las personas, sé que llegarás lejos. Y como antes, si alguien se quedara en el tintero, también es de muy agradecer.

Por último, a mi pupila, Natalia García San Martín, porque como siempre, es mejor maestra de lo que cree.

En décimo lugar, a todos los técnicos del CIC de la universidad de Granada. Que cual escritor en la sombra, han realizado mucho de este trabajo. Y pudiendo quedarse ahí, me han enseñado, me han ayudado y me han apoyado tanto. ¡Qué grandes profesionales son! Muchas gracias por no sólo apoyar este proyecto y traerlo a la vida, sino también gracias por todo lo que se sale de vuestro trabajo y aun así aportáis. Gracias a Ana Santos Carro, a Mohamed Tassi Mzamzi, a Isabel Sánchez Almazo, a Fátima Linares Ordoñez, a Gustavo Ortíz Ferrón y a Pablo Álvarez Megías.

Igualmente quiero agradecer al profesor Daniel Kelly del Trinity College de Dublín por aceptarme durante tres meses en su grupo. También gracias a todos mi compañeros y compañeros del Trinity, me llevo un muy grato recuerdo de vosotros y el deseo de visitar Dublín otra vez.

El lector puede ver que hay muchos más nombres de los que aparecen en las publicaciones relacionadas a este artículo. Y le puedo asegurar, de que hay muchas más personas implicadas que por motivos de extensión no puedo incluir. Ruego que me disculpen.

También quiero reflejar en estas páginas una imagen más oculta del doctorado, pues, aunque se vea como un simple documento acreditando las habilidades obtenidas por el/la doctorando, en realidad es un camino arduo, largo y agotador. Hay muchos momentos de baja donde la toalla está más cerca de la lona que del banquillo de entrenamiento. Y, por supuesto, es en esos momentos donde gracias a otras personas y el vínculo que formamos con ellas podemos seguir adelante. Es por ello que me gustaría dejar constancia de su valía y constar mi agradecimiento hacia ellas.

La primera de ellas es mi abuela María Luisa Sánchez Segura. A ella todo lo escrito en este trabajo le sonaría fantástico, puede que mágico. Tampoco conocía el inglés. Pero, en lugar de pensar que podría ser una pérdida de tiempo que un ingeniero se dedicara a hacer investigación, desde antes incluso de empezar me apoyó. Y fue gracias a su apoyo, tanto emocional como económico, que mi persona puede escribirte estas palabras en este trabajo. Sin ella, nada de lo realizado hubiera si quiera existido. Porque en mi caso, han sido muchos las etapas donde las horas de trabajo no iban acompañadas de un salario y gracias a haber tenido familia las pude resistir. Y, aunque siento pena de que ella ya no pueda ver el fin del camino. Gracias a ella he aprendido el valor de seguir adelante e intentar hacer las cosas bien.

Asimismo, voy a agradecer a mi mascota, Pancho, que, aunque a muchos les parezca estúpido y absurdo incluir aquí a un animal, me llevo grandes cosas de haber podido vivir con él. Como perro que fue, lo que yo estuviera haciendo le traería sin cuidado, él estaba más interesado en los palos, las piñas y las piedras. Era feliz de tener comida y cama, y siempre se encargaba de agradecerlo diese igual el día y el momento. Aprendí mucho de su enfermedad, su proceso, y

su muerte. Me enseñó que la vida se puede vivir de forma plena hasta el último instante. Y que, llegado el momento, uno se puede despedir de forma elegante, sin hacer ruido.

Por supuesto agradezco a mis padres, Agustín y Pepa, porque sin ellos yo no existiría. Porque sin ellos, yo no sería lo que soy. Porque sin ellos, yo no habría hecho nada de esto. He aquí, querido lector, que quiero que te tomes un tiempo a reflexionar y honrar sobre tus propios padres. Por otro lado, ya a título personal y humano. Aguantar a un hijo tan quejoso como yo es cansado, y siempre que lo he pedido me han escuchado. Puede que no compartan mis opiniones, ideas o sugerencias. Sin embargo, nada de eso les ha impedido escucharme tanto cuando les venía bien como cuando no. Es también gracias a ellos que he podido realizar la estancia que me permite validar mi doctorado internacional. Así, mi agradecimiento es un agradecimiento triple.

Agradecer a la pareja de uno no es fácil, son tantas cosas las que se comparten que uno no sabe muy bien qué decir. Para aquellos que no la conozcan, Ana ha sido mi compañera incluso antes de embarcarme en este camino. Ha pasado de principio a fin por este proceso junto a mí. Han sido muchas las noches que ha tenido que aguantar mis quejas, mis cabreos y mis manías. Sinceramente no le deseo eso a nadie. Aun así, ella se ha manejado para hacerlo con una solvencia envidiable a la vez que ha crecido como persona, como profesional y como pareja. Ya no es cariño, respeto y agradecimiento lo que tengo por ella, sino admiración. No sé si un día podré devolver todo lo que he recibido de ella. Pero sin duda, el hecho de intentarlo me llena de gozo e ilusión. Gracias Ana, por todo.

En relación al agradecimiento a la familia, qué decir, me gusta mucho mi familia.

Si bien sí podría destacar a mi tía Angustias, hermana de mi abuela, que, como ella, he recibido su apoyo a lo largo de estos años para seguir adelante.

También de mis primos, que, aunque nos vemos poco siempre están ahí para “dejarse ganar” a algún juego de mesa.

A mis tías y tíos, que tanto han hecho y seguirán haciendo por mí. Si pudiera resumirlo con una frase sería esta: “no te sientas apenado por lo recibido, sonrío y di gracias”. Entonces diré gracias, sabiendo que todo lo que soy y todo lo que haga siempre será gracias a vosotros.

No me puedo olvidar de la familia de Ana; Pepi, Emilio, Marta, gracias de corazón por acogerme como uno más, por dar tanto y estar ahí.

Mención especial tienen Juan y María Rosa que han hecho que un español se pueda expresar en inglés sin sentirse idiota.

Y, por último, a mis amigos y amigas por no dejar que la llama se marchite pese al devenir de la vida con sus vientos distantes. Me hubiera gustado tener más tiempo, pero os aseguro, que el que tengamos, lo intentaré apreciar con todo mi ser.

Como material adicional, agradecer a todas esas profesoras y profesores que me han acompañado desde la infancia hasta mis estudios universitarios. Porque un pedacito de ellos ya es parte de mí, camuflado en mis palabras, mis gestos y mis ideas. Pero, sobre todo, por encender la chispa de la curiosidad en mí. Por haber dado el paso de ser buenos profesores a grandes maestros. Sinceramente, gracias.

Para terminar, querido lector, a ti también te quiero dar las gracias por introducirte en estas páginas. He intentado dar mi mejor versión y hacer que pese a tratarse de una tesis doctoral en biomedicina sea entretenida — a su manera— y amena. Y si me dejas, quiero dejarte este mensaje.

La ciencia no es un dogma, es sistemática, es cierto que muchas veces es predecible bajo los conocimientos adecuados. Pero te quiero defender la necesidad de la fe en su proceso. Y sí, digo fe, pues la fe no es sólo propiedad de

la religión. Porque muchas veces tenemos grandes ideas que pensamos que van a funcionar, las intentamos una y otra vez sin resultado. Y es, en última instancia, esa fe indomable en nuestros principios y en la creencia de que estamos en lo cierto lo que nos lleva a continuar. La fe es una herramienta fundamental en la actividad humana, en el progreso social, científico y tecnológico. La fe nos hace mejorar como especie, nos proporciona metas y nos empuja a seguir cuando las fuerzas fallan. Y es responsabilidad nuestra saber usarla sabiamente.

La frontera entre la ilusión y el fanatismo es más difusa de lo que pudiese parecer, siendo más fácil de lo que parece caer en las redes de este último. Porque querido lector, los científicos y científicas primero son personas —recuerda esto— y luego son profesionales.

Con esto me despido hasta que nos volvamos a encontrar.

Si lo hacemos será una alegría y si no, no puede remediarse.

Al final, de mayor o menor manera todos somos compañeros de viaje en la travesía de la vida.

Espero que disfrutes de este.

Gracias por tu tiempo, un saludo de un caminante más

Daniel Martínez Moreno.

Abstract

“If you cannot explain it simply, you do not understand it well enough.”

“Si no puedes explicarlo de forma sencilla, es que no lo entiendes bien.”

Albert Einstein

1. Abstract

Osteoarthritis (OA) is a sizeable socioeconomic condition mainly affecting articular cartilage, a tissue with limited self-healing potential and hence a suitable target for regenerative medicine and tissue engineering (TE). To date, non-effective therapies for cartilage injuries have been discovered. The most pressing requirement in cartilage tissue engineering (CTE) is the development of biomaterials capable of customizing the tissue's complicated extracellular matrix (ECM). Further, novel bioengineered medical devices that stimulate the *ex vivo* growth of biomimetic CTE scaffolds are required.

Regenerative Medicine (RM) is the therapeutical approach that tries organ/tissue repair, replacement, or regeneration to restore decreased function caused by any cause, including congenital deficiencies, illness, trauma, or age. It employs several technology techniques that go beyond typical transplantation and replacement therapy. These methods may include but are not limited to soluble chemicals, gene therapy, stem cell transplantation, TE, and cell and tissue type reprogramming. Alternatively, TE is an interdisciplinary discipline that uses engineering and life science concepts to create biological replacements that restore, maintain, or improve tissue function.

Using cell-based treatments (or CTE products) to regenerate and repair cartilage is not new; techniques like matrix-induced autologous chondrocyte implantation (MACI) and autologous chondrocyte implantation (ACI) have been employed in clinical settings for many years. Even recently, a promised alternative, Instant Mesenchymal Stem Cells (MSC) Product Accompanying Autologous Chondron Transplantation (IMPACT), has been experimented with *in situ* based on fibrin glue containing allogeneic MSCs. Although these methods present some efficacy; however, it is challenging to maintain the proper chondrocyte cell quantity and differentiation stage *in vitro*, and the integration of cells into the surrounding tissue is still subpar. In this sense, the main objective

of this thesis has been to offer solutions to these drawbacks. So, the manuscript has been divided into three chapters.

The first chapter examined how varied geometries and pore sizes (i.e., microstructure) affect the adhesion and proliferation of infrapatellar fat pad-derived mesenchymal stem cells (IPFP-MSCs) in biofabricated 3D thermoplastic scaffolds. These studies used a novel biomaterial for CTE, 1,4-butanediol thermoplastic polyurethane (b-TPUe), and a standardized one (polycaprolactone, PCL). Cell adhesion, proliferation, and mechanical properties were found to alter depending on the form, porosity, and type of biomaterial used. Conclusively, b-TPUe scaffolds more closely mimicked cartilage dynamics, and that triangular geometry with 1.5 mm of fiber distance was the best-adapted morphology for CTE.

In the second chapter, scaffolds of b-TPUe were functionalized using type I collagen and 1-pyrene butyric acid (PBA). After, they were seeded with IPFP-MSCs to verify the effectiveness of these methods in comparison with naive scaffolds. Alamar Blue and confocal tests show that PBA functionalized scaffolds enable superior cell adhesion and proliferation throughout the first 21 days, being cell proliferation and vitality lesser than type I collagen functionalization. Nonetheless, both methods increased the production of ECM and the presence of chondrogenic markers (Sox9, Col2a, and Acan).

The third chapter demonstrates for the first time the chondrogenic evolution of functionalized 3D scaffolds made of b-TPUe in *real-time* in a bioreactor (BR) with low shear pressures. A combination of ultrasonic monitoring and cross-correlation allowed this issue. Applying the signals obtained by a finite element model (FEM) of elastic pulse wave propagation and the empirical signals made it possible to calculate the actual sound speed and density. Further, IPFP-MSCs were utilized as a cellular source for the functionalized b-TPUe-based 3D scaffold. Results showed how the BR induced chondrogenesis in comparison with static 3D cultures. Conclusively, the BR

represented a valuable tool for generating considerable chondrogenesis in a controlled manner.

In summary, a whole process has been developed that uses IPFP-MSCs and functionalized b-TPUe scaffold to generate viable CTE grafts destined for OA treatment. Our highest novelty relies on the absence of an external growth factor to induce chondrogenesis in our 3D scaffolds. Further, a novel system that accelerates the maturation of these grafts and measures the ECM synthesis in *real-time* has been developed and validated.

Therefore, the efficiency of our methodology in terms of cell concentration and ECM production in a relatively short time should imply a possible accurate alternative for CTE.

2. Resumen

La osteoartritis (OA) es una importante afección socioeconómica que afecta principalmente al cartílago articular, un tejido con un potencial de autocuración limitado y, por tanto, un objetivo adecuado para la medicina regenerativa y la ingeniería tisular (TE). Hasta la fecha, se han descubierto terapias poco eficaces para las lesiones del cartílago. El requisito más apremiante en ingeniería tisular del cartílago (CTE) es el desarrollo de biomateriales capaces de personalizar la complicada matriz extracelular (ECM) del tejido. Además, se necesitan nuevos dispositivos médicos de bioingeniería que estimulen el crecimiento *ex vivo* de andamiajes biomiméticos de ETC.

La medicina regenerativa (RM) es el enfoque terapéutico que trata de reparar, sustituir o regenerar órganos/tejidos para restablecer las funciones disminuidas por cualquier causa, incluidas las deficiencias congénitas, las enfermedades, los traumatismos o la edad. Emplea varias técnicas que van más allá de la típica terapia de trasplante y sustitución. Estos métodos pueden incluir, entre otros, sustancias químicas solubles, terapia génica, trasplante de células madre, TE y reprogramación de tipos de células y tejidos. Por su parte, la TE es una disciplina interdisciplinar que utiliza conceptos de ingeniería y ciencias de la vida para crear sustitutos biológicos que restauren, mantengan o mejoren la función de los tejidos.

El uso de tratamientos basados en células (o productos de CTE) para regenerar y reparar el cartílago no es nuevo; técnicas como la implantación de condrocitos autólogos inducida por matriz (MACI) y la implantación de condrocitos autólogos (ACI) se han empleado en entornos clínicos durante muchos años. Incluso recientemente, se ha experimentado con una alternativa prometedora, el producto instantáneo de células madre mesenquimales (MSC) que acompaña al trasplante autólogo de condrocitos (IMPACT), *in situ* a base de pegamento a base de fibrina, que contiene MSC alogénicas. Aunque estos

métodos presentan cierta eficacia, resulta difícil mantener la cantidad adecuada de condrocitos y el estadio de diferenciación *in vitro*, y la integración de las células en el tejido circundante sigue siendo deficiente. En este sentido, el principal objetivo de esta tesis ha sido ofrecer soluciones a estos inconvenientes. Así, el manuscrito se ha dividido en tres capítulos.

En el primer capítulo se examinó cómo las distintas geometrías y tamaños de poro (es decir, la microestructura) afectan a la adhesión y proliferación de células madre mesenquimales derivadas de la almohadilla de grasa infrapatelar (IPFP-MSCs) en andamios termoplásticos 3D biofabricados. En estos estudios se utilizó un biomaterial novedoso para CTE, el poliuretano termoplástico 1,4-butanodiol (b-TPUe), y otro estandarizado (policaprolactona, PCL). Se observó que la adhesión celular, la proliferación y las propiedades mecánicas variaban en función de la forma, la porosidad y el tipo de biomaterial utilizado. En conclusión, los andamios de b-TPUe imitaban mejor la dinámica del cartílago, y que la geometría triangular con 1,5 mm de distancia entre fibras era la morfología mejor adaptada para la ETC.

En el segundo capítulo, los andamios de b-TPUe se funcionalizaron con colágeno de tipo I y ácido 1-pireno butírico (PBA). Después, se sembraron con IPFP-MSCs para verificar la eficacia de estos métodos en comparación con los andamios ingenuos. Las pruebas confocales y con azul de Alamar muestran que los andamios funcionalizados con PBA permiten una adhesión y proliferación celular superiores a lo largo de los primeros 21 días, siendo la proliferación y viabilidad celular menores que la funcionalización con colágeno tipo I. No obstante, ambos métodos aumentaron la producción de ECM y la presencia de marcadores condrogénicos (Sox9, Col2a y Acan).

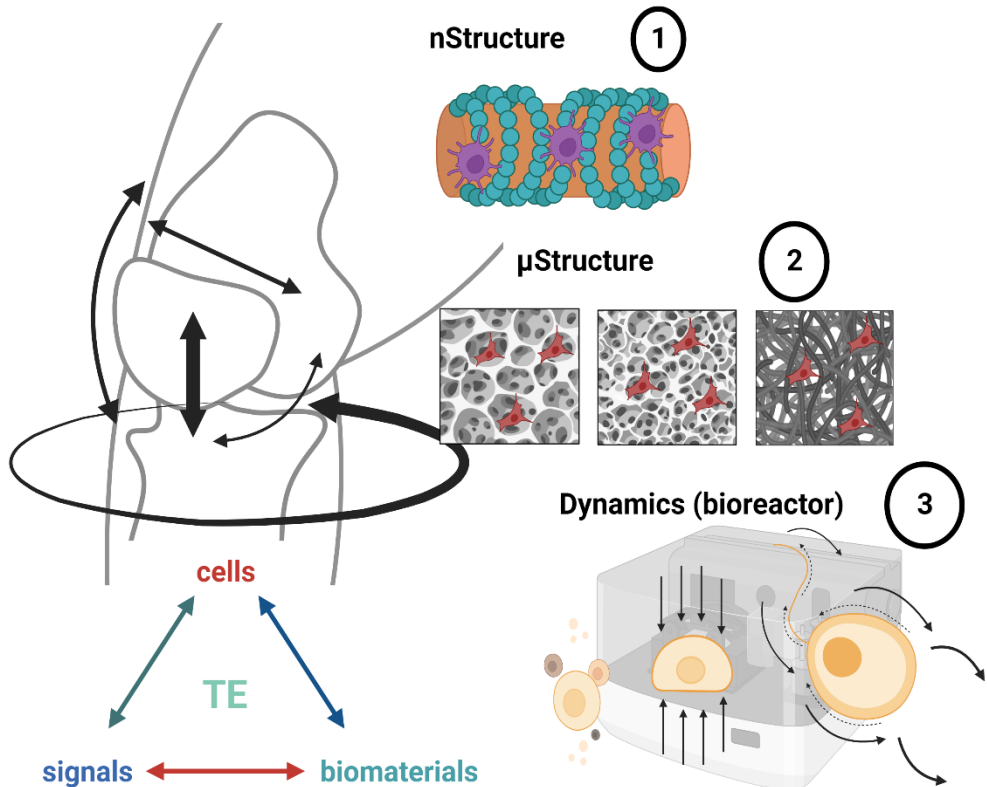
El tercer capítulo demuestra por primera vez la evolución condrogénica de andamios 3D funcionalizados de b-TPUe en tiempo real en un biorreactor (BR) con bajas presiones de cizallamiento. Una combinación de monitorización ultrasónica y correlación cruzada permitió esta cuestión. La aplicación de las

señales obtenidas mediante un modelo de elementos finitos (FEM) de propagación de ondas de pulso elásticas y las señales empíricas permitió calcular la velocidad y la densidad reales del sonido. Además, se utilizaron IPFP-MSC como fuente celular para el andamio 3D funcionalizado basado en b-TPUe. Los resultados mostraron cómo el BR inducía la condrogénesis en comparación con los cultivos 3D estáticos. En conclusión, el BR representa una herramienta valiosa para generar una condrogénesis considerable de forma controlada.

En resumen, se ha desarrollado un proceso completo que utiliza IPFP-MSCs y un andamio b-TPUe funcionalizado para generar injertos de CTE viables destinados al tratamiento de la OA. Nuestra mayor novedad radica en la ausencia de un factor de crecimiento externo para inducir la condrogénesis en nuestros andamios 3D. Además, se ha desarrollado y validado un novedoso sistema que acelera la maduración de estos injertos y mide la síntesis de ECM en tiempo real.

Por lo tanto, la eficacia de nuestra metodología en términos de concentración celular y producción de ECM en un tiempo relativamente corto debería implicar una posible alternativa precisa para la CTE.

BIOMECHANICS OF CARTILAGE TISSUE ENGINEERING



GRAPHICAL ABSTRACT. The core of this doctoral, where Tissue Engineering (TE) and Knee Biomechanics principles were followed. A sophisticated pathway was created, divided into three sections or chapters. 1) Information about nanostructures and scaffold topograph 2) Microstructure and scaffold geometry y 3) Biomechanics and dynamical stimulation. Finally, the three steps produce a product suitable for cartilage tissue engineering (CTE).

RESUMEN GRÁFICO. El núcleo de este doctorado, donde se siguieron los principios de la Ingeniería Tisular (TE) y la Biomecánica de la Rodilla. Se creó un sofisticado itinerario dividido en tres secciones o capítulos. 1) Información sobre nanoestructuras y topografía del andamio 2) Microestructura y geometría del andamio y 3) Biomecánica y estimulación dinámica. Finalmente, los tres pasos dan lugar a un producto adecuado para la ingeniería tisular del cartílago (CTE).

Introduction

“The answers you get depend on the questions you ask.”

“Las respuestas que obtenga dependerán de las preguntas que haga.”

Thomas Samuel Kuhn

3. Regenerative medicine

3.1. Background

The devastating demand for **organ transplantation** has been challenging, as it has the ideal immunosuppression-free strategies. Donor organ allocation may exhibit racial, gender, age, and regional biases, which may intensify as the supply-demand gap expands¹. At the end of 2009, the number of patients in the organ-demanding queue was 28,458; ten years later, in 2019, that quantity increased to 112,568 patients (almost four times higher), but only 39,718 transplants were done^{2,3}. Therefore, the main objective of Regenerative Medicine (RM) is to overcome those limitations, and consequently, it could be defined as the use of different therapies to regenerate human cells, tissues, or organs⁴.

Considering organ transplantation as a technical procedure, its history can be split into three different eras —there are four if the period preceding the first successful transplantation is also taken into account (a pre-transplant age)— which are: i) surgery, ii) immunology, and iii) RM (see **Figure 1**)⁵. Skin transplantation was first mentioned in written literature in the 4th century B.C., with a story from Jacobus De Voragine's 348 ad Legenda Aurea⁶. In 1817, French physician Henri Dutrochet wrote a letter to the editor of Gazette de Santé on skin transplantation. According to the letter, an army subordinate had been punished by having his nose cut off and asked locals to reconstruct him⁶. However, the first register of successful implantation was not confirmed until 1944, during World War II. The patient died at age 84, having lived 60 years after his implant⁵. Nevertheless, this was an exceptional case because of the severe injuries of the patient who received the skin graft; his immunity was compromised to the point of not causing a rejection of the transplantation.

Several years after, in the late 1970s, it was invented a revolutionary drug that would exchange the implant paradigm, cyclosporine, an immunosuppressor

that drastically enhanced long-term survival^{5,7}. Cyclosporine inhibits calcineurin, which is responsible for activating interleukin-2 (Il-2) transcription under normal circumstances. It also inhibits the transcription of lymphokine production and lymphocyte cytokine release⁷.

Regarding RM, which is the consequence of the last transplantation era, its origin is far from being new being the *regeneration* concept first appeared in ancient myths and legends like the Prometheus one when Zeus ordered that every day Prometheus' liver was restored to feed the stormy eagle^{8,9}. The term regeneration has existed since this myth, perhaps even earlier, but it was not until the early 1900s that it became a reality rather than a fantasy thanks to scientists like Alexis Carrel (father of *in vitro* cell culture)⁸. The ability to culture cells outside living organisms may not initially seem very useful. However, thanks to this discovery, studies on cell regeneration, cell differentiation, embryonic induction, pharmacological assays, and an infinite number of other

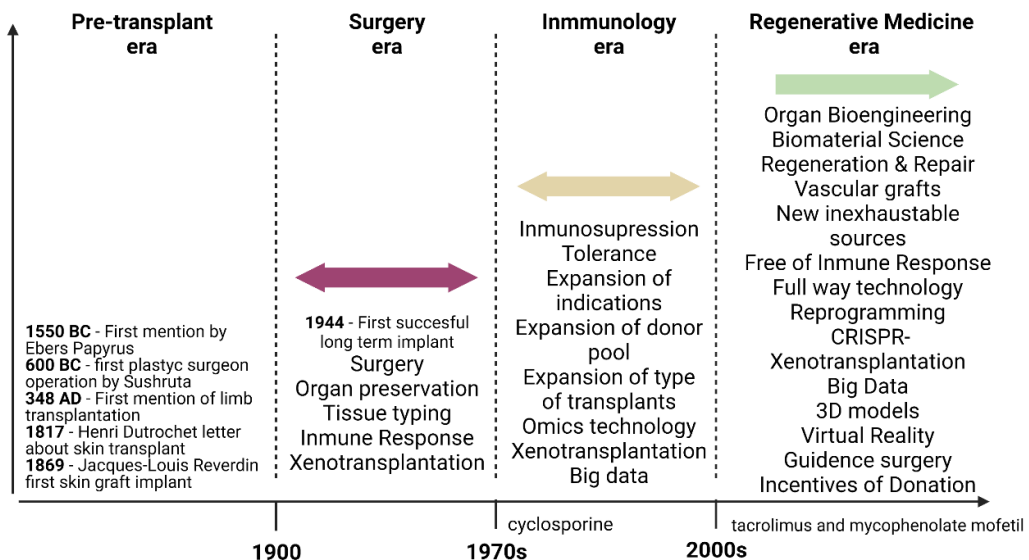


Figure 1. Timeline of organ transplantation. The history of these procedures is divided by three remarkable landmarks: the first successful organ transplantation at 1944, the invention of immunosuppressors as cyclosporine at lates 1970s, and, the start of implementation of vascular grafts thanks to new advanced immunosuppressors. (Figure adapted from Salvatori et al. 2015 with permission).

INTRODUCTION REGENERATIVE MEDICINE

research projects have all been made possible¹⁰. An outstanding example of obtained goals from *in vitro* experimentation was the theory of embryonic induction by Hans Spemann, who won the Nobel Prize in 1935¹¹.

Readers must understand that before this revolutionary invention, scientists used animals to try to analyze those kinds of cellular phenomena¹². Abraham Trembley's research of the hydra, which demonstrated that a whole creature could recover from its severed appendage, is said to have given rise to the present science of regeneration¹³. The extraordinary regenerating ability of amphibian newts, axolotls, and zebrafishes, also caught the attention of scientists in the 18th and 19th centuries. These animals are still regarded as the gold standard models for research on regeneration today¹⁴.

The real beginning of RM dates from 1999 by William Haseltine¹⁵ as a field of research matched with the start of the immunology transplant era; in the late 1970s, Drs Joseph Vacanti and Robert Langer developed the field of tissue engineering (TE)¹⁶. Thus, a new branch of new experts should have been formed as biomedical engineers, biomaterial scientists, and biotechnologists. In favor of simplicity, this interdisciplinary community's first field of work was the skin. In 1979 when Dr. Howard Green et al. realized the first cell-based TE product (Epice), despite its novelty, the final graft was far from being a fully developed new skin tissue, just being a single-layer graft¹⁷. A few years later, a good skin product was developed, Apligraf, which expands the dermis and epidermis layers of the skin¹⁸. Thanks to these two new inventions, TE obtained much popularity during the next decade, and it was no surprise to find researchers starting cartilage tissue engineering (CTE)¹⁹.

Almost ten years later, thanks to the discovery of stem cells, the application of those early TE methodologies with the high regenerative potential of these cells that RM was developed as it is known nowadays^{8,20}. Unfortunately, excess in reducing research times, unacceptable manufacturing costs, and lack of fundamental understanding of tissue synthesis led to a cold period for advances

in RM¹⁶. It lasted several years since the subsequent RM advance was obtained: the first implantable tissue-engineered bladder was developed in 2006²¹. And nowadays, RM is an up-and-coming research field recognized as the forefront of health care²². By 2020, associated market research projects worthed \$67.5 billion²¹.

3.2. Definition

As mentioned previously, due to the vast interconnections between TE and RM, there was controversy differentiating both terms. The first standard definition of RM was established by Greenwood et al. in 2006²³ as:

'Repair, replacement or regeneration of cells, tissues or organs to restore impaired function resulting from any cause, including congenital defects, disease, trauma and aging. It uses a combination of several technological approaches that moves it beyond traditional transplantation and replacement therapies. These approaches may include, but are not limited to, the use of soluble molecules, gene therapy, stem cell transplantation, tissue engineering and the reprogramming of cell and tissue types.'

To synthesize and give a satisfactory global definition for the research community Chris Manson and Peter Dunnill²⁴ established the current description in 2008:

'Regenerative medicine replaces or regenerates human cells, tissue or organs, to restore or establish normal function.'

Almost at the same time, the regulation of regenerative medicine ended in the code from the medical agencies (e.g., EMA or FDA) for all the possible treatments of RM called Advanced Therapy Medicinal Products (ATMPs). Therefore, ATMPs were defined by the EMA as:

'Medicines for human use that are based on genes, tissues or cells. They offer groundbreaking new opportunities for the treatment of disease and injury.'

All the different alternatives of ATMPs must follow Regulation (EC) No 1394/2007²⁵ and Directive 2001/83/EC²⁶.

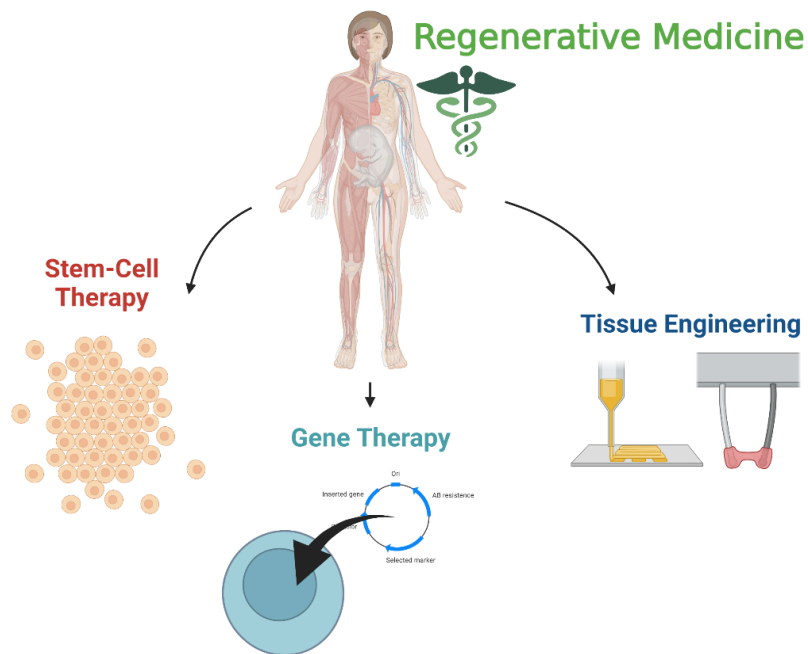


Figure 2. Representation of the three technical approaches for Regenerative Medicine.

Consequently, understanding RM as a valuable therapeutic approach with the same objective as organ transplantation procedures can be divided into three technical methods (Figure 2): **stem-cell treatment**, **gene therapy**, and **tissue engineering**²⁷.

3.3. Stem cell treatment

Stem cells are undifferentiated or partly differentiated cells in multicellular animals that may specialize into numerous types of cells and multiply forever to create more of the same stem cell²⁸. Cell potency refers to a cell's capacity to develop into other types of cells²⁹. The stronger a cell's potency, the more cell types it may develop into. Potency begins with **totipotency** to denote a cell with the maximum differentiation potential, then progresses to **pluripotency**, **multipotency**, **oligopotency**, and eventually **unipotency** (see Figure 3).

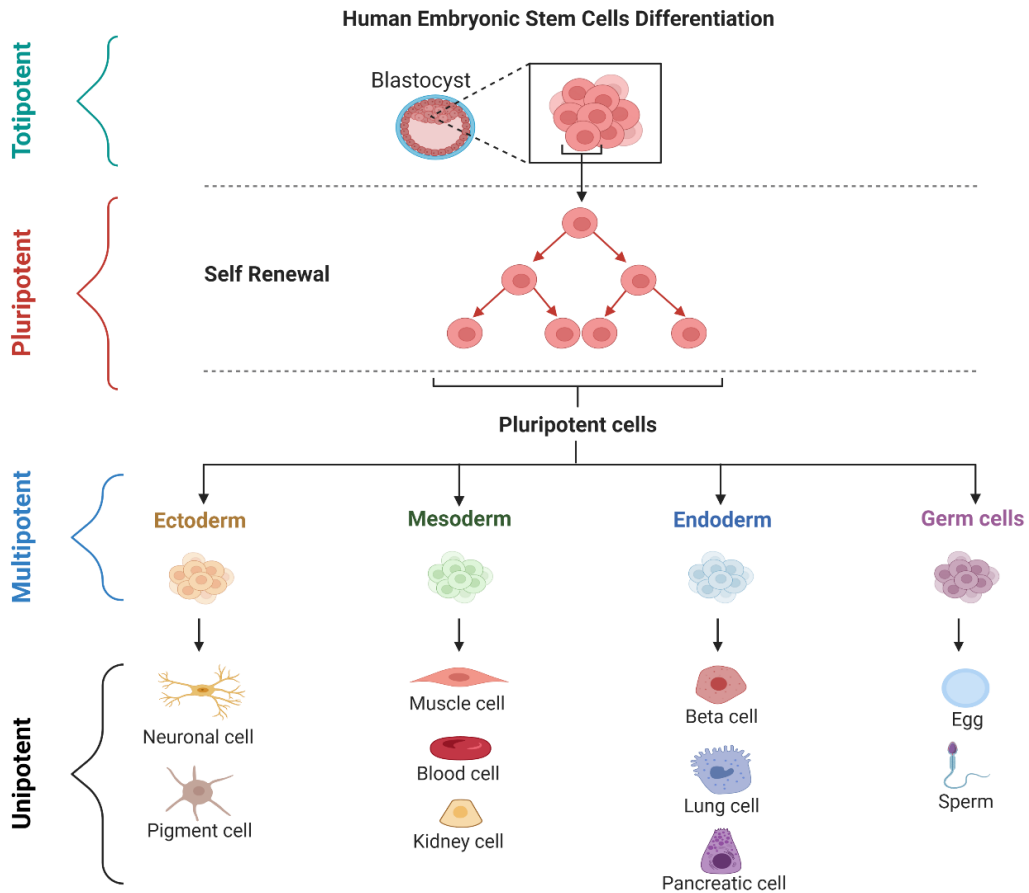


Figure 3. Cell potent lineage.

3.3.1. Pluripotency

The first time **embryonic stem cells** (ESC) were isolated was in 1998; due to their early developmental stage, they can regenerate any defective or damaged cell³⁰. Nonetheless, they are not widely used due to ethical concerns over their harvesting and the risk for teratoma growth and immunological rejection³¹. As a result, it is infrequent only to discover a few examples of their use, such as retina implants (which have a reduced immune response) for individuals with retinitis pigmentosa or dystrophy³².

Realizing all of the constraints of working with ESCs, there was a strong stream of effort seeking to duplicate the practically infinite possibilities of these

INTRODUCTION REGENERATIVE MEDICINE

cells in a more straightforward method, leading to the discovery of **induced pluripotent stem cells** (iPSCs) by Nobel Prize winner Shinya Yamanaka in 2007³³. The earliest uses of iPSCs were to create cardiac³⁴, renal³⁵, liver³⁶, and pancreatic³⁷ tissues. iPSCs can also be used to generate organoids capable of replicating the functional unit of a specific human tissue^{38,39}, allowing the development of novel treatments without animal studies. However, their use has raised several safety concerns, including the potential for dangerous clones to emerge and contamination from undifferentiated cells^{40,41}. In the most recent iPSC report, published in 2016, the guidelines for achieving adequate safety and effectiveness of a final cell therapy product, the quality requirements for source materials, and the ethical limitations of their applications were established⁴².

3.3.2. Multipotency

Another appreciable raw source of RM therapies is the adult stem cells (ASC), which cause their relatively high abundance in the human body, easy obtention, and high regenerative capacities^{43,44}. One valuable source of these cells in the bone marrow is the **Hematopoietic Stem Cells** (HSC), positive for CD34, and the **Mesenchymal Stem Cells** (MSC, aka Stromal Cells), negative for CD34⁴³.

HSCs can differentiate into all blood cell lineages; consequently, they have been used to transplant blood and bone marrow which are increasingly used to treat various ailments, including onco-hematological disorders and refractory autoimmune conditions. The European Group for Blood and Marrow Transplantation has documented some success in patients with multiple sclerosis, rheumatoid arthritis, systemic lupus erythematosus, and other disorders⁴⁵. HSC therapeutic goals have been expanded to include inherited neurologically debilitating metabolic conditions, such as lysosomal storage diseases, peroxisomal storage diseases, and autism spectrum disorders⁴⁶. Also, HSCs are used to restore the functional immune system in a wide range of

immunodeficiencies⁴⁷, reconstruct the myeloablative hematopoietic system in cancer patients⁴⁸, and enhance tolerance to mismatched organ allografts⁴⁹.

The MSC population is sometimes called *stromal* because of its supporting role in establishing a suitable *niche* for HSC differentiation into lymphohematopoietic system cells. MSCs have been isolated from various adult and fetal tissues, including adipose tissue, muscles, skin, liver, kidney, spleen, placenta, amniotic fluid, and umbilical cord⁵⁰. Perhaps, because of their diverse raw sources, there are no specific surface makers to identify MSC yet. Consequently, the International Society for Cellular Therapy has established a protocol to characterize this family of cells⁵¹: i) they present adhesion under conventional culture conditions, ii) they are CD105⁺, CD73⁺, CD90⁺, CD45⁻, CD34⁻, CD14⁻, and, iii) they present *in vitro* differentiation into osteoblasts, adipocytes, and chondroblasts (**Figure 4**).

MSC cells have emerged as an essential player in cell-based therapy because they dampen inflammation and favor tolerance⁵². Further reasons for their attraction are their immense plasticity, easy expansion *ex vivo* with the maintenance of genetic stability, homing to inflamed sites, and repair potential⁵³. An immunoablative conditioning regimen is not required in the application of MSCs because they do not express human class II leukocyte antigens and co-stimulatory molecules on their surface, while they show deficient levels of human class I leukocyte antigen expression⁵⁴; therefore MSCs can be considered as *immunevasive*^{55,56}.

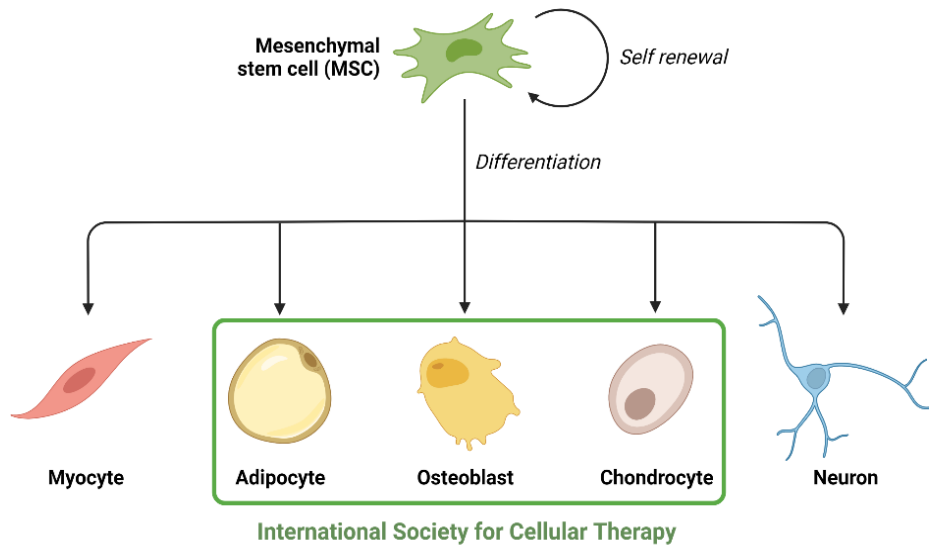


Figure 4 MSCs differentiation potential.

MSCs have been used in the treatment of a variety of diseases, including steroid-refractory acute graft-versus-host disease⁵⁷. MSCs have also been used to treat multiple refractory sclerosis, systemic lupus erythematosus, and intestinal chronic inflammatory diseases⁵⁸. MSCs provide a one-of-a-kind opportunity for Crohn’s disease patients to receive local injections⁵⁹. In literature, there is a vast branch of regenerative procedures using MSCs where can be extracted three overall confirmations: i) MSCs are highly safe, with the most severe risks being transient fever and thromboembolic events^{60,61}. ii) Long-term engraftment and survival rates are extremely low, reducing the risk of malignant transformation ⁶². iii) The standardization of infusion source, dosage, delivery strategy, and timing in each specific clinical setting must be carefully evaluated; the International Society for Cell and Gene Therapy proposed a standard analytical evaluation method⁶³.

3.3.3. Unipotency (or Singlepotency)

In a less manner, Tissue-Specific Stem cells (TSSC) have been used for RM; an example of their application is the Holoclar® (Chiesi Pharma), which is made up of a sheet produced from limbal stem cells that have been plated on a fibrin

matrix and are implanted directly into the patient's eye⁶⁴. Another promising application of TSSCs is in treating junctional epidermolysis bullosa, a debilitating and frequently fatal hereditary condition where; epidermal grafts can be generated using patient-healthy keratinocytes⁶⁵.

3.4. Gene Therapy

Initially, gene therapy was intended to repair a faulty function in monogenic illnesses such as muscular dystrophy, cystic fibrosis, and metabolic disorders. Its applications are expanded to include multifactorial disorders such as cardiovascular disease, neurodegenerative disease, infectious diseases, and cancer⁶⁶. Gene therapy (**Figure 5**) can be defined as the therapeutic introduction of a gene, known as a transgene, into patients' cells (that could be *in vivo* or *in vitro*)⁶⁷. Thus, its most effective applications are i) *Ex vivo* replacement therapy with HSCs, which was first applied to treat severe combined immune deficiency (SCID) *via* an adenosine deaminase retroviral vector (ADA-encoding RV)⁶⁸. ii) *Ex*

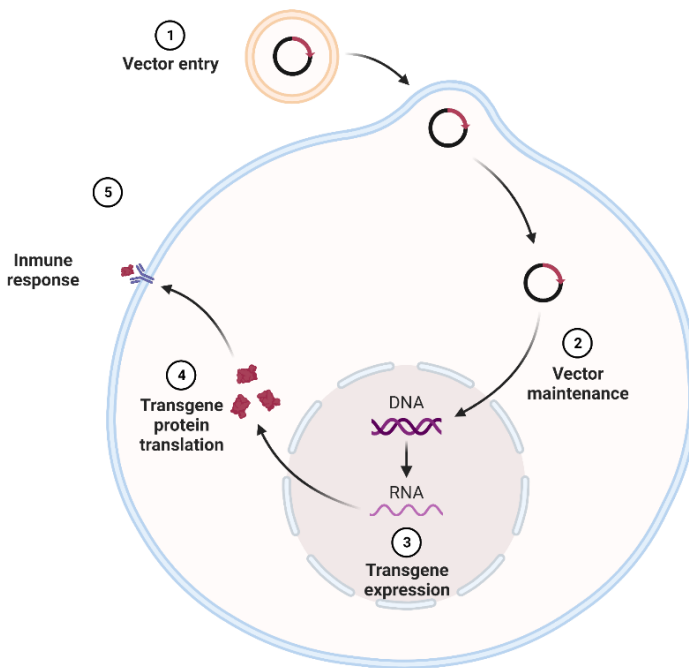


Figure 5. Gene therapy pathway.

INTRODUCTION REGENERATIVE MEDICINE

vivo gene addition therapy as the treatment for Wiskott Aldrich syndrome using lentiviral vectors (LV)⁶⁹, or β -thalassemia⁷⁰. And iii) *in vivo* gene replacement therapy with adeno-associated viral vectors (AAV) where some promising applications have been made in SMA-1 positive children⁷¹ or Parkinson's disease⁷².

A vehicle (called a vector) is needed to target the nucleus to deliver the transgene into cells. Recombinant viral vectors are designed to harness the native viral infection pathways and simultaneously limit replicative life cycles. The combination of transgene and its regulatory components is called an **expression cassette**. Viral vectors can be broadly categorized as integrating and non-integrating depending on their ability to integrate the vector genome into recipient cells' nuclear DNA⁶⁶.

The delivery of a functional form of a mutant gene and the encoded protein that is absent or malfunctioning in target cells is referred to as **gene replacement/addition**⁷³. **Gene subtraction** techniques are designed to mitigate the effects of gain-of-function mutations or to combat infectious illnesses^{74,75}. **Gene editing** is the holy grail of gene therapy, which is theoretically considered predictable and stable. Some examples of gene editing tools are zinc-finger nucleases, transcription activator-like effector nucleases, and CRISPR/Cas9 RNA-guided nucleases⁷⁶. The considerable enthusiasm that resembles this technique is that even if DNA breaks at off-target sites and their effects must be carefully handled, gene editing provides the potential to solve two of the most challenging difficulties in gene therapy: transgene expression control and insertional mutagenesis^{77,78}.

Although gene therapy appears to treat practically all of our medical issues potentially, this technique involves a lot of ethical dissertations and severe technical difficulties. Examples are the gene transfection efficiency (which is not so high), the time persistence of the gene transfection to allow an adequate treatment, the control of the transgene expression, and an accurate vector

integration that avoids insertional mutagenesis⁷⁹. In addition, the patient's immune response will affect the vector intake and the transgenes⁸⁰.

4. Tissue Engineering

4.1. Background

The goals of TE and RM are inextricably linked because TE is just a technological framework for RM applications. TE is a **biomaterials** development approach that combines **scaffolds, cells,** and **biologically active stimuli** (see **Figure 6**). Considering this, TE creates tissue and organ substitutes that can protect, repair, or enhance the capabilities of their injured or diseased counterparts in vivo⁸¹.

Because TE's history is closely tied to RM, it is usual for both names to be misconstrued as synonyms. In **Figure 7**, a timeline with its most relevant events

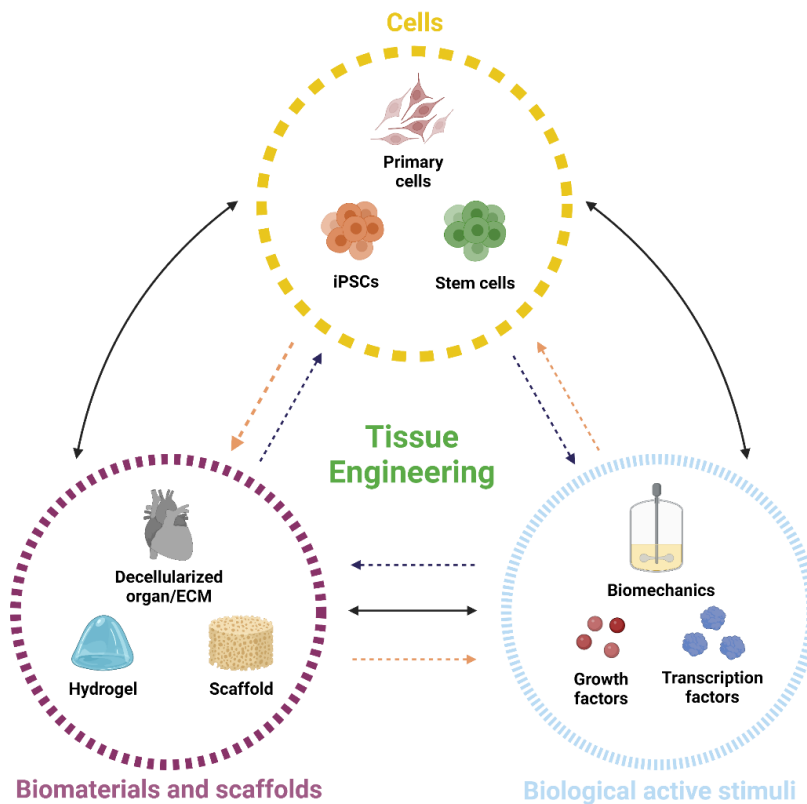


Figure 6. Scheme of the three main pillars of TE. They must be seen as a fully integrated structure with various distinct action channels connecting them.

is represented, where there is especially relevant the development of *in vitro* cryopreservation by Polger⁸². As was exposed above, the beginning of the current conventional RM was a TE application. Nevertheless, most authors consider the beginning of TE to be in the late 1970s when different research groups started to synthesize skin grafts through the formation of keratinizing colonies by James G. Rheinwatd⁸³ or the cultivation of early epidermal grafts by Howard Green⁸⁴ directly harvested from patients' biopsies. At first, this could not be an impressive task. Many years ago, Carrel had already developed *in vitro* cell culture, but keratinocytes needed a specific feed layer made by mouse MSCs⁸⁵.

Perhaps the significance of these advances, and the resulting inflated expectations of TE, were a direct result of the rapid release of the first TE product, the Epicel (by Genzyme, USA)⁸⁶. Further, another invention was quickly released by Integra Life Sciences' (Plainsboro, NJ), a dermal regeneration template used to treat burn wounds where the damage goes deep into the dermis. This time, the TE graft also included a scaffold of a cross-linked bovine type I collagen and shark chondroitin 6-sulfate combination⁸⁷. Almost at the same time, it was synthesized the first skin graft combining dermis and epidermis⁸⁸. A few years later, the second human tissue to be studied by TE was the cartilage; in 1994, a cartilage TE graft was commercialized by Carticel⁸⁹.

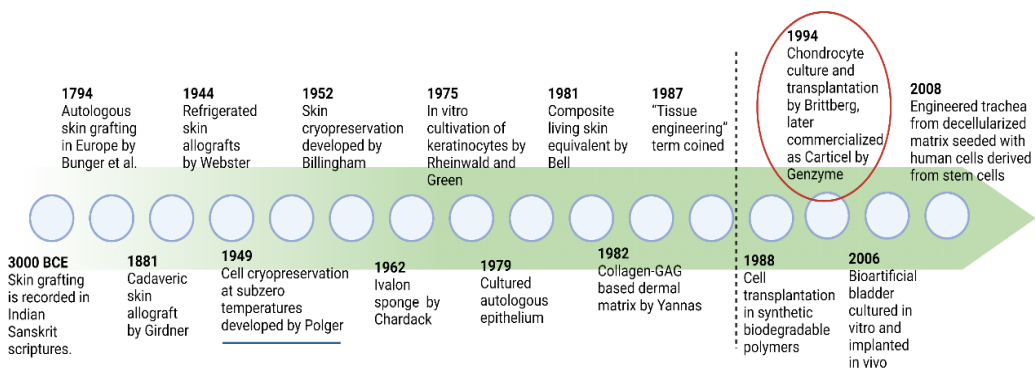


Figure 7. Time-line of more relevant TE history events. The black line represents the most accepted beginning of current TE. Red circle envelops the first iteration of a commercial cartilage TE product, a significant historical landmark for this work.

INTRODUCTION TISSUE ENGINEERING

In the 1990s, diverse TE candidates were tried with insufficient success⁹⁰; skin and cartilage tissues are two with no extended vascularization directly affecting their tissue functions⁹¹. This high-tech market crashed in the early 2000s as jaded investors stopped backing high-risk initiatives such as TE firms⁹². According to a 2004 research, activity in the skin, cartilage, and other structural applications decreased by more than 50%, resulting in the loss of 800 full-time employment⁹³. Despite this, the advances made in the last three decades have ended in top molecular diagnostics, with a market value of more than \$3 billion in 2002 and rising 25% per year⁹⁴.

4.2. Definition

TE was first defined by Langer and Vacanti⁹⁵ in 1993 when they realized the problem of transplant when is a lack of transplantable organs source as follows:

‘Tissue engineering is an interdisciplinary field that applies the principles of engineering and the life sciences toward the development of biological substitutes that restore, maintain, or improve tissue function.’

They proposed a scheme of three pillars to construct the basis of TE: i) isolated cells or cell substitutes, ii) tissue-inducing substances, and iii) cells placed on or within matrices. That representation is mainly preserved, as it was exposed above in previous **Figure 6**; nevertheless, TE is a high-technology field in constant evolution that is constantly nourished by new developments in engineering and biomaterials⁹⁶. Thus, its conventional definition can be exchanged after future relevant applicable inventions for TE, although the treatment pathway of TE is mainly the same as the one proposed by Langer and Vacanti, see **Figure 8**. As a cutting-edge technology, TE is exposed to different challenges that are not solved yet, a scarcity of both renewable **sources** of functional cells and accurate **biomaterials** that present good mechanical, biochemical, and biological properties. In addition, the main objective of present

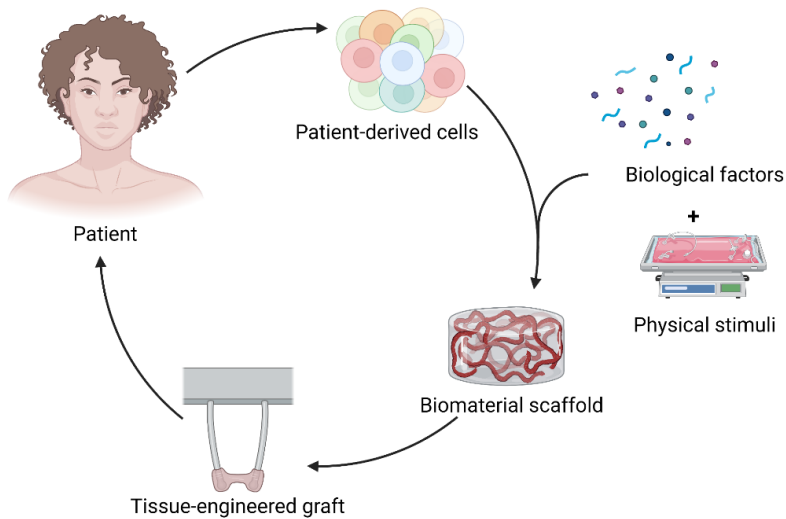


Figure 8. Pathway of TE as an applied therapy.

TE investigations is to create large **vascularization** grafts to simulate larger tissues⁹⁷.

4.3. Challenges and advances in TE

Thanks to technological inventions, TE has experienced many advances in its short history (**Figure 9**). The first one is the development of more sophisticated producing pathways for iPSCs^{98,99}. Respecting MSCs, now that cellular accommodation is better understood. Consequently, the study of ECM has achieved a higher level of relevancy cause its pleasing properties for inducing tissue differentiation; MSCs are programmed to create a pool of desirable growth factors and cytokines¹⁰⁰⁻¹⁰³. In addition, some new cell sources have been identified as adipose-stromal cells¹⁰⁴ and amniotic-fluid-derived stem cells¹⁰⁵. Also of particular interest was the discovery that substrates stiffness influences cell phenotype (i.e., **mechanotransduction**)¹⁰⁶. More surprising was to discover how cells, as with biochemical factors, can remember past mechanical events and adapt to them for any possible subsequent mechanical stimulus¹⁰⁷.

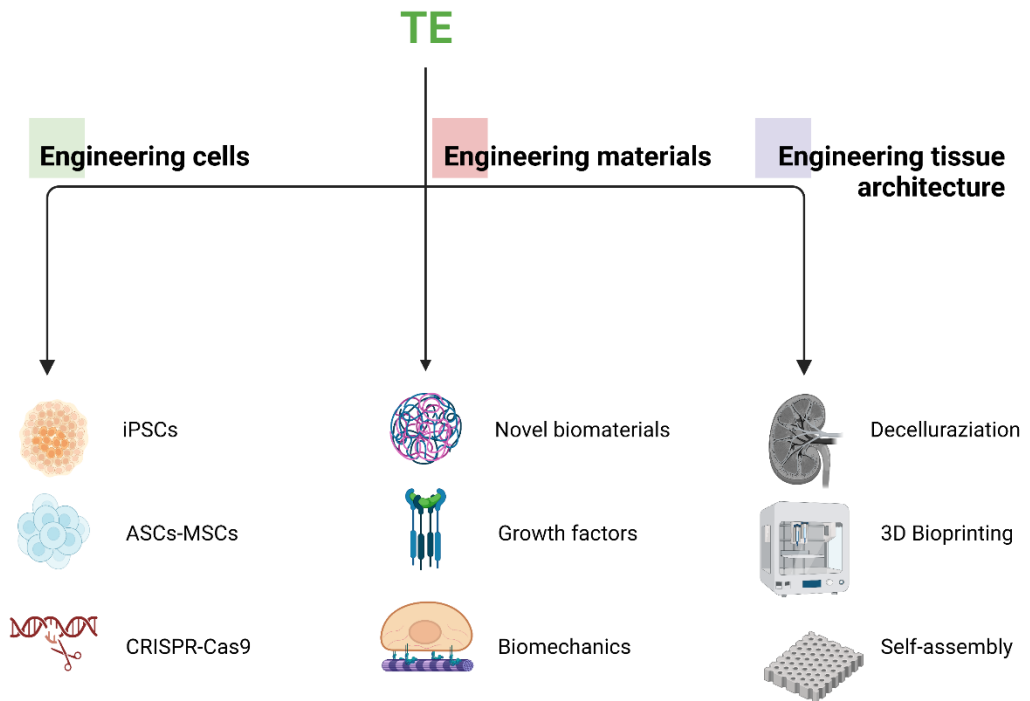


Figure 9. Scheme of new advances acquired in TE during last decade.

Recent advances in biochemistry allowed a considerable increase in **biomaterial conjugations**^{108,109} together with precise bioactive cues **delivery systems**^{110,111}. In addition, our comprehension of the human immune system and graft-host responses is much higher than three decades ago^{112,113}. New biomaterial synthetic procedures allow the creation of **biomimetic** grafts^{114,115}, highly reducing inflammation. Further, thanks to this increase in knowledge, scientists can make more flexible macrophage subsets' proinflammatory responses in response to particular signal induction, which reduces the host immune response^{116,117}.

A combination of gene therapy and TE allows extraordinary results like those obtained by genetic editing of pig organs to adapt them for human transplantation¹¹⁸. Another approach for human transplantation is organ decellularization, where with the use of detergents, cells are completely removed; afterward, iPSCs or ASCs extracted from patients are seeded on that

decellularized organs¹¹⁹⁻¹²². Examples of this methodology are developments of kidney^{123,124}, blood vessels¹²⁵⁻¹²⁷, pancreas¹²⁸, liver^{129,130}, lung^{131,132}, bladder¹³³ and heart¹³⁴.

But perhaps the fundamental advances in TE are due to **biofabrication** innovations, such as **self-assembly**^{135,136} and **three-dimensional (3D) bioprinting**^{137,138} that have been able to create complex structures with integrated **vasculature**^{139,140} and high cell concentrations mixed with **bioinks** composed of biomaterials or ECM components^{140,141}, together with high **spatial resolution**^{142,143}. It had such a profound impact that a new field of study emerged due to the ability to create new in vitro models capable of reproducing organ behavior: **organ-a-chip**¹⁴⁴⁻¹⁴⁹ and **organoids**¹⁵⁰⁻¹⁵³. More recently, the use of biomaterials with the ability to reshape their geometries over time because of external stimuli (e.g., pH and temperature changes, humidity) allowed the development of the novel named technology called four-dimensional (4D) bioprinting^{154,155}.

5. Biomaterials

5.1. Background

Ancient Greeks and Chinese practitioners of biomaterials research exploited natural materials to lessen the symptoms of disease hundreds of years ago¹⁵⁶. However, the development of medical devices made of synthetic and natural materials did not advance significantly until the latter half of the 20th century¹⁵⁷. PMMA, also known as poly(methyl methacrylate), was first used in dentistry in 1937¹⁵⁸. Voorhees experimented with parachute fabric (Vinyon N) as a vascular prosthetic just after World War II¹⁵⁹. The bizarre idea that a conventional fabric could be applied for arterial prosthesis was put out in Rob's 1958 textbook on cardiovascular surgery¹⁶⁰. Early in the 1960s, Charnley performed complete hip replacements using PMMA, ultrahigh-molecular-weight polyethylene, and stainless steel¹⁶¹. Since that time, our understanding of the anatomy of vertebrates and human tissue has increased sharply. We understand that studying substances like those found in woolly mammoth skin will help to better understand collagen in human tissue¹⁵⁷.

5.2. Definition

The definition of biomaterials was accepted by consensus in 1987 by the European Society for Biomaterials and recorded by David F. Willians¹⁶².

'A biomaterial is a nonviable material used in a medical device, intended to interact with biological systems.'

Even it is essential to understand the previous term **biocompatibility** because it is what distinguishes a material from a biomaterial¹⁶³:

'Biocompatibility is the ability of a material to perform with an appropriate host response in a specific application.'

Homsy coined the word "biocompatible" in 1970 after investigating the relationship between several tiny chemicals and cell toxicity and concluding that

a surgical procedure material must be biocompatible to avoid this¹⁶⁴. In the 1990s, the International Organization for Standardization (ISO) saved the term biocompatibility in ISO 10993¹⁶⁵. Since then, it has been a mandatory step in biomaterial science, and all new biomaterials must follow it.

The previous definition could seem precise enough, but it is surrounded by tricky concerns regarding what should be the host response to the implanted biomaterial. It is essential to illuminate what is understood by foreign-body reaction (FBR) to clarify the presented problematic¹⁶⁶.

Any biomaterial implanted causes a local or systemic reaction in the host tissue if the biomaterial is put into the body by injection or surgery¹⁶⁷. Although several biomaterials and medical devices have been successfully implanted in people, no stealth material that can outperform the human surveillance system has been developed¹⁶⁸. FBR is brought on by protein adsorption on the substance (biofouling), which causes the implant to be encapsulated by a thick collagenous capsule and prevents the implant from interacting with the surrounding tissue further¹⁶⁶. The different FBR stages are represented in **Figure 10**.

Considering the previous definition of FBR, some examples of biomaterial implantation do not follow this path. For instance, the subcutaneously implanted is a solid slab of poly(hydroxyethyl ethyl

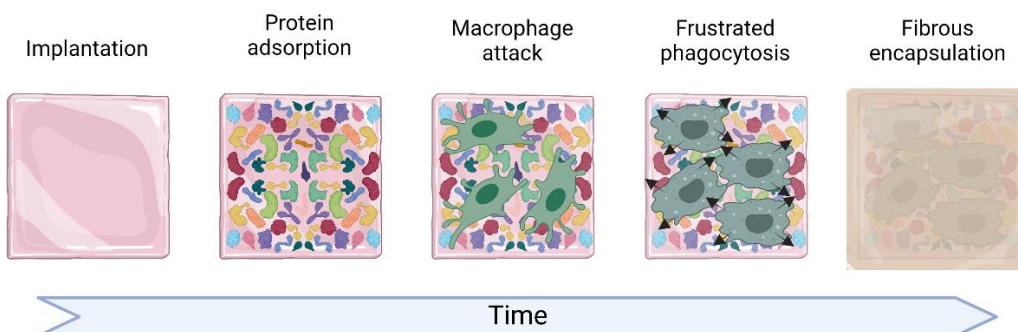


Figure 10. Representation of the Foreign-Body Response steps. At the early stages, the nude scaffold is covered by a layer of coating proteins to attract the macrophages. The phagocytosis is frustrated due to biomaterial size, and, finally the biomaterials is encapsulated by a fibrous layer mostly made by collagen.

INTRODUCTION BIOMATERIALS

methacrylate) (pHEMA) hydrogel, either as a solid slab or as a porous material having 40 μm diameter interconnected pores. The solid slab heals using the traditional FBR. On the other hand, the 40 μm porous pHEMA heals with no capsular sac and a highly vascularized tissue reconstruction¹⁶⁹. So, can a biomaterial have more than one healing process? Or, can a response that isolates a substance from the body be deemed biocompatible?

5.3. Relevant terms related to biomaterials

Along with biomaterial development, some aspects may be clarified to categorize and differentiate one from the others based on their unique characteristics and application. The distinction between **degradation** and **erosion** is an example of the need to clarify these terms; degradation mainly occurs *via* hydrolysis; however it can also occur through oxidative, photodegradation, or enzymatic mechanisms¹⁷⁰. On the other hand, erosion is caused by deterioration of the biomaterial, abrasions, dissolution, or mechanical wear. And one condition does not necessarily imply the other; for instance, an implantable poly(lactic acid) (PLA) scaffold begins to degrade because of the FBR. That degradation is observed due to a reduction of their weight, but no apparent erosion is observed at those early stages. Therefore, erosion is only observable when PLA breakdown is well underway¹⁷⁰. Then the main difference between these terms are:

- **Degradation:** A chemical process that cleaves covalent bonds. **Biodegradation** is used when a biological agent (enzyme, cell, or bacterium) is causing the chemical breakdown of the implanted device, as proposed by the European Society for Biomaterials Consensus Conference¹⁶².
- **Erosion** appears when the biomaterial experiments with size, shape, or mass variations. **Bioerosion** can be used where a non-polar

biomaterial starts its transition to be water-soluble under physiological conditions¹⁷¹.

- **Surface erosion** happens when the conversion rate to water-soluble biomaterial surpasses the water penetration rate, resulting in material surface erosion without altering the biomaterial core¹⁷².
- **Bulk erosion:** Unlike surface erosion, bulk erosion occurs when water penetration overpasses the conversion rate to water-soluble. In this situation, biomaterial degradation occurs through the bulk structure¹⁷².
- **Bioinert:** it is called from a substance that does not elicit a negative response from the body's immune system when it is introduced into the body¹⁷³.
- **Bioactive** refers to an item or material affecting or evoking a reaction from living tissue¹⁷⁴.
- **Biointegration** is the attaching of live tissue to the surface of a biomaterial or implant independent of any mechanical interlocking mechanism. It is frequently used to describe the binding between hydroxyapatite-coated dental implants. Biointegration is critical to the implant's success and lifetime¹⁷⁵.

5.4. Evolution of biomaterials

Regarding the chemical composition and structure, biomaterials can be classified as (**Figure 11**): i) **metallic materials** (e.g., vanadium Steel), which must avoid any possible corrosion¹⁷⁶. ii) **Ceramic materials** (e.g., alumina) are generally complex and can be bioinert, bioactive, biodegradable, or resorbable ceramics¹⁷⁷. iii)

INTRODUCTION BIOMATERIALS

Synthetic polymeric biomaterials (e.g., polyethylene, polyamide) present simpler manufacturability and processability, and they must be biocompatible and present sterilizability¹⁷⁸. iv) **Composite materials** (e.g., natural as bone, synthetic as fiberglass) present hierarchical structures regarding porosity or fibrous structural features¹⁷⁹. v) **Biodegradable polymeric materials** (e.g., poly-3-hydroxybutyrate -PHB-, cellulose) are biomaterials that are absorbable, erodible, or resorbable making them perfect candidates to avoid chronic FBRs and to regenerate tissue¹⁸⁰.

Nevertheless, the evolution of biomaterials presents a higher correlation with biomaterial properties than with their chemical composition. Therefore, it is unsurprising that the first kind of biomaterials was biodegradable because biodegradability is relatively easy to obtain. PLA was initially synthesized in 1944, while poly(glycolic acid) PGA was explored in about 1954¹⁸¹. The Dexon™ suture, a PGA polyester that has been in use since around 1970¹⁸², was an early example of a biodegradable polymer. Despite being created in the 1930s,

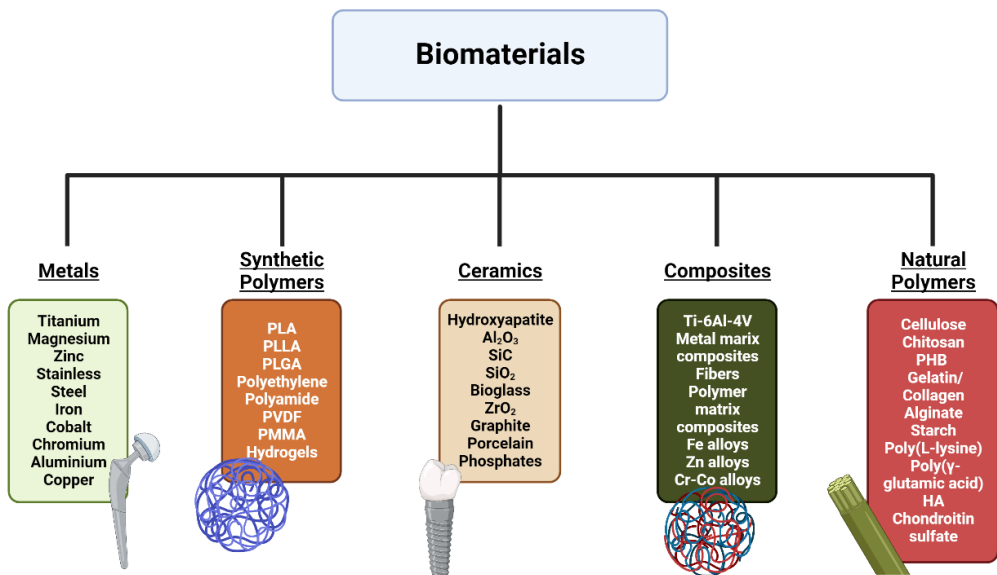


Figure 11. Classificatory scheme of biomaterials depending on their chemical composition.

polycaprolactone (PCL) was also employed in clinical trials of a contraceptive device in the 1980s¹⁸³.

Once biodegradability mainly was obtained, the next developmental step was to create biomaterials capable of response to physiological stimulation, the called **smart** biomaterials¹⁸⁴. Kuhn et al. invented the first intelligent polymeric material in 1950, which was most likely a pH-sensitive, artificial muscle-like, swelling-deswelling hydrogel¹⁸⁵. Later, pH-sensitive hydrogels were created as an early example of a biomolecular system that responded to its surroundings in a medically significant manner¹⁸⁶. However, Dong and Hoffman 1987 showed that the temperature responsiveness of poly(N-isopropyl acrylamide) (pNIPAM) hydrogels began the field of smart polymers¹⁸⁷.

Regarding vascular stent implants or the development of new catheters that do not induce immune response during surgical intervention, biomaterials applied in these procedures must not interact with any external particles (e.g., proteins, platelets). Thus, an excellent relevance goal of biomaterial science is the obtention of **non-fouling** biomaterials¹⁸⁸. The first of their kind was developed in 1983 by Merrill and Salzman¹⁸⁹, and research on platelet resistance by Nagaoka et al.¹⁹⁰. Examples of these non-fouling materials are polysulfobetaines¹⁹¹.

Observing the history of biomaterials, it is true that polymers are the most studied but are far from perfect among all the types of biomaterials. Several mishaps exist since synthetic polymers usually do not present a tailored chain sequence distribution¹⁹², whereas natural polymers depend on the state of the living organisms that produce them¹⁹³. Further, several polymers do present not adequate biocompatible properties, like **hydrophobicity**¹⁹⁴. Being a fundamental adaptability step to modify their surface for inducing bioactivation, with a process called **surface modification**^{195,196}.

Biomedical engineers have been looking for new controlled, and more accurate polymerization methods. Atzet et al. created a biodegradable pHEMA

INTRODUCTION BIOMATERIALS

by employing chain-transfer polymerization (ATRP) to generate pHEMA blocks with a molecular weight of 6,000 Da from a dibromoisobutryl-terminated PCL¹⁹⁷. ARGET (activators regenerated by electron transfer) polymerization was created in 2007 to provide regulated radical polymerization in the presence of oxygen and with very low copper ion concentrations¹⁹⁸. K. B. Sharpless used the phrase "Click Chemistry" in 2001 to characterize high-yielding reactions, broad in scope, produced only by products that can be removed without chromatography. They are stereospecific, simple to perform, and can be carried out in readily removable or benign solvents¹⁹⁹. Thanks to the advances in polymerization protocols, new polymers that, in principle, could not seem biocompatible, like polyurethane, have been able to develop²⁰⁰.

In addition to all these advances, we must also add the advances made by RM and TE, which remarked the importance of 3D structures in cell phenotypic and tissue recapitulation²⁰¹. Recently, 3D organoids²⁰² and patterned two- and 3D organs on a chip²⁰³ have become popular, and both require biomaterials and deep comprehension of how the ECM affects tissue development^{204–206}.

5.5. The importance of the ECM

Collagen fibers are the components that give tissues their tensile strength and prevent tissue creep under continual loads. **Elastic fibers** aid in the recovery of skin and cardiovascular tissue under constant mechanical loads. **Proteoglycans** are abundant in tissues such as cartilage, which are subjected to high compression forces while moving. Shear loading is detected by cells in these tissues, which act as force transducers, converting it into chemical impulses that stimulate the creation of more matrix components. Cell attachment factors (e.g., **glycoproteins**) are essential for maintaining continuity between the cytoskeleton of the cell and the ECM²⁰⁷.

5.5.1. Collagens

Currently, nineteen distinct collagens have been discovered, all of which have particular characteristics and properties²⁰⁸. Collagen comprises three polypeptide chains coiled into a ropelike coil (**Figure 12**)²⁰⁹. This molecule region is responsible for the mechanical characteristics of tendons and ligaments (i.e., the ability to withstand tensile loads). Each chain, known as **α -chain**, is distinguished by three-amino acid repeating patterns, and, depending on each collagen type, chosen α -chains could be identical or not²¹⁰. Changes to the glycine-X-Y amino acid sequence frequently result in collagen molecular failure creating mechanical instability (e.g., osteogenesis imperfecta)²¹¹. Intermolecular interactions between the α -chains of nearby molecules reinforce the helical complex, which is naturally tension-resistant²¹².

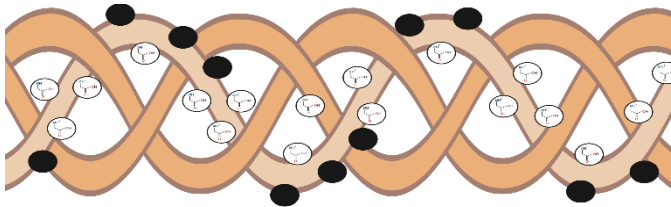


Figure 12. A fragment of a collagen molecule that demonstrates how the alpha chains are wrapped into a triple helix. The amino acids are similarly organized in a helix within each chain, with glycine facing the triple helix's core. The dots stand in for the other amino acids.

5.5.2. Elastic fibers

The elastic fibers of the ECM allow tissues such as the skin, lungs, and blood vessels to withstand repeated stretching and severe deformation while resuming their original shape. Depending on the intensity and direction of the stresses pressing on the tissue, elastin is organized differently²¹⁰. The fibers can be organized as tiny, individual fibers (as in the epidermis or lung) or as a three-dimensional honeycomb-like network of fine fibers (as in the aorta), with concentric fenestrated sheets (as in the aorta) or tiny, individual fibers (e.g., elastic cartilage)²¹⁰.

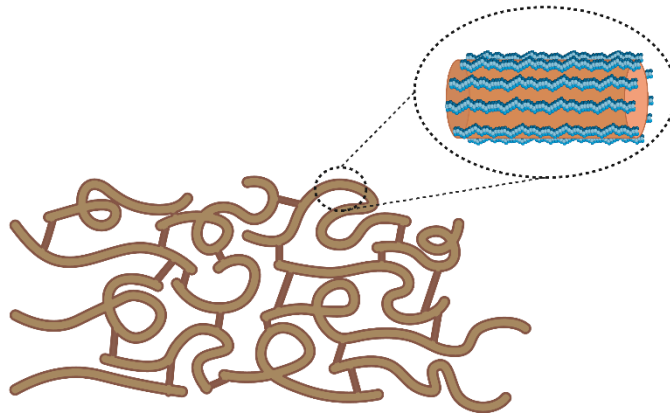


Figure 13. A representation of elastic fibers with a microfibril-containing elastin core is shown.

Regarding elastic fiber composition, it is formed by an elastin core surrounded by several microfibrils (**Figure 13**). The microfibrils, mainly composed of fibrillin, serve as a scaffold for the initial deposition of elastin, but after the production of the fiber's core elastin, the bulk of the microfibrils are relocated to the fiber's exterior²¹¹. Desmosine and isodesmosine, two amino acids found in elastin, create cross-links between neighboring tropoelastin chains, giving elastin its elastic qualities²¹³. Despite the uncertainty over the natural process, the amount of elastin present in the tissue often indicates the degree of its mechanical strain²¹³. Adult humans may produce elastin in response to cyclic strain, injury, UV radiation²¹⁴, and tissues in several disease states, including emphysema²¹⁵; however, adults cannot repair the elastic fiber assembly processes function is not restored²¹³.

5.5.3. Proteoglycans (PGs)

A core protein covalently linked to one or more **glycosaminoglycan** (GAG) side chains define the PGs²¹⁶. The core proteins vary widely in size and are frequently unique to each PG species. The GAG chains are formed of repeating disaccharide units, and the kind and number of units significantly impact the PG's properties (**Figure 14**). Chondroitin sulfates 4 (CS A) and 6 (CS C), keratan sulfate (KS), dermatan sulfate (DS, sometimes known as CS B), heparan sulfate (HS), and **hyaluronic acid** (HA) are the six major GAGs²¹⁷. HA is unique because it is neither sulfated nor linked to a protein core.

All GAGs are negatively charged and have a proclivity to attraction, resulting in an osmotic imbalance that causes the matrix to absorb water from its surroundings²¹⁶. The degree of hydration is determined by the number of GAG chains and the swelling limitation imposed by the surrounding collagen fibers²¹⁶. The proportion of GAG in tissues subjected to high compressive forces (e.g., articular cartilage, AC) differs from that in tension-resisting tissues such as tendons and ligaments²¹⁸. The proportions of PG species vary with mechanical load, with the CS:DS ratio being larger in tissues exposed to compression and lower in tissues resisting tension²¹⁸.

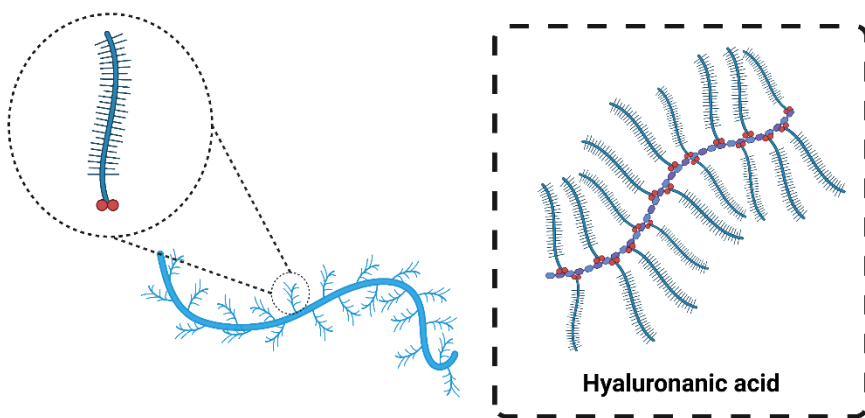


Figure 14. Representation of a conventional PGs with an amplification of their monomers. In the dotted line square there is the Hyaluronic acid obtained by the mixture of the hyaluronan (core molecule) with other PGs.

INTRODUCTION BIOMATERIALS

Substantial evidence supports the claims that appropriate physiological mechanical loading is necessary to maintain proper tissue architecture, and connective tissues vary their PG composition and type in response to applied stress variations²¹⁹. For instance, in healthy AC, joint mobility is essential for the appropriate maintenance and turnover of PG. Joint immobility or disuse causes cartilage shrinkage due to PG loss from the matrix²¹⁹. Cartilage responds to changes in applied stresses by changing its PG content and type²²⁰. Even more, movement is sufficient to sustain PG content in sheep AC without needing weight bearing²²¹.

The production and breakdown of aggrecan are also disturbed in arthritic disorders brought on by trauma or degenerative processes, and the aggrecan monomer is unable to bind to HA and form large aggregates reducing multiple decompressive properties of cartilage²²². This problematic issue is also relevant for the load-bearing intervertebral discs (with high PG content)²²³. It has been known for some time that lateral compression of fetal tendons causes significant alterations in certain PGs and at the gene level. The messenger ribonucleic acids (mRNAs) for aggrecan and biglycan rose without affecting the mRNAs for decorin or type I collagen²²⁴. These alterations appear to be mediated by a specific growth factor, transforming growth factor beta (TGF- β), a potent stimulator for aggrecan and biglycan but not decorin²²⁴. The importance of biomechanics in tissues and, more specifically, in cartilage tissue will be discussed in the following chapters.

5.5.4. Glycoproteins

Glycoproteins are a minor yet significant portion of the overall ECM components; they are soluble, multidomain macromolecules with many functions. Although they do not perform many mechanical functions, they are crucial for maintaining the surrounding matrix and connecting it to the cell, i.e., **cell-ECM interactions (Figure 15)**²²⁵.

Cell-ECM interactions are essential; they control many processes influencing cell shape changes, boosting cell motility, and promoting cell division and proliferation²²⁵. Examples of glycoproteins are: **fibronectin**, which presents an important role in cell attachment²²⁶; **tenascin**, involved in cell attachment modulation²²⁷; **laminin**, with a massive contribution in the structure of the basement membrane^{228,229} **link protein**, which stabilizes PG aggregates embedded in cartilage ECM²³⁰; **thrombospondin**, involved in cell attachment procedures²²⁷; **osteopontin**, endorses tissue calcification through calcium intake²³¹; and, **fibromodulin**, controls collagen fibril formation²³².

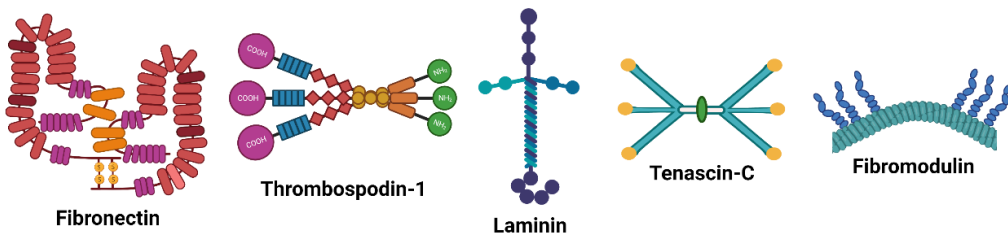


Figure 15. Representation of the most relevant glycoproteins. Osteopontin and link protein are not included due to small size.

6. Biomechanics

6.1. Background

Biomechanics (from Ancient Greek: "life" and "mechanics") is the use of physical concepts in living beings such as people, animals, plants, and the fundamental functional units of life, the cells²³³.

Regarding the history of biomechanics, Aristotle was the first to classify animals' bodies as mechanical systems, where he simplified the motion of the muscles by geometrical forms²³⁴. Several years later, Galileo did early analyses about the different evolution in bone strength related to weight²³⁵, and with Borrelli's calculation concerning human equilibrium, biomechanics became a specific science²³⁶. But it was in the sixteenth century when Leonardo Da Vinci established the origin of biomechanics by studying anatomy in the context of mechanics²³⁷. In the nineteenth century, surgeon Julius Wolff developed the law of bone remodeling based on mechanical stimuli²³⁸. Finally, during the 1960s, biomechanics was taught as part of a medical degree²³⁹. Currently, biomechanics is understood as a subfield of biophysics that studies the structure, operation, and motion of the mechanical components of biological systems, at any level, from complete organisms to organs, cells, and cell organelle^{240,241}.

6.2. Basic solid mechanical concepts

Some basic solid mechanics considerations and definitions must be clarified to follow the explanations below.

A tissue is made up of atoms maintained in equilibrium at the molecular level by repulsive and attraction forces (**Figure 16**)²⁴². There are four sorts of forces in nature: gravitational, electromagnetic, strong nuclear, and weak nuclear²⁴³. For breaking equilibrium, a non-zero force must be applied, and as a

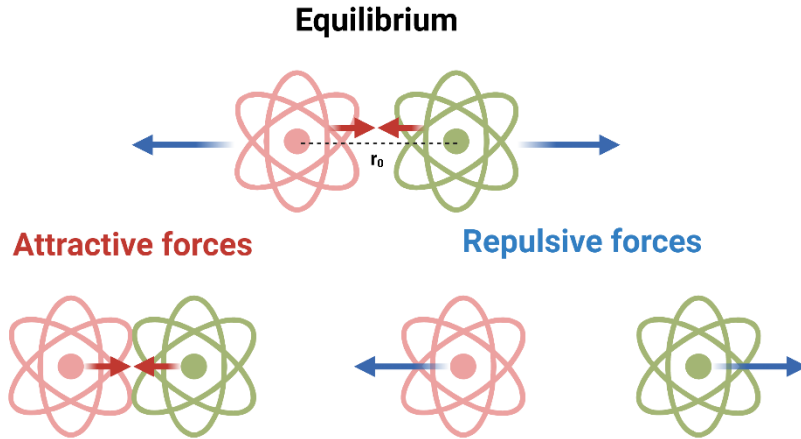


Figure 16. Elastic behaviour from the interatomic forces.

result, the interatomic distance shifts, altering the geometry of the material, i.e., making a deformation. When atoms are placed in a specific position, the repulsive or attractive force (which causes atoms to move towards or away) is proportional to the increase in position²⁴². This force is analogous to that produced by a spring. When applied to the entire body, this concept makes a perfect mesh of springs connecting nearby atoms, i.e., Hooke's law for **continuum mechanics**²⁴⁴. Hooke's linear elasticity's an excellent approximation to reality; however, we must keep in mind that the force-strain relationship in soft tissues is not linear. Furthermore, because atoms have mass, they are susceptible to the concept of *inertia*. This grounds that the transmissions of these forces via tissues (i.e., among atoms) are not instantaneous, so a **wave propagation** phenomenon with a finite wave speed develops.

Solid mechanics is part of the continuum mechanics field, and this is a field of mechanics that studies the mechanical behavior of materials that are represented as a continuous mass rather than discrete particles; these models were developed Augustin-Louis Cauchy²⁴⁵.

A continuum model posits that the object's essence fills the space it occupies²⁴⁶. These models may be used to create differential equations that explain the behavior of such things using physical principles such as

conservations of mass, linear momentum, and energy; together, the constitutive connections offer some information about the material²⁴⁶. Continuum mechanics is concerned with the physical characteristics of solids and fluids unaffected by the coordinate system in which they are seen. To do this, scientists use tensors, mathematical objects independent of coordinate systems, to express physical qualities²⁴⁷. These tensors can be represented computationally using coordinate systems, as explained later²⁴⁸.

6.2.1. Stress in solid mechanics

The force across a "small" border per unit area for all boundary orientations is stress²⁴⁹. Stress (**Figure 17**) is a fundamental number that, like velocity, torque, and energy, can be measured and studied without explicitly taking into account the nature of the material or its physical causes since it is formed from a fundamental physical quantity (force) and a purely geometrical quantity (area).

Stresses are represented with the letter σ for normal stressed and with τ for shear ones. Uniaxial normal stresses are mathematically expressed as follows:

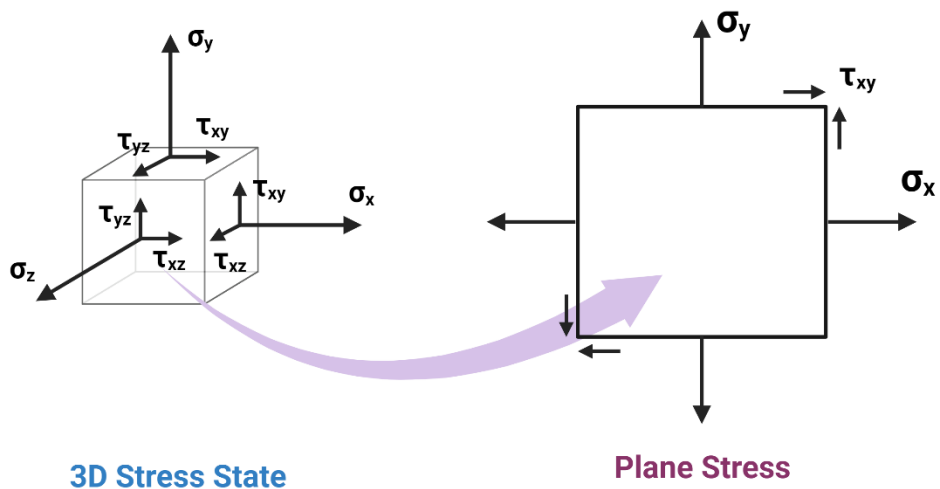


Figure 17. Cartesian representation of tridimensional stresses and the plane stress.

$$\sigma = \frac{F}{A} \quad (1)$$

Cause stress is the ratio between force over area, it has the units of $\text{N} \cdot \text{m}^{-2}$, but it is not uncommon to find it expressed in Pa.

6.2.2. Strain in solid mechanics

When rigid-body movements are not included, **strain** and **deformation** are linked regarding the relative displacement of body components. Depending on whether a strain field is defined about the body's initial or final configuration and whether the metric tensor or its dual is considered, different equivalent options may be made for the formulation of the field.

In the cartesian coordinate system, normal uniaxial strain can be defined as:

$$\varepsilon \stackrel{\text{def}}{=} \frac{\partial}{\partial X}(x - X) \rightarrow \varepsilon_x = \frac{\partial u_x}{\partial x} \quad (2)$$

But, in engineering, most of the time is applied the Cauchy strain is:

$$e = \frac{\Delta l}{L} \quad (3)$$

where Δl is the increment in length (it can be negative), and because it is a ratio between length units over the same units, the result is adimensional, which is a reasonable condition to extrapolate results between models.

On the other hand, shear strains are defined as the change in the angle between two adjacent solid boundaries (see **Figure 18**).

$$\gamma_{xy} = \frac{\partial u_y}{\partial x} + \frac{\partial u_x}{\partial y} \quad (4)$$

In a Cartesian system, the Cauchy's strain tensor looks like:

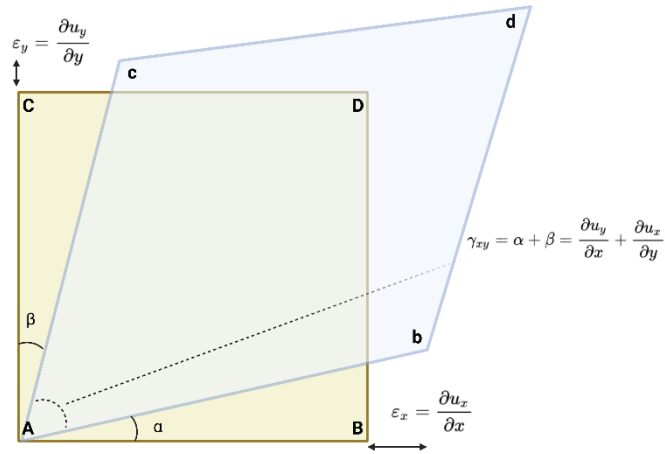


Figure 18. Planar representation of normal and shear strains in Cartesian coordinates.

$$\begin{bmatrix} \varepsilon_{xx} & \varepsilon_{yx} & \varepsilon_{zx} \\ \varepsilon_{xy} & \varepsilon_{yy} & \varepsilon_{zy} \\ \varepsilon_{xz} & \varepsilon_{yz} & \varepsilon_{zz} \end{bmatrix} = \begin{bmatrix} \frac{\partial u_x}{\partial x} & \frac{1}{2} \left(\frac{\partial u_x}{\partial y} + \frac{\partial u_y}{\partial x} \right) & \frac{1}{2} \left(\frac{\partial u_x}{\partial z} + \frac{\partial u_z}{\partial x} \right) \\ \frac{1}{2} \left(\frac{\partial u_y}{\partial x} + \frac{\partial u_x}{\partial y} \right) & \frac{\partial u_y}{\partial y} & \frac{1}{2} \left(\frac{\partial u_y}{\partial z} + \frac{\partial u_z}{\partial y} \right) \\ \frac{1}{2} \left(\frac{\partial u_z}{\partial x} + \frac{\partial u_x}{\partial z} \right) & \frac{1}{2} \left(\frac{\partial u_z}{\partial y} + \frac{\partial u_y}{\partial z} \right) & \frac{\partial u_z}{\partial z} \end{bmatrix} \quad (5)$$

6.2.3. Hooke's law

Elasticity in solid mechanics refers to a body's capacity to withstand a force that causes distortion and to recover its original dimensions once the force has been withdrawn²⁴⁴. Hooke's law establishes that any variation of strain in a solid is proportional to the applied stress; this is true under the consideration of elastic deformation. The relationship between both conditions (i.e., stress and strain) is called **Young's modulus (E)**, the slope of the stress vs. strain curve²⁴⁹.

Thus, simplified Hooke's law in solid mechanics is defined as:

$$\sigma = E\varepsilon \quad (6)$$

that in general form is:

$$\varepsilon = \frac{1}{E} (\sigma - \nu(\text{tr}(\sigma)\mathbf{I} - \sigma)) \quad (7)$$

and, in cartesian coordinates, it is represented as a **tensors** relationship:

$$\begin{bmatrix} \sigma_x \\ \sigma_y \\ \sigma_z \\ \tau_{yz} \\ \tau_{xz} \\ \tau_{xy} \end{bmatrix} = \frac{E}{(1+\nu)(1-2\nu)} \cdot \begin{bmatrix} 1-\nu & \nu & \nu & 0 & 0 & 0 \\ \nu & 1-\nu & \nu & 0 & 0 & 0 \\ \nu & \nu & 1-\nu & 0 & 0 & 0 \\ 0 & 0 & 0 & \frac{1-2\nu}{2} & 0 & 0 \\ 0 & 0 & 0 & 0 & \frac{1-2\nu}{2} & 0 \\ 0 & 0 & 0 & 0 & 0 & \frac{1-2\nu}{2} \end{bmatrix} \begin{bmatrix} \varepsilon_x \\ \varepsilon_y \\ \varepsilon_z \\ \gamma_{yz} \\ \gamma_{xz} \\ \gamma_{xy} \end{bmatrix} \quad (8)$$

where ν is the **Poisson's ratio**, defined as the deformation of a material in the orthogonal direction of the applied stress.

6.3. Pressure waves

Ultrasound (US) are mechanical or acoustic waves that differ from audible waves in that they are generated at frequencies above the audible ones ($f > 20\text{kHz}$) within that they are generated with frequencies above the audible ones ($f > 20\text{kHz}$) to gain temporal resolution by having minimal periods (inverse of frequency)²⁵⁰. They propagate through air, fluids, and solids. For the objectives of the present work, it is relevant to expose the reader's awareness of the simple solution of a linear ultrasonic wave propagation equation.

6.3.1. Linear wave propagation equation

Let there be a solid through which a one-dimensional ultrasonic wave is propagating in the direction of the *X-axis*; as shown in **Figure 19**, we know that the particles move in the same direction of the *X-axis* propagation x .

As a consequence, the only non-zero component is $u_x \neq 0$ and $u_y = u_z = 0$. Following the previous explanations, it can be established that the only non-zero deformation is ε_x , and applying the before mentioned Hooke's law, it is easy to end in the following relation:

$$\sigma_x = \frac{E(1-\nu)}{(1+\nu)(1-2\nu)} \varepsilon_x \quad (9)$$

It is known that to maintain equilibrium; the force balance must be,

INTRODUCTION BIOMECHANICS

$$\sum F_x = 0 \tag{10}$$

and applying Newton's second law²⁵¹, it is obtained:

$$\sum F_x = m \cdot a_x \tag{11}$$

where m is the material mass, and a is its acceleration. Applying the relationships between mass and density (ρ) and acceleration with displacement field, it is obtained:

$$\sum F_x = \rho dx A \frac{d^2 x}{dt^2} \tag{12}$$

that under equilibrium, it is expressed as an equilibrium equation,

$$\frac{d\sigma_x}{dx} = \rho \frac{d^2 u_x}{dt^2} \tag{13}$$

Applying equations (2) and (9) in (13) the standard wave equation can be derived:

$$\frac{d^2 u_x}{dt^2} = \frac{E(1 - \nu)}{\rho(1 + \nu)(1 - 2\nu)} \frac{d^2 u_x}{dx^2} \tag{14}$$

From the basic theory of differential equations²⁵², this **standard wave equation** must have a solution of the form²⁵³:

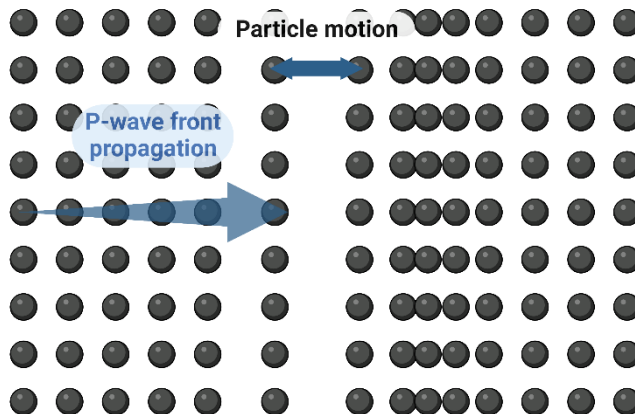


Figure 19. Representation of a linear planar mechanical wave propagation front.

$$u(x, t) = f(x - ct) \quad (15)$$

where x is the propagation space, c is its velocity, and t is the propagation time.

To probe the previous solution can be checked through its second derivative:

$$\frac{d^2 u_x}{dt^2} = c^2 f'' \quad (16)$$

Comparing equations (16) and (14); the only possible solution is obtained when the value of velocity follows the following expression:

$$c = \sqrt{\frac{E(1 - \nu)}{\rho(1 + \nu)(1 - 2\nu)}} \quad (17)$$

6.4. Basic Fluid mechanics concepts

The combined analysis of momentum, mass, and energy transfer, as well as the thermodynamics and kinetics of chemical processes, are all part of the study of transport phenomena²⁵⁴. In introductory biomechanics, the Navier-Stokes equations may be used to solve most transport phenomena problems²⁵⁵. These equations are made up of a time-dependent continuity equation for **mass conservation**, a momentum **conservation** equation, and a time-dependent **energy conservation** equation²⁵⁶:

Conservation of mass (The continuity equation)

$$\frac{\partial \rho}{\partial t} + \mathbf{v} \cdot \nabla \rho = -\rho \nabla \cdot \mathbf{v} \quad (18)$$

where \mathbf{v} is the velocity field of the system.

Conservation of momentum (Newton's second law)

$$\rho \frac{\partial \mathbf{v}}{\partial t} + \rho \mathbf{v} \cdot \nabla \mathbf{v} = -\nabla \mathbf{p} + \mu \nabla^2 \mathbf{v} + \rho \mathbf{g} \quad (19)$$

INTRODUCTION BIOMECHANICS

with p the external pressure field and g the gravity gradient.

Conservation of energy (1st law of thermodynamics)

$$\rho \frac{\partial E}{\partial t} + \mathbf{v} \cdot \nabla E = -\nabla \cdot \mathbf{q} - \nabla \cdot \rho \mathbf{v} + \nabla \cdot (\boldsymbol{\tau} \cdot \mathbf{v}) + \mathbf{F} \cdot \mathbf{v} + \dot{W} + \dot{Q}_p \quad (20)$$

where \dot{Q}_p is the net rate of heat production per unit time volume in the system, \dot{W} is the net rate of work produced in the system, q is the heat conduction field, F is the external forces, and E is the total energy transfer of the system.

The bioengineer's mechanistic knowledge of transport mechanisms is essential to characterize physiological and cellular processes, build and operate various devices, and create novel therapeutics²⁵⁷. Dialysis machines, pacemakers, biosensors, or oxygenators are examples of biomedical equipment impacted by transport processes. Also, transport processes are essential in removing toxins from the blood, creating replacement tissues (for example, bioreactors (BR) for TE), and drug administration²⁵⁸. Molecule transport involves two physical phenomena: **diffusion** and **convection**^{259,260}.

Diffusion is the stochastic movement of molecules caused by thermal energy transfer from molecular collisions²⁵⁹. This phenomenon occurs in gases, liquid solutions, membranes, and interstitial tissue spaces. Diffusing molecules travel from locations of higher concentration to regions of lower concentration (i.e., through **concentration gradients**) as a visible result of random molecular mobility. Flux is the net movement of molecules through a unit area in a given direction per unit of time.

Fick's first law describes the relationship between the diffusion flow and the concentration gradient (also known as the constitutive equation)²⁶¹. Albert Einstein stated that diffusion was: for a 2D random distribution of molecules²⁶²:

$$D_{ij} = \frac{x^2 + y^2}{4t} \quad (21)$$

Convection is a transport mechanism caused by the overall motion of fluids. Fluids flow due to forces such as gravity, pressure, or shear²⁶⁰. Some definitions must be done regarding the bulk motion of a fluid.

The fluid **viscosity** (μ) indicates a fluid's frictional resistance to flow. The frictional force required to cause motion is related to the fluid viscosity. The viscosity of a pure fluid is a thermodynamic function of temperature and pressure²⁵⁶.

Density (ρ) is a material parameter describing how dense molecules are packed together. The density of a system is defined as the ratio of its mass to its volume. The density of a mixture varies with temperature, pressure, and composition²⁵⁶.

Kinematic viscosity is the term for the density-to-viscosity ratio and is represented by the symbol²⁵⁶:

$$\nu = \frac{\mu}{\rho} \quad (22)$$

For simple fluids, the viscosity is a proportional coefficient between the shear stress and the velocity gradient (Newton's law of viscosity):

$$\tau_{yx} = \mu \dot{\gamma}_x = \mu \frac{dv_x}{dy} \quad (23)$$

When a force applied to a moving fluid is withdrawn, it sometimes elapses before the fluid motion stops. The change in velocity over time is caused by a balance of viscous and inertial forces. Viscous forces slow fluid velocity, but inertial forces keep the fluid moving. Because viscous forces are affected by viscosity and inertia is affected by mass or density, the relative contributions of these forces vary amongst fluids. The **Reynolds number (Re)** is a dimensionless set of parameters that describes the ratio between inertial forces and viscous forces²⁶³:

$$Re = \frac{\text{inertial forces/volume}}{\text{viscous forces/volume}} = \frac{\rho v^2/L}{\mu v/L^2} = \frac{\rho L v}{\mu} \quad (24)$$

here, L is the characteristic length, and v is the characteristic velocity for the flow.

A high Re indicates viscous forces are far less critical than inertial forces, such as a guy sprinting against the wind. On the other hand, a small Reynolds numbers indicates highly viscous media on which many viscous forces depend, such as cell migration across the interstitial fluid²⁵⁶.

Therefore, regarding Re , flows can be classified as **laminar** or **turbulent**²⁵⁶. The velocity at any given site does not change with time in continuous laminar flow. When the flow is turbulent, however, the velocity swings arbitrarily due to the production and dissipation of high-energy eddies²⁵⁶. Although turbulent flow analysis is more sophisticated than laminar flow analysis, most fluids in human physiology are laminar²⁵⁸.

In biological systems, these two processes, diffusion and convection control the flow of energy and momentum.

6.5. Perfusion flow

In physiology, perfusion is defined as fluid distribution to an organ or tissue through the circulatory or lymphatic systems²⁶⁴. All living tissues require adequate nutrient and oxygen support, and inadequate perfusion (**ischemia**) leads to cell death²⁶⁵.

Observing TE grafts and naïve human tissues, it is widespread to find materials that present embedded porous media; these pores may be empty or filled with fluid and vary widely depending on biomaterial and synthesis techniques²⁶⁶. Micro- or nanofabricated materials may have a structure with a regular array of cylindrical pores²⁶⁷. On the other hand, sponges comprise a continuous solid phase with interconnecting channels or isolated pores²⁶⁷. A

granular structure, such as a sand pile, comprises solid particles and the vacuum space between them. The basic structure of polymeric gels is fiber matrices²⁶⁷.

The interstitial pores are either isolated or linked to create hydrophilic channels, essential for transporting nutrients, metabolites, growth factors, inhibitors, modulators, and other signaling molecules in tissues. The motion of fluid molecules in porous media follows tortuous pathways, being **tortuosity** ($T = (L_{min}/L)^2$) its analytical parameter²⁶⁸.

Porosity is often characterized by the **specific surface** (aka the surface-volume ratio) and **porosity ratio**, which are defined as²⁶⁶:

$$s = \frac{\text{Total interface area}}{\text{Total volume}} \quad (25)$$

and

$$\varepsilon = \frac{\text{Void volume}}{\text{Total volume}} \quad (26)$$

Although porosity is a precise figure representing the bulk size of holes inside a material, it does not indicate how the pores are distributed or if they are effective for fluid transmission **Figure 20**.

William Henry Darcy developed Darcy's law, the idea of fluid flow in porous media, in 1856²⁶⁹. According to the law, the fluid flow rate in a porous media is proportional to the pressure gradient.

$$v = -K\nabla p \quad (27)$$

where ∇p is the gradient of hydrostatic pressure K is a constant defined as **hydraulic conductivity**.

In the case of incompressible and Newtonian fluids, and considering static fluid pressure, the hydraulic conductivity has the form of:

$$K = \frac{k\rho g}{\mu} \quad (28)$$

where k is the medium's permeability and μ the kinematic viscosity of the fluid.



Figure 20. Scheme of different pore shapes. Porous materials present different kind of behaviour for fluid mechanics depending if they are: closed, dead-ended or opened at both sides. This effect cannot be measured by porosity ratio.

Two approaches may be employed to characterize fluid flow in porous materials²⁷⁰. If the structures or pore networks are known, one method is to numerically solve the governing equations for fluid flow in individual pores. Another assumption is that a porous medium is a homogeneous substance. Darcy proposes three length scales in his so-called **continuum approach**²⁷¹. The first one is the average **pore size** (δ). The second is the distance (L) that must be addressed when considering macroscopic changes in physical variables. The continuum technique needs L to be at least two orders of magnitude bigger than δ such that a third length scale, l , can exist between δ and L ²⁷¹.

Thereby, perfusion flows through scaffolds are porous media transport problems with complex solutions. Despite clarifying some considerations used in Part 3 of this project, the solution of a laminar flow development through a pipe will be helpful.

6.5.1. Laminar flow through a cylindrical pipe

Once all the previous considerations are known, the volumetric flow is calculated by applying the conservation laws of mass and momentum:

$$\frac{\partial \rho}{\partial t} = \left(\frac{1}{r} \frac{\partial(\rho r v_r)}{\partial r} + \frac{1}{r} \frac{\partial(\rho v_\theta)}{\partial \theta} + \frac{1}{r} \frac{\partial(\rho v_z)}{\partial z} \right) \quad (29)$$

The constraints imposed by the problem design on the mass conservation law are as follows: because the medium is Newtonian, the volume density remains constant throughout time. At a steady state, the flow is constant and solely relies on the z direction (parallel to the cylinder axis). Finally, gravity was deemed insignificant to simplify the calculations because of the significant difference in the order of magnitude between the flow profile caused by gravitational forces and the one produced by the peristaltic pump. After applying the discussed constraints, the final solution for equation (29) is as follows:

$$\frac{\partial v_z}{\partial z} = 0 \quad (30)$$

The momentum conservation law is applied with the same constraints as in equation (29).

$$\rho \frac{\partial \vec{v}}{\partial t} + \rho \vec{v} \cdot \nabla \vec{v} = -\nabla \vec{p} + \mu \nabla^2 \vec{v} + \rho \vec{g} \quad (31)$$

which are written in cylindrical coordinates (note that the equations already represent a Newtonian fluid):

$$\begin{aligned} \rho \left(\frac{\partial v_r}{\partial t} + v_r \frac{\partial v_r}{\partial r} + \frac{v_\theta}{r} \frac{\partial v_r}{\partial \theta} - \frac{v_\theta^2}{r} + v_z \frac{\partial v_r}{\partial z} \right) \\ = -\frac{\partial P}{\partial r} + \mu \left(\frac{\partial}{\partial r} \left(\frac{1}{r} \frac{\partial(r v_r)}{\partial r} \right) + \frac{1}{r^2} \frac{\partial^2 v_r}{\partial \theta^2} - \frac{2}{r^2} \frac{\partial v_\theta}{\partial \theta} + \frac{\partial^2 v_r}{\partial z^2} \right) + \rho g_r \end{aligned} \quad (32)$$

$$\begin{aligned} \rho \left(\frac{\partial v_\theta}{\partial t} + v_r \frac{\partial v_\theta}{\partial r} + \frac{v_\theta}{r} \frac{\partial v_\theta}{\partial \theta} + \frac{v_r v_\theta}{r} + v_z \frac{\partial v_\theta}{\partial z} \right) \\ = -\frac{1}{r} \frac{\partial P}{\partial \theta} + \mu \left(\frac{\partial}{\partial r} \left(\frac{1}{r} \frac{\partial(r v_\theta)}{\partial r} \right) + \frac{1}{r^2} \frac{\partial^2 v_\theta}{\partial \theta^2} + \frac{2}{r^2} \frac{\partial v_r}{\partial \theta} + \frac{\partial^2 v_\theta}{\partial z^2} \right) \\ + \rho g_\theta \end{aligned} \quad (33)$$

INTRODUCTION BIOMECHANICS

$$\begin{aligned} \rho \left(\frac{\partial v_z}{\partial t} + v_r \frac{\partial v_z}{\partial r} + \frac{v_\theta}{r} \frac{\partial v_z}{\partial \theta} + v_z \frac{\partial v_z}{\partial z} \right) \\ = - \frac{\partial P}{\partial z} + \mu \left(\frac{1}{r} \frac{\partial}{\partial r} \left(r \frac{\partial v_z}{\partial r} \right) + \frac{1}{r^2} \frac{\partial^2 v_z}{\partial \theta^2} + \frac{\partial^2 v_z}{\partial z^2} \right) + \rho g_z \end{aligned} \quad (34)$$

Because v_r solely depends on r , all derivatives of v_r that relies on z , t , or zero in equation (32). Again, gravitational forces are insignificant. In most cases, pipes boundaries ensure that there is a "no-slip" condition, which means that v_r is 0 at the walls of the cylindrical channel; and there is only one entrance and one output, resulting in v_z equal to a constant along the Z direction (steady flow) and v_θ and v_r equal to 0.

Applying previous concepts, equation (33) and equation (34) result into:

$$- \frac{\partial P}{\partial r} = - \frac{\partial P}{\partial \theta} = 0 \quad (35)$$

Thus, it is clear from equation (35) that the pressure field is independent of r or θ . This finding is consistent with the notion of considering the flow as bi-dimensional.

Finally, after applying the boundary conditions, equation 6 may be reduced as follows:

$$\frac{\mu}{r} \frac{d}{dr} \left(r \frac{dv_z}{dr} \right) = \frac{dP}{dz} \quad (36)$$

It is worth nothing that equation (36) has two distinct but equal derivatives. The only way to solve this equation is if the pressure gradient along the Z direction is constant and the shear stress along the r direction is **constant**.

$$C_1 = \frac{dP}{dz} \quad (37)$$

There are two locations in the center of the canal where the pressure may be felt. The pressure will be P_L at the exit ($z = L$) instead of P_0 at the entry ($z = Z_0$). Therefore, $\Delta P = P_L - P_0$. This type of function, pressure, must exist:

$$P = C_1 r + C_2 \quad (38)$$

that can be solved as:

$$P = P_0 - \frac{\Delta P}{L} (z_0 - z) \quad (39)$$

In this instance, the pressure at the input will be highly identical to the pressure at the output, making $\Delta P \cong 0$, and this is because no external forces are acting on the flow (the BR is in a steady state). The Z component of the velocity may now be derived by integrating equation (36) twice and then putting equation (39) into that one.

The first integral is:

$$\left(r \frac{dv_z}{dr} \right) = -\frac{\Delta P r^2}{2\mu L} + C_3 \quad (40)$$

and the second integral:

$$v_z = -\frac{\Delta P r^2}{4\mu L} + C_4 \quad (41)$$

At $r = R$ (the walls), the velocity is 0 because of the no-slip condition, thus:

$$C_4 = \frac{\Delta P r^2}{4\mu L} \quad (42)$$

Finally, the z component of the velocity is:

$$v_z = \frac{\Delta P r^2}{4\mu L} \left(1 - \frac{r^2}{R^2} \right) \quad (43)$$

The *volumetric flow*, Q (**Figure 21**), can be extracted from the *average velocity*, which is $\bar{v} = \frac{1}{2} v_{max}$ being v_{max} the maximum velocity that the flow can reach. That is produced in the middle of the channel ($r = 0$).

INTRODUCTION BIOMECHANICS

$$Q = v_{max}\pi R^2 = \frac{\Delta P\pi R^4}{8\mu L} \quad (44)$$

Additionally, a fully developed channel flow has a shear *stress profile* of:

$$\tau_{rz} = \frac{1}{2}D\left(\frac{\Delta P}{L}\right) \quad (45)$$

Now that all equations have been solved, it is crucial to highlight two principles that allow the theoretical profile to depict the actual process accurately. Pousille's law, typical of a Hagen-Pouseuille flow, is represented by equation (44). But, for it to be true, the channel's entry length, or the minimum length required to create laminar flow in a Newtonian fluid, must be:

$$L_e = 0.058DRe \quad (46)$$

where the channel diameter is D , and Re is the before-mentioned Reynolds number.

In laminar flows, the Re must be less than 2,100. The Re for this situation is given by the following formula, which is dependent on the gradient of pressures:

$$Re = \frac{\rho L}{\mu} \cdot \frac{1}{2} \frac{r^2}{4\mu L} \Delta P \quad (47)$$

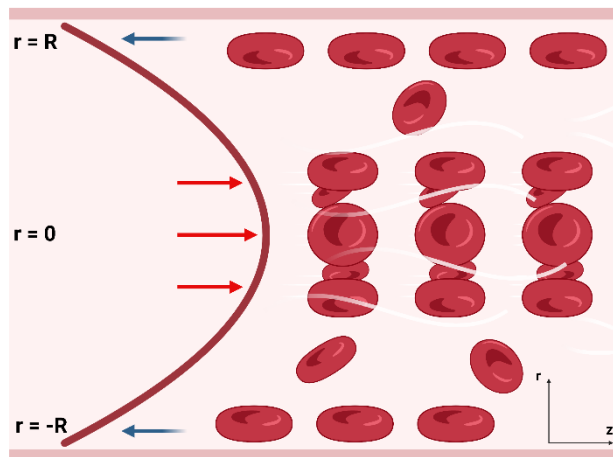


Figure 21. Representation of an ideal Hagen-Poiseuille flow through a capillary.

6.6. Mechanotransduction

It is clear the extraordinary complexities of biofabrication processes, combined with the exceptional organization of AC tissue, where any change in its homeostasis results in a complicated chain of biochemical reactions that leads to OA. Then, why is it necessary to describe all of the physics involved? To put it another way, what is the connection between constitutive mechanical laws and cell physiology? The response could be that mechanical variables might influence changes in tissue homeostasis. But is it essential to explain how such mechanical interactions work? Finally, the aspects that alter the most in diseases are gene expression and protein synthesis. Although it may appear unimportant, how forces affect biochemical activities is essential. It is becoming increasingly clear that epigenetic variables, primarily mechanical and structural signals that affect cell activity, play a critical role in embryogenesis, tissue physiology, and various diseases²⁷². These reasons have sparked increased interest in mechanoregulation in fields ranging from molecular biophysics and cell biology to human physiology and clinical medicine²⁷³⁻²⁷⁵.

At the current time of this work, it is known that a broad group of cells is regulated mechanically; among them are fibroblasts²⁷⁶, keratinocytes²⁷⁷, chondrocytes^{278,279}, osteocytes²⁸⁰, and even stem cells^{281,282}. A growing body of data suggests that the **primary cilium** of most cell types is mechanosensitive and responsive, leading some researchers to conclude that it is a form of universal cellular mechanosensory^{283,284}. However, well-established methods of cellular sensing and reactivity to mechanical stresses include cell-cell, cell-matrix, and cell-lumen interactions²⁸⁵. The process of how cells translate mechanical stimuli into biochemical, cellular responses is called **mechanotransduction**²⁷².

6.6.1. Mechanoreceptors

Mechanoreceptors are somatosensory receptors that transmit external stimuli to intracellular signal transduction *via* mechanically gated ion

INTRODUCTION BIOMECHANICS

channels²⁸⁶. Touch, compression, straining, and mechanical waves are typical external stimuli²⁸⁷. In the cell membrane of animal cells, it can be found next mechanoreceptors (**Figure 22**)²⁸⁸:

- **Stretched-activated ion channels** form gaps in the cell membrane large enough to allow calcium and other cations to flow through. Mechanically generated membrane tension can open the channels depending on the concentration differential across the cell membrane, allowing an inflow or outflow of ions. Ionic balance is essential for many cellular activities and adds to the cell membrane's closely controlled electric potential. Calcium concentrations inside cells regulate intracellular signaling, actin polymerization, cytoskeletal remodeling, and cell motility^{289,290}.
- Growth factor receptors (**GFRs**) bind to external growth factors, activating numerous receptor-mediated second messenger pathways within the cell. GFRs have been discovered to interact with other mechano-sensing receptors in the cell membrane, resulting in additive or complementary signaling effects^{281,291}.
- **Integrins** are transmembrane receptors with two subunits (α and β) that perform different regulatory and signaling activities. They are crucial in force transmission across the cell membrane and cellular perception of matrix stiffness. Integrin activation for ECM binding and signaling can take several forms, including allosteric interactions, clustering to create signaling complexes, and cytoskeletal tensioning via integrin-mediated attachments (e.g., focal adhesions)²⁹². They regulate cell adhesion, proliferation, migration, stem cell differentiation, intracellular signal transduction, and matrix turnover²⁹³⁻²⁹⁷.
- G-protein-coupled receptors (**GPCRs**) are large proteins with seven transmembrane domains. Many effector proteins and chemicals attach to the extracellular region, causing a conformational change in the protein's structure. Once activated, the cytosolic part interacts with intracellular GPCRs to impact the signaling cascade based on the signal's specificity.

Mechanical stresses across the cell surface can activate these receptors, triggering secondary messenger cascades within the cell^{288,297}.

6.6.2. **Tensegrity**

Although evidence establishes forces altering specific molecule routes, these results do not explain how cells can react to far mechanical stimuli in a few seconds. In nature, cells are not isolated systems but they are connected to their ECM and other cells, forming a dense, complex, and hierarchical network. These networks present a preset stress level stabilizing the entire structure, called **tensegrity**²⁹⁸ (Figure 23). The term tensegrity combines the words 'tension' and 'integrity,' and Buckminster Fuller used it for the first time²⁹⁹. At the macroscale, tensegrity may be observed in how pulling forces produced by muscles and resisted by bones maintain the form of our entire bodies³⁰⁰.

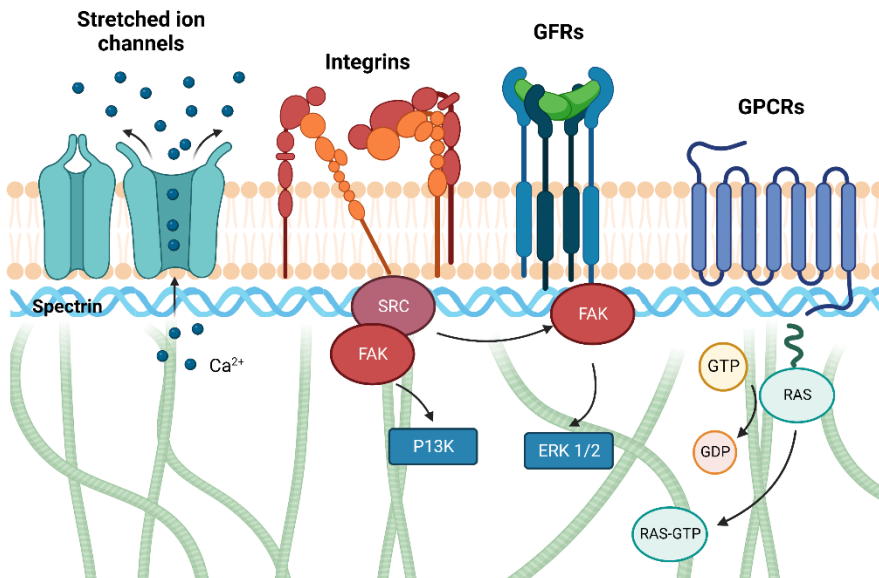


Figure 22. The most common mechanoreceptors and their relationship to gene expression via various signalling pathways are depicted schematically.

As previously stated, the cytoskeleton plays a critical role in the mechanotransduction process.

INTRODUCTION BIOMECHANICS

This tensegrity state is also maintained throughout the cytoskeleton thanks to microtubule architecture, permitting cells to transfer compressive pressures upside/down between microtubules and ECM adhesions³⁰¹. Therefore, in rounded cells with few anchoring sites, microtubules bear most of the prestress, whereas the ECM carries most of the load in spread cells on highly sticky substrates³⁰². The cortical cytoskeleton, which supports the plasma membrane, also forms another tensegrity network by incorporating multiple rigid actin protofilaments held in place by a geodesic (triangulated) array of spectrin molecules that act like tensed cables suspended from the overlying lipid bilayer³⁰³.

The presence of these **tensegrity networks**, as well as their ability to channel mechanical forces across discrete molecular paths to sites deep within the cytoplasm and nucleus, explains how cell distortion or mechanical stress

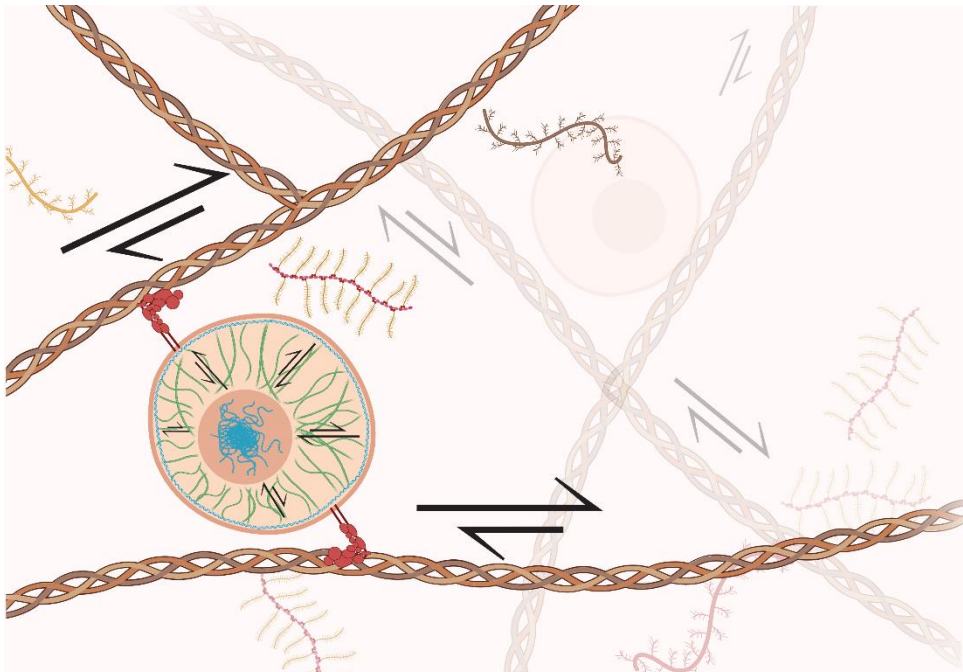


Figure 23. Tensegrity implies a level of prestressing of a whole fiber network connected from the ECM to the cell nucleus. Thanks to this phenomenon, all cells in the same ECM niche are connected and intercommunicated for external stimuli.

application to ECM and bound cell surface integrins results in changes in nuclear shape and induces molecular organization within nucleoli on progressively smaller size scales³⁰⁴. This coupling between integrins and the nucleus is mediated primarily by intermediate filaments that extend from cell surface adhesion sites to the nucleus and, to a lesser extent, by the actin cytoskeleton³⁰⁵, with cytoskeletal prestress governing the efficiency of this multiscale mechanical response³⁰⁶.

The discovery that polycystic kidney disease develops due to mutation or deletion of the polycystin genes, which produce mechanosensitive ion channels that mediate urine flow sensors in kidney epithelium, highlights the significance of mechanical forces for organ regeneration development³⁰⁷.

6.7. Finite Element Analysis

Analytical solutions to stress analysis problems in biomechanics were generally limited to objects with a basic shape and exposed to simple loading circumstances, as was exposed above. Because biological systems are geometrically irregular and have intricate distributions of material mechanical characteristics, classical mechanics analytical solutions were rarely viable or valuable for biomechanical study. These new approximation procedures are required to solve biomechanical problems like finite element analysis (**FEA**), which is undoubtedly the most well-known. Instead of conventional mechanical analytical solutions, a set of simultaneous equations for an array of discrete simplified subdomains in FEA is numerically solved (**elements**). Specific interpolation functions (typically polynomials) are assumed within these individual elements, from which internal variables (e.g., strains) are piecewise estimated and evaluated in a discrete number of points (**nodes**)³⁰⁸.

The early 1940s work of Courant provided the mathematical foundation for this conceptual approach, which saw its initial implementations in physics³⁰⁹ and engineering³¹⁰ in the mid-1950s. R.W. Clough (1960) is widely credited with

INTRODUCTION BIOMECHANICS

coining the term "finite element analysis," which he introduced in a mechanical engineering conference presentation³¹¹. The FEA technique proved suitable for fluid mechanics, electromagnetic field analysis, and other continuum field issues after initially applying it to static structural problems³⁰⁸.

6.7.1. Finite element models in biomechanics

The earliest applications of FEA to biomechanics were isotropic linearly elastic structural studies of bone, undertaken independently by groups in the United States³¹² and the Netherlands³¹³. This new skill's importance to biomechanics science was instantly apparent: for the first time, mechanical stresses could be calculated in bodies with intricate forms, complex material compositions, and nonsymmetrical loadings. Material anisotropy and geometrical nonlinearity, contact and interface nonlinearity, time-variant loadings, adaptive behavior (material and geometrical), and fluid/structure interactions can be studied thanks to FEA^{314,315}.

Nowadays, computational modeling of the biomechanics using FEA, or finite element models (**FEM**), of living systems and their surroundings offers the potential to accelerate medical and biological progress. Imaging advancements have paved the road for patient-specific modeling³¹⁶⁻³²¹, which might transform how doctors identify and treat some illnesses. The usage of highly discretized geometry has been possible because of ongoing developments in high-speed computer technology^{322,323}.

FEM investigations are typically divided into five phases (**Figure 24**): i) The first stage involves the creation of specialized code, if applicable to the topic, and model **design** which implies the selection of the physics (e.g., electromagnetism, solid mechanics, etc.) and domains (e.g., time or frequency). In some studies, the design can be obtained from medical images. ii) The second phase (**preprocessing**) entails establishing the mesh shape, defining the material property distributions, and determining the loading. iii) Third, the finite element solution is computed; this is the **calculation** step. iv) Fourth, it proceeds

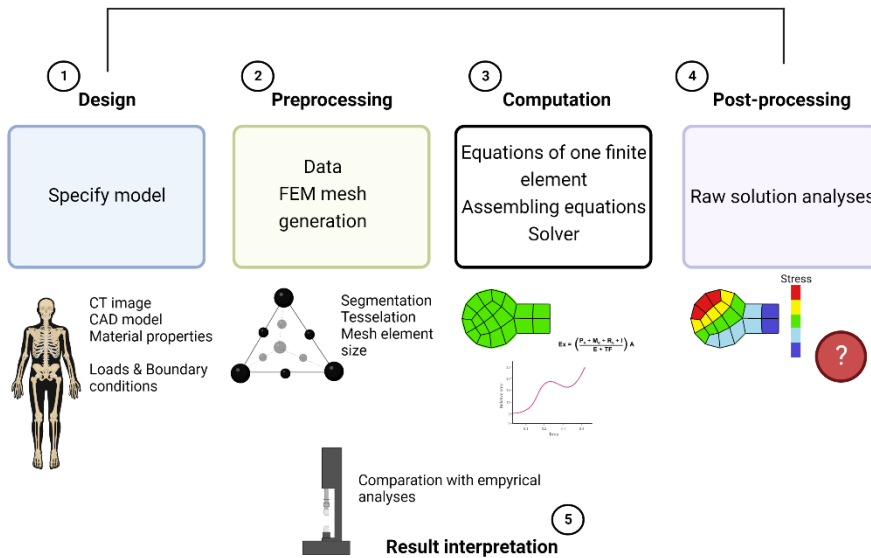


Figure 24. Flow diagram of the developing steps for a FEM.

to a stage known as **postprocessing**, in which the raw output of the FE solution is utilized to compute variables of interest, and chosen information is visually presented. v) The final stage is **result interpretation**, which relies on analyst opinion.

Mesh

To form a mesh for FEMs is based on the mathematical discretization procedure, thus, an infinite-linear problem³²⁴:

$$\begin{aligned}
 & \text{Find } \mathbf{u} \in \mathbf{H}_0^l \text{ such that} \\
 & \forall \mathbf{v} \in \mathbf{H}_0^l - \phi(\mathbf{u}, \mathbf{v}) = \int \mathbf{f} \mathbf{v}
 \end{aligned}
 \tag{48}$$

is simplified into a finite-dimensional version

$$\begin{aligned}
 & \text{Find } \mathbf{u} \in \mathbf{V} \text{ such that} \\
 & \forall \mathbf{v} \in \mathbf{V} - \phi(\mathbf{u}, \mathbf{v}) = \sum \mathbf{f} \Delta \mathbf{v}
 \end{aligned}
 \tag{49}$$

where \mathbf{V} is a finite-dimensional subspace of \mathbf{H}_0^l .

Geometrically, mesh generation divides a continuous geometric space into discrete geometric and topological cells to create a mesh. Mesh cells represent discrete local approximations of a broader region; these are generated through computer algorithms, typically with human assistance via a graphical user interface (GUI). Many meshing approaches are based on the Delaunay triangulation principles³²⁵ and rules for adding vertices, such as Ruppert's algorithm³²⁶. Developing front algorithms begins at the domain perimeter and slowly adds components to fill the inside. The domain is partitioned into large subregions, each a structured mesh in block-structured meshing³²⁷. Applied algebraic algorithms are primarily based on the linear interpolation function:

$$y = y_a + (y_b - y_a) \frac{x - x_a}{x_b - x_a} \text{ at the point } (x, y)$$

$$\frac{y - y_a}{y_b - y_a} = \frac{x - x_a}{x_b - x_a} \quad (50)$$

$$\frac{y - y_a}{x - x_a} = \frac{y_b - y_a}{x_b - x_a}$$

Previous relationships established an equality between slopes of lines $[(x_a, y_a), (x, y)]$ and $[(x_a, y_a), (x_b, y_b)]$. The reader can observe the simplicity and swiftness of linear interpolation, but the error equation (51) has to be managed for adequate accuracy.

$$|f(x) - g(x)| \leq C(x_b - x_a) \text{ where } C = \frac{1}{8} \max_{r \in [x_a, x_b]} |g''(r)| \quad (51)$$

Validation

Because FEM is an approximation approach, it is critical to verify the findings' reliability; to do so, a good technique for determining if a mesh has mathematically converged is whether the solution will not change significantly with further mesh refining^{328,329}. P-convergence³³⁰ testing is rarely used in biomechanical models since it entails progressively higher-order components³³¹. Alternatively, a simplification of the h-convergence test³³², employing multiple different meshes with gradually more excellent resolution but without the consistently systematic subdivisions practicable for simple geometric forms, is commonly performed³³³.

Another model validation is to compare FEA findings with direct consequences; the solution is proven to be acceptable and well-behaved in the sense of being internally consistent and providing a general consistency with current literature. These validation strategies strive to increase the amount of model confidence provided³³⁴.

These models have provided TE with a valuable tool for predicting the ultimate physical characteristics of bioinks and scaffolds before production^{335,336} or even how cells could behave under a particular stress regime³³⁷. Examples include cardiac TE, where the porosities of the scaffolds may be carefully tuned to get the required contraction that heart tissue manages³³⁸. Moreover, RM also benefits from these methods since it may adapt different implants to specific illnesses due to the capacity to reproduce abnormal environments³³⁹.

7. Biofabrication

7.1. Background

The term **biofabrication** was first used in 1994 to describe the biomineralization of pearls³⁴⁰ and, later, for the enamel deposition in mammalian teeth³⁴¹. But, perhaps, the first biofabrication process can be traced back to 1906, when Ross Harrison developed tissue explants *via in vitro* cell culturing³⁴². And it had to go through 60 years to find new advances in this technical procedure; an example was the obtention for 3D tissues *in vitro* thanks to the **self-assembly** process³⁴³. Briefly after, Gabor Forgacs' experimental observations of tissue surface tension³⁴⁴ developed the idea of tissue fluidity and Steinberg's differential adhesion theory, and both concepts are critical biological foundations of biofabrication technology^{345,346}. Later, biofabrication was described as '*the use of biological materials and systems for construction*' by the US Defense Advanced Research Projects Agency in 2003³⁴⁷. Recently, **rapid prototyping** for biomedical applications³⁴⁸ (**computer-aided design (CAD)**³⁴⁹, **layer-by-layer** additive manufacturing³⁵⁰) is an actual example of how mechanical engineering contributes to the burgeoning subject of biofabrication^{351,352}. Changing raw materials from non-living to living organisms or tissues does not affect mechanical engineering's core function in creating fabrication processes and manufacturing technologies. Some thoughts must be considered when moving from one to the other³⁵³; these will be discussed in the following chapter.

It is commonly accepted that biofabrication implies fabricating organic/inorganic materials by living organisms^{354,355}. Biofabrication has many distinguishing features: first, the building blocks are cells or biologics; second, the fabrication techniques are bio-inspired or bio-friendly; and third, the results are biological systems, models, or devices with transformational qualities³⁵⁶.

7.2. Definition

To limit the definition of biofabrication, this term is applied only for TE purposes (see **Figure 25**). The natural concept of biofabrication that persecutes just the construction of viable constructs to fulfill biological functions is not sufficiently accurate for this thesis's purposes. Nevertheless, the development of the biofabrication term was deeply discussed and analyzed by Jürgen Groll and colleagues³⁵⁷. In there, they proposed the following definition:

'The automated generation of biologically functional products with structural organization from living cells, bioactive molecules, biomaterials, cell aggregates such as micro-tissues, or hybrid cell-material constructs, through bioprinting or bioassembly and subsequent tissue maturation processes.'

As an **additive manufacturing** process, bioprinting (also known as 3D bioprinting) directly derives from 3D printing technology; nevertheless, bioprinting is achieved when living single cells, bioactive substances, biomaterials, or cell-aggregates tiny enough to be printed are used for production³⁵⁸. Nowadays is considered the first centrally used methodology in the biofabrication field. Bioassembly, as a second primary strategy of biofabrication, can be defined as³⁵⁹:

'The fabrication of hierarchical constructs with a pre-scribed 2D or 3D organization through automated assembly of preformed cell-containing fabrication units generated via cell-driven self-organization or through preparation of hybrid cell-material building blocks, typically by applying enabling technologies, including micro-fabricated molds or microfluidics'

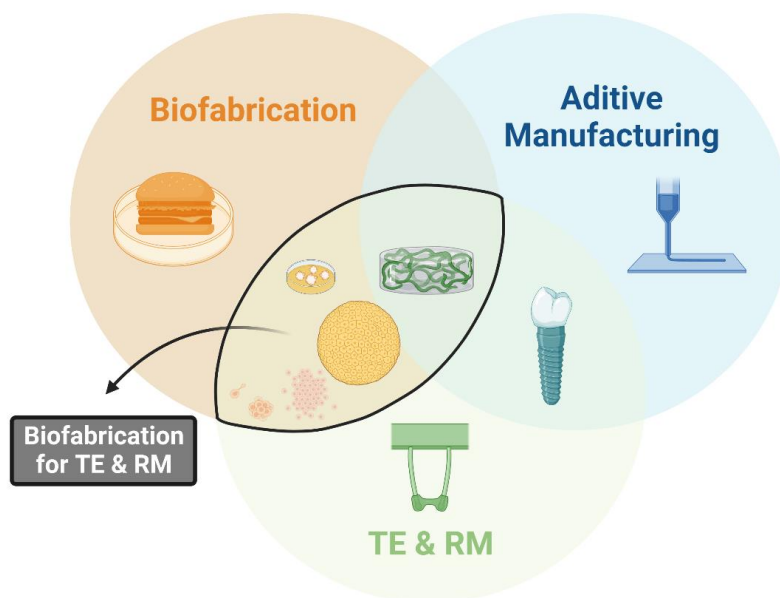


Figure 25. Scheme explaining how the different scientific technologies interact between them.

Aside from their working procedures, the fundamental difference between both technologies is their minimum fabrication unit. In contrast, in bioprinting, this unit can be reduced to the molecular level; it is significantly higher in bioassembly because it must be large enough to achieve automated assembly technologically³⁵⁷.

In summary, biofabrication is a multidisciplinary procedure that uses various technologies for its implementation. Among these technologies are i) light-based technologies such as **selective laser sintering** (SLS), selective laser ablation, **stereolithography** (SLA), and **two-photon polymerization** (2PP); ii) **wet-spun** (WS) automated extrusion systems; iii) **electrospinning**; iv) **3D printing**, and v) **3D and 4D bioprinting**³⁶⁰.

7.3. Biofabrication technologies

7.3.1. Light-based technologies

Carl Deckard patented SLS technology in Texas in 1988; he developed a technology that used a laser to fuse powders rather than liquids³⁶¹. In particular,

SLS employs a laser to selectively focus a light beam onto a powder bed (**Figure 26**), resulting in local heat and fused material patterns. Following solidification, a fresh layer of powder is set down, and the process is repeated over and over to create a scaffold layer by layer³⁶². Among functional biomaterials, thermoplastic metals, polymers, ceramics, and mixtures are mainly used³⁶³⁻³⁶⁵. As a biofabrication technique, SLS has been broadly used in cartilage and bone TE^{366,367}. Thanks to this methodology, it can be developed mixture scaffolds combining polymers with tissue inducer molecules such as hydroxyapatite³⁶⁸.

Even though the process resembles thermal sintering through laser incidence, adding any pharmacological compound to a cell in the scaffold synthesis process is impossible, which is necessary to do the cell-integration process after the scaffold synthesis³⁶⁹⁻³⁷¹. To solve this inconvenience, **surface selective laser sintering (SSLS)**, which employs an infrared laser to sinter powder substrates, has been developed³⁷². Under this situation, radiation is absorbed by carbon microparticles dispersed on the surface of the polymer particles rather than by the polymer particles themselves. Additionally,

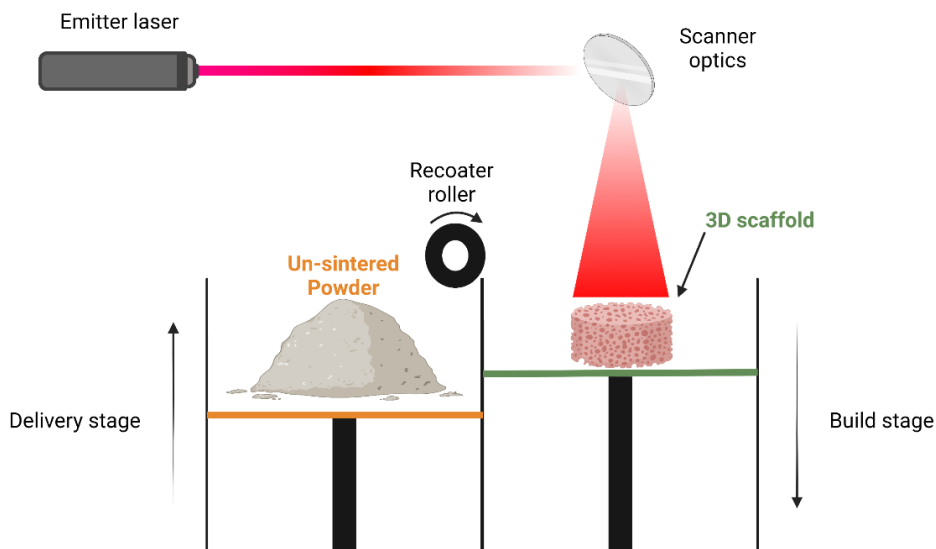


Figure 26. Scheme for SLS fabrication technique.

INTRODUCTION BIOFABRICATION

compared to other methods, such as SLA and FFF, the downside of SLS is that the detail is not as refined and precise³⁷³.

On the other hand, SLA is based on photopolymerization (**Figure 27**), which is used to harden a photosensitive resin. Habitually, it was used for harmful molds filled with ceramic or metallic slurries after³⁷⁴ or for curing dental fillings, among other applications^{375,376}. Charles Hull developed it in the 1980s as the first method for manufacturing 3D constructions using UV light to polymerize materials³⁷⁷. Like many other technologies, SLA is being developed in parallel with its corresponding biomaterials, and many times, one innovation in one field affects the other, as is the case of photosensitive resins used for **digital light processing (DLPTM)**^{378,379}. In addition, recent advances in photocrosslinker molecules and hydrogel synthesis have allowed the incorporation of cells inside the applied material, allowing the use of SLA for 3D bioprinting³⁸⁰. Another relevant advancement in SLA technology was the incorporation of 2PP, which considerably increases both spatial resolution and Z-depth incidence light, resulting in a lower biofabrication time^{381,382}.

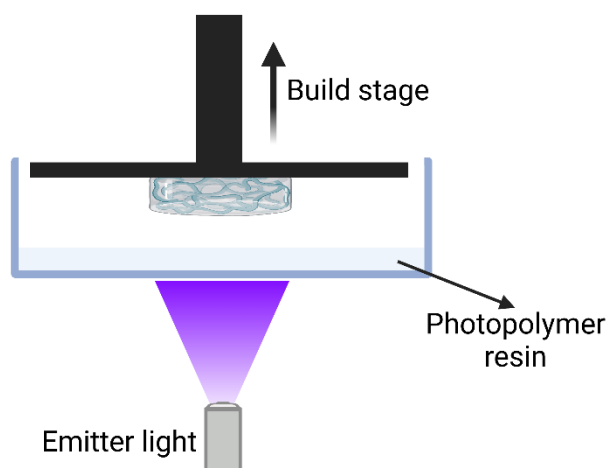


Figure 27. Scheme for SLA fabrication technique.

7.3.2. Wet-spun (aka wet-spinning)

WS of acrylic acid fibers dates from the mid-1850s by Chardonnet, when he synthesized cellulose nitrate fibers from a mixture of raw cotton and sulfuric/nitric acid solution³⁸³. Regarding biofabrication, WS was first developed as a method for creating fibers from polymers produced from natural sources, such as chitosan and collagen, which are vulnerable to heat deterioration when treated by traditional fibers spinning processes³⁸⁴. The ability to readily include various treatments (e.g., antibiotics and chemotherapeutics) using drug incorporation methods thoroughly tested in nano/microparticle technology enlarged the range of polymers for WS³⁸⁵. Examples of those biodegradable polymers included such as chitin³⁸⁶, PLLA^{387,388}, polyacrylonitrile³⁸⁹, poly(L,D-lactic acid)³⁹⁰, and, poly[lactic-co-(glycolic acid)] (PLGA)³⁹¹. Assembling WS polymeric fibers into biodegradable scaffolds with a 3D network of macropores suited for TE applications has also been studied using a variety of methods³⁹².

It is based on the extrusion of a polymeric solution through a syringe pump and nozzle straight into a coagulation bath (**Figure 28**), a non-solvent-induced phase inversion technique³⁹³. Before the filament enters the coagulating

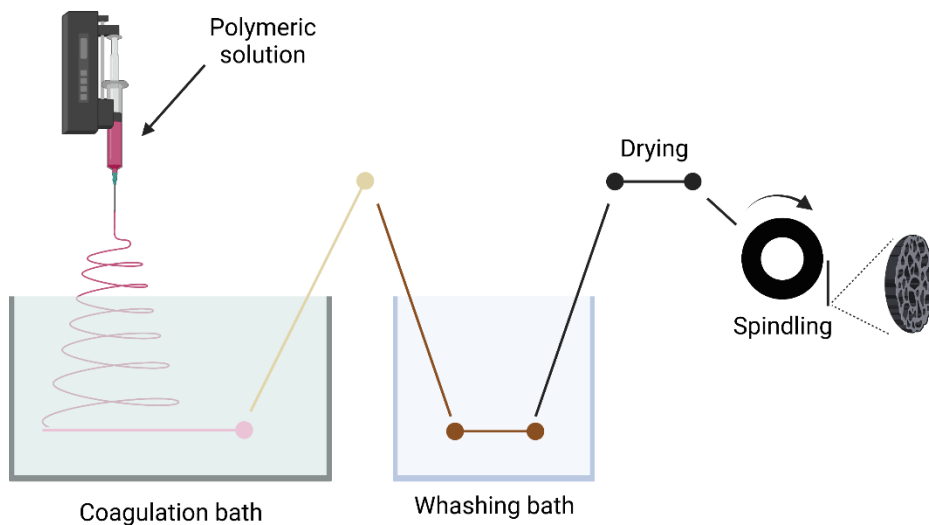


Figure 28. Scheme of WS synthesis process.

solution, the extrusion may be carried out through a tiny air gap, known as dry-jet or air-gap WS³⁹⁴. WS's key point is that it does not experience heat deterioration as fused deposition modeling (FDM) does, and, additionally, it presents higher resolution translated in lower fiber diameter^{395,396}.

7.3.3. **Electrowiring**

The history of electrowiring (aka. electrospinning) can be traced back to several centuries ago when William Gilbert's initial observations of a liquid being attracted electrostatically in 1600. It was not until the nineteenth century that Christian Friedrich Schönbein created highly nitrated cellulose. The first patent for electrospinning was submitted in 1900 by John Francis Cooley³⁹⁷, and since then, it has been applied several times in TE and RM³⁹⁸⁻⁴⁰¹.

Electrospinning uses electricity to create fibers with a nano- or micrometer-sized diameter⁴⁰². A high voltage (**Figure 29**) is used during the electrospinning process to the syringe to produce an electrically charged jet of polymer micro- or nanofibers once the embedded viscoelastic solution is released^{403,404}. When the droplet is linked to the high-voltage power source, charges of the same sign will soon blanket its surface. The spherical drop form is unstable due to the attraction between these charges. Consequently, droplets deform into a conical shape (known as a Taylor cone) to overcome the surface tension, and a jet will emerge from the cone's tip. Charges on the fibers' surface provide repulsive forces that whip the liquid jet toward the collector⁴⁰⁵. The released liquid jet by electrospinning nanofibers causes the polymer chains present in the solution to stretch and glide past one another, forming the electrowiring characteristically nanofibers⁴⁰⁶. The polymeric solution affects the

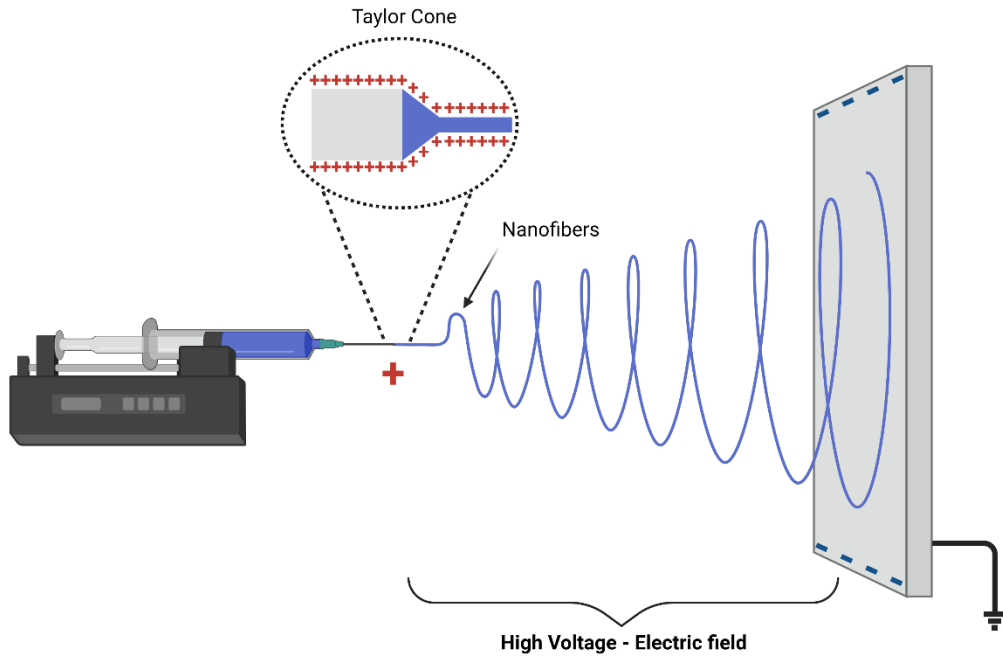


Figure 29. Scheme of electrospinning process.

distance between the needle and the collector, which is crucial for determining the shape of the electrospun nanofiber^{407,408}.

The capacity to govern fiber deposition at the scale of a single fiber achieved utilizing the near-field electrospinning technology, and melt electrospinning writing for liquid polymers, is a new achievement in the area of electrospinning⁴⁰⁹. Electrospinning's flexibility and a great capacity for producing scaffolds comparable to actual ECM make it the most promising and attractive technique in bioprinting approaches. Even though cells can survive electrospinning⁴⁰⁹, electrospinning cell-laden hydrogels have few uses^{410,411}.

7.3.4. Fused Deposition Modeling - 3D printing

3D bioprinting and 3D printing are two recent technologies with closely related technological development; therefore, their state-of-the-art qualities will be presented in the next theme regarding 3D bioprinting.

INTRODUCTION BIOFABRICATION

FDM has been widely employed to build new scaffolds and modify their mechanical characteristics for TE applications, encouraging results^{412,413}. FDM filaments are formed by extruding molten thermoplastic polymers (**Figure 30A**); a 3D scaffold is created layer by layer by depositing these filaments to build a layer. The CAD design serves as the overall process controller. Due to its relatively low melting temperature and commercial availability in medical grades, PCL⁴¹⁴ has been utilized as the preferred polymer in the bulk of published work, but several other polymers have also been used^{415,416}. As a result of FDM, several novel extrusion-based methods for producing 3D scaffolds, such as 3D fiber deposition methods (3DF), have been created, allowing the deposition of diverse materials while also creating constructs with spatially changing physicochemical properties (**Figure 30B**)^{417,418}.

Although FDM 3D printing technologies have considerably improved the functional performance of TE structures, the high temperatures required to create molten polymers may limit the direct integration of biological components using this technology^{413,419–421}. Surface modification approaches

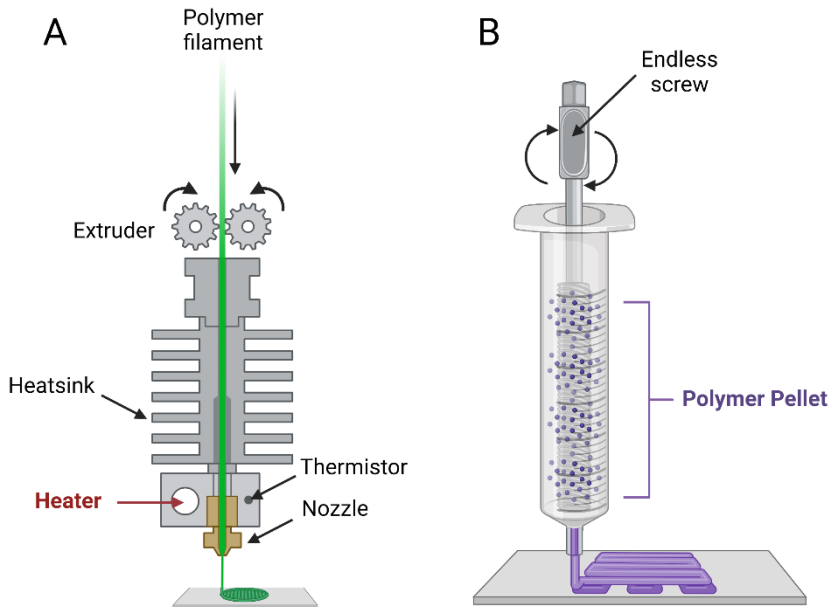


Figure 30. Scheme of 3D printing techniques applied in biofabrication. A) Corresponds to FDM method and B) to 3DF.

might be used to functionalize the fibers and enable the grafting of bioactive compounds in specific locations⁴²². Hydrogels containing biological components might be used with thermoplastic polymers to overcome the limitations imposed by high temperatures^{423,424}.

8. Bioprinting

8.1. Background

Bioprinting is an innovative technology promising for fabricating functional tissues and organs. Currently, bioprinting is a novel, complex, and exciting TE technique and might overcome the lack of tissues and organs suitable for their regeneration and transplantation⁴²⁵. 3D printing, called additive manufacturing techniques, is based on the principle of layer-by-layer material addition allowing the manufacturing of different 3D complex structures. In contrast with the conventional making process, which is based on subtractive manufacturing, 3D printing implies the possibility of managing biomaterials for TE; generally, much more restrictive than metals and daily used plastics⁴²⁶. Bioprinting can be defined as the adaptation of 3D printing for TE, which implies controlling layer-by-layer stacking of biomaterials and living cells⁴²⁷. Thus, the applicability of 3D bioprinting in TE brings several advantages in contrast to previous manufacturing methods: rapid fabrication of scaffolds and constructs, controlled porosity, tailored architecture, adapted biomechanical properties, and the possibility to imbed drugs, cells, or other molecules to enhance the structure of tissue or organ to biofabricate⁴²⁸.

3D printing was invented in 1986 by Charles W. Hull when he adapted the photo-curation process for mending tables; thus, he developed a system for using ultraviolet (UV) light for stereolithography⁴²⁹. On the other hand, the invention of bioprinting dates from 1988 by Keble et al., which consisted of modifying a Hewlett Packard inkjet into a drop-by-drop bioprinting system. Further, its invention was not considered as bioprinting but as cytoscribing technology, a method of micropositioning cells and constructing 2D synthetic

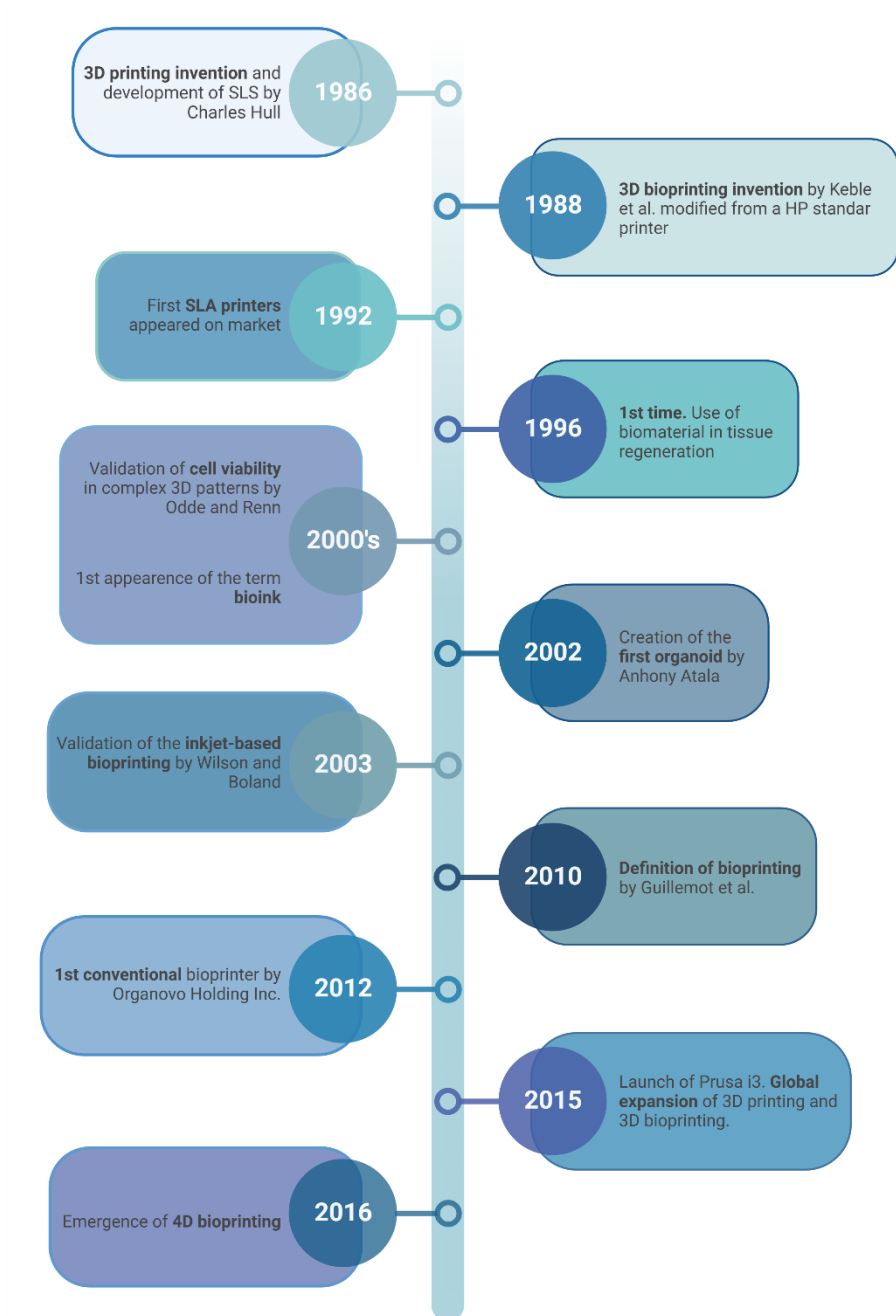


Figure 31. Timeline of 3D bioprinting.

tissues⁴³⁰. Nevertheless, it was not until the launch of a printer named Prusa i3, developed by Josef Průša in 2015, that the concept of 3D printing was globally extended⁴³¹. That was in part due to the simplicity of its work and because it was

INTRODUCTION BIOPRINTING

a 3D printer with open software (Replicating Rapid-Prototypers (RepRap project))⁴³². Thus, the framework and firmware were completely configurable and without copyright protection, allowing this technology to quickly adapt to different fields such as metallurgy, aeronautics, the construction industry, etc. Despite several pieces of research about bioprinting that appeared in 1988⁴³³. Years after, in 1999, Odde and Renn synthesized complicated 3D patterns, which reached the micrometer scale, ensuring the cell viability of bioprinted product⁴³⁴. Closely in time, another modification of a Hewlett Packard printer resulted in the validation of inkjet-based bioprinting by Wilson and Boland⁴³⁵. Years later, in the early 2000s, the term bioink appeared for the first time to define inks used in 3D bioprinting⁴³⁶. Then, in 2010, the term 'bioprinting' was defined by Guillemot et al. They considered 'bioprinting' a computer-aided protocol that allows the precise 2D or 3D alignment patterning of biomaterials loaded with living cells to create bioengineered products for TE, pharmacological drug screening protocols, or fundamental research³⁵⁸. Finally, there were some developments in the extrusion-based technique for 3D bioprinting, but it was not until 2012 when Organovo Holdings Inc. (San Diego, California) developed its first commercial bioprinter NovoGen MMX®^{437,438} (**Figure 31**).

Currently, 3D bioprinting represents an advanced and relatively recent technology that allows manufacturing 3D bioprinting-based ATMPs as organs or functional tissues. The development of ATMPs is focused on designing innovative medicinal products to regenerate damaged tissues and organs, responding to current limitations in the availability of organs and tissue to be transplanted^{439,440}. The main goal of bioprinted organs can be the total replacement of a diseased (or elder) organ with a healthy artificial one that does not present any possible patient rejection⁴⁴¹.

Moreover, 3D bioprinting offers the possibility of manufacturing bioprinted 3D models⁴²⁷, obtaining a high reproducibility of *in vivo* 3D models of tissues (lab-on-a-chip) and organs (organ-on-a-chip)^{442,443}. These 3D models

represent an alternative to animal models or human subjects to test new drugs⁴⁴⁴. Thus, bioprinted 3D *in vivo* models offer a revolutionary system for pharmacological analysis, encompassing the reduction of animal experimentation, high throughput drug screening, optimization of study time, and cost reduction, among others⁴⁴⁵.

3D bioprinting still has some limitations, such as the standardization applicability protocol for clinical use, regulatory framework, the definition of the aseptic process, maintaining the cell viability after the bioprinting process, design of specific bioinks, etc⁴⁴⁶. To focus on the authentic relevancy of this technology, Gao et al. exposed the current limits in technology for developing clinically available organs nowadays, only possible for synthesizing grafts for saving medium/small implant regions⁴⁴⁷. On the other hand, Nie et al. related the pertinent aspects of 3D bioprinting in the drug discovery industry, dividing its implementation into mini-tissues, organ-on-a-chip models, and organ/tissue constructs⁴⁴⁸. Nie et al. also exposed the need to standardize the transfer process.

8.2. Definition

Because of the vast range of procedures encompassed by this umbrella term, defining 3D bioprinting is a complex undertaking. The use of this term is older than the definition imposed by Guillemot in 2010, perhaps due to its similarity with the globally accepted term 3D printing. Nevertheless, the first time scientists coordinated a common term for differentiating 3D printing for 3D bioprinting was in Manchester's First International Workshop Bioprinting and Biopatterning in 2004⁴³³. It was proposed the following definition:

'The use of material transfer processes for patterning and assembling biologically relevant materials —molecules, cells, tissues, and biodegradable biomaterials— with a prescribed organization to accomplish one or more biological functions.'

INTRODUCTION BIOPRINTING

The omission of the term 'bioink' in the preceding definition proves that the previous statement is unclear and cannot precisely determine which approach might be employed.

The final accepted definition (that is currently used) is the one proposed by Guillemot et al. in 2010³⁵⁸, as exposed above:

'The use of computer-aided transfer processes for patterning and assembling living and non-living materials with a prescribed 2D or 3D organization to produce bioengineered structures serving in regenerative medicine, pharmacokinetic and basic cell biology studies.'

8.3. Bioinks

Similar to the 3D bioprinting definition, the term **bioink** is rich in controversy, and it was not until 2019 (i.e., three years before the redaction of this memory) that scientists reached a global consensus regarding their terminology. Thereby, Groll and colleagues disposed of the following definition for bioink⁴⁴⁹:

'A formulation of cells suitable for processing by an automated biofabrication technology that may also contain biologically active components and biomaterials.'

The previous definition clearly states that a bioink must include **living cells** in its formulation. However, as will be seen later in this paper, the bioprinting process is multi-step, and many bioinks need **post-bioprinting** modification (e.g., application of cross-linkers)⁴⁵⁰.

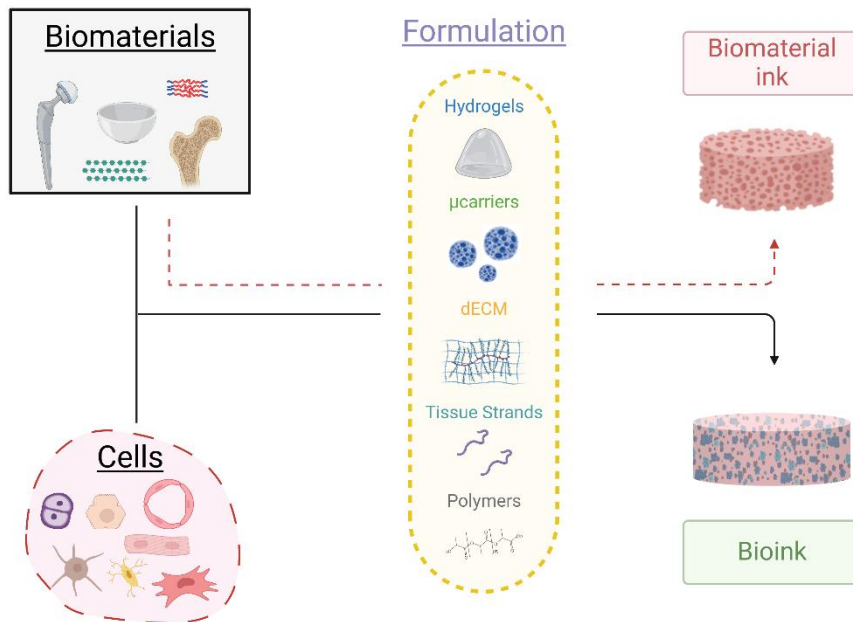


Figure 32. Representation of bioink and biomaterial ink compositions. In biomaterial inks, the cells are added in parallel or after bioprinting step.

Nevertheless, they remark that bioink is not a mandatory condition to impose bioprinting categorization. As explained in this work, a broad branch of different biomaterials could not be conditioned for the previous definition of bioink (e.g., synthetic thermoplastic polymers, ceramics), but they are used for both techniques, biofabrication, and bioprinting. To solve this issue, the same authors also proposed **biomaterial ink**. This concept is used to define the synthesis of scaffolds for cell seeding to introduce them inside BRs⁴⁵¹, implants, or to work in parallel with bioinks⁴⁵²; it can also be applied for those sacrificial biomaterials which will be dissolved in the post-bioprinting stage⁴⁵³. **Figure 32** shows how both formulations do not depend on their matrix content and process form.

An ideal bioink or biomaterial ink presents i) a high printability, described as an easy a high accurate printing procedure; ii) good scalability to bioprint large replacement areas; iii) good mechanical properties, similar to the tissue that tries to replicate; iv) biodegradability and v) immunogenicity⁴⁵⁴.

INTRODUCTION BIOPRINTING

Besides, the post-bioprinting incubation time must be considered to design a bioink, maintaining cell viability.

Bioinks can be formulated from different biomaterials, which can be formulated in different types of matrices, such as hydrogels, tissue strands, decellularized ECM (dECM), microcarriers, and tissue spheroids.

8.3.1. Hydrogels

Hydrogels are very hydrophilic polymers that exhibit a gel-liquid phase due to cross-linking. They are categorized as natural (e.g., gelatin, chitosan) or synthetic (e.g., pluronic and PEG) based on their origin. Crosslinking is a crucial characteristic that characterizes the bioprinting state; it can be urged at the time of printing or later⁴⁵⁰. Hydrogels employ three distinct cross-linking techniques (**Figure 33**): i) physical crosslinking (no external agent required; minimum contamination risk); ii) chemical crosslinking (covalent bonds), which are mechanically the most stable; and iii) enzymatic crosslinking (fibrinogen and thrombin)⁴²⁴. Hydrogels are good options for cell encapsulation and the fabrication of 3D scaffolds because of their high hydrophilicity⁴⁵⁵.

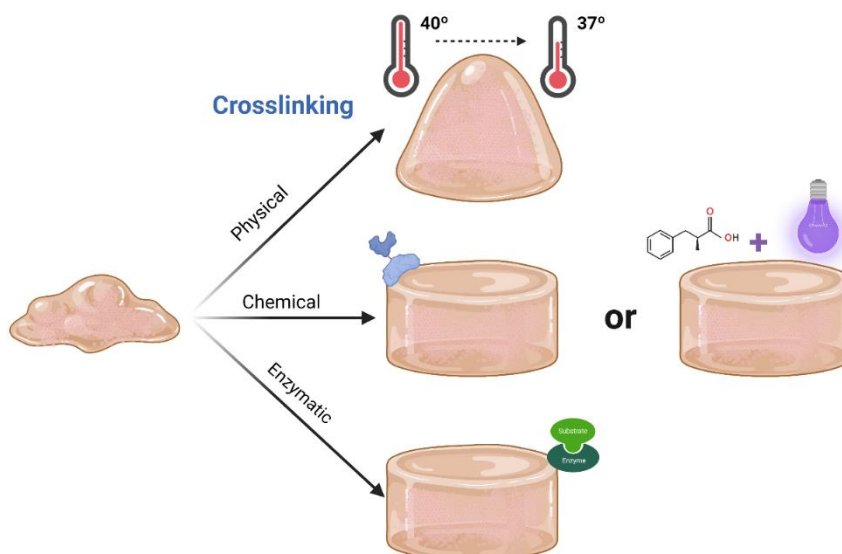


Figure 33. Representation of an arbitrary hydrogel bioink and their three different crosslinking methods applied in bioprinting.

Comparing hydrogels to the optimal bioinks criteria reveals that bioinks created using hydrogels have excellent printing resolution and accuracy; also, the survival of cells within them is among the highest inside bioinks⁴⁵⁶.

On the contrary, their low viscosity makes their stiffness smaller than the rest of the bioinks. Despite this, they could be considered the most versatile bioinks easy to obtain thanks to their commercial spread availability, such as the bioinks series from CELLINK, BioInk®, and Osteoink™ from RegenHU, Bio127, and BioGel from Biobot. Another remarkable case is the company Bioink Solutions that commercializes its Gel4GCell® bioink and its derivate compounds depending on the target tissue: Gel4GCell®-BMP (osteoconductive), Gel4GCell®-VEGF (angiogenic), and Gel4GCell®-TGF (chondrogenic). Finally, Tissue Strads are an evolution of hydrogels, but in this biomaterial, cells should be injected in hollow tubes, which present higher stiffness than conventional bioinks⁴⁵⁷. Their most significant benefit is their robustness of bioinks, making them an appropriate option for their use in TE. Despite this, they are tedious to bioprint⁴⁵⁸.

8.3.2. Decellularized Extracellular Matrix

Alternatively to hydrogels, dECM from different tissues and organs has been proposed as an excellent component for bioinks due to their mimeticity with the natural ECM (**Figure 34**). To replicate all the biochemical and biomechanical aspects of the cell niche, dECM is manufactured by removing cells from the surrounding material⁴²³. In contrast with the rest of the biomaterials, bioinks formulates with dECM present the highest biomimicry. However, its synthesis is expensive and labor-intensive, and they are structurally weak⁴⁵⁹. Thus, correlating with hydrogels, dECM resolution is lower.

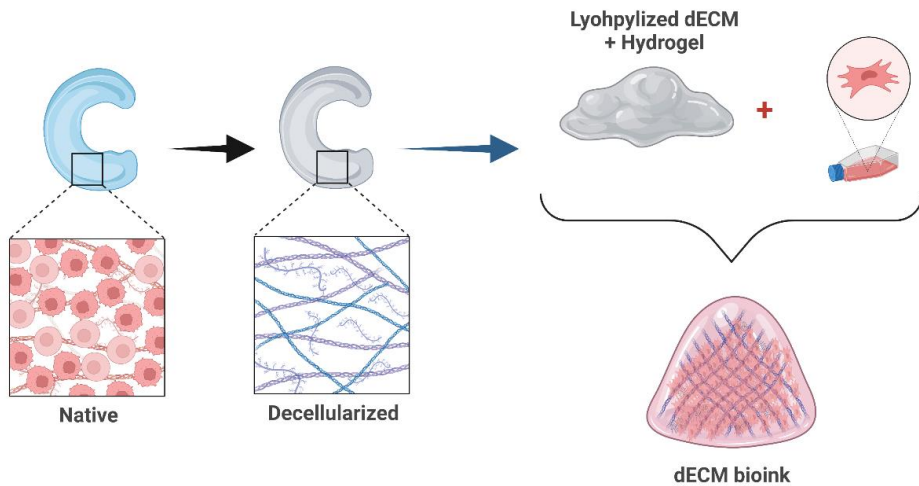


Figure 34. Pathway for dECM bioink synthesis.

8.3.3. Microcarriers based bioinks

Microcarriers are arrays formulated from synthetic polymers (PEG) or natural polymers (cellulose) with interconnected pores in a spherical arrangement (**Figure 35**). Their function is to increase the surface exposure area for cell attachment exponentially to increase cell proliferation⁴⁶⁰. Thus, they serve as a stimulus to the final constructs, saving space and increasing cell density. Bioinks formulated with microcarriers are more oriented to manufacture ATMPs in which a proliferation process should be performed ⁴⁶¹.

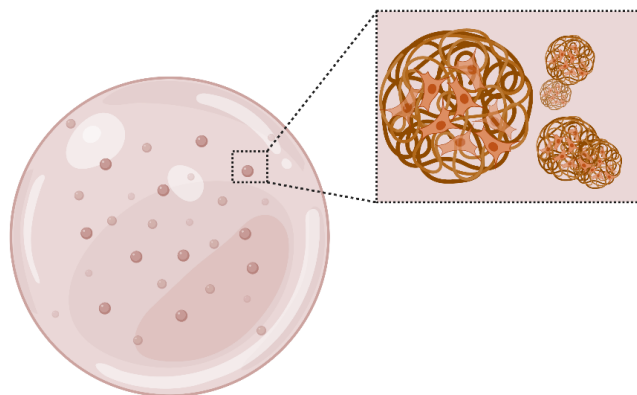


Figure 35. Representation of a microcarrier bioink. Adhesion cells are attached to these microcarriers allowing high expansion of

These types of bioinks have a reduced cost and high availability. Nevertheless, they have a low printing resolution⁴⁶².

8.3.4. Tissue spheroids-based bioinks

Tissue spheroids are sphere-like cell organization architectures with a diameter of less than 500 μm . They need an extremely delicate bioprinting procedure (**Figure 36**). Since the advance published by Mironov et al. in 2009, few kinds of research have been carried out with these structures to formulate bioinks⁴⁶³. The bioinks based on tissue spheroids present high cell-cell interactions; consequently, they offer one of the lowest printing resolutions together with microcarriers⁴⁶².

Future investigations in novel biomaterials are almost mandatory because they will be translated into increased simplicity during the bioprinting process⁴⁶⁴. Nowadays, considering production costs, manufacturing procedure, and cell viability, the most used bioinks are hydrogels that can be found alone or with biomaterial inks as supports.

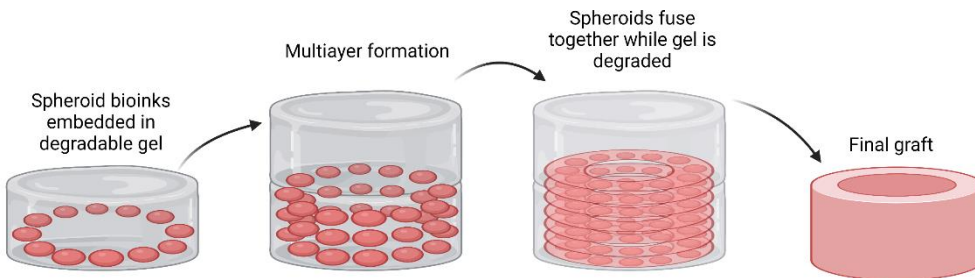


Figure 36. The pathway developed by Mironov to develop tubular structures (e.g., capillaries).

8.4. 3D bioprinting techniques

8.4.1. Droplet-based bioprinting (DBB):

It is the oldest technology applied in 3D bioprinting, also '*inkjet bioprinting*', which was a preliminary attempt to replicate the conventional

INTRODUCTION BIOPRINTING

inkjet printers⁴⁶⁵. DBB technique manipulates the bioink through physical stimuli (thermal, acoustic, electro-hydrodynamic, or micro-valves) to release droplets with embedded cells. This methodology has drastically evolved, and it is used because of its simplicity, agility and versatility, and high resolution, which could reach almost μm scale^{466,467}. However, due to these approaches, the dehydration of the bioinks involves most cells dying in the process. Therefore, the use of BRs is recommended in the post-bioprinting stage.

8.4.2. Extrusion-based bioprinting (EBB):

It is the first system and, perhaps, the most worldwide used by its versatility, affordability, and ability to bioprint porous constructs and scaffolds⁴⁵⁶. In most cases, the extruder is a sterile syringe on which external forces are applied to control the output of the bioink through a needle. (volume and position)⁴⁶⁸. An excessive extrusion pressure could alter morphology and cell function⁴⁶⁹. Thus, the major disadvantage of this technique is the necessity of a complete viscoelastic study of the bioinks before initiating the 3D bioprinting process⁴⁷⁰. Besides, this methodology presents an abrupt resolution of 100 μm in the most advanced cases.

8.4.3. Laser-assisted bioprinting (LAB):

This technique was based on a common practice of computer numerical control (CNC) in metals ⁴⁷¹. Three different parts mainly shape this procedure: a donor-slide, a laser pulse, and a receiver slide. Using two different slides is mandatory because any direct radiation of the laser pulse onto cells will produce immediately cell-dead. Consequently, this process is much more complex than the other technologies described. It has a higher associated cost but also presents higher accuracy (resolution of 10-50 μm); even more, there are pieces of evidence where only one cell per droplet was printed using LAB ⁴⁷².

8.4.4. Laser-based bioprinting (LBB):

Charles W. Hull invented it in 1985, and it is considered the most novel technology of 3D bioprinting and the one with the highest resolution (5-300 μm), allowing the manufacture of blood capillaries or nerves⁴⁷³. This technique is called SLA, based on UV radiation or visible light to cure photosensitive polymers. The scaffold is expected to be printed in this technique, and cells are seeded after bioprinting. However, SLA times are slower than other technologies, and the viability of cells in the 3DBBP may be reduced by UV radiation, photocrosslinking toxicity, or long bioprinting times⁴⁷⁴.

Cell viability, tissue homogeneity, and reproducibility are critical aspects that must be considered before deciding which technique is the most suitable for

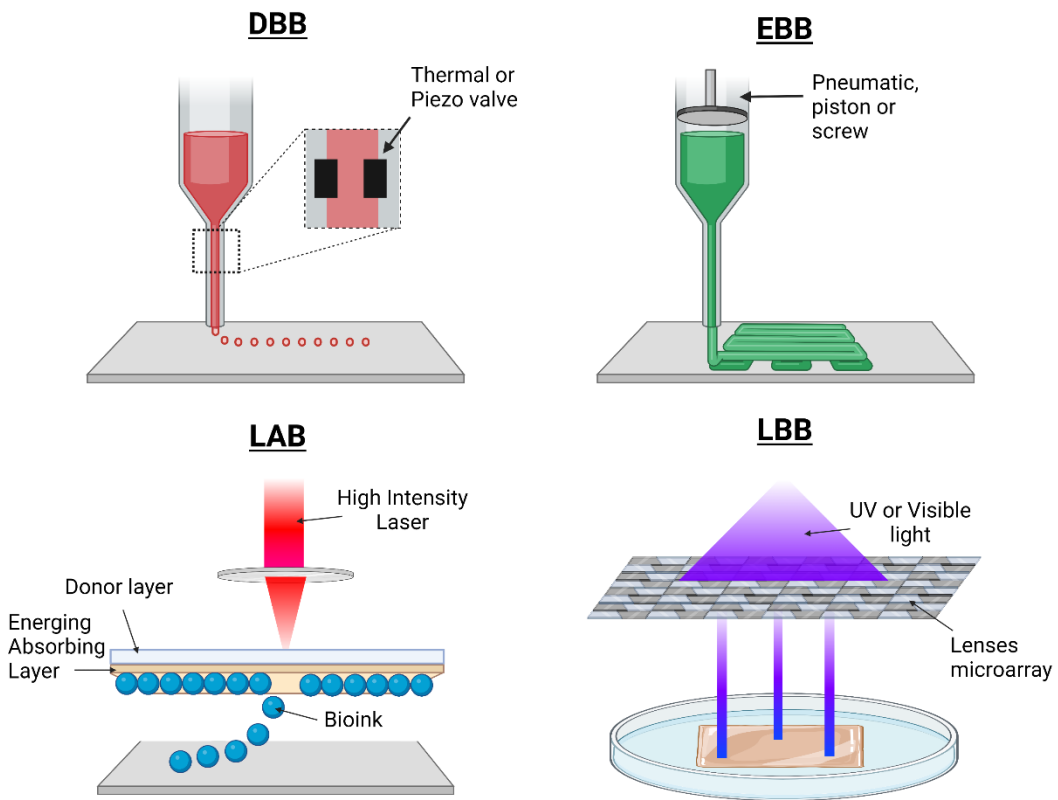


Figure 37. Representation of the most common bioprinting methods.

INTRODUCTION BIOPRINTING

the biofabrication necessities⁴⁶⁵. Thus, each method should be defined and adapted (**Figure 37**).

The latest advances in printing have allowed 3D bioprinting to evolve towards more complex strategies, such as 4D bioprinting, which requires relative intensification on post-bioprinting protocols. The 4D bioprinted constructs can change over time depending on the stimuli⁴⁷⁵. This evolution of conventional 3D bioprinting allows the manufacture of scaffolds and constructs, in which other bio-mimicking features improved (involved in the post-printing step), as could be the case of pediatric implants where the constructs need to grow with the patient⁴⁷⁶. Many TE types of research have led to the consensus of applying mechanical or chemical stimulation to the tissue-engineered constructs after bioprinting. These post-bioprinting processes remark the innovative treatment that supposes 3D bioprinting. Because bioprinted constructs are living, they constantly evolve and adapt.

4D bioprinting requires biomaterials that can be re-shaped over time; thus, recent advances in 3D bioprinting involve using innovative materials such as abilities⁴⁷⁷. This effect is called the shape-morphing effect (SME), a change in morphology because of a preset-stimuli⁴⁷⁸. SME is a relevant aspect of bioprinted constructs; it allows them to accommodate and adapt to specific treatment regions; it also supposes a fundamental difference between conventional implants and bioprinted replacements or patches. This geometrical rearrangement is printer-independent, and it only depends on the resilience of the biomaterials composing the scaffolds. Typically, hybrid ones mix a more rigid polymer with a hydrogel^{479–481}.

3D bioprinting is still evolving rapidly, and numerous bioprinters have been commercialized^{482,483} (**Table 1**).

Table 1. Available commercial 3D bioprinters. This table shows that the most extended methodology for bioprinting is the FDM model; although SLA bioprinting has a higher resolution than FDM, the necessary investment in developing any prototype is a vast wall against commercialization.

Bioprinter	Company	Country	Year of Market	Mechanism	Technique
nSrypt	Sciperio/nScrypt	USA	2002	Pneumatic Extrusion	FDM/EDM/EBB
3D-BioPlotter	EnvisionTec	Germany	2003	Pneumatic Extrusion	
Fab@Home	Seraph Robotics	USA	2006	Mechanical Extrusion	
Novogen MMX	Organovo	USA	2009	Mechanical Extrusion	
3D Discovery	RegenHU	Switzerland	2012	Pneumatic Extrusion	
BioFactory	RegenHU	Switzerland	2012	Pneumatic Extrusion	
The Alpha Bioprinter	3Dynamic Systems	UK	2013	Pneumatic Extrusion	
Regenovo	Regenovo Biotechnology Co. Ltd.	China	2013	Mechanical Extrusion	
The Omega Bioprinter	3Dynamic Systems	UK	2014	Pneumatic Extrusion	
BioAssembly Bot	Advanced solutions	USA	2014	Pneumatic Extrusion	
Inkredible	Cellink	USA	2015	Mechanical Extrusion	
BioBot 1	Biobots	USA	2015	Pneumatic Extrusion	
Regemat 3D v1	Regemat 3D	Spain	2015	Mechanical Extrusion	
Fab@Home MD4	Seraph Robotics	USA	2016	Pneumatic Extrusion	
Scientist 3D printer	Seraph Robotics	USA	N/A	Pneumatic Extrusion	
Bio3D SYN	Bio3D technologies	Singapore	N.A.	Mechanical Extrusion	
Bio3D Explorer	Bio3D technologies	Singapore	N.A.	Mechanical Extrusion	
MicroFab JetLab II	MicroFAB Technologies, Inc.	USA	2000	Piezo Drop-on-demand	Droplet

INTRODUCTION BIOPRINTING

Autodrop AD-P-8000	Microdrop Technologies	Germany	2004	Piezo Drop-on-demand
Fujifilm Dimatrix Printer	Fujifilm Dimatrix, Inc.	USA	2005	Piezo Drop-on-demand
MicroFab JetLab 4	Piezo Drop-on-demand	USA	2006	Piezo Drop-on-demand
Autodrop Compact	Microdrop Technologies	Germany	2008	Piezo Drop-on-demand
Cluster Technology DeskViewer	Cluser Technology Co., Ltd.	Japan	2013	Piezo Drop-on-demand
Cell Jet Cell Printer	Digilab, Inc	USA	2015	Micro-valve and Syringe Pump

8.5. Steps of the 3D bioprinting process

The development of ATMPs is focused mainly on manufacturing artificial organs and tissues, which can be applied in regenerative medicine and advanced therapies as innovative medicines to repair, replace, restore or regenerate damaged tissue or organ in a patient⁴⁸⁴.

The development of ATMPs involves different phases ranging from the design phase to administration to the patient (**Figure 38**). This process is performed in three steps: pre-bioprinting, bioprinting, and post-bioprinting.

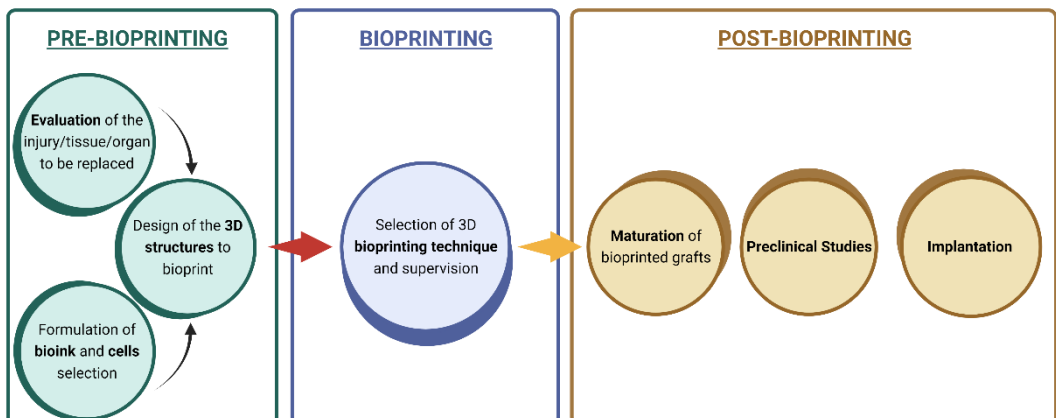


Figure 38. Outline of the development process of a 3D bioprinting TE graft.

8.5.1. Pre-bioprinting

As with any other development process, a conceptual design phase of the ATMPs should be performed; each design is case-dependent and unique. During this phase, several aspects must be considered, such as i) the evaluation of the injury to define the tissue or organ to be bioprinted; ii) histological and physiological analysis of the target tissue/organ; iii) selection of biomaterials and cell types suitable for the formulation of bioink and biomaterial ink; and, iv) the design of the 3D structures to bioprint a construct. Designing tissues or organs needs to be converted into a compatibility geometry that the bioprinter can understand, depending on how the bioprinter works. The digital models can come from computed tomography (CT) or magnetic resonance imaging (MRI) scans⁴⁵⁶.

8.5.2. Bioprinting

In the bioprinting process, there are mainly two options: a) to bioprint a construct directly, from bioinks and biomaterial inks, which have cells embedded inside, or b) to bioprint a 3D cell-free scaffold from only biomaterial inks, and after the bioprinting process injecting cells into the bioprinted scaffold (also named construct)⁴⁴⁹. During this phase, several prototypes (always without cells) should be bioprinted to calibrate and tailor all the parameters involved in the bioprinting process. Once the stability of the procedure is reached, and prototypes are manufactured with pleasing shapes, the final constructs can be bioprinted.

8.5.3. Post-bioprinting

In this step, the maturation process of ATMPs plays a vital role in creating functional and living organs or tissues⁴⁵⁶. Nevertheless, it is not a mandatory step and, in some cases, is not applied. The maturation process requires mechanical and chemical stimulations over time which are applied in almost all cases by BRs⁴⁵⁶.

INTRODUCTION BIOPRINTING

Once 3DBBP is manufactured, *in vitro* preclinical studies should be carried out to guarantee its safety and efficacy as medicine⁴⁸⁵. These studies include i) studies of biological characteristics such as viability, proliferation, toxicity, differentiation assays, ECM production assays⁴⁸⁶; ii) physical-chemical studies such as degradation, swelling, porosity, tensile studies, friction studies⁴⁸⁷; and iii) microbiological studies as sterility test, endotoxins assay, mycoplasma, and virus detection. Also, *in vivo* studies have to perform to evaluate: implant rejection, cytotoxicity, large-time response, degradation rate, wound healing assays, etc⁴⁸⁸. If obtained results from the *in vitro* and *in vivo* studies determine that the ATMP is safe and effective, its clinical evaluation could be studied under a clinical trial. Once the safety and efficacy of the ATMP are verified in humans, the registration process for its market can be started. Finally, if the competent health authorities approve the bioprinted graft, it could be implanted in patient ⁴⁸⁶. Therefore, the development of ATMPs is a complex process, which is based on six essential pillars: i) definition of the cell component; ii) formulation of adequate bioinks and biomaterial inks; iii) selection of bioprinter and fine-tuning the 3D bioprinting process; iv) to evaluate if a maturation process in a BRs is required; v) preclinical and clinical studies and vi) regulatory pathway to be approved and commercialization.

9. Bioreactors

9.1. Background

The **bioreactor (BR)** is a historical device (**Figure 39**) used since antiquity. From observation and experience, ancient societies could address biotechnological design issues for practical uses like wine and beer production⁴⁸⁹. The idea that microscopic life represents a sizeable economic resource came to man gradually despite some pushback from established scientific society⁴⁹⁰; among especially relevant themes are the description of the fermentation mechanisms by Pasteur⁴⁹¹ and the role of bacteriology in disease propagation by Emily Roux and Robert Koch⁴⁹². These contemporary cell biology and medicine advancements supplied the foundation for using cells' industrial potential⁴⁹³. In the twentieth century, the use of glycerol for manufacturing explosives, which used yeast for conversion from glucose, is an example. Another method is to use butyric acid bacteria to produce butanol and acetone on a big scale, as pioneered by Chaim Weizmann⁴⁹⁴. However, these techniques were quickly abandoned in favor of petroleum-based products with more significant process economies.

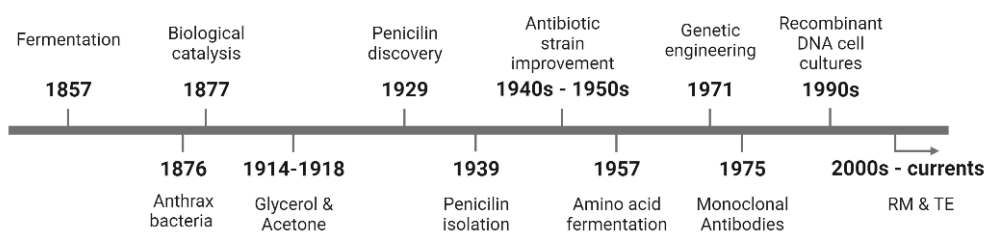


Figure 39. Timeline representing the most relevant advances in BR history.

The tale of antibiotic development is an outstanding illustration of how industrial biotechnology evolved through a combination of academic research and commercial product development. Alexander Fleming discovered the antibiotic property of a *Penicillium* culture in 1929 as part of a series of

INTRODUCTION BIOREACTORS

procedures for increasing the output and activity of cultures moved into large-scale manufacturing⁴⁹⁵. Years after, scientists could detect, stabilize, exploit, and select strains and use genetics and mutational approaches to build bioproduction in BRs to address worldwide medical demands⁴⁹⁶.

The expanding industrial usage of animal cells in the mid-1950s gave rise to bioprocess with the synthesis of microbial polymers (e.g., xanthan)⁴⁹⁷. The next difficulty in BR engineering was large-scale cultivation due to lower cell densities than fungi and yeasts⁴⁹⁸. Later, the discovery by Köhler and Milstein (1975) of expressing monoclonal antibodies in hybridoma cell culture inaugurated a new era in industrial biotechnology and bioengineering⁴⁹⁹.

Genetic engineering and technologies transformed industrial biotechnology by creating macromolecular products from cells⁵⁰⁰. After this novelty, several biotechnological companies appeared in the biotechnology limelight. Cetus and Genentech were made in the early 1970s in California⁵⁰¹. Biogen, Amgen, Chiron, and Genzyme joined the fray in the years that followed⁵⁰². Recently in BR engineering, science has been concerned about cell production and applications with RM products and pluripotent stem cells⁵⁰³. Because of more sensitive cell types and more sophisticated development and activity, BR's controllability demands are higher.

9.2. Definition

BRs are defined by the IUPAC (International Union of Pure and Applied Chemistry) as *devices that manage any biological process*. In the biotechnology field, their use is standardized, unlike in TE, where its use is currently introduced to control and induce some biological reactions for culturing aerobic cells in controlled conditions⁵⁰⁴.

TE uses BRs to offer controlled and reproducible cell and tissue development⁵⁰⁵. Tissue development outcomes include constructing size, shape/architecture, biochemical content, biological function, and morphology⁵⁰⁶.

While cell proliferation is required to form most tissue, a distinct cell cycle phase (interphase) allows cells to specialize⁵⁰⁷. Considering this, a BR can be defined as:

'A BR is a reactor that creates an environment where cells may proliferate and differentiate as they would in vivo while maintaining appropriate nutrient concentrations and allowing for efficient mass transfer to the tissue.'

Although BRs are still in the early phases of TE, essential general qualities aid in the logical construction of these reactors.

9.3. Relevant design aspects

Concerning design (**Figure 40**), it may be evident that the first aspect could be treated to replicate synthetically the naïve tissue ECM and its physiological mechanisms, which implies tissue architecture, the cell-ECM and cell-cell interactions, and cell metabolisms⁵⁰⁸. Even more, a BR system should allow for aseptic feeding and sampling to reduce the possibility of infection.

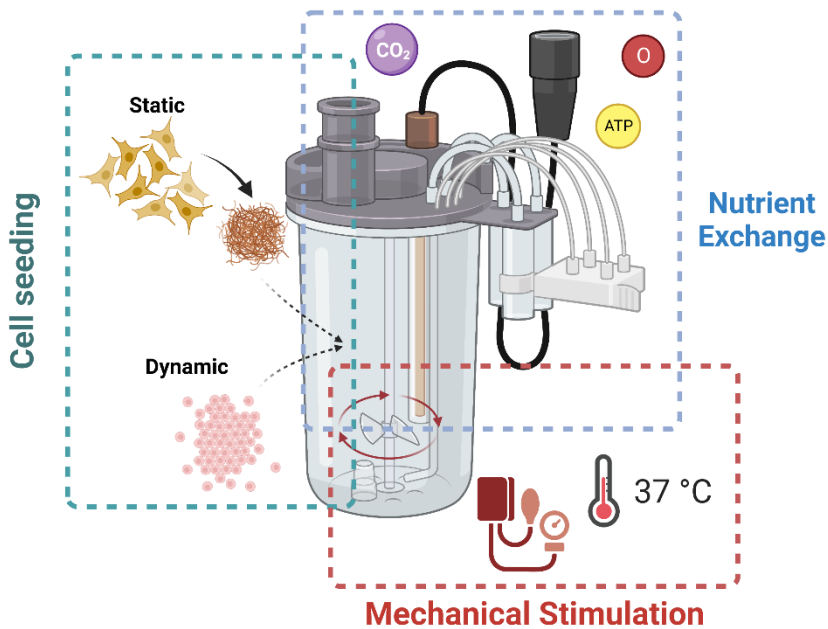


Figure 40. A schematic representation of the main aspects that a BR destined for TE must have.

INTRODUCTION BIOREACTORS

Thus, the technology should also be built to work in a **sterile** environment, fulfilling the pre-sterilization of equipment, creating a sterile medium, and preserving sterility during culture⁵⁰⁹. The second aspect of the design regards how cells are introduced in the system (scaffold seeding) and, more importantly, how the system allows adequate nutrient transport that ensures cell viability and expansion⁵¹⁰⁻⁵¹². Finally, biomechanical stimuli aspects will promote tissue differentiation⁵¹³ once BR can comfortably accommodate cells, as explained in the previous chapter.

9.3.1. **Scaffold seeding**

Frequently, TE involves many cells, which must be cultivated and expanded from biopsy to be later incorporated into the bioink; this *in vitro* cell expansion process is long, which implies time-consuming and a high economic burden. Thus, using BRs for TE is a fundamental tool to enhance development^{514,515} since BRs provide a higher comprehensive level thanks to their monitoring and control capabilities over specific 3D cultures; thereby, transitioning from the laboratory benchwork to the clinics or pharma industry will be accelerated⁵¹⁶.

Seeding can be done as a separate procedure, where cells are allowed to adhere to the scaffold before the BR is used, or cells can be seeded directly within the BR. In both manners, scaffold seeding is done in batches to guarantee maximal cell adhesion⁵¹⁷. The ability to evenly distribute large starting cell counts onto a 3D scaffold is a critical barrier for seeding⁵¹⁸. Although static seeding is the most often used method, dynamic seeding has advantages. Higher attachment efficiencies and more uniform cell distribution on the scaffold result in higher-quality tissue structure and content⁵⁰⁶. Simple mixing, spinner flasks, and convective seeding in perfusion reactors are just a few examples of dynamic seeding techniques that have been ^{519,520}.

9.3.2. **Nutrient transport**

The typical distance between tissues and nutrient-supplying capillaries is 100 micrometers⁵²¹. This size tissue segment, which has 500–1000 cells, is comparable to the size of functioning organ components. An essential **microenvironment** for tissue is a cube with 100-micrometer sides⁵²². Based on this standard TE length scale, it is possible to define a microenvironment; that is unique due to neighboring cells, the chemical environment, and shape^{523–525}. For BRs, a porous scaffold could also be placed to simulate this microenvironment⁵²⁶.

Mass transfer in TE is the delivery of nutrients and gases from their source to the location of the cells. As explained, the mass transfer of nutrients is based on convective and diffusion. The ratio of convective to diffusive transport is a paramount concern (Péclet number)⁵²⁷.

$$Pe = \frac{\text{advective transport rate}}{\text{diffusive transport rate}} = \frac{Lu}{D} \quad (52)$$

where L is the characteristic length, u the local flow velocity, and D the mass diffusion coefficient, for $Pe \gg 1$ means diffusion transport is much higher than convection (e.g., cartilage tissue)⁵²⁸.

The nutrients first reach the cell surface, where there is a balance between the rate at which they are taken up and the rate at which they are provided through diffusion (Damkohler number)⁵²⁹.

$$Da = \frac{\text{reaction rate}}{\text{diffusion mass transfer rate}} = kC_0^{n-1}\tau \quad (53)$$

where k is the kinetics reaction rate, C_0 the initial concentration, and τ the mean residence time. When this ratio is high, nutrients are digested faster than they can diffuse to the surface, decreasing surface concentration. When it is modest, absorption is sluggish, and diffusion keeps nutrient concentrations near constant.

INTRODUCTION BIOREACTORS

Another mass transfer concern is selecting an appropriate medium flow rate to provide a continual supply of new nutrients and the removal of contaminants⁵³⁰. Additionally, balancing the flow rate to ensure the shear rate influences nascent tissue and supports the nutritional demand needs is necessary⁵³¹. Based on an average cellularity of 500 million cells per cm^3 , overall *in vivo* oxygen absorption rates⁵²⁹ of $25 - 250 \frac{\text{mol } O_2}{\text{cm}^3}/h$ and perfusion rates of $0.07 \frac{\text{mL}}{\text{cm}^3}/min$ may be suitable starting points⁵²².

9.3.3. **Biomechanical stimuli**

BRs for TE applications have evolved from mechanobiology, which studies tissue embryology, as its functions of external stimuli and how cells interact with those physical signals (mechanotransduction)^{532,533}. In previous chapters it was deeply exposed the relevance of biomechanics in tissue development and homeostasis; BRs are devices that adopt these kinds of stimulation *in vitro*; sometimes, these cultures are called *ex vivo* to distinguish a dynamic 3D culture from conventional cell cultures^{534,535}. Different tissues, organs, and consecutively, each TE product requires further stimulation to work appropriately (thermal, pressure, electrical, ionic, pH, oxygen concentration)⁵⁰⁸. Concretely, mechanical inputs (fluid flow generated shear stresses) during *in vitro* growth give tissues properties more similar to *in vivo* structures⁵⁰⁶. Pulsed BRs with customizable stroke volumes and rates were employed to develop cardiac patches consisting of PGA or collagen⁵³⁶. As cultures evolve, specific reactors are being designed to produce stimuli.

It is crucial to remember that the culture and tissue-specific factors are **dynamic**. The tissue culture process is not stable, and specific characteristics are dynamic. A BR design must provide optimum tissue or organ growth and development conditions. It includes a control unit (a computer or a microcontroller) and input and output devices that keep the culture material fresh⁵³⁷. Sometimes, it also has sensors that monitor the tissue development inside the BR.

9.4. Sensors

Most bioprocesses are divided into cells (solid phase), disseminated in a liquid-medium phase, and aerated by a gas phase⁵³⁸. The relationships between these three phases are intricate. Biological components are frequently susceptible to environmental changes (e.g., pH, temperature, partial pressure of dissolved oxygen -pO₂-, nutrients), which might harm cell activity or process repeatability⁵³⁹.

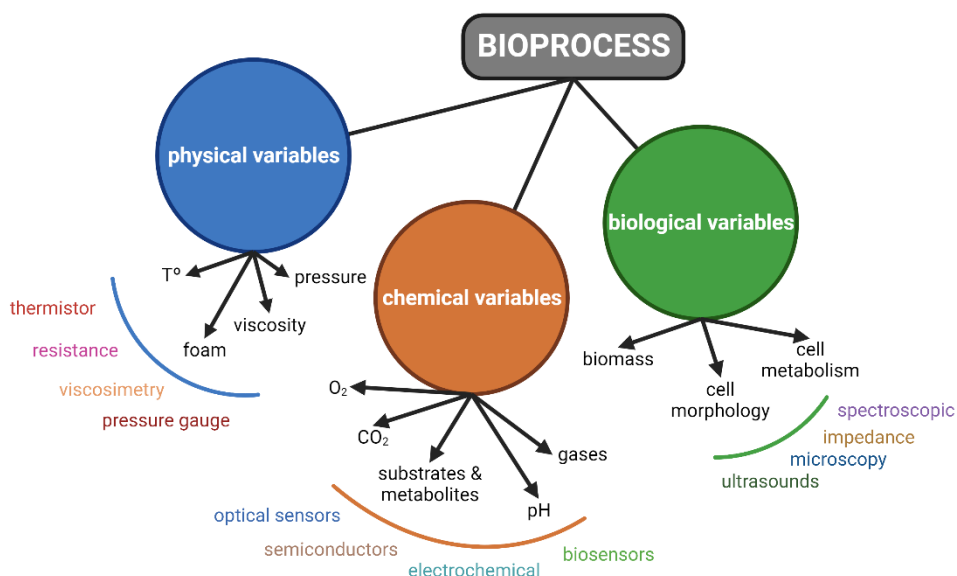


Figure 41. A spider diagram of the diverse bioprocess variables and their most common applied sensors.

For monitoring bioprocesses, three different categories of variables must be measured: physical variables (such as pressure, temperature, viscosity, and density), chemical variables (such as pH, pO₂, nutrients, and metabolites), and biological variables (biomass, concentration, cell metabolism)^{540,541} (**Figure 41**). The three main categories of sensor applications are in-line, at-line, and off-line⁵⁴². In-line or in-situ sensors directly contact the process media and the reactor. At-line systems relied on a sample taken out of the BR and examined elsewhere⁵⁴³. If data are continually captured and the sensor signal's reaction

INTRODUCTION BIOREACTORS

time is quick compared to the process dynamics, the measurement of in-line or at-line sensors can be regarded as on-line⁵⁴³. On-line sensors are not invasive but require that the sensor signal's reaction time has to be minimal concerning the dynamics of the process to have a small signal-to-noise (S/N) ratio⁵⁴⁴. **Figure 42** clarifies this classification.

9.4.1. Gas phase monitoring

To record exchanges in the gas phase inside the BR, semiconductors, electrochemical cells, and paramagnetic sensors are used. Semiconductors rely on the ionic conductivity of a semiconducting oxide, such as zirconia⁵⁴⁵. Electrochemical galvanic cells are composed of an anode and cathode, commonly silver and lead⁵⁴⁶. Paramagnetic sensors use paramagnetic gases' high attraction to magnetic fields⁵⁴⁷. The partial pressure and temperature fluctuations in the surroundings must be considered in these kinds of measurements.

9.4.2. Liquid phase monitoring

Biosensors for various analytes have been developed⁵⁴⁸. Biosensors enable accurate glucose and analyte monitoring^{549,550}. Biosensors face several issues, including sensitivity to pH changes caused by the detecting response⁵⁵¹.

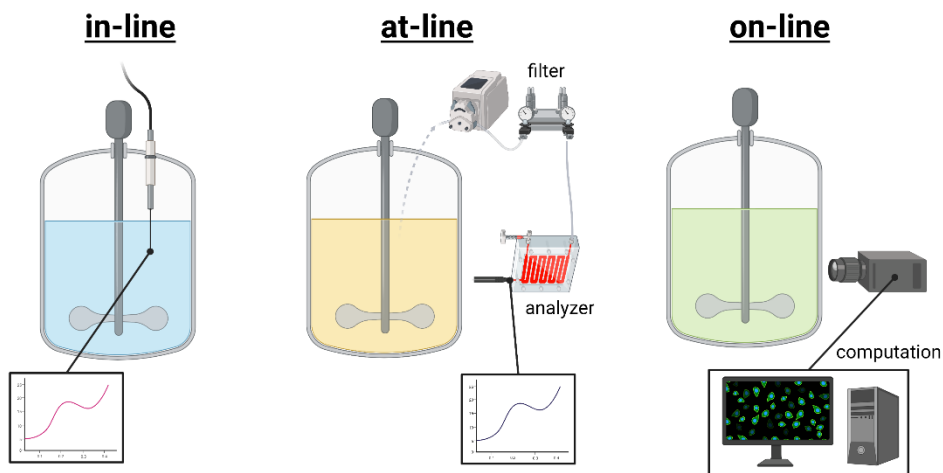


Figure 42. Classification of biosensors depending on their interaction with the BR.

Flow injection analysis (FIA) enables the creation of a predetermined reaction environment (for example, appropriate pH and dissolved oxygen content)^{552,553} by introducing chemicals into the FIA carrier stream, where samples can be diluted and preconditioned. Conventional electrochemical sensors (e.g., Clark-type electrodes, ISFETs, etc.) detect changes in electrical potentials⁵⁵³⁻⁵⁵⁶. The three most critical chemical parameters continually recorded by electrochemical sensors are the pO₂, dissolved carbon dioxide (pCO₂), and the pH value.

Usually, optical chemosensors are made by a matrix-embedded indication, and the analyte interacts to form optical chemosensor devices, also known as optodes⁵⁵⁷. Their function is based on a light source that immobilizes the indicator at the sensor's tip and illuminates it through a fiber optic wire (such as a light-emitting diode). The analyte concentration is related to changes in the optical properties of the indicator, such as photoluminescence intensity, absorption, or reflection. The opposite fiber end is attached to a light detector, such as a photodiode⁵⁵⁸; a dichroic mirror or optical filter separates the light's excitation and emission such that only one fiber may monitor both wavelengths.

On the other hand, spectroscopic sensors are based on the electromagnetic radiation emitted by molecules and their bonds; the different spectra measured can be found from UV to mid-infrared (MIR) and Raman spectroscopy⁵⁵⁹⁻⁵⁶². In contrast with optical chemosensors, no interaction between the sensor and the analytes allows parallel acquisition through sensor arrays.

9.4.3. Solid phase monitoring

Previous biosensors are perhaps the simplest to produce than those which measure the biomass. But, because cells and ECM are part of the solid phase, solid phase monitoring is the most critical aspect to control in a BR.

Optical density (OD) measurement, known as turbidity, is one of the most straightforward and widely used biomass monitoring procedures. In-line optical fiber probes based on transmission, absorption, reflection, or light scattering are

INTRODUCTION BIOREACTORS

available⁵⁶³. A sinusoidal electrical field can be used to assess the **impedance** of a cell suspension⁵⁶⁴. In situ microscopy uses microscopy systems directly in a BR (ISM). Image-processing techniques may capture images of suspended organisms and automatically examine cell concentration, size, dispersion, and shape⁵⁶⁵.

In medicine, **ultrasonic** transmissions are frequently employed. Ultrasonic therapy can acquire information on bioprocesses in addition to the well-known medical imaging, mixing, and emulsifying uses. The primary measuring parameters are sound velocity, attenuation, and acoustic impedance⁵⁶⁶. These factors may be used to identify pure liquids' chemical identity, the components' concentration in pure and mixed solutions, and particle sizes⁵⁶⁷. Sound velocity is estimated by measuring the resonance frequency or the time difference between different echoes over a certain distance⁵⁶⁸.

9.4.4. **Soft sensors**

Digital converters are attached to the sensors to convert the signal to binary digits to manipulate the data computationally^{569,570}. Soft sensors combine a measuring component (sensor) with a software-based estimating method⁵⁷¹. The software component makes predictions about process variables like substrate concentration and particular growth rates based on sensor data⁵⁷². Soft sensors can gather, consolidate, and analyze all data from probes that measure various process factors [8]. **Model-driven** and **data-driven** soft sensors are the two main categories mentioned in the literature. Data-driven soft sensors are based on chemometric models and predict other process variables on-line using past process data^{573,574}. The "First Principles" of processes, known as mass and energy balances, serve as the foundation for the model-driven soft sensors⁵⁷².

9.5. Types of bioreactors

Suspension BRs and attached BRs are the two primary categories into which BRs are often divided. Attached BRs reproduce bioprocesses where cells are bound or immobilized, whereas suspension BRs duplicate bioprocesses where cells are. Regarding mechanotransduction pathways, tissues react at two levels according to mechanical stimuli: macroscopic and microscopic. Thus, it is not uncommon to differentiate BRs depending on the methods of physical stimuli (**Figure 43**).

Spinner flask BRs laid in higher nutrient support in comparison with purely diffusional transportal (2D cultures), which results, for instance, in an increase in osteoblastic marker alkaline phosphatase (ALP)⁵⁷⁵. Rotating Wall Vessel BRs is an extensive example of characteristic stimulation under a microgravity environment where small shear stresses can interact with the graft sources⁵⁷⁶. Perfusion BRs also produce flow shear stress without altering the conventional gravity; besides, depending on the flow rate, those shear stresses making mandatory to precisely control such parameters⁵⁷⁷⁻⁵⁷⁹. Hydrostatic

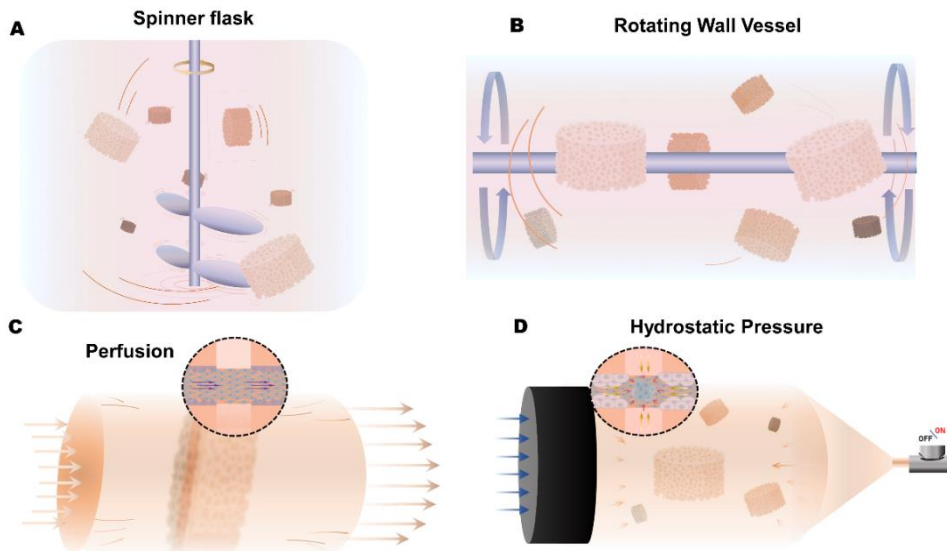


Figure 43. Basic types of BRs are classified depending on the kind of mechanical stimuli that they exert.

INTRODUCTION BIOREACTORS

pressure has been demonstrated to be beneficial for osteochondral tissue many times, and it takes place many times in our organism; BRs that use this mechanism should be prepared to maintain the increase in pressure without leak risks⁵⁸⁰⁻⁵⁸².

9.5.1. Bioreactors for mimicking pathological conditions and drug screening

The term biomimetic microsystems (Bio-MEMS) was first described by Ingber et al. (2010)¹⁴⁹, who defined this system as microchips oriented to *in vitro* drug screening processes made with poly-dimethylsiloxane (PDMS), see **Figure 44**. Different materials have already been used, like agarose⁵⁸³ and PMMA⁵⁸⁴. It is a non-toxic polymer and almost bioinert, making the perfect capsule for this system thanks to its transparency and biocompatibility. Depending on their complexity, these Bio-MEMS can be categorized into mini-tissue, organ-on-a-chip, and tissue/organ construct⁴⁴⁸.

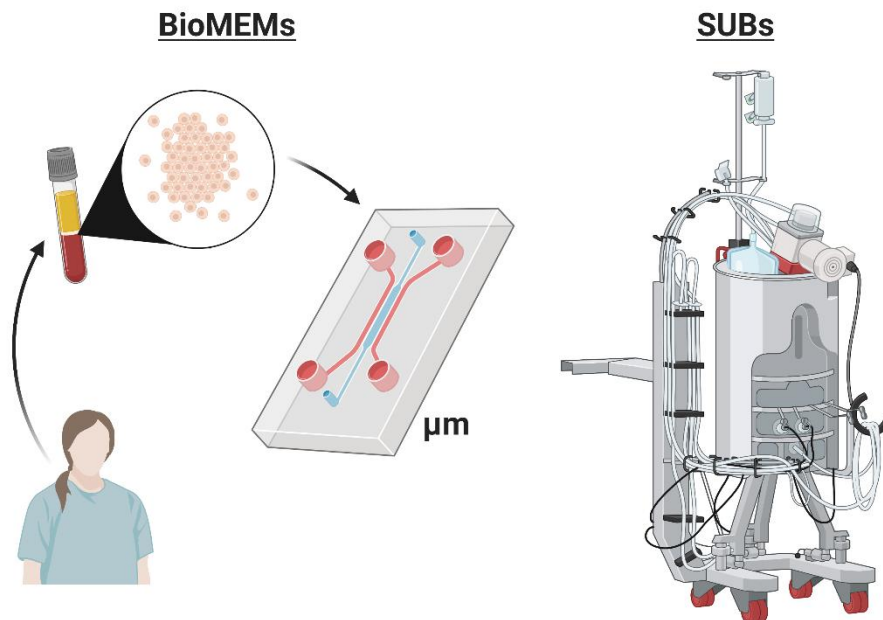


Figure 44. Bio-MEMs are chip kind BRs that can simulate tissues or organs. SUBs are very relevant BRs to produce TE products under sterile conditions.

Ultimately, they are a mixture of bioprinting products, BR, and bioinks, which have obtained a substantial relevancy thanks to the reproducibility of *in vivo* conditions and considering that any reduction of experimental time and animal costs are more significant than the inversion of these techniques.

9.5.2. Single-use bioreactors

Single-use BRs (SUBs) are becoming increasingly popular in the biopharmaceutical sector^{585,586} (**Figure 44**). They have replaced traditional stainless steel reactor systems in many manufacturing sectors, particularly for producing high-value goods in small numbers⁵⁸⁷. Because sophisticated and labor-intensive cleaning processes become unnecessary, disposable reactor technology provides enhanced facility flexibility with cheaper investment and energy costs, and a more straightforward production provided Good Manufacturing Practice (GMP) criteria are fulfilled⁵⁸⁸. SUB systems are swirled, shaken, or pneumatically blended to ensure adequate mixing of all nutrients inside the reactor system and effective gas exchange into the medium. Although primarily employed for mammalian cell culture, yeast, and other microbes have been grown in disposable bag reactors^{589,590}.

Table 2 lists the main applications of BRs; remarkably, most of them are specifically designed for each experiment, making a correlation with 3D bioprinting, where there is a lack of standardization.

Table 2. Compilation of the most suitable BR in RM research in the last 5 years.

Name	Tissue/Cell	Biomechanics	Year	Ref.
Custom-Made	Bone	Perfusion	2017	Beşkardeş et al. ⁵⁹¹
Very Large-Scale Liver-Lobule (VLSLL)	Liver	organ on a chip	2017	Banaeiyan et al. ⁵⁹²
Liver Acinus MicroPhysiology System (LAMPS)	Liver	Oxygen tension	2017	Lee-Montiel et al. ⁵⁹³
Two-leaflet model valves	Heart	Pulsed flow, valves	2018	Hu et al. ⁵⁹⁴

INTRODUCTION BIOREACTORS

Custom-Made	Bone	Hydrostatic Pressure	2018	Stavenschi et al. ⁵⁹⁵
Custom-Made	Heart Valves	Perfusion	2018	Amadeo et al. ⁵⁹⁶
Custom-Made	Ear cartilage	Perfusion	2018	Duisit et al. ⁵⁹⁷
Custom-Made	Osteoarthritis Screening	Microenvironment (Perfusion, shear strain)	2018	Nichols et al. ⁵⁹⁸
Custom-Made	Cartilage	Bioacoustofluidics	2018	Jonnalagadda et al. ⁵⁹⁹
Instron HP bioreactor				
(Tissue Growth Technologies, Minnetonka, MN)	Nucleus Pulposus	Hydrostatic Pressure	2018	Shah et al. ⁶⁰⁰
Custom-Made	HUVECs	Perfusion, 2P-FLIM	2018	Shen et al. ⁶⁰¹
Custom-Made	Ewing Sarcoma	Mechanical Loads	2018	Marturano-Kruik et al. ⁶⁰²
Hydrostatic Pressure Bioreactor (TGT/Instron, USA)				
	Bone Marrow	Hydrostatic Pressure	2018	Reinwald and El Haj ⁶⁰³
Custom-Made	Cornea	Flow exchange and Air-liquid phase	2018	Schmid et al. ⁶⁰⁴
Custom-Made	Lungs	Gas exchange	2018	Engler et al. ⁶⁰⁵
Custom-Made	Vascular tissue (MSCs)	Rotatory Perfusion	2018	Stefani et al. ⁶⁰⁶
Custom-Made	Cartilage	Knee simulation	2018	Vaineiri et al. ⁶⁰⁷
T-CUP perfusion bioreactor	Cartilage	Perfusion	2019	Vukasovic et al. ⁶⁰⁸
Custom-Made and Spinner Flask	Bone	Shear Strain and Perfusion	2019	Tsai et al. ⁶⁰⁹
BOSE, TA Instruments®	Cartilage	Perfusion	2019	Theodoridis et al. ⁶¹⁰
PLLA-MTA membrane bioreactor	Neuronal-like	Capillary feeding	2019	Morelli et al. ⁶¹¹
Custom-Made	Heart	Dynamic stretch	2019	Beca et al. ⁶¹²
Custom-Made	Bone	Perfusion	2019	Yaghoobi et al. ⁶¹³

DOCTORAL THESIS DANIEL MARTÍNEZ MORENO

Custom-Made	hiPSCs (cell expansion)	Capillary feeding	2019	Greuel et al. ⁶¹⁴
Benchtop Bioreactor System	hPDCs	Perfusion and sensors	2019	de Bournonville et al. ⁶¹⁵
Advanced microphysiological systems (MPSs)	Liver	Microfluidic	2019	Bale et al. ⁶¹⁶
PBS-0.1 MAG (PBS biotech®)	MSCs (cell expansion)	Rotatory Well	2019	de Sousa Pinto et al. ⁶¹⁷
Custom-Made	Tumor constructs	Perfusion and Metabolic monitoring	2019	Karami et al. ⁶¹⁸
Custom-Made	MSCs (cell expansion)	Shear Perfusion Bioreactor	2019	Gharravi et al. ⁶¹⁹
Custom-Made	T1 murine breast cancer cells	Perfusion compatible with: FLIM and MRS	2019	Cox et al. ⁶²⁰
TC-3 Bioreactor System (Ebers Medical Technology, ESP)	Skeletal muscle	Stretch	2019	Turner et al. ⁶²¹
3DHFR perfusion platform	Bone Marrow	Perfusion	2019	Allenby et al. ⁶²²
Custom-Made	Mouse Tail Tendon Fascicles (MTTFs)	Tensile Load	2019	Raveling et al. ⁶²³
Cardiac Valve Bioreactor	Heart Valves	Hydrodynamic Performance	2019	Tefft et al. ⁶²⁴
Cyclic Strain Bioreactor	Tendon	Strain	2020	Deniz et al. ⁶²⁵
Custom-Made	Cartilage	Perfusion	2020	Silva et al. ⁶²⁶
Custom-Made	Heart	Perfusion	2021	Cetnar et al. ⁶²⁷
Custom-Made	Bone	Perfusion	2021	Zhang et al. ⁶²⁸
LiveBox1 bioreactor (IVTech, Massarosa, Italy)	Follicles	Microfluidic	2021	Mastrorocco et al. ⁶²⁹
Custom-made	Periodontal Ligament	Laminar flow	2021	Lin et al. ⁶³⁰

INTRODUCTION BIOREACTORS

Custom-made: CyMAD	Hydrogels	Magnetic compression	2022	Czichy et al. ⁶³¹
Custom-made	Bone	Fluid dynamic	2022	Mainardi et al. ⁶³²
Non specified	Cartilage	Hydrostatic Pressure	2022	Zhao et al. ⁶³³
Custom-made	Bone	Loading	2022	Zhang et al. ⁶³⁴
Sartorius Ambr 250 modular bioreactor	MSCs (cell expansion)	Automated Bioreactors	2022	Ho et al. ⁶³⁵
Custom-made	Cardiac Tissue	Perfusion	2022	Zhang et al. ⁶³⁶
Custom-made	Spheroids (cell expansion)	Automated Bioreactor	2022	Kronenberg et al. ⁶³⁷

10. Cartilage

10.1. Main aspects

Since cartilage is a flexible and avascular kind of connective tissue, it is believed that nutrients enter its cells by diffusion from the synovial fluid, which is a fluid containing a lot of blood plasma and joint tissue molecules (HA, PRG4)⁶³⁸. The developed and specialized version of chondroblasts, chondrocytes, are the cells that makeup cartilage. Similar to other tissues, chondrocytes arise from MSCs through a process called **chondrogenesis**⁶³⁹.

Depending on its composition and physiology, three types of cartilage can be observed in a human adult: **hyaline cartilage** is a translucent tissue composed of type II collagen and chondroitin sulfate that can be found in the articular joints, the nose, larynx, and the trachea⁶⁴⁰. **Fibrocartilage** is a mixture of white fibrous and cartilaginous tissue, resulting in a more rigid than hyaline cartilage but also has some elastic behavior⁶⁴¹. The ECM of the fibrocartilage has type I and II collagens in contrast with hyaline cartilage. Furthermore, it is the only cartilage structure that does not present perichondrium⁶⁴². It is widespread that when a scar is produced in a joint, fibrocartilage is formed to substitute the damaged hyaline cartilage⁶⁴³. **Elastic cartilage** (aka yellow cartilage) is very similar to hyaline cartilage, but its ECM contains large quantities of elastin, a very elastic protein⁶⁴⁴. It can be found in the larynges and external ear.

10.2. Anatomy

Anatomically, cartilage is a translucent, elastic tissue that varies in color from pale blue to yellow-white depending on subtype and collagen content (**Figure 45**). A layer of thick fibrous tissue covers the bulk of the cartilage, termed the **perichondrium**, except for the articular surfaces⁶⁴⁵. The

INTRODUCTION CARTILAGE

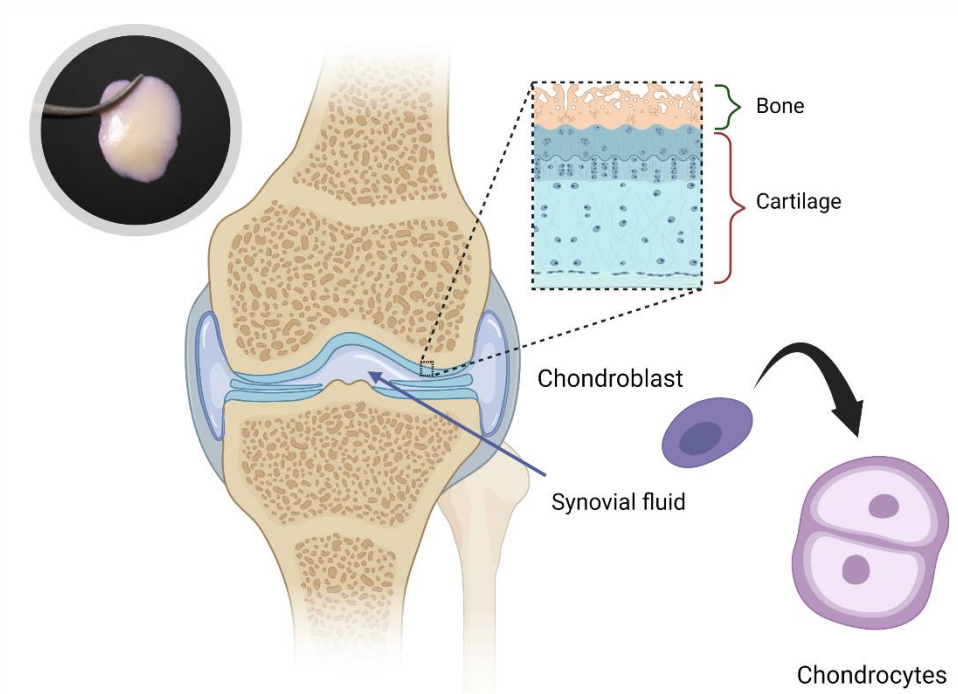


Figure 45. Image of human cartilage tissue. Graphical representations expose and example of hyaline cartilage in the knee joint. Chondroblasts are embedded in the perichondrium.

perichondrium's primary duties are to protect the bones, nourish the cartilage, and promote cartilage formation⁶⁴⁶. The perichondrium protects bones from short- and long-term injury, reduces friction, promotes suppleness in various body regions, and restricts outward expansion when the cartilage is crushed⁶⁴⁶. The fibrous perichondrium also includes blood arteries, which strengthen and nourish cartilage through long-distance diffusion, promote cell renewal, and speed up recovery after injury.

Because of perichondrium presence, all nutrients are delivered through diffusion; even the most significant animals follow this criterion, which restricts the thickness of cartilage surfaces to a few millimeters⁶⁴⁵. Due to pigment deposits from aging and dryness, cartilage changes from blue-white to yellowish and opaque as it matures. Radial collagen fibers that pass from the underlying bone into the cartilage *via* a challenging 3D interface are what hold the cartilage

to the underlying bone. However, the cartilage's specific collagen fibers do not penetrate the subchondral bone.

In addition, the inner layer of the perichondrium contains **chondroblasts**, cartilage-producing cells that aid in cartilage development (**Figure 45**). Chondroblasts generate the extracellular matrix, which is made up of a variety of elements that give cartilage its structure and strength. Chondroblasts also mature into **chondrocytes**, the cartilage's building blocks. At the edge of the cartilages, immature chondrocytes have an elliptic shape with a long axis parallel to the cellular surface. The curve becomes rounded as the frame turns inward.

Additionally, isogenous groupings of up to eight cells may include chondrocytes—cellular grouping results from the mitotic cell division of individual chondral cells⁶⁴⁷. The uneven form of cartilage is caused by the contraction of chondrocytes and their matrix during histological growth, which pulls the cells back into the capsule. Chondrocytes serve as factories for creating collagen and consistently fill the oblong lacunae seen inside tissues⁶⁴⁷.

10.2.1. Histology and surface characterization

Cartilage tissue under a microscope can be observed using histological dyes such as Alcian blue or specific antibodies against proteoglycans, chondroitin, keratan sulfate, or type I and II collagen stain photomicrographs of histological sections of various sample cartilages⁶⁴⁸. Another highly used dye for marking collagens is Sirius Red⁶⁴⁹. The significance analysis of microarrays (SAM) approach has also been utilized by researchers to identify samples of chondrocytes with limited chondrogenic ability⁶⁵⁰. These samples showed more significant amounts of insulin-like growth factor 1 and catabolic genes (aggrecanase 2, matrix metalloproteinase 2). Regarding membrane markers, flow cytometry examination revealed a considerable distribution of CD44, CD49c, and CD151 in chondrocytes with better chondrogenic ability. Furthermore, the data showed that CD151 and CD44 had the potential to identify

INTRODUCTION CARTILAGE

more chondrogenic clones. The tissues produced by chondrocytes with brighter CD49c or CD44 signal expression contained more type II collagen mRNA (3.4-fold max) and GAG/DNA (1.4-fold max) than non-brightened cells⁶⁵⁰.

10.3. Cartilage functions

Numerous roles of cartilage include its capacity to withstand compressive stresses, increase bone resiliency, and offer support to bony regions where flexibility is required⁶⁵¹. Because physical properties depend widely on the ECM composition, each kind of cartilage has a different function. Hyaline cartilage creates a robust surface with less **friction**; additionally, it does a great job of resisting **compressive stresses** at bone articulation points⁶⁵². Elastic cartilage delivers **flexibility** and is **pressure resistant**⁶⁵³. Fibrocartilage can struggle with high **tensions** and **compressions**⁶⁴².

Regarding general cartilage properties, **endochondral ossification** is required for skeletal development, particularly in preexisting cartilaginous models. The diaphysis, the area of a long bone between two ends that grows into the bone's shaft, is where the main ossification center first occurs in long bones⁶⁵⁴. Chondrocytes expand and hypertrophy at ossification sites, where cellular necrosis and matrix calcification occur⁶⁵⁵. The SOX9 transcription factor and the coactivator-associated arginine methyltransferase 1 (CARM1) play other roles in the regulation of osteochondral ossification^{656,657}. Long bones elongate at the junction of the diaphyseal and epiphyseal bones. Elongation is intimately connected to the proliferation of cartilage plates, which are made of collagen and chondral matrix and participate in endochondral osteogenesis and postnatal development⁶⁵⁸.

Chondrocytes frequently operate in low oxygen situations because it is an avascular tissue⁶⁵⁹. In contrast to the bulk of body cells, which use aerobic respiration to fuel cellular activity, hyaline chondrocytes use lactic acid fermentation to give energy⁶⁶⁰. Hyaline chondrocytes employ anaerobic

glycolysis to metabolize glucose, which results in the production of lactic acid at the end of the process. The deep-stored chondrocytes obtain the nutrients required for glycolysis *via* the perichondrium⁶⁴⁶. Two primary processes regulate nutrient movement: i) **diffusion** (as above exposed) and ii) occasional **compression** and **decompression** pumping of cartilage⁶⁶¹.

The chondral function also depends on proper endocrine balance⁶⁶². Somatotropin, also known as hypophyseal growth hormone, primarily controls cartilage development⁶⁶³. This hormone encourages the liver's synthesis of somatomedin C, which indirectly aids in forming chondrocytes. Growth hormone (GH), thyroxin, and testosterone speed up the creation of chondral proteoglycans made of sulfated GAGs^{664,665}.

10.4. Pathophysiology

As early exposure, chondrocytes maintain homeostasis, playing between the production and breakdown of ECM components. Chondrocytes produce these elements and the enzymes that break them down under the influence of environmental variables, polypeptide growth factors, and cytokines⁶⁶⁶. Any slight alteration in this delicate equilibrium will end in a specific pathology. Under pathological conditions, cartilage surfaces degrade mechanically and chemically, producing cartilage wear particles (CWP).

Joint biomechanics can also be affected by trauma to the synovial joint, such as meniscal tears, ligament ruptures, or cartilage damage^{667,668}. Production of CWPs prevents the systematic breakdown of such particles, which causes inflammation and triggers the release of degradative enzymes by chondrocytes^{669,670}. The ECM water content rises due to homeostatic disturbance while its proteoglycan content falls due to a decrease in type II collagen production and an increase in the breakdown of preexisting collagen; this change weakens the collagen network⁶⁶⁶. Depending on the origin of cartilage

INTRODUCTION CARTILAGE

degradation, the involved pathways and the affected cartilage can be distinguished by different pathologies (**Figure 46**):

- In **rheumatoid arthritis (RA)**, the body's immune system targets the synovial cells. RA often impacts both sides of the shoulders, wrists, fingers, knees, hips, feet, and ankles body⁶⁷¹. It is a chronic, progressive autoimmune condition that damages joint tissue by causing inflammation. Anti-inflammatory drugs like aspirin or ibuprofen are often used in treatment⁶⁷¹. RA patients may receive treatment with more potent immunosuppressants such as methotrexate and cyclosporine⁶⁷². Other drugs, such as TNF- α , explicitly work to decrease inflammatory cytokines⁶⁷². Additionally, surgery and more advanced gene therapy medications are options for treatment.
- Injuries to the cartilage can result in **perichondritis**, also known as perichondrium injury⁶⁷³. Microtraumas to the perichondrium tissue, such as piercings, insect bites, or burns, resulting in inflammation and, rarely, an infection commonly cause this⁶⁷⁴. Some symptoms, such as pain, redness, and swelling, may require medical intervention⁶⁷⁴.
- **Achondroplasia** is an autosomal dominant condition often resulting in dwarfism and defective endochondral ossification, turning cartilage into bone⁶⁷⁵.
- **Costochondritis**, an inflammation of the cartilage that connects the ribs to the sternum, is a common cause of chest discomfort⁶⁷⁶.
- Also possible are cartilage-based tumors, which can be benign or cancerous. Although these tumors seldom penetrate already-existing cartilage and often develop in the bone, they can do so⁶⁷⁷. **Chondromas** are benign tumors, whereas chondrosarcomas are malignant tumors⁶⁷⁸.

- In **osteoarthritis (OA)**, the whole articular joint is affected⁶⁷⁹. OA is less commonly considered a disease and is viewed as the consequence of "wear and tear" since it affects the most stressed joints (the knees, elbows, and hips)^{680,681}. The importance of this pathology in this work will be deeply discussed in the following chapter.

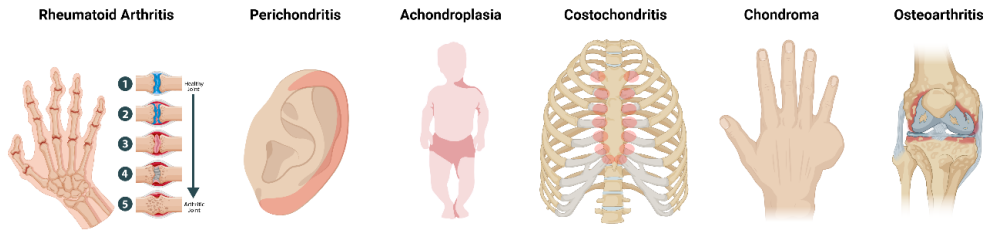


Figure 46. Most relevant pathologies present in cartilage tissues.

10.5. Chondrogenesis

Chondrogenesis is the process through which cartilage is produced from the **mesoderm** germ layer⁶⁸²; **Figure 47** represents a scheme of the whole process. The **β -catenin** levels control the percentages of lineage commitment to chondrogenesis and osteogenesis in the **Wnt signaling** system. This early development is when **bone morphogenic proteins (BMPs)** first appear. Endogenous chondrocyte development is regulated by: growth differentiation factor 5 (**GDF5**), **HOX gene** proteins, **TGF- β** , and other signaling molecules aided by BMPs⁶⁸³.

The cells in early mesenchyme are stellate or polymorphous, forming a network filled with a jelly-like, amorphous intercellular material⁶⁸⁴. MSCs can develop in various ways, but when destined to become cartilage, they form **condensations** due to multiple changes in the morphology of the component cells⁶⁸⁵. These cells grow spindlier or rounder, and the cytoplasmic to nuclear volume ratio decreases. MSCs appear to 'dedifferentiate' in producing such condensations, now known as cartilage **blastemata**⁶⁸⁶. The blastema cells subsequently secrete a homogenous hyaline intercellular material comprising

INTRODUCTION CARTILAGE

fibrils with a similar refractive index as the hyaline binding substance, which is not visible in conventional histological preparations⁶⁸⁶. The increased **sulfated mucoprotein** is linked to the formation of intercellular material in growing cartilage^{687,688}. As cartilage grows, it takes on various characteristics, including fibrous, hyaline, and elastic properties, which are dictated mainly by the fibers' makeup in the intercellular material.

The blastema's peripheral cells condense to produce a **bilaminar perichondrium**, the outer layer becoming fibrous. Simultaneously, the inner develops as a layer of densely packed, spherical, or polymorphous cells known as chondroblasts, responsible for the cartilage rudiment's appositional formation. Matured chondroblasts are chondrocytes distinguished from other cells because they can synthesize large amounts of chondroitin sulfate proteoglycan and type II collagen⁶⁸⁹. Chondrocytes are stable cells and are not thought to 'dedifferentiate' into pluripotent⁶⁹⁰. Since juvenile cartilage cannot grow by mitosis after initial chondrification, it grows primarily *via* evolving into a more mature condition. Cartilage's size and mass do not considerably alter after initial chondrification since there is little cell division in cartilage⁶⁵¹.

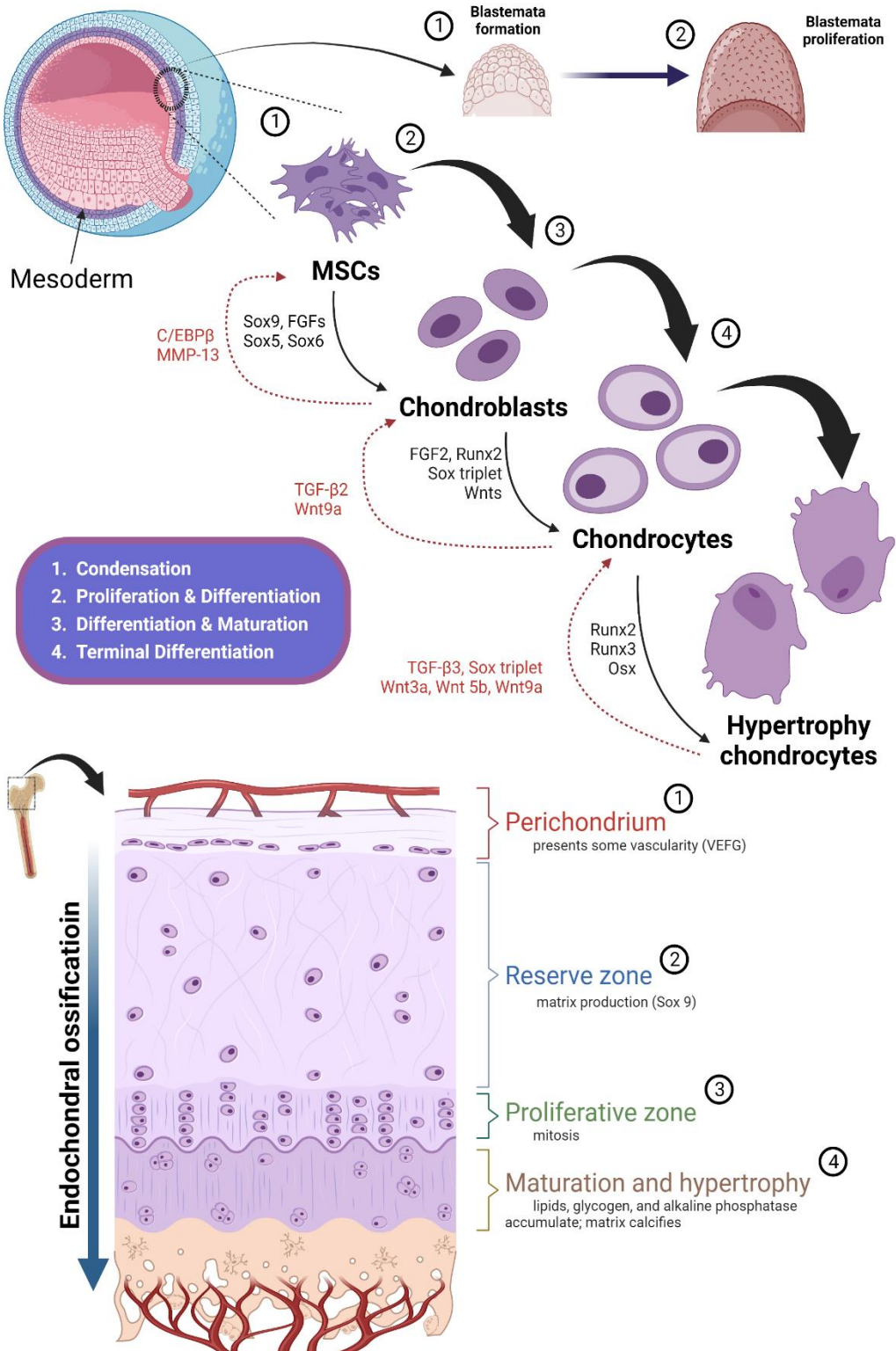


Figure 47. Graphical representation of the chondrogenic process and the endochondral ossification process.

INTRODUCTION CARTILAGE

10.5.1. Biochemistry of chondrogenesis

From the biochemical point of view, chondrogenesis occurs due to the condensation of MSC that expresses type I, II, and IV collagens, as well as the differentiation of chondroprogenitor cells⁶⁸⁴. These cells proliferate thanks to overexpression of type VI collagen and matrilin 1, which are under the control of the parathyroid hormone-related protein (PTHrP)/Ihh axis⁶⁹¹. During limb development, chondrocytes at the ends of the opposing bones stop their multiplication, resulting in hypertrophy and apoptosis and promoting endochondral ossification⁶⁵⁵. Endochondral ossification occurs when calcified hypertrophic cartilage is resorbed and replaced by bone. The hypertrophic zone is distinguished by the expression of type X collagen and matrix calcification⁶⁹².

Converting a non-vascularized and hypoxic tissue, such as cartilage, into bone; matrix remodeling through metalloproteinases (MMPs, 9,13 and 14)⁶⁹³ and vascularization through vascular endothelial growth factor (VEGF)⁶⁹⁴ are necessary. Sox9 and Runx2 are critical transcriptional regulators required for AC development and hypertrophic maturation^{656,695}. Additionally, Sox9 directly inhibits Runx2, and TGF- β and BMP signals differently control Wnt/ β -catenin signaling by activating Runx2⁶⁹⁶. Epidermal growth factor receptor (EGFR) signaling controls endochondral ossification in the growth plate⁶⁹⁷. TGF α , its ligand, inhibits the phenotype of articular chondrocytes by triggering the Rho-associated protein kinase (Rho/ROCK) and mitogen-activated protein/extracellular signal-regulated kinase (MEK)/extracellular-regulated kinase (ERK) signaling pathways⁶⁹⁸.

Due to the complexity of biochemical routes and metabolic cascade regulating chondrogenesis, below are explained the main molecules (or tissue growth factors, TFG) involved in chondrogenesis:

Indian hedgehog (Ihh). The discovery of the PTHrP/Ihh feedback loop contributed significantly to our understanding of growth plate regulation⁶⁹⁹. The interaction between PTHrP and Ihh determines when chondrocytes leave the

proliferative zone and enter the hypertrophic zone⁷⁰⁰. When the diffusion distances between PTHrP-producing cells become too long, the effector cells are no longer sufficiently stimulated by PTHrP, resulting in a delay in proliferation and the synthesis of *Ihh*, a hedgehog family member⁶⁹⁹.

Fibroblast Growth Factor (FGFs). Regarding skeletal development, the most common FGF members found in developing human cartilage are FGF1, FGF2, FGF17, and FGF19⁷⁰¹. Multiple FGFs and FGFR2 are expressed in condensing mesenchymal cells during the early stages of endochondral bone formation, which is thought to stimulate SOX9 expression⁷⁰². In the human growth plate, FGFR3 is expressed by proliferating chondrocytes⁷⁰³, whereas FGFR1 is found in pre-hypertrophic and hypertrophic chondrocytes⁷⁰⁴.

Bone morphogenetic proteins (BMPs) are a group of TGF- β superfamily that promote ectopic cartilage and bone development. The *Ihh*-PTHrP signaling loop incorporates BMPs⁷⁰⁵. They can induce *Ihh* expression, increasing chondrocyte proliferation. In the perichondrium, BMP2, BMP 3, BMP4, BMP 5, and BMP 7 are expressed; hypertrophic chondrocytes express BMP2 and BMP 6, whereas proliferating cells express BMP7⁷⁰⁶. Furthermore, BMP pathways restrict FGF signaling by limiting the expression of FGFR1 (fibroblast growth factor receptor 1)⁷⁰⁷. A BMP concentration gradient inside the development plate may be a crucial component responsible for the spatial modulation of chondrocyte proliferation and differentiation⁷⁰⁸.

Sox9. Sox proteins belong to the High-Mobility-Group (HMG) superfamily of DNA-binding proteins whose sequence is at least 50% similar to the sequence of the HMG domain of the sex-determining region on the Y chromosome of humans and other^{709,710}. In chondroprogenitor cells, the genes *Sox9*, *Sox6*, and *Sox5* coexpress, and there is solid evidence that these genes are essential for bone production^{711,712}. *Sox9* is required for mesenchymal cell clustering during early embryonic development⁷¹³ to express many extracellular matrix components, particularly types II, IX, XI, collagen, and aggrecan⁶⁸⁹. Later

INTRODUCTION CARTILAGE

in development, Sox9, mediated in part by Sox5 and Sox6, is required for chondrocyte proliferation and the alignment of proliferative clones into columns parallel to the longitudinal axis of the developing bone, indicating their importance in the growth plate proliferative zone⁷¹¹. The previous statement is further supported by the fact that the Sox5, Sox6, and Sox9 genes are silenced in hypertrophic chondrocytes⁷¹². Sox9 suppresses the transition of proliferating chondrocytes into hypertrophic chondrocytes in the proliferative zone of the growth plate and is thus implicated in the regulation of future endochondral ossification⁷¹¹; even, though there are pieces of evidence of BMP regulation by Sox9⁶⁸⁹. For all these reasons, Sox9 has a crucial function in the chondrogenesis of isolated human articular chondrocytes⁷¹⁴.

Runx2 promotes chondrocyte terminal differentiation, making room for ossification⁷¹⁵. Previous research demonstrates that Runx2 and Runx3 interactions with Ihh signaling are crucial for chondrocyte proliferation and differentiation⁷¹⁶.

10.6. Articular cartilage

AC is specialized hyaline cartilage with a 2-4 mm thickness. The ECM of AC can retain high quantities of water due to its abundance of sulfated GAGs, which possess strong hydrophilicity and negative charges⁷¹⁷. This property is intrinsically connected with the primary function that AC has, namely allowing movement without friction and counteracting the impact of compression forces applied onto the joint⁶³⁸. Given that AC is a viscoelastic "composite" dominated by two phases (**gel** and **solid**), it can respond to mechanical stimuli in two different ways: i) by deforming the porous matrix, which implies an increase in the number of contact points and a decrease of contact stresses; ii) by releasing interstitial fluid through the porous matrix consequently raising the lubrication of AC⁷¹⁸. Concerning biomechanics, a deep comprehension of the ECM components of AC is required beforehand:

10.6.1. Cartilage collagens

AC contains different collagens classified as fibril-forming or non-fibril-forming; types II and XI create fibrils, while types VI, IX, and X do not but contribute to the ECM structure. Type II collagen fibrils contribute to cartilage tensile strength⁷¹⁹. *In vitro* studies have presented how MSCs at early stages start synthesizing type I collagen, and after, once cell aggregates are formed, it is gradually exchanged to type II⁷²⁰. The thickness of its fibrils is controlled by the other collagen types and changes with cartilage depth; those less common collagens are crucial for the biomechanical behavior of the whole structure⁷²¹.

Type II collagen is the most prevalent in AC, accounting for 90-95% of the matrix's collagen. Type VI collagen is a type of microfibrillar collagen that creates elastic fibers and is found primarily in the pericellular zone of chondrocytes⁷²². Type IX collagen is fibril-associated collagen with interrupted triple helices that may serve as a bridge between collagen fibrils and aggrecan^{723,724}. Type X collagen is network-forming collagen, and while its function is unknown, it is mineralized in the calcified cartilage zone. Type XI collagen regulates fibril diameter and is attached to type II collagen to produce a mesh. The collagen fibrils are held together by cartilage oligomeric matrix protein (COMP), a 100,000-kDa protein found in cartilage and tendons with numerous binding sites⁷²⁵.

10.6.2. Proteoglycans

Other vital molecules involved in the composition of the ECM are the PGs, mainly aggrecan and, in lesser amounts, biglycan, decorin, and others (e.g., fibromodulin, lumican)²¹⁶. These uncommon PGs have been involved in the arrangement of the AC natural structure thanks to several interactions with type II collagen and TGF- β and keeping the fixed charge density constant which regulates water concentration⁷²⁶.

Aggrecan comprises a high molecular weight core protein with connected GAG side chains, primarily chondroitin sulfate and keratan sulfate. Its

INTRODUCTION CARTILAGE

geometry seems a cylindrical comb because SO_4^{2-} and COO^- groups repelled each other. This specific kind of GAG is primarily expressed in cartilage tissues, forming a dense network in addition to hyaluronan. This network is essential to understand AC biomechanical behavior due to its role in the **Gibbs-Donnan effect**.

Gibbs-Donnan effect

According to the Donnan ion distribution law, there are always more charged particles in the tissue than in the bathing fluid⁷²⁷. The fixed-charge density (FCD) of aggrecan pulls cations from the fluid phase due to its overall negative charge⁷²⁷. As a result of this difference in ion concentration, a positive osmotic pressure, known as Donnan osmotic pressure, is created, causing the matrix to expand⁷²⁸. This swelling force is counteracted by crosslinked collagen fibrils containing aggrecan; the collagen is put under strain, causing the cartilage to curl up⁷²⁹. When cartilage is compressed, the interstitial water gets pressured and bears a large percentage of the stress⁷³⁰. Cartilage tries to equilibrate the load levels by adapting osmotic pressure⁷³¹. When the load is removed, fluid returns to the aggrecan network.

Aggrecan is involved in the two principal functions of the cartilage from a biomechanical point of view: i) together with other molecules (i.e., chondroitin sulfate), it modulates the **fluid pressurization** (water permeability) of the tissue. Thus, the structure can be maintained, and the articular surface resists deformations allowing adequate lubrication *via* Donnan osmotic pressure effect⁷³²; ii) the concentration of aggrecan increases through the superficial zone and this gradient is correlated with the amount of extracellular water retention that **inhibits external compressions**⁷³³.

10.6.3. Glycosaminoglycans

In AC, keratan sulfate and chondroitin sulfate are the primary forms of GAGs⁷³⁴; both present a high ratio of sulfated groups (SO_4^{2-}). Disaccharide units, sulfation, and amino acid epimerization are differences between chondroitin and

keratan sulfate within their own family. In addition, chondroitin sulfate is about 20 kDa⁷³⁵, whereas keratan sulfate chains are between 5 and 15 kDa⁷³⁶. The biosynthesis and regulation of GAGs are both poorly understood. It has been demonstrated that cartilage contains more keratan sulfate as people age⁷³⁷. The depth of the cartilage also has an impact on the two GAG ratios. They reduce cartilage inflammation, possibly interacting with aggrecan in regulating the Donnan osmotic pressure⁷³⁸.

10.6.4. **ECM organization of AC**

AC is structured in a **superficial zone**, a **transitional zone**, a **deep zone**, and a **calcified layer**, all with distinctive compositions and cell populations (**Figure 48**). The *superficial zone* protects the rest of the layers from shear stresses and is in direct contact with the synovial fluid. Chondrocytes composing this region segregate a glycoprotein called *superficial zone protein* (SZP), conforming to a mucosa that reduces articular friction⁷³⁹. Next to the superficial zone is the *middle (transitional) zone*; its main action is to serve as a bridge between the superficial zone and deep zones⁷⁴⁰. In contrast with the layer above, collagen is obliquely oriented (compression resistance) among the tissue, whereas chondrocytes have a spherical shape and are highly dispersed and scarce⁷⁴¹. The *deep zone* is the bulk responsible for opposing any compressive force. Collagen fibrils are arranged perpendicular to the tissue surface. Even

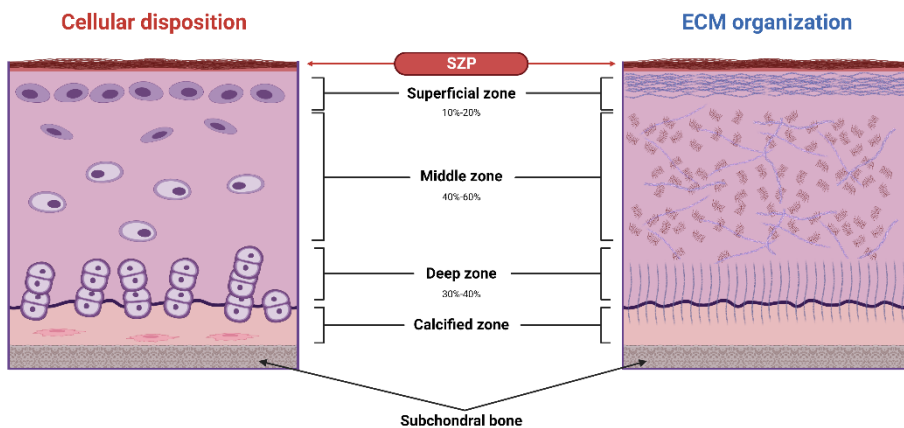


Figure 48. AC zones and their different cell distribution and ECM organization.

INTRODUCTION CARTILAGE

more, chondrocytes have columnar orientation parallel to collagen fibers⁷⁴¹. This region is also characteristic because its high PGs concentration implies low water concentration. Finally, a calcified layer attaches the cartilage to the adjacent bone⁷⁴².

In summary, ECM variations can be explained as water, and PG contents increase inversely with depth, from 84% to 40-60% and 15 to 25-20%, respectively. At the same time, the collagen content varies from 86% to 67% at the AC surface⁷⁴¹.

10.6.5. Mechanical aspects of AC

According to this biphasic hypothesis, cartilage comprises an incompressible, porous-permeable solid and incompressible viscous fluid⁷⁴³. When cartilage is loaded, the fluid-flow drag of the interstitial fluid with the concrete matrix balances the force exerted on the cartilage⁷²⁷. When modeled using biphasic theory, an indentation test generates three independent variables: the equilibrium compressive modulus, the Poisson's ratio, and the permeability. Thus, human AC has an aggregate modulus ranging from 0.53 MPa to 1.34 MPa, a Poisson's ratio ranging from 0.00-0.14, and a permeability ranging from $0.90 \cdot 10^{-15} \text{ m}^4/\text{Ns}$ to $4.56 \cdot 10^{-15} \text{ m}^4/\text{Ns}$ ⁷⁴⁴. The pore size of the solid matrix varies in a range between 30 to 60 Å⁷⁴⁵. Nevertheless, AC cannot be considered isotropic, depending not only on the joint but even on the zone of AC, as its properties differ; **Table 3** summarizes those variations. Also, AC mechanical properties are not equal between spaces, which has sense due to the exerted loads being also different⁷⁴⁶.

As explained earlier, one cartilage function is to reduce articular joint friction. Physically speaking, the squeezing film lubrication model suggests that loaded cartilage deforms to increase the load-bearing surface and decrease the movement of the lubricating fluid film⁷⁴⁷. Tensile hoop stress arises at the cartilage surface due to the radial movement of the interstitial fluid in the

cartilage layer, making the presence of surfactants like glycoprotein-I necessary to reduce those shear loads⁷⁴⁸.

Conclusively, AC is a very complex biomaterial from the biomechanical point of view, and it is evident that their adequate homeostasis also depends on external-internal physical equilibrium.

Table 3. Mechanical properties of different AC joints. H_A = aggregate modulus; ν_s = Poisson's ratio; h = thickness; μ_s = shear modulus.

Joint	H_A (MPa)	ν_s	h (mm)	μ_s (MPa)
Knee ⁷⁴⁹	0.60±0.2	0.06±0.07	3±1	0.28±0.07
Ankle ⁷⁵⁰	1.1±0.4	0.03±0.05	1.2±0.3	0.5±0.2
Hip ⁷⁴⁴	1.2±0.6	0.05±0.06	1.3±0.4	0.6±0.3
Elbow ⁷⁵¹	0.8±0.3	0.07±0.08	1.1±0.3	0.4±0.1

11. Osteoarthritis

11.1. Background

OA is the most representative degenerative disease related to the joints. It has been estimated that 250 million people worldwide suffer from knee OA (2012), a significant cause of pain and disability in adults⁷⁵². The Global Burden of Disease (GBD) estimated that OA approximates 0.6% of all disability-adjusted life-years (DALYs) and 10% in musculoskeletal conditions⁷⁵³. The pathological pathway leading to OA consists of a chronic low-grade degradation of AC, which is the primary driver of ongoing joint degeneration⁷⁵⁴. In such a way, OA should not be considered a disease but a typical end of multiple secondary pathways related to aging, possible traumas, obesity, and their correspondence altered biomechanics of the joint⁷⁵⁵. More and more researchers have supported this idea, which could seem ambitious in the last few years. Ganz et al. in 2008 first introduced the suggestion that the early steps of the OA process are related to biomechanical aspects of the cartilage tissue⁷⁵⁶; recently, other authors have experimentally confirmed this statement⁷⁵⁷.

Inside the biomedical research community, it is globally accepted that biomechanical properties of the tissue behave as a function of the ultrastructural organization, which depends on the biochemistry and cell-cell and ECM-cell interactions⁷⁵⁸ to such an extent that any slight alteration in these properties will drastically alter tissue biomechanics⁷⁵⁹. The central axis of the development of OA is a precedent of mechanical derangement that produces low-grade damage in the AC⁷⁶⁰. Thus, from the biomechanical point of view, three stages can be established in OA development: i) the proteolytic breakdown of the ECM, ii) the fibrillation and erosion of the cartilage surface, and iii) the beginning of synovial inflammation⁷⁶¹.

11.2. Definition

As a "whole joint" disease, OA causes pathologic changes in all tissues, including AC degradation, thickening of the subchondral bone, the production of osteophytes, synovial inflammation, and meniscal and ligament degeneration. The cartilage at the joint surface, where mechanical forces like shear stress are most prominent, shows the earliest alterations⁷⁶². The ordinarily dormant chondrocytes undergo a phenotypic change, becoming "active" cells that proliferate, form clusters, and produce more matrix proteins and enzymes that break down the matrix⁷⁶³.

Kellgren and Lawrence documented the first official attempts to create a radiographic categorization scheme for OA in 1957⁷⁶⁴. Kellgren looked at the inter- and intraobserver reliability of radiographic changes associated with rheumatism seen in the hand⁷⁶⁵ after researching rheumatism in coal miners at the Bedford Colliery in North West England⁷⁶⁶. KL attempted to create a categorization method with an accompanying set of standardized radiographs for OA of diarthrodial joints after establishing a significant discrepancy among various observers. Although a general description that includes cartilage lesions, osteophytes, bone marrow lesions (BMLs), synovitis, and effusion has been established (**Figure 49**)⁷⁶⁷, there is currently no accepted definition of OA analyzing the pathology under MRI. Thus, the standard KL definition establishes that the following statements must be observed:

For radiology^{764,768}:

- 1. It is necessary to form osteophytes on the joint margins or, in the case of the knee joint, on the tibial spines.*
- 2. Periarticular ossicles; were found chiefly on the distal and proximal interphalangeal joints*
- 3. Narrowing of joint cartilage associated with sclerosis of subchondral bone*
- 4. Small pseudocysts areas with sclerotic walls situated usually in the subchondral bone*
- 5. The altered shape of the bone ends in the head of the femur*

For MRI⁷⁶⁷:

INTRODUCTION OSTEOARTHRITIS

1. *Definite osteophyte formation*
2. *Full-thickness cartilage loss*
3. *Subchondral bone marrow lesion or cyst not associated with meniscal or*
4. *ligamentous attachments*
5. *Meniscal subluxation, maceration, or degenerative (horizontal) tear*
6. *Partial thickness cartilage loss (where complete thickness loss is not present)*
7. *Bone attrition*

11.3. Development of OA

Concerning genetics, OA presents polymorphisms or mutations in asporin, GDF5, secreted Frizzled-related protein 3 (sFRP3), deiodinase 2 (DIO₂), and mothers against decapentaplegic homolog 3 (Smad3) genes that may affect OA susceptibility⁷⁶⁹. These genes produce chemicals in the TGF-, BMP-, and Wnt signaling pathways (which maintain chondrocyte homeostasis and differentiation). In case of disruption, it would cause chondrocytes to reenact a molecular developmental program, including the expression of markers of chondrocyte hypertrophy, like COL10A1, MMP-13, and Runx2⁷⁶⁹. In OA cartilage, modifications in gene expression patterns unrelated to changes in DNA sequences have also been noted. Through processes involving microRNA and the epigenome, these modifications enable the cell to react quickly to environmental changes^{770,771}. Numerous studies have started investigating whether changes in the expression of specific miRNAs impact cartilage homeostasis^{772,773} as opposed to the OA disease state since miRNAs might have multiple downstream targets⁷⁷⁴.



Figure 49. Radiography of a healthy knee joint VS. an OA knee joint. Image obtained by permissions of Shivanand et al. ⁷⁶⁸.

AC surfaces degrade mechanically and chemically in an osteoarthritic environment, producing CWPs. Injuries to the synovial joint, such as meniscal tears, ligament ruptures, or cartilage damage, can significantly alter the biomechanics of the joint, leading to increased instability and roughness of the surface^{667,668}. The degree of the illness has been linked to changes in cartilage particle number and characteristics, including size and roughness^{669,670}. These early degradations result in cartilage thinning, worsening cartilage thickness, and superficial layer fibrillation, which, over time, resulted in the collapse of the AC (**Figure 50**)⁶⁷⁹. After this severe event, chondropathy develops a condition that exposes the underlying subchondral bone plate. Current research on the variety of cellular response patterns that define osteoarthritic cartilage degradation has concentrated on apoptotic chondrocyte death and the processes that underpin it⁷⁷⁵.

11.3.1. Biochemical and biomechanical pathways

Synovitis is a frequent symptom of RA. The primary site of cartilage breakdown by proteinases produced primarily by the synovium is the junction between the cartilage and the overlying synovial pannus also has a high presence in OA⁷⁷⁶. Inflammation is a significant risk factor for both cartilage loss progression and disease signs and symptoms⁷⁷⁷. Synovitis has been associated

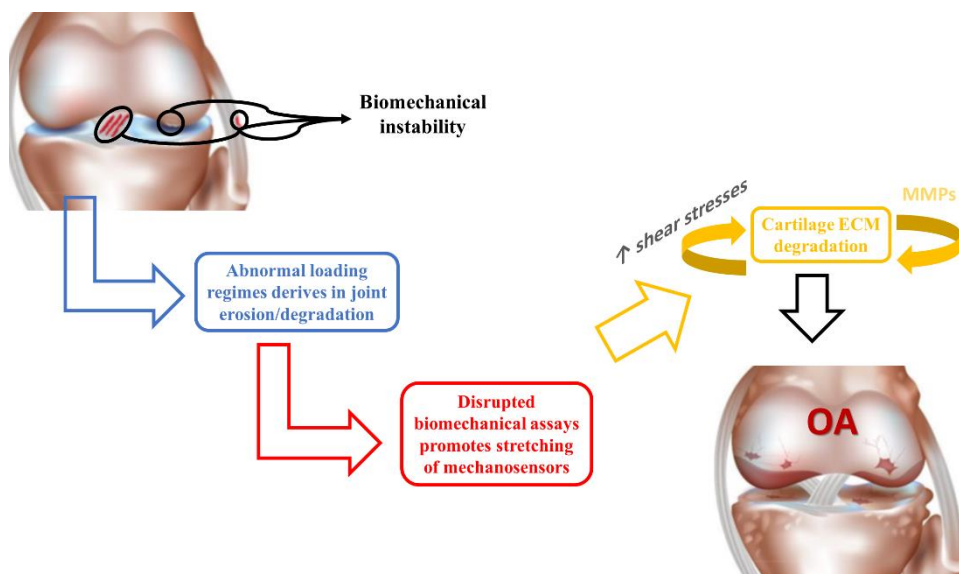


Figure 50. Osteoarthritis mechanical feedback cycle.

INTRODUCTION OSTEOARTHRITIS

with progression in OA⁷⁷⁸; it is unclear if synovitis precedes the beginning of symptomatic OA^{779,780}. **Figure 51** shows a schematic of the whole process regarding this question. Many studies have shown how the homeostatic balance of healthy cartilage is disrupted and leads to sickness. Proteolytic degradation of cartilage matrix proteins threatens cartilage's excellent physical properties, such as elasticity, compressive resistance, and tensile strength⁷⁸¹. In addition to biomechanical stressors, pharmacological and genetic factors have a role in the genesis and development of AC in OA⁷⁷⁵. They contribute to the breakdown of chondrocyte-ECM connections, which alters cell metabolism⁷⁸². Chondrocyte matrix gene expression is changed in OA because it contains collagen molecules (types X, III, VI) absent in healthy adult AC⁷⁸³.

At the beginning of OA, mononuclear cells infiltrate the synovial membrane and release proinflammatory mediators such as interleukin 1 β (IL-1 β), TNF, and chemokines in early and late-stage OA disease⁷⁸⁰. Synovial effusions in the joint can be seen *via* magnetic resonance imaging or US⁷⁸⁴. In patients with traumatic meniscal injury but no radiographic signs of OA, the synovium retrieved following arthroscopic meniscectomy is frequently inflammatory and has rising inflammation scores⁷⁸⁵. Therefore, shear stresses produced by friction between the adjacent bones of the articulation increases⁷⁸⁶. Anterior cruciate ligament (ACL) rupture is associated with an increased risk of developing OA in life⁷⁸⁷.

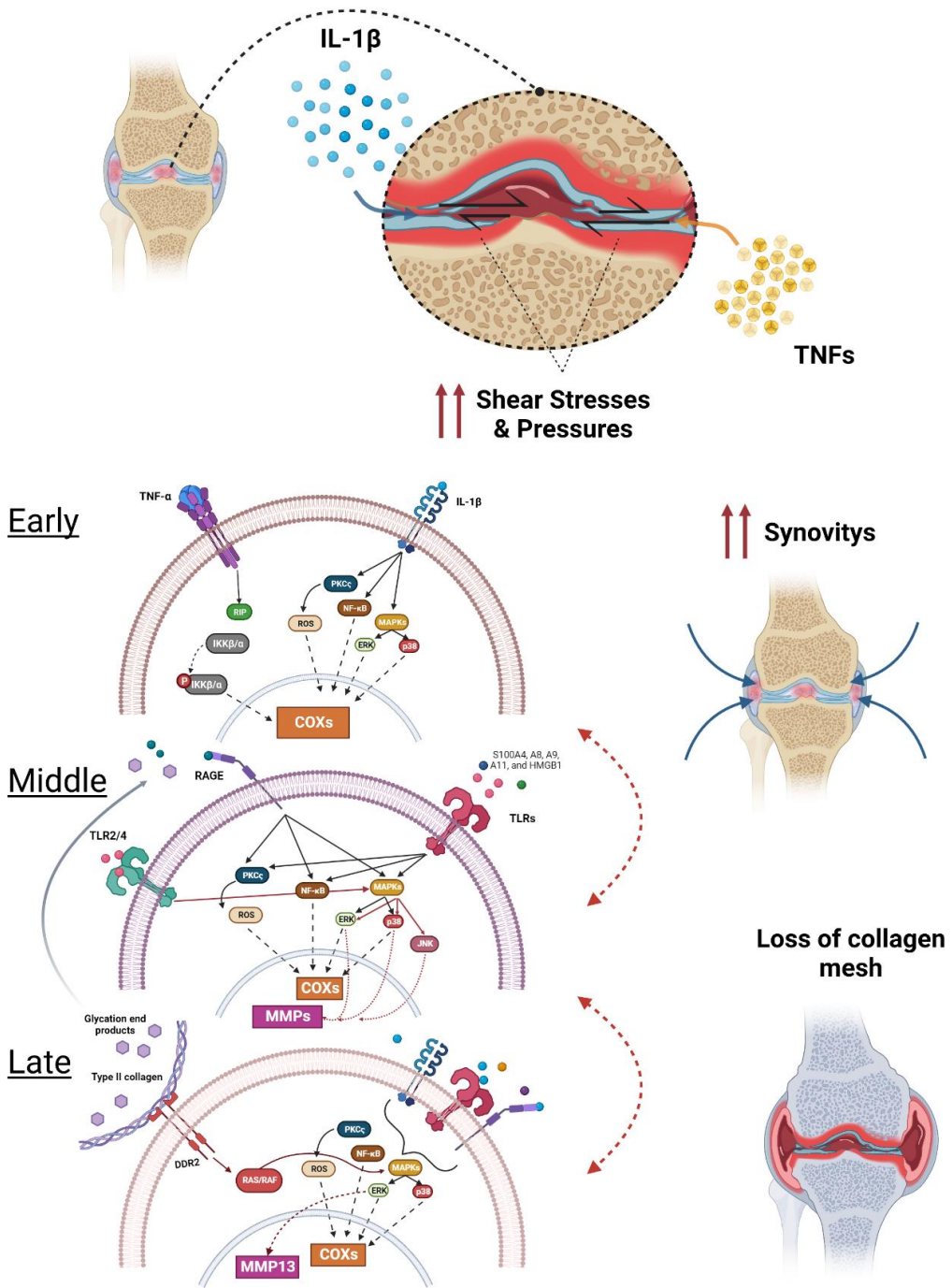


Figure 51. Schematic representation of the diverse biochemical and biomechanical pathways affecting OA joints.

INTRODUCTION OSTEOARTHRITIS

A study of the high abundance synovial fluid proteome found distinct patterns in healthy people compared to patients with early OA who underwent arthroscopy after medial meniscus injury and patients with late-received total joint replacement⁷⁸⁸. According to these studies, low-grade synovitis manifests preclinical disease throughout the early posttraumatic period and may impact long-term prognosis⁷⁸⁹.

Growth of bone spurs thereby progresses during disease development, leading to articular inflammation and joint pain⁶⁶⁷. In this state, the presence of IL-1 β and TNF- α ⁷⁹⁰ induces the synthesis of other inflammatory factors like cyclooxygenases (COX-1, COX-2)⁷⁹¹; mitogen-activated protein kinase (MAPK)⁷⁹², as the I κ -1 and -2 kinases⁷⁹³. Abnormal mechanical stress on cartilage induces catabolic and additional inflammatory processes *via* intracellular signaling pathways similar to those generated by oxidative stress, inflammatory cytokines, and matrix damage products⁷⁹⁴⁻⁷⁹⁶. Inflammatory cytokines also lower the expression of numerous genes associated with the differentiated chondrocyte phenotype, such as aggrecan (ACAN) and type II collagen (COL2A1)⁷⁹⁵. Canonical NF- β (p65/p50) and stress-induced and MAPK signaling must be activated for chondrocytes to create MMPs, a desintegrin and metalloproteinases with thrombospondin motifs (ADAMTSs), and inflammatory cytokines⁷⁹⁷.

Articular chondrocytes from OA patients exhibit phenotypic plasticity similar to MSCs undergoing hypertrophic chondrogenesis⁷⁹⁸; it may be a direct consequence of activating specific receptors in OA chondrocytes due to the positive feedback amplification event by innate immune responses⁷⁹⁹⁻⁸⁰¹. Some receptor activator molecules are the alarmins, particularly S100A4, A8, A9, A11, and HMGB1, which activate RAGE and TLRs to cause inflammation-associated matrix degradation and increase reactive oxygen species (ROS) *via* upregulating cytokines and chemokines^{802,803}. OA chondrocytes also express chemokine receptors, including CXCR3, CXCR4, CXCR5, and CCR6⁸⁰⁴, as well as chemokines

like IL-8⁸⁰⁵, macrophage inflammatory protein 1 (MIP)-1 β ⁷⁹⁸, GRO⁸⁰⁶, monocyte chemoattractant protein 1 (MCP-1)⁸⁰⁷, and RANTES⁸⁰⁸ which may play essential roles in catabolic pathways and chondrocyte hypertrophy. Toll-like receptors (TLRs) and OA chondrocytes express the receptor for advanced glycation end products (RAGE); the secreted damage-associated molecules may act as TLR or RAGE ligands to activate inflammatory and catabolic processes in AC⁸⁰⁹⁻⁸¹¹. Further, TLR2 and TLR4 lead to increased expression of inflammatory and catabolic genes such as MMP-3, MMP-13, and NOS2 *via* the cytosolic adaptor myeloid differentiation factor 88 and subsequent N-B signaling⁸¹². MMP-13 inhibits the β -activating inhibitor of kinases (IKK α and IKK β)^{813,814} and produces changes in the expression and cellular localization of regulators such as Runx2, β -catenin, and Sox9⁸¹⁴.

Thus, the early try to restore cartilage homeostasis results in the leakage of proteoglycans and the breakdown of type II collagen, which starts at the cartilage surface⁸¹⁵. Consequently, the water concentration increases, implying a critical reduction of the tensile strength of the ECM⁷⁸². The posterior step is aggrecan degradation produced by aggrecanases 1 and 2 (ADAMTS4 and 5), a family of the ADAMTs attached to type 1 thrombospondin (TS1)⁸¹⁶⁻⁸¹⁸. The collagen network was partly shielded from destruction by the collagenases MMP-1, 8, and MMP-13 (collagenases I, II, and III) until the proteoglycan layer was removed when the collagen network degraded. In addition, discoidin domain receptor 2 (Ddr2) is overexpressed in OA condition, and OA chondrocytes expressing this receptor probed and induced expression of MMP-13, accelerating the type II collagen proteolysis⁸¹⁹, causing an irreversible point that ends in AC total degradation⁸²⁰.

12. Cartilage Tissue Engineering

12.1. Background

Concerning AC treatment history (**Figure 52**), Pridie's resurfacing approach (1959) was used to treat AC abnormalities for the first time, which was motivated by the fact that entire thickness defects could be repaired⁸²¹. After the first identification of bone marrow MSCs⁸²², some bone marrow stimulation procedures, such as subchondral drilling⁸²³ and arthroscopic abrasion⁸²⁴, were developed. After, the microfracture technique became popular because of its low cost, short and uncomplicated procedure, and brief recovery period⁸²⁵⁻⁸²⁸. Younger patients had a stronger proclivity to repair, most likely owing to MSC regeneration potential diminishing with age⁸²⁹.

Graft transplantation for the treatment of cartilage disorders became popular in the 1970s^{830,831}. It resurfaced as an autograft or allograft in the 1990s, depending on the origin of the graft⁸³²⁻⁸³⁴. Autologous grafting has significant downsides, such as a shortage of accessible tissue and donor site morbidity⁸³⁵. Oppositely, allografts can be employed for more substantial defect sites, but they also raise the prospect of graft against host immunological responses and the chance of organ rejection⁸³⁶. Mosaicplasty has been used to enhance the integration of two tissues in treating minor to medium-sized abnormalities⁸³⁷⁻⁸³⁹. This procedure involves drilling several tiny full-thickness flaws into which autografts from a non-load-bearing donor site are implanted⁸³⁷. Due to the difference in mechanical properties between cartilages, naïve joint properties are not achieved⁸⁴⁰. The chondral grafts fail to integrate correctly in lateral and bottom integration when the subchondral bone is not connected⁸⁴¹.

Brittberg and colleagues presented the first cell transplantation procedure for AC repair in 1994: autologous chondrocyte implantation (ACI)⁸⁹.

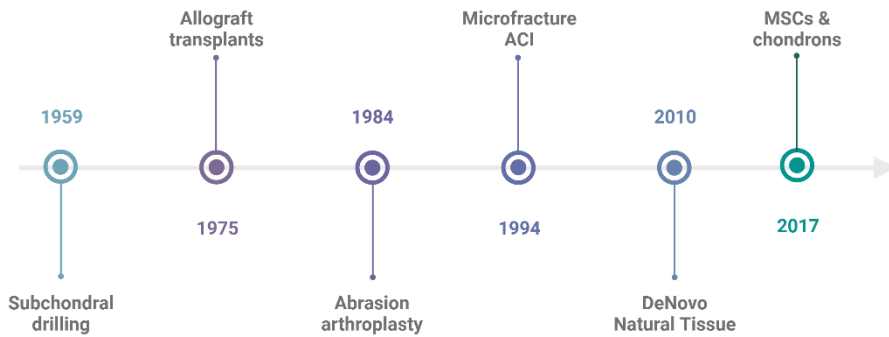


Figure 52. Time-line of CTE.

The original procedure involves transplanting *in vitro* culture-expanded chondrocytes from a biopsy collected from a non-load-bearing region under a periosteal flap. Re-operation rates owing to periosteal graft hypertrophy ranged between 10 and 20%^{842,843}, with some instances reaching almost 40%⁸⁴⁴. This inflammation replaced the periosteal flap approach with a collagen membrane to reduce the problem⁸⁴⁵⁻⁸⁴⁷. Chondrocyte transplantation is considered the gold standard in AC healing for patients with substantial injuries (up to 12 cm²) or when microfracture fails⁸⁴⁸⁻⁸⁵⁰. The second-generation ACI (MACI) uses a bioabsorbable 3D scaffold and is employed as a cell carrier for implantation into the location of the defect⁸⁵¹.

Alternative to conventional ACI, a non-culture-based technique is used to transport chondrocytes to the site of damage⁸⁵². A similar amount of cartilage was manually chopped and integrated into a fibrin-coated polymeric scaffold as was utilized for the ACI. The device was implanted in a full-thickness chondral defect model from a goat⁸⁵².

Frisbie et al. (2009) demonstrate in a horse knee joint chondral lesion that ECM may be generated from cadaveric cartilage cubes (DeNovo Natural Tissue)⁸⁵³. This procedure's first human case report described pain alleviation, full defect filling, and virtually complete healing of preoperative subchondral bone edema after 2 years postoperatively⁸⁵⁴. The interim findings of prospective,

single-arm cohort research were compared to the outcomes of microfracture and first-generation ACI⁸⁵⁵. In 2017, an allogenic MSCs one-step method can give proof of stable repair tissue while significantly lowering the cost of an ACI treatment⁸⁵⁶. The Instant MSC Product Accompanying Autologous Chondron Transplantation (IMPACT) trial employed in situ qualifying fibrin glue containing allogenic MSCs in a 90:10 or an 80:20 ratio with autologous chondrons⁸⁵⁷.

However, existing bioengineered neocartilage is far from ideal compared to mature equivalent. The remark mentioned above is that it is challenging to design a construct that accumulates anisotropy and homogeneity in its structure, resulting in typical AC mechanical qualities⁸⁵⁸. The original AC is replaced with mechanically inferior fibro-cartilaginous tissue in these ways^{840,859}, and all of the treatments reported thus far have failed mechanically, which may limit the intervention's efficacy⁸⁶⁰. As a result, the primary difficulty in bringing cartilage TE (CTE) to the clinic is to develop biomechanical qualities of the final implant that are similar to natural tissue.

12.2. Cell source: mature chondrocytes or MSCs?

Autologous chondrocytes are not the best cellular source for making this autologous explant since the percentage of these cells inside the AC is less than 5%, among other drawbacks. In addition, during the time of *in vitro* expansion, monolayer cell cultures present an overexpression of type I collagen and versican in lieu of type II collagen and aggrecan production⁸⁶¹. This process, by itself, results in a reorganization of the microfilament structure of the 3D ECM, implying that biomechanical stresses of the microstructure, which are crucial for the correct tissue performance, change⁸⁶².

On the other hand, MSCs have demonstrated a real potential in differentiating healthy chondrocytes⁸⁶³. In addition, MSCs promote chondrocytes' resilience when co-cultured *in vitro*⁸⁶⁴. But not everything in the

field of MSCs is an advantage. Nowadays, no conventional cell therapy approach is approved for therapeutic interventions⁸⁶⁵, although the use of MSCs derived from the umbilical cord for AC treatment has been approved within the last year. Even more, the differentiation potential of MSCs is age-dependent, being a limitational factor for autologous implants⁸⁶⁶.

12.3. Biomaterials for cartilage tissue engineering

Among biomaterials applied in CTE, it can be found **synthetic polymers** like PLA⁸⁶⁷ and PCL⁸⁶⁸, **polysaccharide gels** like agarose^{869,870} and alginate^{871,872}, as well as **protein-based materials** such as collagen, gelatin, and fibrin gels⁸⁷³⁻⁸⁷⁶.

Materials have been created as macroporous structures to allow cell seeding into their porous sections, hydrated polymeric networks, and hydrogels, enabling cell embedding. The influence of the synthetic network composition is crucial in the early moments of chondrogenesis when chondrocytes have not yet formed their matrix⁸⁷⁷. The creation and accumulation of a cartilage ECM are influenced by network density, degradation, and stiffness, which vary significantly⁸⁷⁸⁻⁸⁸¹. The impact of matrix structure and mechanical factors in a controlled environment has been studied using synthetic hydrogels. Despite this, these blank matrices do not fully replicate ECM's chemical and biological properties. An appealing approach is to improve the function of natural materials by adding AC ECM components such as collagen^{882,883}, HA^{884,885}, and chondroitin sulfate^{886,887}. Chitosan, a polycationic polysaccharide, has shown various interesting therapeutic features, including the potential to increase GAG synthesis and promote aggrecan and collagen type II formation^{888,889}.

The natural evolution of previous technology is that the actual cartilage ECM for regeneration might be provided by **dECM material**⁸⁹⁰. MSCs embedded in dECM grafts have already probed their *in vitro* capacities to induce chondrogenesis regarding cell proliferation and type II collagen gene

expression⁸⁹¹. In addition to dECM molecules, TGF- β 3 has been used in these materials (as microparticles) to stimulate chondrogenesis^{892,893}. Crosslinking collagen or combining natural ECM components with synthetic polymers is thought to be beneficial in solving the weak mechanical properties of dECM grafts^{894–899}. Another disadvantage of the ECM cartilage-derived scaffold is cell contraction during *in vitro* culture, implying the use of physical and chemical crosslinkers in the mixture⁹⁰⁰. Thus, although dECM gels have demonstrated high potential, more research is needed to evaluate the therapeutic uses of this biomaterial method⁸⁹².

12.3.1. Scaffold architecture

Chondrocytes are implanted in their lacuna inside normal AC, where they maintain a **spherical shape** and **no stress fibers** are present. Chondrocyte separation from AC and traditional monolayer cultures result in phenotypic alterations linked with cytoskeleton modifications during tissue processing. In 2D monolayer culture (**Figure 53**), chondrocytes resemble fibroblasts in form and feature stress fibers in their cytoskeleton^{901–903}. Scientists have discovered that most chondrocytes within sponge scaffolds retain their spherical shape⁹⁰⁴, implying a correlation between this cellular arrangement and the surface area of tiny scaffold fibers and fiber distance⁹⁰⁴. On aligned electrospun nano- and microfibrous PCL scaffolds, cell orientation and chondrogenic ability of human MSCs were examined. Cells seeded on **nanofibrous** PCL scaffolds revealed dramatically increased GAG deposition and type II collagen mRNA expression⁹⁰⁴. Type I and type II collagen fibers were used to create a five-layer scaffold (by electrospinning) that encouraged the migration and differentiation of human BM-MSCs⁹⁰⁵.

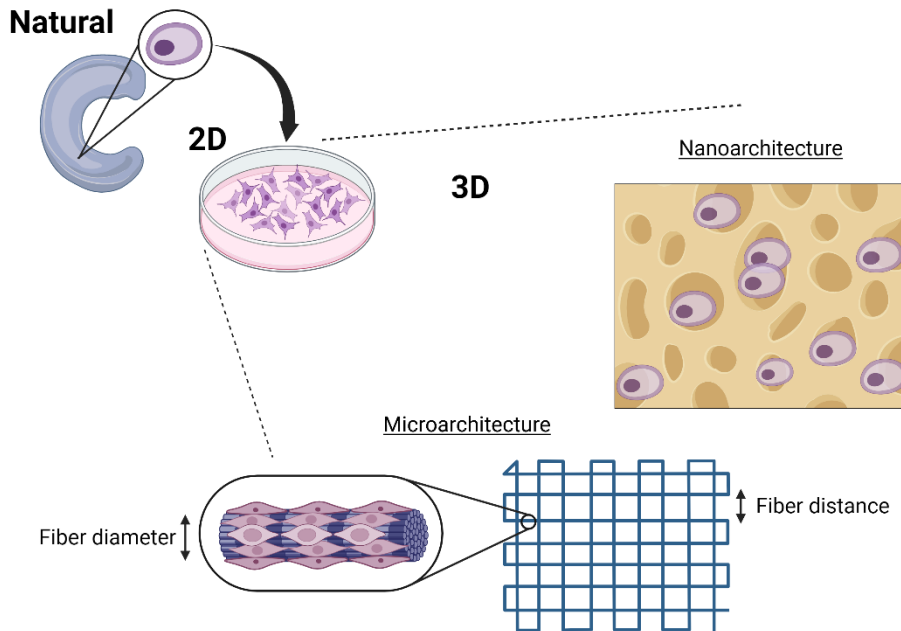


Figure 53. For CTE, it is very important to adequate the architecture of the final graft because it will affect cell metabolism.

Elisseff's group was the first to show that the interaction of chondrocytes from various zones influences tissue-produced products' biological and mechanical aspects⁹⁰⁶. To stimulate MSC proliferation and differentiation, **bi-zonal cartilage** TE was recently performed utilizing a thermoresponsive hydrogel based on chitosan-g-poly(N-isopropyl acrylamide). Results exposed a precise alignment of the cells recreating the macroscale of AC tissue⁹⁰⁷. An AC **layer-mimicking** gel reinforced with nanofibers of PLA and hydroxyapatite has shown upregulation of Sox9 and PRG4 in the superficial layer-mimicking gel, the maximum expression of type II collagen, aggrecan, and GAG content in the mid-layer-mimicking gel, and calcified cartilage in the final gel⁹⁰⁸. Conclusively, any approach mimics the cartilage compositional and zonal structure presents a higher potential for practical clinical application⁹⁰⁹⁻⁹¹¹.

12.4. Biomechanics for *in vitro* cartilage development

The articular chondrocyte is the mechanical unit of cartilage that governs genetic responses under physiologic joint loadings, such as shear stress, osmotic pressure, compression, tension, and hydrostatic pressure²⁷⁹. It is contained in a chondron, a thin pericellular matrix (PCM) within the AC ECM that transfers stresses between the cartilage and the surrounding environment⁹¹².

Mechanosensors in chondrocytes and osteoblasts include transient receptor potential vanilloid 4 (TRPV4), Piezo1, and Piezo2^{913–915}. Bone and cartilage tissue are very related, and both present an acute mechanosensitivity to maintain homeostasis: suppression of Piezo 1 is related to osteoporosis⁹¹⁶, and TRPV4 mediates the anabolic response of chondrocytes to osmotic or mechanical stress⁹¹⁷. The differential orientation of chondrocyte primary cilia in AC vs. those in epiphyseal cartilage suggests the possibility of directed mechanical signals for proliferation and directional synthesis of ECM in response to compression^{912,918}. In health and illness, chondrocytes are exposed to various mechanical stresses and can respond precisely to different mechanical stimuli to control metabolism and matrix synthesis^{278,279,912}.

Among all possible mechanical stimuli applied to cartilage cells in TE, the most reliable ones are hydrostatic pressure, direct compression, and the application of fluid shear stresses. Dynamic, cyclic, and hydrostatic pressure have all been demonstrated to increase the transcription and translation of the ECM proteins aggrecan and type II collagen, whereas static compression decreases both^{919,920}. A similar effect is observed under shear stresses where excessive stress deregulates NFκB⁹²¹, whereas, under controlled shear stresses, higher ECM synthesis is observed⁹²². Thus, a deeper understanding of these mechanisms is necessary to success the objectives of this work.

12.4.1. Hydrostatic Pressure

AC is a highly hydrated tissue (70-80% of water content), so the entrapped water will “resist” the deformation when applying external compression. Translated to the cells, this results in an over-exerted force that will be homogeneous along the whole cell surface producing isotropic deformation and hydrostatic pressure (HP)⁵⁸⁰. Regarding how HP and cartilage interact, various studies have suggested a direct correlation between the HP stimulation on the cells and the behavior of cell membrane channels⁹²³. Despite the fact that HP does not imply a measurable deformation in the cartilage tissue, it interacts with the transporter proteins compressing the void spaces created by the folding orientations of these complexes⁹²⁴.

It has been found that the Na/K pump is dramatically constrained under a static HP load (2.5-5 MPa) or even completely suppressed under 50 MPa^{923,925}. It also inhibits Na/K/2Cl transport activity. On the other hand, Browning et al. showed that Na/H pump activity was increased, and they also found that HP modulates the phosphorylation of the pump⁹²⁵. Mizuno discovered that exercising an HP in the middle zone of the cartilage results in an expansion of the intracellular calcium concentration (Ca^{2+}) due to the stretching of activated calcium channels⁹²⁶.

The usual range of stresses affecting any given common lie between 3-10 MPa, but can reach up to 18 MPa, the maximum measured stress at the hip joint⁹²⁷. In addition, the frequency of these stresses when walking is 1 Hz in humans⁹²⁸. Some authors have studied the relevance of these parameters by applying an HP in the TE of cartilage tissue. For instance, studying responses of monolayer cultures to HP, Suh et al. identified an increase of 40% in proteoglycan synthesis after applying 0.8 MPa alternating function times⁹²⁹. In addition, Jortikka et al. demonstrated that the GAG absorption rises due to an HP at 5 MPa and 0.5 Hz (dynamic compression) in contrast with static compression⁹³⁰.

INTRODUCTION CARTILAGE TISSUE ENGINEERING

Dynamic HP has also promoted a higher synthesis of aggrecan and type II collagen mRNAs in mature chondrocytes (monolayer cultures)⁹³¹.

Concerning 3D matrices, the conclusions that can be drawn are slightly different compared to *in vivo* observations. Applying similar parameters to Jortikka's group, Parkkinen et al. showed a high increase in the incorporation of GAGs, but at much lesser rates⁹³². Another exciting discovery from 3D scaffolds is that adult and juvenile cell lines (chondrocytes) respond differently to mechanical stimuli (3-7 MPa at 0.25 Hz). Adult cells showed increased GAGs and typed II collagen production, while immature cells only presented increased GAGs synthesis. This result implies collagen synthesis is much more sensitive to HP than GAGs⁹³³. Elder et al. showed that static HP (5 or 10 MPa) was beneficial to scaffold-less explants to develop GAG and collagen synthesis, consequently implying a higher compression stiffness of the generated ECM⁹³⁴. Thus, it can be argued that there are no clear responses or accurate controls concerning the timing for HP application⁵⁸⁰.

Also, HP has a differentiation role exercised on MSCs. A research group studied how the HP (0.1 MPa at 0.25 Hz) increased GAG and collagen concentrations in bone marrow MSCs (BMMSCs) compared with the control cases⁹³⁵. Other authors showed the rise of chondrogenesis markers Sox9, aggrecan, and type II collagen mRNAs in this model⁹³⁶. More interestingly, it has been demonstrated that HP leads to chondro-induction in other cell lines like fibroblasts, where applying these forces leads to doubling the production of GAG and collagen⁹³⁷.

Together with HP, the delivery of TGFs, like TFG- β 1 and TFG- β 3, significantly helps the matrix construction in MSCs. For instance, TFG- β 1 with HP almost double ECM production and biomechanical properties (compressive and tensile stiffness)⁹³⁸. Another relevant pathway of applying HP over chondrocytes is the proliferation of pro-inflammatory signals, like IL-6, MMP-2, and MCP-1⁹³⁹.

12.4.2. Mechanical loads

Mechanical loads can be essentially explained as direct contact between two surfaces. In AC, the regular loads range from 0.5 to 8 MPa⁹⁴⁰. In the same manner that HP does, interstitial fluid supports the external compression *via* liquid pressurization⁹⁴¹. This fact is responsible for increasing the stiffness of AC under dynamic loads⁷⁴³. Nevertheless, Armstrong et al. proved that interstitial fluid pressurization only supports 33% of the compression load⁹⁴²; thus, the “solid” ECM supports the rest of the percentage of stresses.

Perhaps because of its simplicity and ease of use, applying uniaxial stress over tissue surface is the most extended experimentation of mechanobiology⁹⁴³. This technique shows how physical stresses interact with the integrin receptors attached to the cell membrane activating G proteins and the adenosine 3',5'-cyclic monophosphate (cAMP) signaling cascade⁹⁴⁴. Furthermore, it has been reported that the phospholipid membrane can activate G proteins under biomechanical stimulation by itself⁹⁴⁵.

Mechanical stimuli directly interact with actin polymerization and depolymerization. Protein kinase A (PKA) phosphorylates Sox9 protein in adult chondrocytes, which enhances its transcriptional activity⁹⁴⁶. In addition, Yoon et al. showed how PKA regulates chondrogenesis in MSCs in a PKC α -dependent manner⁹⁴⁷. Juhász et al. determined that the chondrogenic response to compression regimes is related to elevated pSox9 levels. This result may be derived from increased PKA enzyme activity from mechanically induced cartilage colonies. They also observed Sox9 and cAMP response element-binding (CREB) expression and phosphorylation rise after mechanical stimulation⁹⁴⁸. External forces increase the quantity of Ser211 (a specific phosphorylated form of Sox9) directly involved in ECM synthesis. Furthermore, Sox9 is activated by CREB due to physical interactions at the Ser133⁹⁴⁹. Mechanical stimuli trigger the cAMP-PKA-dependent, the heterotrimeric G α s-subunit, cAMP, and the transcription factor CREB⁹⁵⁰.

INTRODUCTION CARTILAGE TISSUE ENGINEERING

The mechanism behind how chondrocytes interact with external forces is still a hypothesis and is yet to be fully supported by experimental observations. Nevertheless, there is strong evidence that primary cilia, a sensory organelle, links the mechanical and chemical cues⁹⁵¹. The primary cilium has also been observed in chondrocytes, MSCs, and arthritic chondroprogenitor cells (CPCs) used as mechanosensor⁹⁵². These cilia from chondrocytes are aligned with the ECM to respond to external forces. Wann et al. stimulated mutated chondrocytes (without cilia formation) and found these chondrocytes were insensitive to loading stimuli⁹¹⁸. In addition, Farnum et al. demonstrated a difference in the orientation of chondrocyte cilia between load-bearing cartilage and non-load-bearing one⁹⁵³.

In contrast with other cells with cilia, the primary cilium in chondrocytes is essential for modulating the downstream process, which is called intra-flagellar transport (IFT), but not for early mechanoreception. These regulatory pathways are associated with type II and IV collagen, G proteins, Ihh, Ca²⁺ channels, connexins, purine, cAMP, and the PKA pathway⁹⁵⁴. For instance, in the case of Ca²⁺ channels as polymodal TRPV-4, which is present in the chondrocyte cilia⁹⁵⁵, were induced by mechanical loading in porcine articular chondrocytes⁹⁵⁶. Another important example of a membrane receptor of the cilia is the case of connexin 43, a mechanosensitive ATP-release channel⁹⁵⁷. Thanks to these previous discoveries, it is possible that mechanical stimulation activates signal transduction of the focal adhesion complexes (e.g., integrins), activating adenylate cyclase to promote PKA by cAMP^{948,958}. Also interesting is the finding that OA chondrocytes and healthy chondrocytes have differences in cilia length, which may act as a new biomechanical marker. In addition, it was proven that the length of cilia depends on II β ⁹⁵⁴. Rich et al. also found how chondrocyte cilia respond within minutes to changes in osmolarity, which implies an adjustment in cilia length⁹⁵⁹.

The role of the interstitial fluid in AC is so critical that it is considered a biomarker for OA⁹⁶⁰. The interstitial fluid acts as low mechanical shear stress over the chondrocytes producing stimulations previously discussed⁹⁴¹. Perfusion flows (PFs) are applied in cartilage TE to mimic this natural *in vitro* interaction. Pazzano et al. demonstrated that after applying a PF, the chondrocytes were aligned in the same direction of the flow, resulting in an advantageous cartilage TE⁹⁶¹. In previous studies, PF is a reliable tool for growing cartilage and bone TE⁹⁶².

Recent literature remarks on tailoring the flow velocity to acquire chondrogenesis and enhance cell viability. Low flow velocity (10 $\mu\text{m/s}$ and 7 $\mu\text{m/s}$) is appropriate for the early stages of the process to protect matrix deposition in the porous scaffolds and the type II collagen and GAGs synthesis⁹⁶³. After that, it is advisable to develop a slow increase in velocity (from 7 to 19 $\mu\text{m/s}$)⁹⁶⁴.

Perfusion systems are also beneficial for treating OA. It has been found that PF decreases the hypertrophic regime of the pathological ECM. The synthesis of type I collagen under this bioengineered protocol is reduced even more; adult arthritic chondrocytes displayed initial steps of redifferentiation⁹⁶⁵.

12.4.3. Ultrasound

Low-intensity pulsed US (LIPUS) is an acoustic wave that produces mechanical stimuli over cells, and FDA approves them for clinical therapy and bone fracture healing⁹⁶⁶. The applicability of LIPUS ($< 1 \text{ W/cm}^2$) for bone fracture healing has been demonstrated for several years⁹⁶⁷. LIPUS enhances calcium deposition and the synthesis of the BMP-2⁹⁶⁸. Moreover, LIPUS is also beneficial for fibroblasts, osteoblasts, and chondrocyte proliferation *in vitro* and *in vivo*⁹⁶⁹. Furthermore, there is evidence that LIPUS promotes the gene expression of type II collagen⁹⁷⁰ and improves the synthesis of chondrogenic ECM⁹⁷¹.

Revising previous literature about LIPUS cell responses, several mechanotransduction routes are involved in chondrocytes: the

INTRODUCTION CARTILAGE TISSUE ENGINEERING

integrin/P13K/AKT pathway⁹⁷², the integrin-mediated p38 MAPK pathway⁹⁷³, and the integrin-FAK/Src/p130Cas/CrkII/Erk pathway⁹⁷⁴.

Recently, Nishida et al. found a positive feedback pathway that implied MAPK and the CCN family member 2, also known as connective TGF (CCN2)⁹⁷⁵. Alterations modulate this TGF in the cytoskeleton of fibroblasts and osteoblasts⁹⁷⁶. Specifically, it is known that CCN2 is expressed *via* actin polymerization. The same researchers have proven how CCN2 interacts with β - and γ - actin *in vitro* in human chondrosarcoma-derived chondrocytic cell line (HCS)⁹⁷⁷. In addition to the previous metabolic path, MAPK signaling is involved in the CCN2 induction under LIPUS stimulation⁹⁷⁸; LIPUS promotes the Ca^{2+} influx through TRPV4, a BK_{Ca} channel that activates MAPKs to induce CCN2 synthesis. Consequently, LIPUS stimulates two different ways the CCN2

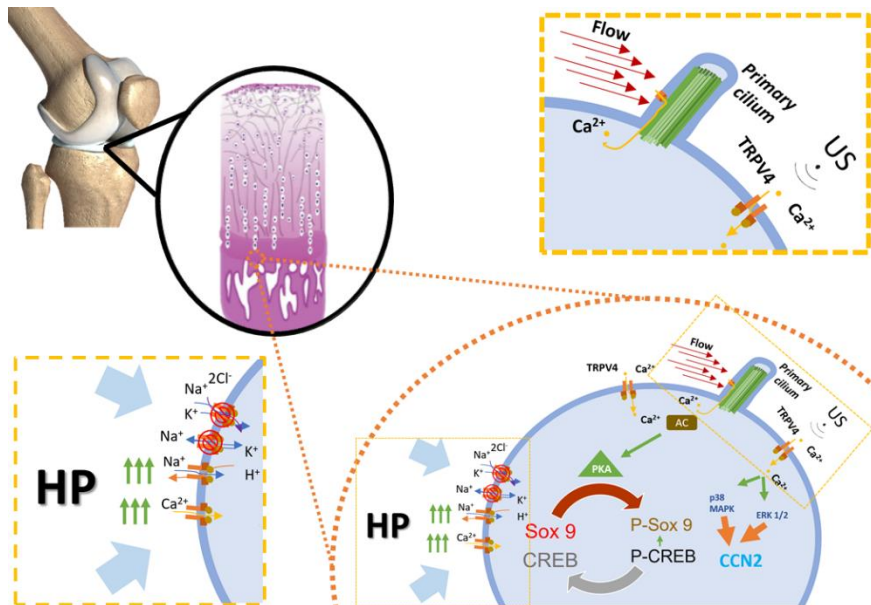


Figure 54. Schematic representation of the biomechanical pathways involved in cartilage synthesis. Hydrostatic Pressure (HP) enhances Ca^{2+} and Na^+ channels and the Na^+/K^+ pump which interacts with PKA that regulates chondrogenesis (Sox9/CREB). Shear stress induced by flow stimulate the primary cilium of chondrocytes that also plays a key role in the Sox9/CREB cycle. Finally, US stimulation activates the TRPV4 channels and actin polymerization that induces chondrogenesis as well

molecule through actin polymerization and MAPKs, which in turn increases chondrogenesis (Col2a and Acan over-expression).

LIPUS has also shown therapeutic results on OA, inhibiting protein expression of type I collagen and bone sialoprotein and the gene expression of hypertrophic Col X⁹⁷⁹. In addition, LIPUS suppresses IL-1 β (which implies MMP13 and ADAMTS 5, OA markers) and helps with chondrocyte migration, proliferation, and differentiation⁹⁶⁶.

In conclusion, in the last few years, many researchers have shown biomechanics' great benefits of biomechanics (**Figure 54**) in treating AC disorders (i.e., OA).

12.5. Future Perspectives of CTE

Thanks to all the previous investigations done in cartilage TE, it is not uncommon to find many diagnostic or analytical devices used in the clinic to clarify the biomechanics of the whole musculoskeletal system before applying any treatment or to avoid possible lesions. Namely, Auckland Bioengineering Institute (2014) developed an open software platform to cover all mechanisms behind the biomechanical behavior of the human body⁹⁸⁰. Furthermore, it would be interesting to modulate neo-cartilage biogenesis from the biomechanical point of view to control tissue development and tailor it for any application. The possibility of reproducing these biomechanical patterns in an *ex vivo* model for cartilage TE is also an attractive target. The use of BRs as a medical tool for tissue formation is highly recommended, not only for studying cartilage development but also as therapeutic devices to develop ATMPs for OA treatment (**Figure 55**) for reducing inflammation and promoting ECM synthesis in the implanted area⁹⁸¹.

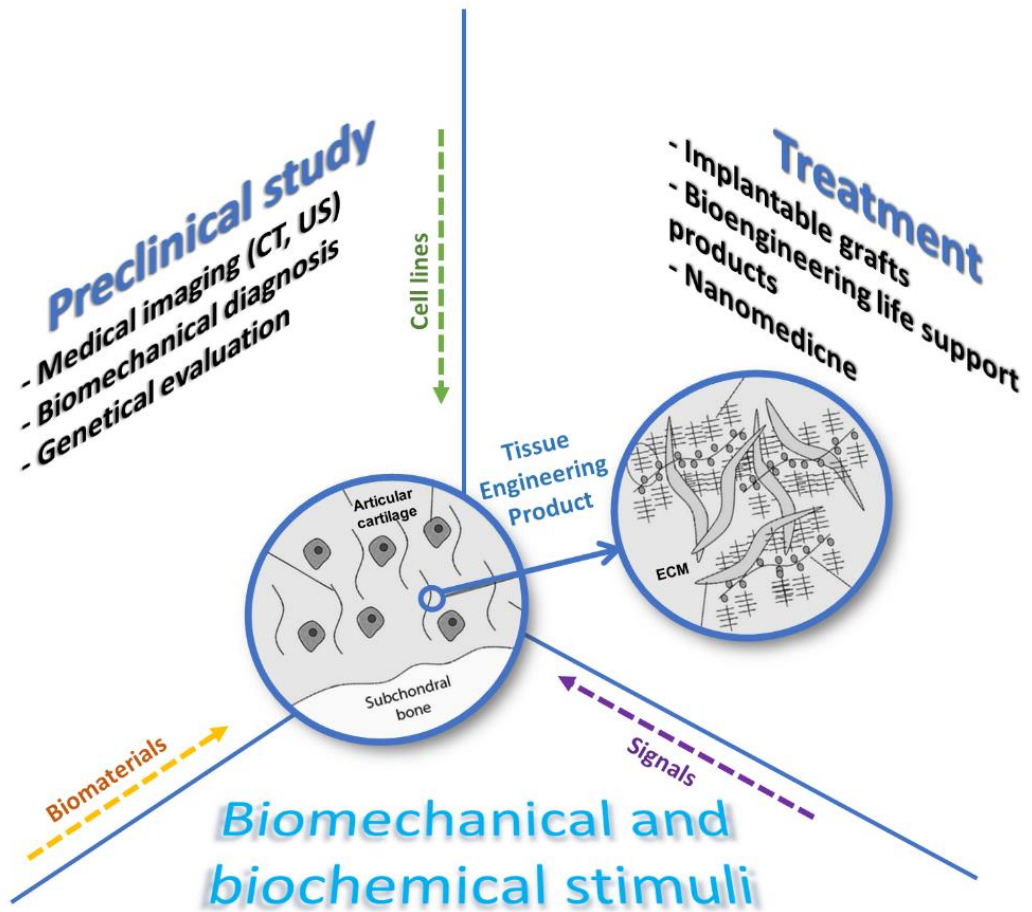


Figure 55. Basis of Biomedical Engineering of the future of cartilage tissue engineering.

13.Motivation

13.1. Clinical development process

The early stages of **clinical development** occurred much time before, in a long process called **preclinical development**⁹⁸². Broadly, preclinical analyses are divided into screening, choice of "lead treatment compound," *in vitro* assays (i.e., synthesis, viability, etc.), *in vivo* assays (e.g., toxicology), scale-up, and clinical promotion⁹⁸³. This time-consuming process could take many years; even worse, the success ratio (i.e., commencing a clinical development) of any preclinical medicine is thought to be 250,000 targets to 1 successful candidate (i.e., 0.004‰)⁹⁸⁴. Moreover, the "survivors" of the previous sieve are just the starter points of the clinical development process, which implies a more extended pathway than the previous one. It is divided into four phases with an increased level of complexity between them. The final number of products (**Figure 56**) that reaches the clinics is less than 10%⁹⁸⁵; it is evident that something is not working correctly, but what?

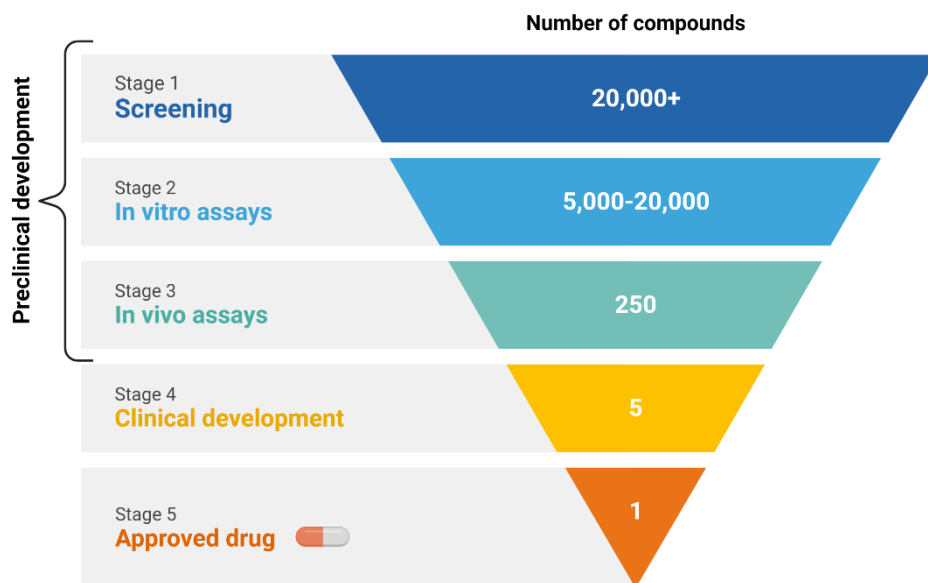


Figure 56. The current drug development process has an acute bottleneck that is still unsolved.

13.2. No time for old drugs

For the past ten years, the pharmaceutical industry's yearly output has practically flatlined⁹⁸⁶. Clinical trial attrition rates have also risen sharply^{987,988}, and government regulations and market goals are getting more stringent⁹⁸⁹⁻⁹⁹¹. At each step of development, the number of candidate therapeutical products necessary to obtain approval for a single new medicine grows⁹⁸⁶. Because there are few unresolved health issues, most new medications will compete with current ones. Several new approaches appear to have a little extra benefit over established therapies⁹⁹². It seems reasonable to explain these tendencies due to high-risk early inversions⁹⁹³ and the previous crisis periods that occidient has suffered⁹⁹⁴. The effectiveness of new medications against placebos has been found to have decreased with time which makes the problem worse⁹⁹⁵. Medication copyright expirations weaken major pharmaceutical firms' financial positions and limit their ability to create new medications⁹⁹⁶. Drug prices are rising so much that important drugs are becoming inaccessible in the developing world, Europe, and the United States⁹⁹⁷. It is common to find that support for the pharma industry has been reduced⁹⁹⁸.

Contemporary biomedical innovations rely on public-private collaborations, where universities (i.e., research groups) grow the company interests to remedy this dearth of private investment⁹⁹⁹. Despite this, the number of novel medications developed by university spin-offs has been disappointing, causing the extinction of most of these early small companies^{1000,1001}. The few surviving brands do that due to appealing products, not their relevancy¹⁰⁰². Moreover, the expenditure incurred by university transfer offices to maintain their intellectual property is much higher than the return¹⁰⁰³. In reality, patents from prior medication research have been transferred. Businesses and academics are attempting to cover the treatment implementation: the discovery process, the product, the formulation (if any), the delivery, and the application techniques¹⁰⁰⁴. In terms of numbers, the pharmaceutical business has the most

applications to the European Patent Office (EPO)¹⁰⁰⁵. So, the reader maybe asking why there is no correlation between the number of patents and the discovery of new treatments (see **Figure 57**)⁹⁸⁶.

13.3. A paradigm shift

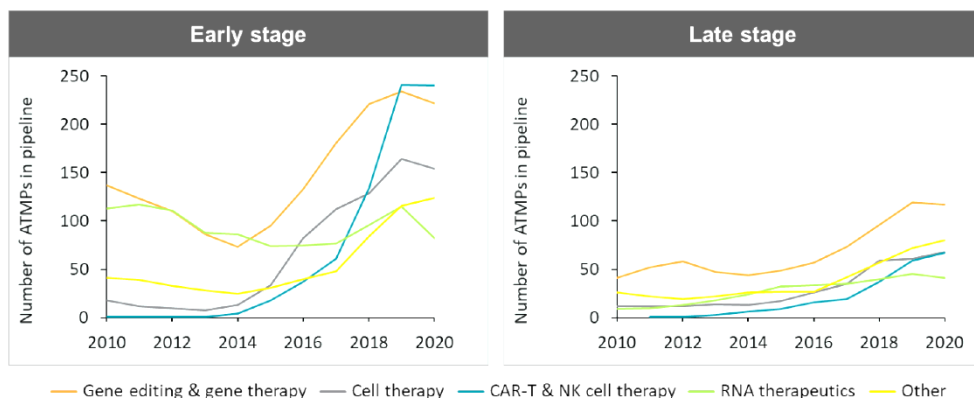


Figure 57. Evolution pipeline of ATMPs divided in different techniques. Figure exposed with permission of the European Federation of Pharmaceutical Industries and Associations (EFPIA)⁹⁸⁶.

Pharmaceutical and biotechnology industries are aware of their current situation; the times for the old paradigm— one target, one drug, one effect—are over¹⁰⁰⁶. As explained during the introduction, simplifying biomedical problems lead to misleading critical information¹⁰⁰⁷. *In vitro* models with full-length proteins interacting with their usual protein partners must adequately address the complexity exhibited *in vivo*. Additionally, many diseases with significant unmet treatment need still lack distinct therapeutic targets today. Identifying these spots that influence specific illness-related characteristics may be the most promising path for disease modification or mitigation¹⁰⁰⁸. Phenotypic screens reveal chemicals that impact an observable cellular feature by simultaneously acting on a previously unknown target or multiple targets¹⁰⁰⁹.

These advancements will encourage using model systems that better mimic human *in vivo* circumstances throughout the early stages of drug discovery¹⁰¹⁰. Furthermore, nontraditional pharmacological target groups,

INTRODUCTION MOTIVATION

including scaffolding, regulatory, and structural proteins, are presenting more and more alluring potential for altering cellular function, and it is now feasible to build medicines with focused poly-pharmacology^{1011,1012}. As mentioned above, BRs can be a beneficial tool to fulfill these objectives.

Since the last decade, the scientific world has been trying to exchange the previous concept of stratified medicine for **personalized medicine**. Personalized medicine was minted in 2008 by the President's Council of Advisors on Science and Technology (PCAST)¹⁰¹³. A correlated solution of personalized medicine is **ATMPs**, just one year before they were regulated²⁵. Even though the regulatory part of customized medicine has been around for more than 10 years (at the time of this paper), its global implementation is far from perfect. Because the ATMP value proposition is built on a long-term or curative impact, the patient follow-up period required to demonstrate such efficacy is substantially longer than a conventional trial duration¹⁰¹⁴. Cost-effectiveness ratios may be problematic in some situations due to a lack of comparative data or surrogate outcomes, which may be compounded by data extrapolation¹⁰¹⁵.

Recently, this idea has evolved into a **precision medicine** concept (**Figure 58**); it refers to tailoring medical therapy to a patient's genetic makeup and particular illness features¹⁰¹⁶. Nevertheless, industry and academia need to realize that the difference between radical change and *toasting in the sun* often lies in small acts. Therefore, to advance precision medicine from idea to reality, the fundamental paradigm shift relies on change "simplicity" by "diversification". To do that, **multidisciplinary** research that involves, by necessity, inter-, and intra- collaborations will be mandatory.

13.4. Multidisciplinary: the role of bioengineering

The term translational medicine was developed with precision medicine to accelerate the abovementioned problem. Translational Medicine (TM) is

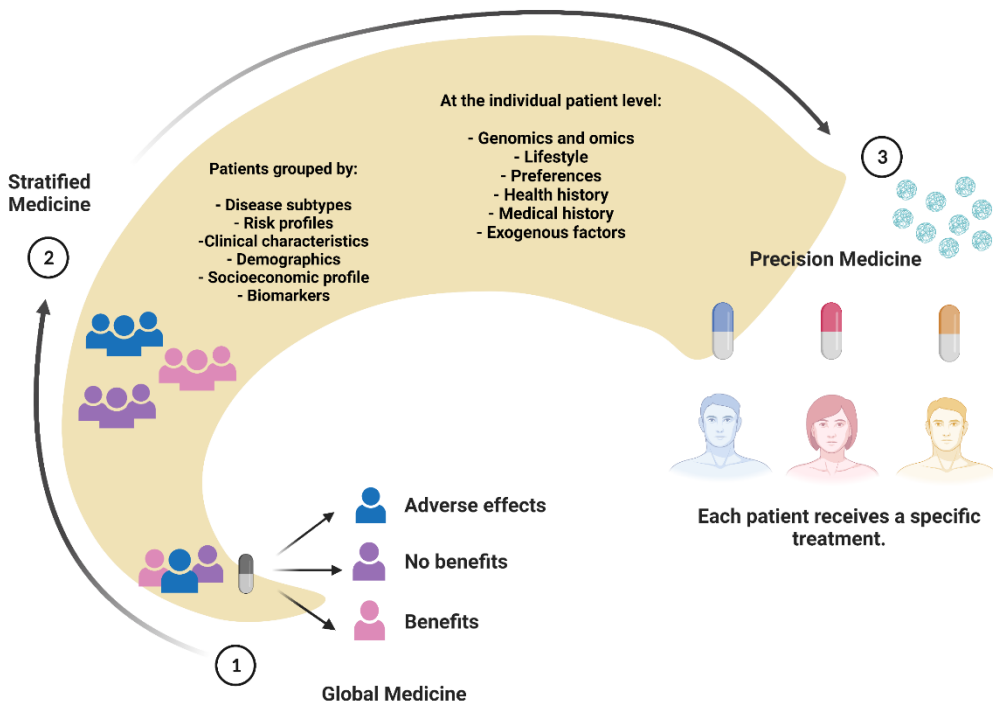


Figure 58. Precision medicine involves one hypothetical scenario where every person will receive a personalized and specific treatment.

defined by the European Society of Translational Medicine (EUSTM) as *an interdisciplinary branch of the biomedical field supported by three main pillars: benchside, bedside, and community. The goal of TM is to combine disciplines, resources, expertise, and techniques within these pillars to promote enhancements in prevention, diagnosis, and therapies*¹⁰¹⁷. It arose as a response to the last paradigm change, but lacking a scientific backbone is a significant problem in TM's current growth; consequently, the problem is still unsolved. The definition and evaluation of crucial indications in the translational process, known as **biomarkers**, is a significant component. Biomarkers are the primary tools for predicting efficacy and safety in the animal-to-human transition¹⁰¹⁸. Biomarkers and other translational research methodologies have applications beyond pharmaceutical development into medical devices¹⁰¹⁹.

The engineering industry and biomedical institutions have developed biomedical engineering professionals to ensure that their products are safe,

INTRODUCTION MOTIVATION

effective, and function as intended for the patient's benefit¹⁰²⁰. They can convert clinical development to a more industrialized state thanks to varied engineering disciplines such as mechanical, materials, signal processing, and market analysis¹⁰²¹. Biomedical engineers comprehend clinical medicine's significant problems and challenges, whereas clinicians respect the quantitative and systems components of biomedical research and education^{1022,1023}. Furthermore, medical devices are becoming "smarter," with the ability to conduct complete monitoring, alert, and control functions that define clinical best practices. This "smart gadget" revolution is spreading BME into ever-expanding fields of creative and professional practice, extending healthcare services beyond hospitals^{1024,1025}.

Concerning this 'new try to rearrange different modalities of science together' to induce a higher speed development in TM (and RM), it is essential to remark that the way of treating the problem also differs. Conventional biomedical science is based on analytical procedures or cause-effect studies, but multidisciplinary research will let, as a direct consequence, in **system** research (**Figure 59**). Furthermore, two essential aspects of systems must be clarified: i) The System is something besides, and not the same, as its elements¹⁰²⁶. ii) System behavior does not depend on **exogenous** factors but on **intrinsic** parts of itself. By necessity, to understand systems, it is more relevant to be aware of the connections among parts than just focus on isolated factors¹⁰²⁷.

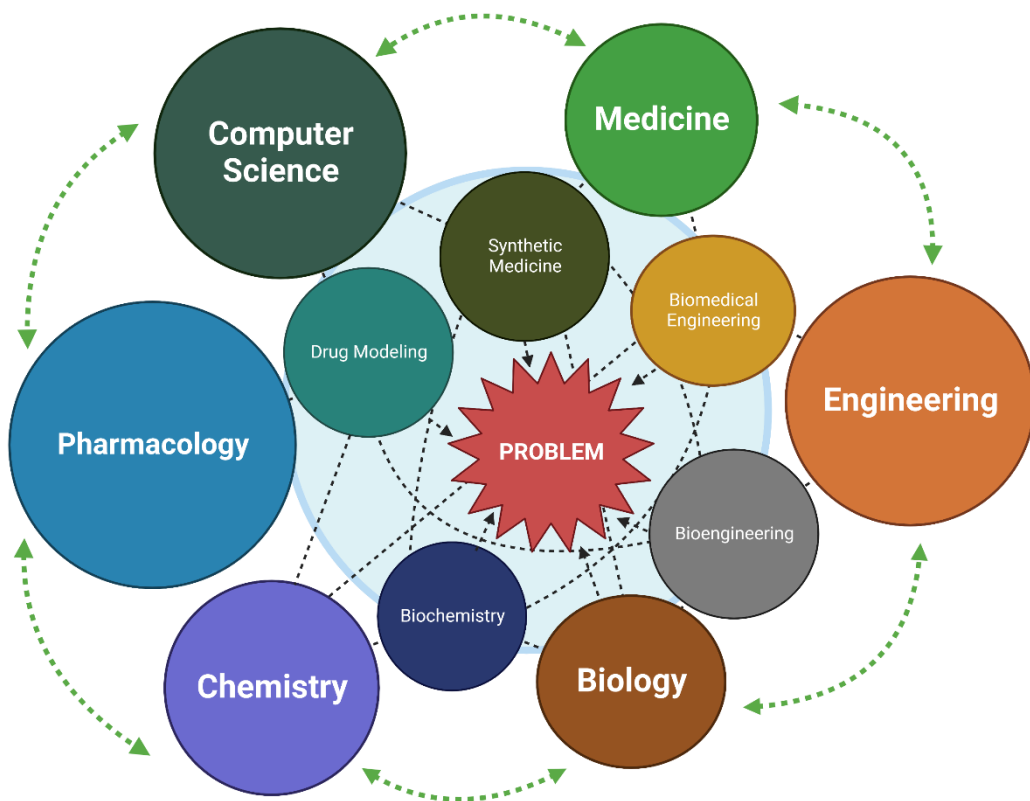


Figure 59. A system envelops a complex connection web: green arrows represent, multidisciplinary connections, black arrows the interdisciplinary ones, and the blue circle is the transdisciplinary field of biomedicine.

Further, precision medicine has to confront the expense of new tailored treatments compared to conventional ones, and big pharmaceutical corporations have little interest in gathering genomic, proteomic, or metabolomic data from massive clinical trials. As a result, their products have a tiny market¹⁰²⁸. After all, we live in a society with preestablished rules, and it is also relevant for researchers to manage those rules during their treatment development.

13.5. A bioreactor for cartilage

The introduction covered the history of RM and how it relies on TE to achieve significant advances in clinical practice. We have seen how it has gone from being an advanced science, self-absorbed by rapid and unattainable growth, to a more mature area, aware of its limitations but excited about its incredible feats and possibilities. It is curious to see how today we are closer to the dreams of the 1970s and, on the contrary, we think we still have a long way to go. We have also seen the importance of selecting an appropriate biomaterial for the treatment we want since the behavior of the cells, tissue, organ, and patient depends on its interactions. Moreover, how external forces shape, stimulate, and characterize us, and how the complex interconnections these stimuli have with the cells, thanks to mechanotransduction, modulate tissue development.

Subsequently, we have immersed ourselves in the latest advances that bioengineering and biomedicine have brought to the field of TE, developing new complex manufacturing systems within biofabrication and bioprinting. The latest technological advances allow us to adapt technologies as old as BRs into complete agents specialized in stimulating and expanding RM. After, we better understand what cartilage is at the cellular and tissue level and the development of such severe pathologies as OA, where we have seen how biomechanics profoundly influences its progression. Furthermore, we have finished with a summarized state-of-the-art of how RM and TE are trying to alleviate this pathology.

Now, with all this knowledge gathered and updated, we can expose the idea of this project which is nothing more than adding a new treatment for OA. One where aspects such as biomechanics, biomaterials, simplicity, and engineering take relevance. Beyond creating a fictitious and pretentious solution, we are looking for one that is practical and oriented to today's clinic.

The cell-material interaction is the earliest contact of cells with their surroundings. As a result, the first feature that must be modified for CTE is the scaffold (if applied). Three main conditions can be customized for scaffold manufacturing: the biomaterial, the microstructure, and the topography. Scaffold biomechanics has been a required element in the CTE process since Engler's studies on matrix elastic and MSC differentiation in 2006¹⁰⁶.

In recent years, the application of BRs in TE has been almost standardized, as shown in chapter 10. However, due to the complexity of the modality (modeling of biological systems), there is still no consensus on BR design and function applied to cartilage TE. Therefore, it was decided to use low-shear stress to induce mechanical stimulation for simplicity. Chondrocyte cilia are membrane receptors for ATP-release channels, connexins, purine, cAMP, and the PKA pathway⁹⁵⁴.

The use of this kind of stimulation directly implies two conditions: i) the design of a perfused BR and ii) the synthesis of a porous scaffold that allows cell growth at the same time that lets the fluid flow through it. Thus, using a hydrogel was impossible because it does not allow fluid convection, and the risk of scaffold degradation is almost inevitable. Consequently, it was selected as a synthetic polymer; the development of these polymer cartilage grafts will be discussed in Part I and Part II.

The second design aspect of our treatment was based on "oriented to today's clinic." Thus, adopting an autonomous system that could induce chondrogenesis and monitor the cartilage synthesis process was considered. As explained in chapter 7, nowadays, the variety of sensors applied in BRs is wide. Nevertheless, not all can monitor a 3D graft oriented to human transplantation without invasion. That explains the decision to use an on-line ultrasonic sensor because it was a relatively low-cost technique that could be implemented and already proved its functionality *in vivo*¹⁰²⁹.

Hypothesis

“It is difficult to say what is impossible, for the dream of yesterday is the hope of today and the reality of tomorrow.”

“Es difícil decir qué es imposible, el sueño de ayer es la esperanza de hoy y la realidad del mañana.”

Robert H. Goddard

14.Hypothesis

Because of its inherent properties, AC is extremely sensitive to injury and has a low capability for regeneration. As part of the OA clinical syndrome, progressive deterioration of AC causes joint discomfort and dysfunction. OA is one of the ten most debilitating illnesses in developed nations, with significant socioeconomic consequences. As a result, the demand for innovative treatment techniques has grown in recent years, including TE solutions.

Biofabrication is a rapidly evolving technology that has demonstrated tremendous applicability for RM. Its use, however, has needed the selection of biocompatible biomaterials that can provide support when utilized with cells. Biomechanics has proven relevant in inducing biochemical responses in tissues and cells in recent decades. These interactions are mainly exerted in two ways: cell-biomaterial interactions that depend on biomaterial mechanical properties and external stimuli exerted by external forces. BRs are increasingly used devices to increase and improve the *ex vivo* tissue production for ATMPs. They benefit from better nutrient transport and induce cell differentiation through mechanotransduction pathways. Even these devices can be designed as simple, user-friendly, and “smart” to be more adapted to current clinics.

CTE is based on three pillars: i) cells, ii) 3D structures to support cell implantation, and iii) stimuli. All of them work together to create a viable treatment solution for AC.

The following hypothesis will be validated in this work:

1. Adipose-derived stem cells are multipotent, highly proliferative somatic cells with chondrogenic differentiation¹⁰³⁰. Furthermore, using 3D culture systems creates an appropriate cell niche, promoting development toward a mature chondrocyte phenotype. OA patients' Infrapatellar Fat Pad-

Derived Mesenchymal Stem Cells (IPFP-MSCs) can be tailored to healthy and viable AC grafts.

2. Previous works by Engler and colleagues demonstrated the differentiation capacities of matrix elasticity¹⁰⁶. Therefore, it is demonstrable that IPFP-MSCs can also be modulated for chondrogenesis regarding mechanical scaffold properties that depend on the following:
 - a. Scaffold micro- and macro-architecture, i.e., porosity.
 - b. Biomaterial elastic bulk properties.
3. It seems sensible to propose that adapting scaffold surface topography will induce IPFP-MSCS chondrogenesis. It was demonstrated by Ross Harrison how surface biomaterial properties influence cell migration¹⁰³¹. Since then, cell-material surface interactions have proved high relevancy in conditioning cell expansion and differentiation^{1032,1033}.
4. In conjunction with creating biomechanical stimulations promoted by a BR, the 3D cultures discussed in points 1, 2, and 3 will significantly facilitate tissue growth under *ex vivo* conditions. From the literature, it can be extracted how biomechanical stimulation causes MSCs to develop cartilage by phosphorylating Sox9 via PKA, cAMP, Ser133, and CREB⁹⁴⁶⁻⁹⁵⁰.
5. It is proposed to use US technology as an on-line sensor monitoring to analyze tissue growth *ex vivo*. The US has been used in medical imaging for more than 70 years. Even LIPUS has also probed *in vivo* their capacity to monitor the evolution of ECM¹⁰²⁹.

Objectives

“The architect of the future will be based on imitation of nature, because it is the most rational, durable and economical of all methods.”

“El arquitecto del futuro se basará en la imitación de la naturaleza, porque es la forma más racional, duradera y económica de todos los métodos.”

Antoni Gaudí i Cornet

15.Objectives

The main objective of this thesis was to bioengineer a biomimetic tissue based on the bioprinting of a 3D biological construct (scaffold+cells) that meets the main conditions of healthy AC and to mature it in an ex-vivo BR system that simultaneously measures at real-time the AC differentiation of the biomimetic construct.

For this aim, the work has been divided into three chapters, each one with different specific objectives:

15.1. Specific Objectives of Chapter I

1. To obtain, characterize and expand MSCs from OA-affected patients and subjects undergoing liposuction.
2. To generate AC biomimetic constructs using the biofabrication technique.
3. Optimize the bioprinter parameters and the scaffold architecture by modifying porosity and filament orientation to adapt it for CTE.
4. To evaluate and correlate the resulting mechanical properties of the biomimetic construct with naïve human AC.

15.2. Specific Objectives of Chapter II

5. To improve the microarchitecture and topography of scaffolds to reduce biomaterial hydrophobicity *via* chemical functionalization.
6. To analyze the cell-material interaction depending on topography.
7. To evaluate the chondrogenic potential of the fabricated biomimetic scaffolds.

15.3. Specific Objectives of Chapter III

8. To design and fabricate a perfusion-based BR that promotes ex-vivo chondrogenesis.
9. To develop a system based on LIPUs that can monitor biomimetic scaffold AC maturation in the proposed BR in real time.

Chapter I

Pore geometry influences growth and cell adhesion of infrapatellar mesenchymal stem cells in biofabricated 3D thermoplastic scaffolds useful for cartilage tissue engineering

*“What we observe is not nature itself,
but nature exposed to our method of
questioning.”*

*“Lo que observamos no es la naturaleza
en sí, sino la naturaleza expuesta a
nuestro método de interrogación.”*

Werner Heisenberg

16. Abstract of Chapter I

The most pressing need in CTE is creating a biomaterial capable of tailoring the complex extracellular matrix of the tissue. Despite the standardized use of PCL for osteochondral scaffolds, the pronounced stiffness mismatch between the PCL scaffold and the tissue it replaces remarks the biomechanical incompatibility as the main limitation. The present work was focused on designing and analyzing several geometries and pore sizes and how they affect cell adhesion and proliferation of IPFP-MSCs loaded in biofabricated 3D thermoplastic scaffolds. The 1,4-butanediol thermoplastic polyurethane (b-TPUe), a novel biomaterial for CTE, and PCL were studied to compare their mechanical properties. Three different geometrical patterns were included: hexagonal (H), square (S), and triangular (T); each one was printed with three different pore sizes (PS): 1-, 1.5-, and 2 mm. Results showed differences in cell adhesion, cell proliferation, and mechanical properties depending on the geometry, porosity, and type of biomaterial used. Finally, the microstructure of the two optimal geometries (T1.5 and T2) was deeply analyzed using multiaxial mechanical tests, with and without perimeters, μ CT for microstructure analysis, DNA quantification, and degradation assays. In conclusion, our results showed that IPFP-MSCs-loaded b-TPUe scaffolds had higher similarity with cartilage mechanics and that T1.5 was the best-adapted morphology for CTE.

Keywords: cartilage tissue engineering, polycaprolactone, 1,4-butanediol thermoplastic polyurethane, rheology, microstructure, porosity, infrapatellar mesenchymal stem cells.

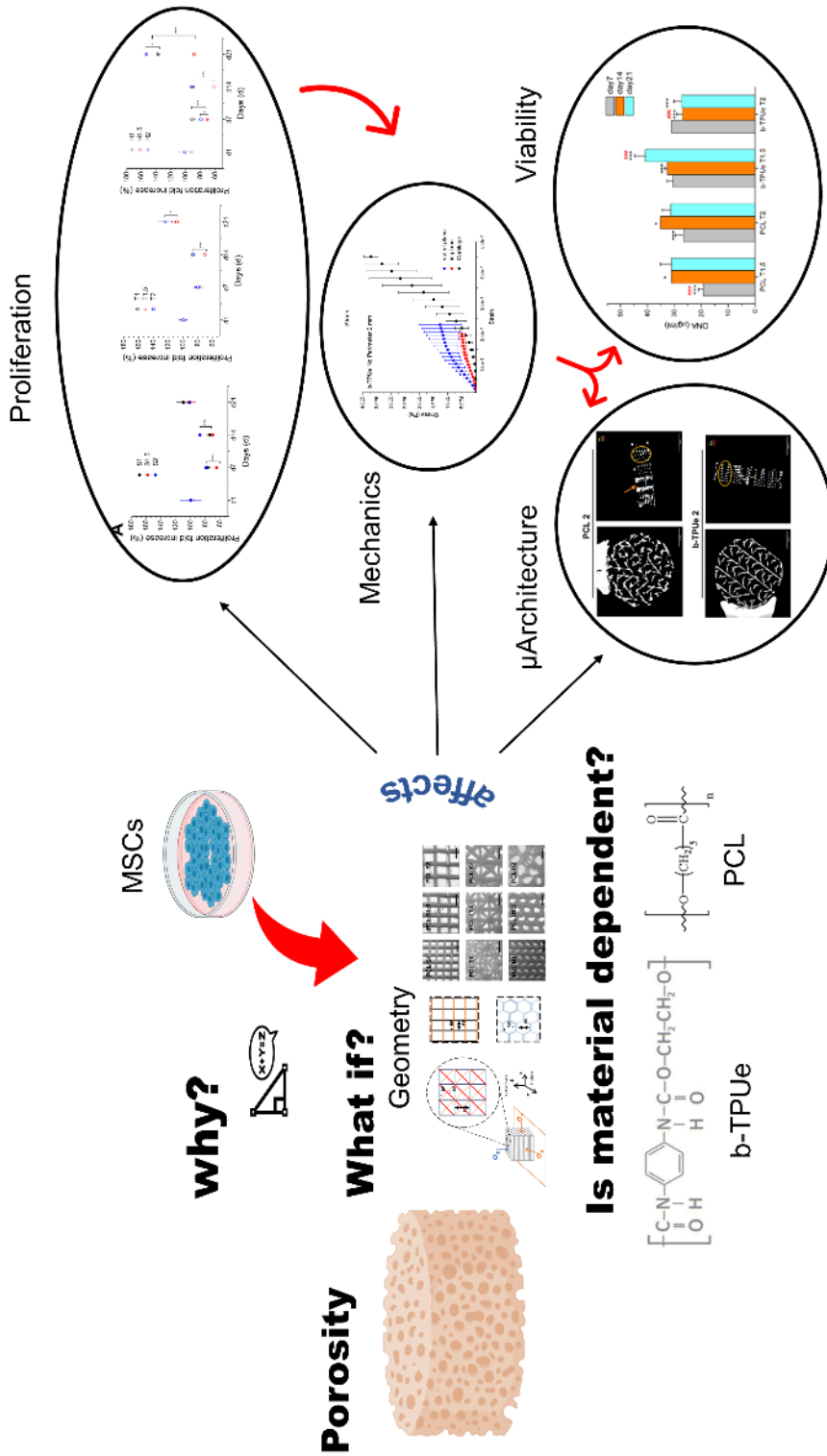


Figure 60. Graphical abstract of Chapter I. Porosity is an important feature in biomechanics and cell-biomaterial interaction.

17. Background for Chapter I

TE is a multidisciplinary research area focused on assembling functional constructs that restore, maintain, or improve damaged tissues or whole organs¹¹⁵. TE is based on three essential pillars: cells, biomaterials, and external stimuli. In this context, 3D bioprinting is a manufacturing methodology that uses biomaterials, cells, proteins, DNA, drugs, and growth factors to ease the restoration and regeneration of injured organs. Among the vast diversity of 3D bioprinting strategies, DBB, EBB, and LBB are the most commonly used⁴²⁸. Each has its strengths and weaknesses: high cost, accuracy, or time-consuming. Perhaps the main difference between the standard 3D bioprinting manufacturing methods is the ability to control the microstructure geometry accurately. In tailoring fibers, it is essential to consider their chemical composition and spatial arrangement because the spatial distribution directly modifies the biomechanical behavior of construct¹⁰³⁴.

Interestingly, how cells interact with the material also depends on the fiber distribution. Thus, controlling the pore interconnectivity, size, and scaffold geometry are pivotal to achieving a suitable cell maturation and extracellular matrix formation to succeed in 3D bioprinting-based tissue engineering purposes¹⁰³⁵. Even more, tailoring porosity (e.g., pore size, geometry, and orientation), the interconnectivity of the whole scaffold is controlled, and the surface chemistry is the parameter that determines the behavior of nutrient flow¹⁰³⁶. EBB is possibly the easiest way to parametrize the fiber orientation, thanks to the possibility of customizing the layer degree lay-down pattern. More precisely, changing fiber orientation during printing will modify the microstructure's final arrangement without modifying the material's chemical structure¹⁰³⁶. On the other hand, traditional methodologies like gas foaming, salt-leaching, or cross-linking provide high porosity, but the resulting porous interconnectivity depends on several factors that make mandatory the precise control of porous distribution, size and geometry^{1037,1038}.

One of the most widely used thermoplastic biomaterials for CTE is PCL, which contrary to conventional thermoplastic materials with high melting temperatures (above 200°C), presents a relatively low glass transition temperature (60°C) that is attractive in bioresorbable polymers¹⁰³⁹. Its thermal stability is also remarkable since its decomposition temperature is around 350°C, whereas other aliphatic polyesters only have a gap of 20-30°C from their melting point¹⁰⁴⁰. Among mechanical aspects, PCL is one of the most flexible biomaterials (Young's modulus, $E \approx 16$ MPa in the solid state) and is relatively easy to work with¹⁰⁴¹. Moreover, b-TPUe is a biomaterial with no prior studies in TE. Compared with other TPUs (petrochemical-based), b-TPUe uses bio-based chain extenders, increasing their biocompatibility and biodegradability, and, at the same time, their thermal and mechanical properties are improved^{200,1042}. Also, b-TPUe is closer to the viscoelastic properties of the cartilage with a storage modulus (G') of 9.6 MPa and a damping factor ($\tan \delta$) of 0.18¹⁰⁴³.

Previous studies reported an array of mechanical and biological analyses of the porous architectures of scaffolds¹⁰⁴⁴⁻¹⁰⁴⁷. Most conclude that porosity depends on two principal aspects: the tissue composition and the cell used¹⁰⁴⁸⁻¹⁰⁵⁰; however, no conclusive results were reported about the geometry. The main focus of the present study was to investigate and clarify which geometry and pore size tailor the conditions optimally for cell adhesion and proliferation of IPFP-MSCs. IPFP-MSCs have probed their massive chondrogenic potential¹⁰⁵¹⁻¹⁰⁵³, which is the tissue that needs to be replaced. In addition, they do not produce type X collagen (cartilage hypertrophy) when exposed to chondrogenic differentiation¹⁰⁵⁴.

Moreover, IPFP-MSCs maintain chondrogenic potential more significantly times than chondrocytes obtained from OA patients¹⁰⁵⁵. Also, comparing IPFP-MSCs with bone-marrow MSCs, they produced higher cartilaginous ECM; and, comparing with synovium-derived stem cells, IPFP-MSCs under hydrostatic pressure¹⁰⁵⁶ or dynamic compression and a gradient

oxygen tension presented higher chondrogenic response¹⁰⁵⁷. Finally, IPFP-MSCs cultured inside decellularized cartilage grafts also showed cartilage ECM synthesis and the zonal architecture, resembling native tissue¹⁰⁵⁸.

For this purpose, we used the first-time b-TPUe as 3D bioprinting material compared to PCL. For each biomaterial, three different geometries (triangular, square, and hexagonal) and three ranges of PS (1, 1.5, and 2 mm) were used. Compression mechanical tests and μ CT technology analyzed patterns from the mechanical perspective. Besides, the biological behavior of IPFP-MSCs was evaluated using Alamar blue assay, DNA content, and environmental scanning electron microscopy.

This article's complex structure (see **Figure 86**) suggests the necessity of mixing several material properties with its cell response. Due to many treated variables and samples, non-adequate samples were reduced after preliminary studies. Thereby: nine different geometries were proposed for the proliferation assay, and each was analytically studied. After, some of those geometries were discarded to simplify deeper analyses, reducing the sample number. Finally, selected geometries were exposed to mechanical assays, microarchitecture analyses, viability tests, and cell-material interaction inquiries.

18. Materials and methods for

Chapter I

18.1. Bioprinter setup

REGEMAT 3D V1 bioprinter (Regemat 3D S.L., Granada, Spain) was used to represent the EBB technique, and the software REGEMAT 3D DESIGNER was used to build scaffold geometries. PCL was obtained from Esun Industrial Co Ltd (Shenzhen, China) and b-TPUe from Recreus Inc (Elda, Spain). Their manufacturer parameters are detailed in **Table 5**.

The layer height (LH = 200 μm), the scaffold diameter (14 mm), and the number of perimeters (2 perimeters of 0.4 mm of thickness) were kept constant. No bottom or top layers were created to ensure that the cells attach to the filaments. Retract Speed was 20 mm/s; Perimeter/Skirt Speed 10 mm/s; Infill Speed 12 mm/s for PCL and 25 mm/s for b-TPUe. Finally, different PS (1, 1.5, and 2 mm) and printing patterns were arranged to modify the porosity. **Table 6**, it is represented the main parameters used to obtain the desired geometries: hexagonal (H), square (S), and triangular (T). Melting points corresponded with manufacturers' ones.

18.2. Isolation and culture of IPFP-MSCs

IPFP-MSCs were obtained from patients with the osteoarthritic knee during joint replacement surgery. Ethical approval for the study was obtained from the Ethics Committee of the Clinical University Hospital of Málaga, Spain (ethics permission number: 02/022010 Hospital Virgen de la Victoria, Málaga). Informed patient consent was obtained for all samples used in this study. IPFP-MSCs isolation and characterization were performed as previously described^{1059,1060}, where samples were extracted directly from OA patients. The IPFP was mechanically and enzymatically (collagenase type I; Sigma-Aldrich)

disaggregated at 37 °C heated ovens, where they remained under stirring for 2 h. When cells were isolated, the excess of collagenase was eliminated with washes (10% phosphate-buffered saline (PBS) fetal bovine serum (FBS; Sigma-Aldrich) and 1% antibiotic penicillin/streptomycin (P/S)), and the obtained pellet was resuspended in culture medium (DMEM (Sigma-Aldrich), 20% FBS, 1% P/S) and it was transferred to a cell culture flask (75 cm²). Afterward, IPFP-MSCs were incubated at 37 °C, and 5% CO₂ with DMEM high glucose (Sigma-Aldrich, St Louis, MO, USA) supplemented with 20% FBS (Lonza, Basel, Denmark) and 1% of penicillin/streptomycin (Sigma-Aldrich, St Louis, MO, USA). At 80% of confluency cells were sub-cultured.

18.3. Cell adhesion and proliferation assays in 3D scaffolds

For cell-seeding experiments, PCL and b-TPUe scaffolds were sterilized as follows: i) first, scaffolds were introduced in glass tubes of 30 mL, rinsed out with 50% ethanol/water solution for 10 min; ii) after, scaffolds were introduced into 70% ethanol/water solution for 24 h. iii) Next day, dried scaffolds were deposited onto Petri dishes, and they were washed with phosphate-buffered saline (PBS) (0.01 M). iv) Then, they were irradiated with UV light for 40 min. iv) Immediately after, scaffolds were fitted inside 24 healthy plates and immersed into DMEM high glucose (Sigma-Aldrich, St Louis, MO, USA) supplemented with 10% FBS (Lonza, Basel, Denmark) and 1% of penicillin/streptomycin (Sigma-Aldrich, St Louis, MO, USA) overnight. All the previous steps and the printing protocol were carried out inside a sterile laminar hood.

Subsequently, to compute similar conditions 2×10^5 cells were seeded onto the scaffolds. The data acquisition intervals were done at day 1(d1), day 7 (d7), day 14 (d14), and day 21 (d21); at those times, scaffolds were introduced in a new 24-well plate to avoid data contamination of viable cells that were attached to the well bottom.

The proliferation rate of IPFP-MSCs in 3D constructs was assessed by colorimetric alamarBlue® (*BIO-RAD*) assay. Samples were withdrawn from the incubation media, rinsed with PBS, and immersed in alamarBlue® for 3 h. The alamarBlue® reduction pattern was analyzed using a fluorescence spectrometer (Ex 530-560 nm / Em 590 nm BIO-TEK synergy4 HT). After that time, the samples were repositioned in a new 24-well plate with 200 µL of fresh culture media.

18.4. Porosity estimation and surface/volume ratio

The porosity (P) and surface/volume (S/V) ratios were theoretically calculated, assuming the fibers had a cylindrical shape. P was also experimentally determined from the relative density ρ_r as follows: $P = 1 - \rho_r$. The relative density was obtained by dividing the experimental density by the theoretical density. More detailed information is described in the supplementary material and methods section.

18.5. Wettability

The degree of scaffold hydrophobicity is one of the principal biomaterial properties determining cell interaction¹⁰⁶¹. Wettability was estimated by measuring the contact angle (CA) of a deposited water droplet (100 µL of distilled water) over a planar section of each material. An orthogonal image was captured after 2 seconds, and the contact angle was measured with ImageJ.

18.6. Angle Frequency

To compute the number of angles that appeared by the superposition of fibers in the different geometries, the Angle Frequency (AF) ($A_f = \frac{n \text{ Angles}}{n \text{ Total Angles}}$) was calculated. Thus, this ratio implies which geometry had higher angles and how the difference was concerning other conformations.

18.7. Mechanical testing of the scaffolds

Mechanical tests were carried out using two different devices to explore a wide strain range of deformations. A commercial rheometer (MCR302, Anton Paar, SE Germany) was used to explore the small strain range (below approx. 0.2). To explore the mechanical behavior in a more extensive strain range (from approx. 1 to 20), a Universal Testing Machine (Shimadzu Autograph AGS-X) was used.

The rheometer was operated with a parallel plate geometry. The experimental protocol consisted of four steps. In the first step, a cylindrical scaffold was placed on top of the bottom plate of the rheometer, and the upper one was displaced downwards from the “lift position” to the “initial position” $h_s = H_s$ (≈ 5 mm). The initial position was always more prominent than the thickness of the scaffolds tested. During this step, the upper plate never touches the scaffold; therefore, data are not recorded. In the second step, the upper plate was displaced downwards at a constant velocity ($10 \mu\text{m/s}$) to compress the scaffold. The third step began when the normal force reached a value of $F_N = 40$ N. At this point, the plate undergoes a small amplitude strain oscillation (strain amplitude $\gamma_0 = 10^{-5}$ % and excitation frequency $f = 1$ Hz) during 10 s to explore the linear viscoelasticity of the scaffold under shear kinematics. In the fourth step, the upper plate was displaced upwards at $10 \mu\text{m/s}$. All steps were performed in triplicates at 25° C. The Young’s modulus was calculated from the compression interval -as the slope of the linear portion of the stress-strain curve (i.e., X-Y strain) by linear fitting- while storage and loss moduli were obtained from the shear interval -in the viscoelastic linear region (strain < 0.01)-.

A Universal Testing Machine was used to explore the mechanical properties of the scaffolds in the extensive strain regime. For this aim, scaffolds with a cubic shape were fabricated and tested in compression along two axes: the Axial ‘out of plane’ direction (i.e., orthogonal to the print plate) and the Radial ‘in plane’ direction (i.e., parallel to the print plate).

18.8. Characterization of the microstructure throughout μ CT technology

μ CT was applied in triangular geometries for PS of 1.5 and 2 mm (T1.5 and T2) To analyze the scaffolds' porosity and microstructure in deeper detail. For each material and PS, three samples were used and analyzed inside an *Xradia 510 Verse (Zeiss)* for 24 hours with an acquisition voltage of 40 kV at 3W. The emitting distance was 50 mm, whereas the detector distance was 91 mm, and the pixel size was 12.1 μ m. The magnification objective was $0.4\times$ and the exposure time was 18-22 seconds.

18.9. DNA quantification

The 4', 6-diamidino-2-phenylindole (DAPI, Sigma-Aldrich, St Louis, MO, USA) assay was used to study the DNA content. Briefly, 50 μ L of papain-digested sample harvested from 3D scaffolds at d7, d14, and d21 were added into a 96-well plate and combined with 50 μ L of DAPI dye. Afterward, the absorbance at 358 nm was read at 461 nm. The DNA standard from Calf Thymus (Sigma-Aldrich, St Louis, MO, USA) was used to determine the DNA content of the samples.

18.10. Environmental scanning electron microscope (ESEM)

The scaffolds were imaged with an FEI Quanta 400 microscope (Thermo Fisher Scientific-FEI, Fremont, CA, USA) with an Everhart-Thornley detector (E-TD) for dry and conductive samples in high vacuum mode and a gaseous SE detector (GSED) for wet samples in the environmental model. Cell-laden PCL and b-TPUe scaffolds with triangular morphology were analyzed at 2 weeks. Afterward, they were fixated with 2% glutaraldehyde for 2 hours at room temperature, and then they were rinsed in 0.1 M cacodylate buffer and incubated at 4^o C. The pressure curve adopted for the measurements was 720-1067 Pa.

18.11. Statistical Analysis

All graphed data represented the mean +/- SD from at least three experiments. All the statistics were performed with $n = 3$ in OriginLab Pro™. For mechanical curves and because of simplicity, linear interpolation applying average was performed over all samples. A two-tailed Students T-test was done to compute statistical significance among geometries, and homoscedasticity and normality tests were done before meaning comparison. In graph representations, P-Value less than 0.05 was represented */#; P-Value < 0.01 with **/## and P-Value < 0.001 ***/###.

19. Results and discussions from

Chapter I

19.1. Fabrication approach

Among different options, thermoplastic polymers can be easily printed using the extrusion EBB technology by fused deposition modeling (FDM) consisting of a nozzle with a heater that melts a thermoplastic filament and deposits it in a controlled and organized manner, layer-by-layer, on a surface¹⁰⁶². The REGEMAT 3D software allows the possibility of tailoring several parameters about the scaffold arrangement. In contrast with other EBB-based bioprinters, it does not apply mesh restrictions configuring patterns slightly different from conventional 3D printers, as could be the triangular and the hexagonal¹⁰⁶³. In contrast with other standard software, it takes a 3D volume (in STL format) and, from such a model, makes the lamination¹⁰⁶⁴. Moreover, this software directly configures the mesh distribution to facilitate the presence of symmetries¹⁰⁶³.

Our study investigated three patterns (triangular, square, and hexagonal) and three porosity sizes PS (1, 1.5, and 2 mm). **Figure 61A-C** shows the layer arrangement for the three different geometries. The triangular geometry presents more possible orientations (4), whereas hexagons only present one. Together with the theoretical porosity, the cylindrical approximation allows us to obtain the available surface (i.e., the exposed material surface for cell contact) for the hypothetical volume (see **Figure 87**) that would take the scaffold in the case of presenting null porosity (see **Table 7**). With all previous considerations, the early defined geometries were fabricated for each biomaterial (**Figure 61D-E**).

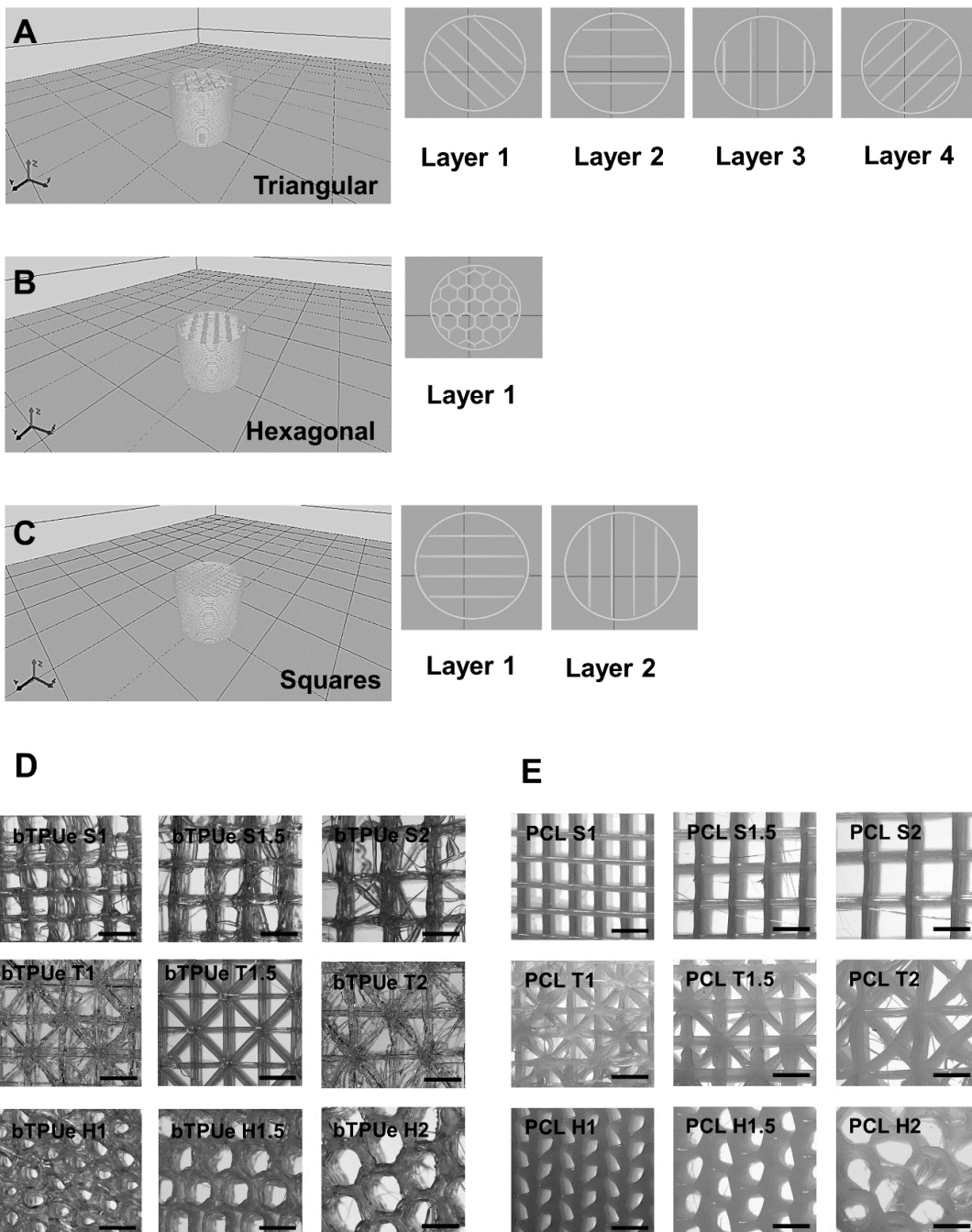


Figure 61. A-C) STL models of the scaffolds of each layer-down topography (PS 1.5 mm). In A) layers 1,2,3,4 are inserted periodically one on top of the next one. B) The hexagonal pattern only has one layer which is repeated along Z axis. C) In the Square pattern there are two different layers intercalated repeatedly. D-E) Cross-sectional images of the fabricated scaffolds. Scale bars correspond to 2 mm in all cases.

A good computer design that controls the thermal conductance and viscosity of the polymer will result in a better fidelity of the final patterns. Comparing **Figure 61D** and **Figure 61E**, it can be distinguished that b-TPUe presents thinner filaments in comparison with PCL, possibly due to the high thermal conductance of PCL¹⁰⁴⁰. Another relevant effect affecting the final design is the stability of the pillars formed because of the fibers' superposition (see **Table 6**). Thus, it is essential to control the initial CAD parameters and the printing properties to ensure an optimal scaffold architecture¹⁰⁶⁵.

19.2. Cell Adhesion/Proliferation assay

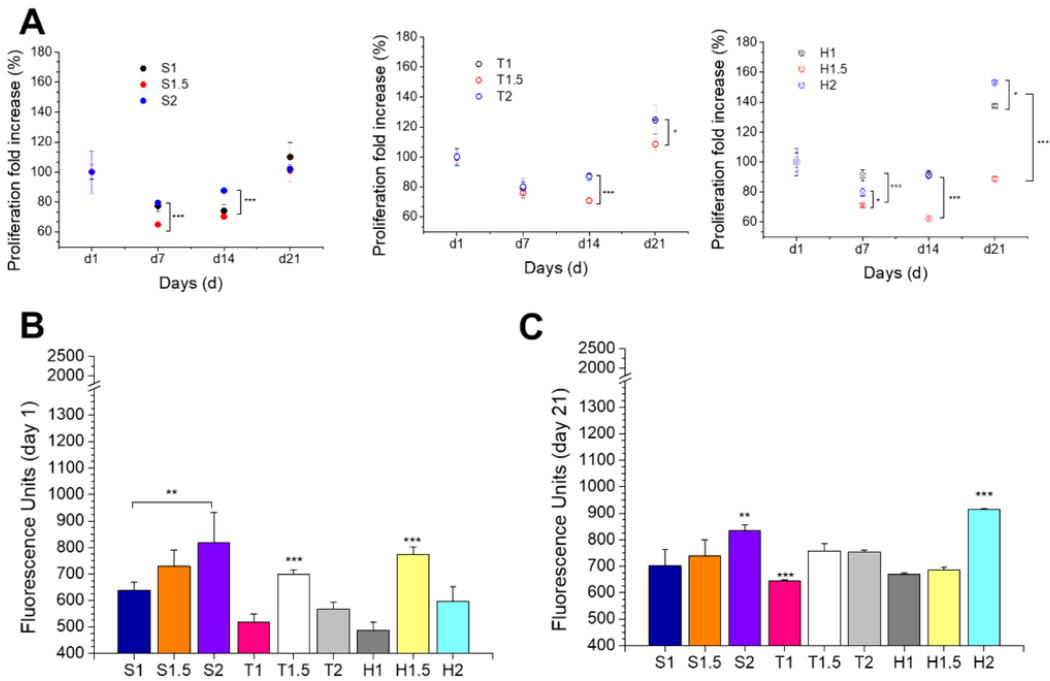
In the previous literature, it has been described several factors that increase cell adhesion and proliferation in 3D bioprinted scaffolds¹⁰⁶⁶. Among others, PS, interconnectivity in the scaffold microstructure, and surface conformation are key determinants^{521,1067,1068}. The exchange of nutrients and cues depends on porosity and interconnectivity¹⁰⁴⁶. Also, surface conformation, hydrophilicity, and PS increase biointegration¹⁹⁶. Here, the interaction of IPFP-MSCs (see **Figure 88** for MSCs characterization) with the two biomaterials (PCL and b-TPUe) was analyzed to characterize their cell adhesion and proliferation profile.

Figure 62 represents the fold increase proliferation of the AlamarBlue® assay for each geometry in both PCL and b-TPUe scaffolds in IPFP-MSCs-loaded scaffolds; the proliferation rate decreased from d1 to d7 and increased up to d21 for all geometries. When the fluorescence units were normalized (fold increase) concerning the values obtained on day 1, it was observed that square and

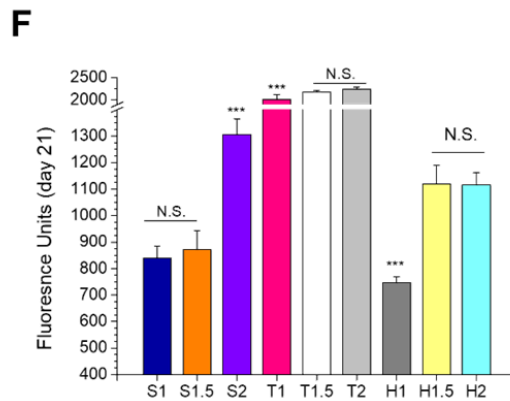
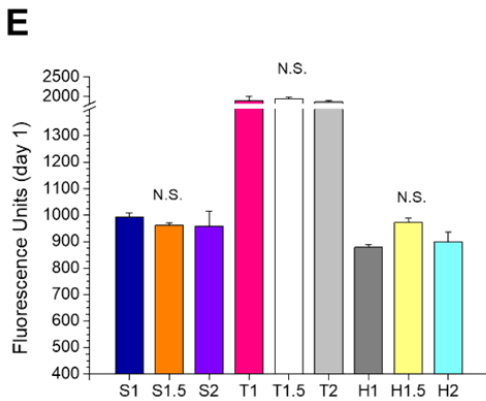
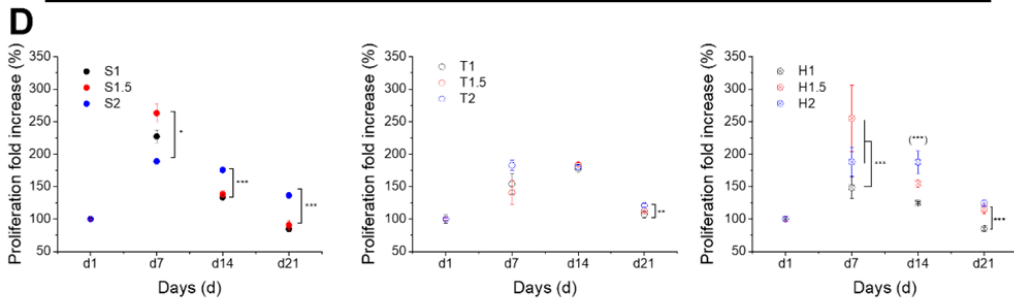
triangular conformations showed similar proliferative levels on day 21, except the hexagonal geometries for PS 1 and 2 mm that showed higher values (**Figure 62A**). **Figure 62B** and **-C** shows the raw fluorescence units of b-TPUe obtained from the AlamarBlue® reduction assay for d1 and d21, respectively.

Figure 62. A & D) Normalized Proliferation assays for b-TPUe and PCL materials, respectively. B) Absorbance of fluorescence emitted at 590 nm for b-TPUe at day 1. C) Same as B at day 21. E) Absorbance of fluorescence emitted at 590 nm for PCL at day 1. F) Same as E at day 21. P-Value less than 0.05 was represented *; P-Value < 0.01 with ** and P-Value < 0.001 ***. Brackets means significance different with the rest of PS inside the same geometry. ↪ *next page*

b-TPUe



PCL



Four conformations, T1.5, H1.5, S1.5, and S2, displayed higher adhesion at the starting point (**Figure 62B**); however, at day 21, all geometries achieved high fluorescence levels when comparing PS for each geometry, being H2 the one with significantly higher values. (**Figure 62C**).

On the other hand, **Figure 62D** represents the fold increase proliferation curves for PCL. As observed, very different behavior is found when compared with b-TPUe. For all geometries, the proliferative response increases from d1 to d7 and afterward decreases until d21 with ratio values similar to d1. Despite this difference in behavior, there is a shared similarity for PS 2 mm, which seems to present a higher proliferative response than the rest of the PS, regardless of spatial conformation. **Figure 62E** and **-F** present the raw data from PCL reduction assays at d1 and d21. The triangular geometry is associated with higher metabolism levels in both cases, implying much higher adhesion. Similarly to b-TPU, S2 and H2 also reached very high fluorescence levels when comparing PS for squares and hexagons.

Overall, cell adhesion in PCL scaffolds was larger than b-TPUe at d1 (see **Figure 62B** and **-E**). This result is the lower contact angle in PCL ($90\pm 1^\circ$) than b-TPUe ($111\pm 2^\circ$), demonstrating a more hydrophilic character of PCL than b-TPUe. These results are in good agreement with previous publications in the literature. In particular, Metwally et al. established that wettability influences cell adhesion and found an inverse correlation between the contact angle and cell proliferation¹⁰⁶⁹.

However, it is remarkable that, in contrast to PCL, the proliferation rate is more extensive for b-TPUe on day 21. These results suggest a better proliferative response for b-TPUe in the long term compared to PCL scaffolds. The higher proliferation response for large PS could be explained by the higher interconnectivity of the pores allowing a better diffusion of the culture medium¹⁰⁷⁰. Conclusively, although the cell adhesion results differ depending on the biomaterial, triangular patterns with large PS showed better response. This

effect is remarkable in PCL, making this geometry the adequate candidate for optimal cell adhesion.

19.3. Correlation of proliferation with experimental porosity and S/V ratio

Based on previous investigations, it can be noticed that the biochemistry and the microstructure of the biomaterial surface affect cell adhesion and proliferation¹⁰⁷¹. Also, it is expected that a higher available surface for cell attachment would result in a higher cell adhesion level¹⁰⁷². Two parameters were used to quantify the surface available for cell attachment: the experimental porosity and the surface-to-volume (S/V) ratio. In **Table 7**, results for the theoretical porosity (under the approximation that cylinders can represent the fibers) are presented together with the experimental porosity (obtained from ρ_r). As observed, a very good agreement is found between the two values suggesting that: i) the scaffolds almost preserved the original computer design; and, ii) the theoretical model is a good approximation. S/V ratios were also calculated using the cylindrical approximation and included in the **Table 7**. The largest S/V ratio is found for the triangular pattern.

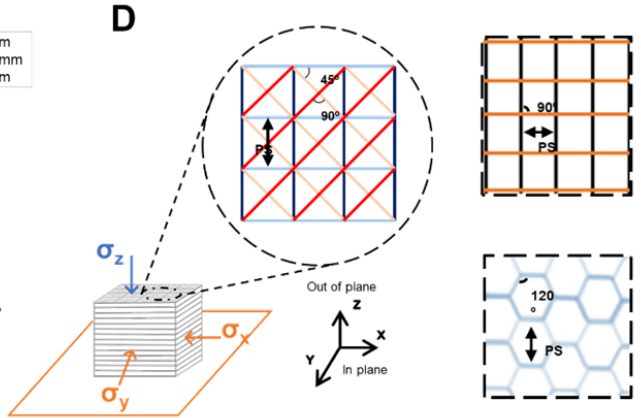
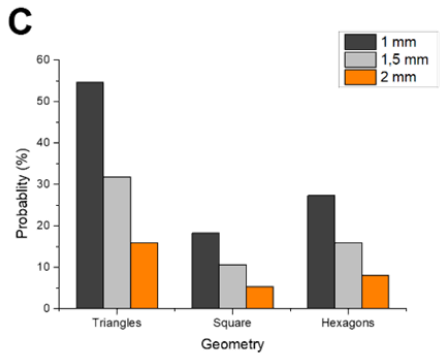


Figure 63. A) Fluorescence units (590 nm) from AlamarBlue© assay for b-TPUe and PCL scaffolds against their experimental porosity at days 1, 7, 14 and 21 (n=3). B) Fluorescence units (590 nm) from AlamarBlue© assay for b-TPUe and PCL scaffolds against their S/V ratio at days 1, 7, 14 and 21 (n=3). C) Angle frequency (AF) for each geometry as obtained from the frequency resulted by dividing the number of angles for each geometry by the total number of angles for all geometries. D) Infographic scheme of how stresses was applied on the scaffolds together with the representation of PS and the different printed angles which affects in cell adhesion.

In an attempt to look for correlations between the proliferation rate and the physical characteristics of the scaffolds (porosity and S/V ratio), **Figure 63A** and **-B** were done. **Figure 63** shows the Alamar Blue® reduction fluorescence at days 1, 7, 14, and 21 for all the patterns investigated as a function of the porosity (**Figure 63A**) and S/V ratio (**Figure 63B**). The fact that the curves are essentially flat in **Figure 63** demonstrates that neither the porosity nor the S/V ratio is the driving factor for cell adhesion and proliferation. Instead, geometry plays a key role; in particular, triangular patterns are associated with a more significant proliferation rate in PCL.

To better understand why the triangular pattern is associated with a more prominent proliferation, in **Figure 63C**, we show the ratio of the number of angular vertices in a particular scaffold concerning the others. In **Figure 63D** is shown a schematic representation of the geometrical unit cells with their corresponding angles. Given **Figure 63C**, the number of angular vertices is larger for patterns with more proliferation. Also important is to note that the connectivity angles in a triangular pattern are also smaller (45° (T) < 90° (T, S) < 120° (H)) hence favoring water entrapment by surface tension¹⁰⁶⁷. From the observation of **Figure 63C**, the higher values for the triangular geometry could explain their good proliferation at day 21 in both materials.

Based on all these results, it can be concluded that the triangular geometry is superior to the rest in terms of cell adhesion and proliferation.

19.4. Mechanical testing

Since these biomaterials and geometrical structures have a potential translation for osteochondral replacements, in this section, we analyze both the compression and shear properties of the scaffolds. Good mechanical behavior is critical for cellular proliferation, as Nam et al. exposed. They showed how stiffness changes in the fibers without altering the microstructure, inducing the expression of different gene expressions¹⁰⁷³. Raw compression curves for the scaffolds are shown in **Figure 89** and **Figure 90**. These curves are obtained with the rheometer to explore the low strain regime and the Universal Testing Machine to explore the extensive strain regime. The compression modulus can be obtained from these curves by fitting the linear region.

Compression modules are summarized in **Table 4**. As observed, the modulus strongly depends on the technique employed in its determination. In particular, the modulus measured with the rheometer is always more significant than the one measured with the Universal Testing Machine. Moreover, in consonance with manufacturers' data, b-TPU is softer than PCL and, therefore, more appropriate for biomedical applications; the modulus of b-TPU is closer to that of cartilage around $E = 10$ kPa. Generally speaking, a decrease in PS is associated with increased stiffness of the scaffold^{1044,1068}. However, for the scaffolds investigated in this work, PS has a minor influence on the compression modulus.

Figure 64 shows the stress versus strain curves under compression tests using the Universal Testing Machine. Two critical observations are as follows: i) out-of-plane measurements generally give larger moduli than in-plane measurements, and ii) specimens with a perimeter generally give larger moduli than samples without a perimeter.

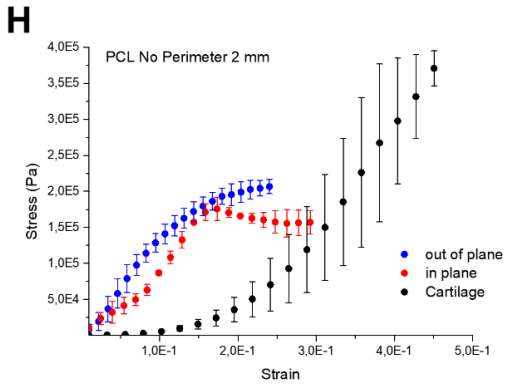
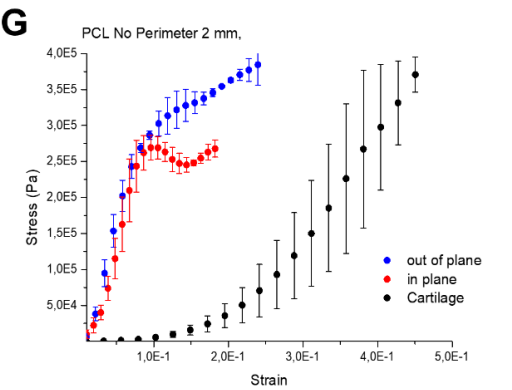
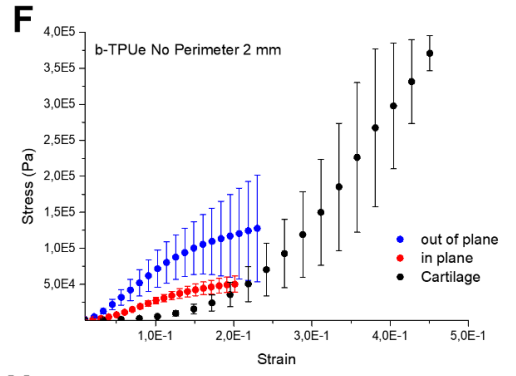
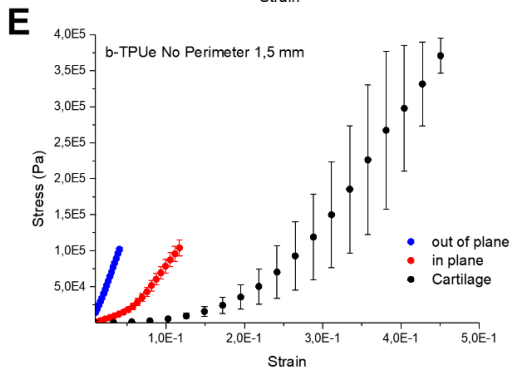
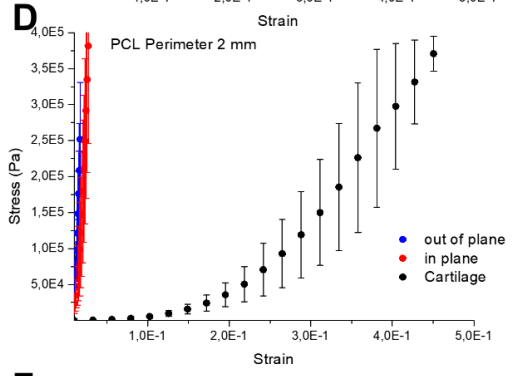
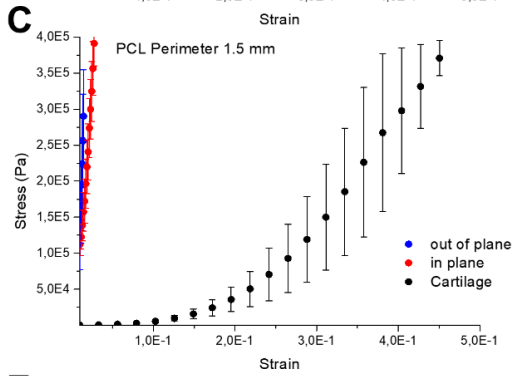
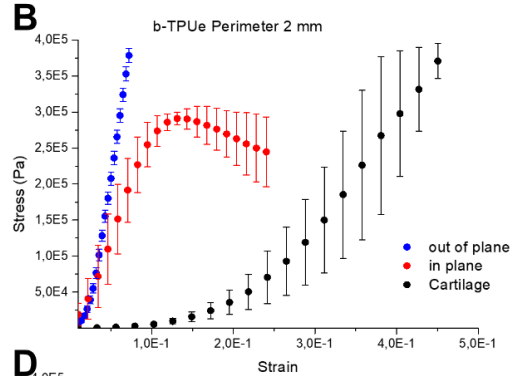
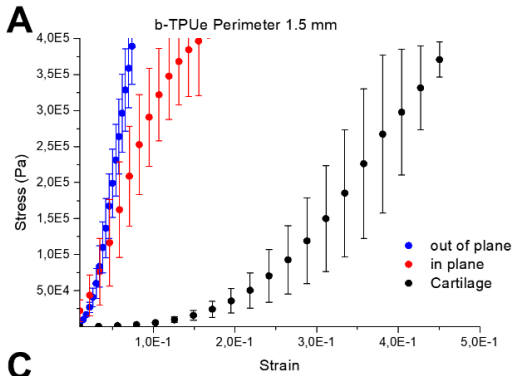


Figure 64. A-H) Stress-strain curves for the optimal architectures in comparison with the average curve from Cartilage samples. A-D) Samples with perimeters. E-H) Samples without perimeters. Each curve corresponds to the average curve applying linear interpolation (n=3).

The mechanical behavior of the scaffolds under shear is summarized in Table 1. In this table, we show the storage modulus. As observed, a very similar value is obtained independently of the direction (in-plane or out-of-plane), material (PCL or b-TPU), or porosity (PS). The only relevant feature was the presence or absence of a perimeter surrounding the scaffold, even though previous works also reported an influence of PS¹⁰⁴³; scaffolds with perimeters exhibited a larger shear modulus.

Table 4. Mechanical properties of the optimal scaffolds (i.e., triangular patterns with PS 1.5 and 2 mm) in the in-plane / out-of-plane. E_{rheo} corresponds to Young’s modulus obtained from the rheometer in the 2nd step of the measuring protocol. E_{UTM} corresponds to Young’s modulus as obtained from the Universal Testing Machine. G_{rheo} corresponds to the Shear (storage) modulus obtained from the rheometer in the 3rd step of the measuring protocol.

<i>With Perimeter</i>	<i>PCL</i>		<i>b-TPU</i>	
	1.5	2	1.5	2
E_{rheo}^*	6400 ± 900 / 1500 ± 700 kPa	2200 ± 100 / 8040 ± 40 kPa	350 ± 10 / 970 ± 90 kPa	1000 ± 70 / 1400 ± 200 kPa
E_{UTM}^{**}	47 ± 8 / 140 ± 20 MPa	250 ± 40 / 150 ± 10 MPa	0.32 ± 0.02 / 11 ± 2 MPa	0.36 ± 0.05 / 10 ± 0.5 MPa
G_{rheo}^{***}	4.2 ± 0.5 / 3.9 ± 0.2 MPa	4.2 ± 0.5 / 4.3 ± 0.3 MPa	4.5 ± 0.4 / 0.4 ± 0.1 MPa	3.1 ± 0.6 / 2 ± 1 MPa

<i>Without Perimeter</i>	<i>PCL</i>		<i>b-TPU</i>	
	1.5	2	1.5	2

E_{rheo}	$1.1 \pm 0.1 /$	$0.099 \pm$	0.14 ± 0.04	0.04 ± 0.01
	0.6 ± 0.5 MPa	$0.003 / 0.6 \pm 0.1$ MPa	$/ 0.67 \pm 0.04$ MPa	$/ 0.11 \pm 0.02$ MPa
E_{UTM}^{**}	$1.0 \pm 0.3 /$	$1.10 \pm 0.06 /$	$2.0 \pm 0.6 /$	$1.7 \pm 0.6 /$
	2.0 ± 0.4 MPa	1.2 ± 0.3 MPa	0.3 ± 0.1 MPa	1.5 ± 0.3 MPa
G_{rheo}^{***}	$3 \pm 2 / 0.4$	$1.0 \pm 0.9 / 5$	0.07 ± 0.03	$1.0 \pm 0.9 /$
	± 0.3 MPa	± 1 MPa	$/ 0.3 \pm 0.05$ MPa	1.3 ± 1 MPa

19.5. Characterization of the microstructure

A deeper study of the microstructure was also performed to understand the apparent differences between candidate geometrical morphologies. In 3D bioprinting, there are differences between the computer design and the final printed scaffold. So, μ CT technology is an outstanding tool for probing the actual architecture of the fibers inside scaffold¹⁰⁷⁴. Considering previous results, the microstructure was characterized in T1.5 and T2 geometries for both biomaterials. **Figure 65A to -D** represents a cross-section corresponding to the middle plane in the axial direction of the scaffolds to analyze the fibers' disposition and the “empty-space” across those fibers¹⁰⁷⁵. The distance (in different colors) between the pillars produced by filament conglomeration can be appreciated in sagittal sections. Although apparently, there were no significant differences among PCL geometries and b-TPUe; however, a deeper analysis showed that b-TPUe presents a lesser distance for both PS, which seems to be related to its higher regularity in fiber distribution.

On the other hand, the analysis of the porous interconnectivity (orange ellipses) in the sagittal middle planes showed that. The accuracy in printing perfect cylindrical fibers was almost lost at PS of 2 mm, although for b-TPUe, they present higher resolution and homogeneity. Also, there is more homogeneity in the fiber disposition in b-TPUe, resulting in continuous lines in the coronal

planes (**Figure 65A** and **-C**). Those irregularities imply direct consequences because a higher irregularity is proportional to lower space, and higher irregularity implies less isotropy, which derives in poor mechanical toughness¹⁰⁷⁶. Nonetheless, although the differences between T1.5 and T2 were lower in the b-TPUe; however, these influenced proliferation rates at day 1, as appreciated in **Figure 62D**, indicating the necessity of high printing resolution to enhance cell viability and ECM synthesis^{1077,1078}.

Further, the analysis of the estimated porosity with image segmentation confirmed our previous results, showing that PS 2 mm had higher porosity than PS 1 mm and that b-TPUe has a higher porosity than PCL at the same PS (**Figure 65E**).

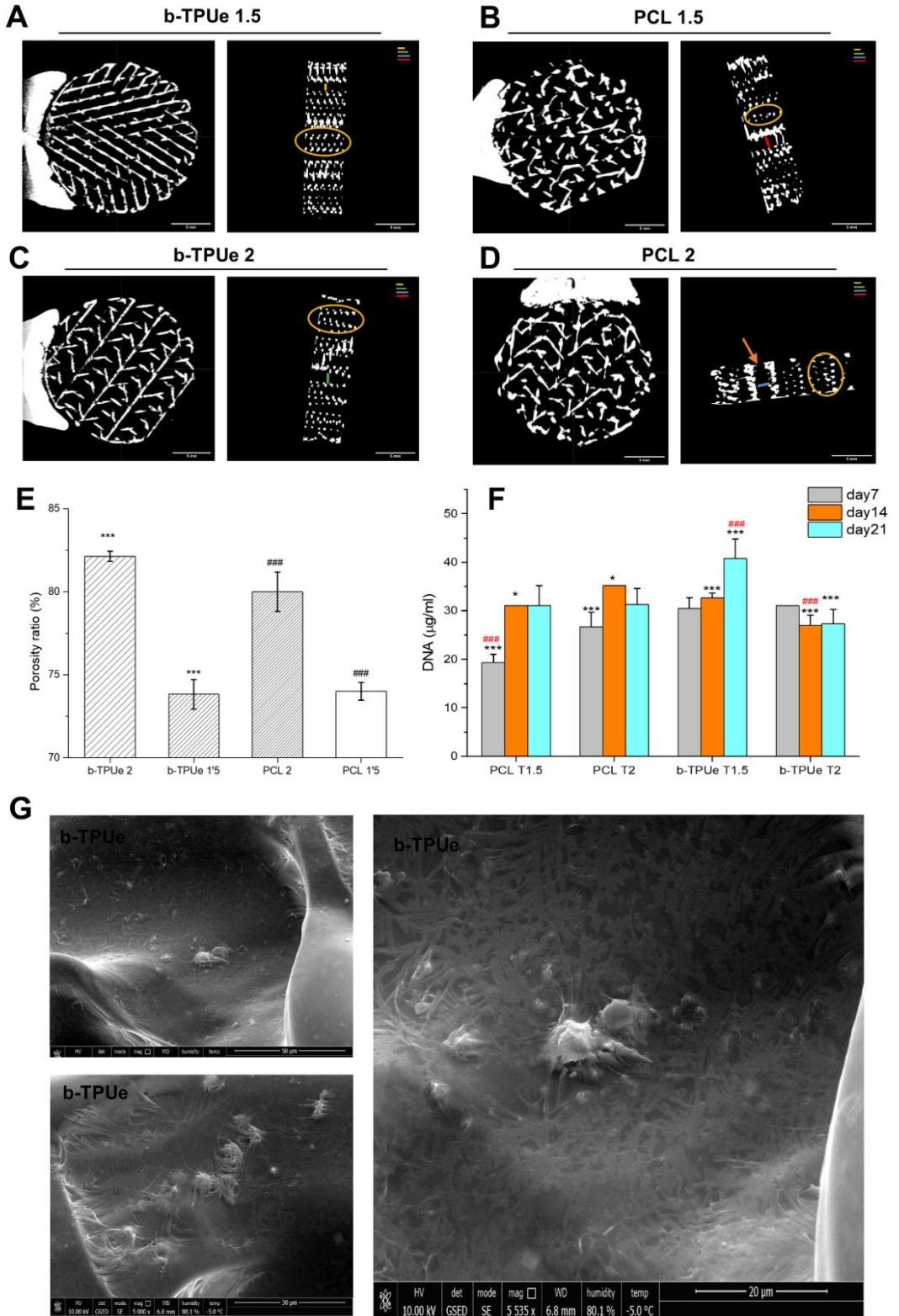
19.6. DNA Quantification

Once it was established that triangular geometries with PS 1.5 and 2 mm combined good optimal mechanical properties and an excellent proliferative response, cell analysis was continued to elucidate the most suitable combination of geometry and PS for IPFP-MSCs. For this purpose, DNA quantification was used since it is a more rigorous technique for measuring the real amount of viable cells inside the 3D scaffolds¹⁰⁷⁹.

The DNA content for each geometry at d7, d14, and d21 was determined (**Figure 65F**). Interestingly, on day 7, the DNA content was higher in b-TPUe in contrast with the proliferation curves, and in T1.5 for PCL, the DNA content was significantly lesser than in the rest of the samples. These results suggest that at early stages, more cells were attached to b-TPUe but with a lower metabolism, indicating a possible poor cell-biomaterial interaction¹⁰⁸⁰. Moreover, DNA increased in a time-dependent manner up to day 21 for both biomaterials in T1.5 and decreased for T2. These results agree with those obtained in the microstructure study since the accurate pillar distance was lowest for triangular geometry and lesser PS in each material. From the DNA quantification assay, it

can be extracted that this final configuration, b-TPUe T1.5, has a better viability response. A foremost requisite for RM applications is maintaining the cell viability of biofabricated scaffolds over time¹⁰⁸¹. Perhaps it is very important to consider how minor mechanics variants also directly affect cell viability^{1078,1082}. In agreement, our results probed that both geometry and porosity modify mechanics and the microstructure and how both parameters influence cell proliferation and viability. Moreover, we demonstrated that IPFP-MSCs-loaded b-TPUe scaffolds are suitable to maintain growth and viability up to day 21, which makes it a good candidate for cartilage tissue engineering as previously has been proved for other polyurethane scaffolds with regenerative properties¹⁰⁷⁷.

Figure 65. A-D) μ CT cross-sectional images (coronal and sagittal middle planes) of T1.5 and T2 geometries. Inside orange circles are presented the ‘pilars’ formed because of filament superposition among layers. Color bars represents the real distance among those ‘pilars’ (which should be PS), in the legend they are aligned for comparing sizes between samples. Orange bar corresponds to T1.5 b-TPUe, red bar T1.5 PCL, green bar T2 b-TPUe and blue bar T2 PCL. E) Porosity ratio obtained from segmentation image analysis from μ CT technique for b-TPUe and PCL, geometries: T1.5 and T2. P-Value less than 0.001 was represented with *** for b-TPUe and with ### for PCL. (n=3) F) DNA content for PCL and b-TPUe in T1.5 and T2 geometries. P-Value less than 0.05 was represented *, P-Value < 0.01 with ** and P-Value < 0.001 *** among equal material. P-Value < 0.001 ### with respect the rest of cases. G) ESEM images of b-TPUe T1. In the amplified picture, it is localized what seems ECM from ifpMSCs. b-TPUe seems to present some rugosity at microstructure, and, consequently there are found more cells attached. \hookrightarrow next page



19.7. Study of interactions between cells and biomaterials by ESEM

All previous results evidenced that cell viability and proliferation were better at d21 for T1.5 b-TPUe and T2 PCL. Then, the interactions between IPFP-MSCs and both biomaterials by ESEM were analyzed, a technique that enables the investigation of both cell and material surface morphology in hydrated conditions¹⁰⁸³. ESEM images on day 21 revealed that IPFP-MSCs attached to the T1.5 b-TPUe scaffolds (**Figure 65G**) actively produced a dense ECM that covered the surface and enhanced their integration with the material. On the other hand, T2 PCL showed less ECM production and areas with lesser cells attached to the biomaterial surface (**Figure 91**).

In future work, it will be interesting to assess whether changes in pore size or geometry will increase or decrease the chondrogenic potency of the scaffold. Heang Oh et al. demonstrated a slight influence on the diameter of cylindrical pores¹⁰⁸⁴. However, a lack of cartilage control of induced chondrogenic MSCs prevents an accurate comparison to extrapolate a real effect on how geometry influences chondrogenesis. Contrarily, Singh et al. showed the importance of scaffold stiffness for chondrogenesis¹⁰⁸⁵ and evidenced that growth factors (like TF β -3) deeply induce this process. Thus, although geometry can optimize the cell niche and ECM production, a combination of tailored scaffold biomechanics with specific growth factors should be recommended for cartilage tissue engineering. However, it would be interesting to analyze the possible effects of geometry in the chemical cues' doses. Despite this, such analyses are out of the scope of this research.

19.8. Conclusions

This work completed an extensive study using two different biomaterials (b-TPU and PCL) oriented to CTE applications. We demonstrated how the pore geometry and PS of biofabricated IPFP-MSCs-loaded scaffolds affected the final

cell viability and adhesion. To fulfill this purpose, EBB was done with both biomaterials tailoring different aspects of their microstructure to quantify the relationships between porosity, design, and mechanical properties. We confirmed that geometry is a crucial parameter for cellular interaction with the biomaterial because of PS and fiber orientation, as suggested by our analysis of the S/V ratio and AF. Thus, it was demonstrated that higher interconnectivity of fibers and, as a consequence of higher exposed angle frequency, presents higher biointegration.

It was shown that decreasing the PS increased the stiffness of the scaffold independently of the biomaterial. Besides, it is the first time that the vast importance of the perimeter in scaffolds rigidity was exposed, making this aspect of scaffold architecture a key factor for good cell integration and biomechanical properties. A deeper analysis playing with the perimeter of cribbed architectures (T1.5 and T2) was inspected, making the T1.5 b-TPUe the optimum geometry and biomaterial for IPFP-MSCs. In summary, our data suggest the necessity of designing the pore geometry and the scaffold microstructure to optimize better 3D constructs for applications on CTE. Consider this will improve the reliability of a good biointegration of 3D constructs in regenerative medicine of cartilage injuries.

Chapter II

Chondro-inductive b-TPUe-based
functionalized scaffolds for
application in cartilage tissue
engineering

“Unlike the Industrial Revolution, the Biomimicry Revolution introduces an era based not on what we can extract from nature, but on what we can learn from her.”

“A diferencia de la Revolución Industrial, la Revolución de la Biomímesis introduce una era basada no en lo que podemos extraer de la naturaleza, sino en lo que podemos aprender de ella.”

Janine M. Benyus

20. Abstract of Chapter II

Osteoarthritis has a tremendous socioeconomic impact and mainly affects AC, a tissue with reduced self-healing capacity. In this work, we functionalized 3D printed b-TPUe scaffolds, and IPFP-MSCs were used as the cellular source. Since b-TPUe is a biomaterial with mechanical properties similar to cartilage but does not provide the desired environment for cell adhesion, scaffolds were functionalized with two methods, one based on type I collagen and the other in 1-pyrene butyric acid (PBA) as principal components. Alamar Blue and confocal assays displayed that PBA functionalized scaffolds support higher cell adhesion and proliferation for the first 21 days. However, type I collagen functionalization induced higher proliferation rates and similar cell viability than the PBA method.

Further, both functionalization methods induced ECM synthesis and the presence of chondrogenic markers (Sox9, Col2a, and Acan). Finally, SEM images probed that functionalized 3D printed scaffolds presented much better cell/biomaterial interactions than controls and confirmed early chondrogenesis. These results indicate that the two methods of functionalization in the highly hydrophobic b-TPUe enhanced the cell-biomaterial interactions and improved the chondro-inductive properties, which has excellent potential for application in cartilage tissue engineering.

Keywords: bioprinting; scaffold; functionalization; osteoarthritis; type I collagen; 1-pyrenebutyric acid

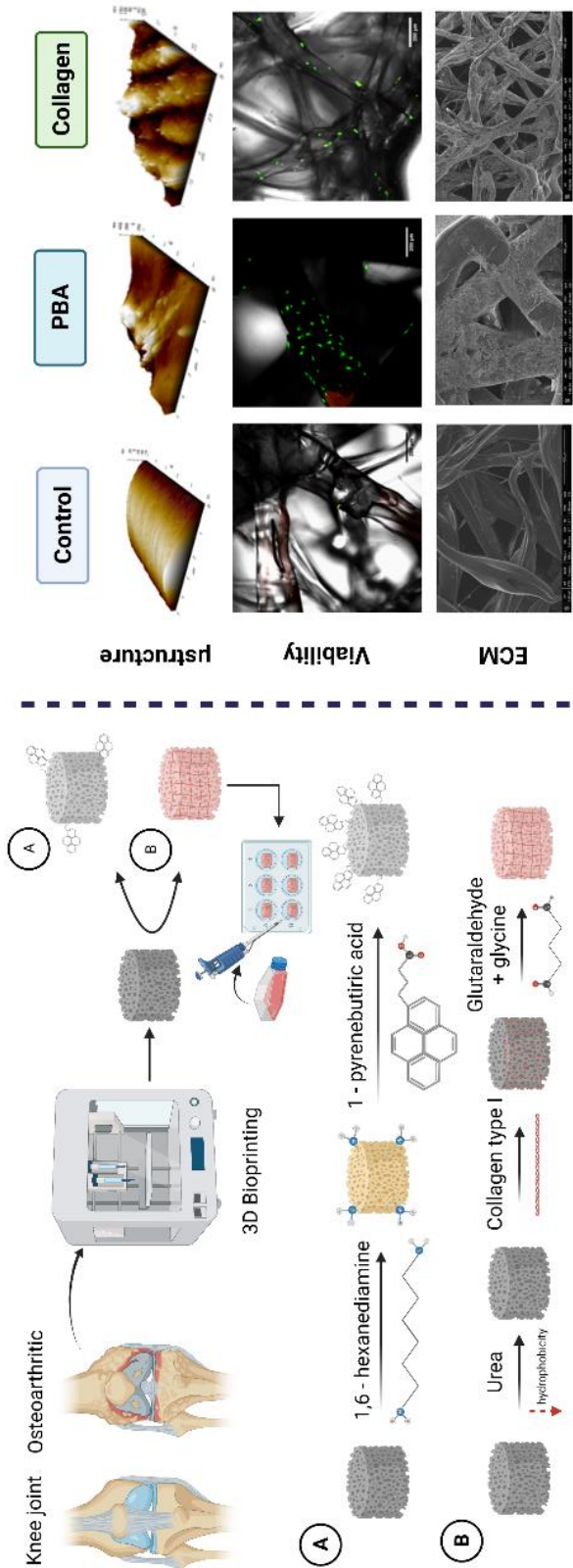


Figure 66. Graphical abstract of Chapter II. Scheme of the whole procedure followed in Part II.

21. Background for Chapter II

RM persecutes the total or partial regeneration of human cells, organs, or tissues to restore or establish normal function¹⁰⁸⁶. On the other hand, TE is a branch of RM based on three pillars: cells, biomaterials, and bioactive molecules¹¹⁵. OA, an irreversible and multifactorial disease, is among the different pathologies that can benefit from the RM. The low regeneration rate in OA is a consequence of the cartilage characteristics, which is an avascular tissue, not lymphatic, and without nerve endings¹⁰⁸⁷. OA leads to pain and loss of joint function due to AC loss¹⁰⁸⁸. It is one of the most common joint disorders resulting from a combination of risk factors, where age and obesity are the most prominent, concerning most frequently in the knees⁶⁴². Until current knowledge, there is no OA treatment for stopping or slowing its progression, being surgical alternatives the treatment of choice¹⁰⁸⁹.

In the last decades, several TE cartilage products like the MACI, Hyalograft® C, NeoCart®, NOVOCART® 3D, Cartipatch®, etc., have tried to mimic AC¹⁰⁹⁰. However, most of these therapies involve fibrocartilage formation. To improve the efficacy of such TE procedures, novel approaches, like 3D biofabrication, are developing to introduce stem cells and avoid the drawback of autologous chondrocytes therapies into a 3D matrix and culture them *in vitro* for more extended periods, 4–6 weeks¹⁰⁹⁰. The 3D matrices are scaffolds that serve as 3D structures to support autologous cells until they synthesize their matrix components temporarily¹⁰⁹¹. This fact allows the creation of a relatively mature tissue *in vitro* before implantation, with biochemical integrity similar to healthy AC, since the presence of matrix around the cells is known to enhance donor cell retention¹⁰⁹² and protect cells from inflammatory agents¹⁰⁹³. Also, scaffolds meet specific requirements such as i) the presence of an adequate surface (roughness and hydrophilicity) to improve cell adhesion, ii) an internal structure (porosity, pore size and structure, and fiber diameter) that supports cellular adherence, proliferation, and differentiation, as well as diffusion of nutrients, oxygen, and

wastes, iii) and also possess mechanical and biochemical properties similar to target tissue¹⁰⁹⁴. Scaffolds can be manufactured with biomaterials, materials intended to interact with biological systems to evaluate, treat, increase, or replace tissues, organs, or functions of the body.

A considerable problem related to biomaterials is how hydrophobicity and lack of biological recognition sites on the material's surface provide an unfriendly environment for cell adhesion¹⁰⁹⁵. Previous functionalization studies focused on modifying biomaterial surfaces have been developed to improve cell adhesion. Further, surface modifications play a role in cell migration, proliferation, and differentiation of stem cells¹⁰⁶⁹. Therefore, cell adhesion enhancement would improve cell-biomaterial interaction¹⁰⁹⁶. Several functionalization methods were used based on interacting components with cell membrane proteins. For example, the surface can be functionalized with the peptide RGD¹⁰⁹⁷, with 1-pyrene butyric acid (PBA)¹⁰⁹⁸, or with different components present in the ECM like fibronectin or collagen¹⁰⁹⁹.

Synthetic polyesters, like b-TPUe, have received considerable attention for cartilage TE due to their appropriate mechanical properties, such as the highly elastic recovery capacity¹¹⁰⁰. However, its hydrophobicity does not provide the desired cell adhesion and proliferation environment. Hence, this study aimed to set up two different functionalization methods based on the biomaterial coating with type I collagen and PBA, probing how it can reduce the hydrophobicity of b-TPUe, improving cell-biomaterial interaction. Two methods were selected to compare a traditional coating method (type I collagen) adapted from literature¹⁰⁹⁹ with a new methodology (PBA) with reduced costs and good results obtained from making graphene biosensors¹⁰⁹⁸. Both methodologies evaluate the efficacy of functionalization by AFM)and ninhydrin reagent.

Then, the biological efficacy of both functionalization methods was analyzed by seeding IPFP-MSCs and performing the subsequent metabolic activity and viability studies. Together with cellular studies, ECM secretion was

analyzed through PCR, GAG quantification, and SEM to verify the chondrogenic potential of both functionalized methods.

22. Materials & methods for

Chapter II

22.1. Sample processing

The IPFP-MSCs were extracted directly from osteoarthritic patients of the Hospital Universitario de Málaga, Spain. Ethical approval for the study was obtained from the Ethics Committee of the Clinical University Hospital of Málaga, Spain (ethics permission number: 02/022010 Hospital Virgen de la Victoria, Málaga). Informed patient consent was obtained for all samples used in this study. Hoffa's fat pad was harvested inside the capsule, excluding vascular and synovial regions. The isolation and culture protocols of IPFP-MSCs were done according to López-Ruiz et al.¹⁰⁵³. IPFP-MSCs were characterized following the established criteria of the International Society for Cellular Therapy (ISCT) (see Supplementary 1.1)⁵¹.

22.2. Printing of 3D scaffolds

The desired scaffold was designed using the Cura 3D program, and its printing with the Monoprice Mini V2 bioprinter inside a class II laminar flow cabinet was carried out. The bioprinter was cleaned in 70 % ethanol and left overnight under UVs.

The scaffolds were designed to fit a multiwell 48-well plate. Therefore, they took cylindrical geometry: a diameter of 10 mm, a height of 2 mm, and a layer height of 200 μm . The extruder's movement speed was set at 14 mm s^{-1} , and the working temperature was 230 $^{\circ}\text{C}$. Finally, the flow rate (the speed at which the filament travels through the extruder) was determined at 1 mm s^{-1} .

To ensure the complete sterility of the scaffolds, they were placed in a Petri dish and washed with 20 %, 50 %, and 70 % ethanol. After washing, UV

radiation was applied for 1 hour on both sides. A new wash with 1% PBS of antibiotic (P/S) was carried out to remove the remaining ethanol. Finally, the b-TPUe scaffolds were immersed in PBS 1% antibiotic and incubated until functionalization protocols.

22.3. Functionalization with PBA

Scaffolds were placed in a multi-well plate and immersed in a 10 % isopropanol solution of 1,6-hexanediamine for 30 minutes at room temperature for the PBA functionalization method. After, scaffolds were rinsed in 1-pyrenebutyric acid (PBA; Sigma-Aldrich) at 5 mM DMSO (Sigma-Aldrich). Finally, several washes were done with PBS^{115,1086}.

22.4. Functionalization with type I collagen

Scaffolds were immersed in urea (Sigma-Aldrich) for 24 hours at room temperature¹⁰⁹⁹. Subsequently, the type I collagen of calfskin (0.1 % in 0.1M Acetic Acid) (Sigma-Aldrich) was added overnight. After, 0.625 % glutaraldehyde in 0.6M monopotassium buffer at pH 7.4 was used in the first functionalization processes¹⁰⁹⁹. Then, a second functionalization protocol was tested to improve cell adhesion. For this purpose, glutaraldehyde concentration was reduced from 0.625% to 0.16 % and used in the same buffer. This reduction of glutaraldehyde was made to ensure cellular viability¹¹⁰¹. Finally, for each glutaraldehyde pump, 0.2 M and 0.5 M glycines were added for 10 minutes to block the unreacted functional groups of glutaraldehyde.

22.5. Magnifying glass and AFM

They were studied before (control) and after surface modification at a macroscopic and microscopic level for surface identification of modified samples. Samples were introduced in different solutions for 24h: MilliQ water (control), 70% and 100% ethanol, in isopropanol, and 0.6 M monopotassium buffer at pH 7.4. For this study, samples were cleaned before being used. Leica

Si9 magnifying glass was used to study scaffold surface properties in different conditions macroscopically. At the microscopic level, AFM NX20 analyses were performed without additional pretreatment.

22.6. Immunofluorescence of type I collagen and PBA after the functionalization process

Indirect immunofluorescent visualization of type I collagen was performed to probe type I collagen in the b-TPUe biomaterial surface after the functionalization method. Collagen-functionalized scaffolds were treated with a primary antibody against type I collagen (Sigma-Aldrich) and a secondary antibody (Thermofischer). PBA possesses autofluorescence, so no staining was necessary, and scaffolds were observed before and after the functionalization process ($\lambda_{\text{exc}} = 340 \text{ nm}$ and $\lambda_{\text{em}} = 405 \text{ nm}$). Images were obtained using a confocal microscope (Nikon Eclipse Ti) and analyzed with Image J software (v. 1.52i, USA).

22.7. Seeding of the scaffolds with cells

IPFP-MSCs suspension (7×10^5 cells) was pipetted onto each scaffold and incubated for 4 h at 37 °C to allow cell attachment. The cell-seeded scaffolds were transferred into new low attachment 48-well culture plates with 1 ml of medium. After, all samples were incubated under a 5% CO₂ atmosphere at 37 °C for 21 days. The culture medium was replaced every 2 days.

22.8. Metabolic activity

The metabolic rate was assessed by colorimetric Alamar Blue assay (Thermo Fisher Scientific) following the manufacturer's instructions on days 1, 3, 7, 14, and 21 days after seeding. Cell-free 3D scaffolds were used as controls, and data were normalized to the appropriate control. The fluorescence intensity was measured using a plate reader (Synergy HT, BIO-TEK).

In addition, DNA was also determined at days 1, 7, 14, and 21 in collagen and PBA samples to check the difference in adhesion and Alamar blue reduction among functionalization protocols. DNA content was also approximated with DAPI, but the extraction protocol was different: samples were inserted in different Eppendorf tubes, and 1 mL of distilled water was added to induce osmotic lysis at 37°C for 1 h. Immediately after, the tubes were transferred to -80°C for 1 h. This protocol was adapted from the one proposed by Sika et al. and was not used to estimate DNA concentration¹¹⁰².

22.9. Cell Viability

The Live/Dead assay (Thermo Fisher Scientific) was used following the manufacturer's instructions to evaluate the viability of IPFP-MSCs before and after the bioprinting process on days 1, 7, and 21. The scaffolds were observed using a confocal microscope (Nikon Eclipse Ti) for visualization and image. Images were analyzed with Image J software (v. 1.52i, USA).

22.10. DNA and GAG quantification

Scaffolds (n=3) were digested with papain (25 uL ml⁻¹ in FBE) after 1 day and 21 days in culture with DMEM Glutamax (Thermo) 1% P/S, 10% FBS. GAG quantification was approached using dimethyl methylene blue (DMMB) colorimetric assay, whereas DNA content was estimated using a fluorometric marker (DAPI staining). The standard curve for the GAG protocol was used using a gradient curve of Chondroitin sulfate (Sigma), and the DNA standard curve was done using DNA from Calf Thymus (Sigma-Aldrich).

22.11. Cartilage gene expression

RNAs for type II collagen, aggrecan, and type I collagen (as a control) were analyzed using PCR assays to determine the cartilage gene expression. Primer sequences were used as in previous works¹⁰³⁰.

Scaffolds were cultivated for 21 days with an initial cell concentration of 2×10^6 cells per scaffold. Both functionalized cases were studied under standard medium (DMEM, 10% FBS, and 1%P/S) and chondrogenic medium (DMEM 1%PS, 1% ascorbic acid, 1% proline, 1% insulin transferrin serum-ITS, 1% of transforming growth factor-beta 3, TGFB3, and 0.1% dexamethasone). After, total messenger RNA (mRNA) from attached IPFP-MSCs was extracted using 1 ml RNazol RT (Sigma) per Eppendorf/scaffold (n=3) at day 21. Then, mRNA was reverse transcribed into cDNA using the Reverse Transcription System kit (Promega) following the manufacturer's protocols. Finally, a quantitative real-time polymerase chain reaction (qRT-PCR) was executed using an SYBR green master mix (Promega) under the company's instructions. Gene expression levels were normalized to the housekeeping gene glyceraldehyde 3-phosphate dehydrogenase (GADPH) and showed a fold change relative to the value of control IPFP-MSCs at day 0.

22.12. Scanning electron microscopy

The scaffolds were imaged with an FEI Quanta 400 microscope (Thermo Fisher Scientific-FEI, Fremont, CA, USA) with an Everhart-Thornley detector (E-TD) for dry and conductive samples in high vacuum mode. Samples were incubated for 21 days (2×10^6 cells per scaffold) and then fixed with 2% glutaraldehyde overnight at room temperature. The next day, they were rinsed in 0.1 M cacodylate buffer and saved at 4°C. Then, samples were prepared for SEM following standard protocols: i) several washed with PBS, ii) dehydration series with ethanol (30-100%), iii) they were critically point dried in an Emscope CPD 750, iv) mounted on aluminum SEM stubs, and v) sputter coating with a conductive material (gold-palladium alloy, Sputter Coater 108 Auto).

22.13. Statistical analysis

Under each condition, three experiments were performed to assess variability (n=3, data representation corresponds to mean \pm SD). The data were

processed and represented using the software Origin 9.0 (OriginLab Corporation, Northampton, MA, USA). Homoscedasticity was verified on all data (Shapiro-Wilk). The Student's two-tailed t-test was applied to analyze the data with a confidence interval of 0.05. If any, outliers were neglected with the IQR (interquartile range) procedure, where the ANOVA test compared multiple samples, and means were compared employing a two-tailed Bonferroni Test with a confidence interval of 0.05. In figures, p-values < 0.001 are represented with '***', < 0.01 '**', and < 0.05 '*'.

23. Results from Chapter II

23.1. Characterization and verification of functionalization protocols on b-TPUe

Functionalization methods involve some aggressive reagents, so evaluating their effect on the biomaterial is necessary. The surface topology of b-TPUe scaffolds was investigated using a magnifying glass and AFM¹¹⁰³, to probe any macrostructure and/or microstructure surface variation of the fibers derivate by functionalization processes.

For this purpose, b-TPUe scaffolds were immersed in different solutions for 24 hours: MilliQ water (**Figure 67A**), which establishes the control; 70% ethanol (**Figure 67B**) used in the sterilization of the scaffolds; isopropanol used in the 1,6-hexanediamine (**Figure 67C**) solution involved in the first step of PBA functionalization; and, finally, 0.6 M monopotassium buffer at pH 7.4, where glutaraldehyde (**Figure 67D**) was dissolved, a fundamental step in functionalization with type I collagen. AFM showed no perceptible surface modification in the monopotassium buffer; however, effects produced by etOH 70% and isopropanol increased rugosity, but no degradation appeared (variation less than 100 nm as can be seen in the legend bars of **Figure 67B** and **-C**)¹¹⁰⁴. In addition, Supplementary Figure S1 shows no significant difference applying 100% EtOH or 70% EtOH.

Scaffolds already functionalized with collagen (**Figure 67E**) and PBA (**Figure 67F**) were analyzed under AFM to compute the presence of any surface modification. **Figure 67E** probed how collagen fibers were aligned surrounding the scaffold's filaments adding rod-likely patterns of 150 nm in diameter. **Figure 67F** confirmed the presence of external material attached to the b-TPUe surface. In this case, PBA formed small mountains of 200-400 nm in height.

CHAPTER II CHONDRO-INDUCTIVE FUNCTIONALIZED SCAFFOLDS FOR CARTILAGE TISSUE ENGINEERING

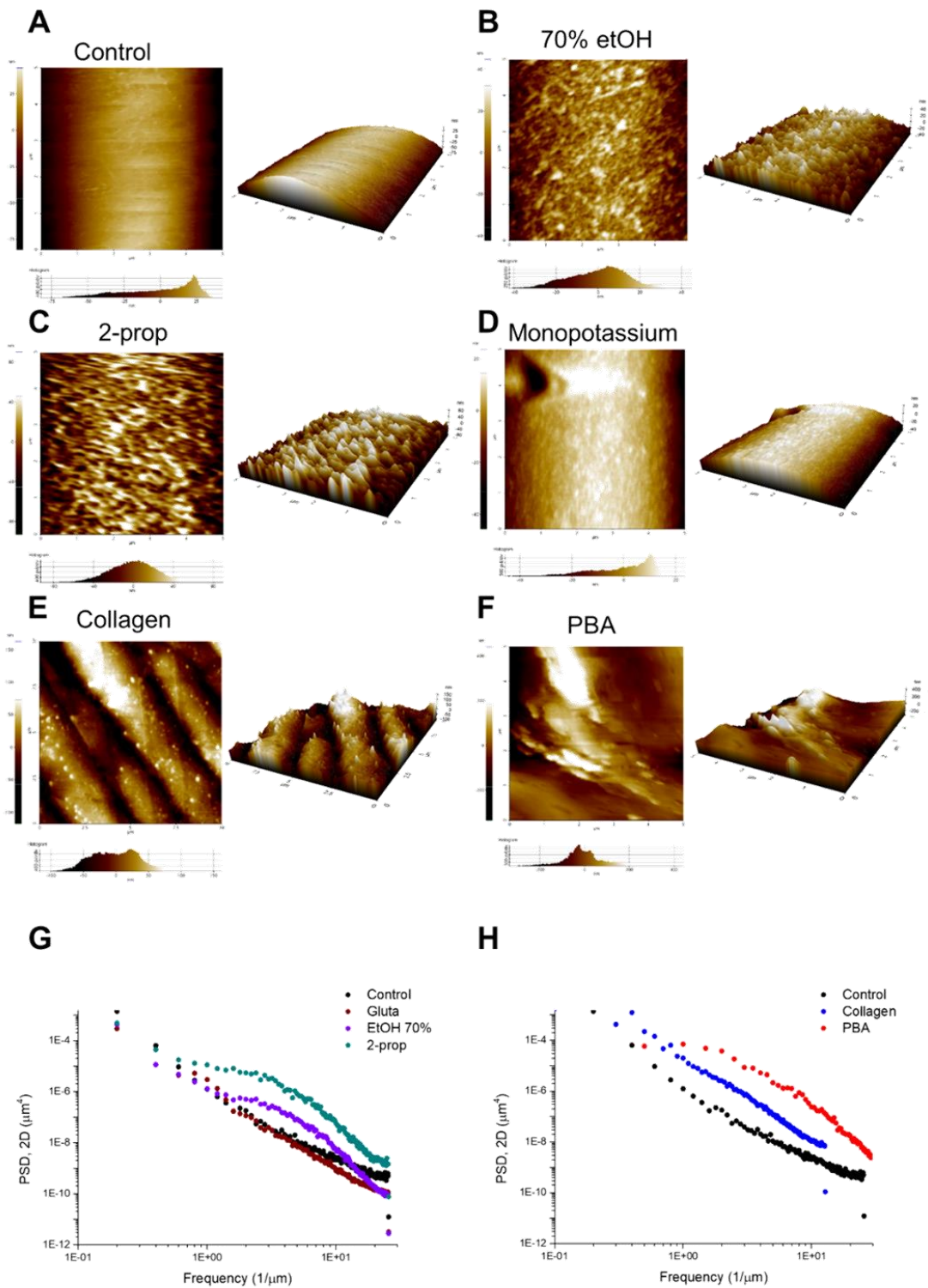


Figure 67. AFM topography analyses. (A-F) Height images captured from AFM for, (A) Mili Q water as control, (B) ethanol 70% (mixed with Mili Q water), used to sterilized scaffolds, (C) 2-propanol 100% buffer, used to diluted hexamethylenediamine (necessary to PBA functionalization) and (D) KH₂PO₄ 0.16 % Glutaraldehyde buffer used to crosslinked collagen fibers in the collagen type I functionalization. (E) Height images for collagen functionalized scaffolds, whereas (F) exposes a PBA functionalized fiber. In all cases, the ROI was 5x5 μm . (G) PSD curves from AFM buffer analyses compared with control. (H) PSD of functionalized scaffolds versus control.

In addition, the power spectra density (PSD) was performed by AFM to compute quantitatively any possible exchange in surface patterns¹¹⁰⁵. **Figure 67G** shows buffers effects over scaffolds vs. control, whereas **Figure 67H** compares functionalized scaffolds concerning control. Here, it is interesting that the glutaraldehyde buffer does not modify the rugosity of scaffold fibers. In contrast, EtOH 70% and 2-prop buffers showed an increase in the height of rugosity, manifested at frequencies lesser than 1 micron. Following previous consideration, collagen functionalization increased the height of rugosity at frequencies higher than 1 micron, inducing those collagen fibers to be distributed over the scaffold surface, letting less than 1 micron between each fiber. Further, comparing PSD curves from PBA functionalization buffer and 2-propanol buffer shares similar tendencies, implying no significant microstructure modification of scaffold beyond the apparition of 400 nm peaks that were not found under 2-prop buffer.

Surface roughness was evaluated at the macroscopic level through images taken with the Leica Si9 magnifying glass, but no differences were found (**Figure 68A**). After comparing these pictures with previous results, it can be estimated that any variation perceived by AFM does not modify scaffold microstructure or fiber integrity. In 70% EtOH and 2-prop buffers, some brighter points for control and glutaraldehyde buffer can be distinguished, which is explained by curves from **Figure 67G**. In addition, it can be appreciated that the size of such points is larger in 2-prop than 70% EtOH as the PSD shows (**Figure 67G**).

Regarding verification of functionalization protocols, with AFM (**Figure 67E** and **-F**), immunofluorescence assays were performed to check the final result. Since the PBA functionalization method consists of two steps, the amination process and PBA addition, to prove that the binding PBA is possible, it is necessary to check the previous amination of the scaffolds (see chapter 34, theme 34.1).

As can be seen in **Figure 68B**, the ninhydrin standard curve follows a dose-response trend, with the following equation¹¹⁰⁴ :

$$y = \frac{A1 + (A2 - A1)}{1 + 10^{(\log x_0 - x) \cdot p}} \quad (R^2 = 0,988) \quad (54)$$

where: A1=2,626; A2=100,640; logx0=34,587

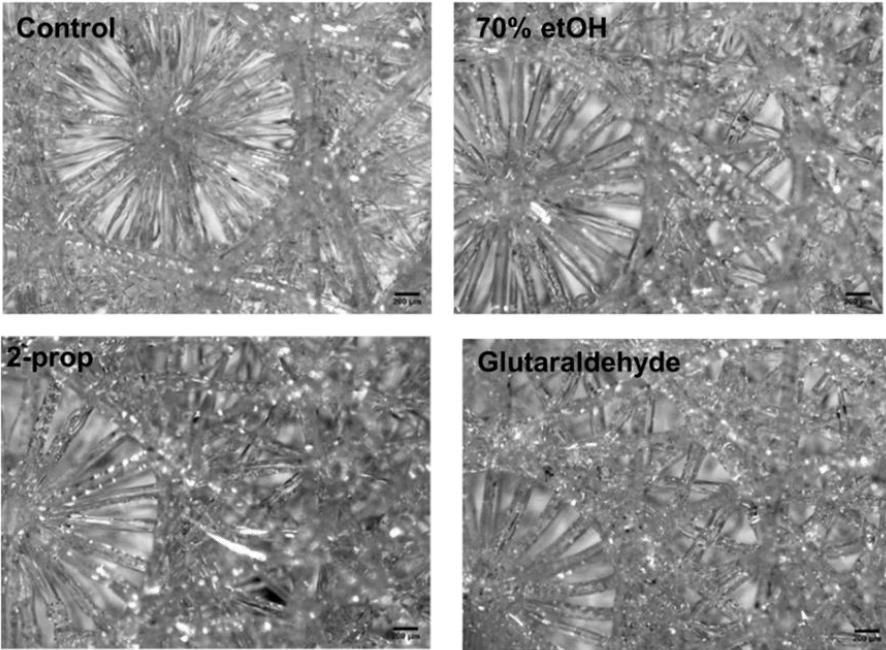
This trend corresponds to the sigmoid or Hill model¹¹⁰⁶, one of the two commonly used pharmacokinetic models to correlate the pharmacological response with drug concentrations. This model follows the following equation:

$$E = \frac{E_{max} \cdot C^{\gamma}}{CE_{50}^{\gamma} + C^{\gamma}} \quad (55)$$

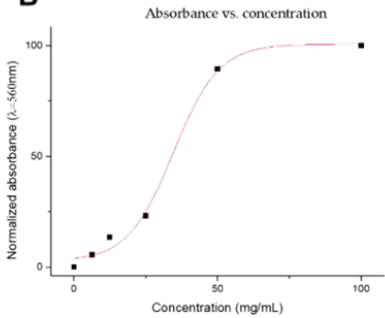
where E_{max} would be the V_{max} , CE_{50} the K_m , corresponding to the Michaelis-Menten equation, and γ a parameter.

B-TPUe scaffolds treated with 1,6-hexanediamine through the addition of ninhydrin showed an average absorbance significantly increased ($p < 0.001$) compared with non-aminated scaffolds, allowing to verify that the amination process was efficient (**Figure 68C**). To finalize with PBA, **Figure 68D** displays the autofluorescence of b-TPUe without functionalization and after PBA treatment, and it can be distinguished the mountain patterns shown in the AFM as brighter fluorescence points.

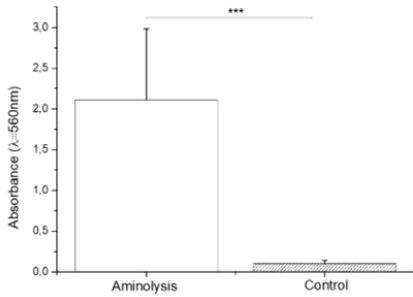
A



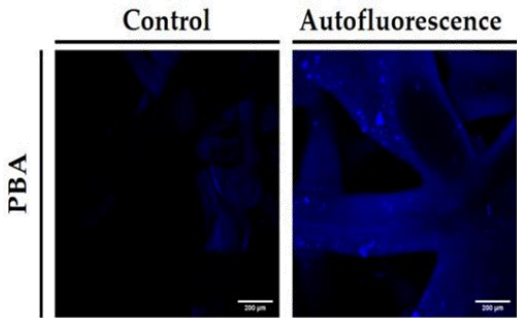
B



C



D



E

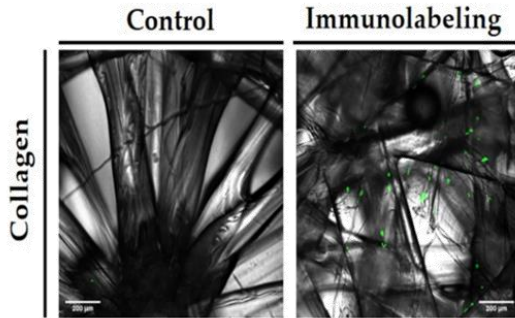


Figure 68. Macroscopic and microscopic characterization. (A) Images captured by magnifying glass under transmitted light from different buffers. Control was Mili Q water, 70% ethanol mixed with Mili Q water, pure isopropanol, and KH₂PO₄ 0.16 % Glutaraldehyde buffer. (B) Ninhydrin standard absorbance curve is done by a spectrophotometer. (C) Ninhydrin assay for aminated scaffolds (scaffolds embedded inside hexamethylenediamine 2-prop buffer) and control (naïve scaffolds). (D) Confocal images from autofluorescence of bTPUe scaffolds functionalized with PBA, and control (non-functionalized). (E) Confocal images from immunohistochemistry scaffolds, Immunolabeling as type I collagen functionalization, and control as naïve scaffolds. Magnifying was 10X.

Also, an immunofluorescence assay was performed to visualize the components of the functionalization. Immunofluorescence in **Figure 68E** to check type I collagen presence (in green) shows the previous homogeneity distribution with no difference between fluorescence points. The collagen can be appreciated over fibers at different focal planes indicating that collagen functionalization was produced on the whole scaffold.

In conclusion, results showed differences in the roughness of the material depending on the condition to which they were subjected, but no apparent degradation was observed, and, more importantly, it can be established that functionalization succeeded in both cases.

23.2. Evaluation of cell metabolic activity and cell viability in PBA and type I collagen functionalized-scaffolds

Functionalization processes aim to improve the superficial properties of b-TPUe since it is a highly hydrophobic material. The reduction of hydrophobicity and the addition of different components to the surface of the scaffolds can enhance cell-biomaterial interaction and consequently maintain cell viability and increase proliferation rate. For this purpose, IPFP-MSCs were seeded in the functionalized b-TPUe scaffolds, and metabolic activity was measured to assess cell attachment and proliferation using the Alamar Blue reagent (**Figure 69A**).

IPFP-MSCs were isolated from osteoarthritic patients and expanded until low passages 3-6. IPFP-MSCs were characterized (**Figure 93**) using the guidelines proposed by the ISCT⁵¹. After that, IPFP-MSCs (700,000 cells per well) were seeded over scaffolds and incubated for 4 h at 37°C; then, a fresh medium was applied. The progression of metabolic activity was monitored for 21 days for all conditions. In the case of type I collagen, we did additional studies to adjust the concentration of glutaraldehyde (**Figure 94**). Results on day 3 confirmed that the optimum glutaraldehyde concentration for collagen functionalization was 0.16 %.

On day 1, the difference in metabolic activity and, therefore, in cell proliferation was found between all conditions ($p < 0.001$) (**Figure 69A**). Both functionalization methods presented higher metabolic activity than controls. Moreover, type I collagen-functionalized scaffolds (0.16% of glutaraldehyde) showed higher metabolic activity than PBA-functionalized scaffolds with a high statistically significant difference ($p < 0.001$). On day 3, metabolic activity increased in control and PBA-functionalized scaffolds while it was maintained in type I collagen-functionalized scaffolds ($p < 0.05$) (**Figure 69A**). Although at day 3, the control showed an increase in its Alamar blue reduction, the metabolic levels dropped again, and they remained the rest of the days (**Figure 69A**). On day 7, metabolic activity increased in type I collagen-functionalized scaffolds while PBA-functionalized was preserved ($p < 0.05$). Even so, both functionalization methods continued to show a higher metabolic activity compared to the control. In contrast, on day 14 and day 21, the decreasing trend continued in type I collagen-functionalized scaffolds, whereas the PBA method expressed maintenance (day 14) or increase (day 21) of proliferation compared with both collagen functionalization and control ($p < 0.001$).

CHAPTER II CHONDRO-INDUCTIVE FUNCTIONALIZED SCAFFOLDS FOR CARTILAGE TISSUE ENGINEERING

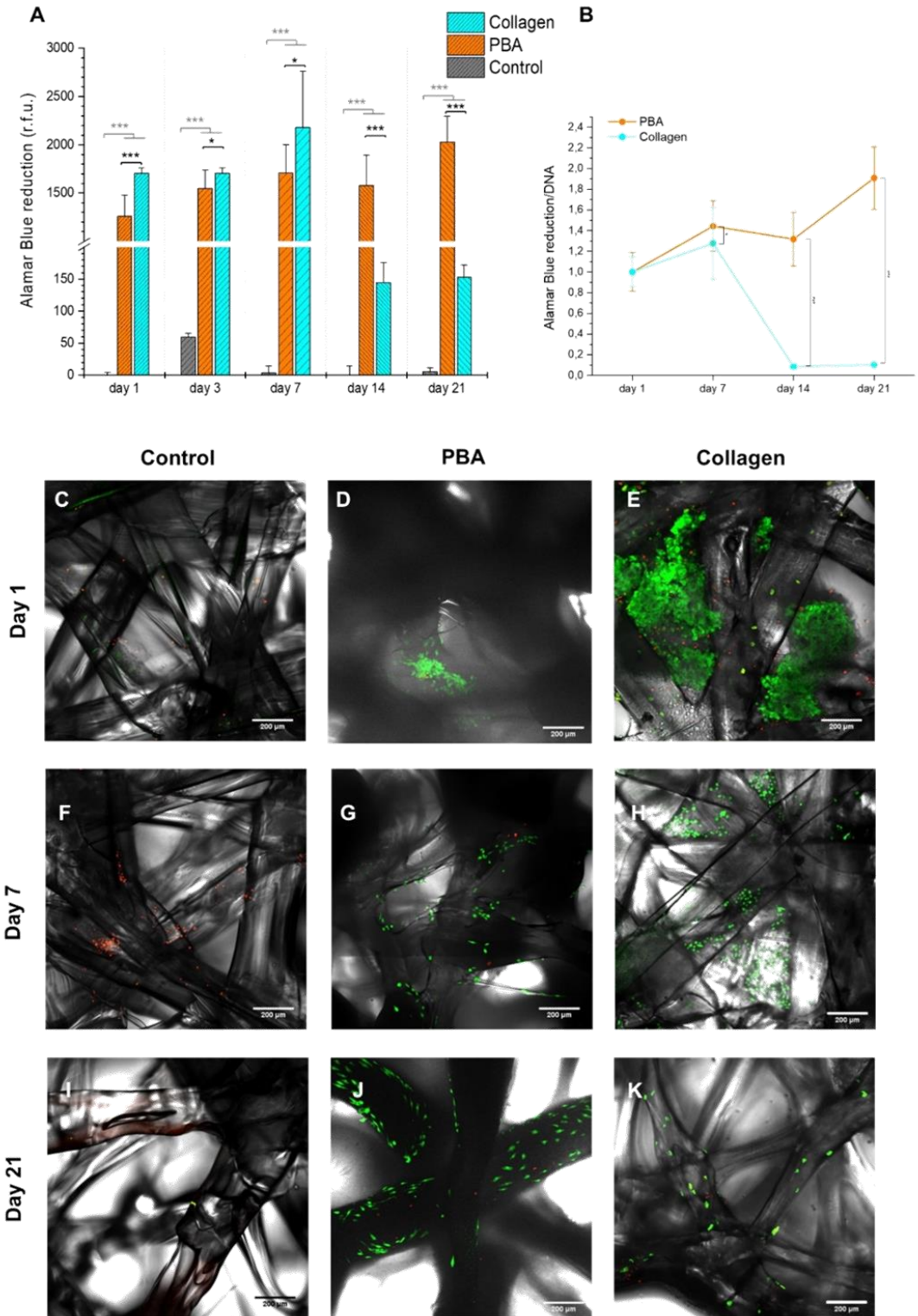


Figure 69. Metabolic and cell proliferation of bTPUe functionalized scaffold loaded with IPFP-MSCs. (A) Alamar Blue reduction fluorescence response ($\lambda = 570$ nm) for bTPUe scaffolds without treatment (control), PBA functionalized scaffolds, and type I collagen functionalized scaffolds at days 1, 3, 7, 14, and, 21. (B) Alamar Blue reduction/DNA fold increase (obtained by dividing Supplementary Figure S4A BY S4B) curves for PBA functionalized scaffolds and type I collagen functionalized scaffolds along 21 days. (n=3) (***, $p < 0.001$; *, $p < 0.05$; N.S., not significance), (C-K) Confocal images from Live/Dead assay (Thermo Fisher Scientific) of naïve bTPUe scaffolds as control and both functionalization protocols. Magnifying was 10X.

Further, to clarify if metabolic responses were in concordance with cellular content in the scaffolds, the Alamar Blue reduction fold increase curve was plotted (**Figure 95A**), and the DNA fold increase curve was obtained (**Figure 95B**). The metabolic ratio (over DNA content) from Alamar Blue reduction versus DNA fold increase¹¹⁰⁷ for functionalized scaffolds shows a correlation between the increase of metabolic activity and DNA content, where PBA functionalized scaffolds presented a higher ratio comparing with type I collagen-functionalized scaffolds at day 21 (**Figure 69B**).

On the other hand, images obtained from the b-TPUe scaffold samples under different conditions using confocal microscopy corroborated the results obtained with the Alamar Blue assay and Alamar Blue reduction fold increase/DNA fold increase. The feasibility study was performed on days 1, 7, and 21 after cell seeding (**Figure 69C-K**). Results were correlated with proliferative assays, with an increase in cell adhesion at day 1 significantly higher in type I collagen scaffolds (**Figure 69E**) than in control (**Figure 69C**) and PBA functionalization (**Figure 69D**). It can be appreciated that cells were found included in the regions between fibers, something that does not happen in other cases. Also, on day 7, viability continued to keep in both functionalized scaffolds (**Figure 69G and -H**), and even more, cell proliferation allowed those cells to colonize the entire surface of the fibers.

On the contrary, the control (**Figure 69F**) did not present living cells on most scaffold surfaces. Finally, on day 21 (**Figure 69I and -K**), the viability was preserved with very poor viability on control. In contrast, the cell distribution

over PBA functionalized and type I collagen functionalized scaffolds was slightly different, whereas in the PBA case, cells surrounded fibers; in type I collagen seems to grow, forming clusters.

23.3. Evaluation of the chondrogenic potential of functionalized scaffolds

Considering the results from metabolic assays and cell viability, we evaluated if cells were producing a chondrogenic matrix. Consequently, GAG quantification vs. DNA concentration was calculated (**Figure 70A-C**), and gene expression by PCR was carried out (**Figure 70D**).

For GAG quantification, scaffolds were seeded over 21 days inside a common cell medium. GAG determination showed significant differences between functionalized samples and controls (**Figure 70A**, $p < 0.001$). Although control scaffolds presented a similar number of cell content (**Figure 70B**), no GAG content was extracted from these scaffolds. After 21 days, although GAG concentration decreased for both functionalization methods, they exhibited higher results than the control. Moreover, PBA-functionalized scaffolds displayed a significantly higher GAG content than type I collagen functionalized scaffolds. Using a more precise DNA extraction method (papain buffer solution assay) showed that in the type I collagen functionalization method, there was a significant reduction of DNA content from day 1 to day 21; however, in PBA functionalization, no difference was founded along time (**Figure 70B**), which is in concordance with **Figure 95B**.

Moreover, type I collagen functionalized scaffolds had higher DNA concentrations on both days ($p < 0.001$). DNA content from controls was not negligible, but, in any case, it was significantly less than functionalization methods. Additionally, the absence of any GAG on both days declares that cells attached to bare filaments do not produce ECM (PBA, $p < 0.05$; Collagen, $p < 0.001$).

Nevertheless, the representation of the ratio between GAG vs. DNA concentrations (**Figure 70C**) showed a significant difference in functionalized scaffolds with control samples ($p < 0.001$). Besides, PBA functionalized scaffolds presented a higher ECM synthesis ratio than type I collagen functionalized scaffolds; however, in type I collagen samples synthesis ratio was preserved along the 21 days, whereas, in PBA protocol, that production was reduced ($p < 0.001$).

Functionalized scaffolds were treated with chondrogenic and regular mediums for 21 days to explore the chondro-inductive potential. Gene expression results (**Figure 70D**) showed that functionalized scaffolds present higher chondrogenic potential than controls ($p < 0.001$), except for Sox9 in differentiated medium cases and PBA and aggrecan (Acan) in differentiated PBA, where no significant differences were found. Surprisingly, in functionalized scaffolds cultivated with a traditional medium, the gene expression for type II collagen, Sox9 and Acan were higher than in those cultured in the medium of differentiation, implying no need to use additional growth factors. Collagen type I functionalized scaffolds with standard medium highlighted over the rest of the cases with almost 10000 times more type II collagen expression and 1000 times more Acan than control ($p < 0.001$). Moreover, type I collagen expression in functionalized scaffolds was significantly lesser than in the control (**Figure 70D**, $p < 0.001$).

Conclusively, GAG/DNA ratios and gene expression assays indicate that, in contrast with control scaffolds, functionalized scaffolds produced more ECM and are chondro-inductive.

CHAPTER II CHONDRO-INDUCTIVE FUNCTIONALIZED SCAFFOLDS FOR CARTILAGE TISSUE ENGINEERING

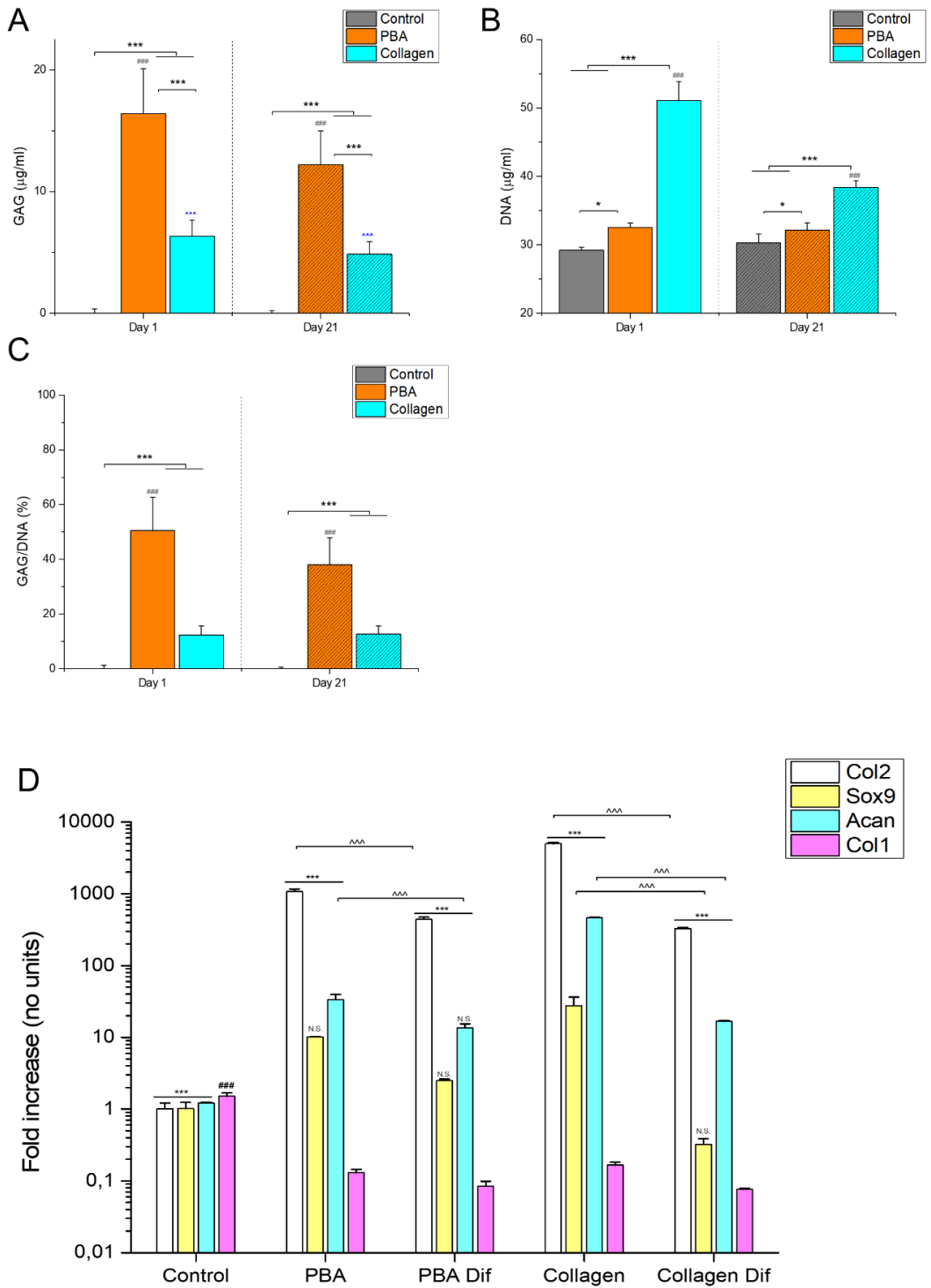


Figure 70. Chondro-inductive properties of bTPUe functionalized scaffold loaded with IPFP-MSCs. (A) GAG concentrations obtain through papain assay for naïve bTPUe scaffold and both functionalization protocols on day 1 and day 21. (B) DNA concentrations were obtained through papain assay for naïve bTPUe scaffolds and both functionalization protocols on day 1 and day 21. (C) GAG/DNA ratios for naïve bTPUe scaffolds and both functionalization protocols at day 1 and day 21 (n=3). (***, $p < 0.001$; *, $p < 0.05$; ###, $p < 0.001$; ^^^, $p < 0.001$). (D) Gene expression fold increase obtained through qPCR. Control used were IPFP-MSCs cultured at day 0. PBA was scaffolds functionalized with PBA under normal cell medium, PBA Dif was the same scaffolds under chondrogenic medium, both at day 21. Collagen scaffolds were collagen type I functionalized scaffolds under normal medium, Collagen Dif was same scaffolds under chondrogenic medium, both at day 21. Col2 was COL2A1. Sox9 was the Transcription factor SOX-9. Acan was Aggrecan. Col1 was COL1A1. (n=3) (***, $p < 0.001$; *, $p < 0.05$; ###, $p < 0.001$; ^^^, $p < 0.001$; N.S., Not Significance). Black bars correlated chondrogenic markers of functionalized scaffolds versus control. N.S: implies exception in previous correlation. Blue # correlates control concerning others. Grey bars correlate PBA with PBA Dif. Green bars correlate Collagen with Collagen Dif.

23.4. Analysis of cell morphology and ECM appearance by scanning electron microscopy

After confirming that functionalized scaffolds showed high cell viability during 21 days and could produce ECM without any additional growth factor, cell morphology and ECM appearance were evaluated by SEM assays after 21 days (**Figure 71**). **Figure 71A, -D, -G** and **-J** represent control scaffolds at different magnifications, where it can perfectly distinguish the presence of living cells attached over the surface of the scaffold, but those cells presented a poor cell/biomaterial interaction (**Figure 71G** and **-J**). It can be pointed out that no presence of ECM was found correlatively with ECM expression results.

In contrast, PBA functionalized scaffolds (**Figure 71B, -E, -H, and -K**) exhibited higher cellular content than the control, and there was a high presence of ECM forming a homogeneous surface that covered scaffold fibers. **Figure 71K** shows how differentiated IPFP-MSCs interact with each other, and **Figure 71H** shows how cells are immersed in a dense ECM and expanded over it.

Type I collagen scaffolds had more cells and a significant amount of ECM (**Figure 71C, -F, -I, and -H**). All the scaffold surfaces were covered by cell content ECM and cells. More interestingly, differentiated IPFP-MSCs produced ECM over angles that formed fiber cross-sections. In **Figure 71L**, a cell with a chondrocyte-like appearance with a spherical shape and some cilium embedded in ECM can be found. Moreover, a much more natural cell-biomaterial response than in other cases was observed, with cells growing through naïve scaffold fibers (**Figure 71I**).

In summary, SEM assay confirmed all previous results where control scaffolds presented very few cells with apoptotic-like morphology, and functionalized methods showed an increased cell number with chondrocyte-like morphology and with a considerable amount of ECM evolving both cells and scaffolds.

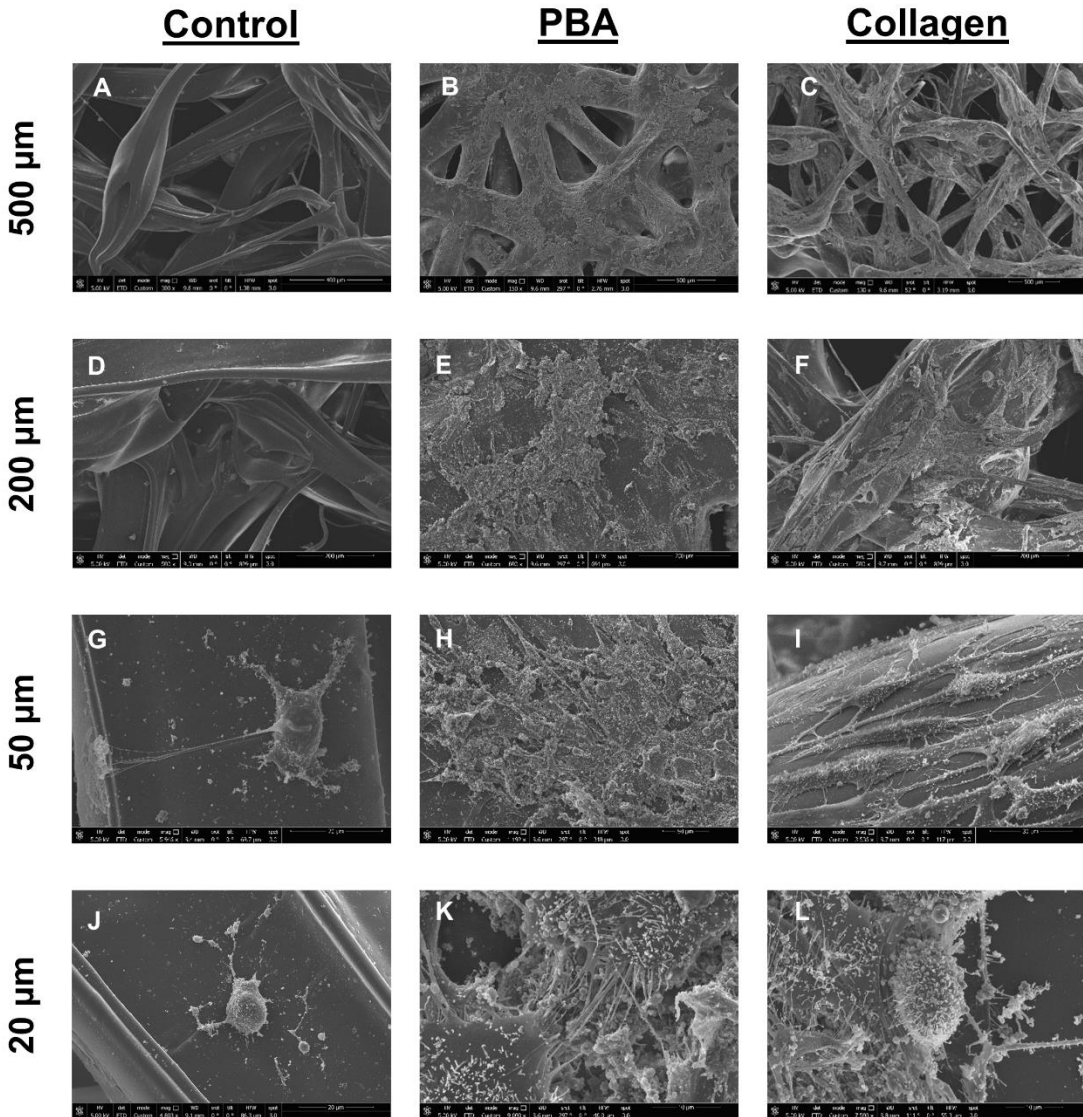


Figure 71. SEM images from control, PBA functionalized and type I collagen functionalized scaffolds at day 21. (A-E) Control images, where (B) shows a magnification of a viable cell. (E) shows poor cell-biomaterial interaction. (F-J) PBA images, (F) clearly show the presence of ECM over scaffold fibers, (G) represents cell-cell interactions. (J) Shows cell-ECM interactions. Collagen images, where (I) shows the presence of ECM over scaffold surface, (K) shows cell-biomaterial interaction and ECM preserved morphology and, (L) shows a chondrocyte-like cell.

24. Discussions from Chapter II

The elasticity and stiffness of the 3D scaffolds are essential for forming AC tissue since it is subjected to cyclic mechanical forces due to corporal movement¹¹⁰⁸. The pore size and scaffold fiber geometry are important factors that regulate previous characteristics in scaffolds. Wang et al. assume that large pore sizes increase ECM production of chondrocytes¹¹⁰⁹, a fact that was contrasted by the previous literature^{1048,1110}. Similarly, it has been established that a pore size between 370 to 400 μm is the optimum for chondrogenesis¹⁰⁸⁴. In this work, we also used a similar pore size (375 μm) that, together, high interconnectivity of scaffold fibers along different layers is essential for conditioning cartilage biomechanics and creating an adequate cellular niche for cell differentiation¹¹¹¹.

The polyurethane (PU) family has been used as a scaffold biomaterial for cartilage TE due to its proper tensile strength, high elasticity, and good biocompatibility¹¹¹²⁻¹¹¹⁵. It has been previously demonstrated¹¹¹² the adequate properties of PU for cartilage substitutes, including their viscoelastic behavior^{1108,1112} and the high elastic recovery (> 99% recovery)¹¹¹⁵. However, its high hydrophobicity makes it necessary to adapt its surface to improve cell-matrix interfaces to ensure good cell adhesion and differentiation^{1116,1117} or by specific surface properties, including topography¹¹¹⁸, potential, and charge^{1119,1120}.

In the present work, 3D scaffolds were printed with b-TPUe, a thermoplastic polyurethane filament comprising methylene diphenyl diisocyanate (MDI) and 1,4-Butanediol, where PU structure consists of three complex monomers: a macrodiol, a diisocyanate, and a chain extender, based on which several different PU materials can be synthesized¹¹²¹. In previous works, we have demonstrated the biocompatibility of b-TPUe¹¹²² and its similar cartilage mechanical behavior¹¹¹¹. The 3D-printed b-TPUe scaffolds were functionalized

using two type I collagen and PBA methodologies to improve their biological properties. In each functionalization method, the solutions to which the material was subjected were diverse, and they exerted an effect on the microstructure of the b-TPUe scaffolds. At the macroscopic level, no differences were observed on the surface; however, AFM analysis showed differential effects in the material's roughness. This superficial characteristic was more remarkable when scaffolds were subjected to 70% ethanol and isopropanol than in other conditions. The roughness obtained does not significantly alter its properties because its increase was less than 1 nm. In addition, in previous literature, it has been described that an increase in roughness implies a decrease in hydrophobicity¹⁰⁷².

Functionalization with components in the ECM is recurrent and mainly offers good results¹¹²³. The chondrogenesis process begins with MSCs, cell proliferation, and differentiation towards chondrocytes occur, finally giving rise to hypertrophy and ossification¹¹²⁴. As differentiation proceeds, a matrix rich in fibronectin and type I collagen is replaced with one containing type II collagen and aggrecan as the main components¹¹²⁵. This statement is why type I collagen was used to functionalize the 3D-printed b-TPUe scaffolds.

Also, functionalization with PBA was performed. Hinnemo et al. reported interesting results using PBA to attach it non-covalently to graphene through π - π stacking, a common approach to non-covalently attaching functional groups¹⁰⁹⁸. No use of PBA over PU surfaces has been previously published, and the only use of PBA with application in TE was done by Luo et al. in 2015¹¹²⁶. The PBA consists of a pyrene group that contains π electrons and a carboxylic group that can be used to facilitate further functionalization. In the present study, b-TPUe has not had a high density of delocalized π -electrons like graphene, so it is not possible to establish a π - π stacking between b-TPUe and PBA¹⁰⁹⁸. For this reason, firstly, the amination process must establish amino groups in the b-TPUe surface and be possible later the interaction between amino groups and PBA by the

carboxylic group. Finally, π - π stacking will be able between PBA and aromatic amino acids of membrane cell proteins.

Collagen has been coated successfully onto numerous hydrophilic biomaterials. Despite the hydrophobic characteristic of b-TPUe, developing a method that reduces its hydrophobicity and allows coating with collagen was necessary. For this reason, type I collagen functionalization was a more complex protocol than PBA, and there were several steps involved. Firstly, urea was necessary to reduce hydrophobicity through the deposition of polysaccharides and proteins to achieve the binding of collagen subsequently¹¹²⁷. Type I collagen must be cross-linked to be used as a functional replacement *in vivo* due to its high degradation rate and low biomechanical strength¹¹²⁸. This fact was obtained when glutaraldehyde was decreased in the protocol, where the absence of it presented an inadequate metabolic cell response. As it is known, glutaraldehyde can become toxic if it is not used in the right concentration and if its unreacted functional groups are not blocked¹¹²⁹. Consequently, different concentrations of glutaraldehyde and glycine (a blocking agent) were tested to optimize the accurate concentration that did not compromise cell viability, and, at the same time, the tertiary structure of type I collagen was preserved. An optimal concentration of 0.16% of glutaraldehyde and 0.5 M of glycine was found to ensure cell viability and preservation of collagen tertiary structure.

In the study of the topographic properties of our 3D printed b-TPUe scaffolds, the AFM results showed how PBA increased the global rugosity height, but frequencies observed in the PSD curves were considerably lesser than control and collagen functionalization. Consequently, the heterogeneity of this functionalization method is higher. Contrary, type I collagen fibers had an estimated diameter of 300 nm¹¹³⁰; therefore, they reached a high level of homogeneity.

Further results showed an increase of cell adhesion in functionalized scaffolds opposite to native scaffolds, implying that our methodology overpasses

the first issue of this research¹¹³¹. Even PBA scaffolds increase cell proliferation over 21 days; type I collagen functionalized scaffolds only preserved that proliferation over 7 days to reduce at days 14 to 21 abruptly. Moreover, DNA content was measured to verify if changes in cell proliferation were in agreement with cellular metabolism. The ratio between Alamar Blue reduction fold increase and DNA fold increase indicated that in PBA, a decrease in cell content was not associated with a decrease in cell metabolism, which suggests that the increase in metabolism activity is in part due to an increase in ECM synthesis as was found in GAG/DNA ratio and SEM, as previously described¹¹³².

Thereby, both functionalized methods reached good cell viability values for 21 days with no apparent difference between them, and obtained results were considerably higher than the previous works^{1111,1122}. Nevertheless, PBA is an inexpensive reagent and a fast process of functionalization that allows obtaining functionalized b-TPUe in 2 hours instead of 3 days, which could be used to manufacture b-TPUe directly coated with PBA.

In addition, it was shocking to verify that functionalized scaffolds did not need any particular medium to induce chondrogenesis. These results concord with literature where type I collagen induced chondrogenesis¹¹²⁸, even in the case of PBA scaffolds where this ability has not been probed before. This effect was confirmed in confocal and SEM assays where living cells were easily founded at the corners formed by fiber's crosslinking between scaffold layers; thus, IPFP-MSCs were more condensed in those regions, a factor that facilitates chondrogenesis¹¹³³. Regarding Col type II and Sox 9 expression, it is interesting to verify how the samples with greater production also presented higher Acan production¹¹³⁴. It is known that in healthy cartilage, chondrocytes are constantly remodeling their ECM, and they use their pericellular matrix for such purpose¹¹³⁵. Our results concurred with previous criteria obtained by other researchers in literature¹¹³⁶. Zhang et al. analyzed the importance of scaffold geometry for enhancing *in vivo* osteogenesis and chondrogenesis without any

additional implementation of cell content before scaffold implantation¹¹³⁷, and also how additional non-physiological materials such as bredigite increased cellular proliferation and ECM synthesis¹¹³⁸, which is in concordance with our results. The importance of biochemical cues inside *in vivo* niche and all the proteomic pathways developed by inflammatory processes present in osteoarticular disorder, such as OA, are essential for regulating cell proliferation and differentiation¹¹³⁹. As discussed in a previous work¹¹⁴⁰, cartilage is trying to remodel at the initial stages of OA with no positive result, and the tensile strength is reduced⁷⁸². Applying biomaterials that avoid such biomechanical instability would be highly beneficial for cartilage repair; thereby, a good functionalization method and an adequate geometry should promote chondrogenesis avoiding the use of chondrogenic medium.

Finally, SEM images concord with all previous results, showing poor cell-biomaterial interaction and, apparently, no cell-cell interactions in non-functionalized scaffolds. Our functionalized methods satisfy cellular demand for a suitable attachment and the cell-cell interactions¹¹⁴¹, a critical factor for adequate biomaterials. In addition, it seems that either PBA as type I collagen induces chondrogenic differentiation, which results in concordance with other research for osteointegration¹¹⁴¹. IPFP-MSCs culture for 21 days changed their characteristic MSC morphology (more elongated and planar) to a spherical conformation embedded in a matrix with some cilium^{952,953,959} indicating what seems differentiation into chondrocyte-like morphology¹¹⁴². Moreover, it was found how differentiated IPFP-MSCs tended to expand their ECM to the fiber's crosslinking regions; an aspect described before¹¹¹¹.

24.1. Conclusions

In this work, we have adapted, for the first time, not one but two different possible methods for bTPUe functionalization in a biomaterial with mechanical properties similar to cartilage^{1111,1112,1115,1143} but with high hydrophobicity. Both of them presented improved IPFP-MSCs adherence, proliferation, and chondro-

inductive properties. Thus, 3D printed b-TPUe scaffolds treated with 1,6-hexanediamine and PBA or type I collagen showed improved cell-biomaterial interaction with increased cell adhesion and proliferation after 21 days. More importantly, IPFP-MSCs attached to the functionalized scaffold increased the chondrogenic differentiation potential even without additional differentiation medium or other growth factors. In addition, SEM images remarked the wide gap in cell/biomaterial interaction between functionalized scaffolds and not functionalized ones.

Regarding the surface modification motifs, AFM displayed an increase in rugosity of both methods, although the patterns differed. SEM images showed how cells adapt better to such patterns; consequently, the functionalized scaffolds significantly increased their adhesiveness and cell properties. Although we probed both type I collagen and PBA functionalization methods, we recommend the PBA functionalized procedure due to its reduced cost in reactive prices and time-consuming.

In summary, the improvement in surface properties of 3D printed b-TPUe scaffolds favoring cell-biomaterial interaction and its chondrogenic properties results in a biomaterial with a highly compliant nature and elastic recovery capacity similar to cartilage, which can overcome the limitations of the current scaffold-based approaches. Nonetheless, further *in vivo* experiments must be done to demonstrate the clinical potential of cartilage TE.

Chapter III

Induction and real time
ultrasonic monitoring of 3D
cartilage-like tissue by a low shear
stresses-based bioreactor

“When a distinguished but elderly scientist states that something is possible, he is almost certainly right. When he states that something is impossible, he is very probably wrong.”

“Cuando un científico distinguido, pero de edad avanzada afirma que algo es posible, es casi seguro que tiene razón. Cuando afirma que algo es imposible, es muy probable que esté equivocado.”

Arthur C. Clarke

25. Abstract of Chapter III

Osteoarthritis is a significant socioeconomic illness that mainly affects articular cartilage, a tissue with a low capacity for self-healing and, hence, an ideal target for regenerative medicine and tissue engineering. To date, non-effective interventions have been developed to treat cartilage injuries.

To solve this problem, a novel bioreactor that creates viscous shear stresses by flow perfusion has been designed for inducing *ex vivo* maturation of biomimetic 3D cartilage scaffolds. IPFP-MSCs were used as a cellular source of the functionalized 3D scaffolds made of b-TPUe. DNA quantification, extracellular matrix determination, and metabolic assay confirmed the chondrogenic differentiation induced by our bioreactor without any conditioned medium.

On the other hand, to control the biomechanical stimulation on IPFP-MSCs, a low intensity ultrasonic transmission system has been developed and embedded in the bioreactor. Combined with a FEM, the tissue growth and differentiation can be deconvoluted in real time from the recorded ultrasonic propagation and interaction across the graft. This complex interaction is reconstructed by the FEM based on the pulse wave speed, viscous and multiphase pore-elastic geometrical dispersion across the graft.

In conclusion, this is the first time a low-shear stresses-based bioreactor can induce and monitor chondrogenic evolution in real time.

Keywords: scaffolds; infrapatellar fat pad, mesenchymal stem cells; b-TPUe; cartilage; osteoarthritis; bioreactor; biomechanics; ultrasound; inverse problem and finite element model (FEM)

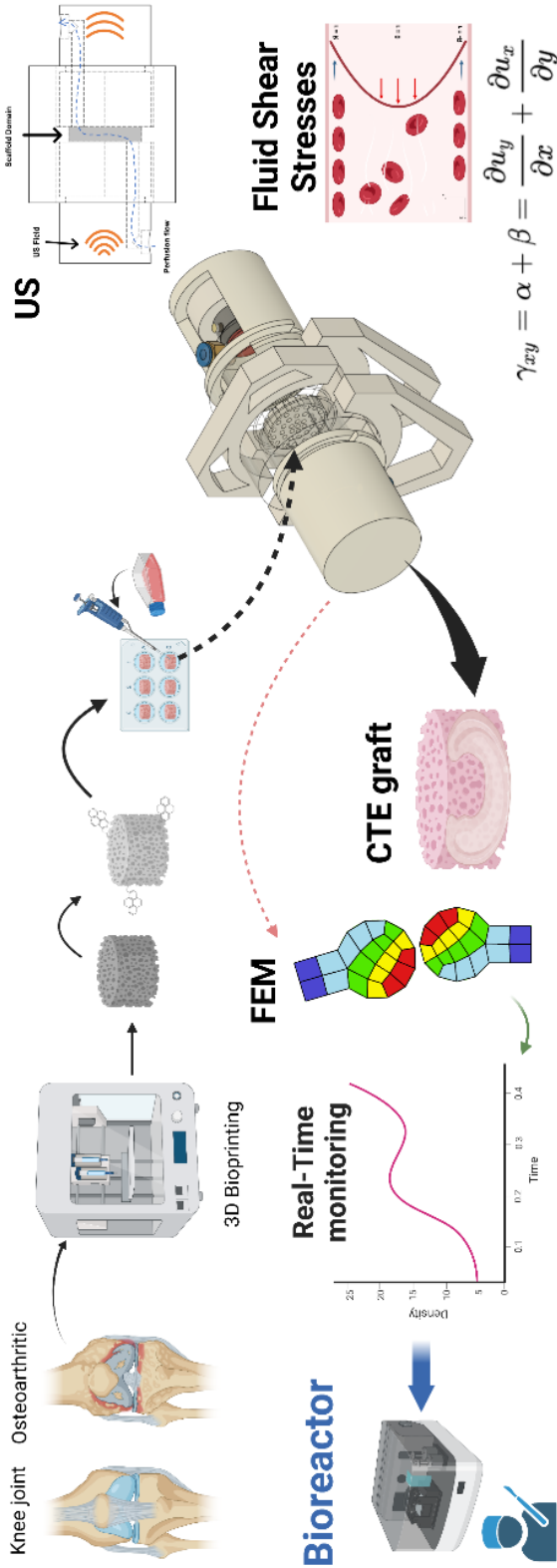


Figure 72. Diagram of the work framework from Chapter III.

26. Background for Chapter III

RM aims to restore or establish normal function by entirely or partially regenerating human cells, organs, or tissues¹⁰⁸⁶. Living cells, biomaterials, and bioactive cues are the three pillars of TE, a subset of RM¹¹⁵. Among the various illnesses that can benefit from the advances in TE is OA, an incurable and complex disorder. The pathogenic process leading to OA is characterized by persistent low-grade AC deterioration, which is the primary cause of continuous joint degeneration⁷⁵⁴. As such, OA should not be regarded as a disease but rather as the common endpoint of several secondary pathways associated with age, possible traumas, obesity, and the resulting changes in the biomechanics of the joint^{642,1144}. Because AC is an avascular tissue with no lymphatic system and nerve endings, OA patients have a limited regeneration rate, making TE an accurate tool to revert that with techniques such as biofabrication¹⁰⁸⁷. Due to the loss of AC, OA causes pain and loss of joint function¹⁰⁸⁸. No known treatment for OA can stop or decrease its progression; surgical treatments are the go-to option¹⁰⁸⁹. Numerous TE based-products and treatments have attempted to simulate AC for a few decades (some of them are still in clinical trials), including ACI, the MACI, NeoCart®, NOVOCART® 3D, Cartipatch®, and Spherox¹¹⁴⁵⁻¹¹⁴⁷. However, clinical, surgical treatments such as ACI or MACI lack long-term effectiveness¹¹⁴⁸⁻¹¹⁵⁰. Another example is mosaicplasty, a treatment for focal chondral lesions which relatively acceptable results for the first 2 years but fails after ($\approx 55\%$)¹¹⁵¹.

A mechanical derangement that causes low-grade injury to the AC is the primary driver in the development of OA⁷⁶⁰. As a result, three distinct stages may be identified from a biomechanical perspective: i) the proteolytic breakdown of the ECM of AC, ii) the fibrillation and erosion of the AC surface, and iii) the onset of synovial inflammation¹¹⁵². A typical mechanical stimulation for AC is mechanical loads, described as direct interactions between two surfaces in the form of stresses varying from 0.5 to 8 MPa¹¹⁵³. On the other hand, frictional loads,

exerted by interstitial fluid, increase cartilage liquid pressurization inducing hydrostatic pressures⁹⁴¹; this contributes to the increase in AC stiffness under dynamic stresses⁷⁴³. On the other hand, the "solid" ECM sustains the remaining proportion (66 %) of the compression load⁹⁴².

Scaffolds for TE applications have been created using synthetic materials such as PLA¹¹⁵⁴, PCL^{1155,1156}, and polylactic-co-glycolic acid (PLGA)^{1157,1158}. These materials do not easily imitate the mechanical properties of real tissue^{1159,1160}. Therefore, the relevancy of novel biomaterials that affront such efforts, like b-TPUe, is pretty promising TE targets for OA¹¹²². Despite this, it is crucial to ensure adequate cell-biomaterial interaction, reducing these synthetic polymers' hydrophobic behavior. A reasonable manner of abording this problem is surface modifications, for example, with RGD peptides¹⁰⁹⁷, with PBA¹⁰⁹⁸, or with various ECM elements like fibronectin or collagen¹⁹⁵.

Mesenchymal stem cells can develop into the chondrogenic lineage¹¹⁶¹⁻¹¹⁶⁵ and have a high rate of in vitro proliferation while retaining their capacity for multipotent differentiation¹¹⁶⁶, making them pretty attractive as therapeutic agents¹¹⁶⁷. The infrapatellar fat pad is one of the sites from which multipotent cells can be isolated¹⁰⁵³; therefore, IPFP-MSCs are a reliable cell source for AC TE¹¹⁶⁸. Before, it was probed how biomechanical stimulation induced chondrogenesis from MSCs by phosphorylation of Sox9 through PKA, cAMP, Ser133, and CREB⁹⁴⁶⁻⁹⁵⁰. So, any pathway that involves the transmission of signals from mechanical stimulation to electrochemical activity is called mechanotransduction¹¹⁶⁹. The mechanosensory TRPV4, piezo1, and piezo 2⁹¹³⁻⁹¹⁵ are found in chondrocytes and osteoblasts—bone tissue and cartilage tissue exhibit acute mechanosensitivity to maintain homeostasis. For example, osteoporosis is linked to the inhibition of Piezo 1, and TRPV4 regulates the anabolic response of chondrocytes to osmotic or mechanical stress^{916,917,946-950}. Although the exact mechanism of action is still unknown, some evidence points to primary cilia as a potential mechanosensory for shear forces^{951,952}. Then,

developing novel devices that induce biomechanical stimulation for chondrogenesis has excellent potential in the TE of OA. In fact, in the past ten years, the use of BR to physically stimulate bone or cartilage tissue has become standardized¹¹⁷⁰⁻¹¹⁷³.

In this paper, a novel BR that promotes chondrogenesis from IPFP-MSCs has been designed and tested. Moreover, an inverse problem based on cross-correlation algorithms forms based on finite element models has been used to quantify tissue growth and differentiation in real-time using LIPUS¹¹⁷⁴.

27. Materials and methods for

Chapter III

27.1. Bioreactor design and construction

A novel BR has been designed to support perfusion flow through scaffold fibers with the capacity to control scaffold elasticity through pulsed US. All designs were performed by Fusion 360™ Education License (Autodesk Inc.). BR parts in direct contact with cells were made in PMMA in the *Centro de Instrumentación Científica* (CIC, UGR). The rest of the parts were 3D printed with our laboratory facilities. The US adapter pieces were printed in white resin in Form 3B (Formlabs Inc.), and the pad of bTPUe was printed in an Artillery X1 (Artillery Inc.). Due to its sterility, a one-use infusion set from CareFusion was applied for the fluid channels. The flow was influenced by a peristaltic pump (Watson Marlow, 400 FD/D2). A tube bore of 0.5 mm was selected due to their flow rate regime: $0.05\text{-}3.3\text{ mL} \cdot \text{min}^{-1}$, and an Arduino Uno Rev3 was chosen for regulating the flow rate and periodicity through an H-bridge.

On the other hand, for the pulse US, contact transducers of 1 MHz were applied (Olympus v103-RM). For generating the 20V sinusoidal pulse waves each 10 ms, the RIGOL DG1022Z (Rigol Inc.) was programmed. The signal obtained by the receiver transducer was preamplified by an Olympus TRPP 5810; after, the signal was captured with an oscilloscope MSO6054A (Agilent Technologies Inc.). A direct trigger connection between the wave generator and Oscilloscope was installed to ensure correct timing between the wave generator and the final captured signal.

To calibrate the flow rate, a weighing method was computed where a precise balance was used. The BR with a blank scaffold was mounted, and distilled water was applied as fluid for measurements. For pressure waves, the

setup for recording the pressure amplitude of the P-wave exerted by the transducer was a high-sensitivity hydrophone (ONDA HNR-0500). Finally, the Arduino Uno and the Oscilloscope were controlled *via* a USB port and VISA protocol with a Raspberry Pi 3.

27.2. Cells isolation and culture

IPFP-MSCs were directly extracted from patients with OA after the approval from the Ethics Committee of the Clinical University Hospital of Malaga, Spain (ethical approval number: 02/022010 Hospital Virgen de la Victoria, Málaga). Informed consent from patients was obtained for all samples used in this study. Hoffa's fat pads were harvested from the inside of the capsule without the vascular and synovial areas. The isolation and culture protocol of IPFP-MSCs was according to López-Ruiz et al.¹⁰⁵³. IPFP-MSCs were characterized according to the established criteria of the ISCT (Supplementary Figure 4)⁵¹.

27.3. Printing 3D scaffolds

The required scaffold was designed using the Cura 3D program, and its printing was carried out in a class II laminar flow cabinet using the Monoprice Mini V2 Bioprinter (Monoprice). The bioprinter was thoroughly cleaned in 70% ethanol and under UV radiation overnight.

The holder was designed to fit inside a multiwell 6-well plate. Therefore, they adopted a cylindrical geometry: 24 mm in diameter, 5 mm in height, and 200 μm in layer height. The movement speed of the extruder was set to 14 mm/s, and the working temperature was set to 230 °C. Finally, the flow rate (the speed of the filament passing through the extruder) was determined to be 1 mm/s. The scaffold's infill geometry and porosity were extracted from previous work (Pore size \approx 375 μm)¹¹¹¹.

To ensure the complete sterility of the scaffolds, they were placed in Petri dishes and washed with an increasing gradient of 20%, 50%, and 70% ethanol.

After washing, scaffolds were irradiated by UV on both sides for 1 h and then rewashed with 1% antibiotic PBS (P/S) to remove any residual ethanol.

27.4. Scaffolds functionalization

Scaffolds were placed in a multiwell plate and immersed in a 10 % isopropanol solution of 1,6-hexanediamine for 30 min at room temperature. After, they were rinsed in PBA (Sigma-Aldrich) at 5 mM DMSO (Sigma-Aldrich). Finally, several washes were done with PBS^{115,1086}.

27.5. Seeding cells in scaffolds

IPFP-MSCs suspension (1×10^6 cells·mL⁻¹) were pipetted onto each scaffold and incubated for 4 h at 37 °C to allow cell attachment. The cells-loaded scaffolds were transferred into new low attachment 48-well culture plates with 1 mL of medium. All samples were incubated under a 5% CO₂ atmosphere at 37 °C for 14 days. The culture medium was replaced every 2 days in control scaffolds, whereas the medium was perfused for BR scaffolds.

27.6. Metabolic activity

The metabolic rate was assessed by colorimetric Alamar Blue assay (Thermo Fisher Scientific) following the manufacturer's instructions on days 1, 3, and 7 after treatment (i.e., 8, 10, and 14 days after seeding). Cells-free 3D scaffolds were used as controls, and data were normalized to the appropriate control. The fluorescence intensity was measured using a plate reader (Synergy HT, BIO-TEK).

27.7. DNA and collagen quantification

Scaffolds (n=3) were digested with papain (25 μL · mL⁻¹ in FBE) after 14 days in culture with DMEM Glutamax (Thermo) 1 % P/S, 10 % FBS. Control scaffolds were maintained inside multi-chamber wells of 6 wells, where cell medium was exchanged every 3 days. On the other hand, BR's scaffolds were

cultured inside the system for 7 days, after 7 days of previous standard cell culture, to ensure adequate cell adhesion. DNA content was estimated using a fluorometric marker (DAPI staining), and a DNA standard curve was done using DNA from Calf Thymus (Sigma-Aldrich).

For collagen quantification, scaffolds were digested in pepsin ($1 \text{ mg} \cdot \text{mL}^{-1}$) buffer in acetic acid (0.5 N) for 48 h at $4 \text{ }^{\circ}\text{C}$, followed by adding a $1 \text{ mg} \cdot \text{mL}^{-1}$ pancreatic elastase solution at $4 \text{ }^{\circ}\text{C}$ for 24 h. Finally, samples were neutralized with 1 M Tris base, and the supernatant was collected for further assays. Collagens were quantified using Sirius Red assay. Samples were placed in microcentrifuge tubes and were embedded in Sirius Red buffer (0.1 % in picric acid) for 1h RT. Then, the tubes were centrifuged for 15 min under 13,000 rpm, and the supernatant was discarded. Then, the pellet was resuspended in $250 \text{ } \mu\text{L}$ of NaOH 0.1 M. Finally, the absorbance supernatant was measured in a microplate reader at 540 nm (Synergy HT, BIO-TEK) for standard collagen from calf skin was used (Sigma). On the other hand, to quantify type II collagen, a commercially available type II collagen ELISA kit (Chondrex) was used according to the manufacturer's instructions and measured at 490 nm on a microplate spectrophotometer (Synergy HT, BIO-TEK).

27.8. Immunofluorescence

Celltracker™ Green (Thermoscientific, 1:1000) was added to the pellet before cell seeding for 30 min at 37°C . After 14 days, scaffolds were fixed with 4% PFA in PBS for 30 min at RT. Samples were treated with a primary antibody against type II collagen (Abcam, 1:200), type I collagen (Abcam, 1:200), and Aggrecan (Abcam, 1:200). Then, they were incubated with AlexaFluor 645 (Abcam, 1:500). Images were obtained using a Nikon Eclipse Ti microscope and analyzed with Image J software.

27.9. Scanning electron microscopy (SEM)

Samples were incubated for 21 days (2×10^6 cells per scaffold) and then fixed with 2 % glutaraldehyde overnight at room temperature. The next day, they were rinsed in 0.1 M cacodylate buffer and stored at 4°C. Samples were then prepared for SEM according to standard protocols: i) washed several times with PBS, ii) dehydration series with ethanol (30-100 %), iii) they were critical point dried in Emscope CPD 750, iv) mounted on aluminum SEM Top stubs and v) sputter coating with conductive material (gold-palladium alloy, Sputter Coater 108 Auto). Finally, samples were imaged using an FEI Quanta 400 microscope (Thermo Fisher Scientific-FEI, Fremont, CA, USA) with an Everhart-Thornley detector (E-TD) for dry and conductive samples in high vacuum mode.

27.10. Statistical Analysis

Three experiments were performed in each condition to assess variability ($n = 3$) and data representation corresponds to mean \pm standard deviation. Data were processed and presented using Origin 9.0 software (OriginLab Corporation, Northampton, MA, USA) and were validated for homoscedasticity (Shapiro-Wilk test). Student's two-tailed t-test was used to analyze data with a confidence interval of 0.05. If present, outliers were ignored using the IQR (interquartile range) method, where multiple samples are compared using the ANOVA test, and means are compared using the two-tailed Bonferroni test with a confidence interval of 0.05. In the figure, p-values <0.001 are indicated by "****", <0.01 "**", and <0.05 "*".

27.11. In silico model

A computational model using Multiphysics FEM software was used to evaluate and understand the effect of the pressure wave exerted by US in the culture. For that purpose, a set of synthetic signals were obtained through an inverse problem, where different model parameters were swept. In addition, shear stresses employed by the laminar flow were also modeled (COMSOL

Multiphysics). A 2D model was applied to reduce computational time and memory consumption. The plane of the simulation was the XZ middle plane of the BR.

The Multiphysics tool was employed to model the piezoelectric effect of the transducer to reproduce the transducer behavior. Due to patent protection, the materials employed for the piezo and the matching layer were unknown; after early trials, PZT-5H for the piezo and Armco iron was selected due to their similarity. The transducer's thickness was established as 13 mm, and its reference impedance to 50 Ω (Olympus v103-RM, the same diameter was used). For charge conservation, the relative permittivity ($\mathbf{D} = \epsilon_0 \epsilon_r \mathbf{E}$) as a dielectric model was chosen. No initial voltage was estimated, letting as input the following electric potential: $V(t) = V_0 * \sin(\omega_0 t) |_{0}^{T_0}$, where $V_0 = 20$ V and $T_0 = 1$ μ s. On the other hand, linear elastic material was selected with isotropic behavior for the solid mechanics' response of the transducer. A fixed restriction was exerted in the outer boundary of the piezo to avoid motion in such a direction. A stress-charge form to describe the constitutive relation was applied to the properties of the piezoelectric material. All parameters and geometries of the transducer were reconstructed by an inverse problem using materials such as water and PLA with known speed, sound, and density from the literature.

The wave propagation was modeled with the Acoustic Pressure tool, whereas the transitory model was linear elastic depending on the speed of sound and density of each material. A converge study was done for Δx (maximum mesh size, using triangular mesh) to ensure adequate wave propagation, and density and speed of sound parameters were obtained through the inverse problem. An acoustic-structure boundary condition was used for boundary intersection. The model was performed in the time domain to obtain a comparable signal with the experimental one; the time-dependent variable (t) varied in a range from 0 μ s to 50 μ s (same range as experimental time windows), $\Delta t = T_0/40$. Transition layers

were marked as interior impedances where $Z_i = \rho_m \cdot c_m$, where ρ_m and c_m are parameters from the reflective material.

Finally, a boundary probe was attached to the receiver transducer for obtaining the final electrical modeled signal. No initial potential was computed for the receiver piezo, and as outer potential was selected, the floating potential was.

28. Results from Chapter III

28.1. Perfusion bioreactor with pulsed ultrasound characterization

A novel BR was designed to promote perfusion flow and to exert direct shear stresses on the cell surface among scaffold fibers to induce chondrogenesis (**Figure 73A**). The final construction material was Polymethyl methacrylate (PMMA) because of its effortless sterility, transparency, and economical manufacturing prices. The BR is mainly composed of 3 different pieces: the culture chamber cylinder (**Figure 73B**) and the input and output cylinders (IO cylinders, **Figure 73C**). The geometry of the cell chamber consisted of a middle ring of 24 mm to save the IPFP-MSC-loaded 3D scaffold and a total length of 45 mm, where only 5 mm corresponded to scaffold size and rest distances (20 mm per side) were selected to avoid the near field effect of the US signal.

Thereby, IO cylinders were 30 mm diameter rods of PMMA and 40 mm in length, and they were perforated from the cell contact face to make fluid channels (**Figure 96**). The viable length of the IO cylinders allows fully developed laminar flow. When a fluid enters a pipe, the minimum length to be fully developed must fulfill the following: $\frac{L}{D} = 4.4Re^{1/6}$. The fluid applied in this research was culture medium (Dulbecco's modified eagle medium (DMEM) high glucose, 10% fetal bovine serum (FBS), which is Newtonian ($\rho = 1009 \text{ kg} \cdot \text{m}^{-3}$; $\mu = 0.93 \text{ mPa} \cdot \text{s}$)¹¹⁷⁵ with $Re = 4.6$. Thus, L to fulfill previous conditions is 22.7 mm; IO cylinders present a pipe length of 35 mm, higher than necessary, before reaching the scaffold chamber. On the other hand, the near field length was (N): $N = \frac{D^2 f}{4c} = 15.4 \text{ mm}$ with $c = 2730 \text{ m} \cdot \text{s}^{-1}$ (longitudinal sound velocity of PMMA) and D the diameter of the transducer.

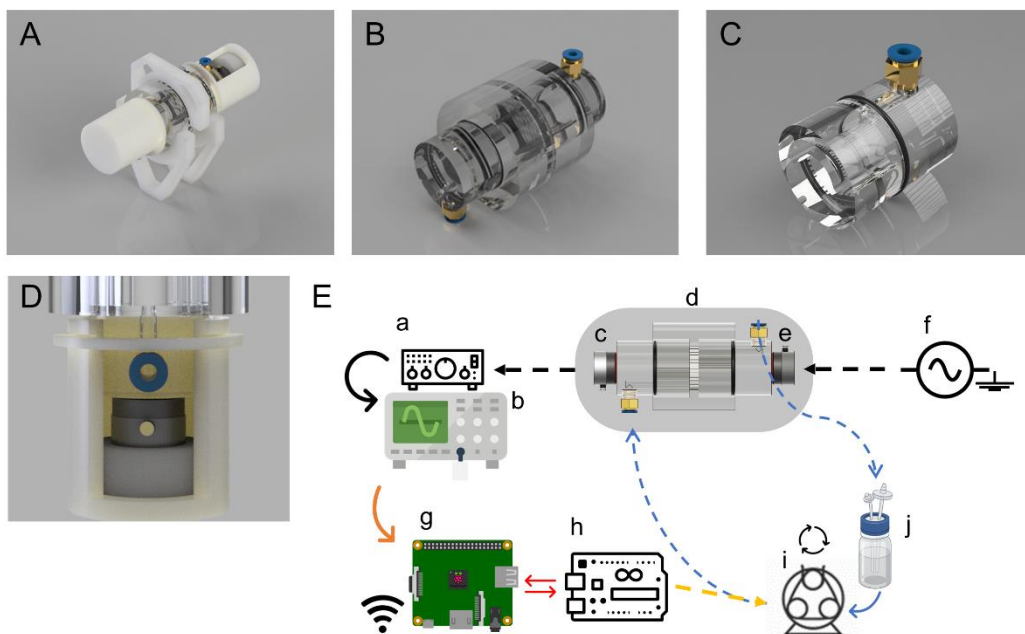


Figure 73. Bioreactor (BR) design. (A) Final design (cell chamber and transducers coupled) renderization. (B) Render image of cell chamber BR and input and output (IO) cylinders. (C) IO channels render images. (D) The visual concept of the transducer with the coupling system. (E) (a) represents the Olympus preamplifier that was connected after the recording oscilloscope (b) and the receiver transducer (c); (d) the cell chamber and BR heart; (e) transmitter transducer, which was directly connected to the wave generator (f); (g) Raspberry PI that is uncharged of received the signals from the Oscilloscope and to control the Arduino board; (h) Arduino Uno that regulates pump rotation speed and flow rate; (i) peristaltic pump that exerts the laminar fluid flow through the bioreactor; (j) the medium reservoir with a $0.22\ \mu\text{m}$ filter for O_2 and CO_2 exchange.

Regarding transducer coupling, a simple system of a hollow cylinder with a restriction ring was designed to retain the transducer and a bTPUe pillow that exerts enough pressure to acquire a precise signal (**Figure 73D**). **Figure 73E** schematically represents the electronic BR assembly. Oscilloscope MSO6054A (Agilent, USA) was programmed to capture each signal between $30\ \mu\text{s}$ to $50\ \mu\text{s}$; the such period was manually established the first time once a time of flight (TOF) of scaffold signals (approximately $35\ \mu\text{s}$) was shown. The caption interval was set to 5 minutes to save memory and to allow enough time for signal transfer

between the Oscilloscope and the Raspberry Pi (Raspberry Foundation, UK), and capture signals were the average of 200 measured signals with 8-bit resolution. In addition, to ensure good communication between Arduino UNO (Arduino Inc., Italy), the microcontroller that regulates the pump (programmed in C++), and the Raspberry Pi, which was then applied computer unit (Python), a parser library was applied (ParserLib by LuisLlamas).

Figure 74A and **-B** show the whole BR assembly and the electronic circuit regulating the peristaltic pump. All components shown in **Figure 74A** were sterilized with Biozidal ZF (WAK – Chemie Medical GmbH) and ethanol 70%, followed by UV light ON inside the laminar hood. After, the BR was coupled and initialized at flows, not over $0.5 \text{ mL} \cdot \text{min}^{-1}$ to ensure no cell damage.

Figure 74C to **-E** represent experimental parameters obtained directly from the BR. **Figure 74C** corresponds to two arbitrary US signals recorded in the Raspberry; the red one resembles a scaffold seeded with cells, whereas the black one is the blank control (i.e., functionalized scaffold without cells). The amplitude of the *cell* signal was almost double that *blank* signal; the rebounds closer to the primary signal (approx. 40-45 μs) were also more attenuated in the *cell* signal. **Figure 74D** represents the incident pressure exerted by the P-waves produced by the transmitter transducer; notice that although our wave generator had a limit output amplitude of 20 V, to verify linear response of exerted pressure concerning input excitation voltage, a curve from 0 to 50 V was computed.

The obtained pressure was extracted through the manufacturer's datasheet formula: $P = 0.35 \frac{V_m}{10^{-\frac{254}{20} + 6}}$ (Onda's Hydrophone Calibration, with V_m the mean voltage), applying linear regression $R^2 = 0.99$ with $P = 72.6 \cdot V_m + 43.8$. For experimentation procedures, it was selected an excitation voltage of $V_{pp} = 20 \text{ V}$, where an acoustic pressure of 1509 Pa was obtained in an immersion tank with abovementioned hydrophone. A weighing protocol was used to calculate the flow rate, where voltage variations from 5 V to 24 V (in steps of 0.5

V) were applied. The extracted results showed flow rates below $1 \text{ mL}\cdot\text{min}^{-1}$ if the power supply was lower than 12 V.

Figure 74F-a to the **-F-d** showed a microfluidic model through scaffold fibers (represented as circles) with two different flows. The scaffold was represented as a matrix of circles, where each circle had a diameter of $200 \mu\text{m}$, and they were separated between them by $600 \mu\text{m}$ cause of the printing layer pattern. Mesh element size was adapted to $100 \mu\text{m}$ caused is $\frac{1}{2}$ of the fiber diameter. The cylindrical approximation of the fibers was demonstrated in the previous work¹¹¹¹. The cell medium density ($\rho = 1.009 \text{ g}\cdot\text{cm}^{-3}$) and dynamic viscosity ($\mu = 0.93 \text{ mPa}\cdot\text{s}$) can be retrieved from prior literature¹¹⁷⁵. Reynolds number was calculated as $Re = \frac{\rho u D_h}{\mu} = 4.6 \ll 2300$, where u is the input flow speed (at $0.8 \text{ mL}\cdot\text{min}^{-1}$ $u = 106.1 \mu\text{m}\cdot\text{s}^{-1}$; at $0.5 \text{ mL}\cdot\text{min}^{-1}$ $u = 66.31 \mu\text{m}\cdot\text{s}^{-1}$) and D_h is the input diameter height, which was 4 mm. The obtained Re is less than 2300, which is regarded the upper limit for laminar flows, whereas turbulent flows develop when Re numbers exceeds 2900^{1176,1177}.

According to model results, the flow rate obtained can be translated by weighing to actual flow speeds incident over cells: a) $0.5 \text{ mL}\cdot\text{min}^{-1}$ corresponds to flows below $800 \mu\text{m}\cdot\text{s}^{-1}$ and b) $0.8 \text{ mL}\cdot\text{min}^{-1}$ to flow speeds below $1000 \mu\text{m}\cdot\text{s}^{-1}$. Notice that although the flow speed is higher between fibers close to the fiber surface (i.e., cell location), the flow speed decreased lower half of the maximum value (**Figure 74F**). From the model, it can be extracted that maximum shear rates are 10 mPa at $0.5 \text{ mL}\cdot\text{min}^{-1}$ (b) and 16 mPa at $0.5 \text{ mL}\cdot\text{min}^{-1}$ (d).

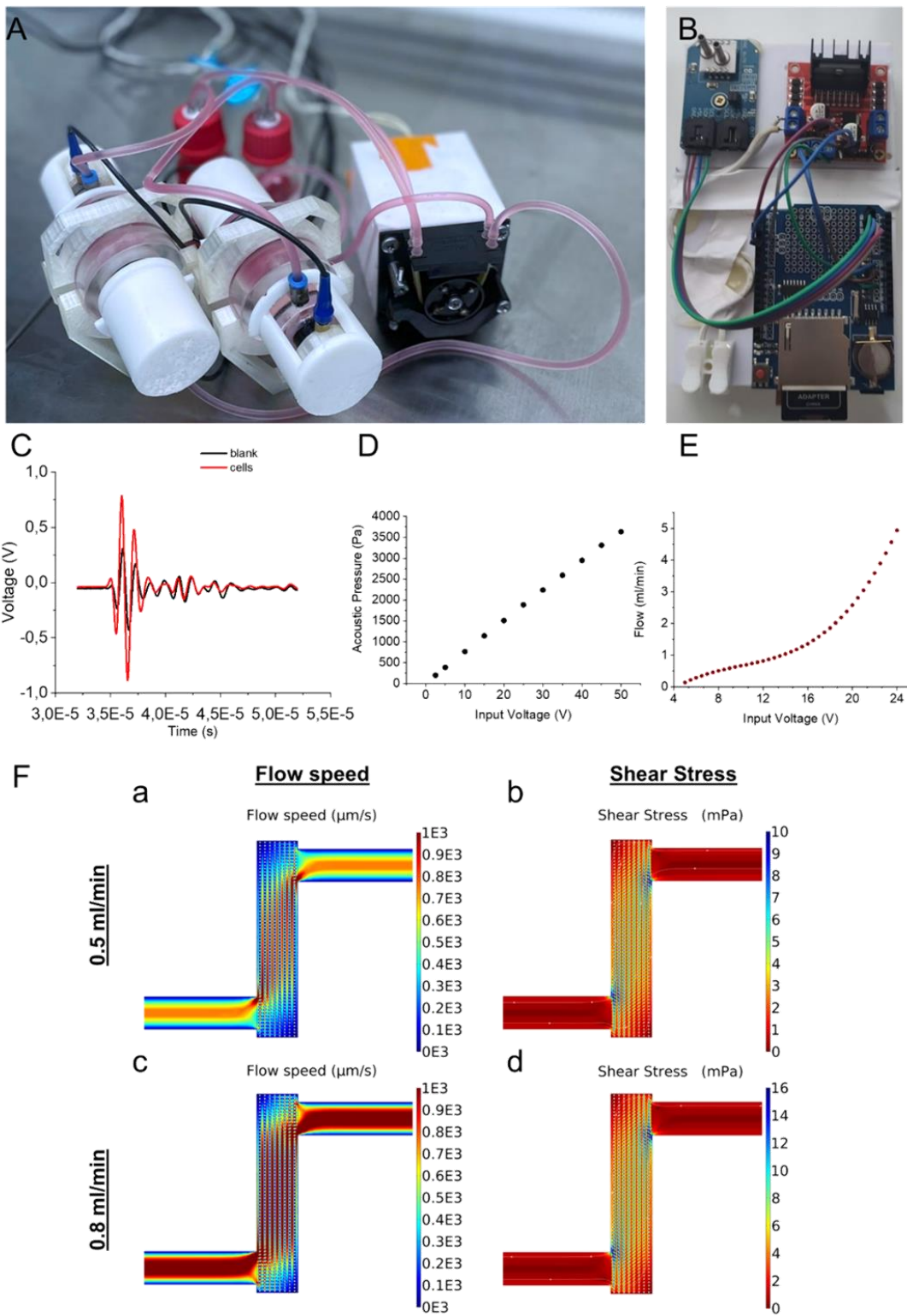


Figure 74. BR final arrangement and global parameters. (A) Photography of the final assembly of the BR inside a laminar hood. (B) Photography of the Arduino circuit that controls the peristaltic pump. (C) Output signals recorder by Raspberry PI. Red represents the functionalized scaffold with seeded cells, and in black, the same scaffold without cells. (D) Pressure amplitude of P-Wave vs. Voltage amplitude exciting transducer. (E) Results from flow rate calibration, Flow rate vs. Voltage amplitude of peristaltic pump. (F) A 2D fluid dynamic model in FEM to evaluate the incidence flow speed (a and c) over scaffold fibers and their corresponding shear stresses (b and d) depending on the flow rate. Two flow rates are represented $0.5 \text{ mL}\cdot\text{min}^{-1}$ and $0.8 \text{ mL}\cdot\text{min}^{-1}$.

28.2. Acoustic Pressure Wave Propagation Model

A complex and novel 2D model applying Multiphysics FEM (COMSOL Multiphysics®) was developed to understand the mechanical behavior of the BR US system. Figure 3 shows the representation of the model and the physics behind its comportment. **Figure 75A** represents the XY plane visualization of the whole geometry, where the modeled plane corresponds to a transversal section in the middle of the BR. This plane was selected in both models (P-wave propagation and fluidic dynamic model) because flow channels have no axial symmetry.

To validate the present model, the BR was assembled in two different manners: without any scaffold (and filled with water) and with a solid disk of PLA (and filled with water). In previous literature, both density and speed sound have been obtained¹¹⁷⁸. PMMA speed sound was empirically calculated to $2630 \text{ m}\cdot\text{s}^{-1}$. **Figure 97** represents the level of correlation between the water (**Figure 97A and -C**) model and the PLA (**Figure 97B and -D**) model. A signal correlation (comparing synthetical signals with experimental ones) higher than 80% was obtained in both cases.

In summary, the signal originated in the transmitter transducer as a mechanical P-wave (**Figure 75B** shows mechanical displacement in the X direction, Y displacement was negligible); the total displacement goes from $-25 \cdot 10^{-5} \mu\text{m}$ (3B.a) at $t = T_0/2$ to $25 \cdot 10^{-5} \mu\text{m}$ (3B.b) at $t = T_0$. After that, the P-wave is propagated through the acoustic pressure module (**Figure 75C**), where

dependent variables were material densities and material sound speeds (ρ and c_s Respectively): $\frac{1}{\rho c_s^2} \frac{\partial^2 p_t}{\partial t^2} + \nabla \cdot \left(-\frac{1}{\rho} (\nabla p_t - \mathbf{q}_d) \right) = Q_m$, where Q_m is the Monopole Domain Source, \mathbf{q}_d is the dipole domain source, and $p_t = p + p_b$, where p_b is the background pressure field. Notice that interior impedance, a boundary condition that simulates the reflection/transmission phenomena, depends on both parameters (ρ and c_s respectively). Thus, the attenuation of the signal will depend on the density and sound speed of the scaffold domain. For the external boundaries that represent the walls of the BR $-\mathbf{n} \cdot \left(-\frac{1}{\rho} (\nabla p_t - \mathbf{q}_d) \right) = 0$.

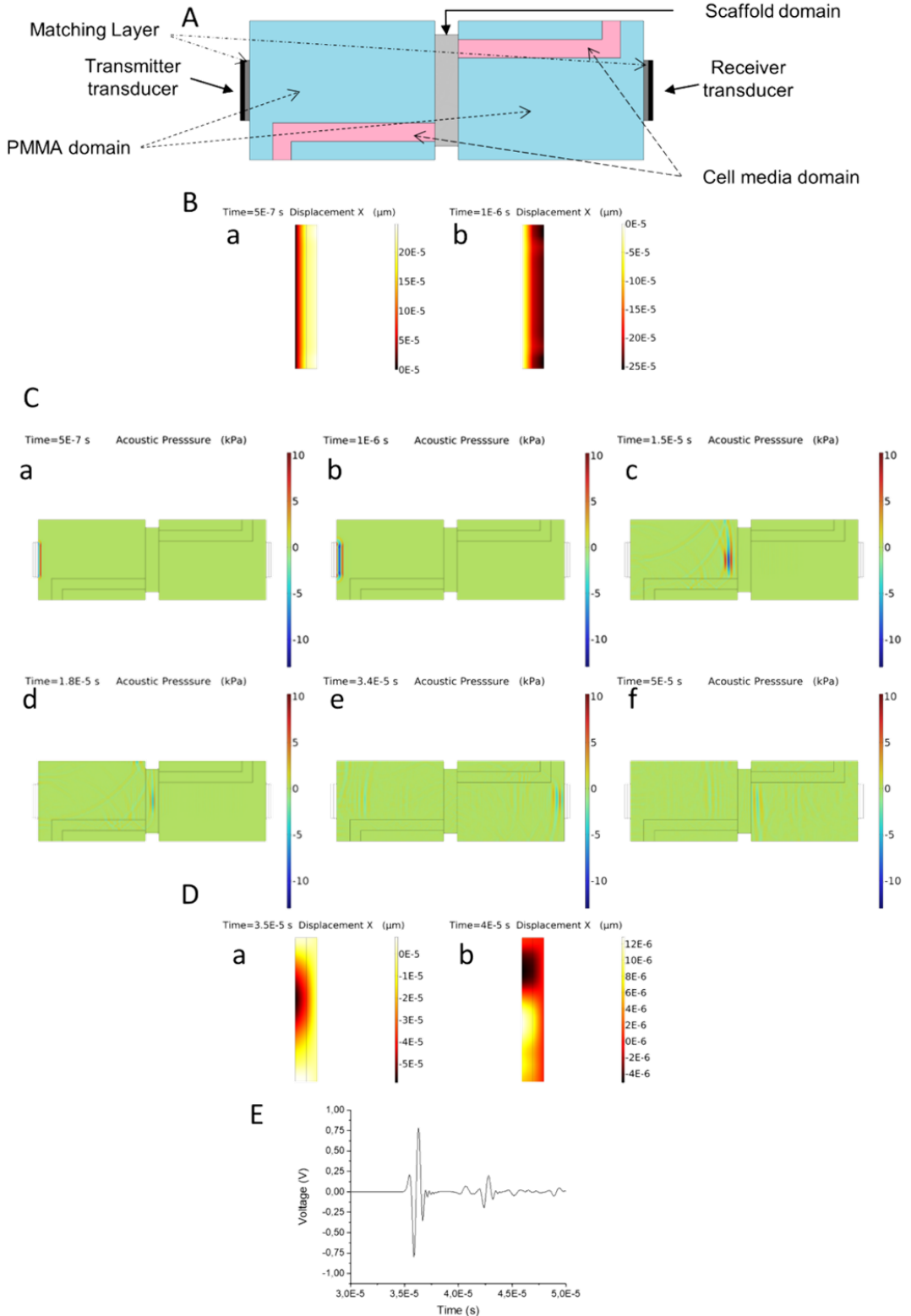
Figure 753C-a, which corresponds to $T_0/2$, the P-wave is partially developed; in **Figure 753C-b** is fully developed and shows that the P-wave contact the scaffold domain at $t = 15 \mu\text{s}$ (**Figure 753C-c**); at $t = 18 \mu\text{s}$ (**Figure 753C-d**) at the middle of the scaffold domain, implying that the primary wave travels through the scaffold domain in $6 \mu\text{s}$ approximately. Next, at $34 \mu\text{s}$, the main wave reaches the receiver transducer (**Figure 753C-e**), and at $t = 50 \mu\text{s}$ (last experimental time), there are only rebounds obtained from different boundary conditions (**Figure 753C-f**). As done in the transmitter transducer, **Figure 75D** shows the displacement in the X direction of the mechanical P-wave over receiver transducer domains. The P-wave is fully developed at $t = 35 \mu\text{s}$, and rebound waves are transmitted at $t = 40 \mu\text{s}$. Finally, **Figure 75E** represents an US wave obtained by the proposed model as a floating potential of the receiver.

A 2D model was chosen because it drastically reduces the computational time, the memory requirements, and the representation complexity. All previous parameters are essential to computing inverse problem studies where parametric sweeps are performed. Contrasting the previous model that describes the microfluidic flow, in this model, porosity has not been modeled due wavelength of the US P-wave through the scaffold domain is much higher than the pore size¹¹⁷⁹: $\lambda_{SD} = c_{SD}/f_0$, $c_{SD} > 1480 \text{ m} \cdot \text{s}^{-1}$, $f_0 = 1 \text{ MHz}$; thus, $\lambda_{SD} > 1.48$

mm and the $PS < 400 \mu m$ (SD: scaffold domain, PS: pore size, c_{SD} means the sound speed of the scaffold domain, f_0 = cutoff frequency). Mesh element size was selected through parameter sweep to verify model convergence (**Figure 98**); it was established that an element size below $400 \mu m$ was sufficient to acquire a stable signal. In **Figure 98G to -J**, no significant variance over amplitudes in mesh sizes below $400 \mu m$ can be appreciated. Rest of parameters (*i. e.* c_{PMMA} , c_{H_2O} , ρ_{PMMA} , ρ_{H_2O}) were reconstructed through inverse problem.

Figure 75. FEM model of P-wave propagation phenomena. (A) 2D representation of the different domains of the FEM model. (B) Thermal image of the “u” component of the displacement of the transmitter ultrasound transducer (*i. e.*, X component) at $t = 0.5 \mu s$ (a) and $t = 1 \mu s$ (b). (C) P-wave propagation at different times: (a) $t = 0.5 \mu s$, (b) $t = 1 \mu s$, (c) $t = 15 \mu s$, (d) $t = 18 \mu s$, (e) $t = 34 \mu s$, and (f) $t = 50 \mu s$. (D) Thermal image of the “u” component (*i. e.*, X component) of the displacement of the receiver ultrasound transducer at $t = 35 \mu s$ (a) and $t = 40 \mu s$. (b). (E) The final electrical modeled signal was obtained from the FEM model. \hookrightarrow next page

CHAPTER III CARTILAGE-LIKE TISSUE BY A LOW SHEAR STRESSES-BASED BIOREACTOR



28.3. Viability and chondrogenic characterization

Alamar Blue reagent was used to detect metabolic activity in the PBA functionalized bTPUe scaffolds after seeding IPFP-MSCs. Different flow regimes and flow rates were performed (**Figure 76A**) to evaluate cell proliferation and viability.

IPFP-MSCs were isolated and grown from OA patients until passages 3 to 5. IPFP-MSCs were identified using the standards recommended by the ISCT⁵¹ (**Figure 99**). Following this, 10^6 cells·mL⁻¹ were seeded over scaffolds and incubated for 4 h at 37°C before receiving new media (DMEM Glutamax, 10% FBS, 1% P/S). Scaffolds with cells were cultivated for 1 week in a 6-well plate to ensure adequate cell-scaffold integration. After, scaffolds were introduced inside the BR for another week, while control cell-loaded scaffolds were maintained in the well plate that week. All conditions' metabolic activity was tracked on days 1,3, and 7 of BR experimental time.

Results indicated a different response in cellular metabolism as a function of flow rates (**Figure 76A**). Following literature recommendations⁵³⁰, a continuous flux of 0.5 mL·min⁻¹ was probed with negative results. Next, a discrete (1 h of work separated by each 6 h) form of the previous flow rate was applied to reduce the exposure stress over cells; negative results were obtained with a dramatic reduction of cell metabolism at day 3. On the other hand, once the flow rate was increased to 0.8 mL·min⁻¹, the metabolism increased similarly with respect control scaffolds. In fact, at day 7 in BR 0.8 mL·min⁻¹, the metabolism continued its growth compared to the rest of the conditions, reaching almost double the rate of day 1. Consequently, the following experiments were performed with a flow rate of 0.8 mL·min⁻¹.

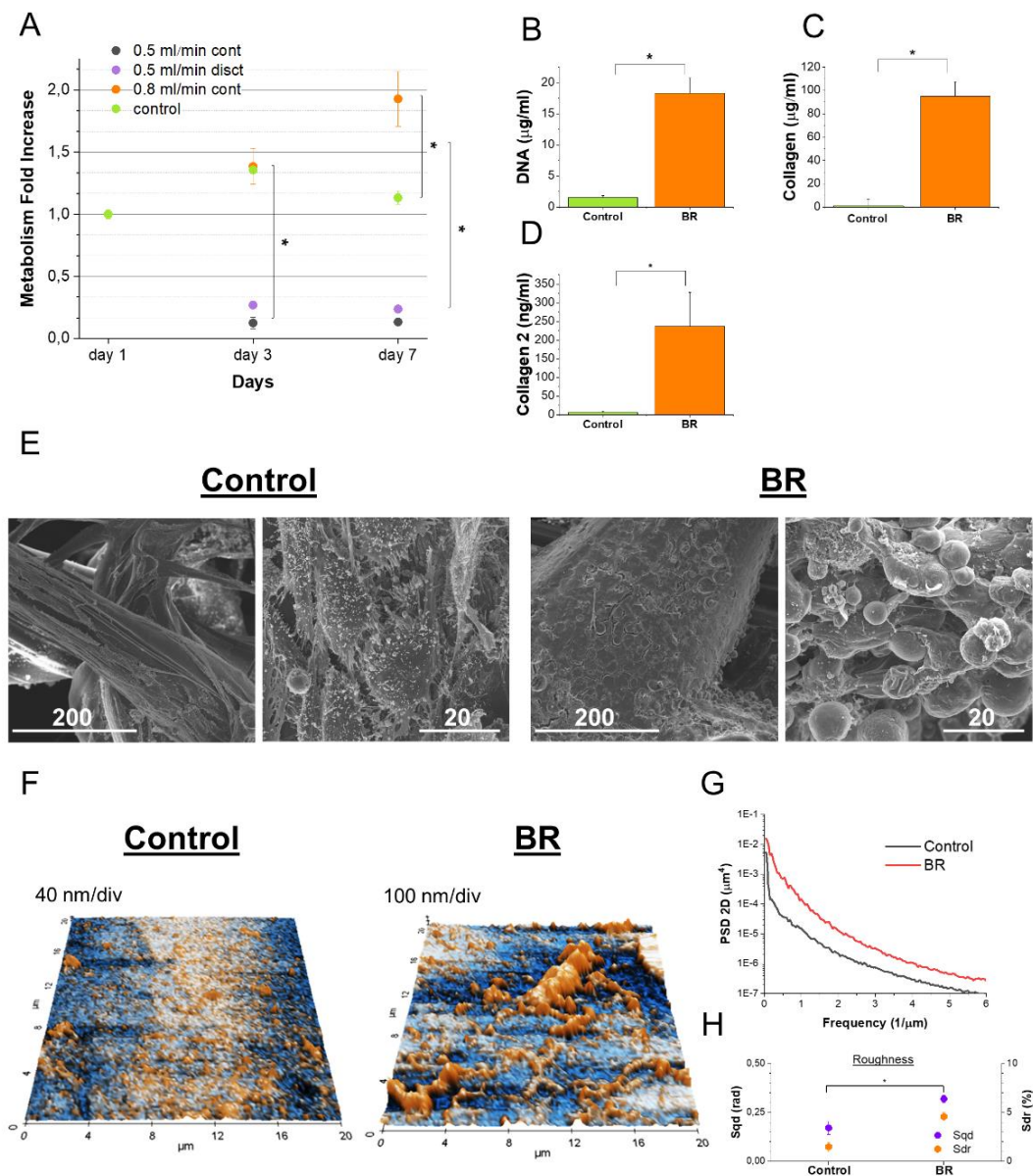


Figure 76. (A) Alamar Blue assay with different flow rates and control. Values were normalized for day 1. (B) DNA quantification at day 7 of experimentation of control and BR $0.8 \text{ mL}\cdot\text{min}^{-1}$. (C) General collagen quantification with Sirius Red assay of the control and BR samples ($0.8 \text{ mL}\cdot\text{min}^{-1}$). (D) Collagen type II quantification using Elisa kit for both control and BR ($0.8 \text{ mL}\cdot\text{min}^{-1}$) samples. (E) SEM images at day 7 of both scaffolds and scale bars are expressed in microns. (* means p -value < 0.001 ; cont. = continuous perfusion flow, disct. = discrete perfusion flow).

Additionally, DNA quantification for BR scaffolds and control one was carried out to see if changes in metabolic activity were associated with differences in cell density. The results presented in **Figure 76B** show a clear difference between BR samples and control ones, with a significant increase in BR scaffolds ($p < 0.001$) (see a standard curve in **Figure 100A**). Concerning ECM synthesis, both general collagen quantification based on Sirius Red dye (see the standard curve in **Figure 100B**) and type II collagen quantification were exerted. **Figure 76C** shows similar results to DNA content and a much higher collagen presence in BR samples ($p < 0.001$). On the other hand, a much higher type II collagen concentration (see the standard curve in **Figure 100C**) in BR samples in comparison to control one (p -value < 0.001) was obtained (**Figure 76D**).

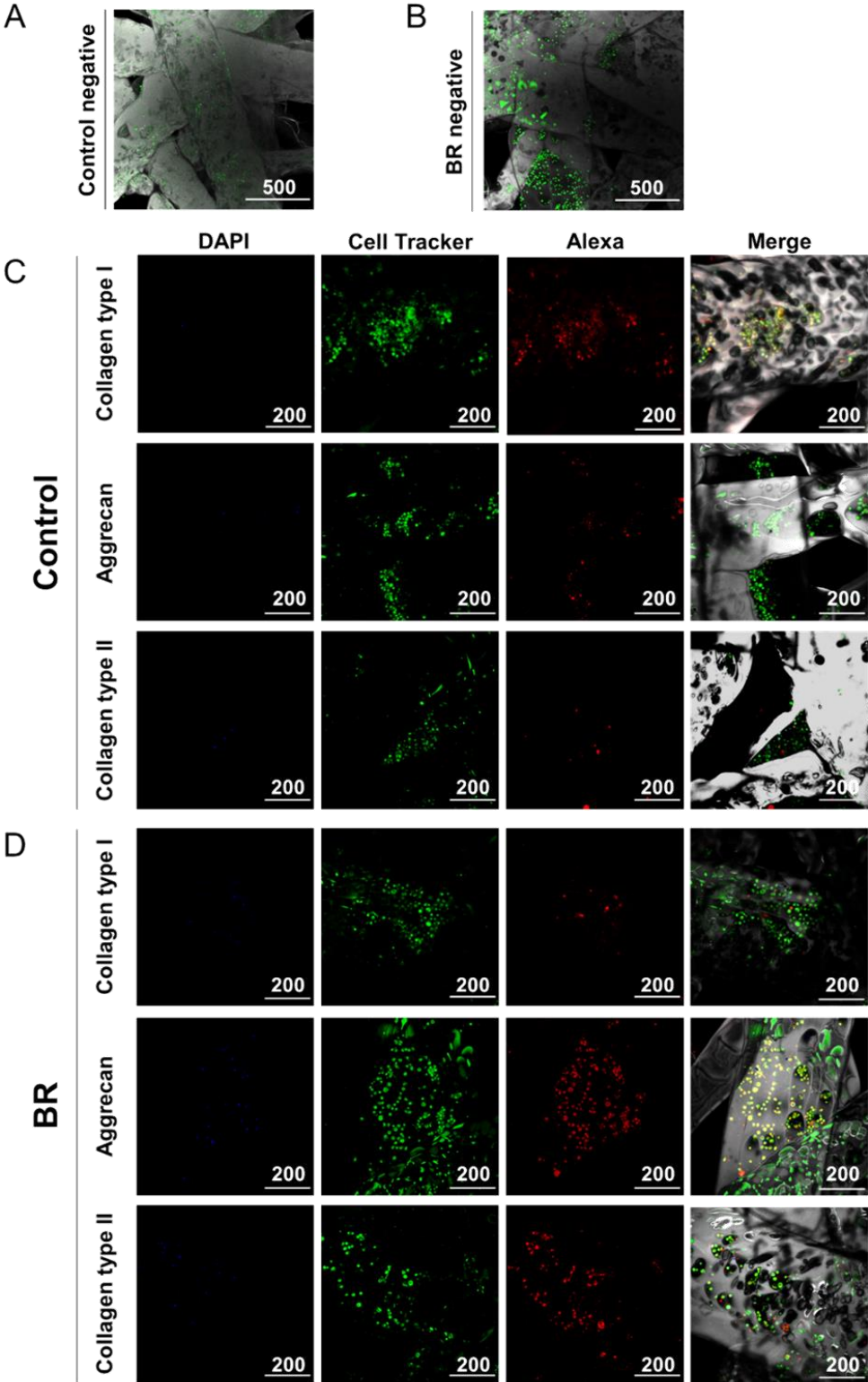
SEM and immunofluorescence techniques were applied to verify the increased amount of ECM in 3D scaffolds included in BR. SEM results showed that scaffold fibers in both samples were covered by cells (**Figure 76E**). Nonetheless, in the control scaffold, there were empty spaces between cells. Something different happened on BR samples where scaffold fibers were entirely covered by cells and ECM. Additionally, IPFP-MSc shape differed between control and BR samples; BR ones displayed a more circular cellular shape. Nevertheless, cell viability and adequate cell-biomaterial interaction were shown in both cases.

In addition to SEM images, AFM was applied to characterize the rugosity of the surface of the scaffold fibers between cells. In **Figure 4F** it can be observed enhanced contrast images of a region of interest (ROI) of both conditions. Results express an observable increase in rugosity in quantity and size of grain in BR scaffolds than control samples. Even more, the presence of some fibrils (collagen) is manifested in BR cases. The power spectral density (PSD) profile of the average of three samples was computed in **Figure 76G** to quantify the degree of exchange in rugosity. Curves show a higher signal power in BR samples than in control ones, implying the presence of higher structures attached to the

scaffold surface, as observed previously in **Figure 76F**. Finally, typical roughness parameters as the root mean square gradient (Sqd) and the developed interfacial ratio (Sdr) were also computed, founding a statistical difference ($p < 0.001$) between control samples and BR condition, implying that the rugosity of the scaffold increased with the exerted perfusion flow.

Figure 77A and **-B** correspond to images without primary antibody (negative) to verify if the secondary antibody presented no corresponding interactions for immunofluorescence images. Alexa Deep Red was selected as the secondary antibody to avoid scaffold autofluorescence. Thus, each ECM protein was represented separately (**Figure 76C** and **-D**). Results clearly expressed the abundant presence of all the common AC ECM proteins and high cell viability on BR samples: type I collagen, type II collagen, and aggrecan. BR scaffolds presented much higher expression of type II collagen and aggrecan, with a few amounts of type I collagen. In contrast, control scaffolds presented much lower cellular content, no aggrecan proteins, and a much higher content of type I collagen. Conclusively, from quantification assays, SEM, and immunofluorescence, it is demonstrated the active chondrogenic induction potential of the BR over IPFP-MSCs.

Figure 77. Immunofluorescence merges images without primary antibody (i.e., negative) of the control sample (A) and BR sample (B). (C) Control and BR samples with primary type II collagen antibody + 2nd Ab and primary aggrecan antibody + 2nd Ab. Cell Tracker™ green is represented in green. Secondary Ab (Alexa 647 nm) is shown in red. In blue, the DAPI marker is represented. ↪ *next page*



28.4. Biomechanical correlation analysis

Since US are a valuable non-invasive characterization method, in this research, LIPUS (1 MHz) were employed to study the mechanical evolution of the scaffold for one week inside the BR. Free-cells (blank) scaffolds were also evaluated with US and replying to the same conditions as *ex vivo* experimentation to neglect any background information. **Figure 78A** and **-B** show arbitrary signals for cell-seeded and blank scaffolds of each experimental day. In both cases, a decrease in the V_p was observed after 24 hours of treatment, accomplished with a signal delay. The presence of this phenomenon in both conditions implies a no-cell-dependent behavior. On the other hand, it can be observed how V_p increased from day 2 to day 7 in cell-loaded scaffolds (from 1.3 V to 2.1 V), whereas, in blank scaffolds, no substantial variance was revealed (0.04 V to 0.043 V).

Figure 78C represents the evolution of signal amplitudes over time; in blank conditions, no significant difference was observed during one week of experimentation. Although a decrease in amplitude from day 1 to day 3 was observed in both cases, only in cell-loaded scaffolds was an appreciable increase in amplitude. Another important consideration, which can also be observed in **Figure 78A**, **-B**, and **-C**, is the significant difference in amplitude value on all days ($p < 0.001$). The same difference was evident for the computed ToF signal (**Figure 78D**), where blank scaffold signals were slightly slower than cell-loaded ones ($p < 0.001$). In summary, results observed in **Figure 78C** and **-D** imply that received US signals expressed considerable differences when cells were seeded in the scaffolds.

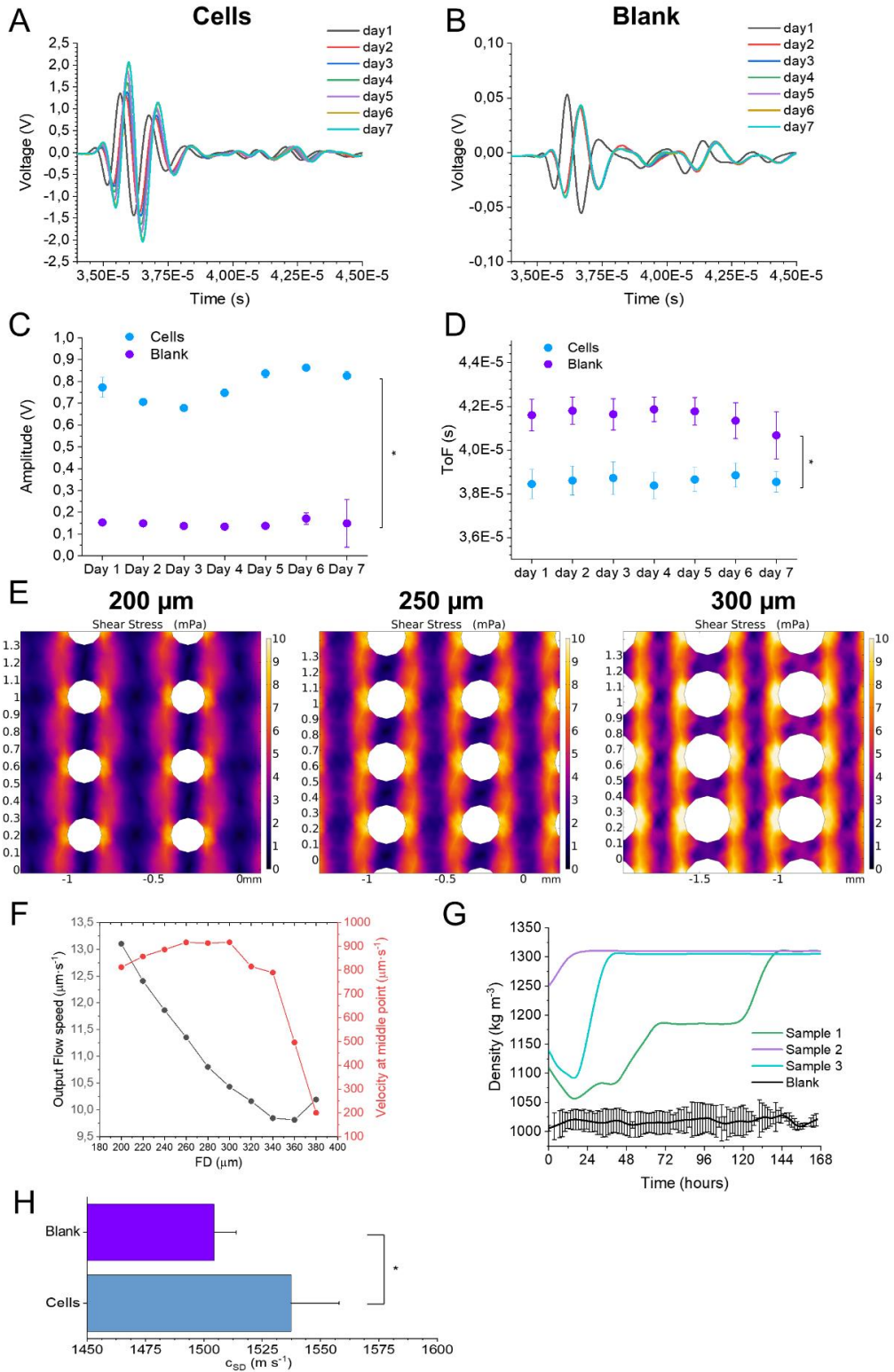


Figure 78. (A) P-wave arbitrary signals obtained from the cell content scaffolds during BR experimentation. (B) P-wave arbitrary signals obtained from the blank scaffolds (no cells) during BR experimentation. (C) Amplitude evolution curve of average amplitude signals. (D) Time of flight (ToF) curves. (E) Thermal 2D images of fluid shear stress (CFD) model using different scaffold fiber diameters. (F) Output Flow speed from the BR vs. the scaffold fiber diameter (FD) in black; and the instant velocity of the middle point ($X = 0, Y = 0$) inside the scaffold domain. (G) Density evolution along time of BR cell content in scaffold samples and blank scaffolds obtained by cross-correlation empirical signals with synthetical ones. (H) Speed of sound of scaffold domain (c_{SD}) (scaffold + water) obtained by cross-correlation. (*: P-value < 0.001).

Raw recorded data does not comprehensively predict the ECM synthesis rate. As explained, computational models were developed to describe the fluid dynamics and the P-wave propagation phenomena. Thanks to such models, it can be estimated how the fluid could affect the cells if scaffold fibers fatten over time. The idea behind the previous argument is expressed in **Figure 78E**, where three different fiber diameters are proposed: an initial fiber diameter of 200 μm , an intermediate of 250 μm , and a final estimated diameter of 300 μm (approximately the one obtained from the SEM images). It is not uncommon to confirm that shear stresses ($\tau = \mu \frac{\partial u}{\partial y}$, with μ the dynamic fluid viscosity) will increase directly proportional to the fiber diameter; notably, there is a range from an initial 4-7 mPa to a final 8-10 mPa. But more important is the presence of high shear stresses in the orthogonal direction of fluid flow once the diameter fiber overpasses the diameter of 250 μm .

Figure 78F shows the BR output flow speed, which is very similar to Figure 6E in that the boundary probe recorded data as instant flow speed (at the axial origin point) and output flow velocity magnitude. Previous magnitudes were compared to an estimated increase in scaffold fiber diameters (FD). Both magnitudes are shown to be connected and exhibit distinct patterns. The output velocity decreased linearly for FD 360 μm , although the instantaneous speed increased from 200 to 320 μm . For FD > 320 μm , the output flow speed began to decline slightly, but at FD = 360 μm , there was a sharp drop followed by a tendency change. This observation implies that when the FD exceeds 340 μm , the

permeability of the scaffold decreases and the fluid channel may not cross the scaffold but rather passes around the scaffold walls.

P-wave propagation models must consider the mechanical behavior of three different materials (PMMA, water, and bTPUe). Thus, the final electrical signal representing the ultrasonic pulse envelops all such parameters making it a very complex task to extract information from that. Again, the computer model helped focus on the reconstructive parameters that had more variability over time. Thereby, for P-wave propagation it can be highlighted the speed of the longitudinal wave: $c_p = \sqrt{\frac{E(1-\nu)}{\rho(1+\nu)(1-2\nu)}} \rightarrow c_p = \sqrt{\frac{K}{\rho}}$, E = Young's Modulus, and $K = \frac{E(1-\nu)}{(1+\nu)(1-2\nu)}$. The previous equation estimates that the final signal obtained by receiver transducers will mostly depend on the scaffold's sound speed and density.

With that in mind, a set of signals varying c_{SD} (sound speed of Scaffold Domain) from 1300 to 1600 $\text{m}\cdot\text{s}^{-1}$ and ρ_{SD} (density of Scaffold Domain) from 1000 to 1400 $\text{kg}\cdot\text{m}^{-3}$ were synthetically created. After that, empirical signals obtained from the BR *ex vivo* experiments were compared with such a set of signals. After each empirical signal was cross-correlated, $(f \star g)(x) \stackrel{\text{def}}{=} \sum_j f_j^* g_{i+j}$, with each synthetical signal generated with the computational model. Every synthetical signal was tagged with its corresponding ρ_{SD} and c_{SD} . Then, it was estimated that the maximum cross-correlation (and always > 80%) was the most acceptable density and sound speed value.

In **Figure 78G** and **-H** such extracted parameters (c_{SD} and ρ_{SD}) are shown. **Figure 78G** indicates two pieces of evidence: the first is that no significant density variation was observed in blank scaffolds; the second is an increase in the scaffold domain densities over time in cells-seeded scaffolds. The non-average curve was computed in cells-seeded scaffolds to show the capacity to record different growth patterns. On the other hand, Figure 6H shows the sound speeds of both cells-seeded scaffolds and blank ones. Average values are

represented due to much lesser variation ($SD < 1\%$) of this parameter than density. The figure shows again a significant difference between blank scaffolds and cell content ones ($p < 0.001$), being higher the c_{SD} of cells-loaded scaffolds. It is essential to considerate that: $c_{TPU} = 1740 \text{ m} \cdot \text{s}^{-1}$ and $c_{H_2O} = 1480 \text{ m} \cdot \text{s}^{-1}$ from literature are pretty close to the obtained by our experimentation and model¹¹⁸⁰. Moreover, the porous ratio of printed scaffolds was 0.3, seeing $c_{SD} = 0.3 \cdot c_{TPU} + 0.7 \cdot c_{H_2O} = 1558 \text{ m} \cdot \text{s}^{-1}$. From this can be extracted that the results obtained from the model are highly accurate and that a higher sound speed implies less water content in the scaffold domain.

29. Discussions from Chapter III

OA is a gradual and degenerative condition based on the loss of functionality in cartilage tissue, which has a limited ability for regeneration. The great potential of RM products will therefore be advantageous to OA's long-term treatment¹¹⁴⁵. For RM development, the applied biomaterial properties are significant. For instance, the stiffness of 3D bioengineered scaffolds is essential for forming AC tissue because it is subjected to cyclic mechanical pressures from bodily activity¹¹⁰⁸. So, prior characteristics of scaffolds are significantly influenced by scaffold fiber geometry and pore size^{1048,1109,1110}. Every joint in the musculoskeletal system relies on connective tissues (such as cartilage)¹¹⁸¹; AC experiences baseline amounts of mechanical strain within their constituent fibers due to growth and swelling¹¹⁸². These strains provide local cells with biophysical signals, ultimately affecting cellular phenotype and function¹¹⁸³. Here, we drew inspiration from the cartilage ECM, their physical stimuli, and 3D TE principles to develop an alternative to preceding therapeutic strategies.

Previous works have studied the benefits of perfusion flows over MSCs and chondrocytes^{1173,1184–1186}. But, even nowadays, there is no clear definition of standard conditions for such mechanical cues. Despite this, it is interesting to remark that those studies relate perfusion flows with the primary cilia stimulation¹¹⁸⁷ and the IFT of chondrocytes, which involves the TRPV4 channels⁹¹⁴. This transport regulates the gene expression of type II and type IV collagen, G proteins, *Ihh*, Ca²⁺ channels, connexins, purine, cAMP, and the PKA pathway among others^{954,1188}.

Most of the previous literature only expresses the quantities of flow rates^{530,1173}; in contrast, this article exposes this magnitude and the exerted shear stresses thanks to FEM results. In addition, it was modeled by two-phase fluid dynamics in the BR filing, where no significant turbulences appeared, and the exerted shear stresses were very similar to the last ones. Moreover, those planar

representations also expose the regions of higher stresses, implying that not all scaffolds will suffer the same regime of loads. A small region close to the corners of the IO channels has the highest tensions, whereas the rest of the scaffold suffers from minor stimulation. As a result, homogeneous (i.e., isotropic) stimulation over the whole scaffold in BR experimentation cannot be assumed, as some previous literature claims^{530,1184}.

Further, FEM analysis also enhances global comprehension, causing its possibility to simulate estimated evolutions of our study case. A hypothesis of FD increases over time was assumed and it was evident that shear stresses increased with the diameter of scaffold fibers (from 6 mPa to 10 mPa). Previous parameters are lower than those applied in the previous research^{530,1185,1189,1190}, but it is essential to control precisely the evolution of those shear stresses because it can cause possible cell damage^{1173,1185,1191,1192}. On the other hand, if insufficient perfusion flow is exerted, poor nutrient transport will likely result in cell death, as possibly happened with flow rates of $0.5 \text{ mL}\cdot\text{min}^{-1}$. Extrapolating these observations and comparing them with the simulation obtained our work, it can be concluded that as the FD increases, the flow through the scaffold decreases and, consequently, the nutritional intake decreases. This consideration concurs with results obtained by the cross-correlation model of the experimental P-waves, where a limit of ρ was observed.

Concerning the biological assays, where the metabolism of scaffolds inside the BR was analyzed together with their chondrogenic potential to generate cartilage-like structures, it can be extracted the following statements. Once the input flow rate was optimized, that is, the final continuous $0.8 \text{ mL}\cdot\text{min}^{-1}$, it was observed how the cell metabolism increased earlier than in control scaffolds, reaching almost 200 % of growth. Meanwhile, in the control scaffold, cell metabolism was reduced from day 3 to day 5. Cell metabolism is highly determined by nutrient transport, and perfusion flows enhance metabolite intake, promoting that increase in metabolism^{1193,1194}. Our results show that the

cell metabolism increased, and the cell content was significantly higher, indicating that cells were expanded under the BR stimulation protocol. The available collagen quantification assay and the obtained type II collagen values prove the chondrogenic potential of the scaffold embedded inside the BR. In previous studies¹¹⁹⁵, we already demonstrated the chondrogenic potential of PBA functionalized scaffold at 21 days, and comparing the current obtained values at day 7 of experimentation inside the BR; it is observed that in less manner, there is the presence of collagens and increased production of type II collagen. These results indicate that our BR drastically enhances the chondrogenic potential of cell-loaded scaffolds.

Image techniques (SEM and immunofluorescence) corroborated the presence of cells attached to the scaffold fibers in both control and BR samples. In control samples, how cells preserved their elongated and planar MSC morphology could be distinguished, and some ECM surrounding cells could also be observed. In contrast, the MSC morphology was lost in BR samples, presenting a rounder shape embedded in a matrix with some cilium^{952,953,959} typical chondrocyte-like morphology¹¹⁴². Besides, the ECM in the BR samples was considerably higher than in the control samples, and the scaffold filaments seem to be wholly covered by such a matrix. Previous results obtained by SEM experiments were confirmed by AFM analyses, where a higher rugosity was obtained in the BR samples, and the presence of similar AC ECM¹¹⁹⁶ was found together with thicker fibers, which are a marker of healthy AC¹¹⁹⁷.

Finally, BR samples' immunofluorescence was performed to detect specific chondrogenic ECM proteins. Both collagen type I, collagen type II, and aggrecan were observed in BR and control samples. For controls, much lower amounts were observed for collagen type II and aggrecan, and an increased expression of type I collagen was detected. In contrast, BR samples showed higher levels of viable cells attached to the fibers, a lower expression of type I collagen, and higher amounts of both type II collagen and aggrecan, implying

chondrogenesis¹¹⁹⁸. Even more, immunofluorescence images displayed how these proteins were distributed between cells along the BR scaffold fibers, whereas control samples concentrated on the interlacing of fibers. In previous literature, MSCs express type I collagen and hyaluronan¹¹⁹⁹, an early stage of precartilaginous condensation; the digestion of type I collagen matrix; and the expression of N-cadherin, tenascin-C, and other adhesion proteins regulated by TFG- β , Wnt/ β -catenin and Sox9 signaling pathways^{713,1200-1203}. Finally, precartilaginous ECM is converted into AC ECM rich in collagen type II and aggrecans^{1204,1205}.

Moreover, the expression of Sox9 and Col2a1¹¹⁹⁵ is correlated in chondrogenesis with collagen type II synthesis¹¹⁹⁸. Here, there was quantified and observed after BR stimulation the increased expression levels of collagen type II and the overexpression of such genes. In conclusion, our results indicate that PBA functionalized scaffolds embedded inside the BR enhance cell proliferation and chondrogenesis, reducing the differentiation times compared to previous research and without the necessity of an additional chondrogenic medium.

Besides, this work was centered on considering the chondrogenic effect that fluid low-shear stress can induce in IPFP-MSCs and on developing a compact system that analyzes both growth and differentiation in real-time. The final goal was to obtain an autonomous system that could predict and quantify the viability of the cartilage-like graft implant. In the past, monitoring BRs using different techniques based on light have been applied for directly analyzing the cell behavior^{1171,1206}; however, they only provided a qualitative measurement retrieved from several sensors that would require external verification but did not infer a quantitative result that would establish the tissue growth over time. BR sensor application types are often categorized as in-line, at-line, or off-line. In-line or in-situ sensors are directly connected to the BR (invasive), whereas at-line systems rely on a withdrawn and evaluated outside sample. On-line

measurement of in-line or at-line sensors occurs when data is continuously captured and the sensor signal response time is short compared to the process dynamics. Every other measurement is regarded as off-line, implying a temporal lag from biological activities¹²⁰⁷. Here, we focused on on-line systems (at-line sensors) due to their lack of contamination. Among the themes that can be found are: optical chemo-sensors^{1208,1209}, spectroscopic sensors^{1210,1211}, impedance spectroscopy sensors^{1212,1213}, ultrasonic sensors^{566,1214}, and free-floating wireless sensors¹²¹⁵.

LIPUS has been applied for quantifying the densitometry of scaffold samples inside BR over time in rheumatological studies¹²¹⁶, but this is the first time that an *ex vivo* system has been built to quantify scaffold chondrogenesis in real-time. In our BR, the application of US transducers for exerting the excitatory P-wave and recording the final emitted pulsed together with a FEM model that predicts possible physical events was done. In our system, the scaffold domain (SD) was considered a homogeneous domain formed by the mixture of water and bTPUe (with attached cells and ECM). This approximation is based on the link between the size of the FEM element to be examined and the excitation wavelength, being its ratio crucial for deriving information from the received wave in the field of non-destructive evaluation utilizing ultrasonic waves. When the wavelength is more significant than the element's size to be examined, data from the medium, which is thought to be homogeneous, is obtained¹¹⁷⁹.

However, when the wavelength is smaller than the element's size to be characterized, mechanical data from the element in question is recognized in the received wave. The scaffold has been treated as a homogenous medium without modeling it because the excitation wavelength (~1.5 mm) is larger than the size of the pores (400 μm) or the fiber diameter (200 μm). This consideration has been demonstrated by the findings obtained in the BR. In this instance, the interaction of the wave with the assumption of the scaffold as a homogenous medium result in the validation of the obtained wave information. Thus, based

on the mechanical characteristics of both the scaffold's bioprinting material and its printing percentage, as well as the mechanical properties rebuilt with the culture model, the obtained velocity of the wave is estimated to correspond to the empirically recorded ToF.

Results extracted from the BR assays showed that the amplitude of the cells-loaded scaffolds was higher than in blank scaffolds, implying that the stiffness of the seeded scaffolds was higher¹²¹⁵. A shared characteristic between cells-loaded scaffold samples and blank samples was the decrease of amplitude from day 1 to day 3, indicating an external cause of such phenomena and probably due to plastic deformation of the materials exerting the contact tension of the transducers. On the other hand, the ToF value is a non-adequate parameter for tissue expansion prediction because its variations are much lower than the rates of cell proliferation and ECM synthesis. More interesting is the absence of considerable near rebounds in study samples compared with blank scaffolds, implying smaller pore sizes. Our empirical signals differentiate between measuring the scaffold with cells attached to their fiber surface and no cells attached (blank). Thus, applying a FEM to induce big data analysis tools as signal cross-correlation is an accurate tool for expanding the information of extracted results and, in this case, transforming a qualitative approximation into a quantitative one.

Moreover, since an apparent increase in the scaffold domain density was obtained over time into the BR, and this was not due to any degradation in bTPUE after 14 days¹¹²², this result can be only explained by ECM synthesis and cellular proliferation. As a consequence, it is probed that our system can determine tissue development in real-time. In addition, cellular scaffolds' noticeable sound speed increase indicates that the K component of the speed sound equation increased higher than the density increase, implying a higher Elastic modulus (E) or lower viscosities (ν). Perhaps the most exciting result is the asymptotic value of 1300 $\text{kg}\cdot\text{m}^{-3}$ obtained by cells-loaded scaffolds, which could be explained as causing a

decrease in nutrient support associated with higher shear stresses. But curiously, the obtained value is similar to literature results for collagen ($1.3 \text{ g}\cdot\text{cm}^{-3}$)¹²¹⁵, suggesting that the final reached density is mainly composed of collagen.

29.1. Conclusions

In this work, we have developed a unique BR that, when compared to static cultures, improves chondrogenesis through fluid-low shear stresses. Our BR boosts the growth of IPFP-MSCs seeded in bTPUe scaffolds functionalized with PBA and induces increased ECM production with a high type II collagen content. SEM and confocal imaging prove scaffolds stimulated by the BR increased cell presence and AC ECM. The results not only agree with our earlier research¹¹⁹⁵, but they also suggest a significant improvement over it. To confirm that our AC grafts display a similar conformation to naive AC tissue, long-term evaluation, *in vivo* experiments, and histological assays would be advised in further research. Using FEM to analyze the current fluid dynamics reveals the need to regulate the initial flow rate and modify it over time to accommodate tissue growth.

Additionally, a system that can independently track the rise in tissue graft density over time and determines that graft speed of sound has been developed using inverse problem characterization through FEM. As a result of the fact that both metrics are closely associated with an increase in material stiffness and collagen content, it can be concluded that our method can monitor tissue growth over time. In summary, we have developed a BR for the first time to induce chondrogenesis in cells-loaded scaffolds and measure tissue growth in real time. Although further studies are necessary, our results suggest the great potential of our BR as a medical device in AC bioengineered therapeutic strategies.

Final discussion

*“The most radical revolutionary will
become a conservative the day after the
revolution.”*

*“El revolucionario más radical se
convertirá en conservador al día
siguiente de la revolución.”*

Hannah Arendt

30. Final discussions

30.1. Overarching concerns

As predicted throughout this work, OA is an attractive target for TE due to its pathological training that is both persistent and irreversible¹¹⁴⁵. A basic PUBMED search for "osteoarthritis" yields more than 100,000 papers¹⁸, including over 80,000 from the recent two decades¹⁸. To put it into context, "cancer" has about 3 million publications¹²¹⁷, while "cardiovascular disease" has over 1.5 million (in the last 20 years)¹²¹⁸. OA appears to be much less relevant; however, when compared to specific diseases such as "breast cancer" (> 300,000 results)¹²¹⁹ or "diabetes" (> 650,000 results)¹²²⁰, the attention gap is much reduced. It is also worth noting the findings for RM, 94,297, and TE, 174,822^{1221,1222}. These findings have two immediate consequences. The first is that OA appears to be significantly relevant for RM and TE. The second is dependent on the high intricacy of innovation.

This work has focused on biomechanics to impose innovation in the experimental process. This fact is pretty exposed in the different chapters; the first two were oriented toward scaffold structure and biomechanics, while the third chapter focused on tissue biomechanics. Mechanics are complex due to their highly required abstraction capacity and mathematical background. Nevertheless, biomechanics is even more difficult because we do not know precisely physical cell interactions yet¹²²³. Moreover, to make matters worse, we do not have sufficiently developed technology to measure mechanical responses at the cellular level. A powerful image that exposes this gap in humankind's knowledge is cell mechanical sensitivity. In fact, cells sense pressures lesser than 1 mN¹²²⁴, where simultaneously, they can resist loads of more than 1 kN¹²²⁵. No sensor made by humankind can be so sensitive and robust simultaneously.

Through the introduction, it was described how biomechanics regulates chondrogenesis. It is well known that MSCs produce TGF- β 1 in response to the

interaction of shear and dynamic^{1226,1227}. Additionally, previous research probed that MSCs secrete stromal-derived factor-1 (SDF-1) in response to low levels of shear stress, resulting in enhanced MSC migration *in vitro*¹²²⁶. Also, the mechanical strain has boosted MSC angiogenic capacity by inducing VEGF production¹²²⁶. Mechanical loading increased the secretion of factors such as MMP-2 and essential fibroblast growth factor (bFGF) but did not influence VEGF production during the subsequent loading¹²²⁸. It is possible to infer that a large body of data illustrates how mechanical stimuli impact MSC gene expression and modify chondrogenesis; nevertheless, all prior studies have been based on results acquired.

Science should not depend on the results acquired but on what can be done with those results. It is mandatory to understand that "data" and "information" are not the same¹²²³. We could let the message of this work in something so simple as "biomechanical stimuli induce chondrogenesis". However, this oversimplification will not provide information on the next steps because there will be questions without answers. What is the limit in biomechanics to induce chondrogenesis, and where does osteogenesis begin? Why do some loads kill cells and others induce tissue regeneration? Why can tissue development be acquired without mechanical stimuli? Is biomechanics an additional sophisticated tool to conventional RM methodologies? Or, in contrast, is it a mandatory step? Nevertheless, tissues do not have external pharmacological molecules in standard physiological conditions.

30.2. The role of microstructure

Mass transfer restrictions significantly impede the therapeutic use of RM implants¹²²⁹⁻¹²³¹. In general, cells must be within 100-200 μm of a blood vasculature to acquire adequate oxygen and nutrients and maintain optimal activity¹²³². As previously mentioned, Darcy's law explains how porosity affects diffusion; and nutrient transport²⁷¹. For reviewing concepts, porosity is the void space ratio over material-filled one¹²³³. Therefore, previous literature analyzes

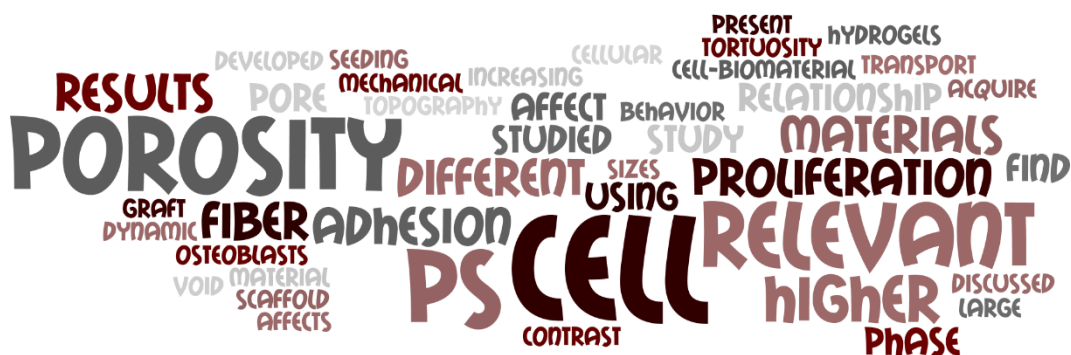


Figure 79. Word cloud of the role of microstructure.

how porosity could affect cell behavior, e.g., cell migration and orientation^{1234,1235} (Figure 79). These investigations show how lower porosities cause higher cell aggregations, whereas they exhibited reduced proliferation¹²³⁶. However, increasing the PS is not easy; large pores may risk the mechanical stability of the polymer network due to the excessive void^{1237,1238}. This problem has appeared in our results, where the mechanical strength of FD over 2 mm resulted in less stable grafts.

Concerning studies that regarded different PSs, it is common to find that each study focused on single materials. For instance, angiogenesis analyses were done using other hydrogels (e.g., HA-methacrylate, PEG, or GelMA), and results exposed that PS differed a lot between materials with a global range between 10 to 250 μm ^{1239–1241}. In contrast, chondrogenesis—the topic of study—has demonstrated a completely different degree of PS (250-500 μm)¹²⁴². Furthermore, as discussed before, the PS obtained in our experimentation fulfilled the conditioning of approximately 380 μm .

Further, osteogenesis is a highly related process in CTE, and understanding which kind of microstructure induces it is relevant to tailor graft properties. PSCs developed into osteoblasts in bone morphogenetic protein-2

(BMP-2)-containing hydrogels with pore sizes ranging from 100 to 600 μm ¹²⁴³. In contrast, HBMSCs developed into osteoblasts using 92% porosity silk fibroin scaffolds with pore sizes around 900 μm ¹²⁴⁴. Interestingly, chondrogenesis was seen in PGA scaffolds with a 97% porosity and fiber thickness of $\sim 15 \mu\text{m}$ ¹²⁴⁵.

In light of the external investigations studied, it seems relevant to establish the lack of consensus among them on what would be most appropriate for tissue growth¹²³⁹⁻¹²⁴⁵. It appears that more than the size of the pore, what is relevant is the manufacture of the scaffold. However, all of them conclude that there is a direct relationship between porosity and cellular response. What is not so obvious is to establish what this relationship is. We analyzed two different materials using the same manufacturing method to find such a relation. It was surprising to discover how we did not find a direct relationship between PS and cell adhesion, nor did we notice differences in proliferation. Nevertheless, we found that angles produced by the cross-section of fibers were more relevant than PS.

On the other hand, comparing the results from Chapter II with Chapter I, it can be extracted, at least in large PS, that cell attachment is more relevant depending on the scaffold topography than the fiber distance. Previously, it was studied how cell adhesion, contact guidance, migration, and general gene regulation were affected by topography¹²⁴⁶⁻¹²⁵⁰. Further, fiber diameter will profoundly affect the porosity and PS, which result in influence cell morphology and proliferation¹²⁵¹⁻¹²⁵³.

How substrate affects cell adhesion has been studied so far; from the physical point of view is a multivariable problem where different aspects, like hydrophobicity, participate¹²⁵⁴. Again, proposing that a higher hydrophilic material will perform better cell-biomaterial interactions is common sense. However, that is not necessarily the truth; a significantly stiff material, although hydrophilic, could not present an adequate cell expansion medium. In our work, we have demonstrated how seeding protocols are relevant at the end; cells

FINAL DISCUSSION

behave as a liquid in this step of graft synthesis. Another relevant criterion that most articles do not take into account is tortuosity¹²⁵⁵. This phenomenon will affect nutrient transport dramatically under dynamic seeding. Therefore, porosity studies regarding conditions, tortuosity, and dynamic feeding could highlight deeper relations between porous and cell behavior.

In this study, fiber distributions with higher tortuosities present a higher number of zones that allows liquid retention (thru surface tensions) and, consequently, higher cellular concentrations. At the same time, only adapting stiffness and microstructures was not enough to acquire optimum cell-biomaterial interactions. That was the decisive reason for proposing the two functionalization methods adopted in Chapter II. The efficiency of this methodology in increasing hydrophilicity on polymer materials has been discussed before¹²⁵⁶. Again, our results showed a dramatic difference in cell adhesion and proliferation applying these procedures.

30.3. Tissues as dynamic systems

Heraclitus said: "No man ever steps in the same river twice, for it is not the same river, and he is not the same man¹²⁵⁷." Cells and growing organisms are also susceptible to changes. Cytoplasmic fluxes, mainly, are involved in asymmetric cell division and occur during amoeba migration^{1258,1259}. Previously it has been demonstrated how rotational cytoplasmic streaming is mediated by



Figure 80. Word cloud of tissues as dynamic systems.

myosin-coated organelles interacting with an organized actin cortex on the inner wall of plant cells¹²⁶⁰. Furthermore, the hydrodynamic description of active gels demonstrates that the cytoskeleton is susceptible to spontaneous flows^{1261,1262} (**Figure 80**).

Regarding the previous assumption, scientists could conclude that no external stimuli are required because cells are in constant motion. Nevertheless, using traditional 2D cultures already implies a biomechanical interaction based on cell-material responses. Culture flasks are commonly made of polystyrene because they are cheap and highly resistant. In addition, polystyrene's Young modulus varies between 3000-3600 MPa¹²⁶³, whereas human cells offer one below 2 kPa¹²⁶⁴. This vast difference in magnitude order negatively affects the cells. As explained several times in this work, it is naïve to reduce cellular behavior to just one parameter. Thus, the real question should be why scientists still use polystyrene for cell culturing instead of asking for the necessity of external physical stimuli.

Biomechanics is all around us; it describes us from conception to our last breath. It is present when a newborn's first cry reacts to air entering their new lungs¹²⁶⁵. It is also present when a patient requires treatment for a lesion¹²⁶⁶. Biomechanics is also heavily implicated in cancer development^{1267,1268}. The first time a body manifests itself in a system, it is exposed to the stimuli that characterize that system¹²⁶⁹. It is absurd to question whether external mechanical stimulation is reasonable or necessary. However, we must first comprehend how they affect us, how we may engage with them, and how we can adapt to them.

This work has exposed the diverse ways of mechanical stimuli for both chondrocytes and MSCs to induce AC maturation. Even some of these reports have presented a high concordance with the obtained results in Chapter III. For instance, Miyanishi et al. discussed how HP promoted chondrogenesis in both conditions, using TFG- β 3 and without it¹²⁷⁰. Another relevant example is the

FINAL DISCUSSION

results obtained by Schätti et al., where applying compression and also shear stresses induce chondrogenesis, again without TFG- β ³¹²⁷¹. Nevertheless, both used other chondrogenic medium factors like FGF, ascorbic acid, or ITS¹²⁷²⁻¹²⁷⁴.

Additionally, Schätti et al. did a precondition of MSCs to induce chondrogenesis. Nonetheless, they did not obtain a substantial increase in using mechanical stimuli to employ a chondrogenic media. Shear stresses created by our BR have rapidly increased ECM production and AC indicators without any chondrogenic medium factor. The chondrogenic response of our graft was already demonstrated in Chapter II. Therefore, BR's chondrogenic capacity results from a process that began with the microstructure customization of CTE grafts and ended with the BR.

TERM's ultimate goal is to discover the chemicals and structures that mediate this cascade of multiscale activities in somatic organs during mechanotransduction. In Chapter III, a physical property-based monitoring approach was created and compared with traditional biochemical markers, such as immunofluorescence. The findings could be construed as a novel incorporation of a conventional imaging technique (echographies) in an ex vivo system. Looking deeper, however, the potential for discovering new physiological markers is more extensive due to this mechanical research.

30.4. Future perspectives

To face the new challenges ahead of us after this project, we must first analyze the repercussions of our research on the different fronts to be addressed. We can divide these fronts into technical, biological, ethical, and clinical applications.

30.4.1. Technical implications

Although, as with the first approach, technology may appear to be the most restricting element. The fundamental restriction in TERM research is cell

expansion, which was also the most significant in our findings. Obtaining the required cell concentrations for these tests was difficult and time-consuming. The research community has tried to solve this problematic applying down-scaling processes during the last decade. This change in the way of studying is reflected in the published articles. Again, using PUBMED, the results using "biomems"¹²⁷⁵ are more than the double applying "bioreactor AND tissue engineering"¹²⁷⁶. In the case of the present work, downscaling will reduce procedure times for analyses and open the applicability of other biomedical imaging techniques, such as luminescence and fluorescence.

Concerning electronics, our prototype, based on Raspberry Pi and Arduino Uno, does not fulfill the current regulations (in Spain, based on Royal Decree 908/1978)¹²⁷⁷. Medical electrical (ME) equipment and systems must be designed and constructed under the general requirements of DIN EN 60601-1¹²⁷⁸. One of the main requirements imposed in the previous order is the protective earth (PE) connection. Therefore, our prototype does not comply with present regulations, although high-class insulations were not required because they would not be directly connected to the patient. Consequently, the electronic manufacture must be modified under these concerns, and circuits should be exchanged by a Printed Circuit Board (PCB)¹²⁷⁹.

Finally, tools such as Deep Learning (DL) will help the level of information our system can manage¹²⁸⁰. However, establishing the training architecture for DL in the healthcare sector is difficult because of the requirement for a vast quantity of data. Our model required a powerful computer and more than a month of sophisticated computations. Feedforward neural networks (FNNs)¹²⁸¹ combined with customized multilayer perceptrons (MLPs) might significantly reduce time consumption¹²⁸². Furthermore, there is much study on this network in the Python programming language¹²⁸³. The benefits of these networks in helping microcontrollers have already been demonstrated,

FINAL DISCUSSION

even without suitable sensors¹²⁸⁴, manifesting the valuable information these networks create by themselves.

30.4.2. Biological implications

From a biological point of view, the most relevant goal has been to induce early chondrogenesis without additional growth factors. Nevertheless, markers like collagen type X production and the Sox9 expression along long periods should be considered to analyze if this chondrogenesis is maintained over time. Even analyses of calcium deposition for late chondrogenesis must be done under mechanical stimuli to understand better the stress limit at MSCs can be stimulated to avoid osteogenesis. On the other hand, regarding histological and *in vivo* assays. The obtention of histological samples from polymer scaffolds biofabricated by FDM is not an easy task⁵⁹⁷ since the risk of scaffold disintegration is high. To solve this issue, studies involving the mixture of scaffold polymers with embedded hydrogels are applied^{1285,1286}; thus, subsequent studies should study this possibility.

Even though we have talked severally about inducing chondrogenesis because of mechanical stimuli, we have done a considerable branch of assays trying different experiments tracking the response of mechanotransducers together with their metabolic reaction would increase the overall obtained graft response. As explained in theme 10, chondrocytes present several known mechanosensors like TRPV4, Piezo1, Piezo2, and the primary cilia^{912-915,918}. Measuring the over- or underexpression of these complexes in real-time is challenging, but the calcium concentration $[Ca^{2+}]$ in the intracellular space can be measured *via* ratiometric fluorescence imaging¹²⁸⁷. These $[Ca^{2+}]$ gradients and post-quantification mechanosensors' expression, together with our methods to measure the density, would better understand which force levels manifest the limits of chondrogenesis and the starting points of osteogenesis^{1288,1289}.

30.4.3. Ethical implications

This project involves diverse bioethical constraints because human cells are the prime material for all experiments¹²⁹⁰. Although stem cells do not exert an immune response, using them in any bioprinting therapy, including cells taken from the patient, includes dangers such as tumor formation, immunological reactions, unpredictable cell behavior, and long-term health implications unknown^{1291,1292}. Reports of kidney lesions or osteogenic corpuscles around a patient's eye are two examples of these consequences involving MSCs^{1293,1294}.

TERM therapies will be particularly customized and created to target a single patient's specific ailment (and only that patient). Testing safety in a randomized clinical study on a distinct set of non-specific volunteers would be ineffective and unethical¹²⁹⁵⁻¹²⁹⁷. A patient waiting for a biofabricated graft would be their test subject or "guinea pig" for their biofabricated transplant¹²⁹⁸. Ethical problems and questions remain: since 3D biofabricated items (tissues) are now exempt from regulation. Again, regarding ethics, our methodology to induce a cartilage graft by stimulating MSCs without growth factors will presumably reduce the risk of unexpected future pathologies.

30.4.4. Clinical application

As the final objective of this work is to develop an accurate and applicable ATMP, it is crucial to be aware of the current protocols and regulations required for its implementation in the medical system. In the EU, somatic cell therapy medicinal products (SCTMP) and tissue-engineered products (TEP) are distinct¹²⁹⁹. SCTMP is supplied to humans to treat, prevent, or diagnose a disease by its cells' pharmacological, immunological, or metabolic effects. TEPs are also products made up of created or modified cells that cause regeneration, repair, or replacement in native tissue through the production of paracrine factors¹³⁰⁰. Thus, our product would be released following TEP regulations.

FINAL DISCUSSION

Concerning the Spanish context, the approval of ATMPs not made industrially is governed by Royal Decree 477/2014, issued on June 13¹³⁰¹. According to this, goods created and used following the Hospital Exemption must adhere to quality standards, be approved by the appropriate state body (in Spain, this would be the Agencia Española de Medicamentos y Productos Sanitarios, AEMPS), and fulfill national traceability and pharmacovigilance criteria. Fortunately, there are pre-established collaboration networks imposed by the Instituto de Salud Carlos III, like Advanced Therapies Network (TERAV), to simplify these procedures¹³⁰².

Finally, regarding the necessary preclinical animal experimentation, in 2018, the Dutch government hurred a new program evaluating the actual necessity of the experiments¹³⁰³. Nevertheless, if ATMPs work with already studied and approved biomaterials and naïve human cells. Understandably, previous regulations could not be adequate for these kinds of products¹³⁰³. Further, the biomechanical properties of cartilage differ drastically among species^{746,750}. Thus, should any mouse model be representative of the human joint?

30.5. Closing argument

The conclusion of a Ph.D. thesis is usually a time for introspection. A doctorate thesis aims to demonstrate the doctoral student's technical, didactic, and research abilities. However, we cannot disregard the necessity to construct a watershed moment in the field of study. One rationale for developing this work's comprehensive introduction was to demonstrate that what has been done in this work is not a "reinvention of the wheel" but rather a tiny next step. Moreover, it is only *via* earlier studies that we may produce unique and helpful information that future researchers will use. Recognizing that the final result would not have been feasible without the initial chapters' accomplishments is critical. That is why, even if future obstacles appear complex and insurmountable, our experience has shown us that with time, teamwork, and

planning, we will be able to overcome them. After all, we are attempting to replicate something that nature already accomplishes. Only by fully comprehending it will we be able to recreate it and lead it to nurture possible new remedies.

Conclusions

“Remember, always, that everything you know, and everything everyone knows, is only a model. Get your model out there where it can be viewed. Invite others to challenge your assumptions and add their own.”

“Recuerda siempre que todo lo que sabes, y todo lo que todo el mundo sabe, es sólo un modelo. Exponga su modelo donde pueda ser visto. Invita a los demás a cuestionar tus hipótesis y a añadir las suyas.”

Donella H. Meadows

31. Conclusions

1. The porosity obtained from modifying the construct's microarchitecture utilizing bio- and 3D printing processes may be predicted analytically. This characteristic enables better control of cell distribution and modeling.
2. A porosity of less than 70% is detrimental to cell expansion, being a porosity of 70%-80% ideal for providing both good initial adhesion and subsequent nutrition loading to allow proper proliferation.
3. The porosity value is not directly proportional to the proliferation of the construct, with more critical parameters such as the tortuosity of the pores or the distribution of the fibers, as well as the interconnections between threads of different layers, which help to retain the medium and promote more outstanding adhesion, being more relevant.
4. The mechanical properties of the scaffolds are determined by the material's bulk properties, the distribution of the fibers, the existence and number of perimeters, and the presence of bases.
5. Regardless of the material, microarchitecture is critical for the adherence and proliferation of IPFP-MSCs. The geometry of T1.5 and the b-TPUe material offer a better alternative for the CTE than the other variables.
6. The construct's surface topography is critical in matching the cell-material interaction. Protocols for functionalizing b-TPUe based on type I collagen and PBA that do not compromise the material's or the construct's integrity exponentially increases cell adhesion and proliferation.

7. Both functionalization protocols generate IPFP-MSC chondrogenesis to the same or greater level without requiring extra chondrogenic media.
8. A sterilizing and matching BR capable of creating shear stresses and low-intensity pulsed US has been devised and manufactured.
9. Stimulating low-intensity shear stresses produced by perfusion-flow friction increases cell proliferation of IPFP-MSCs connected to the PBA-functionalized b-TPUe construct.
10. Mechanical stimulation also increases the formation of cartilage ECM, GAG, and type 2 collagen, which promotes chondrogenesis. Furthermore, this mechanical stimulation reduces type 1 collagen formation, implying a more hyaline cartilage-like matrix.
11. Our BR and b-TPUe-based construct with T1.5 geometry and PBA functionalization considerably improve IPFP-MSC chondrogenesis without needing a conditioning medium.
12. US-created pulsed mechanical waves present a technology capable of assessing in real time the fluctuations in the biomaterial-cell construct density *via* applying a FEM model relevant to the specified BR.

32. Conclusiones

1. La porosidad obtenida al modificar la microarquitectura del constructo utilizando procesos de bioimpresión e impresión 3D puede predecirse analíticamente. Esta característica permite un mejor control de la distribución y modelado celular.
2. Una porosidad inferior al 70% es perjudicial para la expansión celular, siendo una porosidad del 70%-80% ideal para proporcionar tanto una buena adhesión inicial como una posterior carga nutritiva que permita una correcta proliferación.
3. El valor de la porosidad no es directamente proporcional a la proliferación del constructo, siendo más relevantes parámetros como la tortuosidad de los poros o la distribución de las fibras, así como las interconexiones entre hilos de diferentes capas, que ayudan a retener el medio y promueven una adhesión más destacada.
4. Las propiedades mecánicas de los andamios vienen determinadas por las propiedades del material a granel, la distribución de las fibras, la existencia y número de perímetros y la presencia de pilares.
5. Independientemente del material, la microarquitectura es crítica para la adherencia y proliferación de las IPFP-MSCs. La geometría de T1.5 y el material b-TPUe ofrecen una mejor alternativa para el CTE que el resto de variables.
6. La topografía de la superficie del constructo es crítica para la interacción célula-material. Protocolos de funcionalización del b-TPUe basados en colágeno tipo I y PBA que no comprometan la integridad del material ni del constructo aumentan exponencialmente la adhesión y proliferación celular.

7. Ambos protocolos de funcionalización generan condrogénesis IPFP-MSc al mismo o mayor nivel que con el uso de medios condrogénicos adicionales.
8. Se ha ideado y fabricado un BR esterelizable y modular capaz de crear tensiones de cizallamiento y US pulsado de baja intensidad.
9. La estimulación de tensiones de cizallamiento de baja intensidad producidas por la fricción perfusión-flujo aumenta la proliferación celular de IPFP-MSCs conectadas al constructo b-TPUe funcionalizado con PBA.
10. La estimulación mecánica también aumenta la formación de ECM de cartílago, GAG y colágeno tipo 2, lo que promueve la condrogénesis. Además, esta estimulación mecánica reduce la formación de colágeno tipo 1, lo que implica una matriz más parecida al cartílago hialino.
11. Nuestro constructo basado en BR y b-TPUe con geometría T1.5 y funcionalización PBA mejora considerablemente la condrogénesis IPFP-MSc sin necesidad de medio acondicionador.
12. Las ondas mecánicas pulsadas creadas por US presentan una tecnología capaz de evaluar en tiempo real las fluctuaciones en la densidad del constructo biomaterial-célula mediante la aplicación de un modelo FEM relevante para la BR especificada.

Annexes

*“Curiosity will conquer fear even
more than bravery will.”*

*“La curiosidad vence al miedo
más fácilmente que el valor.”*

James Stephens

33. Printing settings

The adaptability of various 3D printing and bioprinting processes for biofabrication was explored in the introductory section. However, the intricacy of the entire process could not be revealed to avoid over-extension of such apart. As a result, in this appendix, certain essential features of the 3D printing and bioprinting processes are presented to elucidate how the various factors impact the scaffold's microarchitecture.

33.1. The slicing step

The slicing algorithm is critical in additive manufacturing. It can produce goods with detailed customizable features with no more labor than routine production procedures. The slicing input is a standard STL file typically used to represent CAD models in 3D printing process planning¹³⁰⁴. 3D Systems created

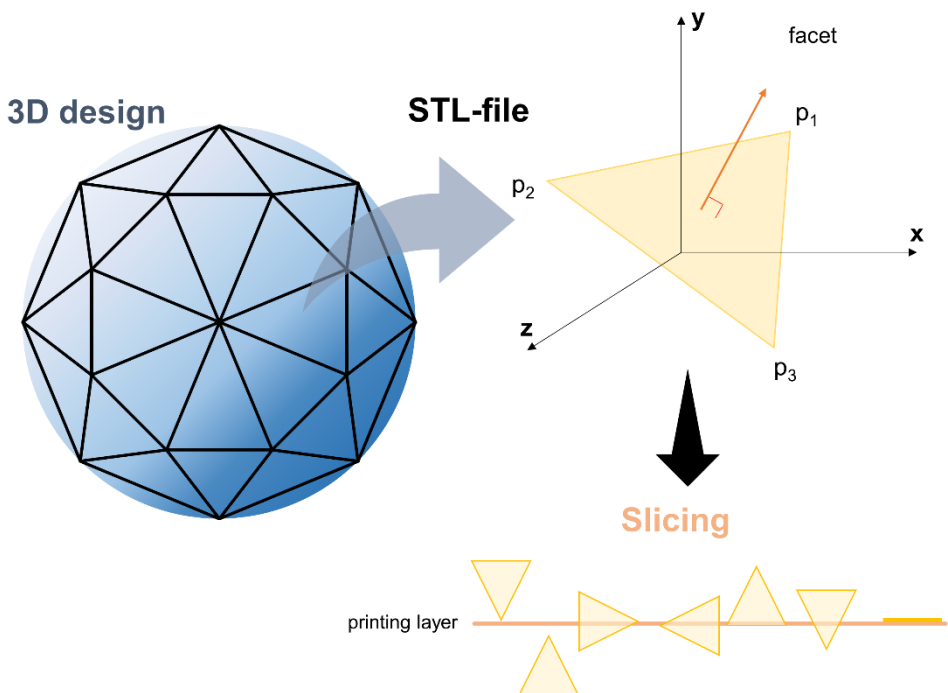


Figure 81. The slicing step is divided in two main steps: i) the STL-file formation and ii) the GCODE formation.

the STL format in 1987 to facilitate the transfer of 3D CAD models to its stereolithography equipment (SLA) machines¹³⁰⁵. Several companies and people have proposed modifying the standard throughout the years but to no result. An STL file is a collection of triangular **facet** data that defines the surface of a three-dimensional object. Each facet forms part of the object's border between its inner and outside (see **Figure 81**), and it is mathematically defined by its three vertexes and its average vector (which follows the right-hand rule). Even the finite set of triangles that conforms to the STL file must satisfy the following conditions: i) each edge is shared by at most two triangles. ii) A vertex shared by any number of triangles. iii) Connectivity: each triangle has at least one point in common with another triangle. iv) Knot-to-knot property: if a second triangle shares a vertex, it is also a vertex of the second triangle. v) No piercing, no overlapping: no triangle has an intersection with the interior of any other triangles¹³⁰⁶.

A slicer program is just software (e.g., Cura, Repetier, and Slic3r) that applies the slicing algorithm in the STL file already obtained¹³⁰⁷⁻¹³¹⁰. A slicing algorithm is a technique for transforming each triangle facet into its line segment. The contour generation method can join these line segments to form contour lines¹³¹¹. Facets in STL format are arbitrary and can be oriented in any direction (see **Figure 81**), implying different mathematical approximations^{1312,1313}. Because a line segment only requires two other points, each interaction must be handled correctly. Finally, the slicing stage produces a G-code file, a sequence of instructions that a Computer Numerical Control (CNC) machine must follow to create the final 3D construct. The G-Code documentation (<http://reprap.org/wiki/G-code>) explains the whole collection of G-codes in detail. It may appear inconvenient, but understanding the G-code language is critical for particular constructions and, more specifically, for some 3D bioprinters.

33.2. Parameters affecting the printing process

Although, as one might think, the printing (or bioprinting) process by the user ends when they send the STL file for being converted into a GCODE, that is not necessarily true. For printing accuracy and structural characteristics of printed products, parameter settings in slicing software are just as important as the printer's designing parameters and the material's attributes^{1314,1315}. Additionally, printing variables like **extrusion rate** and **nozzle speed** are essential for effective printing¹³¹⁶.

33.2.1. Layer height

Every 3D printing process is based on additively manufacturing objects one layer at a time. In slicing software, the Layer height parameter determines the height (and consequently the overall quantity) of the slices or layers. In other words, the layer height parameter is primarily adjusted in G-code by modifying the Z-axis parameter. At the most basic level, when a part is printed with a reduced layer height, it has a smoother surface and can generate finer features

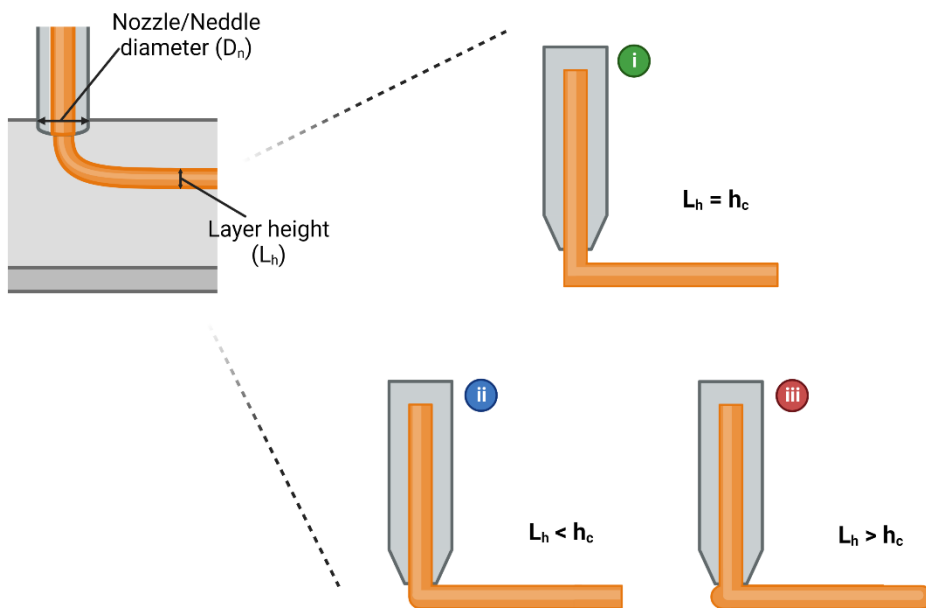


Figure 82. Diagram of layer height and its relation with the critical layer height.

with more precision, but the print time is longer. Thicker layer heights result in quicker printing. Because the nozzle/needle diameter restricts the diameter of extruded filament, layer height is generally connected to it (**Figure 82**). The following equation relates the relationship between the layer height and the nozzle/needle diameter^{1317,1318}:

$$h_c = \frac{V_d}{v_n D_n} \quad (56)$$

where h_c is the critical layer height, V_d is the extruding speed, v_n is the moving speed of the printhead, and D_n is the nozzle/needle diameter.

Concerning equation (56), three different states can happen (see **Figure 82**); if $L_h = h_c$ is the optimal situation, if $L_h < h_c$ the same's diameter decreases, and, if $L_h > h_c$ the filaments settled unevenly on the underlying layer, and the fiber diameter is expanded^{1309,1319}.

33.2.2. Nozzle speed

The nozzle speed is a setting that governs the nozzle's movement velocity while printing curves, infills, bridges, and support materials. This field determines the value of the G-code **F** instruction. Proper nozzle speed settings improve printing efficiency and print quality.

Similarly to the layer height, it is established a critical nozzle speed by:

$$v_N = \frac{4Q}{\pi D_n^2} \quad (57)$$

where v_n is the critical nozzle speed, and Q is the filament extrusion rate.

And again, equation (57) imposes three different conditions affecting the fiber morphology: i) where $v_i = v_N$, being the optimum condition, and consequently, the printed fiber diameter will correspond to D_n . ii) with $v_i < v_N$ implies that filament extrusion is quicker than printhead displacement; as a result, fiber diameter is higher than D_n and the fibers would not present cylindrical morphology. iii) $v_i >$

ANNEX I PRINTING SETTINGS

v_N , the opposite case as the previous one where fiber will present smaller diameters than the nozzle one¹³²⁰.

33.2.3. Extrusion rate

The extrusion rate is a parameter in FDM 3D printing that controls the pace at which slurries are extruded per second. This parameter setting governs the E-axis, linked to the actuator's speed exerted force over the filament or bioink¹³²¹. According to the above sections, the printer's extrusion rate positively correlates with critical layer height and nozzle speed.

Furthermore, a linear relationship was discovered between the extrusion rate and the diameter of the printed filament¹³²⁰. With high extrusion rates (over $0.004 \text{ cm}^3 \cdot \text{s}^{-1}$), the filament diameter was higher than the crucial nozzle diameter, suggesting that the slurry had spread throughout the substrate surface before it was set¹³²². On the other hand, with a low extrusion rate (below $0.002 \text{ cm}^3 \cdot \text{s}^{-1}$), the release of material would be inconsistent, implying the presence of wholes or poorly printed filaments¹³²² when the extrusion rate parameter is fixed; however, the pressure necessary for the actuator to successfully extrude materials of varying viscosity differs¹³²³. In other words, the impact of other slice characteristics, material viscosity, and printer settings should be considered while determining the extrusion rate.

33.2.4. Infill

Infill allows a component to be printed faster in direct proportion to the degree of infill. Most FDM slicer programs produce pieces with a 20% infill by default, which is sufficient for most 3D printing applications. A prototype with a high degree of the form may be created with a very low infill (10%), saving both money and time¹³²⁴. The four most popular infill forms are i) rectangular, the most common infill design for FDM printing. It has strength in all directions and prints quickly. The printer must conduct as little bridging over the infill pattern as possible. ii) triangular, employed when strength in the direction of the walls is required. Printing triangular infill takes longer. iii) Wiggle is a fantastic choice

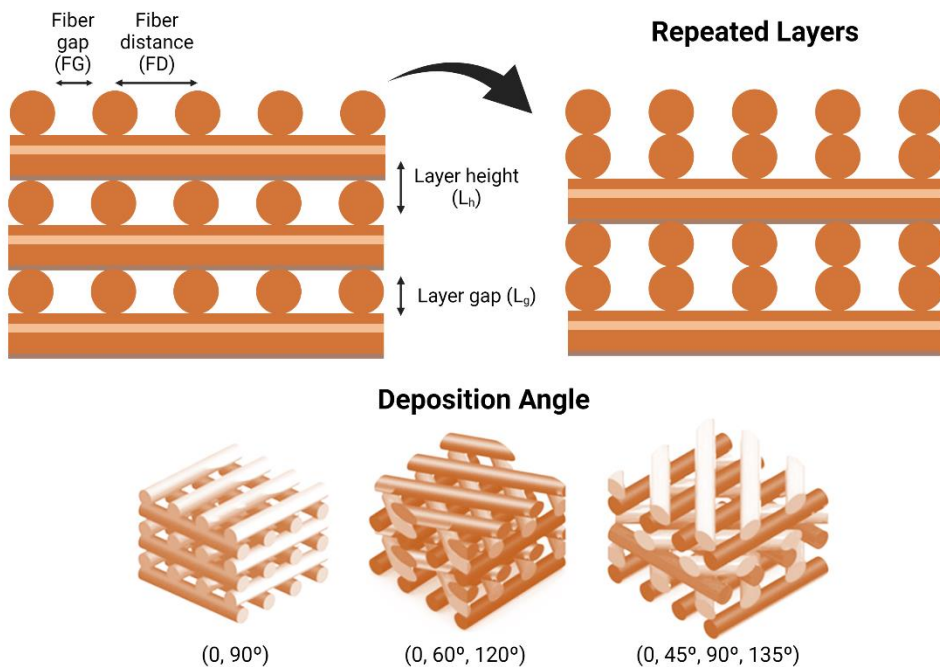


Figure 83. Scheme of different infill arrangements. Image adapted from that one published by Domingo et al.¹⁰⁴⁴

for softness, twisting, or compression designs. iv) honeycomb, a typical infill. It is compelling, offering strength in all directions¹³²⁵.

Rep

Fiber distance (FD) is crucial since it influences scaffold pore size. The shortest distance (see **Figure 83**) between the axes of two filaments within the same layer constitutes this design parameter¹³²⁶. Small lengths between filaments, however, may be troublesome if two contiguous filaments connect.

Repeated layers

Scaffolds with two repeating layers have a lower elastic modulus than those with alternating layers; longer holes along the compression axis result in a mechanically weaker structure¹⁰⁴³. The number of repeated layers used considerably impacts pore size¹³²⁷, but more studies regarding this phenomenon must be done¹³²⁸.

Deposition Angle (or lay-down patterns)

Scaffolds with a 2-angle pattern have a higher compressive modulus and maximum stress than those with a higher number of angle patterns (see **Figure 83**). A decrease in the amplitude of the deposition angle between struts of neighboring layers suggested a greater contact area, resulting in a reduction of the 3D structure's local stress¹³²⁹. As a result, the minor lay-down pattern filaments can readily move apart from one another when the scaffolds are squeezed, enhancing the deformability of the scaffold¹³³⁰.

Although deposition angle could seem a minor parameter, 3D scaffolds must endure mechanical loads in weight-bearing applications such as bone. Cell adhesion/proliferation, vascularization, and tissue ingrowth require proper pore size and interconnectivity. A scaffold not mechanically compatible with the original tissue may induce tissue resorption and aberrant growth¹³³¹.

33.3. Future outlook

Custom software has been built in certain circumstances to provide more precise control over specific features of the additive printing nozzle location and route¹⁴². Simply put, a 3D printer or bioprinter is just a robot that can insert material in a particular site. Therefore, there is much room for entirely new and creative structures to be created^{1332,1333}. Scaffolds, for example, might be created by carefully planning the arrangement of filaments¹³³⁴.

34. Piezoelectric effect

Piezoelectricity is derived from Greek, meaning "electricity through pressure" (Piezo means pressure in Greek). Hankel offered this term in 1881¹³³⁵ to describe a phenomenon noticed a year previously by the Curie brothers¹³³⁶. They discovered that positive and negative charges occurred on various regions of the crystal surfaces when they assembled the crystal in different orientations, which had previously been analyzed based on its symmetry.

34.1. Piezoelectric effect

Before applying external stress to the material, the gravity centers of each molecule's negative and positive charges coincide. As a result, the external effects of negative and positive charges are mutually cancellable. As a consequence, a molecule that is electrically neutral arises. When pressure is applied to the material, its internal reticular structure can deform, causing the separation of the molecules' positive and negative gravity centers and the generation of small dipoles (see **Figure 84**). The confronting poles within the material cancel each other out, and the distribution of a connected charge

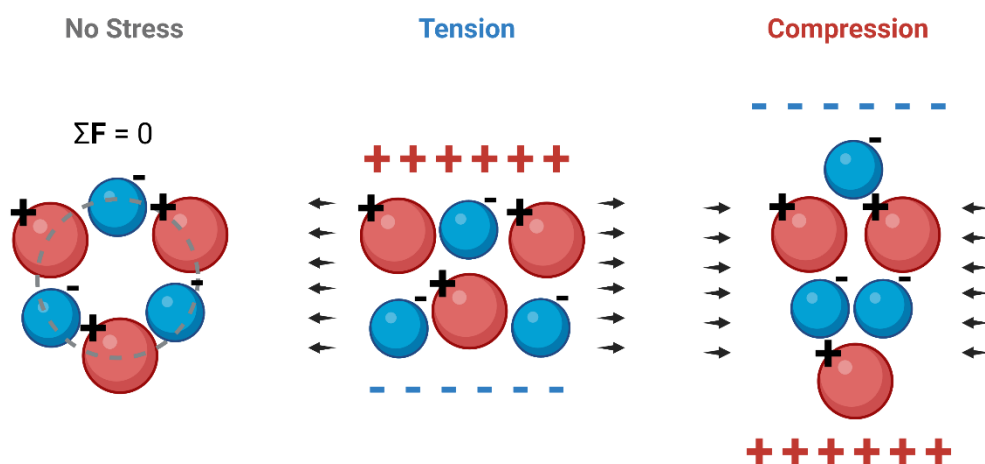


Figure 84. Scheme of piezoelectric effect.

ANNEX II PIEZOELECTRIC EFFECT

develops on the material's surfaces. This polarization produces an electric field, which may be utilized to convert mechanical energy used in material deformation into electrical energy.

In a primary method, the generated connected charge's surface density correlated with the applied pressure:

$$P_p \propto dT \quad (58)$$

where P_p is the piezoelectric polarization vector, d is the piezoelectric strain coefficient, and T is the applied stress.

But for the technological industry was more relevant the reverse process anticipated by Lippmann (1881) a year after their discovery¹³³⁷. That is, if one arbitrarily refers to the generation of an electric charge, and thus of an electric field, due to stress in specific materials and under certain laws, there would also exist a reverse piezoelectric effect in which the application of an electric field, under similar circumstances, would cause deformation in those materials.

Mathematically the reverse piezoelectric effect is formulated as follows:

$$S_p = dE \quad (59)$$

where S_p is the strain produced by the piezoelectric effect and E is the electric field magnitude.

Considering the plastic properties of the material, (59) can be formulated as:

$$P_p = dT = dcS = eS \quad (60)$$

$$T_p = kS_p = kdE = eE \quad (61)$$

where k is the material elasticity constant ($T = kS$).

34.1.1. Electric Displacement

The reverse piezoelectric effect is the ability of speakers to convert electrical information into sound. And in the case of the USs, US transducers also are based on this effect. According to the theoretical foundations, when an external electric field \mathbf{E} is applied between two electrodes where a material of dielectric constant ϵ exists, an electric displacement towards those electrodes is formed, the size of which is unknown⁵⁵⁶:

$$\mathbf{D} = \epsilon \mathbf{E} \quad (62)$$

And in the case of piezoelectric materials, the electric fields also imply induced strains, which will also induce an increase in the material's polarization. Consequently, the total electrical displacement of a piezoelectric material under an external electric field is:

$$\mathbf{D} = \epsilon \mathbf{E} + \mathbf{P}_p = \epsilon \mathbf{E} + ed\mathbf{E} = \bar{\epsilon} \mathbf{E} \quad (63)$$

where $\bar{\epsilon}$ is the effective dielectric constant.

34.2. Ultrasonic transducers

Ultrasonic transducers can be defined as devices that produce mechanical waves (US) from electrical pulses, i.e., they transform electrical energy into mechanical energy and *vice-versa*^{1338,1339}. They can be split into five components (**Figure 85**): i) A crystal/ceramic element (piezoelectric material). ii) positive and negative electrodes. iii) a damping block adhered to the piezo's back. iv) a matching layer, the interface between the piezo and the material to analyze. v) an electrical insulation layer.

Most transducers are **narrow-band** (a few percent bandwidths) and **broad-band** (30-70% bandwidth). Broad-band transducers are commonly employed in detection, measurement, and control applications ranging from

ANNEX II PIEZOELECTRIC EFFECT

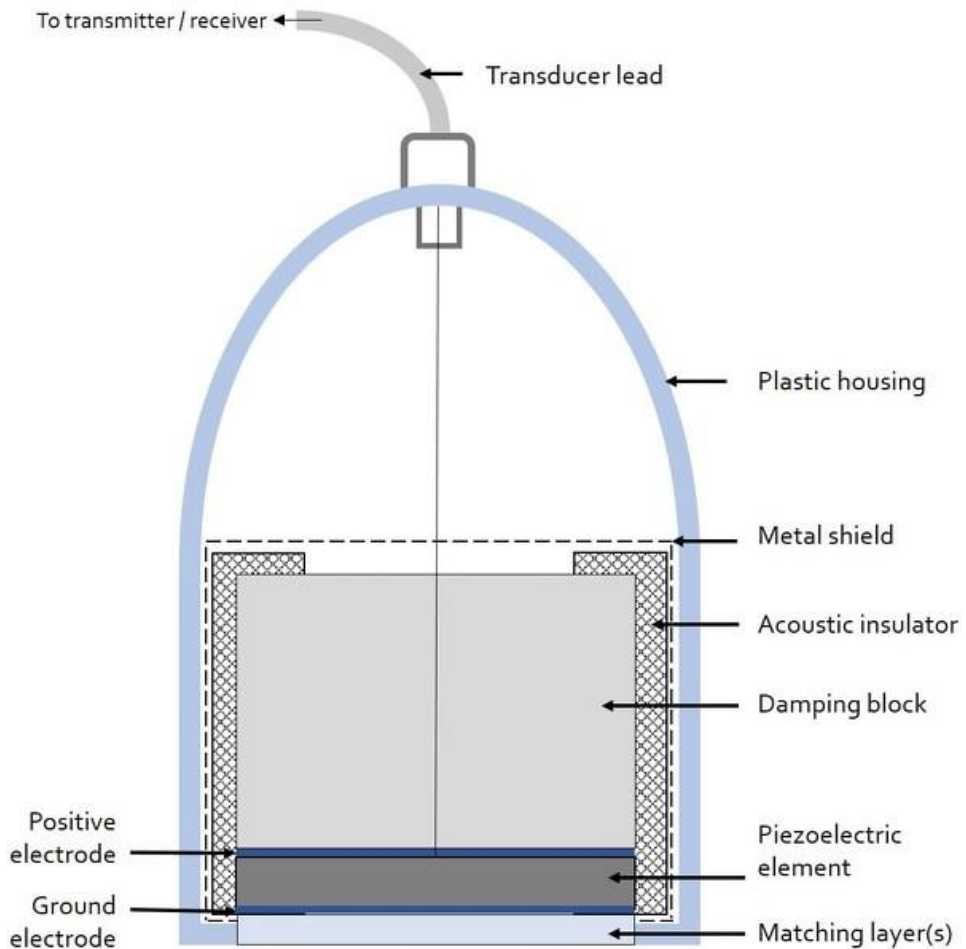


Figure 85. Cross section of an ultrasound transducer and its components. Image courtesy of Dr Rachael Nightingale, Radiopaedia.org, rID: 54040

non-destructive testing or imaging, using extremely brief ultrasonic pulses (typically three or four cycles), frequencies in the range of 0.5-50 MHz. Narrow-band transducers are used for low-frequency applications (20-100 kHz) at very high intensities¹³⁴⁰.

The basic structure of transducers constructed for optimal impulse response consists of a piezoelectric ceramic plate vibrating in its thickness mode, bonded to a backing block and a wear plate¹³⁴¹. The piezoceramic element's acoustic impedance is similar to that of the backing block, which is comprised of

a high-loss material. The core frequency of their bandwidth, which roughly matches those of the resonance, is used to identify transducers. Energy transmission is selective, which impacts the transducer's spectrum properties. Applications of these technologies involve flaw detection and imaging, including non-destructive testing and medical diagnostics. Compared to other medical imaging modalities, ultrasonography offers significant benefits. It gives real-time pictures, is portable, and can thus be transported to the patient's bedside. It is far less expensive than other imaging technologies and does not employ dangerous ionizing radiation¹³⁴².

Two modalities for US imaging are applied: **through transmission** and **pulse-echo**.

- A **transmitter** and **receiver** are situated on opposing sides of an ultrasonic test item to achieve adequate acoustic coupling in the through-transmission approach¹³⁴³. Any defect or impedance change in the path of the US beam causes a dip in or a total lack of the received signal. This approach is not suited for identifying the placement of targets in the material.
- A brief pulse of ultrasonic waves is transmitted to an object *via* the pulse-echo method, and echoes return from flaws, discontinuities, or borders¹³⁴⁴. There is a so-called dead zone in this latter approach because the input voltage of the transmitted pulse saturates the transducer in the receiver mode.

Further, ultrasonic transducers can measure materials and systems' qualities, characteristics, or particular parameters. Lynnworth (1975) has thoroughly evaluated the industrial applications in which the propagation of low-intensity US is affected by the medium's factors, condition, or quality¹³⁴⁵. Several methods for measuring ultrasonic velocity and attenuation have been developed for years¹³⁴⁶.

35. Supplementary Material C1

35.1. Workflow of Chapter I

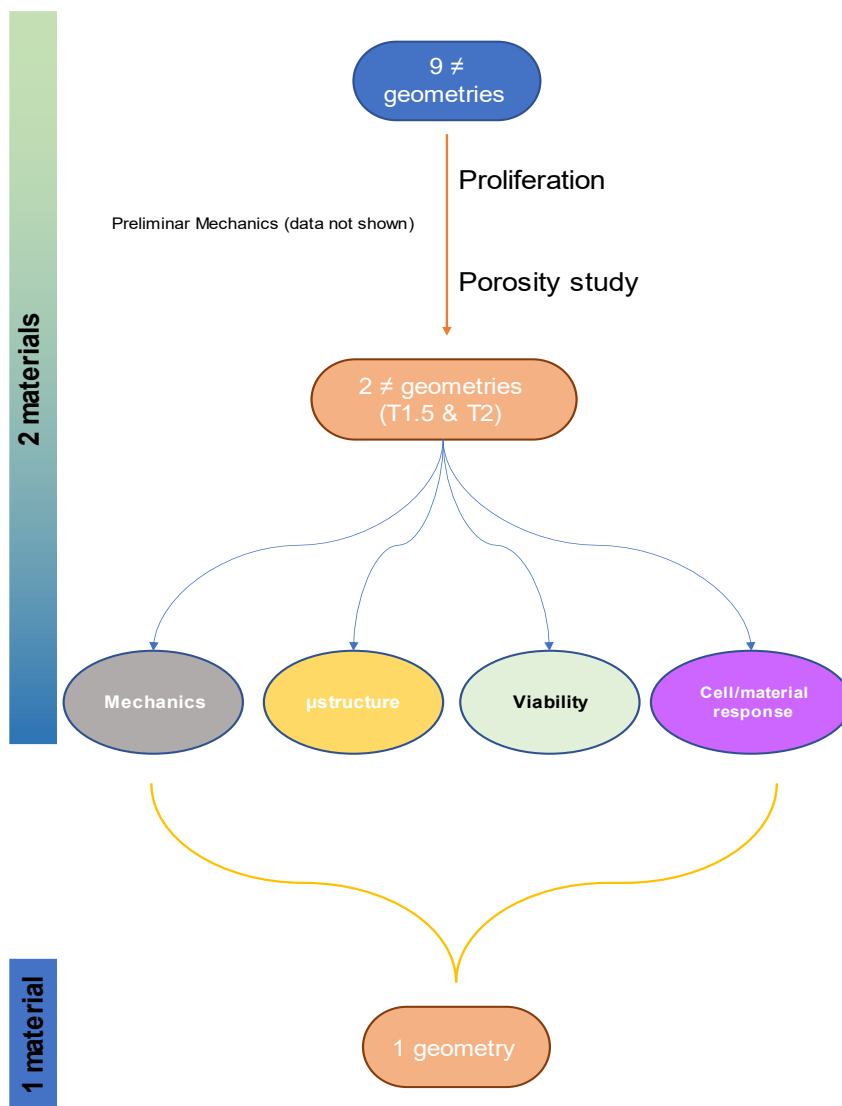


Figure 86. Nine different geometries were proposed for the proliferation assay, each one was carefully studied. After, some of those geometries were discarded to simplify deeper analyses, reducing sample number. Finally, selected geometries were exposed to mechanical assays, microarchitecture analyses, viability tests and cell-material interactions inquiries.

35.2. Volume ratio and surface/volume

The volume occupied by the filaments within the scaffold, the volume ratio, was calculated as described in this section.

For simplicity, the filaments were considered perfect cylinders in shape aligned in parallel within a limiting circumference (see **Figure 87A**). As a result, the length of each filament depends on its position inside the circumference. Given **Figure 87A**, this relation applies:

$$l_f = -2r + D_s = D_s \left(1 - \frac{r}{R_s}\right) \quad (64)$$

Here, l_f is the length of the filament, D_s is the diameter of the scaffold and R_s is the scaffold radius. Thus, at $r = 0$, the length of the filament corresponds to the diameter of the scaffold whereas, at $r = R_s$ it can be estimated that there is no filament.

Equation (64) only works well for triangles and squares. The approximation is different in the case hexagons (see **Figure 87B**). Again, filaments were considered as cylindrical rods but at this time, but they were not straight lines. The number of hexagons in each filament was calculated decomposing them into triangles and equation (65) was used again to approximate the length of the filament. The number of hexagons included in such a filament was calculated dividing the length by the apothem as follows:

$$\text{number of hexagons } (n_{hex}) = \frac{l_f}{2 \cdot \alpha_{hex}} \quad (65)$$

Here, α_{hex} is the apothem of the hexagon and it depends on the pore size. In addition, the bioprinter software vary twice the apothem (e.g. hexagonal porosity of 1 mm, means α_{hex} is 0.5 mm). Because to close a hexagon it is needed

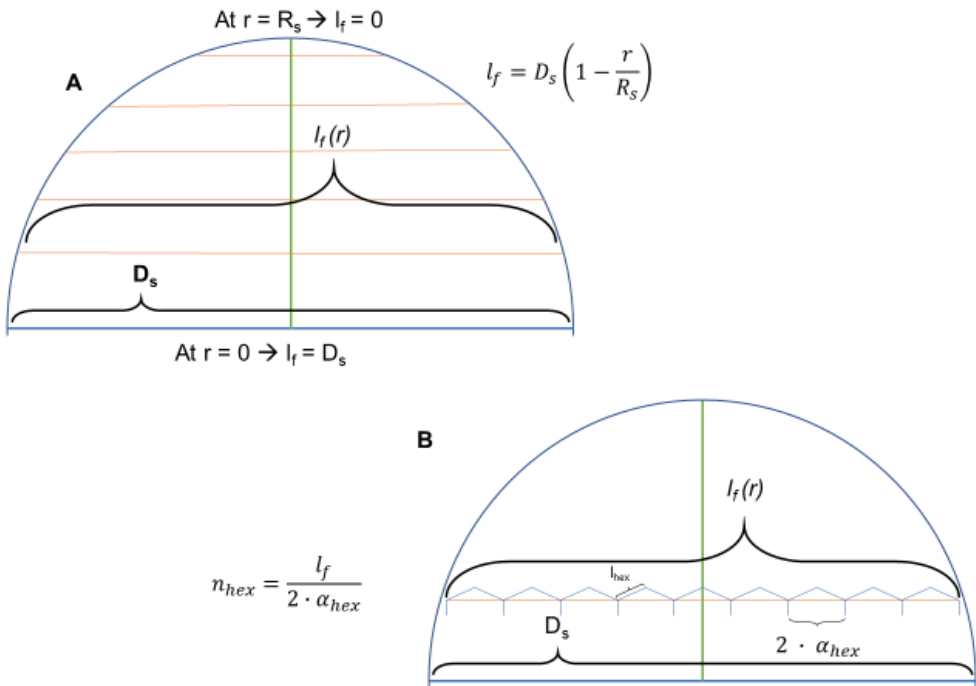


Figure 87. A) Scheme of fiber distribution and dependency of fiber length as a function of scaffold radius (R_s). B) In the hexagonal geometry, the real length of the filaments was slightly larger than square and triangular conformations. It was extracted calculating the number of hexagons approximating a straight filament divided by the apothem (α_{hex}). l_f : length of the filament. D_s : scaffold diameter.

two filaments, the assumption of calculating half of the total result was applied. In addition, instead of using the length of the filament (l_f) it was applied the length of the hexagon sides (l_{hex}), and, knowing that each hexagon has 3 sides printed: $h_s = n_{hex} \cdot 3$ (again, it is considered half of the total). Knowing how the software distributes the filaments, it was analyzed how many filaments were printed in each layer; they are represented in Supplementary Table 2.

With this, the volume occupied by the scaffold is given by:

$$V_{sca} = \pi R_s^2 \cdot H_s \quad (66)$$

And the volume occupied by a single filament:

$$V_{fil} = N_f \cdot \pi R_f^2 \int l_f(r) dr \quad (67)$$

The total volume occupied by the filaments is:

$$V_{Tfil} = N_f \cdot \pi R_f^2 \int_0^{R_s} D_s \left(1 - \frac{r}{R_s}\right) dr \quad (68)$$

And finally, from the definition of the volume ratio $V_{ratio} = \frac{V_{Tfil}}{V_{sca}}$ one can get the porosity $porosity = \frac{V_{pore}}{V_{sca}} = 1 - V_{ratio}$.

For calculating the S/V ratio the previous V_{fil} was used together with the Surface of the filaments $S_{fil} = N_f \cdot 2\pi R_f \int l_f(r) dr$.

$$S/V = S_{fil}/V_{sca} \quad (69)$$

35.3. IPFP-MSCs characterization

Both protocols are extracted from Jimenez et al. 2018 G. Jiménez, M. Hackenberg, P. Catalina, H. Boulaiz, C. Griñán-Lisón, M.Á. García, M. Perán, E. López-Ruiz, A. Ramírez, C. Morata-Tarifa, E. Carrasco, M. Aguilera, J.A. Marchal, Mesenchymal stem cell's secretome promotes selective enrichment of cancer stem-like cells with specific cytogenetic profile., Cancer Lett. 429 (2018) 78–88. <https://doi.org/10.1016/j.canlet.2018.04.042>:

35.3.1. Flow cytometry analysis

The immunophenotype was analyzed by flow cytometry (Supplementary Figure 2A). Cells were washed and resuspended in PBS with 2% bovine serum albumin BSA (Sigma, St. Louis, MO), and 2 mM ethylenediaminetetraacetic acid (EDTA, Sigma). Cells were incubated in dark for 30 minutes at 4° C with the appropriate fluorochrome-conjugated monoclonal antibodies. Markers used were: CD73-APC, CD90-FITC, CD105-PE, CD34-PE, CD45-PerCP, and CD133-APC (Miltenyi Biotec). All cells were washed in PBS and analyzed in a FACS Canto II cytometer (BD Biosciences).

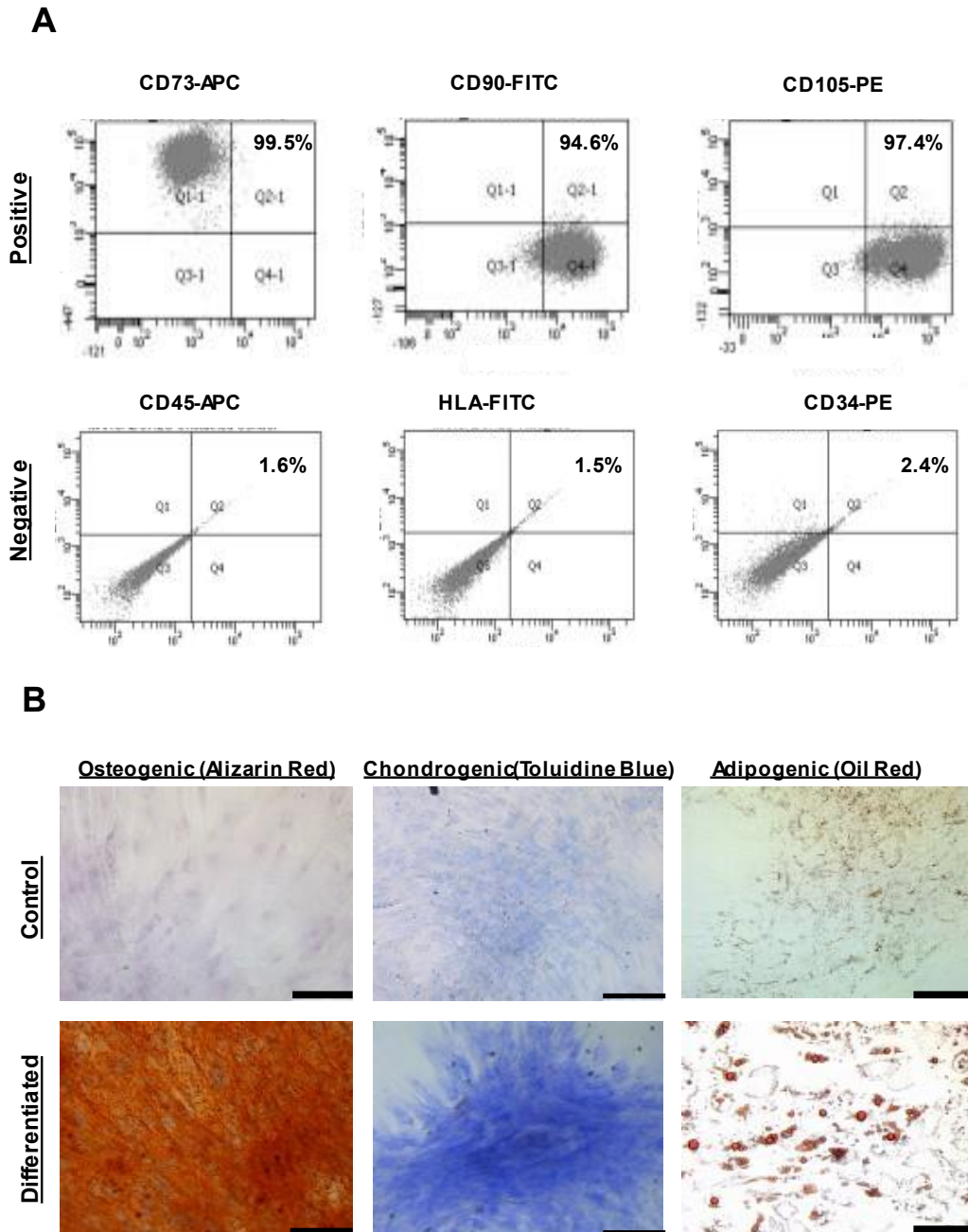


Figure 88. A) FACS markers for stemness. B) Differentiation capacity. Controls were IPFP-MSCs with DMEM, 10%FBS and 1%P/S. Differentiated mediums were: Osteogenic medium applied was StemMACS OsteoDiff 130-091-678, Miltenyi. Adipogenic medium applied was StemMACS adipoDiff 130-091-677, Miltenyi. Chondrogenic medium applied was DMEM supplemented with 10 ng/ml TGF- β 1, 0.1 μ M dexamethasone, 40 μ g/ml L-proline, 50 μ g/ml L-Ascorbate-2-Phosphate, and 50 mg/ml ITS. (Scale bar = 110 μ m).

35.3.2. **Differentiation assays**

MSCs isolated from lipoaspirates were plated at 2×10^3 cells/cm² in DMEM (Sigma) containing 10% FBS (Gibco) with penicillin and streptomycin at 100 µg/ml (Sigma) and allowed to adhere for 24 hours. The culture media was then replaced with specific inductive media. For adipogenic, osteogenic and chondrogenic differentiation, cells were cultured for two weeks in Adipogenic MSCs Differentiation Bullet Kit, Osteogenic MSCs Differentiation Bullet Kit (Lonza) and NH ChondroDiff Medium (Miltenyi Biotec), respectively. Differentiated cell cultures were stained with Oil Red O (Amresco) for adipogenic differentiation, Alizarin Red (Lonza) for osteogenic differentiation or Toluidine Blue (Sigma) for chondrogenic differentiation (**Figure 88**).

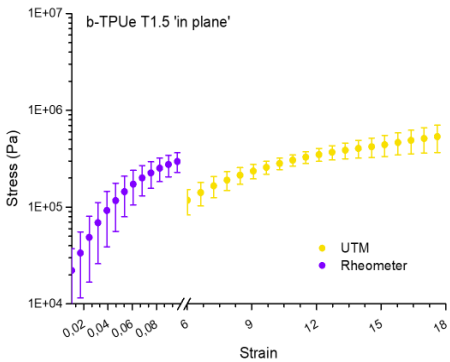
35.4. **Mechanical analysis**

In this section we show stress-strain curves as obtained with the Rheometer and the Universal Tensile Machine (UTM).

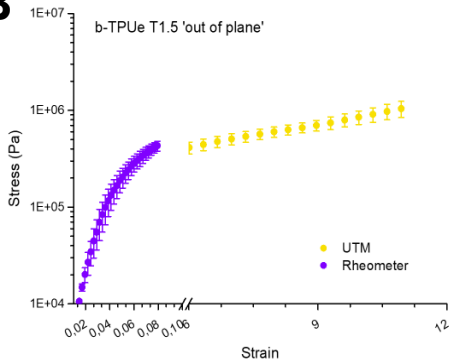
Figure 89. A-B) Stress vs. Strain curve of cube b-TPUe scaffold under compression pattern in the rheometer and UTM for Triangular geometry and PS 1.5 mm, A) 'in plane', and B) 'out of plane'. C-D) Stress vs. Strain curve of cube b-TPUe scaffold under compression pattern in the rheometer and UTM for Triangular geometry and PS 2 mm, C) 'in plane', and D) 'out of plane'. E-F) Stress vs. Strain curve of cube PCL scaffold under compression pattern in the rheometer and UTM for Triangular geometry and PS 1.5 mm, E) 'in plane', and F) 'out of plane'. G-H) Stress vs. Strain curve of cube PCL scaffold under compression pattern in the rheometer and UTM for Triangular geometry and PS 1.5 mm, G) 'in plane', and H) 'out of plane'. (n=3) ↪ *next page*

ANNEX III SUPPLEMENTARY MATERIAL C1

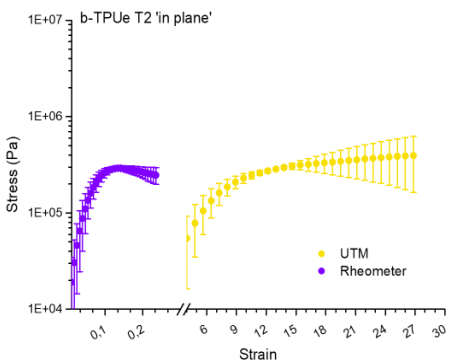
A



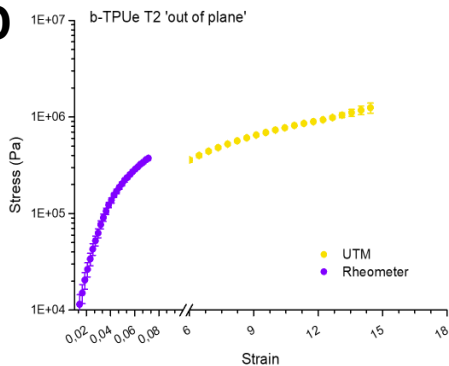
B



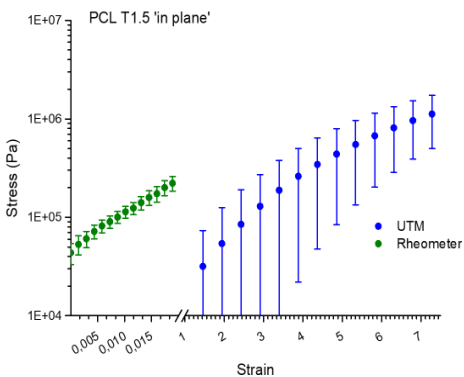
C



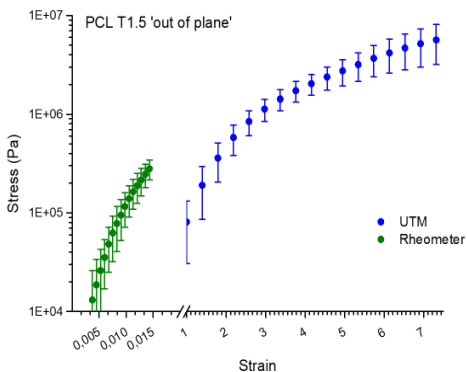
D



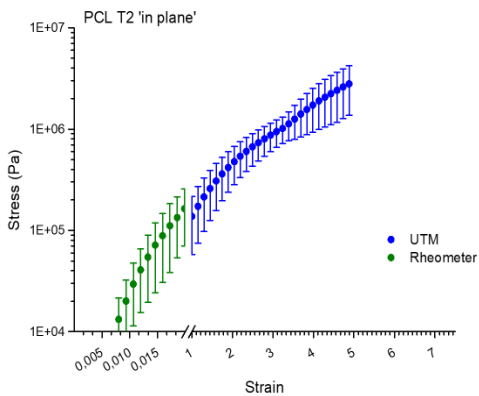
E



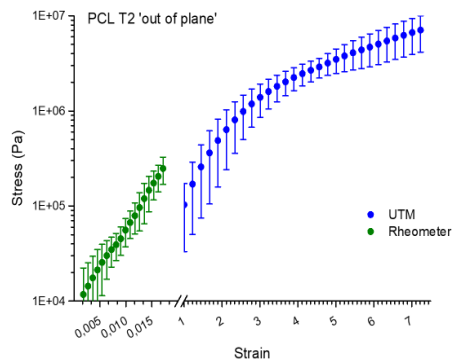
F



G



H



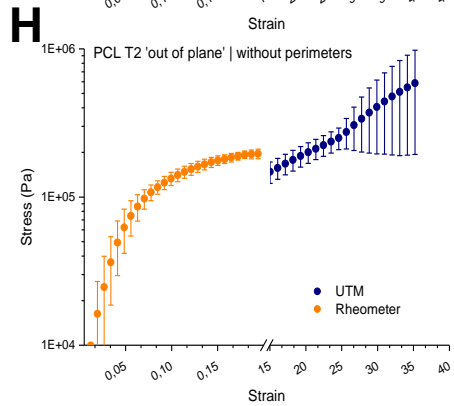
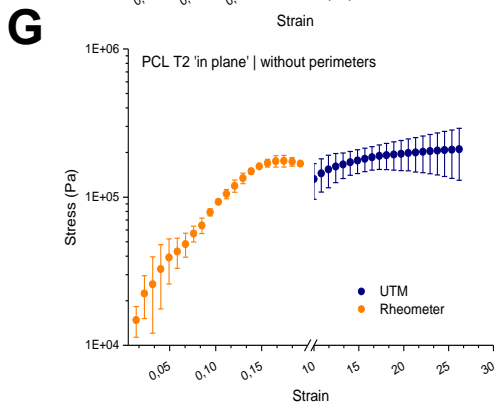
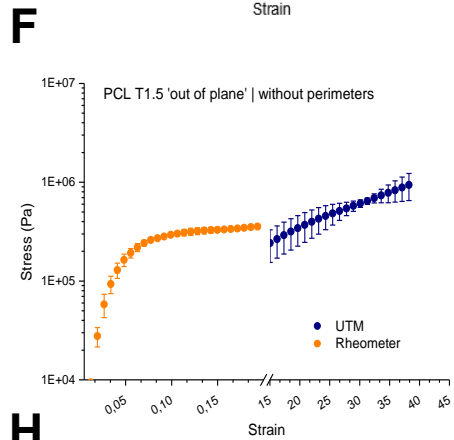
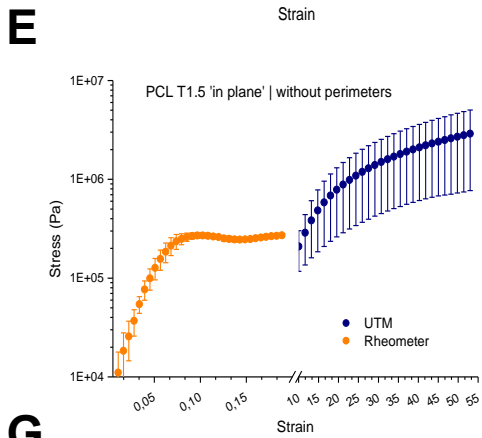
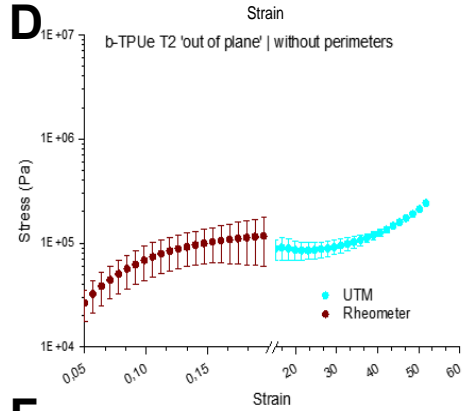
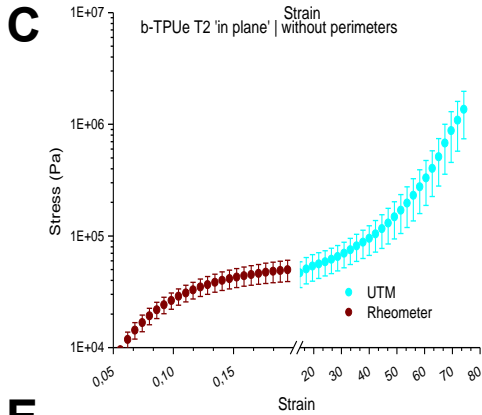
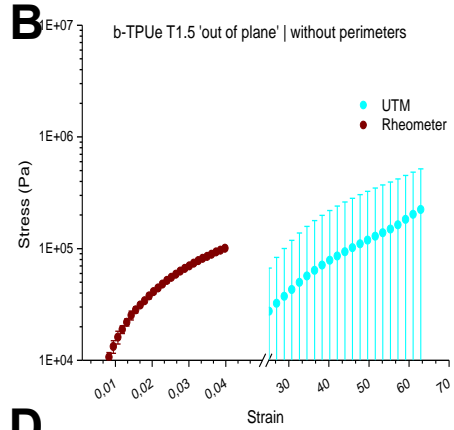
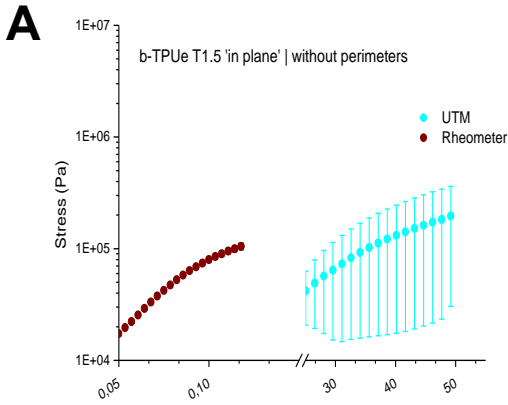


Figure 90. Same as previous figure without perimeters (n=3).

35.5. ESEM

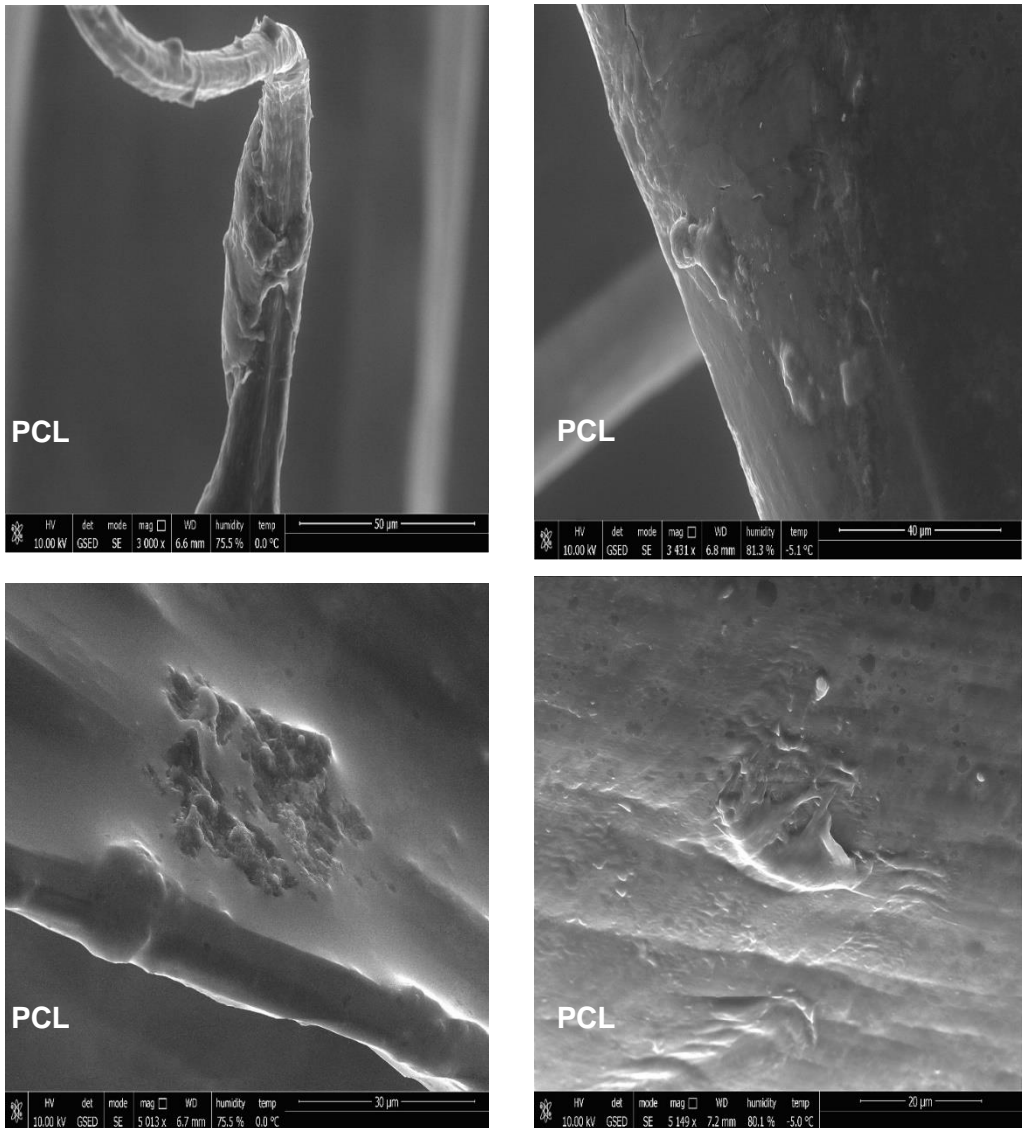


Figure 91. ESEM images of PCL, although there are cells attached to the fibers, it seems to be a coating layer above the scaffold. Possibly due to material degradation because of the assay.

35.6. Supplementary Tables

Table 5. Manufacturer parameters for b-TPUe (Recreus Inc.) and PCL (Esun Inc.).

Physical Properties	b-TPUe	PCL
Melting point	200-240 °C	60-140° C
Density	1.14 g/cm ³	1.16 g/cm ³
Elongation at break	665%	11%
Tensile strength	42 MPa	18 MPa
Tensile modulus (E₀)	350 MPa	483 MPa
Shear modulus (G₀)	10 MPa	1 GPa

Table 6. Depending on the pore geometry, the number of filaments differs. Quadrangular and triangular geometries share the way to bio-print, with the only difference on the printing angle (0°/90° in quadrangular, 0°/45°/90°/135° in triangular). In both cases, the porosity size means the distance between each filament (considering these ones parallel to each other). About the triangular shape, the porous size is a quarter of the corresponding square geometry. The porosity size in hexagonal geometry corresponds to twice the apothem. H_t = triangular height. $layer_n$ = odd layer. $layer_{2n}$ = even layer. a_{hex} = hexagon apothem.

Geometry	Porosity size	Number of filaments by layer
<i>Triangular/Quadrangular</i>	1 mm ($h_t = 500 \mu\text{m}$)	$layer_n = 5 \text{ filaments}$ $layer_{2n} = 6 \text{ filaments}$
	1.5 mm ($h_t = 750 \mu\text{m}$)	$layer_n = 4 \text{ filaments}$ $layer_{2n} = 5 \text{ filaments}$
	2 mm ($h_t = 1000 \mu\text{m}$)	$layer_n = 3 \text{ filaments}$ $layer_{2n} = 4 \text{ filaments}$
	1 mm ($a_{hex} = 500 \mu\text{m}$)	20 filaments
<i>Hexagonal</i>	1.5 mm ($a_{hex} = 750 \mu\text{m}$)	13 filaments
	2 mm ($a_{hex} = 1000 \mu\text{m}$)	10 filaments

ANNEX III SUPPLEMENTARY MATERIAL C1

Table 7. Main geometrical parameters obtained both theoretically and experimentally in order to compare the validation of the filament distribution hypothesis. Thickness of the wall corresponds to the presence of two perimeters for cylindrical scaffolds, each one makes 400 μm . Length of the wall corresponds to the side length of the geometrical patterns; they were calculated from the pore sizes. In the case of triangles, they correspond to $(\sqrt{2}\cdot\text{PS})/2$; squares to PS and hexagons to $\text{PS}/\sqrt{3}$. Size ratios express the tension that will suffer the ‘porous cells’ against the pressured absorbed by the scaffold’s walls. Experimental relative density was obtained by dividing the experimental density by the manufacturer’s density. Finally, the theoretical porosity was obtained applying the methodology early exposed.

	PCL						b-TPUe											
	T		S		H		T		S		H							
Experimental porosity ($P_e = 1 - \rho_r$)	0.73	0.78	0.81	0.73	0.75	0.8	0.44	0.58	0.66	0.77	0.78	0.81	0.71	0.76	0.79	0.47	0.59	0.66
Experimental relative density	0.27	0.22	0.19	0.27	0.25	0.2	0.56	0.42	0.34	0.23	0.22	0.19	0.29	0.24	0.21	0.53	0.41	0.34
Size ratio (t/l)	0.71	0.48	0.46	0.80	0.53	0.4	1.39	0.92	0.69	0.71	0.48	0.46	0.80	0.53	0.4	1.39	0.92	0.69
Length of the edge wall (l)	1.12	1.68	1.73	1.00	1.50	2.00	0.58	0.87	1.15	1.12	1.68	1.73	1.00	1.50	2.00	0.58	0.87	1.15
Thickness of the edge wall (t)	0.8	0.8	0.8	0.8	0.8	0.8	0.8	0.8	0.8	0.8	0.8	0.8	0.8	0.8	0.8	0.8	0.8	0.8
	1	1.5	2	1	1.5	2	1	1.5	2	1	1.5	2	1	1.5	2	1	1.5	2

S/V ratio (m ⁻¹)	Theoretical porosity
2.25	0.71
1.98	0.74
1.65	0.77
1.95	0.74
1.64	0.77
1.29	0.81
0.70	0.43
0.49	0.57
0.38	0.63
2.25	0.71
1.98	0.74
1.65	0.77
1.95	0.74
1.64	0.77
1.29	0.81
0.70	0.43
0.49	0.57
0.38	0.63

36. Supplementary Material C2

36.1. Characterization and verification of functionalization protocols on b-TPUe

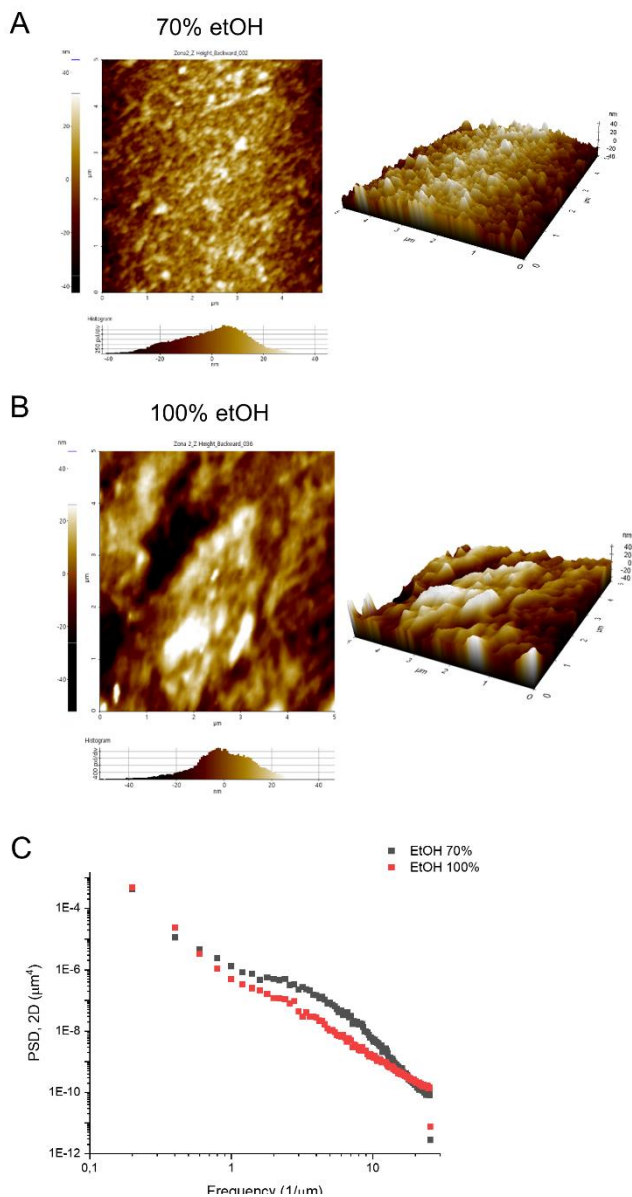


Figure 92. AFM topography analyses. (A-B) Height images captured from AFM for, A) ethanol 70% (mixed with Mili Q water), used to sterilized scaffolds, B) ethanol 70% (mixed with Mili Q water), used to sterilized scaffolds C) PSD curves from AFM ethanol buffers analyses.

36.2. MSCs characterization

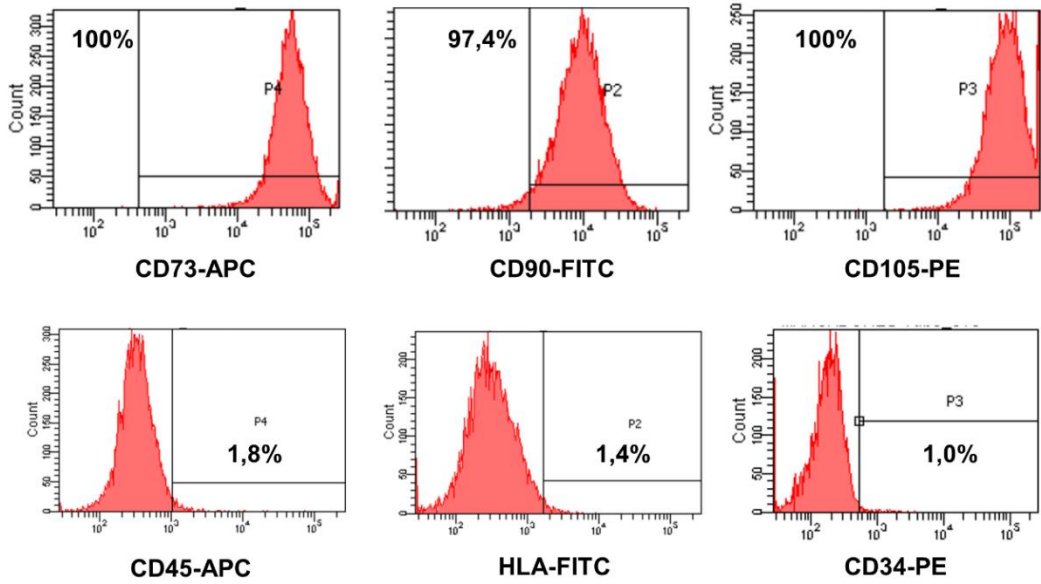
MSCs were trypsinized, washed, and resuspended in PBS with 1% bovine serum albumin (BSA; Sigma-Aldrich). Cells were centrifuged followed by the addition of fluorochrome-conjugated monoclonal antibodies for CD73, CD90, CD105, CD34, CD45, and HLA-II and CD133 (Miltenyi Biotec) according to manufacturer's instructions and incubated at 4 °C, in the dark, for 12 min. After adding BSA, cells were centrifuged and resuspended in PBS and analyzed by flow cytometry in a FACSCanto II cytometer (BD Biosciences).

MSCs isolated from lipoaspirates were plated at 2×10^3 cells/cm² in DMEM (Sigma) containing 10% FBS (Gibco) with penicillin and streptomycin at 100 µg/ml (Sigma) and allowed to adhere for 24 hours. The culture media was then replaced with specific inductive media. For adipogenic, osteogenic, and chondrogenic differentiation, cells were cultured for two weeks in Adipogenic MSCs Differentiation Bullet Kit, Osteogenic MSCs Differentiation Bullet Kit (Lonza), and NH ChondroDiff Medium (Miltenyi Biotec), respectively. Differentiated cell cultures were stained with Oil Red O (Amresco) for adipogenic differentiation, Alizarin Red (Lonza) for osteogenic differentiation, or Toluidine Blue (Sigma) for chondrogenic differentiation (**Figure 93**).

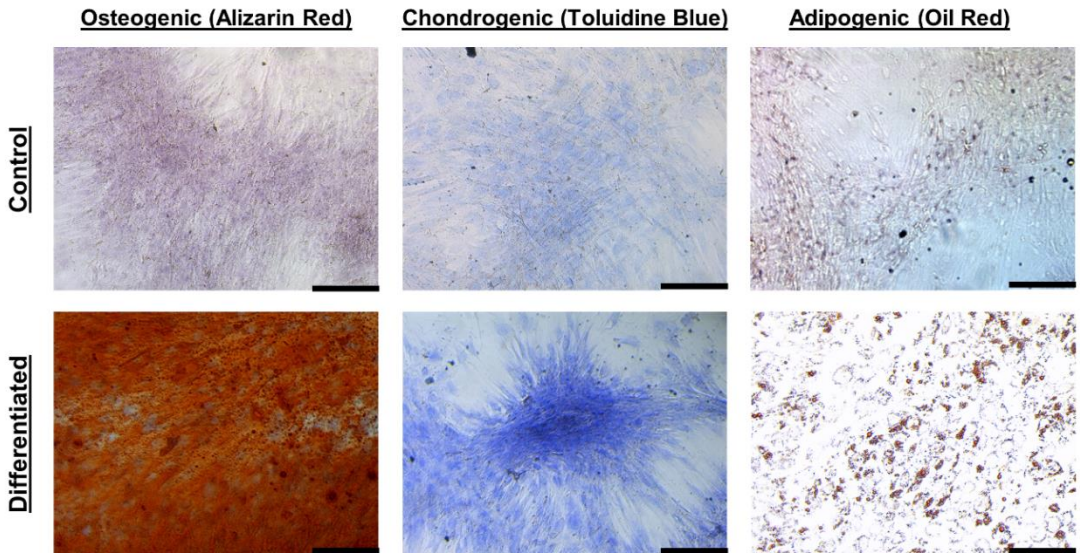
Figure 93. A) FACS markers for stemness. B) Differentiation capacity. Controls were IPFP-MSCs with DMEM, 10%FBS and 1%P/S. Differentiated mediums were: Osteogenic medium applied was StemMACS OsteoDiff 130-091-678, Miltenyi. Adipogenic medium applied was StemMACS adipoDiff 130-091-677, Miltenyi. Chondrogenic medium applied was DMEM supplemented with 10 ng/ml TGF- β 1, 0.1 µM dexamethasone, 40 µg/ml L-proline, 50 µg/ml L-Ascorbate-2-Phosphate, and 50 mg/ml ITS. (Scale bar = 110 µm). ↪ *next page*

ANNEX IV SUPPLEMENTARY MATERIAL C2

A



B



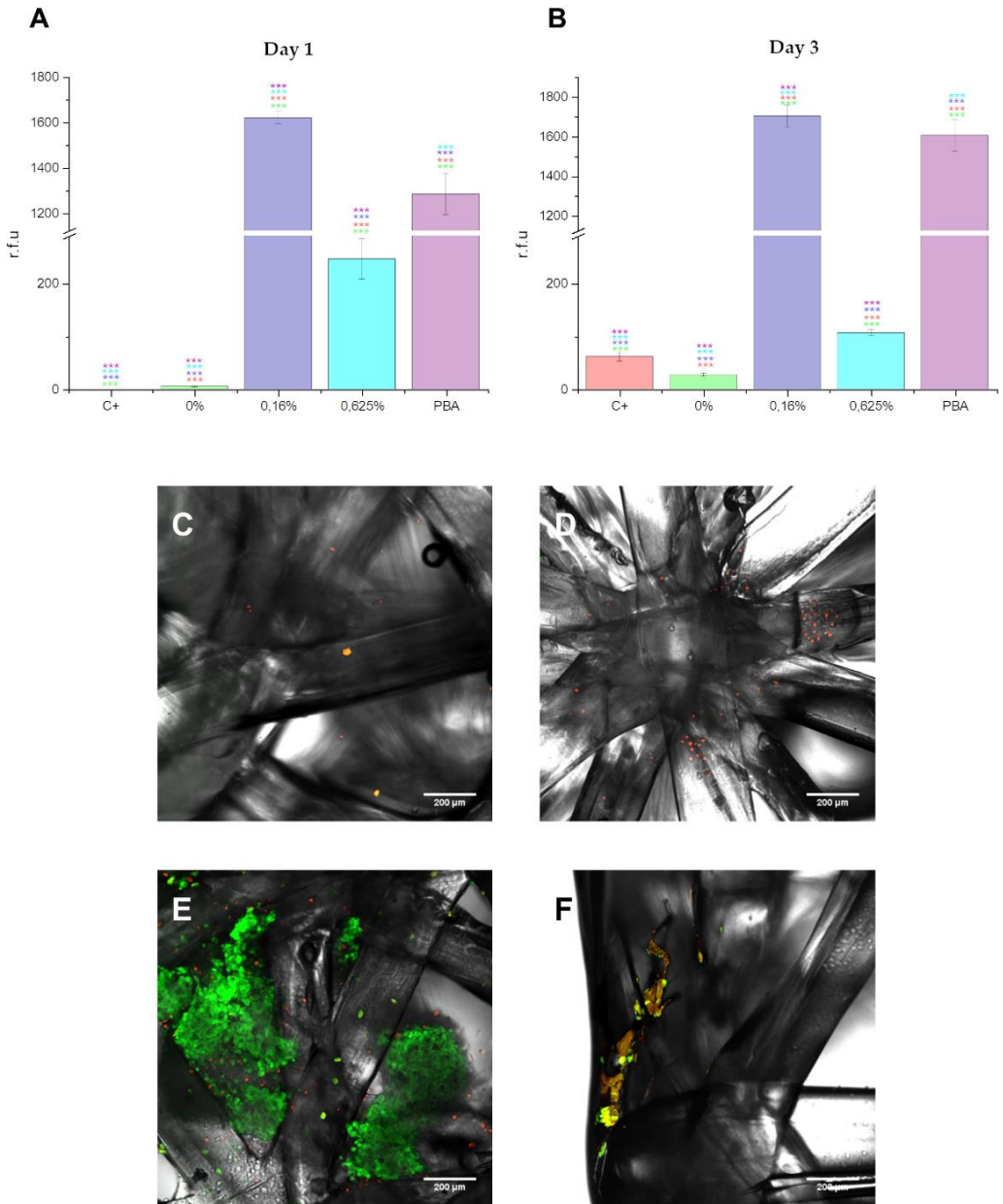
36.3. Preparation of the ninhydrin standard curve.

Aminolysis and ninhydrin treatment.

For the ninhydrin (Sigma-Aldrich) standard curve, it was carried out the preparation of solutions of 1,6-hexanediamine in isopropanol at different concentrations (100 mg/mL; 50 mg/mL; 25 mg/mL; 12.5 mg/mL; 6.25 mg/mL and a blank of 0 mg/mL) and then, in a multiwell plate, 50 μ L of each solution and 50 μ L of 2 M ninhydrin were added. Finally, the plate was incorporated into the plate reader and the absorbance was adjusted to 560 nm. The scaffolds were placed in a multiwell plate and immersed in a 10 % 2-propanol solution of 1,6-hexanediamine for 1 hour at 37 ° C. It was washed with distilled water and dried. They were immersed in a solution of ninhydrin in 1 Methanol for 1 minute.

Figure 94. A), B) Metabolic activity study carried out on days 0 and 3 using the Alamar Blue reagent. FF scaffolds have been functionalized with collagen using different concentrations of glutaraldehyde (0%; 0.16% and 0.625%) and glycine (0M, 0.5M, 0.2M, respectively). The positive control has only been seeded without previous functionalization. (***) $p < 0.001$. Images obtained with the confocal microscope Nikon Eclipse Ti after the treatment of FF scaffolds with the LIVE/DEAD® cytotoxicity/viability kit. C) Positive control. D) 0% glutaraldehyde and 0M glycine E) 0.16% glutaraldehyde and 0.5M glycine. F) 0.625% glutaraldehyde and 0.2M glycine.
↪ next page

36.4. Metabolic activity & Viability of Collagen with and without Glutaraldehyde



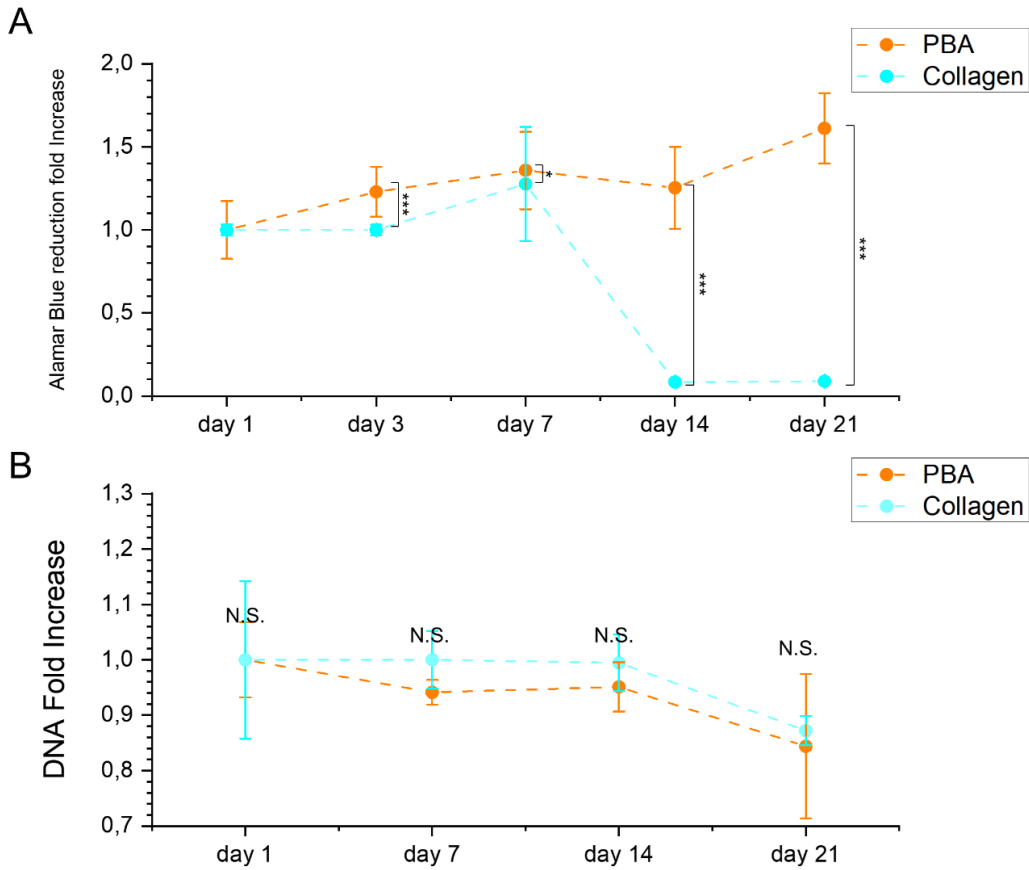


Figure 95. A) Alamar Blue fold increase obtained normalizing Alamar Blue reduction assay fluorescence raw results by day 1. B) DNA fold increase obtained by normalizing fluorescence raw results by day 1. (n=3) (***, $p < 0.001$; *, $p < 0.05$; N.S., not significance).

37. Supplementary Material C3

37.1. Design concepts

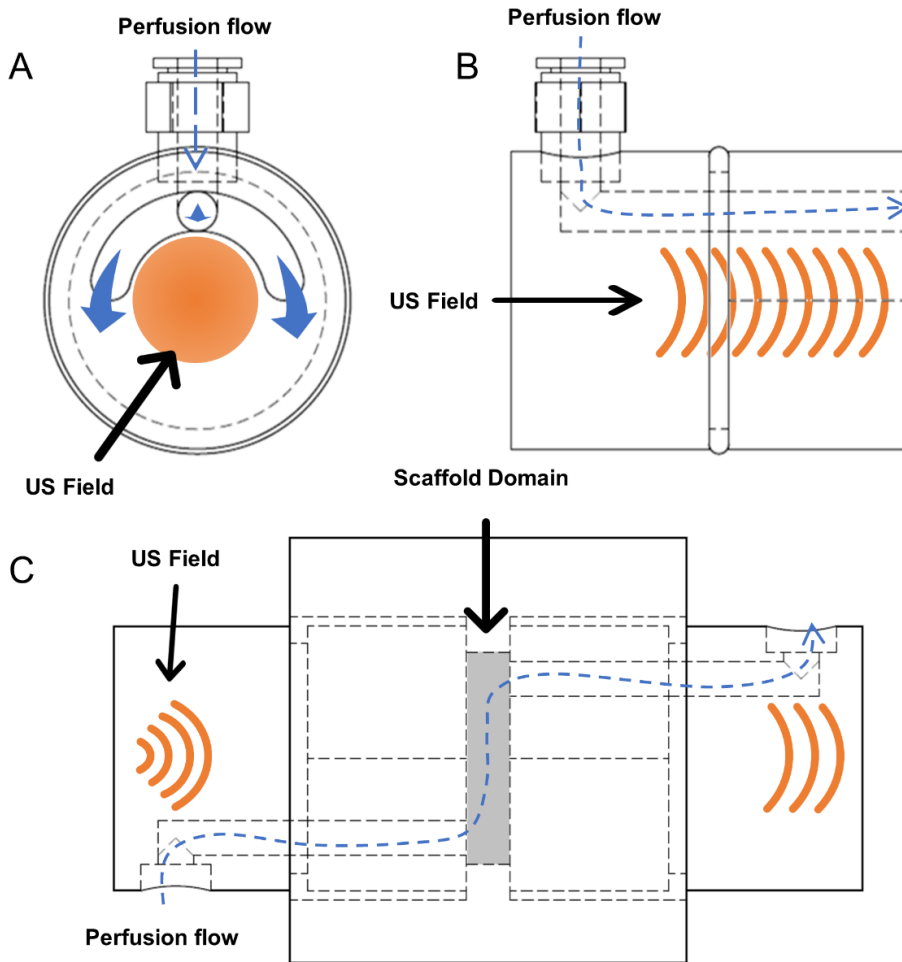


Figure 96. (A) Front view of Input/Output (IO) channels, (B) Profile view of IO channels. (C) Profile view of Scaffold chamber and IO channels. Ultrasound (US) field is represented in orange whereas the perfusion flow are represented in blue.

37.2. Model validation

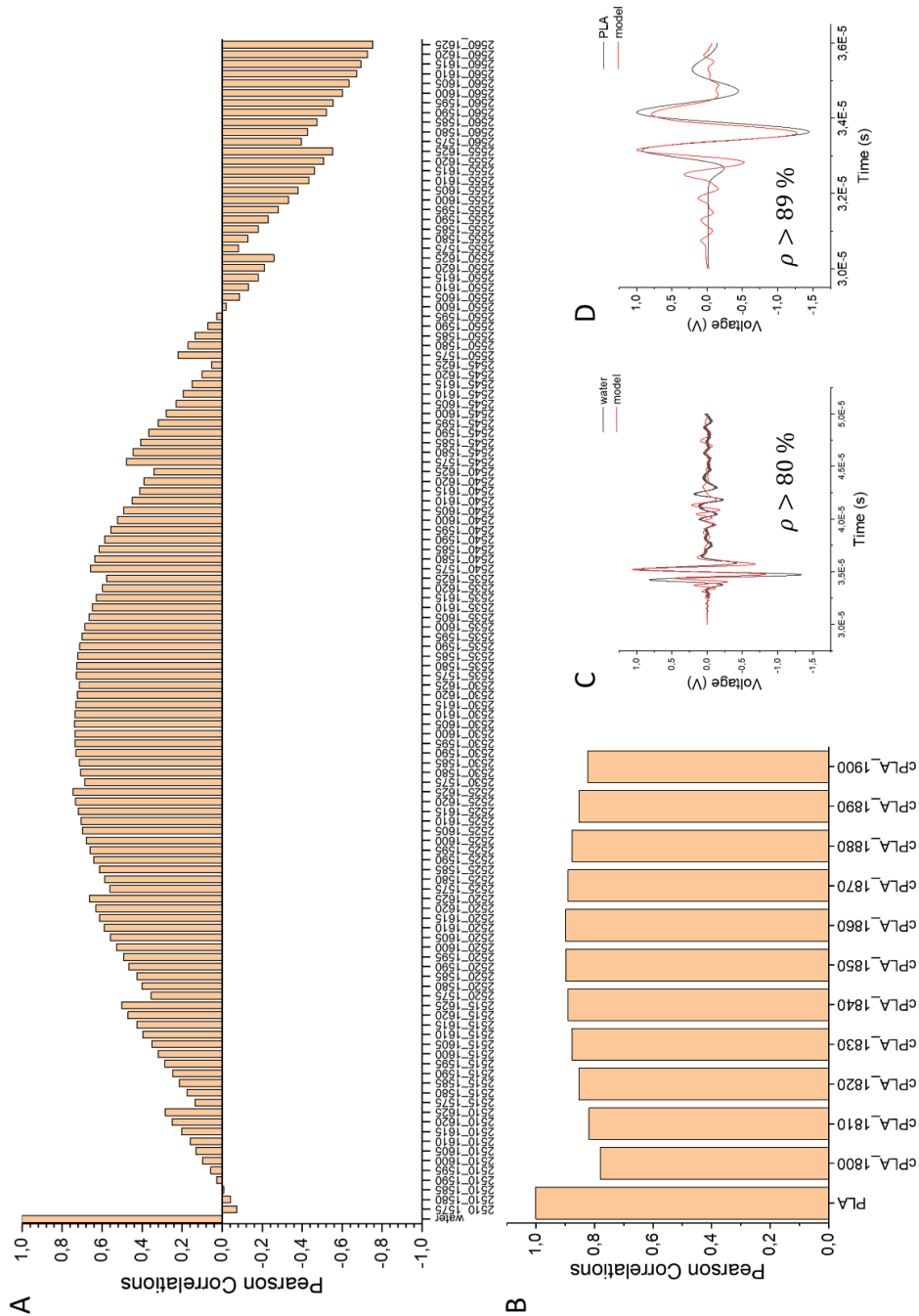
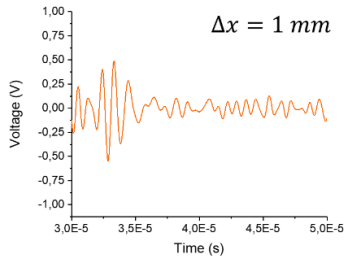


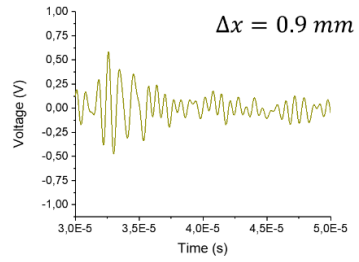
Figure 97. (A) Pearson coefficients obtained from Pearson correlation between water experimental signal and FEM (Finite Element Model) synthetic signals. (B) Pearson coefficients obtained from Pearson correlation between PLA (polylactic acid) experimental signal and FEM (Finite Element Model) synthetic signals. (C) Comparison of experimental water signal with the modeled one. (D) Comparison of experimental PLA signal with the modeled one. (ρ = Pearson coefficient)

ANNEX V SUPPLEMENTARY MATERIAL C3

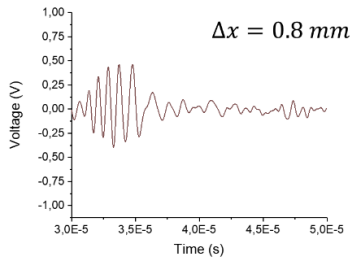
A



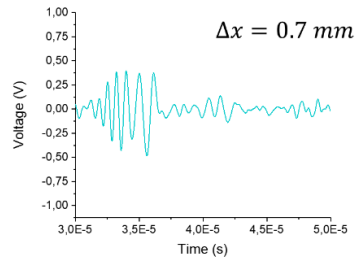
B



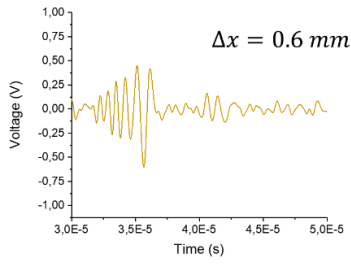
C



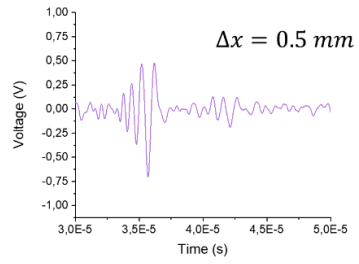
D



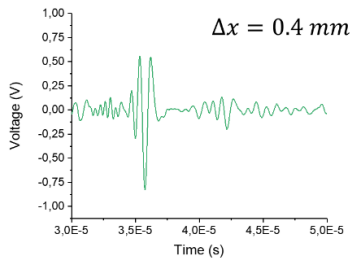
E



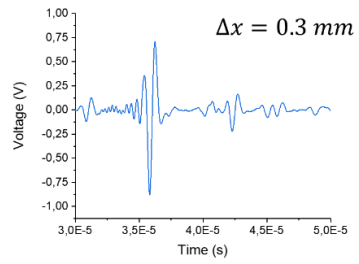
F



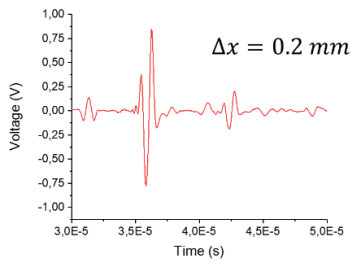
G



H



I



J

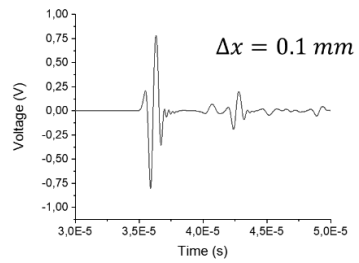
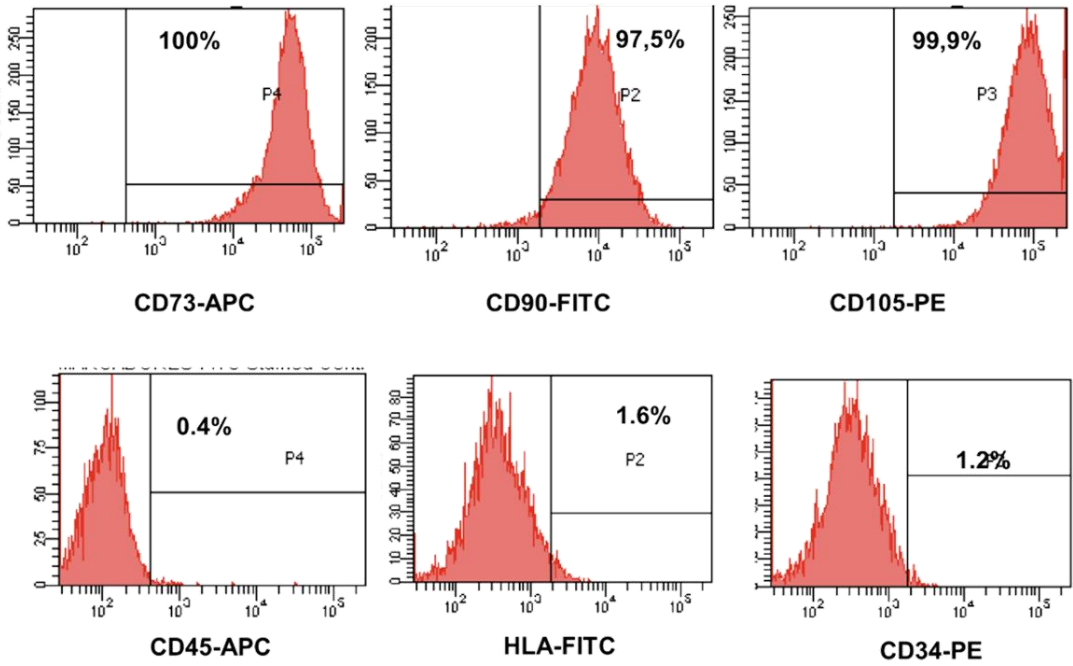


Figure 98. Modeled signals of our pressure wave sweeping mesh size (Δx), each step was 100 μm ; thus, the parametric sweep varied from 1 mm to final 100 μm . (Δx =distance of mesh size, is equal in both directions X and Y)

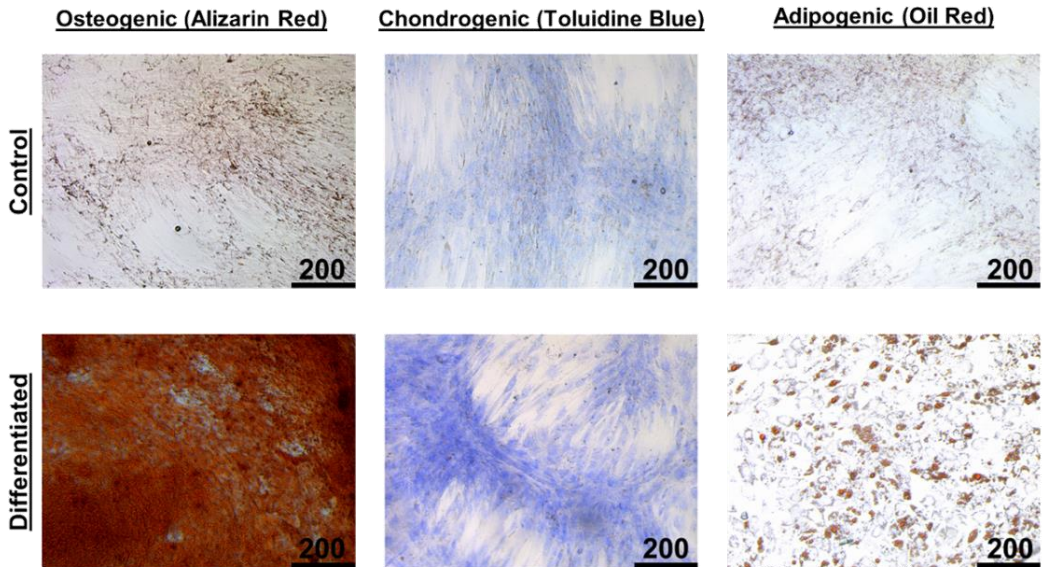
Figure 99. (A) FACS markers for stemness. (B) Differentiation capacity. Controls were IPFP-MSCs with DMEM, 10%FBS and 1%P/S. Differentiated mediums were: Osteogenic medium applied was StemMACS OsteoDiff 130-091-678, Miltenyi. Adipogenic medium applied was StemMACS adipoDiff 130-091-677, Miltenyi. Chondrogenic medium applied was DMEM supplemented with 10 ng/ml TGF- β 1, 0.1 μM dexamethasone, 40 $\mu\text{g/ml}$ L-proline, 50 $\mu\text{g/ml}$ L-Ascorbate-2-Phosphate, and 50 mg/ml ITS. (Scale bar = 200 μm). \hookrightarrow next page

37.3. MSCs characterization

A



B



37.4. Quantification Standard Curves

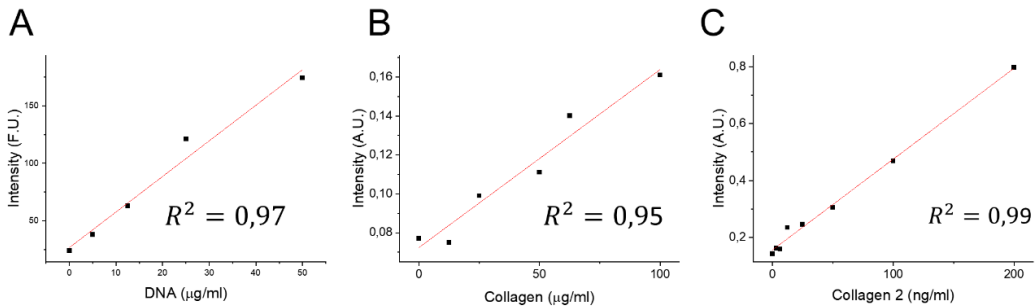


Figure 100. (A) Standard curve of DNA quantification. DNA content was estimated using a fluorometric marker (DAPI staining) and DNA standard curve was done using DNA from Calf Thymus (Sigma-Aldrich). (B) Standard curve of general collagen quantification. Collagen content was measured *via* Sirius Red assay, absorbance supernatant was measured in a microplate reader at 540 nm (Synergy HT, BIO-TEK), for standard collagen from calf skin was used (Sigma). (C) Standard curve of type II collagen quantification following manufacturer's protocols by Chondrex. (R^2 is the coefficient of determination for linearity, 1 means completely linearity, 0 means no linearity).

References

REFERENCES

“People will not look forward to posterity who never look backward to their ancestors.”

“La gente no mirará hacia adelante en la posteridad si nunca mira hacia atrás en sus antepasados.”

Edmund Burke

38. Literature

1. Wedd J, Basu M, Curtis LM, et al. Racial, ethnic, and socioeconomic disparities in web-based patient portal usage among kidney and liver transplant recipients: cross-sectional study. *J Med Internet Res*. 2019;21(4):e11864.
2. McCullough KP, Morgenstern H, Saran R, Herman WH, Robinson BM. Projecting ESRD incidence and prevalence in the United States through 2030. *J Am Soc Nephrol*. 2019;30(1):127-135.
3. Hart A, Lentine KL, Smith JM, et al. OPTN/SRTR 2019 Annual Data Report: Kidney. *Am J Transplant*. 2021;21(S2):21-137. doi:<https://doi.org/10.1111/ajt.16502>
4. Chang Chien GC, Stogicza A. Regenerative Medicine. In: *Pain Care Essentials and Innovations*. Elsevier; 2021:245-253. doi:10.1016/B978-0-323-72216-2.00017-X
5. Salvatori M, Peloso A, Katari R, et al. Semi-xenotransplantation: The regenerative medicine-based approach to immunosuppression-free transplantation and to meet the organ demand. *Xenotransplantation*. 2015;22(1):1-6. doi:10.1111/xen.12122
6. Nordham KD, Ninokawa S. The history of organ transplantation. *Baylor Univ Med Cent Proc*. 2022;35(1):124-128. doi:10.1080/08998280.2021.1985889
7. Colombo D, Ammirati E. Cyclosporine in transplantation - a history of converging timelines. *J Biol Regul Homeost Agents*. 2011;25(4):493-504.
8. Kaul H, Ventikos Y. On the genealogy of tissue engineering and regenerative medicine. *Tissue Eng Part B Rev*. 2015;21(2):203-217.
9. Broughton KM, Sussman MA. Enhancement strategies for cardiac regenerative cell therapy: focus on adult stem cells. *Circ Res*. 2018;123(2):177-187.
10. Mount NM, Ward SJ, Kefalas P, Hyllner J. Cell-based therapy technology classifications and translational challenges. *Philos Trans R Soc B Biol Sci*. 2015;370(1680):20150017.
11. Murillo-González J. Evolution of embryology: a synthesis of classical, experimental, and molecular perspectives. *Clin Anat Off J Am Assoc Clin Anat Br Assoc Clin Anat*. 2001;14(2):158-163.
12. Goss RJ. The natural history (and mystery). *A Hist Regen Res milestones Evol a Sci*. 1991:7.
13. Lenhoff HM, Lenhoff SG. Abraham Trembley and the origins of research on regeneration in animals. *A Hist Regen Res Milestones Evol a Sci*. 1991:47-66.
14. Dinsmore CE. *A History of Regeneration Research: Milestones in the Evolution of a Science*. Cambridge University Press; 1991.
15. Sampogna G, Guraya SY, Forgione A. Regenerative medicine: Historical roots and potential strategies in modern medicine. *J Microsc Ultrastruct*. 2015;3(3):101-107.
16. Kemp P. History of regenerative medicine: looking backwards to move forwards. 2006.
17. Berthiaume F, Maguire TJ, Yarmush ML. Tissue engineering and regenerative medicine: history, progress, and challenges. *Annu Rev Chem Biomol Eng*. 2011;2:403-430.
18. Berthiaume F, Maguire TJ, Yarmush ML. Tissue engineering and regenerative medicine: History, progress, and challenges. *Annu Rev Chem Biomol Eng*. 2011;2:403-430. doi:10.1146/annurev-chembioeng-061010-114257
19. Jacques E, Suuronen EJ. The Progression of Regenerative Medicine and its Impact on Therapy Translation. *Clin Transl Sci*. 2020;13(3):440-450. doi:10.1111/cts.12736

REFERENCES

20. Slingerland AS, Smits AIPM, Bouten CVC. Then and now: hypes and hopes of regenerative medicine. *Trends Biotechnol.* 2013;31(3):121-123.
21. Allickson JG. Emerging translation of regenerative therapies. *Clin Pharmacol Ther.* 2017;101(1):28-30.
22. Terzic A, Pfenning MA, Gores GJ, Harper CM. Regenerative Medicine Build-Out. *Stem Cells Transl Med.* 2015;4(12):1373-1379. doi:10.5966/sctm.2015-0275
23. Greenwood HL, Thorsteinsdottir H, Perry G, Renihan J, Singer P, Daar A. Regenerative medicine: new opportunities for developing countries. *Int J Biotechnol.* 2006.
24. Mason C, Dunnill P. A brief definition of regenerative medicine. *Regen Med.* 2008;3(1):1-5. doi:10.2217/17460751.3.1.1
25. Relevance T with E. REGULATION (EC) No 1394/2007 OF THE EUROPEAN PARLIAMENT AND OF THE COUNCIL of 13 November 2007. *Off J Eur Union.* 2007;121(324):17. <https://eur-lex.europa.eu/legal-content/EN/ALL/?uri=CELEX%3A32007R1394>.
26. Directive 2001/83/EC of the European Parliament and of the Council of 6 November 2001. *Pharm Policy Law.* 2009;11(4):411-499. doi:10.3233/ppl-2009-0234
27. Ciccocioppo R, Cantore A, Chaimov D, Orlando G. Regenerative medicine: the red planet for clinicians. *Intern Emerg Med.* 2019;14(6):911-921. doi:10.1007/s11739-019-02126-z
28. Potten CS, Wilson JW. The development of epithelial stem cell concepts. In: *Essentials of Stem Cell Biology.* Elsevier; 2009:17-27.
29. Mahla RS. Stem Cells Applications in Regenerative Medicine and Disease Therapeutics. Higgins PJ, ed. *Int J Cell Biol.* 2016;2016:6940283. doi:10.1155/2016/6940283
30. Thomson JA, Itskovitz-Eldor J, Shapiro SS, et al. Embryonic stem cell lines derived from human blastocysts. *Science (80-).* 1998;282(5391):1145-1147.
31. Knoepfler PS. Deconstructing stem cell tumorigenicity: a roadmap to safe regenerative medicine. *Stem Cells.* 2009;27(5):1050-1056.
32. Schwartz SD, Regillo CD, Lam BL, et al. Human embryonic stem cell-derived retinal pigment epithelium in patients with age-related macular degeneration and Stargardt's macular dystrophy: follow-up of two open-label phase 1/2 studies. *Lancet.* 2015;385(9967):509-516.
33. Takahashi K, Tanabe K, Ohnuki M, et al. Induction of pluripotent stem cells from adult human fibroblasts by defined factors. *cell* 131: 861-872. 2007.
34. Guyette JP, Charest JM, Mills RW, et al. Bioengineering human myocardium on native extracellular matrix. *Circ Res.* 2016;118(1):56-72.
35. Wilm B, Tamburrini R, Orlando G, Murray P. Autologous cells for kidney bioengineering. *Curr Transplant reports.* 2016;3(3):207-220.
36. Wang B, Jakus AE, Baptista PM, et al. Functional maturation of induced pluripotent stem cell hepatocytes in extracellular matrix—a comparative analysis of bioartificial liver microenvironments. *Stem Cells Transl Med.* 2016;5(9):1257-1267.
37. Wan J, Huang Y, Zhou P, et al. Culture of iPSCs derived pancreatic β -like cells in vitro using decellularized pancreatic scaffolds: a preliminary trial. *Biomed Res Int.* 2017;2017.
38. Múnera JO, Sundaram N, Rankin SA, et al. Differentiation of human pluripotent stem cells into colonic organoids via transient activation of BMP signaling. *Cell Stem Cell.* 2017;21(1):51-64.
39. Takasato M, Er PX, Chiu HS, et al. Kidney organoids from human iPS cells contain multiple

DOCTORAL THESIS DANIEL MARTÍNEZ MORENO

- lineages and model human nephrogenesis. *Nature*. 2015;526(7574):564-568. doi:10.1038/nature15695
40. Kumar D, Anand T, Kues WA. Clinical potential of human-induced pluripotent stem cells. *Cell Biol Toxicol*. 2017;33(2):99-112.
 41. Yoshihara M, Hayashizaki Y, Murakawa Y. Genomic instability of iPSCs: challenges towards their clinical applications. *Stem cell Rev reports*. 2017;13(1):7-16.
 42. Kim J-H, Kurtz A, Yuan B-Z, et al. Report of the international stem cell banking initiative workshop activity: current hurdles and progress in seed-stock banking of human pluripotent stem cells. *Stem Cells Transl Med*. 2017;6(11):1956-1962.
 43. Ilic D, Polak JM. Stem cells in regenerative medicine: introduction. *Br Med Bull*. 2011;98(1):117-126.
 44. Gimble JM, Katz AJ, Bunnell BA. Adipose-derived stem cells for regenerative medicine. *Circ Res*. 2007;100(9):1249-1260.
 45. Farge D, Labopin M, Tyndall A, et al. Autologous hematopoietic stem cell transplantation for autoimmune diseases: an observational study on 12 years' experience from the European Group for Blood and Marrow Transplantation Working Party on Autoimmune Diseases. *Haematologica*. 2010;95(2):284-292.
 46. Sun JM, Kurtzberg J. Cell therapy for diverse central nervous system disorders: inherited metabolic diseases and autism. *Pediatr Res*. 2018;83(1):364-371.
 47. Prunotto G, Offor UT, Samarasinghe S, et al. HSCT provides effective treatment for lymphoproliferative disorders in children with primary immunodeficiency. *J Allergy Clin Immunol*. 2020;146(2):447-450.
 48. Martino M, Lanza F, Pavesi L, et al. High-dose chemotherapy and autologous hematopoietic stem cell transplantation as adjuvant treatment in high-risk breast cancer: data from the European Group for Blood and Marrow Transplantation Registry. *Biol Blood Marrow Transplant*. 2016;22(3):475-481.
 49. Leventhal JR, Ildstad ST. Tolerance induction in HLA disparate living donor kidney transplantation by facilitating cell-enriched donor stem cell infusion: The importance of durable chimerism. *Hum Immunol*. 2018;79(5):272-276. doi:10.1016/j.humimm.2018.01.007
 50. Charbord P. Bone marrow mesenchymal stem cells: historical overview and concepts. *Hum Gene Ther*. 2010;21(9):1045-1056.
 51. Dominici M, Le Blanc K, Mueller I, et al. Minimal criteria for defining multipotent mesenchymal stromal cells. The International Society for Cellular Therapy position statement. *Cytotherapy*. 2006;8(4):315-317. doi:10.1080/14653240600855905
 52. Griffin MD, Elliman SJ, Cahill E, English K, Ceredig R, Ritter T. Concise review: adult mesenchymal stromal cell therapy for inflammatory diseases: how well are we joining the dots? *Stem Cells*. 2013;31(10):2033-2041.
 53. Regulski MJ. Mesenchymal Stem Cells: "Guardians of Inflammation". *Wounds a Compend Clin Res Pract*. 2017;29(1):20-27.
 54. Sundin M, Ringdén O, Sundberg B, Nava S, Götherström C, Le Blanc K. No alloantibodies against mesenchymal stromal cells, but presence of anti-fetal calf serum antibodies, after transplantation in allogeneic hematopoietic stem cell recipients. *Haematologica*. 2007;92(9):1208-1215.
 55. Ankrum JA, Ong JF, Karp JM. Mesenchymal stem cells: immune evasive, not immune privileged. *Nat Biotechnol*. 2014;32(3):252-260.

REFERENCES

56. Galipeau J, Sensébé L. Mesenchymal stromal cells: clinical challenges and therapeutic opportunities. *Cell Stem Cell*. 2018;22(6):824-833.
57. Chen X, Wang C, Yin J, Xu J, Wei J, Zhang Y. Efficacy of mesenchymal stem cell therapy for steroid-refractory acute graft-versus-host disease following allogeneic hematopoietic stem cell transplantation: a systematic review and meta-analysis. *PLoS One*. 2015;10(8):e0136991.
58. Wang L-T, Ting C-H, Yen M-L, et al. Human mesenchymal stem cells (MSCs) for treatment towards immune-and inflammation-mediated diseases: review of current clinical trials. *J Biomed Sci*. 2016;23(1):1-13.
59. Panés J, García-Olmo D, Van Assche G, et al. Expanded allogeneic adipose-derived mesenchymal stem cells (Cx601) for complex perianal fistulas in Crohn's disease: a phase 3 randomised, double-blind controlled trial. *Lancet*. 2016;388(10051):1281-1290.
60. Toyserkani NM, Jørgensen MG, Tabatabaeifar S, Jensen CH, Sheikh SP, Sørensen JA. Concise review: a safety assessment of adipose-derived cell therapy in clinical trials: a systematic review of reported adverse events. *Stem Cells Transl Med*. 2017;6(9):1786-1794.
61. Lalu MM, McIntyre L, Pugliese C, et al. Safety of cell therapy with mesenchymal stromal cells (safecell): A systematic review and meta-analysis of clinical trials. *PLoS One*. 2012;7(10):e47559.
62. Spees JL, Lee RH, Gregory CA. Mechanisms of mesenchymal stem/stromal cell function. *Stem Cell Res Ther*. 2016;7(1):1-13.
63. Galipeau J, Krampera M, Barrett J, et al. International Society for Cellular Therapy perspective on immune functional assays for mesenchymal stromal cells as potency release criterion for advanced phase clinical trials. *Cytotherapy*. 2016;18(2):151-159.
64. Pellegrini G, Ardighò D, Milazzo G, et al. Navigating market authorization: the path holoclar took to become the first stem cell product approved in the European Union. *Stem Cells Transl Med*. 2018;7(1):146-154.
65. Hirsch T, Rothoefl T, Teig N, et al. Regeneration of the entire human epidermis using transgenic stem cells. *Nature*. 2017;551(7680):327-332.
66. Dunbar CE, High KA, Joung JK, Kohn DB, Ozawa K, Sadelain M. Gene therapy comes of age. *Science (80-)*. 2018;359(6372):eaan4672.
67. Ermak G. *Emerging Medical Technologies*. World scientific publishing company; 2015.
68. Ferrua F, Aiuti A. Twenty-five years of gene therapy for ADA-SCID: from bubble babies to an approved drug. *Hum Gene Ther*. 2017;28(11):972-981.
69. Aiuti A, Biasco L, Scaramuzza S, et al. Lentiviral hematopoietic stem cell gene therapy in patients with Wiskott-Aldrich syndrome. *Science (80-)*. 2013;341(6148):1233-1235.
70. Thompson AA, Walters MC, Kwiatkowski J, et al. Gene therapy in patients with transfusion-dependent β -thalassemia. *N Engl J Med*. 2018;378(16):1479-1493.
71. Mendell JR. Therapy for spinal muscular atrophy. *N Engl J Med*. 2018;378(5):487.
72. Palfi S, Gurruchaga JM, Ralph GS, et al. Long-term safety and tolerability of ProSavin, a lentiviral vector-based gene therapy for Parkinson's disease: a dose escalation, open-label, phase 1/2 trial. *Lancet*. 2014;383(9923):1138-1146.
73. Hartmann J, Schüßler-Lenz M, Bondanza A, Buchholz CJ. Clinical development of CAR T cells—challenges and opportunities in translating innovative treatment concepts. *EMBO Mol Med*. 2017;9(9):1183-1197.
74. Amabile A, Migliara A, Capasso P, et al. Inheritable silencing of endogenous genes by hit-

DOCTORAL THESIS DANIEL MARTÍNEZ MORENO

- and-run targeted epigenetic editing. *Cell*. 2016;167(1):219-232.
75. Davidson BL, McCray PB. Current prospects for RNA interference-based therapies. *Nat Rev Genet*. 2011;12(5):329-340.
 76. Maeder ML, Gersbach CA. Genome-editing technologies for gene and cell therapy. *Mol Ther*. 2016;24(3):430-446.
 77. Schirotti G, Conti A, Ferrari S, et al. Precise gene editing preserves hematopoietic stem cell function following transient p53-mediated DNA damage response. *Cell Stem Cell*. 2019;24(4):551-565.
 78. Kosicki M, Tomberg K, Bradley A. Repair of double-strand breaks induced by CRISPR-Cas9 leads to large deletions and complex rearrangements. *Nat Biotechnol*. 2018;36(8):765-771.
 79. Biasco L, Rothe M, Büning H, Schambach A. Analyzing the genotoxicity of retroviral vectors in hematopoietic cell gene therapy. *Mol Ther Clin Dev*. 2018;8:21-30.
 80. Annoni A, Gregori S, Naldini L, Cantore A. Modulation of immune responses in lentiviral vector-mediated gene transfer. *Cell Immunol*. 2019;342:103802.
 81. Khademhosseini A, Vacanti JP, Langer R. Progress in tissue engineering. *Sci Am*. 2009;300(5):64-71. doi:10.1038/scientificamerican0509-64
 82. Polge C, Smith AU, Parkes AS. Revival of spermatozoa after vitrification and dehydration at low temperatures. *Nature*. 1949;164(4172):666.
 83. Rheinwald JG, Green H. Serial cultivation of strains of human epidermal keratinocytes: the formation keratinizing colonies from single cell is. *Cell*. 1975;6(3):331-343.
 84. Green H, Kehinde O, Thomas J. Growth of cultured human epidermal cells into multiple epithelia suitable for grafting. *Proc Natl Acad Sci*. 1979;76(11):5665-5668.
 85. O'Connor N, Mulliken J, Banks-Schlegel S, Kehinde O, Green H. Grafting of burns with cultured epithelium prepared from autologous epidermal cells. *Lancet*. 1981;317(8211):75-78.
 86. Hefernan J. Genzyme Tissue Repair. In: *ASME International Mechanical Engineering Congress and Exposition*. Vol 19340. American Society of Mechanical Engineers; 2000:31-32.
 87. Yannas I V, Burke JF, Orgill DP, Skrabut EM. Wound tissue can utilize a polymeric template to synthesize a functional extension of skin. *Science (80-)*. 1982;215(4529):174-176.
 88. Bell E, Ehrlich HP, Buttle DJ, Nakatsuji T. Living tissue formed in vitro and accepted as skin-equivalent tissue of full thickness. *Science (80-)*. 1981;211(4486):1052-1054.
 89. Brittberg M, Lindahl A, Nilsson A, Ohlsson C, Isaksson O, Peterson L. Treatment of deep cartilage defects in the knee with autologous chondrocyte transplantation. *N Engl J Med*. 1994;331(14):889-895.
 90. Langer R, Vacanti JP. Artificial organs. *Sci Am*. 1995;273(3):130-133.
 91. Khademhosseini A, Langer R. A decade of progress in tissue engineering. *Nat Protoc*. 2016;11(10):1775-1781. doi:10.1038/nprot.2016.123
 92. Mansbridge JN. Tissue-engineered skin substitutes in regenerative medicine. *Curr Opin Biotechnol*. 2009;20(5):563-567.
 93. Lysaght MJ, Hazlehurst AL. Tissue engineering: the end of the beginning. *Tissue Eng*. 2004;10(1-2):309-320.
 94. Ross JS, Ginsburg GS. The integration of molecular diagnostics with therapeutics:

REFERENCES

- implications for drug development and pathology practice. *Am J Clin Pathol.* 2003;119(1):26-36.
95. Langer R, Vacanti JP. Tissue engineering. *Science.* 1993;260(5110):920-926.
 96. Vacanti J. Tissue engineering and regenerative medicine: from first principles to state of the art. *J Pediatr Surg.* 2010;45(2):291-294. doi:10.1016/j.jpedsurg.2009.10.063
 97. Khademhosseini A, Langer R. Microengineered hydrogels for tissue engineering. *Biomaterials.* 2007;28(34):5087-5092.
 98. Yu J, Vodyanik MA, Smuga-Otto K, et al. Induced pluripotent stem cell lines derived from human somatic cells. *Science (80-).* 2007;318(5858):1917-1920.
 99. Okita K, Ichisaka T, Yamanaka S. Generation of germline-competent induced pluripotent stem cells. *Nature.* 2007;448(7151):313-317.
 100. Levy O, Zhao W, Mortensen LJ, et al. mRNA-engineered mesenchymal stem cells for targeted delivery of interleukin-10 to sites of inflammation. *Blood, J Am Soc Hematol.* 2013;122(14):e23-e32.
 101. Sarkar D, Spencer JA, Phillips JA, et al. Engineered cell homing. *Blood, J Am Soc Hematol.* 2011;118(25):e184-e191.
 102. Ranganath SH, Levy O, Inamdar MS, Karp JM. Harnessing the mesenchymal stem cell secretome for the treatment of cardiovascular disease. *Cell Stem Cell.* 2012;10(3):244-258.
 103. Karp JM, Teo GSL. Mesenchymal stem cell homing: the devil is in the details. *Cell Stem Cell.* 2009;4(3):206-216.
 104. Zuk PA, Zhu M, Ashjian P, et al. Human adipose tissue is a source of multipotent stem cells. *Mol Biol Cell.* 2002;13(12):4279-4295.
 105. De Coppi P, Bartsch G, Siddiqui MM, et al. Isolation of amniotic stem cell lines with potential for therapy. *Nat Biotechnol.* 2007;25(1):100-106.
 106. Engler AJ, Sen S, Sweeney HL, Discher DE. Matrix Elasticity Directs Stem Cell Lineage Specification. *Cell.* 2006;126(4):677-689. doi:10.1016/j.cell.2006.06.044
 107. Yang C, Tibbitt MW, Basta L, Anseth KS. Mechanical memory and dosing influence stem cell fate. *Nat Mater.* 2014;13(6):645-652.
 108. DeForest CA, Anseth KS. Cytocompatible click-based hydrogels with dynamically tunable properties through orthogonal photoconjugation and photocleavage reactions. *Nat Chem.* 2011;3(12):925-931.
 109. DeForest CA, Polizzotti BD, Anseth KS. Sequential click reactions for synthesizing and patterning three-dimensional cell microenvironments. *Nat Mater.* 2009;8(8):659-664.
 110. Martino MM, Briquez PS, Ranga A, Lutolf MP, Hubbell JA. Heparin-binding domain of fibrin (ogen) binds growth factors and promotes tissue repair when incorporated within a synthetic matrix. *Proc Natl Acad Sci.* 2013;110(12):4563-4568.
 111. Pakulska MM, Miersch S, Shoichet MS. Designer protein delivery: From natural to engineered affinity-controlled release systems. *Science (80-).* 2016;351(6279):aac4750.
 112. Vegas AJ, Veiseh O, Doloff JC, et al. Combinatorial hydrogel library enables identification of materials that mitigate the foreign body response in primates. *Nat Biotechnol.* 2016;34(3):345-352.
 113. Veiseh O, Doloff JC, Ma M, et al. Size-and shape-dependent foreign body immune response to materials implanted in rodents and non-human primates. *Nat Mater.* 2015;14(6):643-651.

DOCTORAL THESIS DANIEL MARTÍNEZ MORENO

114. Vacanti JP, Langer R. Tissue engineering: the design and fabrication of living replacement devices for surgical reconstruction and transplantation. *Lancet*. 1999;354:S32-S34.
115. Langer R, Vacanti JP, Vacanti CA, Atala A, Freed LE, Vunjak-Novakovic G. Tissue Engineering: Biomedical Applications. *Tissue Eng*. 1995;1(2):151-161. doi:10.1089/ten.1995.1.151
116. Mokarram N, Bellamkonda R V. A perspective on immunomodulation and tissue repair. *Ann Biomed Eng*. 2014;42(2):338-351.
117. Brown BN, Ratner BD, Goodman SB, Amar S, Badylak SF. Macrophage polarization: an opportunity for improved outcomes in biomaterials and regenerative medicine. *Biomaterials*. 2012;33(15):3792-3802.
118. Reardon S. New life for pig-to-human transplants. *Nat News*. 2015;527(7577):152.
119. Ott HC, Matthiesen TS, Goh S-K, et al. Perfusion-decellularized matrix: using nature's platform to engineer a bioartificial heart. *Nat Med*. 2008;14(2):213-221.
120. Badylak SF, Taylor D, Uygun K. Whole-organ tissue engineering: decellularization and recellularization of three-dimensional matrix scaffolds. *Annu Rev Biomed Eng*. 2011;13(1):27-53.
121. Song JJ, Ott HC. Organ engineering based on decellularized matrix scaffolds. *Trends Mol Med*. 2011;17(8):424-432.
122. Arenas-Herrera JE, Ko IK, Atala A, Yoo JJ. Decellularization for whole organ bioengineering. *Biomed Mater*. 2013;8(1):14106.
123. Song JJ, Guyette JP, Gilpin SE, Gonzalez G, Vacanti JP, Ott HC. Regeneration and experimental orthotopic transplantation of a bioengineered kidney. *Nat Med*. 2013;19(5):646-651.
124. Sullivan DC, Mirmalek-Sani S-H, Deegan DB, et al. Decellularization methods of porcine kidneys for whole organ engineering using a high-throughput system. *Biomaterials*. 2012;33(31):7756-7764.
125. Kaushal S, Amiel GE, Guleserian KJ, et al. Functional small-diameter neovessels created using endothelial progenitor cells expanded ex vivo. *Nat Med*. 2001;7(9):1035-1040.
126. Amiel GE, Komura M, Shapira OZ, et al. Engineering of blood vessels from acellular collagen matrices coated with human endothelial cells. *Tissue Eng*. 2006;12(8):2355-2365.
127. Zhang W, Zhang YS, Bakht SM, et al. Elastomeric free-form blood vessels for interconnecting organs on chip systems. *Lab Chip*. 2016;16(9):1579-1586.
128. Goh S-K, Bertera S, Olsen P, et al. Perfusion-decellularized pancreas as a natural 3D scaffold for pancreatic tissue and whole organ engineering. *Biomaterials*. 2013;34(28):6760-6772.
129. Baptista PM, Siddiqui MM, Lozier G, Rodriguez SR, Atala A, Soker S. The use of whole organ decellularization for the generation of a vascularized liver organoid. *Hepatology*. 2011;53(2):604-617.
130. Uygun BE, Soto-Gutierrez A, Yagi H, et al. Organ reengineering through development of a transplantable recellularized liver graft using decellularized liver matrix. *Nat Med*. 2010;16(7):814-820.
131. Petersen TH, Calle EA, Zhao L, et al. Tissue-engineered lungs for in vivo implantation. *Science (80-)*. 2010;329(5991):538-541.
132. Ott HC, Clippinger B, Conrad C, et al. Regeneration and orthotopic transplantation of a bioartificial lung. *Nat Med*. 2010;16(8):927-933.

REFERENCES

133. Atala A, Bauer SB, Soker S, Yoo JJ, Retik AB. Tissue-engineered autologous bladders for patients needing cystoplasty. *Lancet*. 2006;367(9518):1241-1246.
134. Lu T-Y, Lin B, Kim J, et al. Repopulation of decellularized mouse heart with human induced pluripotent stem cell-derived cardiovascular progenitor cells. *Nat Commun*. 2013;4(1):1-11.
135. Todhunter ME, Jee NY, Hughes AJ, et al. Programmed synthesis of three-dimensional tissues. *Nat Methods*. 2015;12(10):975-981.
136. Qi H, Ghodousi M, Du Y, et al. DNA-directed self-assembly of shape-controlled hydrogels. *Nat Commun*. 2013;4(1):1-10.
137. Cohen DL, Malone E, Lipson HOD, Bonassar LJ. Direct freeform fabrication of seeded hydrogels in arbitrary geometries. *Tissue Eng*. 2006;12(5):1325-1335.
138. Khalil S, Nam J, Darling A, Sun W. Multi-nozzle biopolymer deposition for freeform fabrication of tissue constructs. In: *2004 International Solid Freeform Fabrication Symposium*. ; 2004.
139. Miller JS, Stevens KR, Yang MT, et al. Rapid casting of patterned vascular networks for perfusable engineered three-dimensional tissues. *Nat Mater*. 2012;11(9):768-774.
140. Kolesky DB, Truby RL, Gladman AS, Busbee TA, Homan KA, Lewis JA. 3D bioprinting of vascularized, heterogeneous cell-laden tissue constructs. *Adv Mater*. 2014;26(19):3124-3130.
141. Colosi C, Shin SR, Manoharan V, et al. Microfluidic bioprinting of heterogeneous 3D tissue constructs using low-viscosity bioink. *Adv Mater*. 2016;28(4):677-684.
142. Kang H-W, Lee SJ, Ko IK, Kengla C, Yoo JJ, Atala A. A 3D bioprinting system to produce human-scale tissue constructs with structural integrity. *Nat Biotechnol*. 2016;34(3):312-319.
143. Ober TJ, Foresti D, Lewis JA. Active mixing of complex fluids at the microscale. *Proc Natl Acad Sci*. 2015;112(40):12293-12298.
144. Ebrahimkhani MR, Neiman JAS, Raredon MSB, Hughes DJ, Griffith LG. Bioreactor technologies to support liver function in vitro. *Adv Drug Deliv Rev*. 2014;69:132-157.
145. Huh D, Fujioka H, Tung Y-C, et al. Acoustically detectable cellular-level lung injury induced by fluid mechanical stresses in microfluidic airway systems. *Proc Natl Acad Sci*. 2007;104(48):18886-18891.
146. Wilmer MJ, Ng CP, Lanz HL, Vulto P, Suter-Dick L, Masereeuw R. Kidney-on-a-chip technology for drug-induced nephrotoxicity screening. *Trends Biotechnol*. 2016;34(2):156-170.
147. Kim S, Lee H, Chung M, Jeon NL. Engineering of functional, perfusable 3D microvascular networks on a chip. *Lab Chip*. 2013;13(8):1489-1500.
148. Torisawa Y, Spina CS, Mammoto T, et al. Bone marrow-on-a-chip replicates hematopoietic niche physiology in vitro. *Nat Methods*. 2014;11(6):663-669.
149. Huh D, Matthews BD, Mammoto A, Montoya-Zavala M, Hsin HY, Ingber DE. Reconstituting organ-level lung functions on a chip. *Science*. 2010;328(5986):1662-1668. doi:10.1126/science.1188302
150. Esch EW, Bahinski A, Huh D. Organs-on-chips at the frontiers of drug discovery. *Nat Rev Drug Discov*. 2015;14(4):248-260.
151. Bhatia SN, Ingber DE. Microfluidic organs-on-chips. *Nat Biotechnol*. 2014;32(8):760-772.

DOCTORAL THESIS DANIEL MARTÍNEZ MORENO

152. Zhang YS, Khademhosseini A. Seeking the right context for evaluating nanomedicine: from tissue models in petri dishes to microfluidic organs-on-a-chip. *Nanomedicine*. 2015;10(5):685-688.
153. Huh D, Hamilton GA, Ingber DE. From 3D cell culture to organs-on-chips. *Trends Cell Biol*. 2011;21(12):745-754. doi:10.1016/j.tcb.2011.09.005
154. Sydney Gladman A, Matsumoto EA, Nuzzo RG, Mahadevan L, Lewis JA. Biomimetic 4D printing. *Nat Mater*. 2016;15(4):413-418. doi:10.1038/nmat4544
155. Tibbits S. 4D printing: Multi-material shape change. *Archit Des*. 2014. doi:10.1002/ad.1710
156. Culav EM, Clark CH, Mervyn J. Connective Tissues : Matrix. 1999;79(3):308-319.
157. Silver FH, Christiansen DL. Introduction to Biomaterials Science and Biocompatibility. *Biomater Sci Biocompat*. 1999:1-26. doi:10.1007/978-1-4612-0557-9_1
158. Cascione M, De Matteis V, Pellegrino P, et al. Improvement of PMMA dental matrix performance by addition of titanium dioxide nanoparticles and clay nanotubes. *Nanomaterials*. 2021;11(8):2027.
159. Smith III RB. Arthur B. Voorhees, Jr.: pioneer vascular surgeon. *J Vasc Surg*. 1993;18(3):341-348.
160. Rob CG, Standeven A. Arterial occlusion complicating thoracic outlet compression syndrome. *Br Med J*. 1958;2(5098):709.
161. Charnley J. Anchorage of the femoral head prosthesis to the shaft of the femur. *J Bone Joint Surg Br*. 1960;42(1):28-30.
162. Williams DF. *Definitions in Biomaterials: Proceedings of a Consensus Conference of the European Society for Biomaterials, Chester, England, March 3-5, 1986*. Vol 4. Elsevier Science Limited; 1987.
163. Williams DF. *Progress in Biomedical Engineering: Definitions in Biomaterials*. Elsevier; 1987.
164. Homsy CA. Bio-Compatibility in selection of materials for implantation. *J Biomed Mater Res*. 1970;4(3):341-356.
165. Wallin RF, Arscott EF. A practical guide to ISO 10993-5: Cytotoxicity. *Med Device Diagnostic Ind*. 1998;20:96-98.
166. Anderson JM, Rodriguez A, Chang DT. Foreign body reaction to biomaterials. In: *Seminars in Immunology*. Vol 20. Elsevier; 2008:86-100.
167. Gonzalez-Simon AL, Eniola-Adefeso O. Host response to biomaterials. In: *Engineering Biomaterials for Regenerative Medicine*. Springer; 2012:143-159.
168. Ward WK. A review of the foreign-body response to subcutaneously-implanted devices: the role of macrophages and cytokines in biofouling and fibrosis. *J Diabetes Sci Technol*. 2008;2(5):768-777.
169. Sussman EM, Halpin MC, Muster J, Moon RT, Ratner BD. Porous implants modulate healing and induce shifts in local macrophage polarization in the foreign body reaction. *Ann Biomed Eng*. 2014;42(7):1508-1516.
170. Treiser M, Abramson S, Langer R, Kohn J. *Degradable and Resorbable Biomaterials*. Third Edit. Elsevier; 2013. doi:10.1016/B978-0-08-087780-8.00021-8
171. Okada H, Toguchi H. Biodegradable microspheres in drug delivery. *Crit Rev Ther Drug Carr Syst*. 1995;12(1).

REFERENCES

172. Von Burkersroda F, Schedl L, Göpferich A. Why degradable polymers undergo surface erosion or bulk erosion. *Biomaterials*. 2002;23(21):4221-4231.
173. Tschernitschek H, Borchers L, Geurtsen W. Nonalloyed titanium as a bioinert metal--a review. *Quintessence Int (Berl)*. 2005;36(7).
174. Hua K, Rocha I, Zhang P, et al. Transition from Bioinert to Bioactive Material by Tailoring the Biological Cell Response to Carboxylated Nanocellulose. *Biomacromolecules*. 2016;17(3):1224-1233. doi:10.1021/acs.biomac.6b00053
175. Portillo-Lara R, Goding JA, Green RA. Adaptive biomimicry: Design of neural interfaces with enhanced biointegration. *Curr Opin Biotechnol*. 2021;72:62-68.
176. Kamachimudali U, Sridhar TM, Raj B. Corrosion of bio implants. *Sadhana*. 2003;28(3):601-637.
177. Atala A, Lanza R, Mikos T, Nerem R. *Principles of Regenerative Medicine*. Academic press; 2018.
178. Hai Bang Lee, Gilson Khang JHL. Polymeric Biomaterials. In: *Biomedical Engineering Fundamentals*. ; 2006.
179. Ehrlich H. Hierarchical biological materials. In: *Biological Materials of Marine Origin*. ; 2010.
180. Albertsson A-C, Varma IK. Aliphatic polyesters: Synthesis, properties and applications. *Degrad aliphatic polyesters*. 2002:1-40.
181. Gilding DK, Reed AM. Biodegradable polymers for use in surgery—polyglycolic/poly (actic acid) homo-and copolymers: 1. *Polymer (Guildf)*. 1979;20(12):1459-1464.
182. Hogston P. Suture choice in general gynaecological surgery. *Obstet Gynaecol*. 2001;3(3):127-131.
183. Christen M-O, Vercesi F. Polycaprolactone: How a well-known and futuristic polymer has become an innovative collagen-stimulator in esthetics. *Clin Cosmet Investig Dermatol*. 2020;13:31.
184. Anderson DG, Burdick JA, Langer R. Smart biomaterials. *Science (80-)*. 2004;305(5692):1923-1924.
185. Kuhn W, Hargitay B, Katchalsky A, Eisenberg H. Reversible dilation and contraction by changing the state of ionization of high-polymer acid networks. *Nature*. 1950;165(4196):514-516.
186. Kost J, Horbett TA, Ratner BD, Singh M. Glucose-sensitive membranes containing glucose oxidase: Activity, swelling, and permeability studies. *J Biomed Mater Res*. 1985;19(9):1117-1133.
187. Dong LC, Hoffman AS. Thermally reversible hydrogels: Swelling characteristics and activities of copoly (N-isopropylacrylamide-acrylamide) gels containing immobilized asparaginase. In: ACS Publications; 1987.
188. Tsay R-Y, Imae T. Development of Nonfouling Biomaterials. In: *Encyclopedia of Biocolloid and Bointerface Science 2V Set*. ; 2016:145-160. doi:https://doi.org/10.1002/9781119075691.ch11
189. Merrill EW, Salzman EW. Polyethylene oxide as a biomaterial. *ASAIO J*. 1983;6(2):60-64.
190. Nagaoka S, Mori Y, Takiuchi H, Yokota K, Tanzawa H, Nishiumi S. Interaction between blood components and hydrogels with poly (oxyethylene) chains. In: *Polymers as Biomaterials*. Springer; 1984:361-374.

DOCTORAL THESIS DANIEL MARTÍNEZ MORENO

191. Schlenoff JB. Zwitteration: coating surfaces with zwitterionic functionality to reduce nonspecific adsorption. *Langmuir*. 2014;30(32):9625-9636.
192. Feldman D, Barbalata A. *Synthetic Polymers: Technology, Properties, Applications*. Springer Science & Business Media; 1996.
193. Olatunji O. *Natural Polymers: Industry Techniques and Applications*. Springer; 2015.
194. Pearce AK, O'Reilly RK. Polymers for biomedical applications: the importance of hydrophobicity in directing biological interactions and application efficacy. *Biomacromolecules*. 2021;22(11):4459-4469.
195. Douglas T, Haugen HJ. Coating of polyurethane scaffolds with collagen: Comparison of coating and cross-linking techniques. In: *Journal of Materials Science: Materials in Medicine*. Vol 19. ; 2008:2713-2719. doi:10.1007/s10856-008-3393-6
196. Cheng Z, Teoh SH. Surface modification of ultra thin poly (ϵ -caprolactone) films using acrylic acid and collagen. *Biomaterials*. 2004. doi:10.1016/j.biomaterials.2003.08.038
197. Das D, Srinivasan S, Kelly AM, et al. RAFT polymerization of ciprofloxacin prodrug monomers for the controlled intracellular delivery of antibiotics. *Polym Chem*. 2016;7(4):826-837.
198. Hong D, Hung H-C, Wu K, et al. Achieving ultralow fouling under ambient conditions via surface-initiated ARGET ATRP of carboxybetaine. *ACS Appl Mater Interfaces*. 2017;9(11):9255-9259.
199. Kolb HC, Finn MG, Sharpless KB. Click chemistry: diverse chemical function from a few good reactions. *Angew Chemie Int Ed*. 2001;40(11):2004-2021.
200. Wang Z, Yan J, Wang T, Zai Y, Qiu L, Wang Q. Fabrication and Properties of a Bio-Based Biodegradable Thermoplastic Polyurethane Elastomer. *Polymers (Basel)*. 2019;11(7):1121. doi:10.3390/polym11071121
201. Alhaque S, Themis M, Rashidi H. Three-dimensional cell culture: from evolution to revolution. *Philos Trans R Soc B Biol Sci*. 2018;373(1750):20170216.
202. Simian M, Bissell MJ. Organoids: a historical perspective of thinking in three dimensions. *J Cell Biol*. 2017;216(1):31-40.
203. Ishida S. Organs-on-a-chip: current applications and consideration points for in vitro ADME-Tox studies. *Drug Metab Pharmacokinet*. 2018;33(1):49-54.
204. Crosby CO, Zoldan J. Mimicking the physical cues of the ECM in angiogenic biomaterials. *Regen Biomater*. 2019;6(2):61-73.
205. Hinderer S, Layland SL, Schenke-Layland K. ECM and ECM-like materials—Biomaterials for applications in regenerative medicine and cancer therapy. *Adv Drug Deliv Rev*. 2016;97:260-269.
206. Wade RJ, Burdick JA. Engineering ECM signals into biomaterials. *Mater Today*. 2012;15(10):454-459.
207. Culav EM, Clark CH, Merrilees MJ. Connective tissues: matrix composition and its relevance to physical therapy. *Phys Ther*. 1999;79(3):308-319.
208. Bateman JF, Lamande SR, Ramshaw JAM. Collagen superfamily. *Extracell matrix*. 1996;2:22-67.
209. Kielty CM, Grant ME. The collagen family: structure, assembly, and organization in the extracellular matrix. *Connect tissue its heritable Disord Mol Genet Med Asp*. 2002:159-221.
210. Hay ED. *Cell Biology of Extracellular Matrix*. Springer Science & Business Media; 1991.

REFERENCES

211. Royce PM, Steinmann B. *Connective Tissue and Its Heritable Disorders: Molecular, Genetic, and Medical Aspects*. John Wiley & Sons; 2003.
212. Oryan A. Role of collagen in soft connective tissue wound healing. In: *Transplantation Proceedings*. Vol 27. ; 1995:2759-2761.
213. Chadwick D, Goode J. molecular biology and pathology of elastic tissues. In: *Symposium on the Molecular Biology and Pathology of Elastic Tissues (1994: Nairobi, Kenya)*. J. Wiley; 1995.
214. Chen YQ, Bernstein EF, Tamai K, et al. Enhanced elastin and fibrillin gene expression in chronically photodamaged skin. *J Invest Dermatol*. 1994;103(2):182-186.
215. Pierce RA, Mariani TJ, Senior RM. Elastin in Lung Development and Disease. In: *Ciba Foundation Symposium 192 - The Molecular Biology and Pathology of Elastic Tissues*. Novartis Foundation Symposia. ; 2007:199-214. doi:<https://doi.org/10.1002/9780470514771.ch11>
216. Hardingham TE, Fosang AJ. Proteoglycans: many forms and many functions. *FASEB J*. 1992;6(3):861-870. doi:10.1017/CBO9781107415324.004
217. Heinegård D, Aspberg A, Franzén A, Lorenzo P. Glycosylated Matrix Proteins. In: *Connective Tissue and Its Heritable Disorders*. ; 2002:271-291. doi:<https://doi.org/10.1002/0471221929.ch4>
218. International Conference on Fibrous Proteins: Scientific I and MA (4th : 1979 : MU [Main author], Parry DAD, Creamer LK, University) IC on FP (4th : 1979 : M. *Fibrous Proteins: Scientific, Industrial and Medical Aspects*. London: Academic Press; 1979.
219. Ratcliffe A, Mow VC. *Extracellular Matrix, Volume 1, Tissue Function*. 1996.
220. Wall A, Board T. The biological effect of continuous passive motion on the healing of full-thickness defects in articular cartilage. An experimental investigation in the rabbit. In: *Classic Papers in Orthopaedics*. Springer; 2014:437-439.
221. Houlbrooke K, Vause K, Merrilees MJ. Effects of movement and weightbearing on the glycosaminoglycan content of sheep articular cartilage. *Aust J Physiother*. 1990;36(2):88-91.
222. Burton-Wurster N, Todhunter RJ, Lust G. Animal models of osteoarthritis. *Inflamm Dis Ther*. 1993;12:347.
223. Johnstone B, Bayliss MT. The large proteoglycans of the human intervertebral disc. Changes in their biosynthesis and structure with age, topography, and pathology. *Spine (Phila Pa 1976)*. 1995;20(6):674-684.
224. Robbins JR, Evanko SP, Vogel KG. Mechanical loading and TGF- β regulate proteoglycan synthesis in tendon. *Arch Biochem Biophys*. 1997;342(2):203-211.
225. von der Mark K, Sorokin L. Adhesive glycoproteins. *Connect tissue its heritable Disord Wiley-Liss, New York*. 2002:293-328.
226. Yamada KM. Fibronectin and other cell interactive glycoproteins. In: *Cell Biology of Extracellular Matrix*. Springer; 1991:111-146.
227. Sage EH, Bornstein P. Extracellular proteins that modulate cell-matrix interactions. SPARC, tenascin, and thrombospondin. *J Biol Chem*. 1991;266(23):14831-14834.
228. Martin GR, Timpl R. Laminin and other basement membrane components. *Annu Rev Cell Biol*. 1987;3(1):57-85.
229. Paulsson M. Basement membrane proteins: structure, assembly, and cellular interactions. *Crit Rev Biochem Mol Biol*. 1992;27(1-2):93-127.

DOCTORAL THESIS DANIEL MARTÍNEZ MORENO

230. Hascall VC, Heinegård D. Aggregation of cartilage proteoglycans: I. The role of hyaluronic acid. *J Biol Chem.* 1974;249(13):4232-4241.
231. Sodek J, Ganss B, McKee MD. Osteopontin. *Crit Rev Oral Biol Med.* 2000;11(3):279-303.
232. Hedlund H, Mengarelli-Widholm S, Heinegård D, Reinholt FP, Svensson O. Fibromodulin distribution and association with collagen. *Matrix Biol.* 1994;14(3):227-232.
233. LeVeau BF. Biomechanics: A summary of perspectives. *Phys Ther.* 1984;64(12):1812. doi:10.1093/ptj/64.12.1812
234. Nussbaum MC. *Aristotle's De Motu Animalium: Text with Translation, Commentary, and Interpretive Essays.* Princeton University Press; 1985.
235. Ascenzi A. Biomechanics and galileo galilei. *J Biomech.* 1993;26(2):95-100.
236. Pope MH. Giovanni Alfonso Borelli—The Father of Biomechanics. *Spine (Phila Pa 1976).* 2005;30(20).
https://journals.lww.com/spinejournal/Fulltext/2005/10150/Giovanni_Alfonso_Borelli_The_Father_of.18.aspx.
237. Armentano R. Leonardo Da Vinci, the Great Innovator in Cardiovascular Biomechanics. In: *Latin American Conference on Biomedical Engineering.* Springer; 2019:975-981.
238. Wolff J. *The Law of Bone Remodelling.* Springer Science & Business Media; 2012.
239. Sammarco GJ, Burstein AH, Frankel VH. Biomechanics of the ankle: a kinematic study. *Orthop Clin North Am.* 1973;4(1):75-96.
240. Hatze H. The meaning of the term 'biomechanics.' *J Biomech.* 1974;7(2):189-190. doi:[https://doi.org/10.1016/0021-9290\(74\)90060-8](https://doi.org/10.1016/0021-9290(74)90060-8)
241. Nissan M. Review of some basic assumptions in knee biomechanics. *J Biomech.* 1980;13(4):375-381. doi:10.1016/0021-9290(80)90018-4
242. Leckband D, Israelachvili J. Intermolecular forces in biology. *Q Rev Biophys.* 2001;34(2):105-267.
243. Davies PCW. *The Forces of Nature.* CUP Archive; 1979.
244. Giuliodori MJ, Lujan HL, Briggs WS, Palani G, DiCarlo SE. Hooke's law: applications of a recurring principle. *Adv Physiol Educ.* 2009;33(4):293-296.
245. Maugin GA. Generalized continuum mechanics: what do we mean by that? In: *Mechanics of Generalized Continua.* Springer; 2010:3-13.
246. Spencer AJM. *Continuum Mechanics.* Courier Corporation; 2004.
247. Reddy JN. *An Introduction to Continuum Mechanics.* Cambridge university press; 2013.
248. Shabana AA. *Computational Continuum Mechanics.* John Wiley & Sons; 2018.
249. Chou PC, Pagano NJ. *Elasticity: Tensor, Dyadic, and Engineering Approaches.* Courier Corporation; 1992.
250. Gennisson J-L, Deffieux T, Fink M, Tanter M. Ultrasound elastography: principles and techniques. *Diagn Interv Imaging.* 2013;94(5):487-495.
251. Newton I. Principia mathematica. *B III, Lemma V, Case.* 1934;1:1687.
252. Braun M, Golubitsky M. *Differential Equations and Their Applications.* Vol 1. Springer; 1983.
253. Speiser D. *Discovering the Principles of Mechanics 1600-1800: Essays by David Speiser.* Vol 1. Springer Science & Business Media; 2008.

REFERENCES

254. Bird RB. Transport phenomena. *Appl Mech Rev.* 2002;55(1):R1-R4.
255. Galdi G. *An Introduction to the Mathematical Theory of the Navier-Stokes Equations: Steady-State Problems.* Springer Science & Business Media; 2011.
256. Vlachopoulos J. *Fundamentals of Fluid Mechanics.* Polydynamics Inc; 2016.
257. Fournier RL. *Basic Transport Phenomena in Biomedical Engineering.* CRC press; 2017.
258. Truskey GA, Yuan F, Katz DF. Transport phenomena in biological systems. 2004.
259. Foister RT, Van De Ven TGM. Diffusion of Brownian particles in shear flows. *J Fluid Mech.* 1980;96(1):105-132.
260. Leal LG. *Advanced Transport Phenomena: Fluid Mechanics and Convective Transport Processes.* Vol 7. Cambridge University Press; 2007.
261. Poirier DR, Geiger GH. Fick's Law and diffusivity of materials. In: *Transport Phenomena in Materials Processing.* Springer; 2016:419-461.
262. Einstein A. *Investigations on the Theory of the Brownian Movement.* Courier Corporation; 1956.
263. Reynolds O. IV. On the dynamical theory of incompressible viscous fluids and the determination of the criterion. *Philos Trans R Soc london(a).* 1895;(186):123-164.
264. Michael Peters A. The precise physiological definition of tissue perfusion and clearance measured from imaging. *Eur J Nucl Med Mol Imaging.* 2018;45(7):1139-1141.
265. Gottlieb RA. Cell death pathways in acute ischemia/reperfusion injury. *J Cardiovasc Pharmacol Ther.* 2011;16(3-4):233-238.
266. Bear J, Bachmat Y. *Introduction to Modeling of Transport Phenomena in Porous Media.* Vol 4. Springer Science & Business Media; 2012.
267. Dullien FAL. *Porous Media: Fluid Transport and Pore Structure.* Academic press; 2012.
268. Ghanbarian B, Hunt AG, Ewing RP, Sahimi M. Tortuosity in porous media: a critical review. *Soil Sci Soc Am J.* 2013;77(5):1461-1477.
269. Darcy H. *Les Fontaines Publiques de La Ville de Dijon: Exposition et Application Des Principes à Suivre et Des Formules à Employer Dans Les Questions de Distribution d'eau: Ouvrage Terminé Par Un Appendice Relatif Aux Fournitures d'eau de Plusieurs Villes, Au Filt.* Vol 2. V. Dalmont; 1856.
270. Preziosi L, Farina A. On Darcy's law for growing porous media. *Int J Non Linear Mech.* 2002;37(3):485-491.
271. Whitaker S. Flow in porous media I: A theoretical derivation of Darcy's law. *Transp porous media.* 1986;1(1):3-25.
272. Ingber DE. Cellular mechanotransduction: putting all the pieces together again. *FASEB J.* 2006;20(7):811-827. doi:10.1096/fj.05-5424rev
273. Wang JH-C, Thampatty BP, Lin J-S, Im H-J. Mechanoregulation of gene expression in fibroblasts. *Gene.* 2007;391(1-2):1-15.
274. Isaksson H, Wilson W, van Donkelaar CC, Huijkes R, Ito K. Comparison of biophysical stimuli for mechano-regulation of tissue differentiation during fracture healing. *J Biomech.* 2006;39(8):1507-1516.
275. Gruber EJ, Leifer CA. Molecular regulation of TLR signaling in health and disease: mechano-regulation of macrophages and TLR signaling. *Innate Immun.* 2020;26(1):15-25.
276. Chiquet M, Renedo AS, Huber F, Flück M. How do fibroblasts translate mechanical signals

DOCTORAL THESIS DANIEL MARTÍNEZ MORENO

- into changes in extracellular matrix production? *Matrix Biol.* 2003;22(1):73-80.
277. Wong VW, Akaishi S, Longaker MT, Gurtner GC. Pushing back: wound mechanotransduction in repair and regeneration. *J Invest Dermatol.* 2011;131(11):2186-2196.
278. Wong M, Carter DR. Articular cartilage functional histomorphology and mechanobiology: a research perspective. *Bone.* 2003;33(1):1-13.
279. Chen C, Tambe DT, Deng L, Yang L. Biomechanical properties and mechanobiology of the articular chondrocyte. *Am J Physiol Physiol.* 2013;305(12):C1202-C1208.
280. Santos A, Bakker AD, Klein-Nulend J. The role of osteocytes in bone mechanotransduction. *Osteoporos Int.* 2009;20(6):1027-1031.
281. Brizzi MF, Tarone G, Defilippi P. Extracellular matrix, integrins, and growth factors as tailors of the stem cell niche. *Curr Opin Cell Biol.* 2012;24(5):645-651.
282. Sun Y, Fu J. Mechanobiology: a new frontier for human pluripotent stem cells. *Integr Biol.* 2013;5(3):450-457.
283. Satir P, Pedersen LB, Christensen ST. The primary cilium at a glance. *J Cell Sci.* 2010;123(4):499-503.
284. Seeger-Nukpezah T, Golemis EA. The extracellular matrix and ciliary signaling. *Curr Opin Cell Biol.* 2012;24(5):652-661.
285. Zhang H, Labouesse M. Signalling through mechanical inputs—a coordinated process. *J Cell Sci.* 2012;125(13):3039-3049.
286. Iheanacho F, Vellipuram AR. Physiology, Mechanoreceptors. 2019.
287. Abaira VE, Ginty DD. The sensory neurons of touch. *Neuron.* 2013;79(4):618-639. doi:10.1016/j.neuron.2013.07.051
288. Zöllner AM, Holland MA, Honda KS, Gosain AK, Kuhl E. Growth on demand: reviewing the mechanobiology of stretched skin. *J Mech Behav Biomed Mater.* 2013;28:495-509.
289. Hamill OP, Martinac B. Molecular basis of mechanotransduction in living cells. *Physiol Rev.* 2001;81(2):685-740.
290. Sukharev S, Sachs F. Molecular force transduction by ion channels—diversity and unifying principles. *J Cell Sci.* 2012;125(13):3075-3083.
291. Ross RS. Molecular and mechanical synergy: cross-talk between integrins and growth factor receptors. *Cardiovasc Res.* 2004;63(3):381-390.
292. Boettiger D. Mechanical control of integrin-mediated adhesion and signaling. *Curr Opin Cell Biol.* 2012;24(5):592-599.
293. Wehrle-Haller B. Assembly and disassembly of cell matrix adhesions. *Curr Opin Cell Biol.* 2012;24(5):569-581.
294. Alon R, Feigelson SW. Chemokine-triggered leukocyte arrest: force-regulated bidirectional integrin activation in quantal adhesive contacts. *Curr Opin Cell Biol.* 2012;24(5):670-676.
295. Geiger T, Zaidel-Bar R. Opening the floodgates: proteomics and the integrin adhesome. *Curr Opin Cell Biol.* 2012;24(5):562-568.
296. Roca-Cusachs P, Iskratsch T, Sheetz MP. Finding the weakest link—exploring integrin-mediated mechanical molecular pathways. *J Cell Sci.* 2012;125(13):3025-3038.
297. Shen B, Delaney MK, Du X. Inside-out, outside-in, and inside-outside-in: G protein

REFERENCES

- signaling in integrin-mediated cell adhesion, spreading, and retraction. *Curr Opin Cell Biol.* 2012;24(5):600-606.
298. Levin SM. The tensegrity-truss as a model for spine mechanics: biotensegrity. *J Mech Med Biol.* 2002;2(03n04):375-388.
299. Fuller B. Tensegrity. *Portf Artnews Annu.* 1961;4:112-127.
300. Hohenschurz-Schmidt DJ, Esteves JE, Thomson OP. Tensegrity and manual therapy practice: a qualitative study. *Int J Osteopath Med.* 2016;21:5-18. doi:<https://doi.org/10.1016/j.ijosm.2016.02.001>
301. Coughlin MF. A tensegrity model of the cytoskeleton in spread and round cells. *J Biomech Eng.* 1998;120(6):770-777.
302. Volokh KY, Vilnay O, Belsky M. Cell cytoskeleton and tensegrity. *Biorheology.* 2002;39(1-2):63-67.
303. Vera C, Skelton R, Bossens F, Sung LA. 3-D nanomechanics of an erythrocyte junctional complex in equibiaxial and anisotropic deformations. *Ann Biomed Eng.* 2005;33(10):1387-1404.
304. Maniotis AJ, Chen CS, Ingber DE. Demonstration of mechanical connections between integrins, cytoskeletal filaments, and nucleoplasm that stabilize nuclear structure. *Proc Natl Acad Sci.* 1997;94(3):849-854.
305. Eckes B, Dogic D, Colucci-Guyon E, et al. Impaired mechanical stability, migration and contractile capacity in vimentin-deficient fibroblasts. *J Cell Sci.* 1998;111(13):1897-1907.
306. Hu S, Chen J, Butler JP, Wang N. Prestress mediates force propagation into the nucleus. *Biochem Biophys Res Commun.* 2005;329(2):423-428.
307. Nauli SM, Alenghat FJ, Luo Y, et al. Polycystins 1 and 2 mediate mechanosensation in the primary cilium of kidney cells. *Nat Genet.* 2003;33(2):129-137.
308. Brown TD. Finite element modeling in musculoskeletal biomechanics. *J Appl Biomech.* 2004;20(4):336-366. doi:10.1123/jab.20.4.336
309. Synge JL, Rheinboldt WC. The hypercircle in mathematical physics. *Phys Today.* 1957;10(10):45.
310. Argyris JH, Kelsey S. *Energy Theorems and Structural Analysis.* Vol 60. Springer; 1960.
311. Clough RW. The finite element method in plane stress analysis. In: *Proceedings of 2nd ASCE Conference on Electronic Computation, Pittsburgh Pa., Sept. 8 and 9, 1960.* ; 1960.
312. Rybicki EF, Simonen FA, Weis Jr EB. On the mathematical analysis of stress in the human femur. *J Biomech.* 1972;5(2):203-215.
313. Brekelmans WAM, Poort HW, Slooff T. A new method to analyse the mechanical behaviour of skeletal parts. *Acta Orthop Scand.* 1972;43(5):301-317.
314. Huiskes R, Chao EYS. A survey of finite element analysis in orthopedic biomechanics: the first decade. *J Biomech.* 1983;16(6):385-409.
315. Huiskes R, Hollister SJ. From structure to process, from organ to cell: recent developments of FE-analysis in orthopaedic biomechanics. 1993.
316. Schmid-Schönbein GW, Diller KR. Transport processes in biomedical systems: a roadmap for future research directions. *Ann Biomed Eng.* 2005;33(9):1136-1141. doi:10.1007/s10439-005-5633-y
317. Portnoy S, Yarnitzky G, Yizhar Z, et al. Real-time patient-specific finite element analysis of internal stresses in the soft tissues of a residual limb: a new tool for prosthetic fitting. *Ann*

DOCTORAL THESIS DANIEL MARTÍNEZ MORENO

- Biomed Eng.* 2007;35(1):120-135. doi:10.1007/s10439-006-9208-3
318. Speelman L, Bohra A, Bosboom EMH, et al. Effects of wall calcifications in patient-specific wall stress analyses of abdominal aortic aneurysms. *J Biomech Eng.* 2007;129(1):105-109. doi:10.1115/1.2401189
319. Wang L, Zhang H, Shi P, Liu H. Imaging of 3D cardiac electrical activity: a model-based recovery framework. *Med image Comput Comput Interv MICCAI . Int Conf Med Image Comput Comput Interv.* 2006;9(Pt 1):792-799. doi:10.1007/11866565_97
320. Spilker RL, Feinstein JA, Parker DW, Reddy VM, Taylor CA. Morphometry-based impedance boundary conditions for patient-specific modeling of blood flow in pulmonary arteries. *Ann Biomed Eng.* 2007;35(4):546-559. doi:10.1007/s10439-006-9240-3
321. Anderson AE, Peters CL, Tuttle BD, Weiss JA. Subject-specific finite element model of the pelvis: development, validation and sensitivity studies. *J Biomech Eng.* 2005;127(3):364-373. doi:10.1115/1.1894148
322. Li LP, Herzog W. Arthroscopic evaluation of cartilage degeneration using indentation testing--influence of indenter geometry. *Clin Biomech (Bristol, Avon).* 2006;21(4):420-426. doi:10.1016/j.clinbiomech.2005.12.010
323. Crawford RP, Rosenberg WS, Keaveny TM. Quantitative computed tomography-based finite element models of the human lumbar vertebral body: effect of element size on stiffness, damage, and fracture strength predictions. *J Biomech Eng.* 2003;125(4):434-438. doi:10.1115/1.1589772
324. Yang Y, Webb GI, Wu X. Discretization methods. In: *Data Mining and Knowledge Discovery Handbook.* Springer; 2009:101-116.
325. Delaunay B. Sur la sphere vide. *Izv Akad Nauk SSSR, Otd Mat i Estestv Nauk.* 1934;7(793-800):1-2.
326. Ruppert J. A Delaunay refinement algorithm for quality 2-dimensional mesh generation. *J algorithms.* 1995;18(3):548-585.
327. Lo DSH. *Finite Element Mesh Generation.* CRC Press; 2014.
328. Zhao W, Ji S. Mesh convergence behavior and the effect of element integration of a human head injury model. *Ann Biomed Eng.* 2019;47(2):475-486.
329. Valeš J, Kala Z. Mesh convergence study of solid FE model for buckling analysis. In: *AIP Conference Proceedings.* Vol 1978. AIP Publishing LLC; 2018:150005.
330. Szabo BA. *Estimation and Control Error Based on P-Convergence.* WASHINGTON UNIV ST LOUIS MO CENTER FOR COMPUTATIONAL MECHANICS; 1984.
331. Elhaddad M, Zander N, Bog T, et al. Multi-level hp-finite cell method for embedded interface problems with application in biomechanics. *Int j numer method biomed eng.* 2018;34(4):e2951.
332. Murat F, Tartar L. H-convergence, in "Topics in the mathematical modeling of composite materials", A. Cherkaev and R. Kohn Eds. *Prog Nonlinear Differ Equations Their Appl.* 1997;31.
333. Hart RT, Hennebel V V, Thongpreda N, Van Buskirk WC, Anderson RC. Modeling the biomechanics of the mandible: a three-dimensional finite element study. *J Biomech.* 1992;25(3):261-286.
334. Zeng H, Xu W, Zang M, Yang P, Guo X. Calibration and validation of DEM-FEM model parameters using upscaled particles based on physical experiments and simulations. *Adv Powder Technol.* 2020;31(9):3947-3959.

REFERENCES

335. Hassan CR, Qin Y-X, Komatsu DE, Uddin SMZ. Utilization of Finite Element Analysis for Articular Cartilage Tissue Engineering. *Materials (Basel)*. 2019;12(20). doi:10.3390/ma12203331
336. Soufivand AA, Abolfathi N, Hashemi SA, Lee SJ. Prediction of mechanical behavior of 3D bioprinted tissue-engineered scaffolds using finite element method (FEM) analysis. *Addit Manuf*. 2020;33:101181. doi:https://doi.org/10.1016/j.addma.2020.101181
337. Epari DR, Duda GN, Thompson MS, Tanner KE, Dalby MJ. Mechanobiology of bone healing and regeneration: in vivo models. *Proc Inst Mech Eng Part H J Eng Med*. 2010;224(12):1543-1553. doi:10.1243/09544119JEIM808
338. Jean A, Engelmayer GC. Finite element analysis of an accordion-like honeycomb scaffold for cardiac tissue engineering. *J Biomech*. 2010;43(15):3035-3043. doi:https://doi.org/10.1016/j.jbiomech.2010.06.032
339. Marwan SH, Todo M. Biomechanical Analysis of Left Ventricle Considering Myocardial Infarction and Regenerative Therapy Using Dynamic Finite Element Method. *J Biotechnol Biomed*. 2021;4(2):10-25.
340. Fritz M, Belcher AM, Radmacher M, et al. Flat pearls from biofabrication of organized composites on inorganic substrates. *Nature*. 1994;371(6492):49-51. doi:10.1038/371049a0
341. Fong H, White SN, Paine ML, Luo W, Snead ML, Sarikaya M. Enamel Structure Properties Controlled by Engineered Proteins in Transgenic Mice. *J Bone Miner Res*. 2003;18(11):2052-2059. doi:https://doi.org/10.1359/jbmr.2003.18.11.2052
342. Harrison RG. Observations on the living developing nerve fiber. *Proc Soc Exp Biol Med*. 1906;4(1):140-143.
343. Steinberg MS. Reconstruction of tissues by dissociated cells: some morphogenetic tissue movements and the sorting out of embryonic cells may have a common explanation. *Science (80-)*. 1963;141(3579):401-408.
344. Forgacs G, Foty RA, Shafrir Y, Steinberg MS. Viscoelastic properties of living embryonic tissues: a quantitative study. *Biophys J*. 1998;74(5):2227-2234.
345. Foty RA, Pflieger CM, Forgacs G, Steinberg MS. Surface tensions of embryonic tissues predict their mutual envelopment behavior. *Development*. 1996;122(5):1611-1620.
346. Foty RA, Forgacs G, Pflieger CM, Steinberg MS. Liquid properties of embryonic tissues: measurement of interfacial tensions. *Phys Rev Lett*. 1994;72(14):2298.
347. Liu Y, Kim E, Ghodssi R, et al. Biofabrication to build the biology-device interface. *Biofabrication*. 2010;2(2):22002. doi:10.1088/1758-5082/2/2/022002
348. Hollister SJ. Porous scaffold design for tissue engineering. *Nat Mater*. 2005;4(7):518-524. doi:10.1038/nmat1421
349. Hutmacher DW, Sittinger M, Risbud M V. Scaffold-based tissue engineering: rationale for computer-aided design and solid free-form fabrication systems. *Trends Biotechnol*. 2004;22(7):354-362. doi:10.1016/j.tibtech.2004.05.005
350. Weigel T, Schinkel G, Lendlein A. Design and preparation of polymeric scaffolds for tissue engineering. *Expert Rev Med Devices*. 2006;3(6):835-851. doi:10.1586/17434440.3.6.835
351. Peltola SM, Melchels FPW, Grijpma DW, Kellomäki M. A review of rapid prototyping techniques for tissue engineering purposes. *Ann Med*. 2008;40(4):268-280. doi:10.1080/07853890701881788
352. Sun W, Lal P. Recent development on computer aided tissue engineering — a review.

DOCTORAL THESIS DANIEL MARTÍNEZ MORENO

- Comput Methods Programs Biomed.* 2002;67(2):85-103.
doi:[https://doi.org/10.1016/S0169-2607\(01\)00116-X](https://doi.org/10.1016/S0169-2607(01)00116-X)
353. Yeong W-Y, Chua C-K, Leong K-F, Chandrasekaran M. Rapid prototyping in tissue engineering: challenges and potential. *Trends Biotechnol.* 2004;22(12):643-652. doi:10.1016/j.tibtech.2004.10.004
354. Zaremba CM, Belcher AM, Fritz M, et al. Critical Transitions in the Biofabrication of Abalone Shells and Flat Pearls. *Chem Mater.* 1996;8(3):679-690. doi:10.1021/cm9503285
355. Schröder HC, Wang X, Tremel W, Ushijima H, Müller WEG. Biofabrication of biosilica-glass by living organisms. *Nat Prod Rep.* 2008;25(3):455-474. doi:10.1039/B612515H
356. Luo X. Biofabrication in Microfluidics: A Converging Fabrication Paradigm to Exploit Biology in Microsystems. *J Bioeng Biomed Sci.* 2012;02(03):2-4. doi:10.4172/2155-9538.1000e104
357. Groll J, Boland T, Blunk T, et al. Biofabrication: Reappraising the definition of an evolving field. *Biofabrication.* 2016;8(1). doi:10.1088/1758-5090/8/1/013001
358. Guillemot F, Mironov V, Nakamura M. Bioprinting is coming of age: Report from the International Conference on Bioprinting and Biofabrication in Bordeaux (3B'09). In: *Biofabrication.* ; 2010. doi:10.1088/1758-5082/2/1/010201
359. Guven S, Chen P, Inci F, Tasoglu S, Erkmen B, Demirci U. Multiscale assembly for tissue engineering and regenerative medicine. *Trends Biotechnol.* 2015;33(5):269-279. doi:10.1016/j.tibtech.2015.02.003
360. Moroni L, Boland T, Burdick JA, et al. Biofabrication: A Guide to Technology and Terminology. *Trends Biotechnol.* 2018;36(4):384-402. doi:10.1016/j.tibtech.2017.10.015
361. Deckard CR. *Selective Laser Sintering.* The University of Texas at Austin; 1988.
362. Kruth JP, Wang X, Laoui T, Froyen L. Lasers and materials in selective laser sintering. *Assem Autom.* 2003;23(4):357-371. doi:10.1108/01445150310698652
363. Tan KH, Chua CK, Leong KF, et al. Selective laser sintering of biocompatible polymers for applications in tissue engineering. *Biomed Mater Eng.* 2005;15:113-124.
364. Simpson RL, Wiria FE, Amis AA, et al. Development of a 95/5 poly(L-lactide-co-glycolide)/hydroxylapatite and β -tricalcium phosphate scaffold as bone replacement material via selective laser sintering. *J Biomed Mater Res Part B Appl Biomater.* 2008;84B(1):17-25. doi:<https://doi.org/10.1002/jbm.b.30839>
365. Zhou WY, Lee SH, Wang M, Cheung WL, Ip WY. Selective laser sintering of porous tissue engineering scaffolds from poly(l-lactide)/carbonated hydroxyapatite nanocomposite microspheres. *J Mater Sci Mater Med.* 2008;19(7):2535-2540. doi:10.1007/s10856-007-3089-3
366. Wiria FE, Leong KF, Chua CK, Liu Y. Poly- ϵ -caprolactone/hydroxyapatite for tissue engineering scaffold fabrication via selective laser sintering. *Acta Biomater.* 2007;3(1):1-12.
367. Zhang H, Lin C-Y, Hollister SJ. The interaction between bone marrow stromal cells and RGD-modified three-dimensional porous polycaprolactone scaffolds. *Biomaterials.* 2009;30(25):4063-4069.
368. Du Y, Liu H, Shuang J, Wang J, Ma J, Zhang S. Microsphere-based selective laser sintering for building macroporous bone scaffolds with controlled microstructure and excellent biocompatibility. *Colloids Surfaces B Biointerfaces.* 2015;135:81-89.
369. Sherwood JK, Riley SL, Palazzolo R, et al. A three-dimensional osteochondral composite

REFERENCES

- scaffold for articular cartilage repair. *Biomaterials*. 2002;23(24):4739-4751. doi:[https://doi.org/10.1016/S0142-9612\(02\)00223-5](https://doi.org/10.1016/S0142-9612(02)00223-5)
370. Williams JM, Adewunmi A, Schek RM, et al. Bone tissue engineering using polycaprolactone scaffolds fabricated via selective laser sintering. *Biomaterials*. 2005;26(23):4817-4827. doi:<https://doi.org/10.1016/j.biomaterials.2004.11.057>
371. Sarig-Nadir O, Livnat N, Zajdman R, Shoham S, Seliktar D. Laser Photoablation of Guidance Microchannels into Hydrogels Directs Cell Growth in Three Dimensions. *Biophys J*. 2009;96(11):4743-4752. doi:<https://doi.org/10.1016/j.bpj.2009.03.019>
372. Antonov EN, Bagratashvili VN, Whitaker MJ, et al. Three-Dimensional Bioactive and Biodegradable Scaffolds Fabricated by Surface-Selective Laser Sintering. *Adv Mater*. 2005;17(3):327-330. doi:<https://doi.org/10.1002/adma.200400838>
373. Gu BK, Choi DJ, Park SJ, Kim MS, Kang CM, Kim CH. 3-Dimensional Bioprinting for Tissue Engineering Applications. *Biomater Res*. 2016;20(1):1-8. doi:10.1186/s40824-016-0058-2
374. Chu T-MG, Orton DG, Hollister SJ, Feinberg SE, Halloran JW. Mechanical and in vivo performance of hydroxyapatite implants with controlled architectures. *Biomaterials*. 2002;23(5):1283-1293. doi:[https://doi.org/10.1016/S0142-9612\(01\)00243-5](https://doi.org/10.1016/S0142-9612(01)00243-5)
375. Jakubiak J, Rabek JF. Three-dimensional (3D) photopolymerization in stereolithography. Part I: fundamentals of 3D photopolymerization. *Polimery*. 2000;45(11-12).
376. Lee JH, Prud'Homme RK, Aksay IA. Cure depth in photopolymerization: Experiments and theory. *J Mater Res*. 2001;16(12):3536-3544.
377. Hull CW. Apparatus for production of three-dimensional objects by stereolithography. March 1986.
378. Melchels FPW, Feijen J, Grijpma DW. A poly(D,L-lactide) resin for the preparation of tissue engineering scaffolds by stereolithography. *Biomaterials*. 2009;30(23):3801-3809. doi:<https://doi.org/10.1016/j.biomaterials.2009.03.055>
379. Gauvin R, Chen Y-C, Lee JW, et al. Microfabrication of complex porous tissue engineering scaffolds using 3D projection stereolithography. *Biomaterials*. 2012;33(15):3824-3834. doi:<https://doi.org/10.1016/j.biomaterials.2012.01.048>
380. Wang Z, Abdulla R, Parker B, Samanipour R, Ghosh S, Kim K. A simple and high-resolution stereolithography-based 3D bioprinting system using visible light crosslinkable bioinks. *Biofabrication*. 2015;7(4):45009.
381. Ovsianikov A, Schlie S, Ngezahayo A, Haverich A, Chichkov BN. Two-photon polymerization technique for microfabrication of CAD-designed 3D scaffolds from commercially available photosensitive materials. *J Tissue Eng Regen Med*. 2007;1(6):443-449. doi:<https://doi.org/10.1002/term.57>
382. Ovsianikov A, Chichkov BN. Three-Dimensional Microfabrication by Two-Photon Polymerization Technique BT - Computer-Aided Tissue Engineering. In: Liebschner MAK, ed. Totowa, NJ: Humana Press; 2012:311-325. doi:10.1007/978-1-61779-764-4_19
383. Capone GJ. Wet-spinning technology. *Acrylic fiber Technol Appl*. 1995:69-103.
384. Tuzlakoglu K, Reis RL. Chitosan-based scaffolds in orthopedic applications. In: *Natural-Based Polymers for Biomedical Applications*. Elsevier; 2008:357-373.
385. Mathiowitz E, Lavin DM, Hopkins RA. Wet spun microfibers: potential in the design of controlled-release scaffolds? *Ther Deliv*. 2013;4(9):1075-1077.
386. Hirano S, Zhang M, Nakagawa M. Release of glycosaminoglycans in physiological saline and

DOCTORAL THESIS DANIEL MARTÍNEZ MORENO

- water by wet-spun chitin–acid glycosaminoglycan fibers. *J Biomed Mater Res An Off J Soc Biomater Japanese Soc Biomater Aust Soc Biomater Korean Soc Biomater*. 2001;56(4):556-561.
387. Gao H, Gu Y, Ping Q. The implantable 5-fluorouracil-loaded poly (l-lactic acid) fibers prepared by wet-spinning from suspension. *J Control Release*. 2007;118(3):325-332.
388. Jung M-R, Shim I-K, Kim E-S, et al. Controlled release of cell-permeable gene complex from poly (L-lactide) scaffold for enhanced stem cell tissue engineering. *J Control release*. 2011;152(2):294-302.
389. Nie H-L, Ma Z-H, Fan Z-X, et al. Polyacrylonitrile fibers efficiently loaded with tamoxifen citrate using wet-spinning from co-dissolving solution. *Int J Pharm*. 2009;373(1-2):4-9.
390. Rissanen M, Puolakka A, Ahola N, et al. Effect of protein-loading on properties of wet-spun poly (l, d-lactide) multifilament fibers. *J Appl Polym Sci*. 2010;116(4):2174-2180.
391. Lavin DM, Zhang L, Furtado S, Hopkins RA, Mathiowitz E. Effects of protein molecular weight on the intrinsic material properties and release kinetics of wet spun polymeric microfiber delivery systems. *Acta Biomater*. 2013;9(1):4569-4578.
392. Puppi D, Zhang X, Yang L, Chiellini F, Sun X, Chiellini E. Nano/microfibrous polymeric constructs loaded with bioactive agents and designed for tissue engineering applications: a review. *J Biomed Mater Res Part B Appl Biomater*. 2014;102(7):1562-1579.
393. Puppi D, Dinucci D, Bartoli C, et al. Development of 3D wet-spun polymeric scaffolds loaded with antimicrobial agents for bone engineering. *J Bioact Compat Polym*. 2011;26(5):478-492.
394. Puppi D, Chiellini F. Wet-spinning of biomedical polymers from single-fibre production to additive. *Polym Int*. 2017;66:1690-1696.
395. Puppi D, Mota C, Gazzarri M, et al. Additive manufacturing of wet-spun polymeric scaffolds for bone tissue engineering. *Biomed Microdevices*. 2012;14(6):1115-1127. doi:10.1007/s10544-012-9677-0
396. Vozzi G, Previti A, De Rossi D, Ahluwalia A. Microsyringe-Based Deposition of Two-Dimensional and Three-Dimensional Polymer Scaffolds with a Well-Defined Geometry for Application to Tissue Engineering. *Tissue Eng*. 2002;8(6):1089-1098. doi:10.1089/107632702320934182
397. Tucker N, Stanger JJ, Staiger MP, Razzaq H, Hofman K. The history of the science and technology of electrospinning from 1600 to 1995. *J Eng Fiber Fabr*. 2012;7(3):63-73. doi:10.1177/155892501200702s10
398. Jiang T, Carbone EJ, Lo KW-H, Laurencin CT. Electrospinning of polymer nanofibers for tissue regeneration. *Prog Polym Sci*. 2015;46:1-24.
399. Sun B, Long YZ, Zhang HD, et al. Advances in three-dimensional nanofibrous macrostructures via electrospinning. *Prog Polym Sci*. 2014;39(5):862-890.
400. Liu W, Thomopoulos S, Xia Y. Electrospun nanofibers for regenerative medicine. *Adv Healthc Mater*. 2012;1(1):10-25.
401. Agarwal S, Wendorff JH, Greiner A. Use of electrospinning technique for biomedical applications. *Polymer (Guildf)*. 2008;49(26):5603-5621.
402. Cooley JF. Electrical method of dispersing fluids. November 1903.
403. Huang Z-M, Zhang Y-Z, Kotaki M, Ramakrishna S. A review on polymer nanofibers by electrospinning and their applications in nanocomposites. *Compos Sci Technol*. 2003;63(15):2223-2253.

REFERENCES

404. Teo WE, Ramakrishna S. A review on electrospinning design and nanofibre assemblies. *Nanotechnology*. 2006;17(14):R89.
405. Xue J, Xie J, Liu W, Xia Y. Electrospun nanofibers: new concepts, materials, and applications. *Acc Chem Res*. 2017;50(8):1976-1987.
406. Haider A, Haider S, Kang I-K. A comprehensive review summarizing the effect of electrospinning parameters and potential applications of nanofibers in biomedical and biotechnology. *Arab J Chem*. 2018;11(8):1165-1188.
407. Sill TJ, Von Recum HA. Electrospinning: applications in drug delivery and tissue engineering. *Biomaterials*. 2008;29(13):1989-2006.
408. Lannutti J, Reneker D, Ma T, Tomasko D, Farson D. Electrospinning for tissue engineering scaffolds. *Mater Sci Eng C*. 2007;27(3):504-509.
409. Brown TD, Dalton PD, Hutmacher DW. Direct Writing By Way of Melt Electrospinning. *Adv Mater*. 2011;23(47):5651-5657. doi:<https://doi.org/10.1002/adma.201103482>
410. Ji Y, Ghosh K, Li B, Sokolov JC, Clark RAF, Rafailovich MH. Dual-Syringe Reactive Electrospinning of Cross-Linked Hyaluronic Acid Hydrogel Nanofibers for Tissue Engineering Applications. *Macromol Biosci*. 2006;6(10):811-817. doi:<https://doi.org/10.1002/mabi.200600132>
411. Jin G, Lee S, Kim S-H, Kim M, Jang J-H. Bicomponent electrospinning to fabricate three-dimensional hydrogel-hybrid nanofibrous scaffolds with spatial fiber tortuosity. *Biomed Microdevices*. 2014;16(6):793-804. doi:10.1007/s10544-014-9883-z
412. Moroni L, de Wijn JR, van Blitterswijk CA. 3D fiber-deposited scaffolds for tissue engineering: Influence of pores geometry and architecture on dynamic mechanical properties. *Biomaterials*. 2006;27(7):974-985. doi:<https://doi.org/10.1016/j.biomaterials.2005.07.023>
413. Woodfield TBF, Blitterswijk CA Van, Wijn J De, Sims TJ, Hollander AP, Riesle J. Polymer Scaffolds Fabricated with Pore-Size Gradients as a Model for Studying the Zonal Organization within Tissue-Engineered Cartilage Constructs. *Tissue Eng*. 2005;11(9-10):1297-1311. doi:10.1089/ten.2005.11.1297
414. Critchley S, Sheehy EJ, Cunniffe G, et al. 3D printing of fibre-reinforced cartilaginous templates for the regeneration of osteochondral defects. *Acta Biomater*. 2020;113:130-143. doi:10.1016/j.actbio.2020.05.040
415. Suo H, Zhang J, Xu M, Wang L. Low-temperature 3D printing of collagen and chitosan composite for tissue engineering. *Mater Sci Eng C Mater Biol Appl*. 2021;123:111963. doi:10.1016/j.msec.2021.111963
416. Anadioti E, Kane B, Soulas E. Current and Emerging Applications of 3D Printing in Restorative Dentistry. *Curr Oral Heal Reports*. 2018;5(2):133-139. doi:10.1007/s40496-018-0181-3
417. Yan Y, Xiong Z, Hu Y, Wang S, Zhang R, Zhang C. Layered manufacturing of tissue engineering scaffolds via multi-nozzle deposition. *Mater Lett*. 2003;57(18):2623-2628. doi:[https://doi.org/10.1016/S0167-577X\(02\)01339-3](https://doi.org/10.1016/S0167-577X(02)01339-3)
418. Woodfield TBF, Malda J, De Wijn J, Péters F, Riesle J, Van Blitterswijk CA. Design of porous scaffolds for cartilage tissue engineering using a three-dimensional fiber-deposition technique. *Biomaterials*. 2004. doi:10.1016/j.biomaterials.2003.10.056
419. Hoque ME, Hutmacher DW, Feng W, et al. Fabrication using a rapid prototyping system and in vitro characterization of PEG-PCL-PLA scaffolds for tissue engineering. *J Biomater Sci Polym Ed*. 2005;16(12):1595-1610. doi:10.1163/156856205774576709

DOCTORAL THESIS DANIEL MARTÍNEZ MORENO

420. Schantz J-T, Brandwood A, Hutmacher DW, Khor HL, Bittner K. Osteogenic differentiation of mesenchymal progenitor cells in computer designed fibrin-polymer-ceramic scaffolds manufactured by fused deposition modeling. *J Mater Sci Mater Med*. 2005;16(9):807-819. doi:10.1007/s10856-005-3584-3
421. Hutmacher DW, Ng KW, Kaps C, Sittinger M, Kläring S. Elastic cartilage engineering using novel scaffold architectures in combination with a biomimetic cell carrier. *Biomaterials*. 2003;24(24):4445-4458. doi:https://doi.org/10.1016/S0142-9612(03)00350-8
422. Hubbell JA. Hydrogel systems for barriers and local drug delivery in the control of wound healing. *J Control Release*. 1996;39(2):305-313. doi:https://doi.org/10.1016/0168-3659(95)00162-X
423. Pati F, Jang J, Ha DH, et al. Printing three-dimensional tissue analogues with decellularized extracellular matrix bioink. *Nat Commun*. 2014. doi:10.1038/ncomms4935
424. Hennink WE, van Nostrum CF. Novel crosslinking methods to design hydrogels. *Adv Drug Deliv Rev*. 2012. doi:10.1016/j.addr.2012.09.009
425. Atala A. Engineering organs. *Curr Opin Biotechnol*. 2009. doi:10.1016/j.copbio.2009.10.003
426. Paris H, Mokhtarian H, Coatanéa E, Museau M, Ituarte IF. Comparative environmental impacts of additive and subtractive manufacturing technologies. *CIRP Ann - Manuf Technol*. 2016. doi:10.1016/j.cirp.2016.04.036
427. Ozbolat IT. Bioprinting scale-up tissue and organ constructs for transplantation. *Trends Biotechnol*. 2015. doi:10.1016/j.tibtech.2015.04.005
428. Ozbolat IT. Introduction. *3D Bioprinting*. 2017:1-12. doi:10.1016/B978-0-12-803010-3.00001-9
429. Hull CW. Apparatus for Production of Three-Dimensional Objects By Stereo Thography. *Patent*. 1984.
430. Klebe RJ. Cytoscribing: a method for micropositioning cells and the construction of two- and three-dimensional synthetic tissues. *Exp Cell Res*. 1988;179(2):362-373. doi:10.1016/0014-4827(88)90275-3
431. Průša J. What's up with Original Prusa i3? Prusa Printers.
432. Bowyer A (Bath U. Wealth Without Money. University of Bath. https://reaprap.org/wiki/Wealth_Without_Money. Published 2004. Accessed July 16, 2020.
433. Mironov V, Reis N, Derby B. Bioprinting: A beginning. *Tissue Eng*. 2006;12(4):631-634.
434. Odde DJ, Renn MJ. Laser-guided direct writing for applications in biotechnology. *Trends Biotechnol*. 1999. doi:10.1016/S0167-7799(99)01355-4
435. Wilson WC, Boland T. Cell and organ printing 1: Protein and cell printers. *Anat Rec - Part A Discov Mol Cell Evol Biol*. 2003. doi:10.1002/ar.a.10057
436. Mironov V. Printing technology to produce living tissue. *Expert Opin Biol Ther*. 2003. doi:10.1517/14712598.3.5.701
437. Rai B, Teoh SH, Hutmacher DW, Cao T, Ho KH. Novel PCL-based honeycomb scaffolds as drug delivery systems for rhBMP-2. *Biomaterials*. 2005. doi:10.1016/j.biomaterials.2004.09.052
438. Murphy K, Dorfman S, Law RJ, LE VA. Devices, systems, and methods for the fabrication of tissue utilizing uv cross-linking. 2012:68.

REFERENCES

439. Ozbolat IT, Yu Y. Bioprinting toward organ fabrication: Challenges and future trends. *IEEE Trans Biomed Eng.* 2013. doi:10.1109/TBME.2013.2243912
440. Bajaj P, Schweller RM, Khademhosseini A, West JL, Bashir R. 3D Biofabrication Strategies for Tissue Engineering and Regenerative Medicine. *Annu Rev Biomed Eng.* 2014. doi:10.1146/annurev-bioeng-071813-105155
441. Cui H, Nowicki M, Fisher JP, Zhang LG. 3D Bioprinting for Organ Regeneration. *Adv Healthc Mater.* 2017. doi:10.1002/adhm.201601118
442. Faulkner-Jones A, Fyfe C, Cornelissen DJ, et al. Bioprinting of human pluripotent stem cells and their directed differentiation into hepatocyte-like cells for the generation of mini-livers in 3D. *Biofabrication.* 2015. doi:10.1088/1758-5090/7/4/044102
443. Dittrich PS, Manz A. Lab-on-a-chip: microfluidics in drug discovery. *Nat Rev Drug Discov.* 2006;5(3):210-218.
444. Peng W, Datta P, Ayan B, Ozbolat V, Sosnoski D, Ozbolat IT. 3D bioprinting for drug discovery and development in pharmaceuticals. *Acta Biomater.* 2017. doi:10.1016/j.actbio.2017.05.025
445. Vermeulen N, Haddow G, Seymour T, Faulkner-Jones A, Shu W. 3D bioprint me: a socioethical view of bioprinting human organs and tissues. *J Med Ethics.* 2017;43(9):618-624. doi:10.1136/medethics-2015-103347
446. Sun W, Starly B, Daly AC, et al. The bioprinting roadmap. *Biofabrication.* 2020;12(2). doi:10.1088/1758-5090/ab5158
447. Gao G, Huang Y, Schilling AF, Hubbell K, Cui X. Organ Bioprinting: Are We There Yet? *Adv Healthc Mater.* 2018;7(1):1-8. doi:10.1002/adhm.201701018
448. Nie J, Gao Q, Fu J, He Y. Grafting of 3D Bioprinting to In Vitro Drug Screening: A Review. *Adv Healthc Mater.* 2020;1901773:1-18. doi:10.1002/adhm.201901773
449. Groll J, Burdick JA, Cho DW, et al. A definition of bioinks and their distinction from biomaterial inks. *Biofabrication.* 2019;11(1). doi:10.1088/1758-5090/aaec52
450. Rutz AL, Hyland KE, Jakus AE, Burghardt WR, Shah RN. A multimaterial bioink method for 3D printing tunable, cell-compatible hydrogels. *Adv Mater.* 2015. doi:10.1002/adma.201405076
451. Schuurman W, Khristov V, Pot MW, Van Weeren PR, Dhert WJA, Malda J. Bioprinting of hybrid tissue constructs with tailorable mechanical properties. *Biofabrication.* 2011. doi:10.1088/1758-5082/3/2/021001
452. Shim J-H, Kim JY, Park M, Park J, Cho D-W. Development of a hybrid scaffold with synthetic biomaterials and hydrogel using solid freeform fabrication technology. *Biofabrication.* 2011;3(3):34102.
453. Ahlfeld T, Guduric V, Duin S, et al. Methylcellulose—a versatile printing material that enables biofabrication of tissue equivalents with high shape fidelity. *Biomater Sci.* 2020;8(8):2102-2110.
454. Gungor-Ozkerim PS, Inci I, Zhang YS, Khademhosseini A, Dokmeci MR. Bioinks for 3D bioprinting: An overview. *Biomater Sci.* 2018. doi:10.1039/c7bm00765e
455. Ahmed EM. Hydrogel: Preparation, characterization, and applications: A review. *J Adv Res.* 2015;6(2):105-121. doi:10.1016/j.jare.2013.07.006
456. Ozbolat IT, Hospodiuk M. Current advances and future perspectives in extrusion-based bioprinting. *Biomaterials.* 2016. doi:10.1016/j.biomaterials.2015.10.076
457. Yu Y, Ozbolat IT. Tissue strands as “bioink” for scale-up organ printing. In: *2014 36th*

DOCTORAL THESIS DANIEL MARTÍNEZ MORENO

- Annual International Conference of the IEEE Engineering in Medicine and Biology Society, EMBC 2014.* ; 2014. doi:10.1109/EMBC.2014.6943868
458. Ozbolat IT. *The Bioink* [With Contributions by Monika Hospodiuk and Madhuri Dey, The Pennsylvania State University.]; 2017. doi:10.1016/b978-0-12-803010-3.00003-2
459. Dzobo K, Motaung KSCM, Adesida A. Recent trends in decellularized extracellular matrix bioinks for 3D printing: An updated review. *Int J Mol Sci.* 2019;20(18):1-28. doi:10.3390/ijms20184628
460. Goh TKP, Zhang ZY, Chen AKL, et al. Microcarrier culture for efficient expansion and osteogenic differentiation of human fetal mesenchymal stem cells. *Biores Open Access.* 2013. doi:10.1089/biores.2013.0001
461. Li B, Wang X, Wang Y, et al. Past, present, and future of microcarrier-based tissue engineering. *J Orthop Transl.* 2015. doi:10.1016/j.jot.2015.02.003
462. Ozbolat IT. *The Bioink.* In: *3D Bioprinting.* ; 2017.
463. Mironov V, Visconti RP, Kasyanov V, Forgacs G, Drake CJ, Markwald RR. Organ printing: Tissue spheroids as building blocks. *Biomaterials.* 2009. doi:10.1016/j.biomaterials.2008.12.084
464. Tappa K, Jammalamadaka U. Novel biomaterials used in medical 3D printing techniques. *J Funct Biomater.* 2018;9(1). doi:10.3390/jfb9010017
465. Murphy S V., Atala A. 3D bioprinting of tissues and organs. *Nat Biotechnol.* 2014. doi:10.1038/nbt.2958
466. Christensen K, Xu C, Chai W, Zhang Z, Fu J, Huang Y. Freeform inkjet printing of cellular structures with bifurcations. *Biotechnol Bioeng.* 2015. doi:10.1002/bit.25501
467. Lee VK, Lanzi AM, Ngo H, Yoo SS, Vincent PA, Dai G. Generation of multi-scale vascular network system within 3D hydrogel using 3D bio-printing technology. *Cell Mol Bioeng.* 2014. doi:10.1007/s12195-014-0340-0
468. Xu C, Chai W, Huang Y, Markwald RR. Scaffold-free inkjet printing of three-dimensional zigzag cellular tubes. *Biotechnol Bioeng.* 2012. doi:10.1002/bit.24591
469. Pati F, Jang J, Lee JW, Cho DW. Extrusion bioprinting. In: *Essentials of 3D Biofabrication and Translation.* ; 2015. doi:10.1016/B978-0-12-800972-7.00007-4
470. Chimene D, Lennox KK, Kaunas RR, Gaharwar AK. Advanced Bioinks for 3D Printing: A Materials Science Perspective. *Ann Biomed Eng.* 2016. doi:10.1007/s10439-016-1638-y
471. Kim BF, Bohandy J, Adrian FJ. Method and apparatus for the thin film deposition of materials with a high power pulsed laser. 1988:6. <https://patents.google.com/patent/US4970196A/en>.
472. Keriquel V, Oliveira H, Rémy M, et al. In situ printing of mesenchymal stromal cells, by laser-assisted bioprinting, for in vivo bone regeneration applications. *Sci Rep.* 2017. doi:10.1038/s41598-017-01914-x
473. Yue K, Trujillo-de Santiago G, Alvarez MM, Tamayol A, Annabi N, Khademhosseini A. Synthesis, properties, and biomedical applications of gelatin methacryloyl (GelMA) hydrogels. *Biomaterials.* 2015. doi:10.1016/j.biomaterials.2015.08.045
474. Guvendiren M, Molde J, Soares RMD, Kohn J. Designing Biomaterials for 3D Printing. *ACS Biomater Sci Eng.* 2016;2(10):1679-1693. doi:10.1021/acsbiomaterials.6b00121
475. Wan Z, Zhang P, Liu Y, Lv L, Zhou Y. Four-dimensional bioprinting: Current developments and applications in bone tissue engineering. *Acta Biomater.* 2020;101:26-42. doi:10.1016/j.actbio.2019.10.038

REFERENCES

476. Morrison RJ, Hollister SJ, Niedner MF, et al. Mitigation of tracheobronchomalacia with 3D-printed personalized medical devices in pediatric patients (Science Translational Medicine (2015) 7 (287er4)). *Sci Transl Med.* 2015;7(287):1-12. doi:10.1126/scitranslmed.aac4749
477. Tibbits S. 4D printing: multi-material shape change. *Archit Des.* 2014;84(1):116-121.
478. Momeni F, Liu X, Ni J. A review of 4D printing. *Mater Des.* 2017;122:42-79.
479. Liu X, Zhao K, Gong T, et al. Delivery of growth factors using a smart porous nanocomposite scaffold to repair a mandibular bone defect. *Biomacromolecules.* 2014;15(3):1019-1030.
480. Hager MD, Bode S, Weber C, Schubert US. Shape memory polymers: past, present and future developments. *Prog Polym Sci.* 2015;49:3-33.
481. Kuksenok O, Balazs AC. Stimuli-responsive behavior of composites integrating thermo-responsive gels with photo-responsive fibers. *Mater Horizons.* 2016;3(1):53-62.
482. Ozbolat IT, Moncal KK, Gudapati H. Evaluation of bioprinter technologies. *Addit Manuf.* 2017;13:179-200. doi:10.1016/j.addma.2016.10.003
483. Choudhury D, Anand S, Naing MW. The arrival of commercial bioprinters - Towards 3D bioprinting revolution! *Int J Bioprinting.* 2018;4(2). doi:10.18063/IJB.v4i2.139
484. Oberweis CV, Marchal JA, López-Ruiz E, Gálvez-Martín P. A Worldwide Overview of Regulatory Frameworks for Tissue-Based Products. *Tissue Eng Part B Rev.* 2020;26(2):181-196. doi:10.1089/ten.TEB.2019.0315
485. López-Beas J, Guadix JA, Clares B, Soriano-Ruiz JL, Zugaza JL, Gálvez-Martín P. An overview of international regulatory frameworks for mesenchymal stromal cell-based medicinal products: From laboratory to patient. *Med Res Rev.* February 2020. doi:10.1002/med.21659
486. Guadix JA, López-Beas J, Clares B, Soriano-Ruiz JL, Zugaza JL, Gálvez-Martín P. Principal Criteria for Evaluating the Quality, Safety and Efficacy of hMSC-Based Products in Clinical Practice: Current Approaches and Challenges. *Pharmaceutics.* 2019;11(11). doi:10.3390/pharmaceutics11110552
487. Singh YP, Bandyopadhyay A, Mandal BB. 3D Bioprinting Using Cross-Linker-Free Silk-Gelatin Bioink for Cartilage Tissue Engineering. *ACS Appl Mater Interfaces.* 2019;11(37):33684-33696. doi:10.1021/acsami.9b11644
488. Piard C, Baker H, Kamalidinov T, Fisher J. Bioprinted osteon-like scaffolds enhance in vivo neovascularization. *Biofabrication.* 2019;11(2):25013. doi:10.1088/1758-5090/ab078a
489. Soetaert W, Vandamme EJ. *Industrial Biotechnology: Sustainable Growth and Economic Success.* John Wiley & Sons; 2010.
490. Mason SF. A History of the Sciences. 1962.
491. Pasteur L. Sur la fermentation appelee lactique. *Ann Chim Phys.* 1858;3.
492. Gillen AL, Sherwin F. Louis Pasteur's views on creation, evolution, and the genesis of germs. 2008.
493. Ciferri O, Tiboni O. The biochemistry and industrial potential of Spirulina. *Annu Rev Microbiol.* 1985;39(1):503-526.
494. Santangelo JD, Dürre P. Microbial production of acetone and butanol: Can history be repeated? *Chim Oggi.* 1996:29-36.
495. Brown K, Dosani S. Reviews-MULTIMEDIA-Book: Penicillin Man: Alexander Fleming and the Antibiotic Revolution. *BMJ-British Med Journal-International Ed.* 2005;330(7481):48-

- 49.
496. Aminov RI. A brief history of the antibiotic era: lessons learned and challenges for the future. *Front Microbiol.* 2010;1:134.
497. Ratledge C, Kristiansen B. *Basic Biotechnology.* Cambridge University Press; 2001.
498. Freshney RI. *Culture of Animal Cells: A Manual of Basic Technique and Specialized Applications.* John Wiley & Sons; 2015.
499. Köhler G, Milstein C. Continuous cultures of fused cells secreting antibody of predefined specificity. *Nature.* 1975;256(5517):495-497.
500. Butler M, Meneses-Acosta A. Recent advances in technology supporting biopharmaceutical production from mammalian cells. *Appl Microbiol Biotechnol.* 2012;96(4):885-894.
501. Hamilton WF. Corporate strategies for managing emerging technologies. In: *Technology in the Modern Corporation.* Elsevier; 1986:103-118.
502. Pisano G. Can science be a business. *Harv Bus Rev.* 2006;10:1-12.
503. Serra M, Brito C, Correia C, Alves PM. Process engineering of human pluripotent stem cells for clinical application. *Trends Biotechnol.* 2012;30(6):350-359.
504. Mabvuure N, Hindocha S, S. Khan W. The Role of Bioreactors in Cartilage Tissue Engineering. *Curr Stem Cell Res Ther.* 2012;7(4):287-292. doi:10.2174/157488812800793018
505. Wang S-J, Zhong J-J. Chapter 6 - Bioreactor Engineering. In: Yang S-TBT-B for V-AP from RR, ed. Amsterdam: Elsevier; 2007:131-161. doi:https://doi.org/10.1016/B978-044452114-9/50007-4
506. Freed LE. Tissue culture bioreactors: chondrogenesis as a model system. *Princ tissue Eng.* 1997.
507. Strehl R, Schumacher K, De Vries U, Minuth WW. Proliferating cells versus differentiated cells in tissue engineering. *Tissue Eng.* 2002;8(1):37-42.
508. Selden C, Fuller B. Role of bioreactor technology in tissue engineering for clinical use and therapeutic target design. *Bioengineering.* 2018;5(2):1-10. doi:10.3390/bioengineering5020032
509. Sinclair A, Ashley MH. Sterilization and containment. *Bioprocess Technol.* 1995;21:553-588.
510. Cummings LJ, Waters SL. Tissue growth in a rotating bioreactor. Part II: fluid flow and nutrient transport problems. *Math Med Biol.* 2007;24(2):169-208.
511. Abdullah NS, Jones DR, Das DB. Nutrient transport in bioreactors for bone tissue growth: why do hollow fibre membrane bioreactors work? *Chem Eng Sci.* 2009;64(1):109-125.
512. Hutmacher DW, Singh H. Computational fluid dynamics for improved bioreactor design and 3D culture. *Trends Biotechnol.* 2008;26(4):166-172.
513. Martin I, Wendt D, Heberer M. The role of bioreactors in tissue engineering. *Trends Biotechnol.* 2004;22(2):80-86. doi:10.1016/j.tibtech.2003.12.001
514. Kumar A, Starly B. Large scale industrialized cell expansion: Producing the critical raw material for biofabrication processes. *Biofabrication.* 2015;7(4). doi:10.1088/1758-5090/7/4/044103
515. Grayson W, Stephenson M. Recent advances in bioreactors for cell-based therapies [version 1; referees: 2 approved]. *F1000Research.* 2018;7(0):1-9. doi:10.12688/f1000research.12533.1

REFERENCES

516. Martin I, Wendt D, Heberer M. The role of bioreactors in tissue engineering. *Trends Biotechnol.* 2004;22(2):80-86. doi:10.1016/j.tibtech.2003.12.001
517. Shokrani H, Shokrani A, Sajadi SM, et al. Cell-seeded biomaterial scaffolds: the urgent need for unanswered accelerated angiogenesis. *Int J Nanomedicine.* 2022;17:1035.
518. Huang BJ, Brown WE, Keown T, Hu JC, Athanasiou KA. Overcoming challenges in engineering large, scaffold-free neocartilage with functional properties. *Tissue Eng Part A.* 2018;24(21-22):1652-1662.
519. Wendt D, Marsano A, Jakob M, Heberer M, Martin I. Oscillating perfusion of cell suspensions through three-dimensional scaffolds enhances cell seeding efficiency and uniformity. *Biotechnol Bioeng.* 2003;84(2):205-214.
520. Vunjak-Novakovic G, Obradovic B, Martin I, Bursac PM, Langer R, Freed LE. Dynamic cell seeding of polymer scaffolds for cartilage tissue engineering. *Biotechnol Prog.* 1998;14(2):193-202.
521. Yang S, Leong KF, Du Z, Chua CK. The design of scaffolds for use in tissue engineering. Part I. Traditional factors. *Tissue Eng.* 2001. doi:10.1089/107632701753337645
522. Palsson B. Tissue engineering, Chapter 12 in Introduction to Biomedical Engineering,(Editors). J. Enderle, S. Blanchard, and J. Bronzino. 2000.
523. Howlett AR, Bissell MJ. The influence of tissue microenvironment (stroma and extracellular matrix) on the development and function of mammary epithelium. *Epithelial Cell Biol.* 1993;2(2):79-89.
524. Schmeichel KL, Weaver VM, Bissell MJ. Structural cues from the tissue microenvironment are essential determinants of the human mammary epithelial cell phenotype. *J Mammary Gland Biol Neoplasia.* 1998;3(2):201-213.
525. Rosso G, Guck J. Mechanical changes of peripheral nerve tissue microenvironment and their structural basis during development. *APL Bioeng.* 2019;3(3):36107.
526. McCoy RJ, Jungreuthmayer C, O'Brien FJ. Influence of flow rate and scaffold pore size on cell behavior during mechanical stimulation in a flow perfusion bioreactor. *Biotechnol Bioeng.* 2012;109(6):1583-1594.
527. Huysmans M, Dassargues A. Review of the use of Péclet numbers to determine the relative importance of advection and diffusion in low permeability environments. *Hydrogeol J.* 2005;13(5):895-904.
528. Michael LW, C. M Van. Ultrafiltration of Synovial Fluid by Cartilage. *J Eng Mech Div.* 1978;104(1):79-96. doi:10.1061/JMCEA3.0002329
529. Oldham CE, Farrow DE, Peiffer S. A generalized Damköhler number for classifying material processing in hydrological systems. *Hydrol Earth Syst Sci.* 2013;17(3):1133-1148.
530. Bancroft GN, Sikavitsas VI, Van Den Dolder J, et al. Fluid flow increases mineralized matrix deposition in 3D perfusion culture of marrow stromal osteoblasts in a dose-dependent manner. *Proc Natl Acad Sci U S A.* 2002;99(20):12600-12605. doi:10.1073/pnas.202296599
531. Mazzei D, Guzzardi MA, Giusti S, Ahluwalia A. A low shear stress modular bioreactor for connected cell culture under high flow rates. *Biotechnol Bioeng.* 2010;106(1):127-137.
532. Jansen KA, Donato DM, Balcioglu HE, Schmidt T, Danen EHJ, Koenderink GH. A guide to mechanobiology: Where biology and physics meet. *Biochim Biophys Acta - Mol Cell Res.* 2015;1853(11):3043-3052. doi:10.1016/j.bbamcr.2015.05.007
533. Ramage L, Nuki G, Salter DM. Signalling cascades in mechanotransduction: Cell-matrix

DOCTORAL THESIS DANIEL MARTÍNEZ MORENO

- interactions and mechanical loading. *Scand J Med Sci Sport*. 2009;19(4):457-469. doi:10.1111/j.1600-0838.2009.00912.x
534. LeBaron RG, Athanasiou KA. Ex vivo synthesis of articular cartilage. *Biomaterials*. 2000;21(24):2575-2587.
535. Shachar M, Cohen S. Cardiac tissue engineering, ex-vivo: design principles in biomaterials and bioreactors. *Heart Fail Rev*. 2003;8(3):271-276.
536. Hoerstrup SP, Sodian R, Sperling JS, Vacanti JP, Mayer Jr JE. New pulsatile bioreactor for in vitro formation of tissue engineered heart valves. *Tissue Eng*. 2000;6(1):75-79.
537. Ravichandran A, Liu Y, Teoh SH. Review: bioreactor design towards generation of relevant engineered tissues: focus on clinical translation. *J Tissue Eng Regen Med*. 2018;12(1):e7-e22. doi:10.1002/term.2270
538. Bluma A, Höpfner T, Lindner P, et al. In-situ imaging sensors for bioprocess monitoring: state of the art. *Anal Bioanal Chem*. 2010;398(6):2429-2438.
539. Spadiut O, Rittmann S, Dietzsch C, Herwig C. Dynamic process conditions in bioprocess development. *Eng Life Sci*. 2013;13(1):88-101.
540. Glindkamp A, Riechers D, Rehbock C, Hitzmann B, Scheper T, Reardon KF. Sensors in disposable bioreactors status and trends. *Dispos Bioreact*. 2009:145-169.
541. Zhao L, Fu H, Zhou W, Hu W. Advances in process monitoring tools for cell culture bioprocesses. *Eng Life Sci*. 2015;15(5):459-468.
542. O'Mara P, Farrell A, Bones J, Twomey K. Staying alive! Sensors used for monitoring cell health in bioreactors. *Talanta*. 2018;176(July 2017):130-139. doi:10.1016/j.talanta.2017.07.088
543. Shek CF, Betenbaugh M. Taking the pulse of bioprocesses: at-line and in-line monitoring of mammalian cell cultures. *Curr Opin Biotechnol*. 2021;71:191-197.
544. Rajan NK, Routenberg DA, Reed MA. Optimal signal-to-noise ratio for silicon nanowire biochemical sensors. *Appl Phys Lett*. 2011;98(26):264107.
545. Suresh S, Srivastava VC, Mishra IM. Techniques for oxygen transfer measurement in bioreactors: a review. *J Chem Technol Biotechnol Int Res Process Environ Clean Technol*. 2009;84(8):1091-1103.
546. Liu J, Liu L, Gao B, Yang F. Integration of bio-electrochemical cell in membrane bioreactor for membrane cathode fouling reduction through electricity generation. *J Memb Sci*. 2013;430:196-202.
547. Pohlscheidt M, Charaniya S, Bork C, Jenzsch M, Noetzel TL, Luebbert A. Bioprocess and fermentation monitoring. *Encycl Ind Biotechnol bioprocess, Biosep cell Technol*. 2009:1469-1491.
548. Mulchandani A, Bassi AS. Principles and applications of biosensors for bioprocess monitoring and control. *Crit Rev Biotechnol*. 1995;15(2):105-124.
549. Karube I, Mitsuda S, Suzuki S. Glucose sensor using immobilized whole cells of *Pseudomonas fluorescens*. *Eur J Appl Microbiol Biotechnol*. 1979;7(4):343-350.
550. Lee S-J, Saleemuddin M, Scheper T, Loos H, Sahn H. A fluorometric fiber-optic biosensor for dual analysis of glucose and fructose using glucose-fructose-oxidoreductase isolated from *Zymomonas mobilis*. *J Biotechnol*. 1994;36(1):39-44.
551. Wang J. Electrochemical glucose biosensors. *Chem Rev*. 2008;108(2):814-825.
552. Garn M, Gisin M, Thommen C, Cevey P. A flow injection analysis system for fermentation

REFERENCES

- monitoring and control. *Biotechnol Bioeng*. 1989;34(4):423-428.
553. Forman LW, Thomas BD, Jacobson FS. On-line monitoring and control of fermentation processes by flow-injection analysis. *Anal Chim Acta*. 1991;249(1):101-111.
554. Harms P, Kostov Y, Rao G. Bioprocess monitoring. *Curr Opin Biotechnol*. 2002;13(2):124-127.
555. Clark JR LC, Wolf R, Granger D, Taylor Z. Continuous recording of blood oxygen tensions by polarography. *J Appl Physiol*. 1953;6(3):189-193.
556. Henkel S, Beutel S. Messung des pH-Werts in der Biotechnologie. *Chemie Ing Tech*. 2013;6(85):872-885.
557. Rehbock C, Beutel S, Brueckerhoff T, et al. Bioprozessanalytik. *Chemie Ing Tech*. 2008;80(3):267-286.
558. Lam H, Kostov Y. Optical instrumentation for bioprocess monitoring. *Opt Sens Syst Biotechnol*. 2009:125-142.
559. Cannizzaro C, Rhiel M, Marison I, von Stockar U. On-line monitoring of *Phaffia rhodozyma* fed-batch process with in situ dispersive Raman spectroscopy. *Biotechnol Bioeng*. 2003;83(6):668-680.
560. Haack MB, Eliasson A, Olsson L. On-line cell mass monitoring of *Saccharomyces cerevisiae* cultivations by multi-wavelength fluorescence. *J Biotechnol*. 2004;114(1-2):199-208.
561. Noui L, Hill J, Keay PJ, et al. Development of a high resolution UV spectrophotometer for at-line monitoring of bioprocesses. *Chem Eng Process Process Intensif*. 2002;41(2):107-114.
562. Card C, Hunsaker B, Smith T, Hirsch J. Near-infrared spectroscopy for rapid, simultaneous monitoring of multiple components in mammalian cell culture. *Bioprocess Int*. 2008;6(3):58.
563. Vojinović V, Cabral JMS, Fonseca LP. Real-time bioprocess monitoring: Part I: In situ sensors. *Sensors Actuators B Chem*. 2006;114(2):1083-1091.
564. Carvell JP, Dowd JE. On-line measurements and control of viable cell density in cell culture manufacturing processes using radio-frequency impedance. *Cytotechnology*. 2006;50(1):35-48.
565. Bjørnsen PK. Automatic determination of bacterioplankton biomass by image analysis. *Appl Environ Microbiol*. 1986;51(6):1199-1204.
566. Henning B, Rautenberg J. Process monitoring using ultrasonic sensor systems. *Ultrasonics*. 2006;44:e1395-e1399.
567. Becker T, Mitzscherling M, Delgado A. Ultrasonic velocity—a noninvasive method for the determination of density during beer fermentation. *Eng Life Sci*. 2001;1(2):61-67.
568. Hauptmann P, Hoppe N, Püttmer A. Application of ultrasonic sensors in the process industry. *Meas Sci Technol*. 2002;13(8):R73.
569. Yurish SY, Kirianaki N V, Pallàs-Areny R. Universal frequency-to-digital converter for quasi-digital and smart sensors: specifications and applications. *Sens Rev*. 2005.
570. Reverter F. The art of directly interfacing sensors to microcontrollers. *J Low Power Electron Appl*. 2012;2(4):265-281.
571. Chérury A. Software sensors in bioprocess engineering. *J Biotechnol*. 1997;52(3):193-199.
572. Luttmann R, Bracewell DG, Cornelissen G, et al. Soft sensors in bioprocessing: a status report and recommendations. *Biotechnol J*. 2012;7(8):1040-1048.

DOCTORAL THESIS DANIEL MARTÍNEZ MORENO

573. Warth B, Rajkai G, Mandenius C-F. Evaluation of software sensors for on-line estimation of culture conditions in an *Escherichia coli* cultivation expressing a recombinant protein. *J Biotechnol.* 2010;147(1):37-45.
574. Ödman P, Johansen CL, Olsson L, Gernaey K V, Lantz AE. Sensor combination and chemometric variable selection for online monitoring of *Streptomyces coelicolor* fed-batch cultivations. *Appl Microbiol Biotechnol.* 2010;86(6):1745-1759.
575. Sikavitsas VI, Bancroft GN, Mikos AG. Formation of three-dimensional cell/polymer constructs for bone tissue engineering in a spinner flask and a rotating wall vessel bioreactor. *J Biomed Mater Res.* 2002;62(1):136-148. doi:10.1002/jbm.10150
576. Radtke AL, Herbst-Kralovetz MM. Culturing and applications of rotating wall vessel bioreactor derived 3D epithelial cell models. *J Vis Exp.* 2012. doi:10.3791/3868
577. Yeatts AB, Fisher JP. Bone tissue engineering bioreactors: Dynamic culture and the influence of shear stress. *Bone.* 2011. doi:10.1016/j.bone.2010.09.138
578. Radisic M, Marsano A, Maidhof R, Wang Y, Vunjak-Novakovic G. Cardiac tissue engineering using perfusion bioreactor systems. *Nat Protoc.* 2008. doi:10.1038/nprot.2008.40
579. Jaasma MJ, Plunkett NA, O'Brien FJ. Design and validation of a dynamic flow perfusion bioreactor for use with compliant tissue engineering scaffolds. *J Biotechnol.* 2008. doi:10.1016/j.jbiotec.2007.11.010
580. Elder BD, Athanasiou KA. Hydrostatic pressure in articular cartilage tissue engineering: From chondrocytes to tissue regeneration. *Tissue Eng - Part B Rev.* 2009. doi:10.1089/ten.teb.2008.0435
581. Shaikh FM, O'Brien TP, Callanan A, et al. New pulsatile hydrostatic pressure bioreactor for vascular tissue-engineered constructs. *Artif Organs.* 2010. doi:10.1111/j.1525-1594.2009.00766.x
582. Henstock JR, Rotherham M, Rose JB, El Haj AJ. Cyclic hydrostatic pressure stimulates enhanced bone development in the foetal chick femur in vitro. *Bone.* 2013. doi:10.1016/j.bone.2013.01.010
583. Fujii S, Nobukawa A, Osaki T, et al. Pesticide vapor sensing using an aptamer, nanopore, and agarose gel on a chip. *Lab Chip.* 2017;17(14):2421-2425. doi:10.1039/c7lc00361g
584. Cardoso RM, Santos RO Dos, Munoz RAA, Garcia CD, Blanes L. A Multi-Pump Magnetohydrodynamics Lab-On-A-Chip Device for Automated Flow Control and Analyte Delivery. *Sensors (Basel).* 2020;20(17). doi:10.3390/s20174909
585. Rader RA, Langer ES. Upstream single-use bioprocessing systems. *Bioprocess Int.* 2012;10:12-18.
586. Singh V. Disposable bioreactor for cell culture using wave-induced agitation. *Cytotechnology.* 1999;30(1):149-158.
587. Allison N, Richards J. Current status and future trends for disposable technology in the biopharmaceutical industry. *J Chem Technol Biotechnol.* 2014;89(9):1283-1287.
588. de Vries I, Busse C, Kopatz J, Neumann H, Beutel S, Scheper T. Polysialic acid production using *Escherichia coli* K1 in a disposable bag reactor. *Eng Life Sci.* 2017;17(7):723-731.
589. Jonczyk P, Schmidt A, Bice I, et al. Strictly anaerobic batch cultivation of eubacterium ramulus in a novel disposable bag reactor system. *Chemie Ing Tech.* 2011;83(12):2147-2152.
590. Jonczyk P, Takenberg M, Hartwig S, Beutel S, Berger RG, Scheper T. Cultivation of shear stress sensitive microorganisms in disposable bag reactor systems. *J Biotechnol.*

REFERENCES

- 2013;167(4):370-376.
591. Beşkardeş IG, Hayden RS, Glettig DL, Kaplan DL, Gümüşderelioğlu M. Bone tissue engineering with scaffold-supported perfusion co-cultures of human stem cell-derived osteoblasts and cell line-derived osteoclasts. *Process Biochem.* 2017. doi:10.1016/j.procbio.2016.05.008
592. Banaeiyan AA, Theobald J, Paukstyte J, Wolf S, Adiels CB, Goksor M. Design and fabrication of a scalable liver-lobule-on-a-chip microphysiological platform. *Biofabrication.* 2017;9(1):15014. doi:10.1088/1758-5090/9/1/015014
593. Lee-Montiel FT, George SM, Gough AH, et al. Control of oxygen tension recapitulates zone-specific functions in human liver microphysiology systems. *Exp Biol Med (Maywood).* 2017;242(16):1617-1632. doi:10.1177/1535370217703978
594. Hu X-J, Wu W-C-H, Dong N-G, et al. Role of TGF-beta1 Signaling in Heart Valve Calcification Induced by Abnormal Mechanical Stimulation in a Tissue Engineering Model. *Curr Med Sci.* 2018;38(5):765-775. doi:10.1007/s11596-018-1943-9
595. Stavenschi E, Corrigan MA, Johnson GP, Riffault M, Hoey DA. Physiological cyclic hydrostatic pressure induces osteogenic lineage commitment of human bone marrow stem cells: a systematic study. *Stem Cell Res Ther.* 2018;9(1):276. doi:10.1186/s13287-018-1025-8
596. Amadeo F, Boschetti F, Polvani G, Banfi C, Pesce M, Santoro R. Aortic valve cell seeding into decellularized animal pericardium by perfusion-assisted bioreactor. *J Tissue Eng Regen Med.* 2018;12(6):1481-1493. doi:10.1002/term.2680
597. Duisit J, Amiel H, Wuthrich T, et al. Perfusion-decellularization of human ear grafts enables ECM-based scaffolds for auricular vascularized composite tissue engineering. *Acta Biomater.* 2018;73:339-354. doi:10.1016/j.actbio.2018.04.009
598. Nichols DA, Sondh IS, Litte SR, Zunino P, Gottardi R. Design and validation of an osteochondral bioreactor for the screening of treatments for osteoarthritis. *Biomed Microdevices.* 2018;20(1):4-11. doi:10.1007/s10544-018-0264-x
599. Canadas RF, Marques AP, Reis RL, Oliveira JM. Acoustically modulated biomechanical stimulation for human cartilage tissue engineering. *Lab Chip.* 2018;18(3):473-485. doi:10.1039/c7lc01195d
600. Shah BS, Chahine NO. Dynamic Hydrostatic Pressure Regulates Nucleus Pulposus Phenotypic Expression and Metabolism in a Cell Density-Dependent Manner. *J Biomech Eng.* 2018;140(2). doi:10.1115/1.4038758
601. Shen N, Riedl JA, Carvajal Berrio DA, et al. A flow bioreactor system compatible with real-time two-photon fluorescence lifetime imaging microscopy. *Biomed Mater.* 2018;13(2). doi:10.1088/1748-605X/aa9b3c
602. Marturano-Kruik A, Villasante A, Yaeger K, et al. Biomechanical regulation of drug sensitivity in an engineered model of human tumor. *Biomaterials.* 2018;150:150-161. doi:10.1016/j.biomaterials.2017.10.020
603. Reinwald Y, El Haj AJ. Hydrostatic pressure in combination with topographical cues affects the fate of bone marrow-derived human mesenchymal stem cells for bone tissue regeneration. *J Biomed Mater Res A.* 2018;106(3):629-640. doi:10.1002/jbm.a.36267
604. Schmid R, Tarau I-S, Rossi A, et al. In Vivo-Like Culture Conditions in a Bioreactor Facilitate Improved Tissue Quality in Corneal Storage. *Biotechnol J.* 2018;13(1). doi:10.1002/biot.201700344
605. Engler AJ, Le A V, Baevova P, Niklason LE. Controlled gas exchange in whole lung bioreactors. *J Tissue Eng Regen Med.* 2018;12(1):e119-e129. doi:10.1002/term.2408

DOCTORAL THESIS DANIEL MARTÍNEZ MORENO

606. Stefani I, Asnaghi MA, Cooper-White JJ, Mantero S. A double chamber rotating bioreactor for enhanced tubular tissue generation from human mesenchymal stem cells: a promising tool for vascular tissue regeneration. *J Tissue Eng Regen Med.* 2018;12(1):e42-e52. doi:10.1002/term.2341
607. Vainieri ML, Wahl D, Alini M, van Osch GJVM, Grad S. Mechanically stimulated osteochondral organ culture for evaluation of biomaterials in cartilage repair studies. *Acta Biomater.* 2018;81:256-266. doi:10.1016/j.actbio.2018.09.058
608. Vukasovic A, Asnaghi MA, Kostesic P, et al. Bioreactor-manufactured cartilage grafts repair acute and chronic osteochondral defects in large animal studies. *Cell Prolif.* 2019;52(6):1-14. doi:10.1111/cpr.12653
609. Tsai H-H, Yang K-C, Wu M-H, Chen J-C, Tseng C-L. The Effects of Different Dynamic Culture Systems on Cell Proliferation and Osteogenic Differentiation in Human Mesenchymal Stem Cells. *Int J Mol Sci.* 2019;20(16). doi:10.3390/ijms20164024
610. Theodoridis K, Aggelidou E, Manthou M, Demiri E, Bakopoulou A, Kritis A. Assessment of cartilage regeneration on 3D collagen-polycaprolactone scaffolds: Evaluation of growth media in static and in perfusion bioreactor dynamic culture. *Colloids Surf B Biointerfaces.* 2019;183:110403. doi:10.1016/j.colsurfb.2019.110403
611. Morelli S, Piscioneri A, Curcio E, Salerno S, Chen C-C, De Bartolo L. Membrane bioreactor for investigation of neurodegeneration. *Mater Sci Eng C Mater Biol Appl.* 2019;103:109793. doi:10.1016/j.msec.2019.109793
612. Beca BM, Sun Y, Wong E, Moraes C, Simmons CA. Dynamic Bioreactors with Integrated Microfabricated Devices for Mechanobiological Screening. *Tissue Eng Part C Methods.* 2019;25(10):581-592. doi:10.1089/ten.TEC.2019.0121
613. Yaghoobi M, Hashemi-Najafabadi S, Soleimani M, Vasheghani-Farahani E. Osteogenic induction of human mesenchymal stem cells in multilayered electrospun scaffolds at different flow rates and configurations in a perfusion bioreactor. *J Biosci Bioeng.* 2019;128(4):495-503. doi:10.1016/j.jbiosc.2019.03.015
614. Greuel S, Hanci G, Bohme M, et al. Effect of inoculum density on human-induced pluripotent stem cell expansion in 3D bioreactors. *Cell Prolif.* 2019;52(4):e12604. doi:10.1111/cpr.12604
615. de Bournonville S, Lambrechts T, Vanhulst J, Luyten FP, Papantoniou I, Geris L. Towards Self-Regulated Bioprocessing: A Compact Benchtop Bioreactor System for Monitored and Controlled 3D Cell and Tissue Culture. *Biotechnol J.* 2019;14(7):e1800545. doi:10.1002/biot.201800545
616. Bale SS, Manoppo A, Thompson R, et al. A thermoplastic microfluidic microphysiological system to recapitulate hepatic function and multicellular interactions. *Biotechnol Bioeng.* 2019;116(12):3409-3420. doi:10.1002/bit.26986
617. de Sousa Pinto D, Bandejas C, de Almeida Fuzeta M, et al. Scalable Manufacturing of Human Mesenchymal Stromal Cells in the Vertical-Wheel Bioreactor System: An Experimental and Economic Approach. *Biotechnol J.* 2019;14(8):e1800716. doi:10.1002/biot.201800716
618. Karami D, Richbourg N, Sikavitsas V. Dynamic in vitro models for tumor tissue engineering. *Cancer Lett.* 2019;449:178-185. doi:10.1016/j.canlet.2019.01.043
619. Gharravi AM. Encapsulated explant in novel low shear perfusion bioreactor improve cell isolation, expansion and colony forming unit. *Cell Tissue Bank.* 2019;20(1):25-34. doi:10.1007/s10561-019-09749-8
620. Cox BL, Erickson-Bhatt S, Szulczewski JM, et al. A novel bioreactor for combined magnetic

REFERENCES

- resonance spectroscopy and optical imaging of metabolism in 3D cell cultures. *Magn Reson Med*. 2019;81(5):3379-3391. doi:10.1002/mrm.27644
621. Turner DC, Kasper AM, Seaborne RA, et al. Exercising Bioengineered Skeletal Muscle In Vitro: Biopsy to Bioreactor. *Methods Mol Biol*. 2019;1889:55-79. doi:10.1007/978-1-4939-8897-6_5
622. Allenby MC, Panoskaltzis N, Tahlawi A, Dos Santos SB, Mantalaris A. Dynamic human erythropoiesis in a three-dimensional perfusion bone marrow biomimicry. *Biomaterials*. 2019;188(August 2018):24-37. doi:10.1016/j.biomaterials.2018.08.020
623. Raveling AR, Theodossiou SK, Schiele NR. A 3D printed mechanical bioreactor for investigating mechanobiology and soft tissue mechanics. *MethodsX*. 2018;5:924-932. doi:10.1016/j.mex.2018.08.001
624. Tefft BJ, Choe JA, Young MD, et al. Cardiac Valve Bioreactor for Physiological Conditioning and Hydrodynamic Performance Assessment. *Cardiovasc Eng Technol*. 2019;10(1):80-94. doi:10.1007/s13239-018-00382-2
625. Deniz P, Guler S, Çelik E, Hosseinian P, Aydin HM. Use of cyclic strain bioreactor for the upregulation of key tenocyte gene expression on Poly(glycerol-sebacate) (PGS) sheets. *Mater Sci Eng C*. 2020;106:110293. doi:https://doi.org/10.1016/j.msec.2019.110293
626. Silva JC, Moura CS, Borrecho G, et al. Extruded Bioreactor Perfusion Culture Supports the Chondrogenic Differentiation of Human Mesenchymal Stem/Stromal Cells in 3D Porous Poly(ϵ -Caprolactone) Scaffolds. *Biotechnol J*. 2020;15(2):1-14. doi:10.1002/biot.201900078
627. Cetnar AD, Tomov ML, Ning L, et al. Patient-Specific 3D Bioprinted Models of Developing Human Heart. *Adv Healthc Mater*. 2021;10(15):e2001169. doi:10.1002/adhm.202001169
628. Zhang J, Eyisoğlu H, Qin X-H, Rubert M, Müller R. 3D bioprinting of graphene oxide-incorporated cell-laden bone mimicking scaffolds for promoting scaffold fidelity, osteogenic differentiation and mineralization. *Acta Biomater*. 2021;121:637-652. doi:10.1016/j.actbio.2020.12.026
629. Mastroiocco A, Cacopardo L, Lamanna D, et al. Bioengineering Approaches to Improve In Vitro Performance of Prepubertal Lamb Oocytes. *Cells*. 2021;10(6). doi:10.3390/cells10061458
630. Lin H-H, Chao P-HG, Tai W-C, Chang P-C. 3D-Printed Collagen-Based Waveform Microfibrous Scaffold for Periodontal Ligament Reconstruction. *Int J Mol Sci*. 2021;22(14). doi:10.3390/ijms22147725
631. Czichy C, Kilian D, Wang T-C, et al. CyMAD bioreactor: A cyclic magnetic actuation device for magnetically mediated mechanical stimulation of 3D bioprinted hydrogel scaffolds. *J Mech Behav Biomed Mater*. 2022;131:105253. doi:10.1016/j.jmbbm.2022.105253
632. Mainardi VL, Rubert M, Sabato C, et al. Culture of 3D bioprinted bone constructs requires an increased fluid dynamic stimulation. *Acta Biomater*. 2022;153:374-385. doi:10.1016/j.actbio.2022.09.011
633. Zhao X, Hua Y, Wang T, et al. In vitro Cartilage Regeneration Regulated by a Hydrostatic Pressure Bioreactor Based on Hybrid Photocrosslinkable Hydrogels. *Front Bioeng Biotechnol*. 2022;10:916146. doi:10.3389/fbioe.2022.916146
634. Zhang J, Griesbach J, Ganeyev M, et al. Long-term mechanical loading is required for the formation of 3D bioprinted functional osteocyte bone organoids. *Biofabrication*. 2022;14(3). doi:10.1088/1758-5090/ac73b9
635. Ho DLL, Lee S, Du J, et al. Large-Scale Production of Wholly-Cellular Bioinks via the Optimization of Human Induced Pluripotent Stem Cell Aggregate Culture in Automated

DOCTORAL THESIS DANIEL MARTÍNEZ MORENO

- Bioreactors. *Adv Healthc Mater.* October 2022:e2201138. doi:10.1002/adhm.202201138
636. Zhang Z, Wu C, Dai C, et al. A multi-axis robot-based bioprinting system supporting natural cell function preservation and cardiac tissue fabrication. *Bioact Mater.* 2022;18:138-150. doi:10.1016/j.bioactmat.2022.02.009
637. Kronemberger GS, Miranda GASC, Silva TIG, Gonçalves RM, Granjeiro JM, Baptista LS. Large-Scale, Automated Production of Adipose-Derived Stem Cell Spheroids for 3D Bioprinting. *J Vis Exp.* 2022;(181). doi:10.3791/63430
638. Hu JCY, Athanasiou KA. Structure and Function of Articular Cartilage. In: *Handbook of Histology Methods for Bone and Cartilage.* Totowa, NJ: Humana Press; 2003:73-95. doi:10.1007/978-1-59259-417-7_4
639. Mow VC, Ratcliffe A, Poole AR. Cartilage and diarthrodial joints as paradigms for hierarchical materials and structures. *Biomaterials.* 1992;13(2):67-97.
640. Lehner KB, Rechl HP, Gmeinwieser JK, Heuck AF, Lukas HP, Kohl HP. Structure, function, and degeneration of bovine hyaline cartilage: assessment with MR imaging in vitro. *Radiology.* 1989;170(2):495-499.
641. Benjamin M, Evans EJ. Fibrocartilage. *J Anat.* 1990;171:1.
642. Chen S, Fu P, Wu H, Pei M. Meniscus , articular cartilage and nucleus pulposus : a comparative review of cartilage-like tissues in anatomy , development and function. 2017:53-70. doi:10.1007/s00441-017-2613-0
643. Junqueira LC, Carneiro J, Kelley RO. Connective tissue. *Basic Histol text atlas.* 2005;11:91-122.
644. Cox RW, Peacock MA. The fine structure of developing elastic cartilage. *J Anat.* 1977;123(Pt 2):283.
645. Kronenberg HM. The role of the perichondrium in fetal bone development. *Ann N Y Acad Sci.* 2007;1116(1):59-64.
646. Colnot C, Lu C, Hu D, Helms JA. Distinguishing the contributions of the perichondrium, cartilage, and vascular endothelium to skeletal development. *Dev Biol.* 2004;269(1):55-69.
647. Nahian A, Sapra A. Histology, Chondrocytes. In: *StatPearls [Internet].* StatPearls Publishing; 2022.
648. Musumeci G, Castrogiovanni P, Mazzone V, Szychlinska MA, Castorina S, Loreto C. Histochemistry as a unique approach for investigating normal and osteoarthritic cartilage. *Eur J Histochem.* 2014;58(2):2371. doi:10.4081/ejh.2014.2371
649. Junqueira LCU, Cossermelli W and, Brentani R. Differential staining of collagens type I, II and III by Sirius Red and polarization microscopy. *Arch Histol Jpn.* 1978;41(3):267-274.
650. Grogan SP, Barbero A, Diaz-Romero J, et al. Identification of markers to characterize and sort human articular chondrocytes with enhanced in vitro chondrogenic capacity. *Arthritis Rheum.* 2007;56(2):586-595. doi:10.1002/art.22408
651. Horvai A. Anatomy and Histology of Cartilage BT - Cartilage Imaging: Significance, Techniques, and New Developments. In: Link TM, ed. New York, NY: Springer New York; 2011:1-10. doi:10.1007/978-1-4419-8438-8_1
652. Loy BN, Zimel M, Gowda AL, et al. A Biomechanical and Structural Comparison of Articular Cartilage and Subchondral Bone of the Glenoid and Humeral Head. *Orthop J Sport Med.* 2018;6(7):2325967118785854. doi:10.1177/2325967118785854
653. Safshekan F, Tafazzoli-Shadpour M, Abdouss M, Shadmehr MB. Viscoelastic Properties of Human Tracheal Tissues. *J Biomech Eng.* 2017;139(1). doi:10.1115/1.4034651

REFERENCES

654. Grave KC, Brown T. Skeletal ossification and the adolescent growth spurt. *Am J Orthod.* 1976;69(6):611-619.
655. Mackie E, Ahmed YA, Tatarczuch L, Chen K-S, Mirams M. Endochondral ossification: how cartilage is converted into bone in the developing skeleton. *Int J Biochem Cell Biol.* 2008;40(1):46-62.
656. Nishimura R, Hata K, Ono K, Takashima R, Yoshida M, Yoneda T. Regulation of endochondral ossification by transcription factors. *J Oral Biosci.* 2012;54(4):180-183.
657. Ito T, Yadav N, Lee J, et al. Arginine methyltransferase CARM1/PRMT4 regulates endochondral ossification. *BMC Dev Biol.* 2009;9(1):1-10.
658. Kreuz PC, Steinwachs M, Erggelet C, et al. Classification of graft hypertrophy after autologous chondrocyte implantation of full-thickness chondral defects in the knee. *Osteoarthr Cartil.* 2007;15(12):1339-1347. doi:10.1016/j.joca.2007.04.020
659. Rajpurohit R, Koch CJ, Tao Z, Teixeira CM, Shapiro IM. Adaptation of chondrocytes to low oxygen tension: relationship between hypoxia and cellular metabolism. *J Cell Physiol.* 1996;168(2):424-432. doi:10.1002/(SICI)1097-4652(199608)168:2<424::AID-JCP21>3.0.CO;2-1
660. Holm S, Maroudas A, Urban JPG, Selstam G, Nachemson A. Nutrition of the Intervertebral Disc: Solute Transport and Metabolism. *Connect Tissue Res.* 1981;8(2):101-119. doi:10.3109/03008208109152130
661. Roberts S, Urban JPG, Evans H, Eisenstein SM. Transport properties of the human cartilage endplate in relation to its composition and calcification. *Spine (Phila Pa 1976).* 1996;21(4):415-420.
662. Khalkhali-Ellis Z, Seftor EA, Nieva DR, et al. Estrogen and progesterone regulation of human fibroblast-like synoviocyte function in vitro: implications in rheumatoid arthritis. *J Rheumatol.* 2000;27(7):1622-1631.
663. Paatsama S, Rokkanen P, Jussila J, Sittnikow K. Somatotropin, thyrotropin and corticotropin hormone-induced changes in the cartilages and bones of the shoulder and knee joint in young dogs* An experimental study using histological OTC, bone labelling and microradiographic methods. *J Small Anim Pract.* 1971;12(11):595-601.
664. Demoor M, Ollitrault D, Gomez-Leduc T, et al. Cartilage tissue engineering: molecular control of chondrocyte differentiation for proper cartilage matrix reconstruction. *Biochim Biophys Acta (BBA)-General Subj.* 2014;1840(8):2414-2440.
665. Cicuttini FM, Wluka A, Bailey M, et al. Factors affecting knee cartilage volume in healthy men. *Rheumatology.* 2003;42(2):258-262.
666. Holmes DF, Lu Y, Starborg T, Kadler KE. Collagen Fibril Assembly and Function. *Curr Top Dev Biol.* 2018;130:107-142. doi:10.1016/bs.ctdb.2018.02.004
667. Scanzello CR, Goldring SR. The role of synovitis in osteoarthritis pathogenesis. *Bone.* 2012;51(2):249-257. doi:10.1016/j.bone.2012.02.012
668. Stachowiak GW, Stachowiak GB, Campbell P. Application of numerical descriptors to the characterization of wear particles obtained from joint replacements. *Proc Inst Mech Eng Part H J Eng Med.* 1997;211(1):1-10.
669. Kuster MS, Podsiadlo P, Stachowiak GW. Shape of wear particles found in human knee joints and their relationship to osteoarthritis. *Br J Rheumatol.* 1998;37(9):978-984.
670. Podsiadlo P, Kuster M, Stachowiak GW. Numerical analysis of wear particles from non-arthritic and osteoarthritic human knee joints. *Wear.* 1997;210(1-2):318-325.

DOCTORAL THESIS DANIEL MARTÍNEZ MORENO

671. McInnes IB, Schett G. The pathogenesis of rheumatoid arthritis. *N Engl J Med.* 2011;365(23):2205-2219.
672. Majithia V, Geraci SA. Rheumatoid arthritis: diagnosis and management. *Am J Med.* 2007;120(11):936-939.
673. Bassiouny A. Perichondritis of the auricle. *Laryngoscope.* 1981;91(3):422-431.
674. Prasad HKC, Sreedharan S, Prasad HSC, Meyyappan MH, Harsha KS. Perichondritis of the auricle and its management. *J Laryngol Otol.* 2007;121(6):530-534.
675. Horton WA, Hall JG, Hecht JT. Achondroplasia. *Lancet.* 2007;370(9582):162-172.
676. Proulx AM, Zryd TW. Costochondritis: diagnosis and treatment. *Am Fam Physician.* 2009;80(6):617-620.
677. Chung EB, Enzinger FM. Chondroma of soft parts. *Cancer.* 1978;41(4):1414-1424.
678. LICHTENSTEIN L, HALL JE. Periosteal chondroma: a distinctive benign cartilage tumor. *JBJS.* 1952;34(3):691-697.
679. Man GS, Mologhianu G. Osteoarthritis pathogenesis - a complex process that involves the entire joint. *J Med Life.* 2014;7(1):37-41.
680. Shrier I. Muscle dysfunction versus wear and tear as a cause of exercise related osteoarthritis: an epidemiological update. *Br J Sports Med.* 2004;38(5):526-535.
681. Davis MA. Epidemiology of osteoarthritis. *Clin Geriatr Med.* 1988;4(2):241-255.
682. Von Der Mark K, Von Der Mark H. Immunological and biochemical studies of collagen type transition during in vitro chondrogenesis of chick limb mesodermal cells. *J Cell Biol.* 1977;73(3):736-747. doi:10.1083/jcb.73.3.736
683. Goldring MB. Chondrogenesis, chondrocyte differentiation, and articular cartilage metabolism in health and osteoarthritis. *Ther Adv Musculoskelet Dis.* 2012;4(4):269-285. doi:10.1177/1759720X12448454
684. Goldring MB, Tsuchimochi K, Ijiri K. The control of chondrogenesis. *J Cell Biochem.* 2006;97(1):33-44.
685. Thorogood P V, Hinchliffe JR. An analysis of the condensation process during chondrogenesis in the embryonic chick hind limb. 1975.
686. Dessau W, Mark H Von Der, Mark K Von Der, Fischer S. Changes in the patterns of collagens and fibronectin during limb-bud chondrogenesis. 1980.
687. Curran RC, Kennedy JS. The distribution of the sulphated mucopolysaccharides in the mouse. *J Pathol Bacteriol.* 1955;70(2):449-457.
688. Bostrom H, Odeblad E. The influence of cortisone upon the sulphate exchange of chondroitin sulphuric acid. *Ark Kemi.* 1953;6:39-42.
689. Lefebvre V, de Crombrughe B. Toward understanding SOX9 function in chondrocyte differentiation. *Matrix Biol.* 1998;16(9):529-540.
690. Burgess AMC. Genome control and the genetic potentialities of the nuclei of dedifferentiated regeneration blastema cells. In: *Neoplasia and Cell Differentiation.* Karger Publishers; 1974:106-152.
691. Smeriglio P, Dhulipala L, Lai JH, et al. Collagen VI enhances cartilage tissue generation by stimulating chondrocyte proliferation. *Tissue Eng Part A.* 2015;21(3-4):840-849.
692. Shen G. The role of type X collagen in facilitating and regulating endochondral ossification of articular cartilage. *Orthod Craniofac Res.* 2005;8(1):11-17.

REFERENCES

693. Krane SM, Inada M. Matrix metalloproteinases and bone. *Bone*. 2008;43(1):7-18.
694. Dai J, Rabie ABM. VEGF: an essential mediator of both angiogenesis and endochondral ossification. *J Dent Res*. 2007;86(10):937-950.
695. Chen H, Ghori-Javed FY, Rashid H, et al. Runx2 regulates endochondral ossification through control of chondrocyte proliferation and differentiation. *J Bone Miner Res*. 2014;29(12):2653-2665.
696. Hattori T, Müller C, Gebhard S, et al. SOX9 is a major negative regulator of cartilage vascularization, bone marrow formation and endochondral ossification. *Development*. 2010;137(6):901-911.
697. Zhang X, Siclari VA, Lan S, et al. The critical role of the epidermal growth factor receptor in endochondral ossification. *J Bone Miner Res*. 2011;26(11):2622-2633.
698. Appleton CTG, Usmani SE, Mort JS, Beier F. Rho/ROCK and MEK/ERK activation by transforming growth factor- α induces articular cartilage degradation. *Lab Invest*. 2010;90(1):20-30.
699. Vortkamp A, Lee K, Lanske B, Segre G V, Kronenberg HM, Tabin CJ. Regulation of rate of cartilage differentiation by Indian hedgehog and PTH-related protein. *Science (80-)*. 1996;273(5275):613-622.
700. Mak KK, Kronenberg HM, Chuang P-T, Mackem S, Yang Y. Indian hedgehog signals independently of PTHrP to promote chondrocyte hypertrophy. 2008.
701. Krejci P, Krakow D, Mekikian PB, Wilcox WR. Fibroblast growth factors 1, 2, 17, and 19 are the predominant FGF ligands expressed in human fetal growth plate cartilage. *Pediatr Res*. 2007;61(3):267-272.
702. Murakami S, Kan M, McKeehan WL, De Crombrugge B. Up-regulation of the chondrogenic Sox9 gene by fibroblast growth factors is mediated by the mitogen-activated protein kinase pathway. *Proc Natl Acad Sci*. 2000;97(3):1113-1118.
703. Havens BA, Velonis D, Kronenberg MS, Lichtler AC, Oliver B, Mina M. Roles of FGFR3 during morphogenesis of Meckel's cartilage and mandibular bones. *Dev Biol*. 2008;316(2):336-349.
704. Tan Q, Chen B, Wang Q, et al. A novel FGFR1-binding peptide attenuates the degeneration of articular cartilage in adult mice. *Osteoarthr Cartil*. 2018;26(12):1733-1743.
705. Wozney JM. Bone morphogenetic proteins. *Prog Growth Factor Res*. 1989;1(4):267-280.
706. Grimsrud CD, Romano PR, D'Souza M, et al. BMP signaling stimulates chondrocyte maturation and the expression of Indian hedgehog. *J Orthop Res*. 2001;19(1):18-25.
707. Yoon BS, Pogue R, Ovchinnikov DA, et al. BMPs regulate multiple aspects of growth-plate chondrogenesis through opposing actions on FGF pathways. 2006.
708. Nilsson O, Parker EA, Hegde A, Chau M, Barnes KM, Baron J. Gradients in bone morphogenetic protein-related gene expression across the growth plate. *J Endocrinol*. 2007;193(1):75-84.
709. Sinclair AH, Berta P, Palmer MS, Hawkins JR, Griffiths BL, Matthijs J, Smith, Jamie W, Foster, Anna-Maria Frischauf, Robin Lovell-Badge, and Peter N. Goodfellow (1990) A gene from the human sex-determining region encodes a protein with homology to a conserved DNA-binding motif. *Nature* 346: 240–244. *Sex Brain*. 2007:117.
710. Wegner M. From head to toes: the multiple facets of Sox proteins. *Nucleic Acids Res*. 1999;27(6):1409-1420.
711. Akiyama H, Chaboissier M-C, Martin JF, Schedl A, de Crombrugge B. The transcription

DOCTORAL THESIS DANIEL MARTÍNEZ MORENO

- factor Sox9 has essential roles in successive steps of the chondrocyte differentiation pathway and is required for expression of Sox5 and Sox6. *Genes Dev.* 2002;16(21):2813-2828.
712. Lefebvre V, Li P, De Crombrughe B. A new long form of Sox5 (L-Sox5), Sox6 and Sox9 are coexpressed in chondrogenesis and cooperatively activate the type II collagen gene. *EMBO J.* 1998;17(19):5718-5733.
713. Bi W, Deng JM, Zhang Z, Behringer RR, De Crombrughe B. Sox9 is required for cartilage formation. *Nat Genet.* 1999;22(1):85-89.
714. Hardingham TE, Oldershaw RA, Tew SR. Cartilage, SOX9 and Notch signals in chondrogenesis. *J Anat.* 2006;209(4):469-480.
715. Komori T. Roles of Runx2 in skeletal development. *RUNX Proteins Dev cancer.* 2017:83-93.
716. Kim E-J, Cho S-W, Shin J-O, Lee M-J, Kim K-S, Jung H-S. Ihh and Runx2/Runx3 signaling interact to coordinate early chondrogenesis: a mouse model. *PLoS One.* 2013;8(2):e55296.
717. Buckwalter JA, Mankin HJ. Articular cartilage: tissue design and chondrocyte-matrix interactions. *Instr Course Lect.* 1998;47:477-486.
718. Mow VC. *Cell Mechanics and Cellular Engineering.*; 1994. doi:10.1007/978-1-4613-8425-0
719. Kempson GE, Tuke MA, Dingle JT, Barrett AJ, Horsefield PH. The effects of proteolytic enzymes on the mechanical properties of adult human articular cartilage. *Biochim Biophys Acta (BBA)-General Subj.* 1976;428(3):741-760.
720. Von Der Mark K, Von Der Mark H. Immunological and biochemical studies of collagen type transition during in vitro chondrogenesis of chick limb mesodermal cells. *J Cell Biol.* 1977;73(3):736-747. doi:10.1083/jcb.73.3.736
721. Mayne R. Cartilage collagens. What Is Their Function, and Are They Involved in Articular Disease? *Arthritis Rheum.* 1989;32(3):241-246. doi:10.1002/anr.1780320302
722. Ayad S, Evans H, Weiss JB, Holt L. Type VI collagen but not type V collagen is present in cartilage. *Coll Relat Res.* 1984;4(2):165-168.
723. Smith Jr GN, Brandt KD. Hypothesis: can type IX collagen "glue" together intersecting type II fibers in articular cartilage matrix? A proposed mechanism. *J Rheumatol.* 1992;19(1):14-17.
724. Vaughan L, Mendler M, Huber S, et al. D-periodic distribution of collagen type IX along cartilage fibrils. *J Cell Biol.* 1988;106(3):991-997.
725. Hedbom E, Antonsson P, Hjerpe A, et al. Cartilage matrix proteins. An acidic oligomeric protein (COMP) detected only in cartilage. *J Biol Chem.* 1992;267(9):6132-6136.
726. Heinegrd D, Lorenzo P, Saxne T. Noncollagenous Proteins; Glycoproteins and Related Proteins. In: *Dynamics of Bone and Cartilage Metabolism.*; 2006:71-84. doi:10.1016/B978-012088562-6/50005-4
727. Lai WM, Mow VC, Zhu W. Constitutive modeling of articular cartilage and biomacromolecular solutions. *J Biomech Eng.* 1993;115(4B):474-480.
728. Maroudas A, Mizrahi J, Benaim E, Schneiderman R, Grushko G. Swelling pressure of cartilage: roles played by proteoglycans and collagen. In: *Mechanics of Swelling.* Springer; 1992:487-512.
729. Broom ND, Poole CA. A functional-morphological study of the tidemark region of articular cartilage maintained in a non-viable physiological condition. *J Anat.* 1982;135(Pt 1):65.
730. Soltz MA, Ateshian GA. Experimental verification and theoretical prediction of cartilage

REFERENCES

- interstitial fluid pressurization at an impermeable contact interface in confined compression. *J Biomech.* 1998;31(10):927-934.
731. Maroudas A. Balance between swelling pressure and collagen tension in normal and degenerate cartilage. *Nature.* 1976;260(5554):808-809.
732. Ateshian GA, Warden WH, Kim JJ, Grelsamer RP, Mow VC. Finite deformation biphasic material properties of bovine articular cartilage from confined compression experiments. *J Biomech.* 1997;30(11-12):1157-1164.
733. Roughley PJ, Mort JS. The role of aggrecan in normal and osteoarthritic cartilage. *J Exp Orthop.* 2014;1(1):8. doi:10.1186/s40634-014-0008-7
734. Mankin HJ, LIPPIELLO L. The glycosaminoglycans of normal and arthritic cartilage. *J Clin Invest.* 1971;50(8):1712-1719.
735. Mikami T, Kitagawa H. Biosynthesis and function of chondroitin sulfate. *Biochim Biophys Acta (BBA)-General Subj.* 2013;1830(10):4719-4733.
736. Pomin VH. Keratan sulfate: An up-to-date review. *Int J Biol Macromol.* 2015;72:282-289.
737. Nagase H, Woessner JF. Joint cartilage degradation. 1993.
738. Ronca F, Palmieri L, Panicucci P, Ronca G. Anti-inflammatory activity of chondroitin sulfate. *Osteoarthr Cartil.* 1998;6:14-21. doi:https://doi.org/10.1016/S1063-4584(98)80006-X
739. Swann DA, Hendren RB, Radin EL, Sotman SL. The lubricating activity of synovial fluid glycoproteins. *Arthritis Rheum Off J Am Coll Rheumatol.* 1981;24(1):22-30.
740. Schinagl RM, Gurskis D, Chen AC, Sah RL. Depth-dependent confined compression modulus of full-thickness bovine articular cartilage. *J Orthop Res.* 1997;15(4):499-506.
741. Maroudas A. Physicochemical properties of cartilage in the light of ion exchange theory. *Biophys J.* 1968;8(5):575-595.
742. Sophia Fox AJ, Bedi A, Rodeo SA. The basic science of articular cartilage: structure, composition, and function. *Sports Health.* 2009;1(6):461-468.
743. Mow VC, Kuei SC, Lai WM, Armstrong CG. Biphasic Creep and Stress Relaxation of Articular Cartilage in Compression: Theory and Experiments. *J Biomech Eng.* 1980;102(1):73. doi:10.1115/1.3138202
744. Athanasiou KA, Agarwal A, Dzida FJ. Comparative study of the intrinsic mechanical properties of the human acetabular and femoral head cartilage. *J Orthop Res.* 1994;12(3):340-349.
745. Knudson CB. Hyaluronan receptor-directed assembly of chondrocyte pericellular matrix. *J Cell Biol.* 1993;120(3):825-834.
746. Athanasiou KA, Agarwal A, Muffoletto A, Dzida FJ, Constantinides G, Clem M. Biomechanical properties of hip cartilage in experimental animal models. *Clin Orthop Relat Res.* 1995;(316):254-266.
747. Hou JS, Mow VC, Lai WM, Holmes MH. An analysis of the squeeze-film lubrication mechanism for articular cartilage. *J Biomech.* 1992;25(3):247-259.
748. Swann DA, Slayter HS, Silver FH. The molecular structure of lubricating glycoprotein-I, the boundary lubricant for articular cartilage. *J Biol Chem.* 1981;256(11):5921-5925.
749. Athanasiou KA, Rosenwasser MP, Buckwalter JA, Malinin TI, Mow VC. Interspecies comparisons of in situ intrinsic mechanical properties of distal femoral cartilage. *J Orthop Res.* 1991;9(3):330-340.

DOCTORAL THESIS DANIEL MARTÍNEZ MORENO

750. Athanasiou KA, Niederauer GG, Schenck RC. Biomechanical topography of human ankle cartilage. *Ann Biomed Eng.* 1995;23(5):697-704.
751. Schenck Jr RC, Athanasiou KA, Constantinides G, Gomez E. A biomechanical analysis of articular cartilage of the human elbow and a potential relationship to osteochondritis dissecans. *Clin Orthop Relat Res.* 1994;(299):305-312.
752. Helmick CG, Felson DT, Lawrence RC, et al. Estimates of the prevalence of arthritis and other rheumatic conditions in the United States. Part I. *Arthritis Rheum.* 2008;58(1):15-25. doi:10.1002/art.23177
753. Hunter DJ, Schofield D, Callander E. The individual and socioeconomic impact of osteoarthritis. *Nat Rev Rheumatol.* 2014;10(7):437-441. doi:10.1038/nrrheum.2014.44
754. Libby P. Inflammation in atherosclerosis. *Nature.* 2002;420(6917):868-874. doi:10.1038/nature01323
755. Felson DT. Osteoarthritis of the Knee. *N Engl J Med.* 2006;354(8):841-848. doi:10.1056/NEJMcp051726
756. Ganz R, Leunig M, Leunig-Ganz K, Harris WH. The etiology of osteoarthritis of the hip: An integrated mechanical concept. *Clin Orthop Relat Res.* 2008;466(2):264-272. doi:10.1007/s11999-007-0060-z
757. Saxby DJ, Lloyd DG. Osteoarthritis year in review 2016 : mechanics. *Osteoarthr Cartil.* 2017;25(2):190-198. doi:10.1016/j.joca.2016.09.023
758. Knecht S, Vanwanseele B, Stüssi E. A review on the mechanical quality of articular cartilage - Implications for the diagnosis of osteoarthritis. *Clin Biomech.* 2006;21(10):999-1012. doi:10.1016/j.clinbiomech.2006.07.001
759. Buckwalter JA, Mankin HJ. Articular cartilage: degeneration and osteoarthritis, repair, regeneration, and transplantation. *Instr Course Lect.* 1998;47:487-504.
760. Englund M, Guermazi A, Gale D, et al. Incidental Meniscal Findings on Knee MRI in Middle-Aged and Elderly Persons. *N Engl J Med.* 2008;359(11):1108-1115. doi:10.1056/NEJMoa0800777
761. Martel-Pelletier J. Pathophysiology of osteoarthritis. *Osteoarthritis Cartilage.* 2004;12 Suppl A:S31-S33. doi:10.1053/joca.1998.0140
762. Andriacchi TP, Mündermann A, Smith RL, Alexander EJ, Dyrby CO, Koo S. A framework for the in vivo pathomechanics of osteoarthritis at the knee. *Ann Biomed Eng.* 2004;32(3):447-457.
763. Goldring MB, Marcu KB. Cartilage homeostasis in health and rheumatic diseases. *Arthritis Res Ther.* 2009;11(3):1-16.
764. Kellgren JH, Lawrence J. Radiological assessment of osteo-arthrosis. *Ann Rheum Dis.* 1957;16(4):494.
765. Kellgren JH, Bier F. Radiological signs of rheumatoid arthritis: a study of observer differences in the reading of hand films. *Ann Rheum Dis.* 1956;15(1):55.
766. Kellgren JH, Lawrence JS. Rheumatism in miners. Part II: X-ray study. *Br J Ind Med.* 1952;9(3):197.
767. Hunter DJ, Arden N, Conaghan PG, et al. Definition of osteoarthritis on MRI: results of a Delphi exercise. *Osteoarthr Cartil.* 2011;19(8):963-969. doi:https://doi.org/10.1016/j.joca.2011.04.017
768. Gornale SS, Patravali PU, Hiremath PS. Automatic Detection and Classification of Knee Osteoarthritis Using Hu's Invariant Moments. *Front Robot AI.* 2020;7(November):1-8.

REFERENCES

- doi:10.3389/frobt.2020.591827
769. Loughlin J. Genetics of osteoarthritis. *Curr Opin Rheumatol*. 2011;23(5):479-483.
770. Barter MJ, Bui C, Young DA. Epigenetic mechanisms in cartilage and osteoarthritis: DNA methylation, histone modifications and microRNAs. *Osteoarthr Cartil*. 2012;20(5):339-349.
771. Goldring MB, Marcu KB. Epigenomic and microRNA-mediated regulation in cartilage development, homeostasis, and osteoarthritis. *Trends Mol Med*. 2012;18(2):109-118.
772. Iliopoulos D, Malizos KN, Oikonomou P, Tsezou A. Integrative microRNA and proteomic approaches identify novel osteoarthritis genes and their collaborative metabolic and inflammatory networks. *PLoS One*. 2008;3(11):e3740.
773. Jones SW, Watkins G, Le Good N, et al. The identification of differentially expressed microRNA in osteoarthritic tissue that modulate the production of TNF- α and MMP13. *Osteoarthr Cartil*. 2009;17(4):464-472.
774. Swingler TE, Wheeler G, Carmont V, et al. The expression and function of microRNAs in chondrogenesis and osteoarthritis. *Arthritis Rheum*. 2012;64(6):1909-1919.
775. Aigner T, Kurz B, Fukui N, Sandell L. Roles of chondrocytes in the pathogenesis of osteoarthritis. *Curr Opin Rheumatol*. 2002;14(5):578-584. doi:10.1097/00002281-200209000-00018
776. Rollin R, Marco F, Jover JA, et al. Early lymphocyte activation in the synovial microenvironment in patients with osteoarthritis: comparison with rheumatoid arthritis patients and healthy controls. *Rheumatol Int*. 2008;28(8):757-764.
777. Roemer FW, Guermazi A, Felson DT, et al. Presence of MRI-detected joint effusion and synovitis increases the risk of cartilage loss in knees without osteoarthritis at 30-month follow-up: the MOST study. *Ann Rheum Dis*. 2011;70(10):1804-1809.
778. Baker-LePain JC, Lane NE. Relationship between joint shape and the development of osteoarthritis. *Curr Opin Rheumatol*. 2010;22(5):538.
779. Attur M, Samuels J, Krasnokutsky S, Abramson SB. Targeting the synovial tissue for treating osteoarthritis (OA): where is the evidence? *Best Pract Res Clin Rheumatol*. 2010;24(1):71-79.
780. Sellam J, Berenbaum F. The role of synovitis in pathophysiology and clinical symptoms of osteoarthritis. *Nat Rev Rheumatol*. 2010;6(11):625-635.
781. Man GS, Mologhianu G. Osteoarthritis pathogenesis - a complex process that involves the entire joint. *J Med Life*. 2014;7(1):37-41.
782. Radin EL, Burr DB, Caterson B, Fyhrie D, Brown TD, Boyd RD. Mechanical determinants of osteoarthrosis. *Semin Arthritis Rheum*. 1991;21(3, Supplement 2):12-21. doi:https://doi.org/10.1016/0049-0172(91)90036-Y
783. Aigner T, Dudhia J. Phenotypic modulation of chondrocytes as a potential therapeutic target in osteoarthritis: a hypothesis. *Ann Rheum Dis*. 1997;56(5):287-291. doi:10.1136/ard.56.5.287
784. Hayashi D, Roemer FW, Katur A, et al. Imaging of synovitis in osteoarthritis: current status and outlook. In: *Seminars in Arthritis and Rheumatism*. Vol 41. Elsevier; 2011:116-130.
785. Scanzello CR, McKeon B, Swaim BH, et al. Synovial inflammation in patients undergoing arthroscopic meniscectomy: molecular characterization and relationship to symptoms. *Arthritis Rheum*. 2011;63(2):391-400.
786. Pereira D, Ramos E, Branco J. Osteoarthritis. *Acta Med Port*. 2015;28(1):99-106.

DOCTORAL THESIS DANIEL MARTÍNEZ MORENO

787. Catterall JB, Stabler T V, Flannery CR, Kraus VB. Changes in serum and synovial fluid biomarkers after acute injury (NCT00332254). *Arthritis Res Ther*. 2010;12(6):1-9.
788. Gobezie R, Kho A, Krastins B, et al. High abundance synovial fluid proteome: distinct profiles in health and osteoarthritis. *Arthritis Res Ther*. 2007;9(2):1-15.
789. Lotz MK. New developments in osteoarthritis: posttraumatic osteoarthritis: pathogenesis and pharmacological treatment options. *Arthritis Res Ther*. 2010;12(3):1-9.
790. Goldring MB. The role of cytokines as inflammatory mediators in osteoarthritis: lessons from animal models. *Connect Tissue Res*. 1999;40(1):1-11. doi:10.3109/03008209909005273
791. Goldring MB, Berenbaum F. Human chondrocyte culture models for studying cyclooxygenase expression and prostaglandin regulation of collagen gene expression. In: *Osteoarthritis and Cartilage*. Vol 7. ; 1999:386-388. doi:10.1053/joca.1998.0219
792. Badger AM, Cook MN, Lark MW, et al. SB 203580 inhibits p38 mitogen-activated protein kinase, nitric oxide production, and inducible nitric oxide synthase in bovine cartilage-derived chondrocytes. *J Immunol*. 1998;161(1):467-473.
793. Fuseler JW, Merrill DM, Rogers J a, Grisham MB, Wolf RE. Analysis and quantitation of NF-kappaB nuclear translocation in tumor necrosis factor alpha (TNF-alpha) activated vascular endothelial cells. *Microsc Microanal*. 2006;12(3):269-276. doi:10.1017/S1431927606060260
794. Gabay O, Sanchez C, Salvat C, et al. Stigmasterol: a phytosterol with potential anti-osteoarthritic properties. *Osteoarthr Cartil*. 2010;18(1):106-116.
795. Rogerson FM, Chung YM, Deutscher ME, Last K, Fosang AJ. Cytokine-induced increases in ADAMTS-4 messenger RNA expression do not lead to increased aggrecanase activity in ADAMTS-5-deficient mice. *Arthritis Rheum*. 2010;62(11):3365-3373.
796. Song R, D. Tortorella M, Malfait A, et al. Aggrecan degradation in human articular cartilage explants is mediated by both ADAMTS-4 and ADAMTS-5. *Arthritis Rheum Off J Am Coll Rheumatol*. 2007;56(2):575-585.
797. Goldring MB, Otero M, Plumb DA, et al. Roles of inflammatory and anabolic cytokines in cartilage metabolism: signals and multiple effectors converge upon MMP-13 regulation in osteoarthritis. *Eur Cell Mater*. 2011;21:202.
798. Koch AE, Kunkel SL, Shah MR, et al. Macrophage Inflammatory Protein-1β: A C-C Chemokine in Osteoarthritis. *Clin Immunol Immunopathol*. 1995;77(3):307-314. doi:https://doi.org/10.1006/clin.1995.1157
799. Pulai JI, Chen H, Im H-J, et al. NF-κB mediates the stimulation of cytokine and chemokine expression by human articular chondrocytes in response to fibronectin fragments. *J Immunol*. 2005;174(9):5781-5788.
800. Fichter M, Körner U, Schömburg J, Jennings L, Cole AA, Mollenhauer J. Collagen degradation products modulate matrix metalloproteinase expression in cultured articular chondrocytes. *J Orthop Res*. 2006;24(1):63-70.
801. Homandberg GA, Wen C, Hui F. Cartilage damaging activities of fibronectin fragments derived from cartilage and synovial fluid. *Osteoarthr Cartil*. 1998;6(4):231-244. doi:https://doi.org/10.1053/joca.1998.0116
802. Rasheed Z, Akhtar N, Haqqi TM. Advanced glycation end products induce the expression of interleukin-6 and interleukin-8 by receptor for advanced glycation end product-mediated activation of mitogen-activated protein kinases and nuclear factor-κB in human osteoarthritis chondrocytes. *Rheumatology (Oxford)*. 2011;50(5):838-851. doi:10.1093/rheumatology/keq380

REFERENCES

803. Zreiqat H, Belluoccio D, Smith MM, et al. S100A8 and S100A9 in experimental osteoarthritis. *Arthritis Res Ther*. 2010;12(1):R16. doi:10.1186/ar2917
804. Mazzetti I, Magagnoli G, Paoletti S, et al. A role for chemokines in the induction of chondrocyte phenotype modulation. *Arthritis Rheum*. 2004;50(1):112-122. doi:10.1002/art.11474
805. Chauffier K, Laiguillon M-C, Bougault C, et al. Induction of the chemokine IL-8/Kc by the articular cartilage: possible influence on osteoarthritis. *Jt bone spine*. 2012;79(6):604-609. doi:10.1016/j.jbspin.2011.12.013
806. Merz D, Liu R, Johnson K, Terkeltaub R. IL-8/CXCL8 and growth-related oncogene alpha/CXCL1 induce chondrocyte hypertrophic differentiation. *J Immunol*. 2003;171(8):4406-4415. doi:10.4049/jimmunol.171.8.4406
807. Ni F, Zhang Y, Peng X, Li J. Correlation between osteoarthritis and monocyte chemotactic protein-1 expression: a meta-analysis. *J Orthop Surg Res*. 2020;15(1):516. doi:10.1186/s13018-020-02045-2
808. Alaaeddine N, Olee T, Hashimoto S, Creighton-Achermann L, Lotz M. Production of the chemokine RANTES by articular chondrocytes and role in cartilage degradation. *Arthritis Rheum*. 2001;44(7):1633-1643. doi:https://doi.org/10.1002/1529-0131(200107)44:7<1633::AID-ART286>3.0.CO;2-Z
809. Haglund L, Bernier SM, Onnerfjord P, Recklies AD. Proteomic analysis of the LPS-induced stress response in rat chondrocytes reveals induction of innate immune response components in articular cartilage. *Matrix Biol*. 2008;27(2):107-118. doi:10.1016/j.matbio.2007.09.009
810. Zhang Q, Hui W, Litherland GJ, et al. Differential Toll-like receptor-dependent collagenase expression in chondrocytes. *Ann Rheum Dis*. 2008;67(11):1633-1641. doi:10.1136/ard.2007.079574
811. Geurts J, van den Brand BT, Wolf A, et al. Toll-like receptor 4 signalling is specifically TGF-beta-activated kinase 1 independent in synovial fibroblasts. *Rheumatology (Oxford)*. 2011;50(7):1216-1225. doi:10.1093/rheumatology/ker021
812. Liu-Bryan R, Terkeltaub R. Chondrocyte innate immune myeloid differentiation factor 88-dependent signaling drives pro-catabolic effects of the endogenous Toll-like receptor 2/Toll-like receptor 4 ligands low molecular weight hyaluronan and high mobility group box chromosomal protein. *Arthritis Rheum*. 2010;62(7):2004-2012. doi:10.1002/art.27475
813. Olivetto E, Borzi RM, Vitellozzi R, et al. Differential requirements for IKKalpha and IKKbeta in the differentiation of primary human osteoarthritic chondrocytes. *Arthritis Rheum*. 2008;58(1):227-239. doi:10.1002/art.23211
814. Borzì RM, Olivetto E, Pagani S, et al. Matrix metalloproteinase 13 loss associated with impaired extracellular matrix remodeling disrupts chondrocyte differentiation by concerted effects on multiple regulatory factors. *Arthritis Rheum*. 2010;62(8):2370-2381. doi:10.1002/art.27512
815. Mckenna CH, Hunder GG. Arthritis and Allied Conditions: A Textbook of Rheumatology. *Arthritis Rheum*. 1973;16(4):528-529. doi:10.1002/art.1780160416
816. Plaas A, Osborn B, Yoshihara Y, et al. Aggrecan analysis in human osteoarthritis: confocal localization and biochemical characterization of ADAMTS5-hyaluronan complexes in articular cartilages. *Osteoarthr Cartil*. 2007;15(7):719-734.
817. Cawston TE, Wilson AJ. Understanding the role of tissue degrading enzymes and their inhibitors in development and disease. *Best Pract Res Clin Rheumatol*. 2006;20(5):983-1002.

DOCTORAL THESIS DANIEL MARTÍNEZ MORENO

818. Abbaszade I, Liu RQ, Yang F, et al. Cloning and characterization of ADAMTS11, an aggrecanase from the ADAMTS family. *J Biol Chem.* 1999;274(33):23443-23450. doi:10.1074/jbc.274.33.23443
819. Li X, Chen Y, Xu R, et al. Delay in articular cartilage degeneration of the knee joint by the conditional removal of discoidin domain receptor 2 in a spontaneous mouse model of osteoarthritis. *Ann Transl Med Vol 8, No 18 (September 2020) Ann Transl Med.* 2020. <https://atm.amegroups.com/article/view/52201>.
820. Troeberg L, Nagase H. Proteases involved in cartilage matrix degradation in osteoarthritis. *Biochim Biophys Acta (BBA)-Proteins Proteomics.* 2012;1824(1):133-145.
821. Pridie KH. A method of resurfacing osteoarthritic knee joints. *J Bone Jt Surg Br.* 1959;41:618-619.
822. Friedenstein AJ, Chailakhjan RK, Lalykina KS. THE DEVELOPMENT OF FIBROBLAST COLONIES IN MONOLAYER CULTURES OF GUINEA-PIG BONE MARROW AND SPLEEN CELLS. *Cell Prolif.* 1970;3(4):393-403. doi:<https://doi.org/10.1111/j.1365-2184.1970.tb00347.x>
823. Mitchell N, Shepard N. The resurfacing of adult rabbit articular cartilage by multiple perforations through the subchondral bone. *JBJS.* 1976;58(2). https://journals.lww.com/jbjsjournal/Fulltext/1976/58020/The_resurfacing_of_adult_rabbit_articular.12.aspx.
824. Friedman MJ, Berasi CC, Fox JM, Del Pizzo W, Snyder SJ, Ferkel RD. Preliminary results with abrasion arthroplasty in the osteoarthritic knee. *Clin Orthop Relat Res.* 1984;(182):200-205.
825. Rodrigo JJ. Improvement of full-thickness chondral defect healing in the human knee after debridement and microfracture using continuous passive motion. *Am J Knee Surg.* 1994;7:109-116.
826. Steadman JR, Rodkey WG, Singleton SB, Briggs KK. Microfracture technique for full-thickness chondral defects: Technique and clinical results. *Oper Tech Orthop.* 1997;7(4):300-304.
827. Frisbie DD, Trotter GW, Powers BE, et al. Arthroscopic subchondral bone plate microfracture technique augments healing of large chondral defects in the radial carpal bone and medial femoral condyle of horses. *Vet Surg.* 1999;28(4):242-255.
828. Steadman JR, Rodkey WG, Rodrigo JJ. Microfracture: surgical technique and rehabilitation to treat chondral defects. *Clin Orthop Relat Res.* 2001;391:S362-S369.
829. Stolzing A, Scutt A. Age-related impairment of mesenchymal progenitor cell function. *Aging Cell.* 2006;5(3):213-224.
830. Gross AE, Silverstein EA, Falk J, Falk R, Langer F. The allotransplantation of partial joints in the treatment of osteoarthritis of the knee. *Clin Orthop Relat Res.* 1975;(108):7-14.
831. Bentley G, GREER RB. Homotransplantation of isolated epiphyseal and articular cartilage chondrocytes into joint surfaces of rabbits. *Nature.* 1971;230(5293):385-388.
832. Bobić V. Arthroscopic osteochondral autograft transplantation in anterior cruciate ligament reconstruction: a preliminary clinical study. *Knee Surgery, Sport Traumatol Arthrosc.* 1996;3(4):262-264.
833. Garrett JC. Osteochondral allografts for reconstruction of articular defects of the knee. *Instr Course Lect.* 1998;47:517-522.
834. Bobic V. The utilisation of osteochondral autologous grafts in the treatment of articular cartilage lesions. *Orthopade.* 1999;28(1):19-25.

REFERENCES

835. Clair BL, Johnson AR, Howard T. Cartilage repair: current and emerging options in treatment. *Foot Ankle Spec.* 2009;2(4):179-188.
836. Hamlet W, Liu SH, Yang R. Destruction of a cryopreserved meniscal allograft: a case for acute rejection. *Arthrosc J Arthrosc Relat Surg.* 1997;13(4):517-521.
837. Hangody L, Kish G, Kárpáti Z, Udvarhelyi I, Szigeti I, Bély M. Mosaicplasty for the treatment of articular cartilage defects: application in clinical practice. *Orthopedics.* 1998;21(7):751-756.
838. Hangody L, Vásárhelyi G, Hangody LR, et al. Autologous osteochondral grafting—technique and long-term results. *Injury.* 2008;39(1):32-39.
839. Solheim E, Hegna J, Øyen J, Austgulen OK, Harlem T, Strand T. Osteochondral autografting (mosaicplasty) in articular cartilage defects in the knee: results at 5 to 9 years. *Knee.* 2010;17(1):84-87.
840. Mollon B, Kandel R, Chahal J, Theodoropoulos J. The clinical status of cartilage tissue regeneration in humans. *Osteoarthr Cartil.* 2013;21(12):1824-1833.
841. Bentley G. Articular tissue grafts. *Ann Rheum Dis.* 1992;51(3):292 LP - 296. doi:10.1136/ard.51.3.292
842. Peterson L, Brittberg M, Kiviranta I, Åkerlund EL, Lindahl A. Autologous chondrocyte transplantation: biomechanics and long-term durability. *Am J Sports Med.* 2002;30(1):2-12.
843. Browne JE, Anderson AF, Arciero R, et al. Clinical outcome of autologous chondrocyte implantation at 5 years in US subjects. *Clin Orthop Relat Res.* 2005;436:237-245.
844. Gooding CR, Bartlett W, Bentley G, Skinner JA, Carrington R, Flanagan A. A prospective, randomised study comparing two techniques of autologous chondrocyte implantation for osteochondral defects in the knee: periosteum covered versus type I/III collagen covered. *Knee.* 2006;13(3):203-210.
845. Cherubino P, Grassi FA, Bulgheroni P, Ronga M. Autologous chondrocyte implantation using a bilayer collagen membrane: a preliminary report. *J Orthop Surg.* 2003;11(1):10-15.
846. Gomoll AH, Probst C, Farr J, Cole BJ, Minas T. Use of a type I/III bilayer collagen membrane decreases reoperation rates for symptomatic hypertrophy after autologous chondrocyte implantation. *Am J Sports Med.* 2009;37(1_suppl):20-23.
847. Ferruzzi A, Buda R, Faldini C, et al. Autologous chondrocyte implantation in the knee joint: open compared with arthroscopic technique: comparison at a minimum follow-up of five years. *JBJS.* 2008;90(Supplement_4):90-101.
848. Minas T. Autologous chondrocyte implantation for focal chondral defects of the knee. *Clin Orthop Relat Res.* 2001;391:S349-S361.
849. Peterson L, Minas T, Brittberg M, Nilsson A, Sjögren-Jansson E, Lindahl A. Two-to 9-year outcome after autologous chondrocyte transplantation of the knee. *Clin Orthop Relat Res.* 2000;374:212-234.
850. Peterson L, Minas T, Brittberg M, Lindahl A. Treatment of osteochondritis dissecans of the knee with autologous chondrocyte transplantation: results at two to ten years. *JBJS.* 2003;85(suppl_2):17-24.
851. Behrens P, Bitter T, Kurz B, Russlies M. Matrix-associated autologous chondrocyte transplantation/implantation (MACT/MACI)—5-year follow-up. *knee.* 2006;13(3):194-202.

DOCTORAL THESIS DANIEL MARTÍNEZ MORENO

852. Lu Y, Dhanaraj S, Wang Z, et al. Minced cartilage without cell culture serves as an effective intraoperative cell source for cartilage repair. *J Orthop Res.* 2006;24(6):1261-1270.
853. Frisbie DD, Lu Y, Kawcak CE, DiCarlo EF, Binette F, Mcllwraith CW. In vivo evaluation of autologous cartilage fragment-loaded scaffolds implanted into equine articular defects and compared with autologous chondrocyte implantation. *Am J Sports Med.* 2009;37(1_suppl):71-80.
854. Bonner KF, Daner W, Yao JQ. 2-year postoperative evaluation of a patient with a symptomatic full-thickness patellar cartilage defect repaired with particulated juvenile cartilage tissue. *J Knee Surg.* 2010;23(02):109-114.
855. Farr J, Yao JQ. Chondral defect repair with particulated juvenile cartilage allograft. *Cartilage.* 2011;2(4):346-353.
856. de Windt TS, Vonk LA, Slaper-Cortenbach ICM, van den Broek MP, Nizak R. Allogeneic Mesenchymal Stem Cells Stimulate Recycled Chondron-based Tissue Regeneration and are Safe for Single-stage Cartilage Repair in Humans. *IMPACT Cartil REPAIR KNEE.* 2015:171.
857. Korpershoek J V, Vonk LA, Kester EC, et al. Efficacy of one-stage cartilage repair using allogeneic mesenchymal stromal cells and autologous chondron transplantation (IMPACT) compared to nonsurgical treatment for focal articular cartilage lesions of the knee: study protocol for a crossover randomiz. *Trials.* 2020;21(1):1-11.
858. Camarero-Espinosa S, Rothen-Rutishauser B, Foster EJ, Weder C. Articular cartilage: from formation to tissue engineering. *Biomater Sci.* 2016;4(5):734-767. doi:10.1039/C6BM00068A
859. Newman AP. Articular cartilage repair. *Am J Sports Med.* 1998;26(2):309-324.
860. Kreuz PC, Steinwachs MR, Erggelet C, et al. Results after microfracture of full-thickness chondral defects in different compartments in the knee. *Osteoarthr Cartil.* 2006;14(11):1119-1125.
861. Benya PD, Shaffer JD. Dedifferentiated chondrocytes reexpress the differentiated collagen phenotype when cultured in agarose gels. *Cell.* 1982;30(1):215-224. doi:10.1016/0092-8674(82)90027-7
862. Brown PD, Benya PD. Alterations in chondrocyte cytoskeletal architecture during phenotypic modulation by retinoic acid and dihydrocytochalasin B-induced reexpression. *J Cell Biol.* 1988;106(1):171 LP - 179.
863. Dowthwaite GP. The surface of articular cartilage contains a progenitor cell population. *J Cell Sci.* 2004;117(6):889-897. doi:10.1242/jcs.00912
864. Dahlin RL, Meretoja V V., Ni M, Kasper FK, Mikos AG. Chondrogenic Phenotype of Articular Chondrocytes in Monoculture and Co-Culture with Mesenchymal Stem Cells in Flow Perfusion. *Tissue Eng Part A.* 2014;20(21-22):2883-2891. doi:10.1089/ten.tea.2014.0107
865. Armiento AR, Stoddart MJ, Alini M, Eglin D. Biomaterials for Articular Cartilage Tissue Engineering: Learning from Biology. *Acta Biomater.* 2017. doi:10.1016/j.actbio.2017.11.021
866. Guadix J, Zugaza J, Gálvez-Martín P. Characteristics, applications and prospects of mesenchymal stem cells in cell therapy. *Med Clin (Barc).* 2017;10(148(9)):408-414. doi:10.1016/j.medcli.2016.11.033
867. Haaparanta A-M, Järvinen E, Cengiz IF, et al. Preparation and characterization of collagen/PLA, chitosan/PLA, and collagen/chitosan/PLA hybrid scaffolds for cartilage tissue engineering. *J Mater Sci Mater Med.* 2014;25(4):1129-1136.

REFERENCES

868. Steele JAM, Moore AC, St-Pierre JP, et al. In vitro and in vivo investigation of a zonal microstructured scaffold for osteochondral defect repair. *Biomaterials*. 2022;286(May):121548. doi:10.1016/j.biomaterials.2022.121548
869. Mauck RL, Soltz MA, Wang CCB, et al. Functional tissue engineering of articular cartilage through dynamic loading of chondrocyte-seeded agarose gels. *J Biomech Eng*. 2000;122(3):252-260.
870. Buschmann MD, Gluzband YA, Grodzinsky AJ, Kimura JH, Hunziker EB. Chondrocytes in agarose culture synthesize a mechanically functional extracellular matrix. *J Orthop Res*. 1992;10(6):745-758.
871. Hauselmann HJ, Fernandes RJ, Mok SS, et al. Phenotypic stability of bovine articular chondrocytes after long-term culture in alginate beads. *J Cell Sci*. 1994;107(1):17-27.
872. San MokS S, HauselmannSn J, AydelotteS B. Aggrecan synthesized by mature bovine chondrocytes suspended in alginate. *J Biol Chem*. 1994;26952:33021-33027.
873. Kaplonyi G, Zimmerman I, Frenyo AD, Farkas T, Nemes G. The use of fibrin adhesive in the repair of chondral and osteochondral injuries. *Injury*. 1988;19(4):267-272. doi:https://doi.org/10.1016/0020-1383(88)90043-5
874. Sams AE, Nixon AJ. Chondrocyte-laden collagen scaffolds for resurfacing extensive articular cartilage defects. *Osteoarthr Cartil*. 1995;3(1):47-59. doi:https://doi.org/10.1016/S1063-4584(05)80037-8
875. Schneider U, Schmidt-Rohlfing B, Gavenis K, Maus U, Mueller-Rath R, Andereya S. A comparative study of 3 different cartilage repair techniques. *Knee Surgery, Sport Traumatol Arthrosc*. 2011;19(12):2145-2152. doi:10.1007/s00167-011-1460-x
876. LaPorta TF, Richter A, Sgagliione NA, Grande DA. Clinical Relevance of Scaffolds for Cartilage Engineering. *Orthop Clin North Am*. 2012;43(2):245-254. doi:https://doi.org/10.1016/j.ocl.2012.02.002
877. Nicodemus GD, Bryant SJ. The role of hydrogel structure and dynamic loading on chondrocyte gene expression and matrix formation. *J Biomech*. 2008;41(7):1528-1536. doi:https://doi.org/10.1016/j.jbiomech.2008.02.034
878. Bryant SJ, Anseth KS. Hydrogel properties influence ECM production by chondrocytes photoencapsulated in poly (ethylene glycol) hydrogels. *J Biomed Mater Res An Off J Soc Biomater Japanese Soc Biomater*. 2002;59(1):63-72.
879. Bryant SJ, Anseth KS. Controlling the spatial distribution of ECM components in degradable PEG hydrogels for tissue engineering cartilage. *J Biomed Mater Res Part A An Off J Soc Biomater Japanese Soc Biomater Aust Soc Biomater Korean Soc Biomater*. 2003;64(1):70-79.
880. Bryant SJ, Bender RJ, Durand KL, Anseth KS. Encapsulating chondrocytes in degrading PEG hydrogels with high modulus: engineering gel structural changes to facilitate cartilaginous tissue production. *Biotechnol Bioeng*. 2004;86(7):747-755.
881. Brandl F, Sommer F, Goepferich A. Rational design of hydrogels for tissue engineering: impact of physical factors on cell behavior. *Biomaterials*. 2007;28(2):134-146.
882. Antoine EE, Vlachos PP, Rylander MN. Review of collagen I hydrogels for bioengineered tissue microenvironments: characterization of mechanics, structure, and transport. *Tissue Eng Part B Rev*. 2014;20(6):683-696.
883. Kuo K-C, Lin R-Z, Tien H-W, et al. Bioengineering vascularized tissue constructs using an injectable cell-laden enzymatically crosslinked collagen hydrogel derived from dermal extracellular matrix. *Acta Biomater*. 2015;27:151-166.

DOCTORAL THESIS DANIEL MARTÍNEZ MORENO

884. Bryant SJ, Nicodemus GD, Villanueva I. Designing 3D photopolymer hydrogels to regulate biomechanical cues and tissue growth for cartilage tissue engineering. *Pharm Res.* 2008;25(10):2379-2386.
885. Roberts JJ, Nicodemus GD, Giunta S, Bryant SJ. Incorporation of biomimetic matrix molecules in PEG hydrogels enhances matrix deposition and reduces load-induced loss of chondrocyte-secreted matrix. *J Biomed Mater Res Part A.* 2011;97(3):281-291.
886. Levett PA, Melchels FPW, Schrobback K, Hutmacher DW, Malda J, Klein TJ. A biomimetic extracellular matrix for cartilage tissue engineering centered on photocurable gelatin, hyaluronic acid and chondroitin sulfate. *Acta Biomater.* 2014;10(1):214-223.
887. Wang D-A, Varghese S, Sharma B, et al. Multifunctional chondroitin sulphate for cartilage tissue-biomaterial integration. *Nat Mater.* 2007;6(5):385-392.
888. Lahiji A, Sohrabi A, Hungerford DS, Frondoza CG. Chitosan supports the expression of extracellular matrix proteins in human osteoblasts and chondrocytes. *J Biomed Mater Res.* 2000;51(4):586-595.
889. Nettles DL, Elder SH, Gilbert JA. Potential use of chitosan as a cell scaffold material for cartilage tissue engineering. *Tissue Eng.* 2002;8(6):1009-1016.
890. Benders KEM, van Weeren PR, Badylak SF, Saris DBF, Dhert WJA, Malda J. Extracellular matrix scaffolds for cartilage and bone regeneration. *Trends Biotechnol.* 2013;31(3):169-176.
891. Sutherland AJ, Beck EC, Dennis SC, et al. Decellularized cartilage may be a chondroinductive material for osteochondral tissue engineering. *PLoS One.* 2015;10(5):e0121966.
892. Almeida H V, Eswaramoorthy R, Cunniffe GM, Buckley CT, O'Brien FJ, Kelly DJ. Fibrin hydrogels functionalized with cartilage extracellular matrix and incorporating freshly isolated stromal cells as an injectable for cartilage regeneration. *Acta Biomater.* 2016;36:55-62.
893. Almeida H V, Liu Y, Cunniffe GM, et al. Controlled release of transforming growth factor- β 3 from cartilage-extra-cellular-matrix-derived scaffolds to promote chondrogenesis of human-joint-tissue-derived stem cells. *Acta Biomater.* 2014;10(10):4400-4409.
894. Elder S, Pinheiro A, Young C, Smith P, Wright E. Evaluation of genipin for stabilization of decellularized porcine cartilage. *J Orthop Res.* 2017;35(9):1949-1957. doi:<https://doi.org/10.1002/jor.23483>
895. Cui YL, Qi A Di, Liu WG, et al. Biomimetic surface modification of poly(l-lactic acid) with chitosan and its effects on articular chondrocytes in vitro. *Biomaterials.* 2003;24(21):3859-3868. doi:[https://doi.org/10.1016/S0142-9612\(03\)00209-6](https://doi.org/10.1016/S0142-9612(03)00209-6)
896. Chen G, Sato T, Ushida T, Ochiai N, Tateishi T. Tissue Engineering of Cartilage Using a Hybrid Scaffold of Synthetic Polymer and Collagen. *Tissue Eng.* 2004;10(3-4):323-330. doi:10.1089/107632704323061681
897. Jin R, Moreira Teixeira LS, Dijkstra PJ, et al. Injectable chitosan-based hydrogels for cartilage tissue engineering. *Biomaterials.* 2009;30(13):2544-2551. doi:<https://doi.org/10.1016/j.biomaterials.2009.01.020>
898. Callahan LAS, Ganios AM, McBurney DL, et al. ECM Production of Primary Human and Bovine Chondrocytes in Hybrid PEG Hydrogels Containing Type I Collagen and Hyaluronic Acid. *Biomacromolecules.* 2012;13(5):1625-1631. doi:10.1021/bm3003336
899. Liao J, Qu Y, Chu B, Zhang X, Qian Z. Biodegradable CSMA/PECA/graphene porous hybrid scaffold for cartilage tissue engineering. *Sci Rep.* 2015;5(1):1-16.

REFERENCES

900. Rowland CR, Lennon DP, Caplan AI, Guilak F. The effects of crosslinking of scaffolds engineered from cartilage ECM on the chondrogenic differentiation of MSCs. *Biomaterials*. 2013;34(23):5802-5812. doi:<https://doi.org/10.1016/j.biomaterials.2013.04.027>
901. Benjamin M, Archer CW, Ralphs JR. Cytoskeleton of cartilage cells. *Microsc Res Tech*. 1994;28(5):372-377.
902. Langelier E, Suetterlin R, Hoemann CD, Aebi U, Buschmann MD. The chondrocyte cytoskeleton in mature articular cartilage: structure and distribution of actin, tubulin, and vimentin filaments. *J Histochem Cytochem*. 2000;48(10):1307-1320.
903. Durrant LA, Archer CW, Benjamin M, Ralphs JR. Organisation of the chondrocyte cytoskeleton and its response to changing mechanical conditions in organ culture. *J Anat*. 1999;194(3):343-353.
904. Li W-J, Jiang YJ, Tuan RS. Chondrocyte phenotype in engineered fibrous matrix is regulated by fiber size. *Tissue Eng*. 2006;12(7):1775-1785.
905. Reboredo JW, Weigel T, Steinert A, Rackwitz L, Rudert M, Walles H. Investigation of Migration and Differentiation of Human Mesenchymal Stem Cells on Five-Layered Collagenous Electrospun Scaffold Mimicking Native Cartilage Structure. *Adv Healthc Mater*. 2016;5(17):2191-2198.
906. Sharma B, Williams CG, Kim TK, et al. Designing zonal organization into tissue-engineered cartilage. *Tissue Eng*. 2007;13(2):405-414.
907. Mellati A, Fan C, Tamayol A, et al. Microengineered 3D cell-laden thermoresponsive hydrogels for mimicking cell morphology and orientation in cartilage tissue engineering. *Biotechnol Bioeng*. 2017;114(1):217-231.
908. Karimi T, Barati D, Karaman O, Moeinzadeh S, Jabbari E. A developmentally inspired combined mechanical and biochemical signaling approach on zonal lineage commitment of mesenchymal stem cells in articular cartilage regeneration. *Integr Biol*. 2015;7(1):112-127.
909. Klein TJ, Malda J, Sah RL, Hutmacher DW. Tissue engineering of articular cartilage with biomimetic zones. *Tissue Eng Part B Rev*. 2009;15(2):143-157.
910. Tatman PD, Gerull W, Sweeney-Easter S, Davis JI, Gee AO, Kim D-H. Multiscale biofabrication of articular cartilage: bioinspired and biomimetic approaches. *Tissue Eng Part B Rev*. 2015;21(6):543-559.
911. Motamedian SR, Hosseinpour S, Ahsaie MG, Khojasteh A. Smart scaffolds in bone tissue engineering: A systematic review of literature. *World J Stem Cells*. 2015;7(3):657.
912. Mow VC, Wang CC, Hung CT. The extracellular matrix, interstitial fluid and ions as a mechanical signal transducer in articular cartilage. *Osteoarthr Cartil*. 1999;7(1):41-58.
913. Lee W, Leddy HA, Chen Y, et al. Synergy between Piezo1 and Piezo2 channels confers high-strain mechanosensitivity to articular cartilage. *Proc Natl Acad Sci U S A*. 2014;111(47):E5114-E5122. doi:10.1073/pnas.1414298111
914. Xu X, Liu S, Liu H, et al. Piezo channels: Awesome mechanosensitive structures in cellular mechanotransduction and their role in bone. *Int J Mol Sci*. 2021;22(12). doi:10.3390/ijms22126429
915. Du G, Li L, Zhang X, et al. Roles of TRPV4 and piezo channels in stretch-evoked Ca²⁺ response in chondrocytes. *Exp Biol Med*. 2020;245(3):180-189. doi:10.1177/1535370219892601
916. Sun W, Chi S, Li Y, et al. The mechanosensitive Piezo1 channel is required for bone formation. *Elife*. 2019;8:1-25. doi:10.7554/eLife.47454

DOCTORAL THESIS DANIEL MARTÍNEZ MORENO

917. Agarwal P, Lee H pyo, Smeriglio P, et al. A dysfunctional TRPV4–GSK3 β pathway prevents osteoarthritic chondrocytes from sensing changes in extracellular matrix viscoelasticity. *Nat Biomed Eng*. 2021;5(12):1472-1484. doi:10.1038/s41551-021-00691-3
918. Wann AKT, Zuo N, Haycraft CJ, et al. Primary cilia mediate mechanotransduction through control of ATP-induced Ca²⁺ signaling in compressed chondrocytes. *FASEB J*. 2012;26(4):1663-1671. doi:10.1096/fj.11-193649
919. Shieh AC, Athanasiou KA. Dynamic compression of single cells. *Osteoarthr Cartil*. 2007;15(3):328-334.
920. Fitzgerald JB, Jin M, Dean D, Wood DJ, Zheng MH, Grodzinsky AJ. Mechanical compression of cartilage explants induces multiple time-dependent gene expression patterns and involves intracellular calcium and cyclic AMP. *J Biol Chem*. 2004;279(19):19502-19511.
921. Agarwal S, Deschner J, Long P, et al. Role of NF- κ B transcription factors in antiinflammatory and proinflammatory actions of mechanical signals. *Arthritis Rheum*. 2004;50(11):3541-3548.
922. Waldman SD, Spiteri CG, Grynblas MD, Pilliar RM, Hong J, Kandel RA. Effect of biomechanical conditioning on cartilaginous tissue formation in vitro. *JBJS*. 2003;85(suppl_2):101-105.
923. Hall AC. Differential effects of hydrostatic pressure on cation transport pathways of isolated articular chondrocytes. *J Cell Physiol*. 1999;178(2):197-204. doi:10.1002/(SICI)1097-4652(199902)178:2<197::AID-JCP9>3.0.CO;2-3
924. Kornblatt JA, Kornblatt MJ. The effects of osmotic and hydrostatic pressures on macromolecular systems. *Biochim Biophys Acta - Protein Struct Mol Enzymol*. 2002;1595(1-2):30-47. doi:10.1016/S0167-4838(01)00333-8
925. Browning JA, Walker RE, Hall AC, Wilkins RJ. Modulation of Na⁺ x H⁺ exchange by hydrostatic pressure in isolated bovine articular chondrocytes. *Acta Physiol Scand*. 1999;166(1):39-45.
926. Mizuno S. A novel method for assessing effects of hydrostatic fluid pressure on intracellular calcium: a study with bovine articular chondrocytes. *Am J Physiol Cell Physiol*. 2005;288(2):C329-37. doi:10.1152/ajpcell.00131.2004
927. Buckwalter JA. Articular Cartilage: Injuries and Potential for Healing. *J Orthop Sport Phys Ther*. 1998;28(4):192-202. doi:10.2519/jospt.1998.28.4.192
928. Waters RL, Lunsford BR, Perry J, Byrd R. Energy speed relationship of walking: Standard tables. *J Orthop Res*. 1988;6(2):215-222. doi:10.1002/jor.1100060208
929. Suh JK, Baek GH, Arøen A, et al. Intermittent sub-ambient interstitial hydrostatic pressure as a potential mechanical stimulator for chondrocyte metabolism. *Osteoarthr Cartil*. 1999;7(1):71-80. doi:10.1053/joca.1998.0163
930. Jortikka MO, Parkkinen JJ, Inkinen RI, et al. The role of microtubules in the regulation of proteoglycan synthesis in chondrocytes under hydrostatic pressure. *Arch Biochem Biophys*. 2000;374(2):172-180. doi:10.1006/abbi.1999.1543
931. Smith RL, Rusk SF, Ellison BE, et al. In vitro stimulation of articular chondrocyte mRNA and extracellular matrix synthesis by hydrostatic pressure. *J Orthop Res*. 1996;14(1):53-60. doi:10.1002/jor.1100140110
932. Parkkinen JJ, Ikonen J, Lammi MJ, Laakkonen J, Tammi M, Helminen HJ. Effects of Cyclic Hydrostatic Pressure on Proteoglycan Synthesis in Cultured Chondrocytes and Articular Cartilage Explants. *Arch Biochem Biophys*. 1993;300(1):458-465. doi:https://doi.org/10.1006/abbi.1993.1062

REFERENCES

933. Carver SE, Heath CA. Increasing extracellular matrix production in regenerating cartilage with intermittent physiological pressure. *Biotechnol Bioeng*. 1999;62(2):166-174.
934. Elder BD, Athanasiou KA. Effects of Temporal Hydrostatic Pressure on Tissue-Engineered Bovine Articular Cartilage Constructs. *Tissue Eng Part A*. 2009;15(5):1151-1158. doi:10.1089/ten.tea.2008.0200
935. Luo Z-J, Seedhom BB. Light and low-frequency pulsatile hydrostatic pressure enhances extracellular matrix formation by bone marrow mesenchymal cells: an in-vitro study with special reference to cartilage repair. *Proc Inst Mech Eng H*. 2007;221(5):499-507. doi:10.1243/09544119JEIM199
936. Wagner DR, Lindsey DP, Li KW, et al. Hydrostatic pressure enhances chondrogenic differentiation of human bone marrow stromal cells in osteochondrogenic medium. *Ann Biomed Eng*. 2008;36(5):813-820. doi:10.1007/s10439-008-9448-5
937. Elder SH, Fulzele KS, McCulley WR. Cyclic hydrostatic compression stimulates chondroinduction of C3H/10T1/2 cells. *Biomech Model Mechanobiol*. 2005;3(3):141-146. doi:10.1007/s10237-004-0058-3
938. Elder BD, Athanasiou KA. Synergistic and Additive Effects of Hydrostatic Pressure and Growth Factors on Tissue Formation. Egles C, ed. *PLoS One*. 2008;3(6):e2341. doi:10.1371/journal.pone.0002341
939. Trindade MCD, Shida J, Ikenoue T, et al. Intermittent hydrostatic pressure inhibits matrix metalloproteinase and pro-inflammatory mediator release from human osteoarthritic chondrocytes in vitro. *Osteoarthr Cartil*. 2004;12(9):729-735. doi:https://doi.org/10.1016/j.joca.2004.05.008
940. Afoke NY, Byers PD, Hutton WC. Contact pressures in the human hip joint. *J Bone Joint Surg Br*. 1987;69(4):536-541. doi:10.1302/0301-620X.69B4.3611154
941. Park S, Krishnan R, Nicoll SB, Ateshian GA. Cartilage interstitial fluid load support in unconfined compression. *J Biomech*. 2003;36(12):1785-1796. doi:10.1016/S0021-9290(03)00231-8
942. Armstrong CG, Lai WM, Mow VC. An analysis of the unconfined compression of articular cartilage. *J Biomech Eng*. 1984;106(2):165-173.
943. Schumann D, Kujat R, Nerlich M, Angele P. Mechanobiological conditioning of stem cells for cartilage tissue engineering. *Biomed Mater Eng*. 2006;16(4 Suppl):S37-52. http://www.ncbi.nlm.nih.gov/pubmed/16823112.
944. Meyer CJ, Alenghat FJ, Rim P, Fong JHJ, Fabry B, Ingber DE. Mechanical control of cyclic AMP signalling and gene transcription through integrins. *Nat Cell Biol*. 2000;2(9):666-668. doi:10.1038/35023621
945. Gudi S, Nolan JP, Frangos JA. Modulation of GTPase activity of G proteins by fluid shear stress and phospholipid composition. *Proc Natl Acad Sci U S A*. 1998;95(5):2515-2519. doi:10.1073/pnas.95.5.2515
946. Kumar D, Lassar AB. The Transcriptional Activity of Sox9 in Chondrocytes Is Regulated by RhoA Signaling and Actin Polymerization. *Mol Cell Biol*. 2009;29(15):4262-4273. doi:10.1128/MCB.01779-08
947. Yoon YM, Oh C Do, Kang SS, Chun JS. Protein kinase A regulates chondrogenesis of mesenchymal cells at the post-precartilage condensation stage via protein kinase C- α signaling. *J Bone Miner Res*. 2000;15(11):2197-2205. doi:10.1359/jbmr.2000.15.11.2197
948. Juhász T, Matta C, Somogyi C, et al. Mechanical loading stimulates chondrogenesis via the PKA/CREB-Sox9 and PP2A pathways in chicken micromass cultures. *Cell Signal*. 2014;26(3):468-482. doi:10.1016/j.cellsig.2013.12.001

DOCTORAL THESIS DANIEL MARTÍNEZ MORENO

949. Zhao L, Li G, Zhou GQ. SOX9 directly binds CREB as a novel synergism with the PKA pathway in BMP-2-induced osteochondrogenic differentiation. *J Bone Miner Res.* 2009;24(5):826-836. doi:10.1359/jbmr.081236
950. Wang Y, Huang Z, Nayak PS, et al. Strain-induced Differentiation of Fetal Type II Epithelial Cells Is Mediated via Integrin $\alpha 6\beta 1$ -ADAM17/TACE Signaling Pathway. *J Biol Chem.* 2013;02905:820-828. doi:10.1074/jbc.M113.473777
951. Subramanian A, Budhiraja G, Sahu N. Chondrocyte primary cilium is mechanosensitive and responds to low-intensity-ultrasound by altering its length and orientation. *Int J Biochem Cell Biol.* 2017;91(August):60-64. doi:10.1016/j.biocel.2017.08.018
952. Muhammad H, Rais Y, Miosge N, Ornan EM. The primary cilium as a dual sensor of mechanochemical signals in chondrocytes. *Cell Mol Life Sci.* 2012;69(13):2101-2107. doi:10.1007/s00018-011-0911-3
953. Farnum CE, Wilsman NJ. Orientation of Primary Cilia of Articular Chondrocytes in Three-Dimensional Space. *Anat Rec.* 2011;294(3):533-549. doi:10.1002/ar.21330
954. Knight AKTWMM. Primary cilia elongation in response to interleukin-1 mediates the inflammatory response. 2012:2967-2977. doi:10.1007/s00018-012-0980-y
955. Phan MN, Leddy HA, Votta BJ, et al. Functional characterization of TRPV4 as an osmotically sensitive ion channel in porcine articular chondrocytes. *Arthritis Rheum.* 2009;60(10):3028-3037. doi:10.1002/art.24799
956. O'Connor CJ, Leddy HA, Benefield HC, Liedtke WB, Guilak F. TRPV4-mediated mechanotransduction regulates the metabolic response of chondrocytes to dynamic loading. *Proc Natl Acad Sci.* 2014;111(4):1316-1321. doi:10.1073/pnas.1319569111
957. Knight MM, Mcglashan SR, Garcia M, Jensen CG, Poole CA. Articular chondrocytes express connexin 43 hemichannels and P2 receptors - A putative mechanoreceptor complex involving the primary cilium? *J Anat.* 2009;214(2):275-283. doi:10.1111/j.1469-7580.2008.01021.x
958. Toma CD, Ashkar S, Gray ML, Schaffer JL, Gerstenfeld LC. Signal transduction of mechanical stimuli is dependent on microfilament integrity: Identification of osteopontin as a mechanically induced gene in osteoblasts. *J Bone Miner Res.* 1997;12(10):1626-1636. doi:10.1359/jbmr.1997.12.10.1626
959. Rich DR, Clark AL. Chondrocyte primary cilia shorten in response to osmotic challenge and are sites for endocytosis. *Osteoarthr Cartil.* 2012;20(8):923-930. doi:10.1016/j.joca.2012.04.017
960. Moore AC, Burriss DL. An analytical model to predict interstitial lubrication of cartilage in migrating contact areas. *J Biomech.* 2014;47(1):148-153. doi:10.1016/j.jbiomech.2013.09.020
961. Pazzano D, Mercier KA, Moran JM, et al. Comparison of chondrogenesis in static and perfused bioreactor culture. *Biotechnol Prog.* 2000;16(5):893-896. doi:10.1021/bp000082v
962. Yeatts AB, Fisher JP. Bone tissue engineering bioreactors: Dynamic culture and the influence of shear stress. *Bone.* 2011;48(2):171-181. doi:10.1016/j.bone.2010.09.138
963. Davisson T, Sah RL, Ratcliffe A. Perfusion Increases Cell Content and Matrix Synthesis in Chondrocyte Three-Dimensional Cultures. *Tissue Eng.* 2002;8(5):807-816. doi:10.1089/10763270260424169
964. Shahin K, Doran PM. Strategies for enhancing the accumulation and retention of extracellular matrix in tissue-engineered cartilage cultured in bioreactors. *PLoS One.* 2011;6(8). doi:10.1371/journal.pone.0023119

REFERENCES

965. Mayer N, Lopa S, Talò G, et al. Interstitial perfusion culture with specific soluble factors inhibits type I collagen production from human osteoarthritic chondrocytes in clinical-grade collagen sponges. *PLoS One*. 2016;11(9):1-18. doi:10.1371/journal.pone.0161479
966. Uddin SMZ, Richbrough B, Ding Y, et al. Chondro-protective effects of low intensity pulsed ultrasound. *Osteoarthr Cartil*. 2016;24(11):1989-1998. doi:10.1016/j.joca.2016.06.014
967. Azuma Y, Ito M, Harada Y, Takagi H, Ohta T, Jingushi S. Low-intensity pulsed ultrasound accelerates rat femoral fracture healing by acting on the various cellular reactions in the fracture callus. *J Bone Miner Res*. 2001;16(4):671-680. doi:10.1359/jbmr.2001.16.4.671
968. Zhou X, Castro NJ, Zhu W, et al. Improved Human Bone Marrow Mesenchymal Stem Cell Osteogenesis in 3D Bioprinted Tissue Scaffolds with Low Intensity Pulsed Ultrasound Stimulation. *Sci Rep*. 2016;6. doi:10.1038/srep32876
969. Takayama T, Suzuki N, Ikeda K, et al. Low-intensity pulsed ultrasound stimulates osteogenic differentiation in ROS 17/2.8 cells. *Life Sci*. 2007;80(10):965-971. doi:https://doi.org/10.1016/j.lfs.2006.11.037
970. Korstjens CM, van der Rijt RHH, Albers GHR, Semeins CM, Klein-Nulend J. Low-intensity pulsed ultrasound affects human articular chondrocytes in vitro. *Med Biol Eng Comput*. 2008;46(12):1263-1270. doi:10.1007/s11517-008-0409-9
971. Ebisawa K, Hata K-I, Okada K, et al. Ultrasound enhances transforming growth factor beta-mediated chondrocyte differentiation of human mesenchymal stem cells. *Tissue Eng*. 2004;10(5-6):921-929. doi:10.1089/1076327041348437
972. Cheng K, Xia P, Lin Q, et al. Effects of low-intensity pulsed ultrasound on integrin-FAK-PI3K/Akt mechanochemical transduction in rabbit osteoarthritis chondrocytes. *Ultrasound Med Biol*. 2014;40(7):1609-1618. doi:10.1016/j.ultrasmedbio.2014.03.002
973. Xia P, Ren S, Lin Q, et al. Low-Intensity Pulsed Ultrasound Affects Chondrocyte Extracellular Matrix Production via an Integrin-Mediated p38 MAPK Signaling Pathway. *Ultrasound Med Biol*. 2015;41(6):1690-1700. doi:10.1016/j.ultrasmedbio.2015.01.014
974. Whitney NP, Lamb AC, Louw TM, Subramanian A. Integrin-Mediated Mechanotransduction Pathway of Low-Intensity Continuous Ultrasound in Human Chondrocytes. *Ultrasound Med Biol*. 2012;38(10):1734-1743. doi:10.1016/j.ultrasmedbio.2012.06.002
975. Nishida T, Kubota S, Aoyama E, Yamanaka N, Lyons KM, Takigawa M. Low-intensity pulsed ultrasound (LIPUS) treatment of cultured chondrocytes stimulates production of CCN family protein 2 (CCN2), a protein involved in the regeneration of articular cartilage: mechanism underlying this stimulation. *Osteoarthr Cartil*. 2017;25(5):759-769. doi:10.1016/j.joca.2016.10.003
976. Honjo T, Kubota S, Kamioka H, et al. Promotion of Ccn2 expression and osteoblastic differentiation by actin polymerization, which is induced by laminar fluid flow stress. *J Cell Commun Signal*. 2012;6(4):225-232. doi:10.1007/s12079-012-0177-z
977. Yosimichi G, Kubota S, Hattori T, et al. CTGF/Hcs24 interacts with the cytoskeletal protein actin in chondrocytes. *Biochem Biophys Res Commun*. 2002;299(5):755-761. doi:https://doi.org/10.1016/S0006-291X(02)02739-0
978. Ren L, Yang Z, Song J, Wang Z, Deng F, Li W. Involvement of p38 MAPK pathway in low intensity pulsed ultrasound induced osteogenic differentiation of human periodontal ligament cells. *Ultrasonics*. 2013;53(3):686-690. doi:https://doi.org/10.1016/j.ultras.2012.10.008
979. Wang J, Tang N, Xiao Q, Zhao L, Li Y, Li J. The Potential Application of Pulsed Ultrasound on Bone Defect Repair via Developmental Engineering: An In Vitro Study. *Artificial*.

DOCTORAL THESIS DANIEL MARTÍNEZ MORENO

- 2015;40(5):505-513. doi:10.1111/aor.12578
980. Fernandez J, Zhang J, Heidlauf T, et al. Multiscale musculoskeletal modelling, data-model fusion and electromyography-informed modelling. *Interface Focus*. 2016;6(2):20150084. doi:10.1098/rsfs.2015.0084
981. Schulz RM, Bader A. Cartilage tissue engineering and bioreactor systems for the cultivation and stimulation of chondrocytes. *Eur Biophys J*. 2007;36(4-5):539-568. doi:10.1007/s00249-007-0139-1
982. Ting N. Introduction and new drug development process. In: *Dose Finding in Drug Development*. Springer; 2006:1-17.
983. Brodniewicz T, Gryniewicz G. Preclinical drug development. *Acta Pol Pharm*. 2010;67(6):578-585.
984. Drug T, Process D. The Drug Development Process and the Phases of Clinical Research. 2007:304-328. doi:10.1007/978-88-470-0492-4_12
985. Sun D, Gao W, Hu H, Zhou S. Why 90% of clinical drug development fails and how to improve it? *Acta Pharm Sin B*. 2022;12(7):3049-3062. doi:10.1016/j.apsb.2022.02.002
986. EFPIA. Shifting the paradigm for ATMPs : Adapting reimbursement and value frameworks to improve patient access in Europe Shifting the paradigm for ATMPs. 2022;(January):25. <https://www.efpia.eu/news-events/the-efpia-view/efpia-news/shifting-the-paradigm-for-atmps/>.
987. Kola I, Landis J. Can the pharmaceutical industry reduce attrition rates? *Nat Rev Drug Discov*. 2004;3(8):711-716.
988. Arrowsmith J, Miller P. Phase II and Phase III attrition rates 2011-2012. *Nat Rev Drug Discov*. 2013;12(8):569. doi:10.1038/nrd4090
989. Munos B. Lessons from 60 years of pharmaceutical innovation. *Nat Rev Drug Discov*. 2009;8(12):959-968. doi:10.1038/nrd2961
990. Paul SM, Mytelka DS, Dunwiddie CT, et al. How to improve R&D productivity: the pharmaceutical industry's grand challenge. *Nat Rev Drug Discov*. 2010;9(3):203-214. doi:10.1038/nrd3078
991. Pammolli F, Magazzini L, Riccaboni M. The productivity crisis in pharmaceutical R&D. *Nat Rev Drug Discov*. 2011;10(6):428-438. doi:10.1038/nrd3405
992. Austin DH. Research and development in the pharmaceutical industry. In: Congress of the United States, Congressional Budget Office; 2006.
993. DiMasi JA, Paquette C. The economics of follow-on drug research and development. *Pharmacoeconomics*. 2004;22(2):1-14. doi:10.2165/00019053-200422002-00002
994. Raghavendra MS, Raj JR, Seetharaman A. A STUDY OF DECREASE IN R&D SPENDING IN THE PHARMACEUTICAL INDUSTRY DURING POST-RECESSION. *Int J Acad Res*. 2012;4(5).
995. Olfson M, Marcus SC. Decline In Placebo-Controlled Trial Results Suggests New Directions For Comparative Effectiveness Research. *Health Aff*. 2013;32(6):1116-1125. doi:10.1377/hlthaff.2012.1353
996. Garnier J-P. Rebuilding the R&D engine in big pharma. *Harv Bus Rev*. 2008;86(5):68-70.
997. Barton JH, Emanuel EJ. The Patents-Based Pharmaceutical Development Process Rationale, Problems, and Potential Reforms. *JAMA*. 2005;294(16):2075-2082. doi:10.1001/jama.294.16.2075
998. Bauchner H, Fontanarosa PB. Restoring Confidence in the Pharmaceutical Industry. *JAMA*.

REFERENCES

- 2013;309(6):607-609. doi:10.1001/jama.2013.58
999. Yildirim O, Gottwald M, Schüler P, Michel MC. Opportunities and challenges for drug development: public-private partnerships, adaptive designs and big data. *Front Pharmacol.* 2016;7:461.
1000. Smith HL, Ho K. Measuring the performance of Oxford University, Oxford Brookes University and the government laboratories' spin-off companies. *Res Policy.* 2006;35(10):1554-1568.
1001. Prokop D, Huggins R, Bristow G. The survival of academic spinoff companies: An empirical study of key determinants. *Int Small Bus J.* 2019;37(5):502-535. doi:10.1177/0266242619833540
1002. Jagosh J, Bush PL, Salsberg J, et al. A realist evaluation of community-based participatory research: partnership synergy, trust building and related ripple effects. *BMC Public Health.* 2015;15(1):1-11.
1003. Frangioni J V. The impact of greed on academic medicine and patient care. *Nat Biotechnol.* 2008;26(5):503-507. doi:10.1038/nbt0508-503
1004. Bostyn SJR. Is the European Patent System for (Bio) Pharmaceuticals in Need of Change? *IIC-International Rev Intellect Prop Compet Law.* 2022:1-5.
1005. Kumazawa R. Patenting in the Pharmaceutical Industry. *Intellect Prop Rights.* 2017:23-38.
1006. Chan SY, Loscalzo J. The emerging paradigm of network medicine in the study of human disease. *Circ Res.* 2012;111(3):359-374.
1007. Hart Y, Antebi YE, Mayo AE, Friedman N, Alon U. Design principles of cell circuits with paradoxical components. *Proc Natl Acad Sci.* 2012;109(21):8346-8351.
1008. Eggert US. The why and how of phenotypic small-molecule screens. *Nat Chem Biol.* 2013;9(4):206-209.
1009. Swinney DC, Anthony J. How were new medicines discovered? *Nat Rev Drug Discov.* 2011;10(7):507-519.
1010. Vidal R, Pilar-Cuellar F, dos Anjos S, et al. New strategies in the development of antidepressants: towards the modulation of neuroplasticity pathways. *Curr Pharm Des.* 2011;17(5):521-533.
1011. Besnard J, Ruda GF, Setola V, et al. Automated design of ligands to polypharmacological profiles. *Nature.* 2012;492(7428):215-220.
1012. Makley LN, Gestwicki JE. Expanding the number of 'Druggable' targets: non-enzymes and protein-protein interactions. *Chem Biol Drug Des.* 2013;81(1):22-32.
1013. Behrens MK. Priorities for Personalized Medicine. 2008.
1014. Wilson MK, Karakasis K, Oza AM. Outcomes and endpoints in trials of cancer treatment: the past, present, and future. *Lancet Oncol.* 2015;16(1):e32-e42.
1015. Jönsson B, Hampson G, Michaels J, et al. Advanced therapy medicinal products and health technology assessment principles and practices for value-based and sustainable healthcare. *Eur J Heal Econ.* 2019;20(3):427-438.
1016. Dolsten M, Søggaard M. Precision medicine: an approach to R&D for delivering superior medicines to patients. *Clin Transl Med.* 2012;1(1):1-4.
1017. Cohrs RJ, Martin T, Ghahramani P, Bidaut L, Higgins PJ, Shahzad A. Translational medicine definition by the European society for translational medicine. *New Horizons Transl Med.* 2015;2(3):86-88. doi:10.1016/j.nhtm.2014.12.002

DOCTORAL THESIS DANIEL MARTÍNEZ MORENO

1018. Wehling M. Translational medicine: can it really facilitate the transition of research “from bench to bedside”? *Eur J Clin Pharmacol.* 2006;62(2):91-95. doi:10.1007/s00228-005-0060-4
1019. Wehling M. Translational science in medicine. *Int J Pharm Med.* 2006;20(5):303-310.
1020. Enderle J, Bronzino J. *Introduction to Biomedical Engineering.* Academic press; 2012.
1021. Chien S, Bashir R, Nerem RM, Pettigrew R. Engineering as a new frontier for translational medicine. *Sci Transl Med.* 2015;7(281):1-3. doi:10.1126/scitranslmed.aaa4325
1022. Yock PG, Brinton TJ, Zenios SA. Teaching biomedical technology innovation as a discipline. *Sci Transl Med.* 2011;3(92):92cm18-92cm18.
1023. Meyers FJ, Pomeroy C. Creating the future biomedical research workforce. *Sci Transl Med.* 2011;3(102):102fs5-102fs5.
1024. DeFranco JF, Hutchinson M. Understanding smart medical devices. *Computer (Long Beach Calif).* 2021;54(5):76-80.
1025. Watts-Schacter E, Kral P. Mobile health applications, smart medical devices, and big data analytics technologies. *Am J Med Res.* 2019;6(1):19-25.
1026. Aristotle A, Aristotle. *Metaphysics.* Vol 1. Harvard University Press Cambridge, MA; 1933.
1027. Meadows DH. *Thinking in Systems: A Primer.* chelsea green publishing; 2008.
1028. Feldman AM. Bench-to-Bedside; Clinical and Translational Research; Personalized Medicine; Precision Medicine-What's in a Name? *Clin Transl Sci.* 2015;8(3):171-173. doi:10.1111/cts.12302
1029. Chen Y, Yan Y, Li X, et al. Application of ultrasound on monitoring the evolution of the collagen fiber reinforced nHAC/CS composites in vivo. *Biomed Res Int.* 2014;2014.
1030. López-Ruiz E, Jiménez G, Kwiatkowski W, et al. Impact of TGF- β family-related growth factors on chondrogenic differentiation of adipose-derived stem cells isolated from lipoaspirates and infrapatellar fat pads of osteoarthritic patients. *Eur Cells Mater.* 2018;35:209-224. doi:10.22203/eCM.v035a15
1031. Harrison RG. On the stereotropism of embryonic cells. *Science (80-).* 1911;34(870):279-281.
1032. D'angelo F, Armentano I, Mattioli S, et al. Micropatterned hydrogenated amorphous carbon guides mesenchymal stem cells towards neuronal differentiation. *Eur Cell Mater.* 2010;20(4):231-244.
1033. Kilian KA, Bugarija B, Lahn BT, Mrksich M. Geometric cues for directing the differentiation of mesenchymal stem cells. *Proc Natl Acad Sci.* 2010;107(11):4872-4877.
1034. Jeong CG, Zhang H, Hollister SJ. Three-dimensional poly(1,8-octanediol-co-citrate) scaffold pore shape and permeability effects on sub-cutaneous in vivo chondrogenesis using primary chondrocytes. *Acta Biomater.* 2011;7(2):505-514. doi:10.1016/j.actbio.2010.08.027
1035. Chang BS, Lee CK, Hong KS, et al. Osteoconduction at porous hydroxyapatite with various pore configurations. *Biomaterials.* 2000. doi:10.1016/S0142-9612(00)00030-2
1036. Ozbolat IT, Koc B. 3D hybrid wound devices for spatiotemporally controlled release kinetics. *Comput Methods Programs Biomed.* 2012;108(3):922-931. doi:10.1016/j.cmpb.2012.05.004
1037. Zhang J, Wu L, Jing D, Ding J. A comparative study of porous scaffolds with cubic and spherical macropores. *Polymer (Guildf).* 2005. doi:10.1016/j.polymer.2005.02.120

REFERENCES

1038. Karageorgiou V, Kaplan D. Porosity of 3D biomaterial scaffolds and osteogenesis. *Biomaterials*. 2005. doi:10.1016/j.biomaterials.2005.02.002
1039. Vieira A, Guedes R, Tita V. Considerations for the design of polymeric biodegradable products. *J Polym Eng*. 2013;33:293-302. doi:10.1515/polyeng-2012-0150
1040. Suggs LJ, Moore SA, Mikos AG. Synthetic biodegradable polymers for medical applications. In: *Physical Properties of Polymers Handbook*. Springer; 2007:939-950.
1041. Engelberg I, Kohn J. Physico-mechanical properties of degradable polymers used in medical applications: A comparative study. *Biomaterials*. 1991. doi:10.1016/0142-9612(91)90037-B
1042. Datta J, Kasprzyk P, Błażek K, Włoch M. Synthesis, structure and properties of poly(ester-urethane)s obtained using bio-based and petrochemical 1,3-propanediol and 1,4-butanediol. *J Therm Anal Calorim*. 2017;130(1):261-276. doi:10.1007/s10973-017-6558-z
1043. Moroni L, De Wijn JR, Van Blitterswijk CA. 3D fiber-deposited scaffolds for tissue engineering: Influence of pores geometry and architecture on dynamic mechanical properties. *Biomaterials*. 2006;27(7):974-985. doi:10.1016/j.biomaterials.2005.07.023
1044. Domingos M, Intranuovo F, Russo T, et al. The first systematic analysis of 3D rapid prototyped poly(ϵ - caprolactone) scaffolds manufactured through BioCell printing: The effect of pore size and geometry on compressive mechanical behaviour and in vitro hMSC viability. *Biofabrication*. 2013;5(4). doi:10.1088/1758-5082/5/4/045004
1045. Zhang ZZ, Jiang D, Ding JX, et al. Role of scaffold mean pore size in meniscus regeneration. *Acta Biomater*. 2016;43:314-326. doi:10.1016/j.actbio.2016.07.050
1046. Zeltinger J, Sherwood JK, Graham DA, Müeller R, Griffith LG. Effect of pore size and void fraction on cellular adhesion, proliferation, and matrix deposition. *Tissue Eng*. 2001. doi:10.1089/107632701753213183
1047. Olubamiji AD, Izadifar Z, Si JL, Cooper DML, Eames BF, Chen DXB. Modulating mechanical behaviour of 3D-printed cartilage-mimetic PCL scaffolds: Influence of molecular weight and pore geometry. *Biofabrication*. 2016;8(2). doi:10.1088/1758-5090/8/2/025020
1048. Lee JW, Ahn G, Cho DW, Kim JY. Evaluating cell proliferation based on internal pore size and 3D scaffold architecture fabricated using solid freeform fabrication technology. *J Mater Sci Mater Med*. 2010. doi:10.1007/s10856-010-4173-7
1049. Temple JP, Hutton DL, Hung BP, et al. Engineering anatomically shaped vascularized bone grafts with hASCs and 3D-printed PCL scaffolds. *J Biomed Mater Res - Part A*. 2014;102(12):4317-4325. doi:10.1002/jbm.a.35107
1050. Park S, Kim G, Jeon YC, Koh Y, Kim W. 3D polycaprolactone scaffolds with controlled pore structure using a rapid prototyping system. *J Mater Sci Mater Med*. 2009;20(1):229-234. doi:10.1007/s10856-008-3573-4
1051. Almeida H V, Cunniffe GM, Vinardell T, Buckley CT, O'Brien FJ, Kelly DJ. Coupling Freshly Isolated CD44(+) Infrapatellar Fat Pad-Derived Stromal Cells with a TGF- β 3 Eluting Cartilage ECM-Derived Scaffold as a Single-Stage Strategy for Promoting Chondrogenesis. *Adv Healthc Mater*. 2015;4(7):1043-1053. doi:10.1002/adhm.201400687
1052. Jiménez G, Venkateswaran S, López-Ruiz E, et al. A soft 3D polyacrylate hydrogel recapitulates the cartilage niche and allows growth-factor free tissue engineering of human articular cartilage. *Acta Biomater*. 2019;90:146-156. doi:10.1016/j.actbio.2019.03.040
1053. López-Ruiz E, Perán M, Cobo-Molinos J, et al. Chondrocytes extract from patients with osteoarthritis induces chondrogenesis in infrapatellar fat pad-derived stem cells.

DOCTORAL THESIS DANIEL MARTÍNEZ MORENO

- Osteoarthr Cartil.* 2013;21(1):246-258. doi:10.1016/j.joca.2012.10.007
1054. Wickham MQ, Erickson GR, Gimble JM, Vail TP, Guilak F. Multipotent stromal cells derived from the infrapatellar fat pad of the knee. *Clin Orthop Relat Res.* 2003. doi:10.1097/01.blo.0000072467.53786.ca
1055. English A, Jones EA, Corscadden D, et al. A comparative assessment of cartilage and joint fat pad as a potential source of cells for autologous therapy development in knee osteoarthritis. *Rheumatology.* 2007. doi:10.1093/rheumatology/kem217
1056. Carroll SF, Buckley CT, Kelly DJ. Cyclic hydrostatic pressure promotes a stable cartilage phenotype and enhances the functional development of cartilaginous grafts engineered using multipotent stromal cells isolated from bone marrow and infrapatellar fat pad. *J Biomech.* 2014. doi:10.1016/j.jbiomech.2013.12.006
1057. Luo L, O'Reilly AR, Thorpe SD, Buckley CT, Kelly DJ. Engineering zonal cartilaginous tissue by modulating oxygen levels and mechanical cues through the depth of infrapatellar fat pad stem cell laden hydrogels. *J Tissue Eng Regen Med.* 2017. doi:10.1002/term.2162
1058. Luo L, Chu JYJ, Eswaramoorthy R, Mulhall KJ, Kelly DJ. Engineering Tissues That Mimic the Zonal Nature of Articular Cartilage Using Decellularized Cartilage Explants Seeded with Adult Stem Cells. *ACS Biomater Sci Eng.* 2017. doi:10.1021/acsbiomaterials.6b00020
1059. López-Ruiz E, Perán M, Cobo-Molinos J, et al. Chondrocytes extract from patients with osteoarthritis induces chondrogenesis in infrapatellar fat pad-derived stem cells. *Osteoarthr Cartil.* 2013;21(1):246-258. doi:10.1016/j.joca.2012.10.007
1060. López-Ruiz E, Jiménez G, Kwiatkowski W, et al. Impact of TGF- β family-related growth factors on chondrogenic differentiation of adipose-derived stem cells isolated from lipoaspirates and infrapatellar fat pads of osteoarthritic patients. *Eur Cells Mater.* 2018. doi:10.22203/eCM.v035a15
1061. Mi HY, Jing X, Salick MR, Cordie TM, Peng XF, Turng LS. Properties and fibroblast cellular response of soft and hard thermoplastic polyurethane electrospun nanofibrous scaffolds. *J Biomed Mater Res - Part B Appl Biomater.* 2015;103(5):960-970. doi:10.1002/jbm.b.33271
1062. O'Brien CM, Holmes B, Faucett S, Zhang LG. Three-dimensional printing of nanomaterial scaffolds for complex tissue regeneration. *Tissue Eng - Part B Rev.* 2015. doi:10.1089/ten.teb.2014.0168
1063. Baena JM, Jiménez G, López-Ruiz E, et al. Volume-by-volume bioprinting of chondrocytes-alginate bioinks in high temperature thermoplastic scaffolds for cartilage regeneration. *Exp Biol Med.* 2019. doi:10.1177/1535370218821128
1064. Cortes ARG, Galea K, No-Cortes J, Sammut EJ, Alzoubi EE, Attard NJ. Use of free CAD design software for 3D printing individualized face masks based on face scans. *Int J Comput Dent.* April 2020:1-7.
1065. Rabionet M, Polonio E, Guerra A, Martin J, Puig T, Ciurana J. Design of a Scaffold Parameter Selection System with Additive Manufacturing for a Biomedical Cell Culture. *Materials (Basel).* 2018;11(8):1427. doi:10.3390/ma11081427
1066. Ran Q, Yang W, Hu Y, et al. Osteogenesis of 3D printed porous Ti6Al4V implants with different pore sizes. *J Mech Behav Biomed Mater.* 2018. doi:10.1016/j.jmbbm.2018.04.010
1067. Tanaka M, Takayama A, Ito E, Sunami H, Yamamoto S, Shimomura M. Effect of pore size of self-organized honeycomb-patterned polymer films on spreading, focal adhesion, proliferation, and function of endothelial cells. In: *Journal of Nanoscience and Nanotechnology.* ; 2007. doi:10.1166/jnn.2007.514
1068. Wang H, Pieper J, Péters F, Van Blitterswijk CA, Lamme EN. Synthetic scaffold morphology

REFERENCES

- controls human dermal connective tissue formation. *J Biomed Mater Res - Part A*. 2005. doi:10.1002/jbm.a.30232
1069. Metwally S, Stachewicz U. Surface potential and charges impact on cell responses on biomaterials interfaces for medical applications. *Mater Sci Eng C*. 2019. doi:10.1016/j.msec.2019.109883
1070. Lawrence BJ, Madihally S V. Cell colonization in degradable 3D porous matrices. *Cell Adh Migr*. 2008. doi:10.4161/cam.2.1.5884
1071. Vuoriluoto K, Jokinen J, Kallio K, Salmivirta M, Heino J, Ivaska J. Syndecan-1 supports integrin $\alpha 2\beta 1$ -mediated adhesion to collagen. *Exp Cell Res*. 2008;314(18):3369-3381. doi:10.1016/j.yexcr.2008.07.005
1072. Keshel SH, Azhdadi SNK, Asefnejad A, Sadraeian M, Montazeri M, Biazar E. The relationship between cellular adhesion and surface roughness for polyurethane modified by microwave plasma radiation. *Int J Nanomedicine*. 2011;6:641-647. doi:10.2147/ijn.s17218
1073. Nam J, Johnson J, Lannutti JJ, Agarwal S. Modulation of embryonic mesenchymal progenitor cell differentiation via control over pure mechanical modulus in electrospun nanofibers. *Acta Biomater*. 2011;7(4):1516-1524. doi:10.1016/j.actbio.2010.11.022
1074. Cengiz IF, Oliveira JM, Reis RL. Micro-CT – a digital 3D microstructural voyage into scaffolds: a systematic review of the reported methods and results. *Biomater Res*. 2018;22(1):26. doi:10.1186/s40824-018-0136-8
1075. Gleadall A, Visscher D, Yang J, Thomas D, Segal J. Review of additive manufactured tissue engineering scaffolds: relationship between geometry and performance. *Burn Trauma*. 2018;6(1):19. doi:10.1186/s41038-018-0121-4
1076. Skedros JG, Sorenson SM, Takano Y, Turner CH. Dissociation of mineral and collagen orientations may differentially adapt compact bone for regional loading environments: results from acoustic velocity measurements in deer calcanei. *Bone*. 2006;39(1):143-151. doi:10.1016/j.bone.2005.12.007
1077. Jensen T, Wanczyk H, Sharma I, Mitchell A, Sayej WN, Finck C. Polyurethane scaffolds seeded with autologous cells can regenerate long esophageal gaps: An esophageal atresia treatment model. *J Pediatr Surg*. 2019;54(9):1744-1754. doi:10.1016/j.jpedsurg.2018.09.024
1078. Zhang J, Wehrle E, Vetsch JR, Paul GR, Rubert M, Müller R. Alginate dependent changes of physical properties in 3D bioprinted cell-laden porous scaffolds affect cell viability and cell morphology. *Biomed Mater*. 2019;14(6):65009. doi:10.1088/1748-605X/ab3c74
1079. Quent VMC, Loessner D, Friis T, Reichert JC, Huttmacher DW. Discrepancies between metabolic activity and DNA content as tool to assess cell proliferation in cancer research. *J Cell Mol Med*. 2010. doi:10.1111/j.1582-4934.2010.01013.x
1080. Winograd-Katz SE, Fässler R, Geiger B, Legate KR. The integrin adhesome: From genes and proteins to human disease. *Nat Rev Mol Cell Biol*. 2014;15(4):273-288. doi:10.1038/nrm3769
1081. Levato R, Webb WR, Otto IA, et al. The bio in the ink: cartilage regeneration with bioprintable hydrogels and articular cartilage-derived progenitor cells. *Acta Biomater*. 2017. doi:10.1016/j.actbio.2017.08.005
1082. Yan Y, Li Y, Song L, Zeng C, Li Y. Pluripotent stem cell expansion and neural differentiation in 3-D scaffolds of tunable Poisson's ratio. *Acta Biomater*. 2017;49:192-203. doi:10.1016/j.actbio.2016.11.025
1083. Parvinzadeh Gashti M, Hulliger J, Burgener M, Oulevey-Aboulfad H, Alimohammadi F,

DOCTORAL THESIS DANIEL MARTÍNEZ MORENO

- Bowlin G. Microscopic methods to study the structure of scaffolds in bone tissue engineering: A brief review. In: Vol 1. ; 2012:625-638.
1084. Oh SH, Kim TH, Im G II, Lee JH. Investigation of Pore Size Effect on Chondrogenic Differentiation of Adipose Stem Cells Using a Pore Size Gradient Scaffold. *Biomacromolecules*. 2010;11(8):1948-1955. doi:10.1021/bm100199m
1085. Singh N, Rahatekar SS, Koziol KKK, et al. Directing Chondrogenesis of Stem Cells with Specific Blends of Cellulose and Silk. *Biomacromolecules*. 2013;14(5):1287-1298. doi:10.1021/bm301762p
1086. Mason C, Dunnill P. A brief definition of regenerative medicine. *Regen Med*. 2007;3(1):1-5. doi:10.2217/17460751.3.1.1
1087. Houard X, Goldring MB, Berenbaum F. Homeostatic Mechanisms in Articular Cartilage and Role of Inflammation in Osteoarthritis. *Curr Rheumatol Rep*. 2013;15(11):375. doi:10.1007/s11926-013-0375-6
1088. Heinegård D, Saxne T. The role of the cartilage matrix in osteoarthritis. *Nat Rev Rheumatol*. 2011;7(1):50-56. doi:10.1038/nrrheum.2010.198
1089. Martínez R, Martínez C, Calvo R. Osteoarthritis (artrosis) de rodilla. 2015;56(3).
1090. Makris EA, Gomoll AH, Malizos KN, Hu JC, Athanasiou KA. Repair and tissue engineering techniques for articular cartilage. *Nat Rev Rheumatol*. 2015;11(1):21.
1091. Tatsumura M, Sakane M, Ochiai N, Mizuno S. Off-loading of cyclic hydrostatic pressure promotes production of extracellular matrix by chondrocytes. *Cells Tissues Organs*. 2013;198(6):405-413. doi:10.1159/000360156
1092. Tan AR, Dong EY, Andry JP, Bulinski JC, Ateshian GA, Hung CT. Coculture of engineered cartilage with primary chondrocytes induces expedited growth. In: *Clinical Orthopaedics and Related Research*. Vol 469. Springer New York LLC; 2011:2735-2743. doi:10.1007/s11999-011-1772-7
1093. Sampat SR, O'Connell GD, Fong J V., Alegre-Aguarón E, Ateshian GA, Hung CT. Growth factor priming of synovium-derived stem cells for cartilage tissue engineering. *Tissue Eng - Part A*. 2011;17(17-18):2259-2265. doi:10.1089/ten.tea.2011.0155
1094. Rad MR, Eghbal MJ, Nadjmi N, et al. Polymeric scaffolds in tissue engineering: a literature review. *J Biomed Mater Res Part B Appl Biomater*. 2015;105(2):431-459. doi:10.1002/jbm.b.33547
1095. Tsai WB, Chen CH, Chen JF, Chang KY. The effects of types of degradable polymers on porcine chondrocyte adhesion, proliferation and gene expression. *J Mater Sci Mater Med*. 2006;17(4):337-343. doi:10.1007/s10856-006-8234-x
1096. Sanz-Herrera JA, Reina-Romo E. Cell-Biomaterial Mechanical Interaction in the Framework of Tissue Engineering: Insights, Computational Modeling and Perspectives. *Int J Mol Sci*. 2011;12(11):8217-8244. doi:10.3390/ijms12118217
1097. Zhang H, Hollister S. Comparison of bone marrow stromal cell behaviors on poly(caprolactone) with or without surface modification: Studies on cell adhesion, survival and proliferation. *J Biomater Sci Polym Ed*. 2009;20(14):1975-1993. doi:10.1163/156856208X396074
1098. Hinnemo M, Zhao J, Ahlberg P, et al. On Monolayer Formation of Pyrenebutyric Acid on Graphene. *Langmuir*. 2017;33(15):3588-3593. doi:10.1021/acs.langmuir.6b04237
1099. Douglas T, Haugen HJ. Coating of polyurethane scaffolds with collagen: Comparison of coating and cross-linking techniques. *J Mater Sci Mater Med*. 2008;19(7):2713-2719. doi:10.1007/s10856-008-3393-6

REFERENCES

1100. Haryńska A, Gubanska I, Kucinska-Lipka J, Janik H. Fabrication and characterization of flexible medical-grade TPU filament for Fused Deposition Modeling 3DP technology. *Polymers (Basel)*. 2018;10(12). doi:10.3390/polym10121304
1101. Galisteo-González F, Molina-Bolívar JA, Navarro SA, et al. Albumin-covered lipid nanocapsules exhibit enhanced uptake performance by breast-tumor cells. *Colloids Surf B Biointerfaces*. 2018;165:103-110. doi:10.1016/j.colsurfb.2018.02.024
1102. Chabi Sika K, Kefela T, Adoukonou-Sagbadja H, et al. A simple and efficient genomic DNA extraction protocol for large scale genetic analyses of plant biological systems. *Plant Gene*. 2015;1:43-45. doi:10.1016/j.plgene.2015.03.001
1103. Keshel SH, Azhdadi SNK, Asefnejad A, Sadraei M, Montazeri M, Biazar E. The relationship between cellular adhesion and surface roughness for polyurethane modified by microwave plasma radiation. *Int J Nanomedicine*. 2011;6:641-647. doi:10.2147/IJN.S17180
1104. Makki H, Adema KNS, Hendrix MMRM, et al. Weathering of a polyester-urethane clearcoat: Lateral inhomogeneities. *Polym Degrad Stab*. 2015;122:180-186. doi:10.1016/j.polymdegradstab.2015.10.022
1105. Gircys M, Ross BJ. Image Evolution Using 2D Power Spectra. Johnson C, ed. *Complexity*. 2019;2019:7293193. doi:10.1155/2019/7293193
1106. Goutelle S, Maurin M, Rougier F, et al. The Hill equation: a review of its capabilities in pharmacological modelling. *Fundam Clin Pharmacol*. 2008;22(6):633-648.
1107. Pina S, Canadas RF, Jiménez G, et al. Biofunctional Ionic-Doped Calcium Phosphates: Silk Fibroin Composites for Bone Tissue Engineering Scaffolding. *Cells Tissues Organs*. 2017;204(3-4):150-163. doi:10.1159/000469703
1108. Hung KC, Tseng CS, Hsu SH. Synthesis and 3D Printing of biodegradable polyurethane elastomer by a water-based process for cartilage tissue engineering applications. *Adv Healthc Mater*. 2014;3(10):1578-1587. doi:10.1002/adhm.201400018
1109. Wang C, Feng N, Chang F, et al. Injectable Cholesterol-Enhanced Stereocomplex Poly(lactide Thermogel Loading Chondrocytes for Optimized Cartilage Regeneration. *Adv Healthc Mater*. 2019;8(14):1-10. doi:10.1002/adhm.201900312
1110. Perez RA, Mestres G. Role of pore size and morphology in musculo-skeletal tissue regeneration. *Mater Sci Eng C*. 2016;61:922-939. doi:https://doi.org/10.1016/j.msec.2015.12.087
1111. Martínez-Moreno D, Jiménez G, Chocarro-Wrona C, et al. Pore geometry influences growth and cell adhesion of infrapatellar mesenchymal stem cells in biofabricated 3D thermoplastic scaffolds useful for cartilage tissue engineering. *Mater Sci Eng C Mater Biol Appl*. 2021;122:111933. doi:10.1016/j.msec.2021.111933
1112. Hung KC, Tseng CS, Dai LG, Hsu S hui. Water-based polyurethane 3D printed scaffolds with controlled release function for customized cartilage tissue engineering. *Biomaterials*. 2016;83:156-168. doi:10.1016/j.biomaterials.2016.01.019
1113. Howard GT. Biodegradation of polyurethane: A review. In: *International Biodeterioration and Biodegradation*. Vol 49. ; 2002:245-252. doi:10.1016/S0964-8305(02)00051-3
1114. Dahl JP, Caballero M, Pappa AK, Madan G, Shockley WW, van Aalst JA. Analysis of human auricular cartilage to guide tissue-engineered nanofiber-based chondrogenesis: implications for microtia reconstruction. *Otolaryngol Head Neck Surg*. 2011;145(6):915-923. doi:10.1177/0194599811419092
1115. Wen YT, Dai NT, Hsu S hui. Biodegradable water-based polyurethane scaffolds with a sequential release function for cell-free cartilage tissue engineering. *Acta Biomater*.

DOCTORAL THESIS DANIEL MARTÍNEZ MORENO

- 2019;88:301-313. doi:10.1016/j.actbio.2019.02.044
1116. Kundu B, Eltohamy M, Yadavalli VK, Kundu SC, Kim HW. Biomimetic Designing of Functional Silk Nanotopography Using Self-assembly. *ACS Appl Mater Interfaces*. 2016;8(42):28458-28467. doi:10.1021/acsami.6b07872
1117. Kuo YC, Rajesh R. Nerve growth factor-loaded heparinized cationic solid lipid nanoparticles for regulating membrane charge of induced pluripotent stem cells during differentiation. *Mater Sci Eng C*. 2017;77:680-689. doi:10.1016/j.msec.2017.03.303
1118. Dvir T, Timko BP, Kohane DS, Langer R. Nanotechnological strategies for engineering complex tissues. *Nat Nanotechnol*. 2011;6(1):13-22. doi:10.1038/nnano.2010.246
1119. Li J, Mou X, Qiu J, et al. Surface Charge Regulation of Osteogenic Differentiation of Mesenchymal Stem Cell on Polarized Ferroelectric Crystal Substrate. *Adv Healthc Mater*. 2015;4(7):998-1003. doi:10.1002/adhm.201500032
1120. Sergeeva YN, Huang T, Felix O, et al. What is really driving cell-surface interactions? Layer-by-layer assembled films may help to answer questions concerning cell attachment and response to biomaterials. *Biointerphases*. 2016;11(1):019009. doi:10.1116/1.4943046
1121. Kohli N, Sharma V, Brown SJ, García-Gareta E. Synthetic polymers for skin biomaterials. In: *Biomaterials for Skin Repair and Regeneration*. Elsevier; 2019:125-149. doi:10.1016/b978-0-08-102546-8.00005-4
1122. Chocarro-Wrona C, de Vicente J, Antich C, et al. Validation of the 1,4-butanediol thermoplastic polyurethane as a novel material for 3D bioprinting applications. *Bioeng Transl Med*. 2021;6(1):e10192. doi:10.1002/btm2.10192
1123. Dai W, Kawazoe N, Lin X, Dong J, Chen G. The influence of structural design of PLGA/collagen hybrid scaffolds in cartilage tissue engineering. *Biomaterials*. 2010;31(8):2141-2152. doi:10.1016/j.biomaterials.2009.11.070
1124. Singh P, Schwarzbauer JE. Fibronectin and stem cell differentiation - lessons from chondrogenesis. *J Cell Sci*. 2012;125(16):3703-3712. doi:10.1242/jcs.095786
1125. Cai R, Nakamoto T, Kawazoe N, Chen G. Influence of stepwise chondrogenesis-mimicking 3D extracellular matrix on chondrogenic differentiation of mesenchymal stem cells. *Biomaterials*. 2015;52(1):199-207. doi:10.1016/j.biomaterials.2015.02.033
1126. Luo G, Wang J, Wang Y, Feng B, Weng J. Synthesis and characterisation of multifunctional alginate microspheres via the in situ formation of ZnO quantum dots and the graft of 4-(1-pyrenyl) butyric acid to sodium alginate. *J Microencapsul*. 2015;32(2):129-136. doi:10.3109/02652048.2014.950712
1127. Santin M, Motta A, Denyer SP, Cannas M. Effect of the urine conditioning film on ureteral stent encrustation and characterization of its protein composition. *Biomaterials*. 1999;20(13):1245-1251. doi:10.1016/S0142-9612(99)00026-5
1128. Sallent I, Capella-Monsonís H, Zeugolis DI. Production and characterization of chemically cross-linked collagen scaffolds. In: *Methods in Molecular Biology*. Vol 1944. ; 2019:23-38. doi:10.1007/978-1-4939-9095-5_3
1129. Wan W, Lin Y, Prakash A, Zhou Y. Three-dimensional carbon-based architectures for oil remediation: from synthesis and modification to functionalization. *J Mater Chem A*. 2016;4(48):18687-18705. doi:10.1039/C6TA07211A
1130. Byers PH, Bonadio JF. 4 - The molecular basis of clinical heterogeneity in osteogenesis imperfecta: Mutations in type I collagen genes have different effects on collagen processing. In: Lloyd JK, Scriver CRBT-G and MD in P, eds. *Butterworths International Medical Reviews*. Butterworth-Heinemann; 1985:56-90. doi:https://doi.org/10.1016/B978-0-407-02312-3.50009-0

REFERENCES

1131. Krüger-Genge A, Dietze S, Yan W, et al. Endothelial cell migration, adhesion and proliferation on different polymeric substrates. *Clin Hemorheol Microcirc.* 2018;70:511-529. doi:10.3233/CH-189317
1132. Antich C, Jiménez G, de Vicente J, et al. Development of a Biomimetic Hydrogel Based on Predifferentiated Mesenchymal Stem-Cell-Derived ECM for Cartilage Tissue Engineering. *Adv Healthc Mater.* 2021;10(8):2001847. doi:https://doi.org/10.1002/adhm.202001847
1133. Ghosh S, Laha M, Mondal S, Sengupta S, Kaplan DL. In vitro model of mesenchymal condensation during chondrogenic development. *Biomaterials.* 2009;30(33):6530-6540. doi:10.1016/j.biomaterials.2009.08.019
1134. Masutani T, Yamada S, Hara A, Takahashi T, Green PG, Niwa M. Exogenous Application of Proteoglycan to the Cell Surface Microenvironment Facilitates to Chondrogenic Differentiation and Maintenance. *Int J Mol Sci.* 2020;21(20):7744. doi:10.3390/ijms21207744
1135. Masutani T, Yamada S, Hara A, Takahashi T, Green PG, Niwa M. Exogenous Application of Proteoglycan to the Cell Surface Microenvironment Facilitates to Chondrogenic Differentiation and Maintenance. *Int J Mol Sci.* 2020;21(20):7744. doi:10.3390/ijms21207744
1136. Lu J, Shen X, Sun X, et al. Increased recruitment of endogenous stem cells and chondrogenic differentiation by a composite scaffold containing bone marrow homing peptide for cartilage regeneration. *Theranostics.* 2018;8(18):5039-5058. doi:10.7150/thno.26981
1137. Zhang Y, Liu X, Zeng L, et al. Polymer Fiber Scaffolds for Bone and Cartilage Tissue Engineering. *Adv Funct Mater.* 2019;29(36):1-20. doi:10.1002/adfm.201903279
1138. Kouhi M, Fathi M, Prabhakaran MP, Shamanian M, Ramakrishna S. Enhanced proliferation and mineralization of human fetal osteoblast cells on PHBV-bredigite nanofibrous scaffolds. *Mater Today Proc.* 2018;5(7):15702-15709. doi:10.1016/j.matpr.2018.04.181
1139. Wang Z, Le H, Wang Y, et al. Instructive cartilage regeneration modalities with advanced therapeutic implantations under abnormal conditions. *Bioact Mater.* 2022;11(June 2021):317-338. doi:10.1016/j.bioactmat.2021.10.002
1140. Martínez-Moreno D, Jiménez G, Gálvez-Martín P, Rus G, Marchal JA. Cartilage biomechanics: A key factor for osteoarthritis regenerative medicine. *Biochim Biophys Acta Mol basis Dis.* 2019;1865(6):1067-1075. doi:10.1016/j.bbadis.2019.03.011
1141. He D, Li H. Biomaterials affect cell-cell interactions in vitro in tissue engineering. *J Mater Sci Technol.* 2021;63:62-72. doi:https://doi.org/10.1016/j.jmst.2020.03.022
1142. Stott NS, Jiang TX, Chuong CM. Successive formative stages of precartilaginous mesenchymal condensations in vitro: modulation of cell adhesion by Wnt-7A and BMP-2. *J Cell Physiol.* 1999;180(3):314-324. doi:10.1002/(SICI)1097-4652(199909)180:3<314::AID-JCP2>3.0.CO;2-Y
1143. Accadbled F, Pham TT, Thevenin Lemoine C, Sales de Gauzy J. Implantation of an Actifit® Polyurethane Meniscal Scaffold 18 Months After Subtotal Lateral Meniscectomy in a 13-Year-Old Male Adolescent. *Am J Case Rep.* 2020;21:e920688. doi:10.12659/AJCR.920688
1144. Felson DT. Osteoarthritis of the Knee. *N Engl J Med.* 2006;354(8):841-848. doi:10.1056/NEJMcp051726
1145. Makris EA, Gomoll AH, Malizos KN, Hu JC, Athanasiou KA. Repair and tissue engineering techniques for articular cartilage. *Nat Rev Rheumatol.* 2015;11(1):21-34. doi:10.1038/nrrheum.2014.157
1146. European Medicines Agency. Spherox. Spherox - EMEA/H/C/002736 - II/0020. <https://www.ema.europa.eu/en/medicines/human/EPAR/spherox>. Published 2021.

DOCTORAL THESIS DANIEL MARTÍNEZ MORENO

Accessed July 28, 2022.

1147. Vinatier C, Guicheux J. Cartilage tissue engineering: From biomaterials and stem cells to osteoarthritis treatments. *Ann Phys Rehabil Med.* 2016;59(3):139-144.
1148. Zheng M-H, Willers C, Kirilak L, et al. Matrix-induced autologous chondrocyte implantation (MACI®): biological and histological assessment. *Tissue Eng.* 2007;13(4):737-746.
1149. Legendre F, Ollitrault D, Hervieu M, et al. Enhanced hyaline cartilage matrix synthesis in collagen sponge scaffolds by using siRNA to stabilize chondrocytes phenotype cultured with bone morphogenetic protein-2 under hypoxia. *Tissue Eng Part C Methods.* 2013;19(7):550-567.
1150. Willers C, Chen J, Wood D, Xu J, Zheng MH. Autologous chondrocyte implantation with collagen bioscaffold for the treatment of osteochondral defects in rabbits. *Tissue Eng.* 2005;11(7-8):1065-1076.
1151. Bentley G, Biant LC, Vijayan S, Macmull S, Skinner JA, Carrington RWJ. Minimum ten-year results of a prospective randomised study of autologous chondrocyte implantation versus mosaicplasty for symptomatic articular cartilage lesions of the knee. *J Bone Joint Surg Br.* 2012;94(4):504-509.
1152. Martel-Pelletier J. Pathophysiology of osteoarthritis. *Osteoarthr Cartil.* 1998;6(6):374-376. doi:10.1053/joca.1998.0140
1153. Hodge WA, Fijan RS, Carlson KL, Burgess RG, Harris WH, Mann RW. Contact pressures in the human hip joint measured in vivo. *Proc Natl Acad Sci.* 1986;83(9):2879-2883. doi:10.1073/pnas.83.9.2879
1154. Diomedea F, Gugliandolo A, Cardelli P, et al. Three-dimensional printed PLA scaffold and human gingival stem cell-derived extracellular vesicles: a new tool for bone defect repair. *Stem Cell Res Ther.* 2018;9(1):1-21.
1155. Su Y, Denbeigh JM, Camilleri ET, et al. Extracellular matrix protein production in human adipose-derived mesenchymal stem cells on three-dimensional polycaprolactone (PCL) scaffolds responds to GDF5 or FGF2. *Gene reports.* 2018;10:149-156.
1156. Dao TT-T, Vu NB, Pham LH, et al. In vitro production of cartilage tissue from rabbit bone marrow-derived mesenchymal stem cells and polycaprolactone scaffold. In: *Tissue Engineering and Regenerative Medicine.* Springer; 2017:45-60.
1157. Brown JH, Das P, DiVito MD, Ivancic D, Tan LP, Wertheim JA. Nanofibrous PLGA electrospun scaffolds modified with type I collagen influence hepatocyte function and support viability in vitro. *Acta Biomater.* 2018;73:217-227.
1158. Lin S, Cui L, Chen G, et al. PLGA/ β -TCP composite scaffold incorporating salvianolic acid B promotes bone fusion by angiogenesis and osteogenesis in a rat spinal fusion model. *Biomaterials.* 2019;196:109-121.
1159. Dai Y, Shen T, Ma L, Wang D, Gao C. Regeneration of osteochondral defects in vivo by a cell-free cylindrical poly (lactide-co-glycolide) scaffold with a radially oriented microstructure. *J Tissue Eng Regen Med.* 2018;12(3):e1647-e1661.
1160. Maggi A, Li H, Greer JR. Three-dimensional nano-architected scaffolds with tunable stiffness for efficient bone tissue growth. *Acta Biomater.* 2017;63:294-305.
1161. Caplan AI. Mesenchymal stem cells. *J Orthop Res.* 1991;9(5):641-650.
1162. Johnstone B, Hering TM, Caplan AI, Goldberg VM, Yoo JU. In vitro chondrogenesis of bone marrow-derived mesenchymal progenitor cells. *Exp Cell Res.* 1998;238(1):265-272.
1163. Mackay AM, Beck SC, Murphy JM, Barry FP, Chichester CO, Pittenger MF. Chondrogenic

REFERENCES

- differentiation of cultured human mesenchymal stem cells from marrow. *Tissue Eng.* 1998;4(4):415-428.
1164. Sheehy EJ, Buckley CT, Kelly DJ. Oxygen tension regulates the osteogenic, chondrogenic and endochondral phenotype of bone marrow derived mesenchymal stem cells. *Biochem Biophys Res Commun.* 2012;417(1):305-310.
1165. Vinardell T, Sheehy EJ, Buckley CT, Kelly DJ. A comparison of the functionality and in vivo phenotypic stability of cartilaginous tissues engineered from different stem cell sources. *Tissue Eng Part A.* 2012;18(11-12):1161-1170.
1166. Bruder SP, Jaiswal N, Haynesworth SE. Growth kinetics, self-renewal, and the osteogenic potential of purified human mesenchymal stem cells during extensive subcultivation and following cryopreservation. *J Cell Biochem.* 1997;64(2):278-294.
1167. Jimenez-Puerta GJ, Marchal JA, López-Ruiz E, Gálvez-Martín P. Role of mesenchymal stromal cells as therapeutic agents: potential mechanisms of action and implications in their clinical use. *J Clin Med.* 2020;9(2):445.
1168. Ghosh S, Laha M, Mondal S, Sengupta S, Kaplan DL. In vitro model of mesenchymal condensation during chondrogenic development. *Biomaterials.* 2009;30(33):6530-6540. doi:10.1016/j.biomaterials.2009.08.019
1169. Ross TD, Coon BG, Yun S, et al. Integrins in mechanotransduction. *Curr Opin Cell Biol.* 2013;25(5):613-618. doi:https://doi.org/10.1016/j.ceb.2013.05.006
1170. Tsimbouri PM, Childs PG, Pemberton GD, et al. Stimulation of 3D osteogenesis by mesenchymal stem cells using a nanovibrational bioreactor. *Nat Biomed Eng.* 2017;1(9):758-770. doi:10.1038/s41551-017-0127-4
1171. Bahmaee H, Owen R, Boyle L, et al. Design and Evaluation of an Osteogenesis-on-a-Chip Microfluidic Device Incorporating 3D Cell Culture. *Front Bioeng Biotechnol.* 2020;8(September):1-17. doi:10.3389/fbioe.2020.557111
1172. Li Z, Yao SJ, Alini M, Stoddart M. Chondrogenesis of human bone marrow mesenchymal stem cells is modulated by frequency and amplitude of dynamic compression and shear stress. *Eur Cells Mater.* 2009;18(SUPPL. 1):51.
1173. Kock LM, Malda J, Dhert WJA, Ito K, Gawlitta D. Flow-perfusion interferes with chondrogenic and hypertrophic matrix production by mesenchymal stem cells. *J Biomech.* 2014;47(9):2122-2129. doi:10.1016/j.jbiomech.2013.11.006
1174. Callejas A, Melchor J, Faris IH, Rus G. Viscoelastic model characterization of human cervical tissue by torsional waves. *J Mech Behav Biomed Mater.* 2021;115:104261. doi:10.1016/j.jmbbm.2020.104261
1175. Poon C. Measuring the density and viscosity of culture media for optimized computational fluid dynamics analysis of in vitro devices. *J Mech Behav Biomed Mater.* 2022;126(i). doi:10.1016/j.jmbbm.2021.105024
1176. Holman JP. *Heat Transfer - Si Units - Sie.* McGraw-Hill Education (India) Pvt Limited; 2002. <https://books.google.es/books?id=1wyjAgAAQBAJ>.
1177. Schlichting H, Gersten K. *Boundary-Layer Theory.* Springer Berlin Heidelberg; 2017. <https://books.google.es/books?id=bOUyDQAAQBAJ>.
1178. Tarrazó-Serrano D, Castiñeira-Ibáñez S, Sánchez-Aparisi E, Uris A, Rubio C. MRI compatible planar material acoustic lenses. *Appl Sci.* 2018;8(12). doi:10.3390/app8122634
1179. Watanabe T, Sassa K. Velocity and amplitude of P-waves transmitted through fractured zones composed of multiple thin low-velocity layers. In: *International Journal of Rock*

DOCTORAL THESIS DANIEL MARTÍNEZ MORENO

- Mechanics and Mining Sciences & Geomechanics Abstracts*. Vol 32. Elsevier; 1995:313-324.
1180. Antoniou A, Evripidou N, Giannakou M, Constantinides G, Damianou C. Acoustical properties of 3D printed thermoplastics. *J Acoust Soc Am*. 2021;149(4):2854-2864. doi:10.1121/10.0004772
 1181. Lanir Y. Mechanisms of residual stress in soft tissues. *J Biomech Eng*. 2009;131(4).
 1182. Hotaling NA, Tang L, Irvine DJ, Babensee JE. Biomaterial strategies for immunomodulation. *Annu Rev Biomed Eng*. 2015;17:317.
 1183. Humphrey JD, Dufresne ER, Schwartz MA. Mechanotransduction and extracellular matrix homeostasis. *Nat Rev Mol cell Biol*. 2014;15(12):802-812.
 1184. Gonalves A, Costa P, Rodrigues MT, Dias IR, Reis RL, Gomes ME. Effect of flow perfusion conditions in the chondrogenic differentiation of bone marrow stromal cells cultured onto starch based biodegradable scaffolds. *Acta Biomater*. 2011;7(4):1644-1652. doi:10.1016/j.actbio.2010.11.044
 1185. Bernhard JC, Hulphers E, Rieder B, et al. Perfusion Enhances Hypertrophic Chondrocyte Matrix Deposition, but Not the Bone Formation. *Tissue Eng - Part A*. 2018;24(11-12):1022-1033. doi:10.1089/ten.tea.2017.0356
 1186. Tarng YW, Huang BF, Su FC. A novel recirculating flow-perfusion bioreactor for periosteal chondrogenesis. *Int Orthop*. 2012;36(4):863-868. doi:10.1007/s00264-011-1291-x
 1187. Muhammad H, Rais Y, Miosge N, Ornan EM. The primary cilium as a dual sensor of mechanochemical signals in chondrocytes. *Cell Mol Life Sci*. 2012;69(13):2101-2107.
 1188. Wann AKT, Zuo N, Haycraft CJ, et al. Primary cilia mediate mechanotransduction through control of ATP-induced Ca²⁺ signaling in compressed chondrocytes. *FASEB J*. 2012;26(4):1663-1671.
 1189. Hosseini MS, Tafazzoli-Shadpour M, Haghighipour N, Aghdami N, Goodarzi A. The synergistic effects of shear stress and cyclic hydrostatic pressure modulate chondrogenic induction of human mesenchymal stem cells. *Int J Artif Organs*. 2015;38(10):557-564. doi:10.5301/ijao.5000433
 1190. Molladavoodi S, Robichaud M, Wulff D, Gorbet M. Corneal epithelial cells exposed to shear stress show altered cytoskeleton and migratory behaviour. *PLoS One*. 2017;12(6):1-16. doi:10.1371/journal.pone.0178981
 1191. Blaeser A, Duarte Campos DF, Puster U, Richtering W, Stevens MM, Fischer H. Controlling Shear Stress in 3D Bioprinting is a Key Factor to Balance Printing Resolution and Stem Cell Integrity. *Adv Healthc Mater*. 2016;5(3):326-333. doi:10.1002/adhm.201500677
 1192. Leverett LB, Hellums JD, Alfrey CP, Lynch EC. Red Blood Cell Damage by Shear Stress. *Biophys J*. 1972;12(3):257-273. doi:10.1016/S0006-3495(72)86085-5
 1193. Van de Walle AB, Moore MC, McFetridge PS. Sequential adaptation of perfusion and transport conditions significantly improves vascular construct recellularization and biomechanics. *J Tissue Eng Regen Med*. 2020;14(3):510-520. doi:10.1002/term.3015
 1194. Provin C, Takano K, Sakai Y, Fujii T, Shirakashi R. A method for the design of 3D scaffolds for high-density cell attachment and determination of optimum perfusion culture conditions. *J Biomech*. 2008;41(7):1436-1449. doi:10.1016/j.jbiomech.2008.02.025
 1195. Martínez-Moreno D, Venegas-Bustos D, Guillermo R, Gálvez-Martín P, Jiménez G, Marchal JA. Chondro-inductive b-TPUe-based functionalized scaffolds for application in cartilage tissue engineering. *Adv Healthc Mater*. 2022;In Press.
 1196. Imer R, Akiyama T, F. de Rooij N, et al. The measurement of biomechanical properties of

REFERENCES

- porcine articular cartilage using atomic force microscopy. *Arch Histol Cytol.* 2009;72(4+5):251-259. doi:10.1679/aohc.72.251
1197. Tschalkowsky M, Brander S, Barth V, et al. The articular cartilage surface is impaired by a loss of thick collagen fibers and formation of type I collagen in early osteoarthritis. *Acta Biomater.* 2022;146:274-283. doi:https://doi.org/10.1016/j.actbio.2022.04.036
1198. Zhao Q, Eberspaecher H, Lefebvre V, De Crombrughe B. Parallel expression of Sox9 and Col2a1 in cells undergoing chondrogenesis. *Dev Dyn an Off Publ Am Assoc Anat.* 1997;209(4):377-386. doi:10.1002/(SICI)1097-0177(199708)209:4<377::AID-AJA5>3.0.CO;2-F
1199. Li Y, Toole BP, Dealy CN, Kosher RA. Hyaluronan in limb morphogenesis. *Dev Biol.* 2007;305(2):411-420.
1200. Tuli R, Tuli S, Nandi S, et al. Transforming growth factor- β -mediated chondrogenesis of human mesenchymal progenitor cells involves N-cadherin and mitogen-activated protein kinase and Wnt signaling cross-talk. *J Biol Chem.* 2003;278(42):41227-41236.
1201. Akiyama H, Lyons JP, Mori-Akiyama Y, et al. Interactions between Sox9 and β -catenin control chondrocyte differentiation. *Genes Dev.* 2004;18(9):1072-1087.
1202. Shum L, Coleman CM, Hatakeyama Y, Tuan RS. Morphogenesis and dysmorphogenesis of the appendicular skeleton. *Birth Defects Res Part C Embryo Today Rev.* 2003;69(2):102-122.
1203. Hall BK, Miyake T. All for one and one for all: condensations and the initiation of skeletal development. *Bioessays.* 2000;22(2):138-147.
1204. Chen CW, Tsai YH, Deng WP, et al. Type I and II collagen regulation of chondrogenic differentiation by mesenchymal progenitor cells. *J Orthop Res.* 2005;23(2):446-453. doi:10.1016/j.jorthres.2004.09.002
1205. Rutgers M, Saris DB, Vonk LA, et al. Effect of collagen type I or type II on chondrogenesis by cultured human articular chondrocytes. *Tissue Eng - Part A.* 2013;19(1-2):59-65. doi:10.1089/ten.tea.2011.0416
1206. Cho S, Islas-Robles A, Nicolini AM, Monks TJ, Yoon J-Y. In situ, dual-mode monitoring of organ-on-a-chip with smartphone-based fluorescence microscope. *Biosens Bioelectron.* 2016;86:697-705. doi:10.1016/j.bios.2016.07.015
1207. Biechele P, Busse C, Solle D, Scheper T, Reardon K. Sensor systems for bioprocess monitoring. *Eng Life Sci.* 2015;15(5):469-488.
1208. Ulber R, Frerichs J-G, Beutel S. Optical sensor systems for bioprocess monitoring. *Anal Bioanal Chem.* 2003;376(3):342-348.
1209. Sonnleitner B. Automated measurement and monitoring of bioprocesses: key elements of the M 3 C strategy. *Meas Monit Model Control bioprocesses.* 2012:1-33.
1210. Sandor M, Rüdinger F, Bienert R, Grimm C, Solle D, Scheper T. Comparative study of non-invasive monitoring via infrared spectroscopy for mammalian cell cultivations. *J Biotechnol.* 2013;168(4):636-645.
1211. Claßen J, Aupert F, Reardon KF, Solle D, Scheper T. Spectroscopic sensors for in-line bioprocess monitoring in research and pharmaceutical industrial application. *Anal Bioanal Chem.* 2017;409(3):651-666.
1212. Logan DW, Carvell JP, Lee MPH. Creating new opportunities in process control through radio frequency impedance spectroscopy. In: *BMC Proceedings.* Vol 5. Springer; 2011:1-3.
1213. Downey BJ, Graham LJ, Breit JF, Glutting NK. A novel approach for using dielectric

DOCTORAL THESIS DANIEL MARTÍNEZ MORENO

- spectroscopy to predict viable cell volume (VCV) in early process development. *Biotechnol Prog.* 2014;30(2):479-487.
1214. Stanke M, Lindner P, Holz S, Hitzmann B. Automated sonic velocity calculation based on ultrasonic resonator measurements for on-line process monitoring. *Sensors Actuators A Phys.* 2013;198:69-74.
1215. Zimmermann R, Fiabane L, Gasteuil Y, Volk R, Pinton J-F. Characterizing flows with an instrumented particle measuring Lagrangian accelerations. *New J Phys.* 2013;15(1):15018.
1216. Flöter M, Bittar CK, Zabeu JL, Carneiro AC. Review of comparative studies between bone densitometry and quantitative ultrasound of the calcaneus in osteoporosis. *Acta Reumatol Port.* 2011;36(4):327-335.
1217. NCBI. PubMed: "cancer."
https://pubmed.ncbi.nlm.nih.gov/?term=cancer&filter=years.2003-2023&show_snippets=off&sort=date&sort_order=asc. Accessed November 22, 2022.
1218. NCBI. PubMed: "cardiovascular disease."
https://pubmed.ncbi.nlm.nih.gov/?term=cardiovascular+disease&filter=years.2003-2023&show_snippets=off&sort=date&sort_order=asc. Accessed November 22, 2022.
1219. NCBI. PubMed: "breast cancer."
https://pubmed.ncbi.nlm.nih.gov/?term=breast+cancer&filter=years.2003-2023&show_snippets=off&sort=date&sort_order=asc. Accessed November 22, 2022.
1220. NCBI. PubMed: "diabetes."
https://pubmed.ncbi.nlm.nih.gov/?term=diabetes&filter=years.2003-2023&show_snippets=off&sort=date&sort_order=asc. Accessed November 22, 2022.
1221. NCBI. PubMed: "tissue engineering."
https://pubmed.ncbi.nlm.nih.gov/?term=tissue+engineering&show_snippets=off&sort=date&sort_order=asc. Accessed November 22, 2022.
1222. NCBI. PubMed: "regenerative medicine."
https://pubmed.ncbi.nlm.nih.gov/?term=regenerative+medicine&show_snippets=off&sort=date&sort_order=asc. Accessed November 22, 2022.
1223. Wu P-H, Aroush DR-B, Asnacios A, et al. A comparison of methods to assess cell mechanical properties. *Nat Methods.* 2018;15(7):491-498. doi:10.1038/s41592-018-0015-1
1224. Lewis AH, Grandl J. Mechanical sensitivity of Piezo1 ion channels can be tuned by cellular membrane tension. Aldrich R, ed. *Elife.* 2015;4:e12088. doi:10.7554/eLife.12088
1225. Luo Q, Kuang D, Zhang B, Song G. Cell stiffness determined by atomic force microscopy and its correlation with cell motility. *Biochim Biophys Acta - Gen Subj.* 2016;1860(9):1953-1960. doi:<https://doi.org/10.1016/j.bbagen.2016.06.010>
1226. Li Z, Kupcsik L, Yao S, Alini M, Stoddart MJ. Mechanical load modulates chondrogenesis of human mesenchymal stem cells through the TGF- β pathway. *J Cell Mol Med.* 2010;14(6a):1338-1346.
1227. Gardner OFW, Fahy N, Alini M, Stoddart MJ. Joint mimicking mechanical load activates TGF β 1 in fibrin-poly (ester-urethane) scaffolds seeded with mesenchymal stem cells. *J Tissue Eng Regen Med.* 2017;11(9):2663-2666.
1228. Kasper G, Dankert N, Tuischer J, et al. Mesenchymal stem cells regulate angiogenesis according to their mechanical environment. *Stem Cells.* 2007;25(4):903-910.
1229. White JA, Deen WM. Agarose-Dextran Gels as Synthetic Analogs of Glomerular Basement Membrane: Water Permeability. *Biophys J.* 2002;82(4):2081-2089.

REFERENCES

- doi:[https://doi.org/10.1016/S0006-3495\(02\)75555-0](https://doi.org/10.1016/S0006-3495(02)75555-0)
1230. Moya ML, Cheng M-H, Huang J-J, et al. The effect of FGF-1 loaded alginate microbeads on neovascularization and adipogenesis in a vascular pedicle model of adipose tissue engineering. *Biomaterials*. 2010;31(10):2816-2826. doi:<https://doi.org/10.1016/j.biomaterials.2009.12.053>
1231. Brey EM, King TW, Johnston C, McIntire L V, Reece GP, Patrick CW. A Technique for Quantitative Three-Dimensional Analysis of Microvascular Structure. *Microvasc Res*. 2002;63(3):279-294. doi:<https://doi.org/10.1006/mvre.2002.2395>
1232. Lin C-H, Wang C-W, Fu Y-P. Characterization of Ni-Cu-Zn ferrite prepared from industrial wastes. *Ceram Int*. 2009;35(6):2325-2328. doi:<https://doi.org/10.1016/j.ceramint.2009.01.011>
1233. Martinez-Garcia FD, Fischer T, Hayn A, Mierke CT, Burgess JK, Harmsen MC. A Beginner's Guide to the Characterization of Hydrogel Microarchitecture for Cellular Applications. *Gels*. 2022;8(9):1-20. doi:10.3390/gels8090535
1234. Fischer T, Hayn A, Mierke CT. Fast and reliable advanced two-step pore-size analysis of biomimetic 3D extracellular matrix scaffolds. *Sci Rep*. 2019;9(1):8352. doi:10.1038/s41598-019-44764-5
1235. Doyle AD, Carvajal N, Jin A, Matsumoto K, Yamada KM. Local 3D matrix microenvironment regulates cell migration through spatiotemporal dynamics of contractility-dependent adhesions. *Nat Commun*. 2015;6:8720. doi:10.1038/ncomms9720
1236. Takahashi Y, Tabata Y. Effect of the fiber diameter and porosity of non-woven PET fabrics on the osteogenic differentiation of mesenchymal stem cells. *J Biomater Sci Polym Ed*. 2004;15(1):41-57. doi:10.1163/156856204322752228
1237. Roosa SMM, Kemppainen JM, Moffitt EN, Krebsbach PH, Hollister SJ. The pore size of polycaprolactone scaffolds has limited influence on bone regeneration in an in vivo model. *J Biomed Mater Res Part A*. 2010;92A(1):359-368. doi:<https://doi.org/10.1002/jbm.a.32381>
1238. Ho ST, Hutmacher DW. A comparison of micro CT with other techniques used in the characterization of scaffolds. *Biomaterials*. 2006;27(8):1362-1376. doi:<https://doi.org/10.1016/j.biomaterials.2005.08.035>
1239. Lu D, Zeng Z, Geng Z, et al. Macroporous methacrylated hyaluronic acid hydrogel with different pore sizes for in vitro and in vivo evaluation of vascularization. *Biomed Mater*. 2022;17(2):25006.
1240. Chiu Y-C, Cheng M-H, Engel H, et al. The role of pore size on vascularization and tissue remodeling in PEG hydrogels. *Biomaterials*. 2011;32(26):6045-6051. doi:<https://doi.org/10.1016/j.biomaterials.2011.04.066>
1241. Fischer T, Hayn A, Mierke CT. Effect of Nuclear Stiffness on Cell Mechanics and Migration of Human Breast Cancer Cells. *Front Cell Dev Biol*. 2020;8. <https://www.frontiersin.org/articles/10.3389/fcell.2020.00393>.
1242. Lien S-M, Ko L-Y, Huang T-J. Effect of pore size on ECM secretion and cell growth in gelatin scaffold for articular cartilage tissue engineering. *Acta Biomater*. 2009;5(2):670-679. doi:<https://doi.org/10.1016/j.actbio.2008.09.020>
1243. Kim HD, Valentini RF. Retention and activity of BMP-2 in hyaluronic acid-based scaffolds in vitro. *J Biomed Mater Res*. 2002;59(3):573-584. doi:<https://doi.org/10.1002/jbm.10011>
1244. Kim HJ, Kim U-J, Vunjak-Novakovic G, Min B-H, Kaplan DL. Influence of macroporous protein scaffolds on bone tissue engineering from bone marrow stem cells. *Biomaterials*.

DOCTORAL THESIS DANIEL MARTÍNEZ MORENO

- 2005;26(21):4442-4452. doi:<https://doi.org/10.1016/j.biomaterials.2004.11.013>
1245. Freed LE, Vunjak-Novakovic G, Biron RJ, et al. Biodegradable Polymer Scaffolds for Tissue Engineering. *Bio/Technology*. 1994;12(7):689-693. doi:10.1038/nbt0794-689
1246. de Vicente G, Lensen MC. Topographically and elastically micropatterned PEG-based hydrogels to control cell adhesion and migration. *Eur Polym J*. 2016;78:290-301. doi:<https://doi.org/10.1016/j.eurpolymj.2016.03.020>
1247. Almonacid Suarez AM, van der Ham I, Brinker MGL, van Rijn P, Harmsen MC. Topography-driven alterations in endothelial cell phenotype and contact guidance. *Heliyon*. 2020;6(6). doi:10.1016/j.heliyon.2020.e04329
1248. Al-Haque S, Miklas JW, Feric N, et al. Hydrogel Substrate Stiffness and Topography Interact to Induce Contact Guidance in Cardiac Fibroblasts. *Macromol Biosci*. 2012;12(10):1342-1353. doi:<https://doi.org/10.1002/mabi.201200042>
1249. Almonacid Suarez AM, Brinker MGL, Brouwer LA, van der Ham I, Harmsen MC, van Rijn P. Topography-Mediated Myotube and Endothelial Alignment, Differentiation, and Extracellular Matrix Organization for Skeletal Muscle Engineering. *Polymers (Basel)*. 2020;12(9). doi:10.3390/polym12091948
1250. Almonacid Suarez AM, Zhou Q, van Rijn P, Harmsen MC. Directional topography gradients drive optimum alignment and differentiation of human myoblasts. *J Tissue Eng Regen Med*. 2019;13(12):2234-2245. doi:<https://doi.org/10.1002/term.2976>
1251. Lee IS, Kwon OH, Meng W, Kang I-K, Ito Y. Nanofabrication of microbial polyester by electrospinning promotes cell attachment. *Macromol Res*. 2004;12(4):374-378.
1252. Moroni L, Licht R, de Boer J, de Wijn JR, van Blitterswijk CA. Fiber diameter and texture of electrospun PEOT/PBT scaffolds influence human mesenchymal stem cell proliferation and morphology, and the release of incorporated compounds. *Biomaterials*. 2006;27(28):4911-4922.
1253. Han N, Johnson JK, Bradley PA, Parikh KS, Lannutti JJ, Winter JO. Cell attachment to hydrogel-electrospun fiber mat composite materials. *J Funct Biomater*. 2012;3(3):497-513.
1254. Horbett TA, Waldburger JJ, Ratner BD, Hoffman AS. Cell adhesion to a series of hydrophilic-hydrophobic copolymers studies with a spinning disc apparatus. *J Biomed Mater Res*. 1988;22(5):383-404. doi:<https://doi.org/10.1002/jbm.820220503>
1255. Guerreiro R, Pires T, Guedes JM, Fernandes PR, Castro APG. On the Tortuosity of TPMS Scaffolds for Tissue Engineering. *Symmetry (Basel)*. 2020;12(4). doi:10.3390/sym12040596
1256. Niemczyk-Soczynska B, Grady A, Sajkiewicz P. Hydrophilic surface functionalization of electrospun nanofibrous scaffolds in tissue engineering. *Polymers (Basel)*. 2020;12(11):2636.
1257. Kirk GS. Natural change in Heraclitus. *Mind*. 1951;60(237):35-42.
1258. Hird SN, White JG. Cortical and cytoplasmic flow polarity in early embryonic cells of *Caenorhabditis elegans*. *J Cell Biol*. 1993;121(6):1343-1355.
1259. Choma MA, Ellerbee AK, Yazdanfar S, Izatt JA. Doppler flow imaging of cytoplasmic streaming using spectral domain phase microscopy. *J Biomed Opt*. 2006;11(2):24014.
1260. Williamson RE. Cytoplasmic Streaming in Characean Algae: Mechanism, Regulation by Ca²⁺, and Organization BT - Algal Cell Motility. In: Melkonian M, ed. Boston, MA: Springer US; 1992:73-98. doi:10.1007/978-1-4615-9683-7_3

REFERENCES

1261. Prost J, Jülicher F, Joanny J-F. Active gel physics. *Nat Phys*. 2015;11(2):111-117.
1262. Voituriez R, Joanny J-F, Prost J. Spontaneous flow transition in active polar gels. *EPL (Europhysics Lett)*. 2005;70(3):404.
1263. MatWeb. Polystere material. <https://www.matweb.com/search/DataSheet.aspx?MatGUID=1c41e50c2e324e00b0c4e419ca780304&ckck=1>. Accessed November 29, 2022.
1264. Guz N, Dokukin M, Kalaparthi V, Sokolov I. If cell mechanics can be described by elastic modulus: study of different models and probes used in indentation experiments. *Biophys J*. 2014;107(3):564-575. doi:10.1016/j.bpj.2014.06.033
1265. van Manen MA. The First Cry of the Child. *Qual Health Res*. 2016;27(7):1069-1076. doi:10.1177/1049732316673342
1266. Glatt V, Evans CH, Stoddart MJ. Regenerative rehabilitation: The role of mechanotransduction in orthopaedic regenerative medicine. *J Orthop Res*. 2019;37(6):1263-1269.
1267. Huang S, Ingber DE. Cell tension, matrix mechanics, and cancer development. *Cancer Cell*. 2005;8(3):175-176.
1268. Jonietz E. Mechanics: The forces of cancer. *Nature*. 2012;491(7425):S56-S57.
1269. Lewis GN, Randall M. *Thermodynamics*. Krishna Prakashan Media; 1963.
1270. Miyanishi K, Trindade MCD, Lindsey DP, et al. Effects of hydrostatic pressure and transforming growth factor- β 3 on adult human mesenchymal stem cell chondrogenesis in vitro. *Tissue Eng*. 2006;12(6):1419-1428.
1271. Schätti O, Grad S, Goldhahn J, et al. A combination of shear and dynamic compression leads to mechanically induced chondrogenesis of human mesenchymal stem cells. *Eur Cell Mater*. 2011;22(214-225):b97.
1272. Davidson D, Blanc A, Filion D, et al. Fibroblast growth factor (FGF) 18 signals through FGF receptor 3 to promote chondrogenesis. *J Biol Chem*. 2005;280(21):20509-20515.
1273. Liu X, Liu J, Kang N, et al. Role of insulin-transferrin-selenium in auricular chondrocyte proliferation and engineered cartilage formation in vitro. *Int J Mol Sci*. 2014;15(1):1525-1537.
1274. Temu TM, Wu K-Y, Gruppuso PA, Phornphutkul C. The mechanism of ascorbic acid-induced differentiation of ATDC5 chondrogenic cells. *Am J Physiol Metab*. 2010;299(2):E325-E334.
1275. NCBI. PubMed: "biomems." https://pubmed.ncbi.nlm.nih.gov/?term=biomems&filter=years.2012-2023&show_snippets=off&sort=date&sort_order=asc. Accessed November 30, 2022.
1276. NCB. PubMed: "bioreactor" and "tissue engineering." https://pubmed.ncbi.nlm.nih.gov/?term=bioreactor+AND+tissue+engineering&filter=years.2012-2023&show_snippets=off&sort=date&sort_order=asc. Accessed November 30, 2022.
1277. BOE-A-2019-5577. Ministerio De Sanidad. *Boletín Of del Estado*. 2020:61561-61567. https://www.mscbs.gob.es/profesionales/farmacia/pdf/ACUERDOS_DE_LA_CIPM_2062_web.pdf.
1278. Kramme R, Uhlig H. Technical Safety of Electrical Medical Technology Equipment and Systems. In: *Springer Handbook of Medical Technology*. ; 2011:35-47. doi:10.1007/978-3-540-74658-4_4

DOCTORAL THESIS DANIEL MARTÍNEZ MORENO

1279. Zhao W, Tian S, Huang L, Liu K, Dong L. The review of Lab-on-PCB for biomedical application. *Electrophoresis*. 2020;41(16-17):1433-1445. doi:<https://doi.org/10.1002/elps.201900444>
1280. LeCun Y, Bengio Y, Hinton G. Deep learning. *Nature*. 2015;521(7553):436-444. doi:10.1038/nature14539
1281. Schmidhuber J. Deep learning in neural networks: An overview. *Neural Networks*. 2015;61:85-117. doi:<https://doi.org/10.1016/j.neunet.2014.09.003>
1282. Hastie T, Tibshirani R, Friedman JH, Friedman JH. *The Elements of Statistical Learning: Data Mining, Inference, and Prediction*. Vol 2. Springer; 2009.
1283. Zaccone G, Karim MR. *Deep Learning with TensorFlow: Explore Neural Networks and Build Intelligent Systems with Python*. Packt Publishing Ltd; 2018.
1284. Tran D, Tan YK. Sensorless Illumination Control of a Networked LED-Lighting System Using Feedforward Neural Network. *IEEE Trans Ind Electron*. 2014;61(4):2113-2121. doi:10.1109/TIE.2013.2266084
1285. Zhao F, Yin Y, Lu WW, et al. Preparation and histological evaluation of biomimetic three-dimensional hydroxyapatite/chitosan-gelatin network composite scaffolds. *Biomaterials*. 2002;23(15):3227-3234.
1286. Brown DA, Chou YF, Beygui RE, Dunn JCY, Wu BM. Gelatin-embedded cell-polymer constructs for histological cryosectioning. *J Biomed Mater Res Part B Appl Biomater An Off J Soc Biomater Japanese Soc Biomater Aust Soc Biomater Korean Soc Biomater*. 2005;72(1):79-85.
1287. Kumon RE, Aehle M, Sabens D, et al. Spatiotemporal Effects of Sonoporation Measured by Real-Time Calcium Imaging. *Ultrasound Med Biol*. 2009;35(3):494-506. doi:<https://doi.org/10.1016/j.ultrasmedbio.2008.09.003>
1288. Wang Q, Zhong S, Ouyang J, et al. Osteogenesis of electrically stimulated bone cells mediated in part by calcium ions. *Clin Orthop Relat Res*. 1998;348:259-268.
1289. Tanikake Y, Akahane M, Furukawa A, et al. Calcium concentration in culture medium as a nondestructive and rapid marker of osteogenesis. *Cell Transplant*. 2017;26(6):1067-1076.
1290. Wert G de, Mummery C. Human embryonic stem cells: research, ethics and policy. *Hum Reprod*. 2003;18(4):672-682.
1291. Hyun I. The bioethics of stem cell research and therapy. *J Clin Invest*. 2010;120(1):71-75.
1292. Munsie M, Hyun I. A question of ethics: selling autologous stem cell therapies flaunts professional standards. *Stem Cell Res*. 2014;13(3):647-653.
1293. Thirabanjasak D, Tantiwongse K, Thorner PS. Angiomyeloproliferative lesions following autologous stem cell therapy. *J Am Soc Nephrol*. 2010;21(7):1218-1222.
1294. Jabr F. In the flesh: The embedded dangers of untested stem cell cosmetics. Scientific American. <http://www.scientificamerican.com/article/stem-cell-cosmetics/>. Accessed December 1, 2022.
1295. Bretzner F, Gilbert F, Baylis F, Brownstone RM. Target populations for first-in-human embryonic stem cell research in spinal cord injury. *Cell Stem Cell*. 2011;8(5):468-475.
1296. Gilbert F. The burden of normality: from 'chronically ill' to 'symptom free'. New ethical challenges for deep brain stimulation postoperative treatment. *J Med Ethics*. 2012;38(7):408-412.
1297. Hess P. Intracranial stem cell-based transplantation: Reconsidering the ethics of phase 1 clinical trials in light of irreversible interventions in the brain. *AJOB Neurosci*. 2012;3(2):3-

REFERENCES

- 13.
1298. Gilbert F, Harris AR, Dodds S, Kapsa RMI. Is a 'Last Chance' Treatment Possible After an Irreversible Brain Intervention? *AJOB Neurosci.* 2015;6(2):W1-W2. doi:10.1080/21507740.2015.1037469
1299. Regulation A. Regulation (EC) No 1394/2007 of the European Parliament and of the Council of 13 November 2007 on advanced therapy medicinal products and amending Directive 2001/83. *EC Regul No.* 2004;726.
1300. European Medicines Agency. Reflection paper on classification of advanced therapy medicinal products Reflection paper on classification of Advanced Therapy Medicinal Products Table of contents. *Therapy.* 2012;44(April):1-19.
1301. Ministerio de Sanidad, Servicios Sociales e Igualdad. Real Decreto 477/2014, de 13 de junio, por el que se regula la autorización de medicamentos de terapia avanzada de fabricación no industrial. *Boletín Of del Estado.* 2014;(144):45068-45078.
1302. de Prensa ISCIII G. La AEMPS y la Red TerCel organizan una jornada sobre buenas prácticas en terapia celular. 2019.
1303. van Meer P, Theunissen P, van den Hoorn T, Herberths C, van der Laan JW. Animal-free applications in the development of cell-based therapies. *Br J Clin Pharmacol.* 2021;87(6):2425-2427. doi:10.1111/bcp.14544
1304. Zhou* MY. STEP-based approach for direct slicing of CAD models for layered manufacturing. *Int J Prod Res.* 2005;43(15):3273-3285.
1305. Cătălin Iancu P, Daniela Iancu E, Alin Stăncioiu D. From CAD Model To 3D Print Via "STL" File Format. *Fiability Durab.* 2010;(1):73-80.
1306. Szilvsi-Nagy M, Matyasi GY. Analysis of STL files. *Math Comput Model.* 2003;38(7-9):945-960.
1307. Kim W, Kim M, Kim GH. 3D-Printed Biomimetic Scaffold Simulating Microfibril Muscle Structure. *Adv Funct Mater.* 2018;28(26):1800405. doi:https://doi.org/10.1002/adfm.201800405
1308. Liu Z, Zhang M, Bhandari B, Yang C. Impact of rheological properties of mashed potatoes on 3D printing. *J Food Eng.* 2018;220:76-82. doi:https://doi.org/10.1016/j.jfoodeng.2017.04.017
1309. Severini C, Derossi A, Azzollini D. Variables affecting the printability of foods: Preliminary tests on cereal-based products. *Innov Food Sci Emerg Technol.* 2016;38:281-291. doi:https://doi.org/10.1016/j.ifset.2016.10.001
1310. Yang F, Zhang M, Prakash S, Liu Y. Physical properties of 3D printed baking dough as affected by different compositions. *Innov Food Sci Emerg Technol.* 2018;49:202-210. doi:https://doi.org/10.1016/j.ifset.2018.01.001
1311. Adnan FA, Romlay FRM, Shafiq M. Real-time slicing algorithm for Stereolithography (STL) CAD model applied in additive manufacturing industry. In: *IOP Conference Series: Materials Science and Engineering.* Vol 342. IOP Publishing; 2018:12016.
1312. Brown AC, De Beer D. Development of a stereolithography (STL) slicing and G-code generation algorithm for an entry level 3-D printer. In: *2013 Africon.* IEEE; 2013:1-5.
1313. Topçu O, Taşcıoğlu Y, Ünver HÖ. A method for slicing CAD models in binary STL format. In: *6th International Advanced Technologies Symposium (IATS'11).* Vol 163. ; 2011:141-145.
1314. Dankar I, Haddarah A, Omar FEL, Sepulcre F, Pujolà M. 3D printing technology: The new era for food customization and elaboration. *Trends Food Sci Technol.* 2018;75:231-242.

DOCTORAL THESIS DANIEL MARTÍNEZ MORENO

- doi:<https://doi.org/10.1016/j.tifs.2018.03.018>
1315. Liu Z, Zhang M, Bhandari B, Wang Y. 3D printing: Printing precision and application in food sector. *Trends Food Sci Technol.* 2017;69:83-94. doi:<https://doi.org/10.1016/j.tifs.2017.08.018>
1316. Severini C, Derossi A, Ricci I, Caporizzi R, Fiore A. Printing a blend of fruit and vegetables. New advances on critical variables and shelf life of 3D edible objects. *J Food Eng.* 2018;220:89-100. doi:<https://doi.org/10.1016/j.jfoodeng.2017.08.025>
1317. Guo C, Zhang M, Bhandari B. Model Building and Slicing in Food 3D Printing Processes: A Review. *Compr Rev Food Sci Food Saf.* 2019;18. doi:10.1111/1541-4337.12443
1318. Hao L, Mellor S, Seaman O, Henderson J, Sewell N, Sloan M. Material characterisation and process development for chocolate additive layer manufacturing. *Virtual Phys Prototyp.* 2010;5(2):57-64. doi:10.1080/17452751003753212
1319. Wang J, Shaw LL. Rheological and extrusion behavior of dental porcelain slurries for rapid prototyping applications. *Mater Sci Eng A.* 2005;397(1):314-321. doi:<https://doi.org/10.1016/j.msea.2005.02.045>
1320. Khalil S, Sun W. Biopolymer deposition for freeform fabrication of hydrogel tissue constructs. *Mater Sci Eng C.* 2007;27(3):469-478. doi:<https://doi.org/10.1016/j.msec.2006.05.023>
1321. Derossi A, Caporizzi R, Ricci I, Severini C. Critical variables in 3D food printing. In: *Fundamentals of 3D Food Printing and Applications.* Elsevier; 2019:41-91.
1322. Wang L, Zhang M, Bhandari B, Yang C. Investigation on fish surimi gel as promising food material for 3D printing. *J Food Eng.* 2018;220:101-108. doi:<https://doi.org/10.1016/j.jfoodeng.2017.02.029>
1323. Yang F, Guo C, Zhang M, Bhandari B, Liu Y. Improving 3D printing process of lemon juice gel based on fluid flow numerical simulation. *LWT.* 2019;102:89-99. doi:<https://doi.org/10.1016/j.lwt.2018.12.031>
1324. Mantihal S, Prakash S, Bhandari B. Textural modification of 3D printed dark chocolate by varying internal infill structure. *Food Res Int.* 2019;121:648-657. doi:<https://doi.org/10.1016/j.foodres.2018.12.034>
1325. Liu Z, Bhandari B, Prakash S, Zhang M. Creation of internal structure of mashed potato construct by 3D printing and its textural properties. *Food Res Int.* 2018;111:534-543. doi:<https://doi.org/10.1016/j.foodres.2018.05.075>
1326. Milionis A, Noyes C, Loth E, et al. Water-Repellent Approaches for 3-D Printed Internal Passages. *Mater Manuf Process.* 2016;31(9):1162-1170. doi:10.1080/10426914.2015.1059443
1327. Ruiz-Cantu L, Gleadall A, Faris C, Segal J, Shakesheff K, Yang J. Characterisation of the surface structure of 3D printed scaffolds for cell infiltration and surgical suturing. *Biofabrication.* 2016;8(1):15016.
1328. Serra T, Planell JA, Navarro M. High-resolution PLA-based composite scaffolds via 3-D printing technology. *Acta Biomater.* 2013;9(3):5521-5530.
1329. Moroni L, De Wijn JR, Van Blitterswijk CA. Three-dimensional fiber-deposited PEOT/PBT copolymer scaffolds for tissue engineering: Influence of porosity, molecular network mesh size, and swelling in aqueous media on dynamic mechanical properties. *J Biomed Mater Res Part A An Off J Soc Biomater Japanese Soc Biomater Aust Soc Biomater Korean Soc Biomater.* 2005;75(4):957-965.
1330. Huttmacher DW, Schantz T, Zein I, Ng KW, Teoh SH, Tan KC. Mechanical properties and cell

REFERENCES

- cultural response of polycaprolactone scaffolds designed and fabricated via fused deposition modeling. *J Biomed Mater Res.* 2001;55(2):203-216. doi:[https://doi.org/10.1002/1097-4636\(200105\)55:2<203::AID-JBM1007>3.0.CO;2-7](https://doi.org/10.1002/1097-4636(200105)55:2<203::AID-JBM1007>3.0.CO;2-7)
1331. Leong KF, Chua CK, Sudarmadji N, Yeong WY. Engineering functionally graded tissue engineering scaffolds. *J Mech Behav Biomed Mater.* 2008;1(2):140-152. doi:<https://doi.org/10.1016/j.jmbbm.2007.11.002>
1332. Takahashi H, Miyashita H. Expressive fused deposition modeling by controlling extruder height and extrusion amount. In: *Proceedings of the 2017 CHI Conference on Human Factors in Computing Systems.* ; 2017:5065-5074.
1333. Yuk H, Zhao X. A new 3D printing strategy by harnessing deformation, instability, and fracture of viscoelastic inks. *Adv Mater.* 2018;30(6):1704028.
1334. Yang C, Vora HD, Chang Y. Behavior of auxetic structures under compression and impact forces. *Smart Mater Struct.* 2018;27(2):25012.
1335. Hankel WG. Über die aktinound piezoelektrischen eigenschaften des bergkrystalles und ihre beziehung zu den thermoelektrischen. *Abh Sächs.* 1881;12(s 457).
1336. Curie J, Curie P. Développement par compression de l'électricité polaire dans les cristaux hémihédres à faces inclinées. *Bull minéralogie.* 1880;3(4):90-93.
1337. Lippmann G. Principe de la conservation de l'électricité, ou second principe de la théorie des phénomènes électriques. *J Phys Théorique Appliquée.* 1881;10(1):381-394.
1338. Bushberg JT, Boone JM. *The Essential Physics of Medical Imaging.* Lippincott Williams & Wilkins; 2011.
1339. Heggie JCP, Liddell NA, Maher KP. *Applied Imaging Technology.* St. Vincent's Hospital; 2001.
1340. J A Gallego-Juarez. Piezoelectric ceramics and ultrasonic transducers. *J Phys E.* 1989;22(10):804. doi:10.1088/0022-3735/22/10/001
1341. Gallego-Juarez JA. Piezoelectric ceramics and ultrasonic transducers. *J Phys E.* 1989;22(10):804-816. doi:10.1088/0022-3735/22/10/001
1342. Srivastav A, Bhogi K, Mandal S, Sharad M. An Adaptive Low-Complexity Abnormality Detection Scheme for Wearable Ultrasonography. *IEEE Trans Circuits Syst II Express Briefs.* 2019;66(8):1466-1470. doi:10.1109/TCSII.2018.2881612
1343. Grosse CU, Reinhardt HW, Herb AT. 4.4 Ultrasound in through-transmission. *Adv Test Cem Mater Dur Setting Hardening-Final Rep RILEM TC 185-ATC.* 2005:163-190.
1344. Hunt JW, Arditi M, Foster FS. Ultrasound transducers for pulse-echo medical imaging. *IEEE Trans Biomed Eng.* 1983;(8):453-481.
1345. Lynnworth L. Industrial application of ultrasound. A review. *IEEE Trans Sonics Ultrason SU-22.* 1975:71-99.
1346. Breazeale MA, Cantrell Jr JH, Heyman JS. 2. Ultrasonic Wave Velocity and Attenuation Measurements. In: *Methods in Experimental Physics.* Vol 19. Elsevier; 1981:67-135.

39. Curriculum Vitae

39.1. Educational background

Master's Degree in Translational Research and Personalized Medicine.

Department of Human Anatomy and Embryology, Faculty of Medicine, University of Granada, Spain, 2016.

Bachelor's Degree in Biomedical Engineering.

School of Engineering, University Charles III of Madrid, Spain, 2012-2015.

39.1.1. Courses

- **Introductory course on machine learning to analyze biomedical data.** Duration: 25 hours. ibs.Granada. Date: 20/04/2021.
- **Python applied for Scientific and Technological Research.** Duration: 25 hours. Darwin Eventur - UGR. Date: 20/01/2020.
- **Raspberry Pi: practical course.** Duration: 20 hours. Darwin Eventur - UGR. Date: 16/12/2019.
- **Introductory course on statistical analysis in R.** Duration: 30 hours. Darwin Eventur - UGR. Date: 31/08/2017.

39.2. Contracts

Research fellow. Employing entity: FUNDACION EMPRESA UNIVERSIDAD DE GRANADA. Department: Department of Human Anatomy and Embryology (UGR), Center for Biomedical Research (CIBM). Biomedical Research Center (CIBM) Date of start-finish: 15/11/2017 - 14/03/2018 Duration: 4 months Dedication regime: Full-time.

Research fellow. Employing entity: FUNDACION EMPRESA UNIVERSIDAD DE GRANADA. Department: Department of Human Anatomy and Embryology (UGR), Center for Biomedical Research (CIBM). Biomedical Research Center (CIBM) Date of start-finish: 15/06/2017 - 05/10/2018 Duration: 3 months Dedication regime: Full-time.

Research staff. Employing entity: OTRI - University of Granada Department: Faculty of Science - UGR. Date of start-finish: 14/06/2019 - 03/02/2021 Duration: 2 years Dedication regime: Full time.

Service lease agreement. MECHANICAL PRESS DESIGN AND TESTING. FIBAO. Date: 01/03/2022.

Engineer. Employing entity: VICERRECTORADO DE INVESTIGACIÓN Y TRANSFERENCIA GESTIÓN DE INVESTIGACIÓN – UGR. Department: Department of Structural Mechanics, ETSICCP. Date of start-finish: 15/03/2021-14/09/2022. Duration: 6 months. Dedication regime: Full time.

Engineer. Employing entity: VICERRECTORADO DE INVESTIGACIÓN Y TRANSFERENCIA GESTIÓN DE INVESTIGACIÓN – UGR. Department: Department of Structural Mechanics, ETSICCP. Date of start-finish: 15/10/2021-31/01/2022. Duration: 3 months. Dedication regime: Full time.

Support technician. Employing entity: MINISTERIO DE CIENCIA E INNOVACIÓN. Ayudas para contratos personal técnico de apoyo a la I+D+I (BOE de 28/11/2020). PTA2020-019607-I/AEI/10.13039/501100011033. UGR – CIBM. Dater of start-finish: 01/02/2022-01/02/2025. Duratin: 36 months. Dedication regime: Full time.

39.3. Publications

- **BOOK.** Marchal Juan Antonio, Galisteo Francisco, Rueda Fernando. Almuraza. 2018. ISBN-10: 8417558578.
- Martínez-Moreno, D.; Jiménez, G.; Gálvez-Martín, P.; Rus, G.; Marchal, J.A. Cartilage biomechanics: a key factor for osteoarthritis regenerative medicine. *Biochimica et Biophysica Acta - Molecular Basis of Disease*. 2019 Jun 1;1865(6):1067-1075. **JIF (JCR): 4.352. Q1.**
- Martínez-Molina, Eduardo; Chocarro-Wrona, Carlos; Martínez-Moreno, Daniel; Marchal, Juan A; Boulaiz, Houria. 2020. Large-Scale Production of Lentiviral Vectors: Current Perspectives and Challenges. *Pharmaceutics*. 12-11. ISSN1999-4923. **JIF (JCR): 6.321. Q1.**
- Martínez-Moreno D, Jiménez G, Chocarro-Wrona C, Carrillo E, Montañez E, Galocha-León C, Clares-Naveros B, Gálvez-Martín P, Rus G, de Vicente J, Marchal JA. Pore geometry influences growth and cell adhesion of infrapatellar mesenchymal stem cells in biofabricated 3D thermoplastic scaffolds useful for cartilage tissue engineering. *Mater Sci Eng C Mater Biol Appl*. 2021 Mar;122:111933. doi: 10.1016/j.msec.2021.111933. Epub 2021 Feb 3. PMID: 33641924. **JIF (JCR): 8.457. Q1.**
- Chocarro-Wrona, Carlos; de Vicente, Juan; Antich, Cristina; et al; Marchal, Juan Antonio. 2021. Validation of the 1,4-butanediol thermoplastic polyurethane as a novel material for 3D bioprinting applications

Bioengineering & Translational Medicine. 6, pp.e 10192-e10192. . **JIF** (JCR): 10.684. Q1.

- Ríos-Galacho M, Martínez-Moreno D, López-Ruiz E, Gálvez-Martín P, Marchal JA. An Overview on the Manufacturing of Functional and Mature Cellular Skin Substitutes. Tissue Eng Part B Rev. 2022 Jan 21. doi: 10.1089/ten.TEB.2021.0131. Epub ahead of print. PMID: 34652978. **JIF** (JCR): 7.376. Q1.
- Martínez-Moreno D, Venegas-Bustos D, Rus G, Gálvez-Martín P, Jiménez G, Marchal JA. Chondro-Inductive b-TPUe-Based Functionalized Scaffolds for Application in Cartilage Tissue Engineering. Adv Healthc Mater. 2022 Oct;11(19):e2200251. doi: 10.1002/adhm.202200251. Epub 2022 Jul 29. PMID: 35857383. **JIF** (JCR): 11.092. Q1.
- Martínez-Moreno D, Callejas A, Jiménez G, Gálvez-Martín P, Rus G, Marchal JA. Induction and real-time ultrasonic monitoring of 3D cartilage-like tissue by a low shear stresses-based bioreactor. In Press.
- **COVER.** Martínez-Moreno D, Venegas-Bustos D, Rus G, Gálvez-Martín P, Jiménez G, Marchal JA. Chondro-Inductive b-TPUe-Based Functionalized Scaffolds for Application in Cartilage Tissue Engineering (Adv. Healthcare Mater. 19/2022). Adv Healthc Mater [Internet]. 2022 Oct 1;11(19):2270112. Available from: <https://doi.org/10.1002/adhm.202270112>. **JIF** (JCR): 11.092. Q1.

39.4. Contributions to congress

- ✓ SOUTH SUMMIT 2015. STARTUP COMPETITION. Startup: Skin Engineering Technologies. Over the best 400s startups.
- ✓ CLUBES DE CIENCIA ESPAÑA 2018. REALIZACIÓN CURSO: "Hacking Medicine 2.0". GRANADA, SPAIN. DATES: 03/09/2018-07/09/2018. Duration: 7 days.
- ✓ II JORNADAS DE JÓVENES INVESTIGADORES. Facultad de Farmacia de Granada. GRANADA, SPAIN. POSTER. DATES: 16/01/2020-17/01/2020. Duration. 2 days.
- ✓ III JORNADAS/I CONGRESO NACIONAL DE INVESTIGADORES EN FORMACIÓN: FOMENTANDO LA INTERDISCIPLINARIEDAD (JIFFI). UGR. POSTER. GRANADA, SPAIN. DATES: 20/06/2018-22/06/2018. Duration: 3 days.

- ✓ X REUNIÓN DEL CAPÍTULO NACIONAL ESPAÑOL DE LA SOCIEDAD EUROPEA DE BIOMECÁNICA. ESB. GRANADA. SPEAKING. Dates: 25/10/2021-26/16/2021. Duration 2 days.
- ✓ WEB'BIOMAT. WEBINAIRES SCIENTIFIQUES SUR LES BIOMATERIAUX. "CARTILAGE BIOMECHANICS: A RELEVANT ASPECT FOR SCAFFOLD CONFORMATION". European Symposium on Biomaterials and Related Areas – BioMAT. Date: 02/06/2022.
- ✓ ESMED GENERAL ASSEMBLY 2022. SPEAKING: "Cartilage biomechanics: A key factor for osteoarthritis regenerative medicine. European Society of Medicine. ESME. MADRID, SPAIN. Dates: 04/08/2022-06/08/2022.

39.5. Fellowships and Grants

- **Scholarship holder M.E.C.D.** Purpose: Predoctoral Issuing entity: Ministry of Education and Science and Science Performing entity: University of Granada Start-finish date: 2015- 2016 Faculty, institute, center: Facultad de Medicina.
- **Scholarship holder M.E.C.D.** Purpose: Predoctoral Issuing institution: Ministry of Education and Science and Science Performing entity: Universidad Carlos III de Madrid Start-finish date: 2013-2015 Faculty, institute, center: Escuela Politécnica Superior.
- **Scholarship Award for Excellence in High School.** Purpose: Pre-doctoral Issuing entity: Ministry of Education and Science Issuing entity: Ministry of Education and Science Date awarded: 2010.
- **Grant for Technical Support Personnel for R&D&I.** Ref. PTA2020-019607-i/aei/10.13039/501100011033.019607-I/AEI/10.13039/501100011033. Issuing entity: Ministry of Science and Innovation. Innovation. Performing entity: University of Granada Start-finish date: 2022- 2024 Award date: 2021- 2024. 2024 Award date: 2021.

39.6. Patents

- **Patent:** JUAN ANTONIO MARCHAL CORRALES; CARLOS CHOCARRO WRONA; ELENA LÓPEZ RUIZ; JUAN DE VICENTE ÁLVAREZ-MANZANEDA; CRISTINA ANTICH ACEDO; DANIEL MARTÍNEZ MORENO; GEMA JIMÉNEZ GONZÁLEZ; MACARENA PERÁN QUESADA; Título: BIOMATERIAL FOR USE IN THE TREATMENT OF DISEASES INVOLVING TISSUE REPAIR OR REGENERATION Código: P202030939
- **Patent:** JUAN ANTONIO MARCHAL CORRALES; DANIEL MARTÍNEZ MORNEO; GEMA JIMÉNEZ GONZÁLEZ. Título: MÉTODO DE FUNCIONALIZACIÓN DE MATERIAL POLIMÉRICO CON PBA Y SU USO EN BIOMEDICINA. Código: P202230435

DOCTORAL THESIS DANIEL MARTÍNEZ MORENO

- **Intelectual Property:** Macarena Perán Quesada; Elena López Ruiz; Carlos Chocarro Wrona; Daniel Martínez Moreno. Título: Anatomía Humana: Aprende Jugando (IPR-847) 16/01/2020. Entidad: Universidad de Jaén. Identificador: 2001312985786 <https://www.safecreative.org/work/2001312985786-anatomiahumana-aprende-jugando>